BRANCHED ORGANOMETALLIC COMPLEXES FOR MOLECULAR ELECTRONICS

BY

MICHAEL STEPHEN INKPEN

A Thesis submitted in partial fulfilment of the requirements for the award of

DOCTOR OF PHILOSOPHY OF IMPERIAL COLLEGE

FEBRUARY 2013

Department of Chemistry, Imperial College London

TABLE OF CONTENTS

DECLARATION

The work described in this thesis was carried out between October 2008 and December 2012 at the Department of Chemistry, Imperial College London. Unless stated otherwise, through cited reference or other acknowledgement, it is entirely my own work and has not been previously submitted for a degree at this or any other university.

PUBLICATIONS

Publications resulting from this work are listed below and reproduced in full in the digital content.

(1) "Metal σ–alkynyl complexes as molecular wires: a comparative study of electron density and delocalisation", M. S. Inkpen and N. J. Long, in *Molecular Design and Applications of Photofunctional Polymers and Materials*, eds. W.-Y. Wong and A. S. Abd-El-Aziz, Royal Society of Chemistry, 2012.

(2) "Probing electron transport in proteins at room temperature with single-molecule precision", M. S. Inkpen and T. Albrecht, *ACS Nano*, 2012, **6**, 13.

(3) "Oxidative purification of halogenated ferrocenes", M. S. Inkpen, S. Du, M. Driver, T. Albrecht and N. J. Long, *Dalton Trans.*, 2013, **42**, 2813.

ABSTRACT

To date, investigations concerning single or small groups of molecules for molecular electronics have largely focussed upon the transfer of electrons from donor to acceptor (electrodes or redox centres), through a single molecular pathway (bridging ligand or linear structure). Herein is described the synthesis and electrochemical properties of some branched and macrocyclic compounds containing $\{FeCp_2\}$ and $\{Ru(dppe)_2\}$ centres, with phenylene ethynylene backbones and pyridyl-termini for surface binding *(Chapters 2* and *5*, respectively). Such systems provide *two* well-defined molecular pathways for electron transfer, facilitating the study of quantum interference effects and other phenomena resulting from concurrent, and ultimately convergent, electron transport.

In addition, the large-scale 'oxidative purification' of 1,1'-diiodoferrocene (**1**) is presented *(Chapter 2)*, its usefulness as a starting material being further enhanced by an investigation into the optimisation of its (typically low-moderate yielding) reactions with terminal alkynes under Sonogashira cross-coupling conditions *(Chapter 3)*. As part of this study, attempts to synthesise 1,1'-bis[(4-thioacetylphenyl)ethynyl]ferrocene from **1** and 4-ethynylphenylthioacetate unexpectedly produced a cyclic trimer (**15**) of the latter. This observation afforded an explanation as to why the Fc–C≡C–C_6H_4–SAc motif may not be formed using this approach, and resulted in the realisation of a new route to β-phenylthioketones in general.

The linear complex $Ru(dppe)_2(C{\equiv}C{-}C_5H_4N)_2$ (**17**) has also been prepared – a synthesis complicated by the bifunctional nature of the 4-ethynylpyridine ligand *(Chapter 4)*. It is hoped that future conductance studies of this and extended structures will complement recent work by others on analogous complexes with isonitrile and thiolate-termini. Experiences with protecting the pyridyl nitrogen of 4-ethynylpyridine, and the moderate success of employing *N*-methyl-4-ethynylpyridinium triflate (**19**) as a ligand, are detailed.

Finally, 'mixed-valence' complexes of the type $[\{M(L)_n\}_2(\mu\text{-BL})]$ (μ-BL = bridging ligand) are discussed and evaluated in light of recently observed correlations between their measured $\Delta E_{1/2}^0$ values (the difference between sequential redox events, $\Delta E_{1/2}^0 = E_2^0 - E_1^0$) and IR triple bond frequencies of analogous $\{M(L)_n\}$–R (R = C≡O, $^-$C≡N, $^-$C≡C–Ph) complexes (a indicator of electron density at $\{M(L)_n\}$) *(Chapter 6)*. Trends in individual contributions to the free energy of comproportionation are explored for complexes of the type $[\{M(L)_n\}_2(\mu\text{-}C{\equiv}C{-}C{\equiv}C)]$.

ACKNOWLEDGEMENTS

I will be forever grateful to my supervisors, Nick and Tim, for the opportunity to study at Imperial, their support, patience, advice, and for everything I have learned over the last four years. Working with them has been nothing short of a fantastic experience.

To all the members of the Long and Albrecht groups past and present, thanks for joining me on this roller-coaster. Together we celebrated the highs – and shared many frustrations! A handful deserves special mention here, though I have fond memories of you all. Alex was a constant in the office and always there when you needed him. Lucy took me under her (lab) wing, teaching me a hell of a lot in the early days. Phil was a stand-up guy, savvy with his 'Irish wit', Chris entertained with rap (straight out of Leicester), and the dullest columns were brightened by Myra's fume-sash doodles and 'chicken-dancing' (don't ask). Jay and I shared a love of bourbon, disagreeing only on when is acceptable to start drinking it on a Friday afternoon/evening. To Tom, Mark, Ishan, Iris, James and Gigi: helping in some small way to supervise your projects was challenging at times, but extremely rewarding. I hope you also enjoyed it.

Special thanks go to Dick and Pete for running an exceptional NMR service, as well as for their help over the years. Pete never likes to be beaten by a sample, and he seldom is! I'd also like to acknowledge Andrew White for X-ray analysis of my compounds, and John Barton, John Hill, Lisa Haigh, the NMSSC, Stephen Boyer and Alan Dickerson for mass spectrometric and elemental analyses. I'm grateful to the EPSRC and the Department of Chemistry at Imperial for funding and accommodating my project.

It would have been impossible to complete this PhD without the support of my family and friends. They were always ready with a sympathetic ear, fun distractions, and great laughs when I needed them. To them I express my deepest gratitude. And lastly, but certainly by no means least, I am indebted to the doctors and nurses of St George's, Hammersmith, St Thomas' and The Royal Marsden (Surrey) for giving me the chance to finish what I'd started, and to start new things.

ABBREVIATIONS

°C	degrees Celsius
16-TMC	1,5,9,13-tetramethyl-1,5,9,13-tetraazacyclohexadecane
β	tunnelling decay constant
δ	chemical shift (ppm)
$\Delta_{as}G^0$	free energy of antiferromagnetic superexchange
$\Delta_{co}G^0$	free energy of comproportionation
ΔE_{DB}	energy gap between donor and bridge states
$\Delta E_{1/2}{}^0$	difference between the first ($E_1{}^0$) and second ($E_2{}^0$) equilibrium potentials (= $E_2{}^0$–$E_1{}^0$)
$\Delta_{el}G^0$	electrostatic factor
$\Delta\varphi$	phase difference
$\Delta_{in}G^0$	inductive factor
$\Delta_{ip}G^0$	ion-pairing factor
Δ_rG^0	reaction Gibbs energy
$\Delta_{re}G^0$	free energy of resonance exchange
$\Delta_{so}G^0$	free energy of solvation
$\Delta_{st}G^0$	statistical factor
$\Delta_{str}G^0$	structural factor
$\Delta\nu_{1/2}$	bandwidth at half-height
ε	molar extinction coefficient
ε_0	vacuum permittivity (F m^{-1})
ε_{max}	molar extinction coefficient at maximum absorption
ε_r	relative permittivity
Φ	magnetic flux
Γ	electronic coupling
κ	transmission coefficient
λ	reorganisation energy
λ_{max}	wavelength at maximum absorption
μ	micro-

μ_0	vacuum permeability
μ-BL	bridging ligand
μ_B	Bohr magneton
μ_{eff}	effective magnetic moment
ν	frequency
ν_{el}	Tolman electronic parameter
Ω	ohm
π	mathematical constant (3.14159...)
θ	Tolman cone angle
χ_m	molar susceptibility
Å	angstrom
A	acceptor
A	magnetic vector potential
AB effect	Aharonov–Bohm effect
AC	alternating current
AFM	atomic force microscope/microscopy
aq.	aqueous
ap	2-anilinopyridinate
ATR	attenuated total reflectance
Ar	aryl
B	bridge
B	magnetic field
bipy	bipyridine
bp	boiling point
br	broad
Bu	butyl
Bz	benzyl
c	concentration
C	capacitance
Calc.	calculated
CE	counter electrode

cm	centimetre
cod	1,5-cyclooctadiene
Cp	cyclopentadienyl
Cp*	1,2,3,4,5-pentamethylcyclopentadienyl
CTTS	charge-transfer-to-solvent
Cy	cyclohexyl
d	doublet
D	donor
d_{DA}	donor-acceptor separation distance
dd	doublet of doublets
ddd	doublet of doublet of doublets
dt	doublet of triplets
DEA	diethylamine
DEP	diethynylpyridine
depe	1,2-bis(diethylphosphino)ethane
DFT	density functional theory
dHpe	1,2-bis(dihydridophosphino)ethane
DIP	diiodopyridine
DIPA	diisopropylamine
DIPEA	diisopropylethylamine
diphos	diphosphine
dippe	1,2-bis(diisopropylphosphino)ethane
DMF	dimethylformamide
dmpe	1,2-bis(dimethylphosphino)methane
DMSO	dimethylsulfoxide
DNA	deoxyribonucleic acid
dppe	1,2-bis(diphenylphosphino)ethane
dppf	1,1'-bis(diphenylphosphino)ferrocene
dppm	1,2-bis(diphenylphosphino)methane
e	elementary charge
$E_{1/2}$	half wave potential

E_b	bond strength
E_F	Fermi level
EI+	electron impact ionisation (positive mode)
EP	ethynylpyridine
E_{pa}	anodic peak potential
E_{pc}	cathodic peak potential
EPR	electron paramagnetic resonance
ES+	electrospray ionisation (positive mode)
ESR	electron spin resonance
E_{ST}	singlet-triplet energy gap
eV	electronvolt
fc	1,1'-ferrocenediyl
Fc	ferrocenyl
g	gram
g	the Landé g-factor
G	conductance
$\mathscr{H}$	Heisenberg-Dirac-van Vleck Hamiltonian
h	hour
h	Planck's constant
$\hbar$	reduced Planck's constant
H_{ab}	electronic coupling parameter
HOMO	highest occupied molecular orbital
HR-MS	high resolution mass spectrometry
Hz	Hertz
^{i}	*iso*
I	current
infl	inflection
i_p^a	anodic peak current
i_p^c	cathodic peak current
IR	infrared
IVCT	intervalence charge transfer

$\mathcal{J}$	exchange coupling constant
J	coupling constant (Hz)
J	Joule
K	Kelvin
k_B	Boltzmann's constant
K_{co}	comproportionation constant
k_{et}	rate of electron transfer
k	kilo-
k_{tun}	rate of tunnelling electron transfer
k_{hop}	rate of hopping electron transfer
LMCT	ligand-to-metal charge transfer
LP	lone pair
LUMO	lowest unoccupied molecular orbital
m	*meta*
m	multiplet
m/z	mass/charge ratio
MALDI	matrix-assisted laser desorption/ionization
M	molar
Me	methyl
MHz	megahertz
mL	millilitre
MLCT	metal-to-ligand charge transfer
min	minute
mmol	millimoles
mp	melting point
n	*normal*
N	number of repeat molecular units
N_A	Avogadro constant
NDR	negative differential resistance
NMR	nuclear magnetic resonance
nm	nanometer

o	*ortho*
OPE	oligo(phenylene-ethynylene)
OTf	triflate
p	*para*
Ph	phenyl
PP_3	tris[2-(diphenylphosphino)ethyl]phosphine
ppm	parts per million
Pr	propyl
Py	pyridyl
py	pyrazine
q	quartet
quint.	quintet
R	gas constant
R_0	contact resistance
r_{ab}	distance between the two diabatic states
RE	reference electrode
r_i	ionic radius
$r_{MM'}$	metal-metal separation distance
R_s	solution resistance
R_u	uncompensated resistance
s	singlet
S	spin
S	Siemens
sh	shoulder
STM	scanning tunnelling microscope/microscopy
t	triplet
^{t}	*tert*
T	temperature
T	Tesla
T_e	electron transmission coefficient
TEA	triethylamine

THF	tetrahydrofuran
TIPS	triisopropylsilyl
TMEDA	N,N,N′,N′-Tetramethylethane-1,2-diamine
TMS	trimethylsilyl
UV-vis	ultraviolet-visible
V	voltage
V_s	scan rate
WE	working electrode
z	charge number of the ion

CHAPTER 1 : INTRODUCTION

The transfer of electrons through molecular species is a subject of intensive study, important in numerous subject areas including, but not limited to, chemical biology, molecular catalysis and materials science. Over the last 20 years, such processes have been increasingly considered in terms of 'molecular electronics', towards single, or groups of, molecules which may serve as nanoscale analogues of common electronic components.[1] Interest in this field can be largely attributed to its potential to extend, or even replace, existing solid-state approaches to the fabrication of integrated circuitry. These are currently facing significant challenges.[2] By using molecular networks, large reductions in interconnect/device sizes are possible compared to present day silicon-based equivalents. Bringing *advantages in cost, efficiency, and power dissipation*,[3] the molecular approach also has the potential to improve computing speeds and provide new electronic functionalities.[4] In the words of Richard Feynman, "there's plenty of room at the bottom".[5]

To date, the majority of species studied in this context have been linear (*e.g. Figure 1-1)*. By this it is meant that they provide only one *well-defined* molecular path through which an electron may be transmitted or transferred (though there may of course be multiple 'sub-molecular' routes). Whilst these undoubtedly represent the least complicated class of systems to study and understand, a myriad of other 'architectures' may be considered; including for example, species with parallel conduction pathways, three or more termini (see also early work by Tour *et al.*[6]), helical, or dendrimeric structures *(Figure 1-2)*. More closely resembling solid state *devices* than wires, the effects such large structural variations might have on a molecule's electronic properties are intriguing. It is important however 'not to run, before you can walk'. Charge transport through even a single, linear molecule is theoretically complex, and the investigation of such processes experimentally still presents significant challenges.

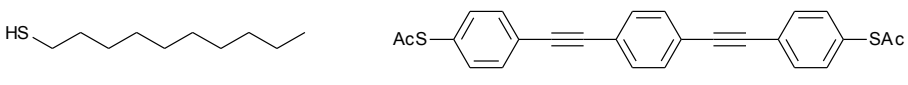

(a) (b)

Figure 1-1. Classic examples of 'molecular wires': (a) a thiol-terminated alkane[7] and (b) a thioacetyl-terminated oligo(phenylene-ethynylene) (OPE).[8]

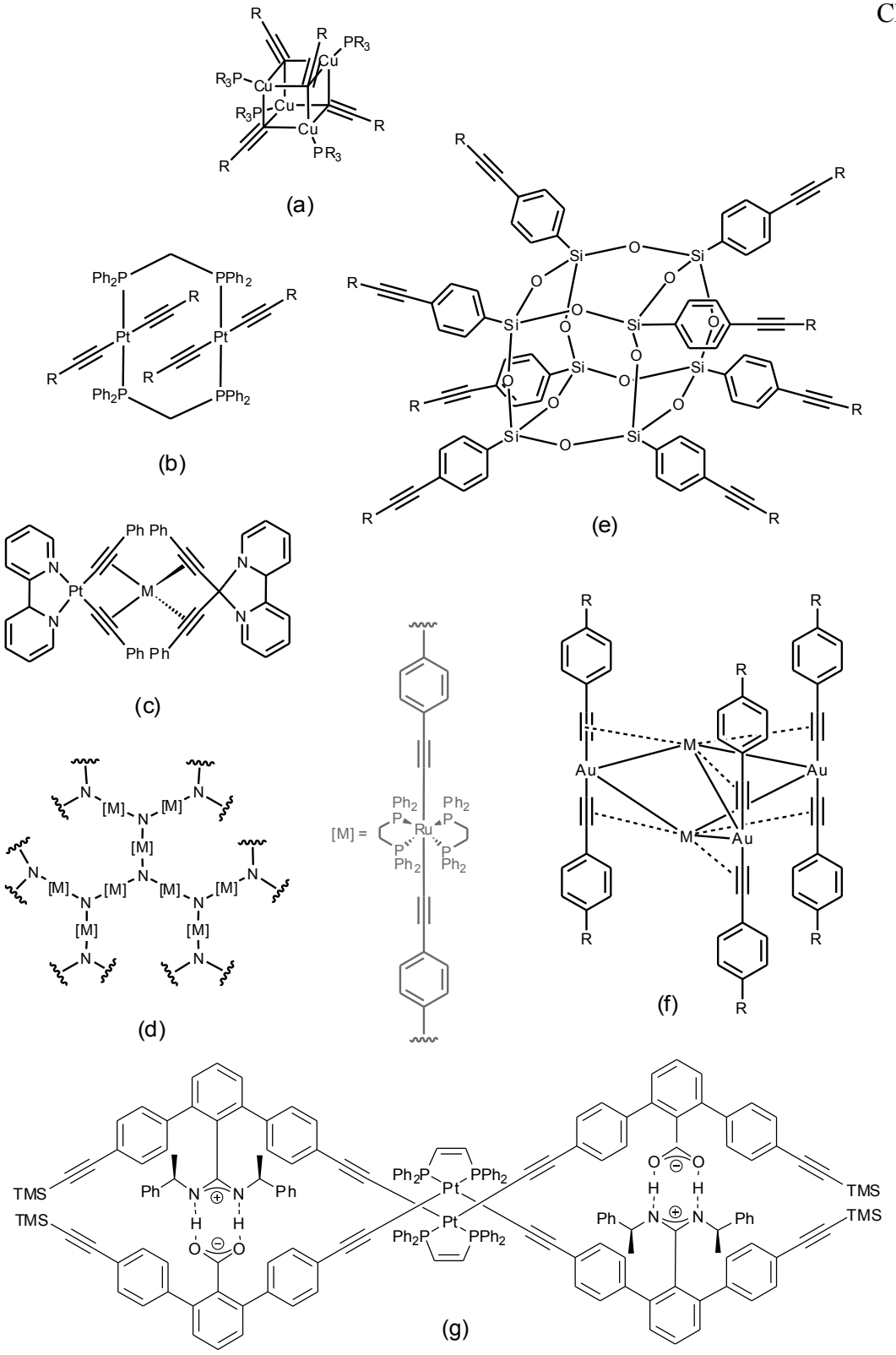

Figure 1-2. Not typically considered for molecular electronics, these selected examples (based on the phenylene-ethynylene/acetylide motif) exemplify the *potential* structural diversity possible in systems (M = Cu, Ag).[9]

Towards improved understanding, the primary focus of this work was to pursue the syntheses of novel *branched complexes* containing two well-defined molecular pathways. As relatively simple (but nonetheless interesting), non-linear materials, these make possible the rational experimental study of quantum interference effects and other phenomena resulting from concurrent electron transport on the nano-scale *(Figure 1-3)*. Critical in this context is the incorporation of *redox-active* groups, to enable the manipulation of electron transfer processes through individual branches. At present, investigations of analogous systems are restricted to a handful of theoretical studies,[10] and some very recent experiments with simple organic structures (see *section 1.1.2)*.[11]

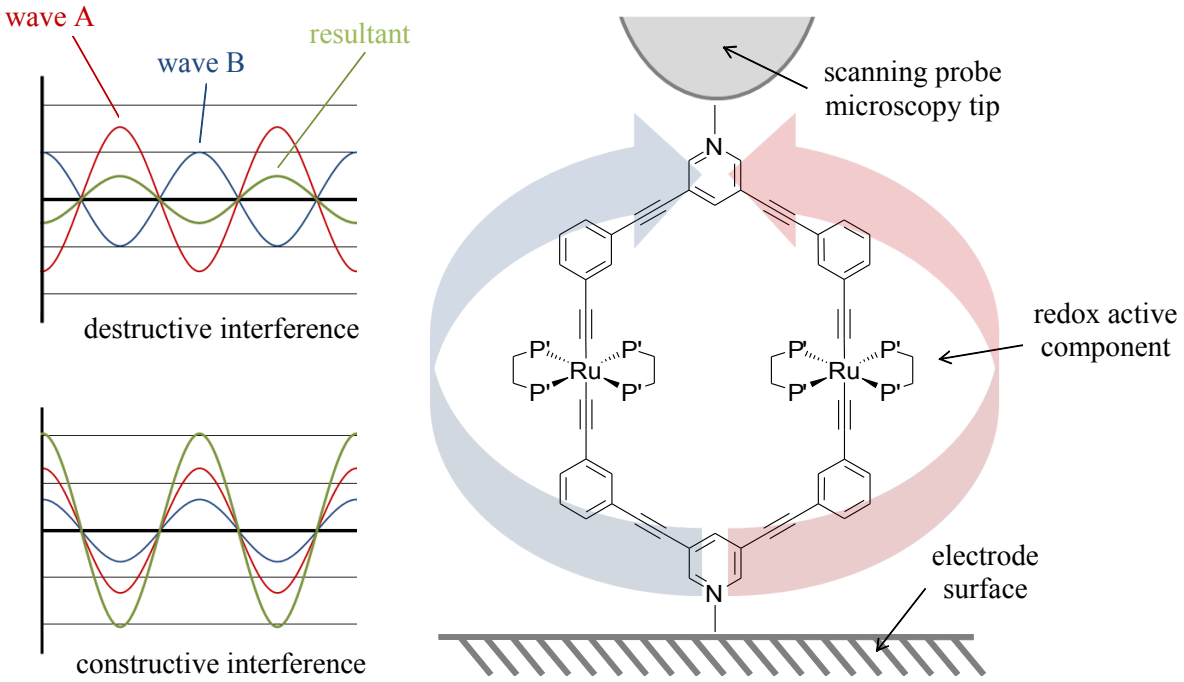

Figure 1-3. The concept of probing quantum interference effects in a single molecule, shown schematically in this case using scanning probe microscopy. Electron transfer through individual branches of the system can be modulated by redox events at $\{Ru(dppe)_2\}$. This could (for example) be used to switch destructive (top left diagram) or constructive (bottom left) interference effects off or on, affecting molecular conductance accordingly.

This chapter aims to provide context for those that follow in this thesis by giving a brief general introduction to molecular electronics, highlighting some important and relevant concepts.

The rationale behind the choice of synthetic targets *(Figure 1-4)* is presented and common strategies for the preparation of macrocycles (a critical branched structure class) are also discussed. Subsequent chapters are introduced in turn, with additional background as appropriate:

- *Chapter 2* discusses known ferrocene-based molecular electronic components and some caveats of ferrocenyl alkyne synthesis
- *Chapter 3* provides an overview of the Sonogashira cross-coupling reaction, focussing on its application to iodoferrocenes.
- *Chapter 4* reviews previously reported {$Ru(dppe)_2$}-containing molecular electronic components and the syntheses of metal-alkynyl complexes.
- *Chapter 5* presents known (all-organic and metal-containing) 'fixed-shape' macrocycles comprising the 3,5-diethynylpyridyl motif.
- *Chapter 6* briefly introduces electron transfer processes in terms of mixed-valence complexes (Marcus-Hush theory), discussing in some detail the factors contributing to $\Delta E_{1/2}^{0}$/comproportionation equilibria.

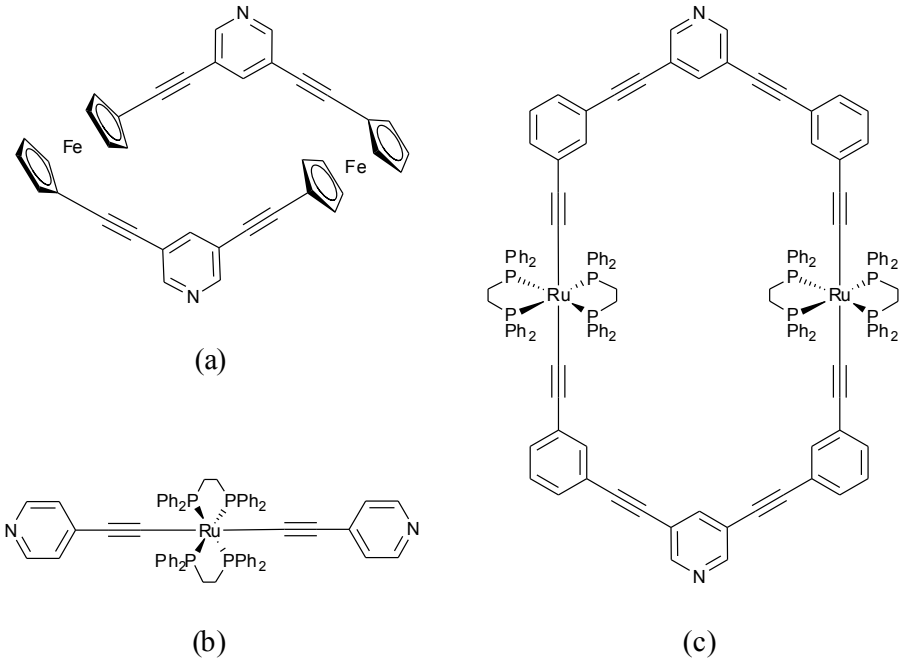

Figure 1-4. Representative synthetic targets pursued in this work. Critical features of the macrocyclic targets are i) surface binding groups (3,5-pyridyl), ii) a conjugated ('conducting') backbone (oligo(phenylene-ethynylene) framework), and iii) redox active centres (Fe/Ru). Efforts involving the linear target (b) are described in *Chapter 4*, providing insights vital for syntheses of (c).

1.1 MOLECULAR ELECTRONICS

Functionalised with suitable moieties for surface binding, the electronic properties of a single molecule, small group of molecules, or monolayer can be probed by self-assembly of the molecular component between two electrodes. Such arrangements are typically called 'molecular junctions',[1j,12] and can be prepared using various techniques. For representative examples, see: crossed-wire[8] and mechanical controllable break junctions,[13] scanning tunnelling microscopy (STM)[14] and conducting probe-atomic force microscopy,[14b] nanopores,[14b] NanoCells[15] and MolePores[16] (also, a*b initio*[17] and theoretical[18] methodologies). Surface binding groups thus far employed include thiol,[13,19] selenium,[20] isocyanide,[19b,21] amine,[19a,22] pyridine,[14c,23] carboxylic acid,[19a] diazonium salt (forming direct Si-C bonds),[24] and trimethylsilyl[25] functionalities, as well

as more elaborate bi- and tri-coordinate anchors such as cyclopentadithiophene[26] and tripodal pyridyl structures.[27]

Efforts towards improving the efficiency of 'molecular wires' (electron or hole conducting species demonstrating a more efficient route to electron transfer than through space) have resulted in the study of a vast array of different structure-types; from alkanes,[19a] alkenes[19e] and alkynes[23c] through to carbon nanotubes,[28] porphyrins[29] and DNA.[30] Though some (perhaps expected) structure-property trends have emerged (*e.g.* unsaturated species generally exhibit a higher conductance than their saturated equivalents (*Table 1-1),* conductance decreases with increasing molecular length),[1e,31] it is important to understand that the properties of a molecular junction are not solely ascribable to those of the individual (*i.e.* isolated) molecule. The nature of the molecule-electrode contact,[19a,b] energies of the molecular bridge HOMO (highest occupied molecular orbital) and LUMO (lowest unoccupied molecular orbital) relative to the Fermi level (E_F) of the electrodes,[18c,32] degree of localisation or delocalisation of the HOMO/LUMO over the entire molecular component,[33] temperature,[32,34] and local molecular environment (single adsorbed molecule/monolayer,[35] vacuum/condensed matter,[36] etc) will all impact upon the electron transport process (see *section 1.1.1)*.

In addition to wire-like behaviour (*i.e.* featureless current-voltage relationships) 'molecules' may exhibit properties more typical of electronic *components* (switches, diodes, etc) and in such cases are generally better described as 'molecular devices'. Interesting phenomena thus far observed include conductance/stochastic switching,[35c,37] hysteresis loops,[24] negative differential resistance,[34a] current rectification,[38] Coulomb blockade[32,39] and Kondo resonance.[40]

Table 1-1. Experimentally determined β-values[a] for selected structure types[41]

structure	formula	terminal group	β (Å^{-1})	ref
saturated alkane	$[-CH_2-]_n$	–SH	1.02-1.08 (± 0.14)	*19a*
		$-NH_2$	0.81-0.88 (± 0.01)	*19a*
		–COOH	0.77-0.81 (± 0.01)	*19a*
acene/oligophenyl	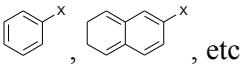 , etc	–SH	0.50 (± 0.09)	*19b*
		–NC	0.49 (± 0.08)	*19b*
oligo(phenylene-vinylene)	$[-CH=CH-C_6H_4-]_n$	–SAc	0.53-0.63 (± 0.13)	*19c*
			0.4 (± 0.12)	*19d*
polyene	$[-CH=CH-CH=CMe-]_n$	$-C_6H_4SH$	0.22 (± 0.04)	*19e*
oligo(phenylene-ethynylene)	$[-C\equiv C-C_6H_4-]_n$	–SAc	0.21 (± 0.01)	*19f*
oligothiophene	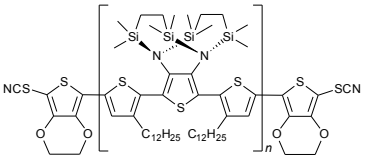	–SCN	0.1	*42*
oligoynes	$[-C\equiv C-]_n$	$-C_5H_4N$	0.06 (± 0.03)	*23c*

[a] β = the tunnelling decay constant (indicative of the efficiency of electron transport along a molecule); $G = Ae^{-\beta L}$ (G and L are molecular conductance (A·V^{-1}) and length (Å), respectively).[43]

The last decade has seen a particular surge of activity exploring the properties of metal complexes in this context (relevant Fe and Ru systems are discussed in *Chapter 2* and *Chapter 4*, respectively). Incorporation of a metal centre potentially enables redox or photochemical addressability of the molecular component,[44] also allowing its electronic properties to be 'tuned' via metal/ligand exchange.[32,45] Of particular interest are metal σ-alkynyl complexes, readily prepared[46] with a wide variety of transition metals. Acetylides have proved excellent mediators of electron transfer in organic systems (extended π-conjugation typically implies small HOMO-LUMO gaps/delocalised electrons), and their rigid and linear nature facilitates the synthesis of molecular species to well-defined, fixed lengths (guaranteeing through-space/through-bond electron transfer between donor and acceptor components by eliminating diffusive aspects).

1.1.1 Electron transport on the nano-scale

How does an electron move through a molecule? Over typical distances (*i.e.* 1-10 nm) three prevalent mechanisms of electron transport may be considered: *coherent tunnelling* (no

relaxation of electrons or nuclei), *hopping* (relaxation of electrons and nuclei) and *Coulomb blockade* (relaxation of electrons but not nuclei). Though one of these often dominates the overall process, they can occur in parallel. The observed *rate* of electron transfer (k_{et}) should therefore be considered as the sum of, for example, tunnelling (k_{tun}) and hopping (k_{hop}) terms, $k_{et} = k_{tun} + k_{hop}$;[1d] with their relative contribution for a given system explored through the temperature and distance dependency of k_{et} or G (molecular conductance, a related parameter) *(vida infra)*. The latter may be described by the Landauer formula (eqn (1-1)), where T_e is the electron transmission coefficient and $2e^2/h$ (= 77.4 μS) is the *quantum of conductance* (*i.e.* the maximum possible conductance for a single transport channel).[1d,e,18c,47]

$$G = \frac{2e^2}{h} T_e(E_F) \tag{1-1}$$

Properties of a typical molecular junction

A simplistic view of a molecular junction is shown in *Figure 1-5*. This denotes two electrodes (conducting surfaces, scanning probe microscopy tips, nanoparticles, etc) separated by a nanoscale gap that is bridged by a single molecule (and perhaps surrounding vacuum, condensed matter, or air). Each (metal) electrode comprises a continuum of energy levels which are filled up to a given energy level (E_F at 0 K), whereas the molecule contains an intrinsic series of discrete energy levels which are filled with electrons up to the energy of the HOMO.[*] Upon contact of the molecule with the metal surface (chemisorption/physisorption), both (a) mixing between the discrete molecule orbitals and metal electron states continuum and (b) charge flow occurs. This results in alignment of the Fermi level of electrodes within the HOMO-LUMO gap.[18c] At zero bias in a symmetrical system E_F for both metal termini is the same. *Figure 1-5* depicts the situation with an applied bias.

[*] In isolation, the Fermi level of a noble metal would be around -5 eV, the HOMO of a molecule around -9 eV (relative to the lowest energy level of a free electron in a vacuum).[18c]

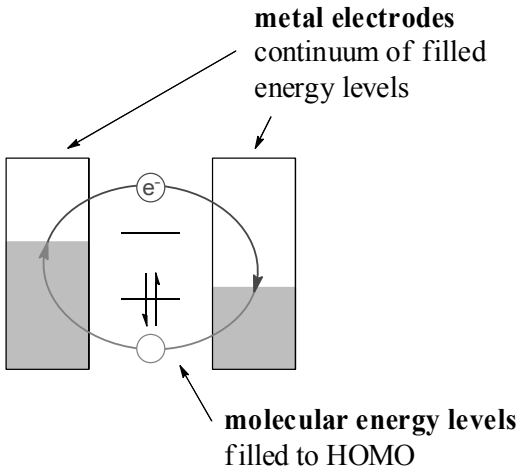

Figure 1-5. A two-electrode setup depicting the electronic energy levels, and *electron* (top arrow) or *hole* (bottom arrow) transfer pathways within a metal-molecule-metal junction (note that the position of the molecular energy levels relative to E_F, the Fermi level of the metal electrodes, changes for every system).[18c]

Other effects resulting from junction formation are worthy of note. First, the localised charge transfer and resulting dipole formation at the interface will perturb the *relative* energies of E_F and molecular orbital levels in the junction.[48] For example, when the dipole is aligned with its negative pole pointing toward the organic layer, the HOMO will be destabilised relative to E_F due to the addition of a repulsive electrostatic energy (and *vice-versa)*. Second, electronic coupling (Γ) between the molecule(s) and electrodes will significantly broaden the molecular energy levels (*caused by the decay of the metal surface states into the molecular region*[49]), also serving to reduce the solid state ('HOMO-LUMO') gap relative to its size in vacuum or as measured in solution.[1d,47a] The magnitude of Γ depends not only on the strength of the bond (E_b) between the termini surface and molecular contact groups (chemisorbed molecule-surface contacts, $E_b \approx$ 0.1-0.5 eV; physisorbed species, $E_b \approx$ 0.001-0.1 eV[47a]), but the extent of (intramolecular) coupling between the latter and the rest of the molecule. Interface effects which *reduce* the conductance of a junction collectively contribute to what is known as 'contact resistance' (R_0) (this term can be determined by extrapolating plots of conductance *vs.* molecular length (R) to zero).

Coherent tunnelling

Tunnelling is the non-classical process by which electrons move from a donor (D) to an acceptor (A) through vacuum, condensed matter or a molecular bridge (B), and in the simplest case this occurs coherently (no inelastic scattering events take place, *i.e.* energy transfer or dephasing). A direct, one-step process, transmitted electrons/holes do not reside on the bridge for any appreciable amount of time (they have only 'virtual' residence[†]). Notably, k_{tun} is faster through a bridging molecule than through vacuum (it can be considered that the former reduces the effective tunnelling barrier height, increasing the transmission probability through the barrier),[52] and through-bond tunnelling (where the current follows the bond overlaps along the molecule) is favoured over through-space tunnelling (direct transfer from terminal to terminal).[1e]

This mechanism is characterised by an exponential dependence of k_{et} on the donor-acceptor separation distance (d_{DA}) (or alternatively, on the number of repeat molecular units, *N)*, with k_{tunn} given by eqn (1-2). Here, $\beta = -(2/a)\ln(H_{BB}/\Delta E_{DB})$ in a superexchange model, H_{BB} = the internal coupling energy between the bridge units, a = the bridge unit length and ΔE_{DB} = the energy of the mediating state (D^+B^-A or DB^+A^-) above the ground state (assumed large relative to H_{BB}).[1d]

$$k_{tun} = k_0 \exp(-\beta d_{DA}) \tag{1-2}$$

Further distinctions between tunnelling processes may be made, depending on the relative energies of D, A, and B. Where the energy difference (ΔE_{DB}) between E_F and the closest molecular frontier orbital is large, transport is described as *off-resonance* tunnelling *(Figure 1-6*a); the suggested situation where molecular junctions are comprised of alkane dithiols (*e.g. Figure 1-1a)*.[47a] In contrast, *resonance* tunnelling *(Figure 1-6b)* occurs when ΔE_{DB} is small (*i.e.* thermally accessible) or zero. Here there is only a minimal dependence of k_{tun} on d_{DA}, due to a small β.[1d,53] This state was postulated for pyridyl-terminated oligoynes (*ab initio* calculations indicating the LUMO in these systems was in resonance with E_F).[23c]

[†] Through-bridge electron transfer (DBA to D^+BA^-) may be considered mediated via the 'virtual' states D^+B^-A (electron transfer) or DB^+A^- (hole transfer) (*i.e.* aided by high lying, empty, or low lying, fully occupied, bridge orbitals).[1d,44,50] Such a process is commonly referred to as *superexchange* (first introduced conceptually by McConnell[51]).

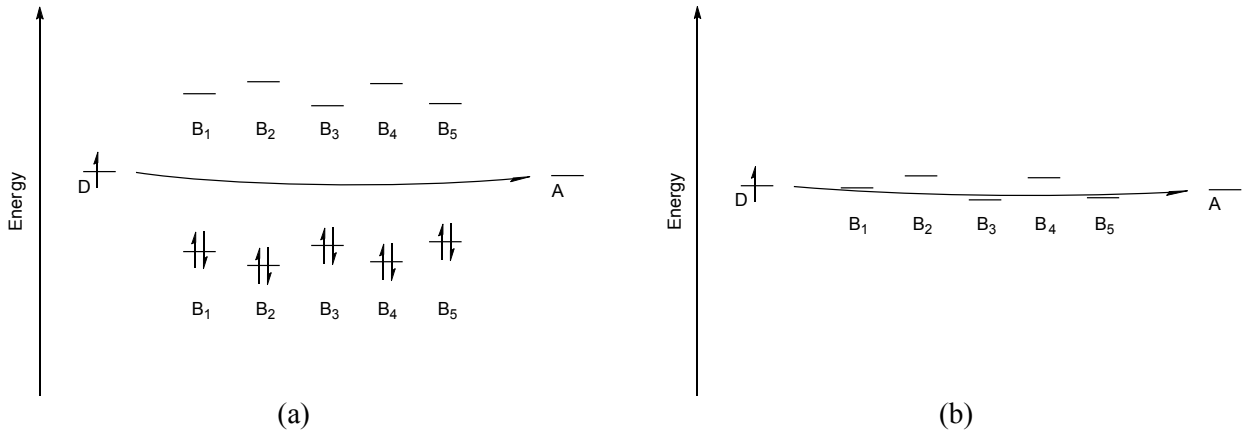

Figure 1-6. Schematic, energy level representations of (a) off-resonance (adapted from Todd *et al.*[50b]) and b) resonance tunnelling through a wire-like DBA device.

Hopping

As E_F approaches the energy of molecular frontier orbitals, direct tunnelling processes come into increasing competition with charge injection onto the bridge.[54] Significant vibrational relaxation is to be expected between successive electron transfer events[47a,55] where, in effect, B is itself reduced or oxidised (*the chemical mechanism*).[1d] Injected charge(s) may be considered localized (DB^+A or DB^-A) or delocalized across two or multiple locations on the bridge or junction, diffusing or *hopping* randomly between bridge sites until they reach the thermodynamic sink at A *(Figure 1-7)*. This mechanism has been observed, for example, in studies of oligo(phenylene-vinylene) structures,[52] and is characterised by $k_{hop} \propto N^{-1}$ (*i.e.* ohmic behaviour), as per eqn (1-3).[1d]

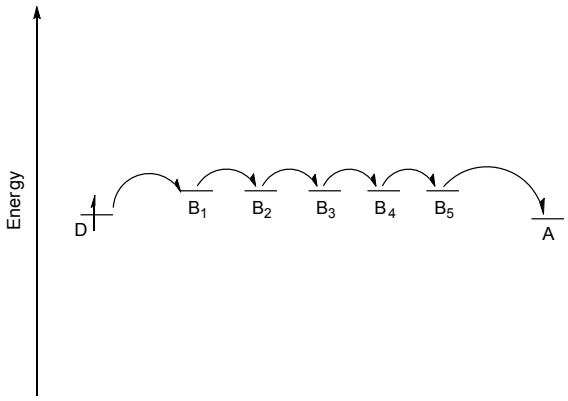

Figure 1-7. A schematic, energy level representation of hopping through a wire-like DBA device (adapted from Todd *et al.*[50b]).

$$k_{\text{hop}} \propto N^{-1} \exp\left(\frac{-\Delta E_{\text{DB}}}{RT}\right) \tag{1-3}$$

Coulomb blockade

A capacitive charge (*i.e.* localised electron(s)) on the molecular component/bridge can limit current flow through a junction due to electron-electron repulsion. For a given charge state *(n)* a voltage-independent steady-state current will be measured until the electrostatic energy (= $e^2/2C$, where e is the electronic charge and C the capacitance of the charged species) is overcome. The resulting charge state (n + 1), having one more transport channel than n, has a higher conductivity. This effect is known as *Coulomb blockade*, and is readily identified by a series of current plateaus interspaced by steep current increases (or alternatively, by sharp peaks in conductance-voltage ($\mathrm{d}I/\mathrm{d}V$-V) plots).

Nanoparticles or quantum dots exhibit Coulomb 'staircase' features with *evenly* separated current increases (these result from evenly spaced energy levels). Though such a spacing of *molecular* energy levels is not typical, Coulomb blockade effects may still be discernable.[39] This mechanism was recently encountered in transport studies of an isonitrile (–NC) terminated trinuclear ruthenium bis(arylacetylide) complex at 5 K (note here R_0 = 4.2 x 10^8 Ω, a relatively large value).[56] Weak coupling between the molecular 'island' and electrodes is considered to promote Coulomb blockade effects, serving to better localise charge(s) on the bridge.

1.1.2 Quantum interference effects

Given that tunnelling can dominate electron transport through a junction, the potential effects of wave interference[18b,57] on molecular conductance are of fundamental interest. *Destructive* effects have been postulated as explanations for the low conductivity[58] of *meta- vs. para*-substituted aromatic systems *(Figure 1-8a* and *b)* (also, reduced electron-transfer rates[11]), and typically provide a focal point for discussions of other cross-conjugated[‡] species *(Figure 1-8c* and *d)*.[59-61] Interference patterns have also been explored theoretically in '*cis*' and '*trans*' connected polycyclic hydrocarbon molecular wires *(Figure 1-8e)* (their total effect on conductance found to be greater for naphthalene-based systems than those containing benzene, anthracene or tetracene; and $G_{trans} > G_{cis}$).[62]

Such effects may be rationalised using a 'path model', whereby electron waves, starting from the donor, are conceived to propagate through different spatial electron paths in the molecule before being superimposed (interfering constructively or destructively) at the acceptor *(Figure 1-3,* left). Whilst sufficient in explaining the properties of many systems, a more complex interpretation may prove necessary; particularly when interference pathways are not spatially separated (*e.g.* in cross-conjugated species).[57b,60] In any case, great insights are obtained from analyses of calculated through junction transmission probabilities (as a function of energy): with destructive interference, large dips/nodes are observed; with constructive interference, high, broad peaks will be seen.[57d] Discussed below, it has been speculated that *interruption* of specific tunnelling pathways can change the total conductance of a junction by altering the through-molecule interference pattern. In this way a molecule might be switched from a high conductance, 'on' state to a low conductance, 'off' state.

[‡] Cross-conjugation describes the situation where atoms (or substituent positions) are connected by a continuous circuit of p orbitals, yet there is no resonance structure that places alternating double and single bonds between them.[59] Recent experimental results suggest through molecule conductance follows the order linear-conjugation > cross-conjugation > broken-conjugation.[59-60]

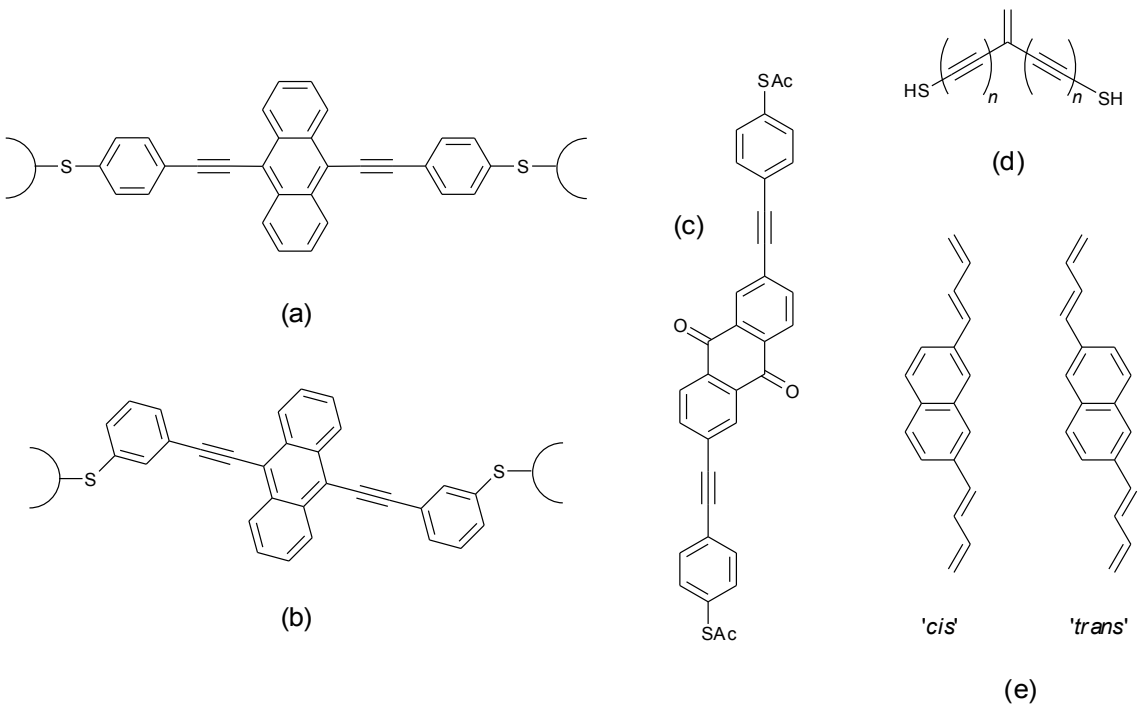

Figure 1-8. The effects of quantum interference on through molecule electron transport have been discussed in terms of the following examples: junctions formed using analogous (a) *para*- (higher conductance) and (b) *meta*-substituted (lower conductance) species;[58a] (c-d) other cross-conjugated compounds;[59,61a,b,61d] (e) '*cis*' and '*trans*' configurations of substituted naphthalene-based wires.[62]

Constructive interference

In 1999, Magoga and Joachim considered the effects of molecules wired in parallel on total conductance, under different 'node' regimes *(Figure 1-9)*.[10c] Using the elastic scattering quantum chemistry (ESQC) technique to numerically evaluate the simple superposition law $G_t = G_1 + G_2$ (for two molecules wired in parallel between electrodes, where G_t = the total conductance, G_n = the conductance of molecule *n; i.e. Figure 1-9a)*, they determined that it holds true when each molecule can be considered as an independent entity (*i.e.* where intermolecular coupling does not occur). This means, for example, that the conductance of a single molecule can be safely determined from the total conductance of a junction when there are a number (X) of identical molecules held between the two electrodes, using $G_n = G_t/X$ (if say, the electrode surface is sparsely populated).

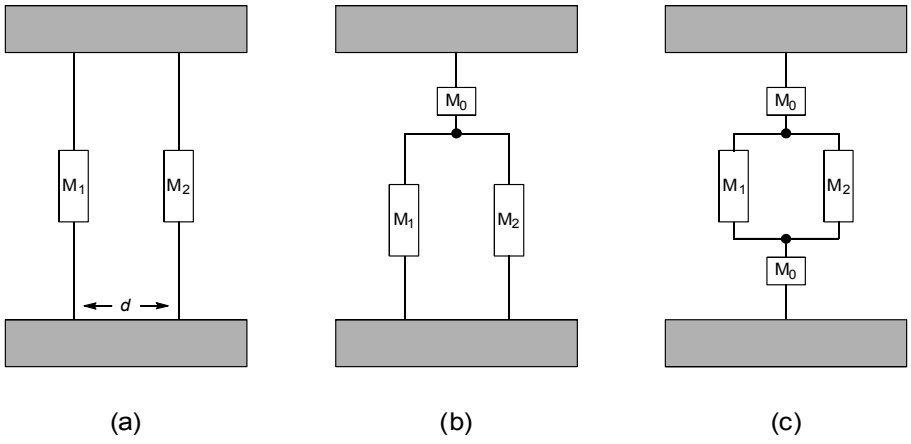

Figure 1-9. Different node regimes considered by Magoga and Joachim: (a) two molecules M_1 and M_2 chemisorbed between two electrodes, separated by a distance, *d* (b) two molecular branches M_1 and M_2 chemisorbed at one electrode (bottom) and via a 'nonresonant node' at the top electrode (disconnecting the molecular energy levels from the electrode energy levels, *i.e.* off-resonance tunnelling through the molecule), (c) two molecular branches connected at either electrode via nonresonant nodes.

As the distance (*d*) between individual molecules becomes smaller, they begin to interact with each other through the surface electronic states. In this case it was found that a similar expression, $G_t = G_1^{eff} + G_2^{eff}$, could be used; where G_n^{eff} describes a modified conductance term taking into account the intermolecular interactions.[§] This relation was also successful in reproducing the conductance of a branched system with one node in the junction (*i.e. Figure 1-9b)*. For the regime with two nodes in the junction (*i.e. Figure 1-9c)*, analogous to systems proposed here *(Figure 1-3)*, G_t was found to be *larger* than the summed conductance of the individual branches. This results from a new *constructivelike* interference term in the conductance expression, now $G_t = G_1 + G_2 + 2\sqrt{G_1G_2}$, attributed to the *transformation of the electronic structure of a molecular circuit when new branches are added to this circuit*.

Of further intrigue, for each case described, $G_t = G_n$ when electron transport through one of the two molecules/branches in the junction was disrupted (where relevant, eliminating the constructive effect). In the model compounds studied (*e.g. Figure 1-10a)* this was achieved via

[§] Linear scaling of conductance with the number of molecular wires has since been verified experimentally[63] in a cross-wire junction (further theoretical investigations of parallel wires in molecular junctions are also noted[64]).

rotation of one aromatic moiety from planarity (high conductance), to 90° (zero conductance through that molecule/branch due to disruption of π-conjugation).

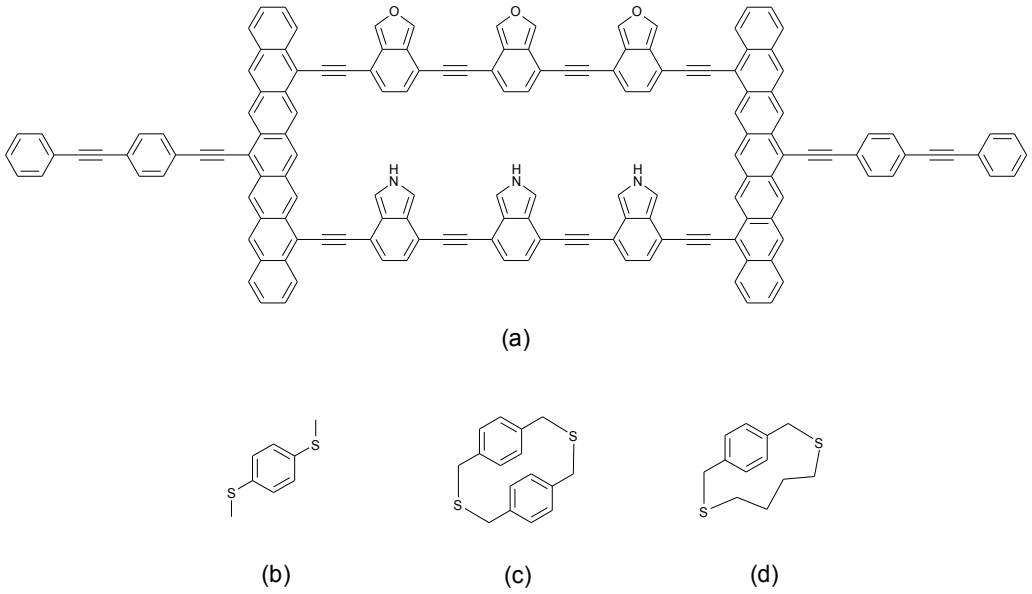

Figure 1-10. (a) Representative theoretical (Magoga and Joachim[10c]) and (b-d) experimental (Vazquez *et al.*[11]) organic structures used to explore superposition laws in single-molecule circuits with parallel paths.

Very recently, Vazquez *et al.* explored these theoretical findings experimentally (STM-break junction technique) using the simple organic structures shown in *Figure 1-10b-d* (as well as via density functional theory (DFT) junction transmission studies).[11,65] Here, structures *b* and *d* (a mechanically constrained analogue) exhibited similar conductance values (3.5×10^{-4} G_0 *vs.* 2.8×10^{-4} G_0; $G_0 = 2e^2/h$), determining that the increased conformational flexibility of *b* played only a minor role in effecting transport. It was subsequently found that the conductance ratio between the single-branched (*b*) and macrocyclic (*c*) structures, $G(b)/G(c) = 2.8$ (= ~3, via DFT; G(c) = 9.7×10^{-4} G_0), was characteristic of constructive interference (in other words, $G(c) > 2G(b)$). The additional 'signature' of this effect was also apparent from computational investigations; that is, a broadened (in this case LUMO) transmission peak in *c* resulting from coherent linear combination of the conjugated backbone orbitals.

Destructive interference

Baer and Neuhauser explored the concept of conductance switching through disruption of an initial destructive process.[10a,b] Interference effects were observed in a series of alkene wires linked at two points by a shorter wire (*Figure 1-11*), with calculated molecular conductance values proving strongly dependent on the length of the cross-linker. Intriguingly, these decreased in the order $L_4 \sim L_8 > L_0 > L_2 > L_6 > L_{10}$ (where L_n = a long alkene wire linked by a shorter wire at two points separated by n carbon-carbon bonds). Critical to interpretation of this result, in their system the electron (de Broglie) wavelength at E_F was 4 multiples of a carbon-carbon bond length, and transport was considered ballistic (the size of the junction being much smaller than the mean free path of the electron in the medium). Low conductance values were accordingly attributed to destructive interference, as $G(L_n) \leq G(L_0)$ only when the cross-linker had a length that was not a multiple of the propagating electron wave.[**] Notable also was $G(L_n) \geq G(L_0)$ when n = 4 and 8, but the authors did not explicitly link this to constructive effects. Further investigations revealed that $G(L_{10})$ could be *increased* by disrupting transmission through one of the branches (*e.g.* by artificially raising the potential energy of one of the CH sites or changing the coupling strength of one bond).

Some close analogues have been prepared by Blaszczyk *et al.*, but to explore intramolecular proximity effects (*i.e.* phenyl ring rotation) on conductance *(Figure 1-12)* rather than quantum interference phenomena.[66] These have not yet been studied in junction measurements.

[**] This concept was discussed further in a subsequent study[62] for a system containing two paths, $4R_{CC}$ and $6R_{CC}$, where the de Broglie wavelength of the conduction electron, $\lambda_F = 4R_{CC}$. Here, the phase difference of the two paths will be $(2R_{CC}/\lambda_F) \times 2\pi = \pi$, thus they will interfere *destructively*.

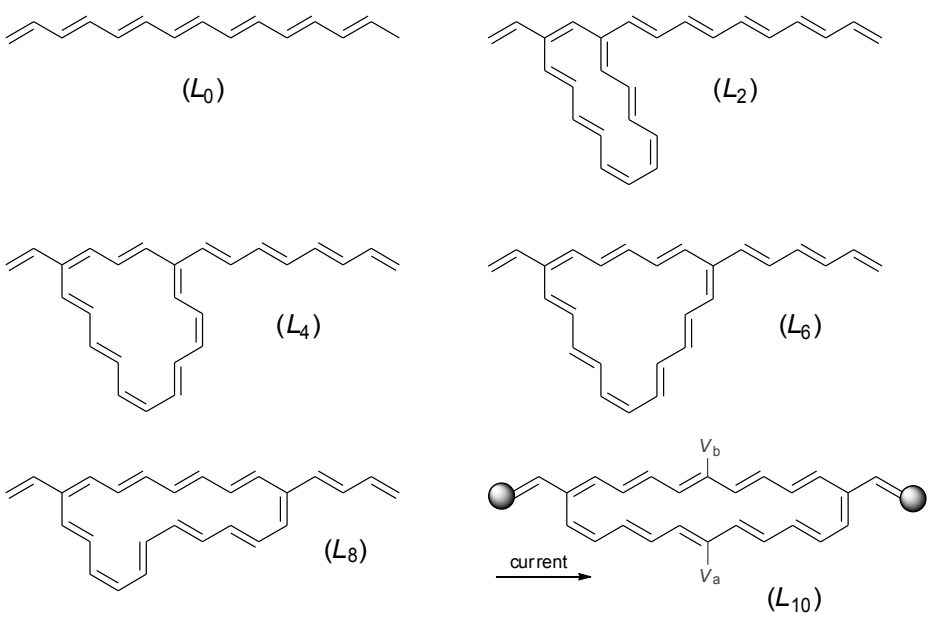

Figure 1-11. A series of cross-linked structures (indexed by the number of carbon-carbon bonds between the cross-linked points) used by Baer and Neuhauser to exemplify switching based on destructive interference.[10a,b] The position of leads/metallic contacts and gate voltages (V_a or V_b) is shown for L_{10}.

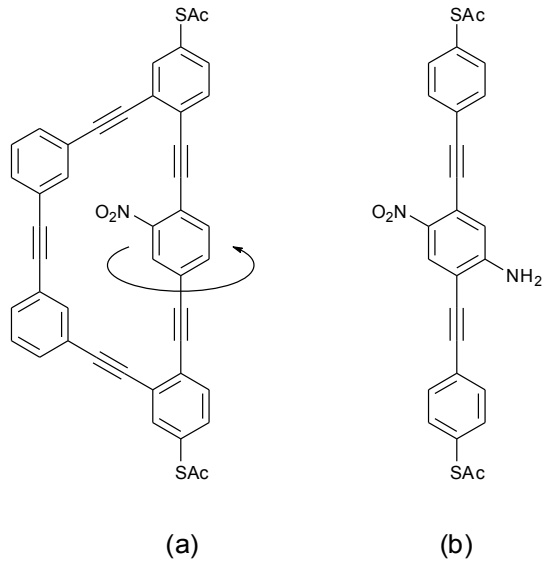

Figure 1-12. A representative macrocycle (a), one of several prepared to study the effect of intramolecular proximity effects on molecular conductance;[66] believed to be the origin of NDR behaviour in monolayers of OPE (b).

For analogous node regimes in real systems, it has been suggested that specific inelastic/elastic processes (*i.e.* deposition of tunnelling electron energy into the vibronic manifold of a bridge site,[67] dephasing without relaxation[68]) might destroy coherence between two electron pathways, removing destructive interference effects and restoring communication between D and A. Using a three terminal approach, Stafford and co-workers have shown how related phenomena may be exploited to switch between conductance states.[69] In their conception, source and drain electrodes are *meta*-connected to a benzene moiety (or analogous positions on [18]-annulene, or other cyclic structure), the junction thus residing in a low conductance state. Coupling of a third electrode to the π-orbitals of the molecule (*para*-connected for the benzene device) can then improve current flow by introducing decoherence (and additional paths that are not cancelled), or elastic scattering. Though alignment of three-terminals on the molecular scale presents a significant technological challenge, their "Quantum Interference Effect Transistor" (QuIET) was patented in 2007.[70]

Effect of magnetic fields on junction conductance

Whilst, in this work, disruption of electron transport through individual branches of a cyclic structure (*e.g.* via redox processes, *Figure 1-3)* would likely form the basis of initial experiments, the potential applications of magnetic fields in affecting molecular junction conductance should also be mentioned. In mesoscopic ring systems this is certainly possible by exploitation of the Aharonov–Bohm (AB) effect,[71] a process underpinned by the general principle that a magnetic vector potential (**A**) can alone affect the phase of an electron wavefunction.[72] Its relevance to work in this thesis may be grasped by describing the original experiment, proposed by Aharonov and Bohm in 1959[71] and undertaken by Chambers in 1960[73]. Here a beam of electrons, split coherently, is allowed to travel along two different paths before recombining (constructively) at a detector. By placing a solenoid between the two electron paths (vanishingly small magnetic field (**B**), but non-zero **A** outside the coil, *Figure 1-13a)* a phase difference ($\Delta\varphi$) is created between the beams such that when reunited they exhibit an interference pattern with destructive character. The extent of interference is related to the magnetic field strength inside the solenoid via eqn (1-4) (where Φ = magnetic flux),[74] and the effective resistance of this 'free electron' circuit, plotted as a function of the magnetic flux intensity, will exhibit oscillations with a period of h/e (integral multiples of h/e change the interference phase by 2π).

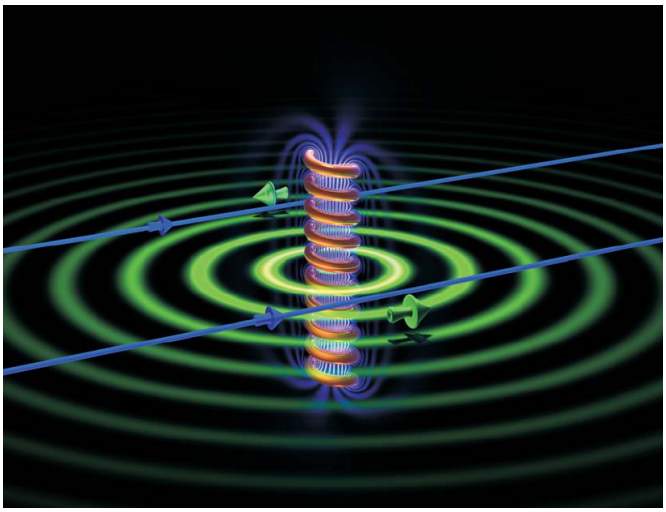

(a)

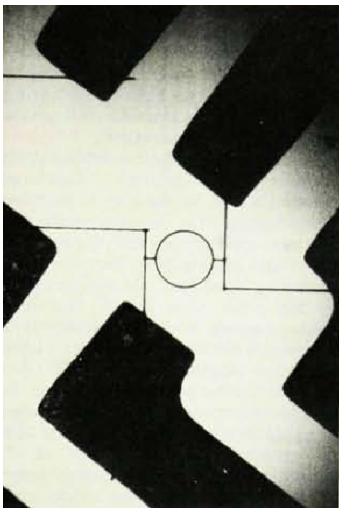

(b)

Figure 1-13. (a) Artistic representation[74] of two electrons passing a solenoid on opposite sides (blue trajectories). The magnetic field (**B**) (purple flux lines) exists predominantly inside the coil, whereas the vector potential (**A**) outside the coil (tangential to the green coaxial circles) falls off as $1/r$ with distance r from the solenoid's axis. The electrons experience a phase shift which is dependent on the path taken (the nearest electron taking a path parallel to **A**, the farthest taking a path anti-parallel to **A**). Image reprinted with permission from reference [74]. Copyright 2009, American Institute of Physics. (b) A photograph of the system used by Webb *et al.* to observe the AB effect in normal-metal rings (internal diameter = 784 nm, width of wire = 41 nm).[72,75] Reprinted with permission from reference [75]. Copyright 1986, American Institute of Physics.

$$\Delta\varphi = (e/h)\Phi \tag{1-4}$$

The AB effect, amongst others,[††] has since been observed in normal-metal rings (*e.g. Figure 1-13b)*,[75,77] and even carbon nanotubes (here, the propagating electron waves are confined within the meso/molecular structure).[78] Though the similarities between *Figure 1-13b* and *Figure 1-3* (or indeed any cyclic molecular system) are striking, it has been speculated that unrealistically large magnetic fields would be required to achieve a full AB period in the conductance of molecular-scale devices.[‡‡] Whilst this problem might readily be circumvented by preparing conjugated molecular ring systems on larger scales (see related work by Mayor and Didschies,[83]

[††] For example, Al'tshuler, Aronov and Spivak proposed an oscillation period of $h/2e$ for rings and cylinders (the AAS effect).[76]

and Iyoda[84]), others have explored circumstances under which much smaller fields may be exploited to affect molecular conductance.

Indeed, work by Hod *et al.* suggests that switching using a field of only 1 T is possible when a cyclic device is weakly electronically coupled to electrodes (for a Cu atom 'corral' of ring diameter ~3 nm,[85] or a 1 nm diameter nanotube[86]). Transmission peaks are thus narrowed, facilitating conductance only in a small energy window. By setting maximal transmission at **B** = 0, they found that an applied magnetic field rapidly shifted (doubly degenerate) molecular levels out of resonance, strongly reducing conductance (this concept was subsequently applied to three terminal devices[79,82]). Rai *et al.* have quite recently extended this work, presenting an improved set of conditions.[87] They argue that weak electrode-ring coupling is a *necessary but insufficient condition to gain magnetic field control over transport*, and that experimentally detectable effects (*i.e.* changes in *I–V* curves) are only possible when molecules are asymmetrically coupled to electrodes (*e.g. ortho*- or *meta*-connected benzene). Under such circumstances, improving conductance with increasing field strength may be understood as *phase adjustment of the interfering electron waves by the field, causing them to interfere constructively until full resonant transmission is reached* (an intriguing destructive to constructive interference mechanism). In line with discussions above, the inherent requirement of weak dephasing (implying low temperatures) in these and related experiments was also stressed.

1.2 SYNTHETIC CONSIDERATIONS

Choice of surface binding group and backbone structure

Following the above discussion, general structural features of the target molecules presented in *Figure 1-4* may be further rationalized (with reasoning behind the choice of $\{FeCp_2\}$ and $\{Ru(dppe)_2\}$ redox centres discussed in subsequent chapters). For stability and consistency of measurement, complexes for molecular electronics should ideally comprise strong (non-labile) bonds and fixed conformations; warranting the use of all-covalent frameworks. Macrocycles

‡‡ ~10^2 to 10^4 T (T = Tesla) for ring systems on the scale of benzene/OPE;[18b] 470 T (≈ $2\pi\hbar/eS$) for a ring with cross-sectional area $S \approx 8.75$ nm^2.[79] To put this in context, the strongest magnetic field thus far created in a laboratory is 91.4 T,[80] with field strengths of typical NMR instruments between 1.4 and 17.5 T (60-750 MHz).[81] For a useful discussion of this and other challenges related to utilisation of the AB effect in nanoscale devices, the reader is directed to a review by Hod, Baer and Rabani.[82]

with these properties are typically referred to as 'shape-persistent'. The π-conjugated oligo(phenylene-ethynylene) motif, also being a good mediator of electron transport *(Table 1-1)*, certainly fulfils this requirement, providing convenient access to *unstrained* cyclic systems using *meta*-connections (= 120° angles).[§§] Indeed, OPEs have already been utilized to great success in the assembly of all-organic macrocycles (see *Chapter 5* for further discussion), and their utilization in analogous (albeit linear) complexes has significant precedence (see *Chapters 2* and *4)*. Complete synthetic control over the organic framework (placement of surface binding groups, solubilizing functionalities, etc) is also possible using established iterative Sonogashira cross-coupling/desilylation methodologies. This capitalizes on the differential reactivity of aryl-iodide/bromide functionalities and cleavage conditions for trimethylsilyl/triisopropylsilyl moieties, where appropriate (exemplified in the synthetic chapters).

In using *meta*-substituted aromatic 'building blocks', appropriate analogues comprising surface binding groups were required *(Figure 1-14)*. Remarkably, with the notable exceptions of 3,5-pyridyl and 3,5-benzoic acid methyl ester[88] species, most materials have yet to be reported outside of the patent literature. Given the commercial availability of 3,5-dibromopyridine (also, 3-bromo-5-iodopyridine, 3-ethynylpyridine, and 4-bromopyridinium chloride), pyridyl containing targets were pursued almost exclusively in this work. For completeness, known or postulated (based on reported syntheses of 1,4-substituted analogues) routes to alternative trifunctional materials are provided in *Scheme 1-1*, *Scheme 1-2* and *Scheme 1-3*.

[§§] Whilst simplifying syntheses, it is acknowledged that the cross-conjugation/destructive interference imparted by *meta*-connectivity *(vida infra)* will likely reduce the conductance of such complexes relative to fully conjugated analogues (*e.g.* cyclic structures based on oligothiophenes[83-84]). This issue could be addressed in 'second generation' structures, if necessary.

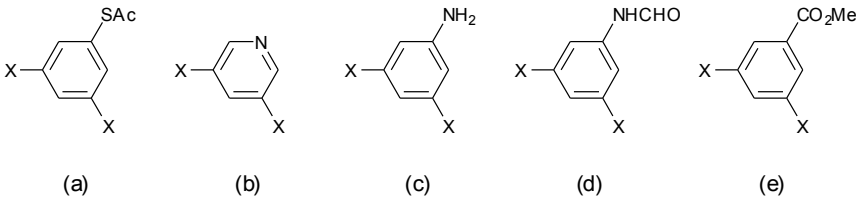

Figure 1-14. Trifunctional starting materials bearing commonly used surface binding groups (X = halogen), required to prepare macrocyclic/branched molecules of interest (*d* and *e* are precursors to –NC and $–CO_2H$ termini).

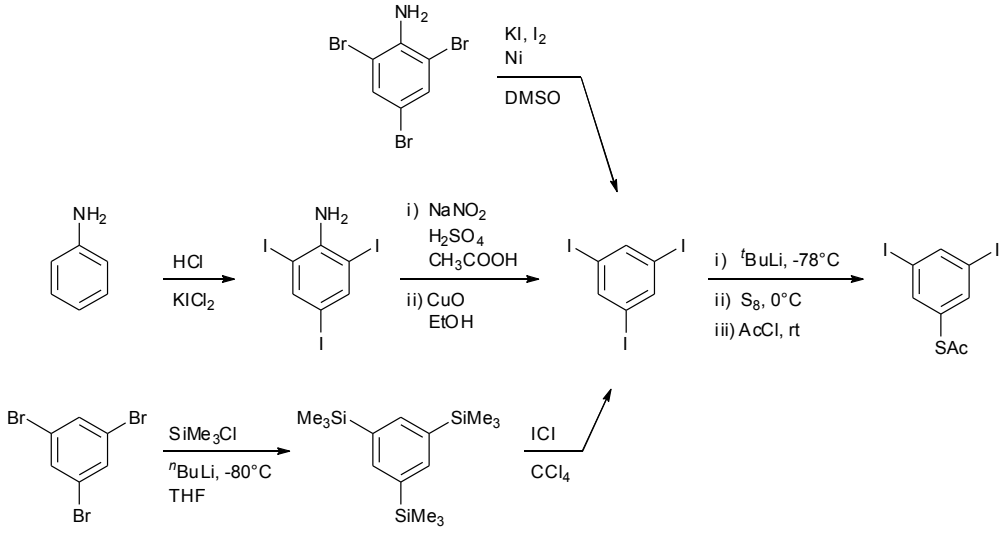

Scheme 1-1. Possible synthetic routes to a relevant thioacetyl functionalised building block, based upon the synthesis of the 1,4-substituted analogue.[89] It should however be noted that problems (also encountered by this author) have been reported with iodo-to-thioacetyl conversion using this approach.[90] The example syntheses of 1,3,5-triiodobenzene shown from (top to bottom) are reported by Müller *et al.*,[91] Vatsadze *et al.* [92] and Mechtler *et al.*[93]

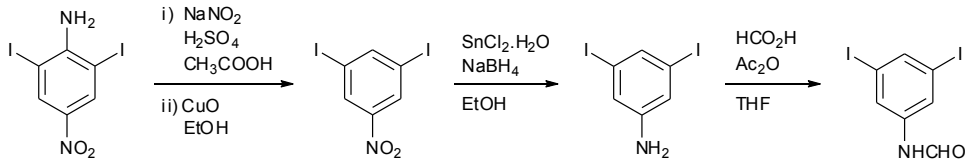

Scheme 1-2. A possible synthetic route to the relevant isonitrile functionalised building block, via 3,5-diiodoaniline,[94] based upon the synthesis of the 1,4-substituted analogue.[95]

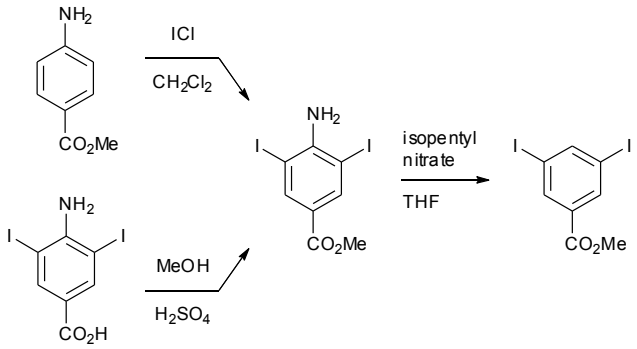

Scheme 1-3. Literature route to a relevant carboxylic acid methyl ester functionalised building block, via aniline derivatives.[88]

Macrocyclization strategies

Though single-branched and double-branched 'control' complexes (*i.e.* zero and one node systems, *Figure 1-9a* and *b)* were also to be synthesized, the most difficult preparations were to be almost certainly those of cyclic structures (*i.e.* two nodes, *Figure 1-9c)*; not least as a result of competitive oligo- or polymerisations.*** This 'overshoot' problem (including the production of cyclic products larger in oligomeric size than the cyclic target) can significantly diminish theoretical yields. Towards relevant, shape-persistent, macrocycles, Zhang and Moore have highlighted four major strategies: (a) cyclo-oligomerization; (b) intramolecular ring closure of α,ω-difunctional oligomers; (c) intermolecular coupling between two or more oligomeric fragments followed by unimolecular cyclization; (d) template cyclization of two or more fragments *(Figure 1-15)*. The following discussion, whilst largely based on their authoritative overview,[97] is also gauged from extensive reviews of the field by others.[98]

*** Related structures may be prepared via synthetic methods resulting in *thermodynamically* controlled product distributions, *i.e.* via alkyne metathesis,[96] but this typically restricts macrocycle design to highly symmetrical species.

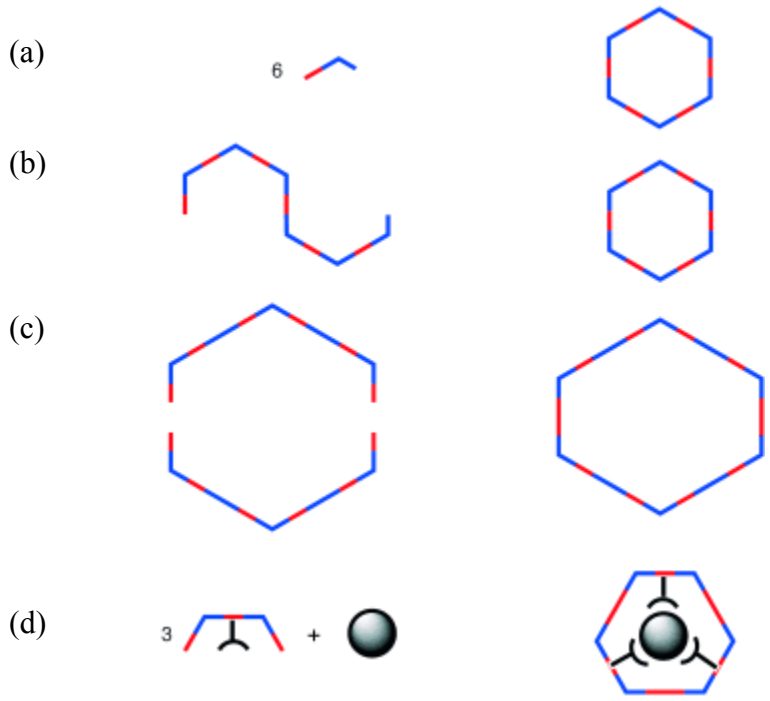

Figure 1-15. Schematic representation of cyclization strategies (reprinted from Zhang and Moore,[97] with permission from Wiley).

With regard to the synthetic targets of this work, the biggest disadvantage of cyclo-oligomerization (oligomerization + cyclization in one-pot, *Figure 1-15a)* is the inability to control placement of site-specific functionalities. Indeed, from a single difunctional monomer AB (where A and B represent different functional groups on the same molecule, and A can only react with B), or AA (identical functional groups, A can react with A) only macrocycles of high symmetry can be produced (small sizes are entropically preferred, but often larger rings result due to unfavourable angle strain). Even if a second, different, monomer (AB*) was mixed with AB, it would likely only be incorporated at indiscriminate ring positions. Low yields (the overshoot problem, multiple bond formation) and difficult to separate product mixtures (multiple species with similar structures) further preclude the utility of cyclo-oligomerization processes here, despite the very attractive prospect of synthesizing desired macrocycles in a single step (also using simple/readily available starting materials).[†††]

[†††] However, syntheses of structures requiring three-fold symmetry (*i.e.* three-terminal molecular devices) may benefit from cyclo-oligomerization approaches involving A_2 + B_2 monomers (where A_2 and B_2 are different monomers, and A can only react with B).[97,99] A 'triangular' amine functionalised oligo(phenylene-ethynylene) has

In contrast, a more involved approach requires the formation of only a single bond in the final step *(Figure 1-15b)*, usually under conditions of high dilution to favour intramolecular, rather than intermolecular, reaction. Higher *cyclization* yields may be expected (due in no small part to the vast preorganization of the structure), but the process involves significant synthetic work through multiple reaction steps to isolate the macrocyclic precursor (*overall* yields may be lower); making it a largely unattractive prospect unless extremely asymmetrical systems are required. As such, a more reasonable strategy, with yields and labour-time intermediate between the first two approaches, is to assemble two appropriate portions of the cycle and join them in one pot via consecutive intermolecular bond-formation and intramolecular cyclization steps (*i.e. Figure 1-15c)*. Here, non-identical branches or non-identical surface binding groups can readily be combined, with only partial loss of structural control in the final product. As will be seen, this was the strategy of choice for the majority of this work.

Template synthesis, whilst offering an interesting and 'intelligent' approach *(Figure 1-15d)*, has not yet been proven as a *reliable* method for increasing yields of macrocycle formation. Furthermore, it typically requires additional synthetic steps (*i.e.* in preparing covalently bound templates), and the approach can restrict, or even dictate, the design of the resulting macrocycle.

1.3 SUMMARY

This chapter has introduced key concepts relevant to the study and understanding of electron transport through single or small groups of molecules, also highlighting some of the intriguing properties that may be associated with branched components (*i.e.* the two node regime, *Figure 1-9c)*. Towards ratification of theoretical investigations and the realization of molecular conductance switching by manipulation of quantum interference effects, subsequent chapters detail efforts towards the synthesis of relevant macrocyclic complexes and their analogues. In these materials, the presence of redox active functionalities should enable the modulation of electron transport through individual branches by redox events. Destructive/constructive interference effects may thus be explored by measuring total molecular conductance as a function of oxidation state, either through step-wise chemical oxidation, isolation and study of

been synthesized using a related approach and studied in two-terminal junction measurements.[100]

the mixed-valence (see *Chapter 6* for relevant discussions), as well as the fully reduced/oxidized, species; or alternatively, using *in situ* electrochemical STM techniques.[101]

Regardless of whether quantum interference effects can be detected in these 'first generation' materials, they remain of significant interest. In addition to the synthetic challenge presented, it is not, for example, unreasonable to consider that they may exhibit *three* distinct conductance states (*i.e.* 0 – both branches reduced, 1 – one branch oxidized, 2 – two branches oxidized). Should this be the case, it is tentatively suggested that in extending beyond typical *binary* molecular/semiconductor devices (*i.e.* two states, 0 = off/low conductance, 1 = on/high conductance), such systems are perhaps well suited to *ternary* computing.‡‡‡ Seldom discussed in the field, despite the fact that multiple conductance states in molecular systems are by no means a new phenomena,[105] it is mentioned here essentially *post scriptum* as an enticing notion, requiring further consideration.

1.3.1 Chapter synopsis

Work presented in this thesis is organized as follows:

Chapter 2 describes the syntheses of some branched ferrocene-containing complexes (*Figure 1-16,* top; and also the macrocycle shown in *Figure 1-4a)*. Electrochemical and UV-vis spectroscopic studies of these materials are also discussed (similar investigations are included in subsequent chapters for relevant novel compounds).

‡‡‡ Prior to the widespread adoption of the binary number system in computing, both decimal (base 10) and ternary (base 3) were contemplated. The relative merits of decimal *vs.* binary representation are discussed by Buchholz in his 1959 paper *Fingers or Fists* (binary numbers are more compact, multiplication is longer in the decimal system, etc);[102] the former certainly being considered more *naturally adapted* given that typical electronic switches/devices have two states (*i.e.* the "flip-flop" circuit[103]). On ternary *vs.* binary it is intriguing to note that 'balanced ternary' (-1, 0, 1) was referred to as *perhaps the prettiest number system of all* by Knuth (in the *Art of Computer Programming*), who suggested that it might one day prove quite important *when the "flip-flop" is replaced by a "flip-flap-flop"*.[104]

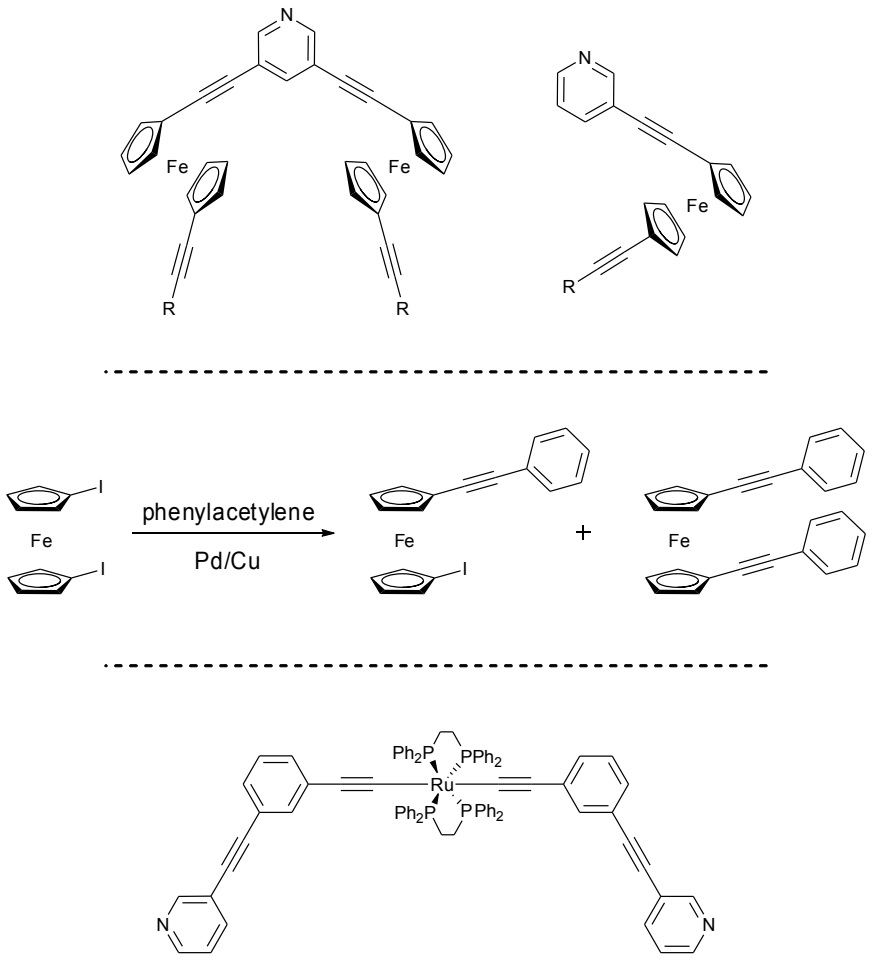

Figure 1-16. Further examples of work presented in this thesis (R = 3-pyridine, 4-(*tert*-butylthio)benzene, trimethylsilane).

Chapter 3 details attempts to optimize the typically low-yielding Sonogashira cross-coupling reactions between terminal alkynes and iodoferrocenes, using the model system shown in *Figure 1-16* (middle). Attempts to synthesise 1,1'-bis[(4-thioacetylphenyl)ethynyl]ferrocene from 1,1'-diiodoferrocene and 4-ethynylphenylthioacetate are described.

In *Chapter 4*, the problematic synthesis of $Ru(dppe)_2(C{\equiv}C{-}C_5H_4N)_2$ (*Figure 1-4b)* is presented. Experiences with protecting the pyridyl nitrogen of 4-ethynylpyridine, and the moderate success of employing *N*-methyl-4-ethynylpyridinium triflate as a ligand, are detailed.

Chapter 5 concerns preparation of the ruthenium macrocycle shown in *Figure 1-4c*, and its single branched analogue *(Figure 1-16,* bottom). Here, problems encountered with the pyridyl nitrogen in *Chapter 4* are circumvented by introducing the pyridyl moiety at a later stage

(avoiding its contact with coordinatively unsaturated 16e$^-$ ruthenium centres). Efforts towards a macrocycle based on {Ru(PP_3)} centres are also described (PP_3 = tris[2-(diphenylphosphino)ethyl]phosphine).

Chapter 6 marks a departure from the synthetic theme, discussing instead some critical thermodynamic aspects of 'mixed-valence' complexes. An intriguing link between electron density and $\Delta E_{1/2}^0$ values (the difference between sequential redox events, $\Delta E_{1/2}^0 = E_2^0 - E_1^0$) is explored in some detail. Focussing on complexes of the type [{M(L)$_n$}$_2$(μ-C≡C–C≡C)], the use of voltammetric methods as a probe of electron delocalisation is discussed.

Finally, *Chapter 7* summarizes what has been learnt during the course of this project, highlighting possible areas of future interest, and *Chapter 8* contains all relevant experimental details.

1.4 REFERENCES

1. (a) J. C. Ellenbogen and J. C. Love, *Proc. IEEE*, 2000, **88**, 386; (b) J. M. Tour, *Acc. Chem. Res.*, 2000, **33**, 791; (c) R. L. Carroll and C. B. Gorman, *Angew. Chem., Int. Ed.*, 2002, **41**, 4379; (d) D. M. Adams, L. Brus, C. E. D. Chidsey, S. Creager, C. Creutz, C. R. Kagan, P. V. Kamat, M. Lieberman, S. Lindsay, R. A. Marcus, R. M. Metzger, M. E. Michel-Beyerle, J. R. Miller, M. D. Newton, D. R. Rolison, O. Sankey, K. S. Schanze, J. Yardley and X. Zhu, *J. Phys. Chem. B*, 2003, **107**, 6668; (e) A. Salomon, D. Cahen, S. Lindsay, J. Tomfohr, V. B. Engelkes and C. D. Frisbie, *Adv. Mater.*, 2003, **15**, 1881; (f) N. Robertson and C. A. McGowan, *Chem. Soc. Rev.*, 2003, **32**, 96; (g) D. K. James and J. M. Tour, *Aldrichimica Acta*, 2006, **39**, 47; (h) N. J. Tao, *Nat. Nanotechnol.*, 2006, **1**, 173; (i) N. Weibel, S. Grunder and M. Mayor, *Org. Biomol. Chem.*, 2007, **5**, 2343; (j) H. Haick and D. Cahen, *Prog. Surf. Sci.*, 2008, **83**, 217; (k) R. L. McCreery and A. J. Bergren, *Adv. Mater.*, 2009, **21**, 1; (l) A. Erbe and S. Verleger, *Acta Phys. Pol., A*, 2009, **115**, 455; (m) J. D. Nero, F. M. d. Souza and R. B. Capaz, *J. Comput. Theor. Nanosci.*, 2010, **7**, 1; (n) H. Song, M. A. Reed and T. Lee, *Adv. Mater.*, 2011, **23**, 1583; (o) A. Coskun, J. M. Spruell, G. Barin, W. R. Dichtel, A. H. Flood, Y. Y. Botros and J. F. Stoddart, *Chem. Soc. Rev.*, 2012, **41**, 4827.
2. R. Chau, B. Doyle, S. Datta, J. Kavalieros and K. Zhang, *Nat. Mater.*, 2007, **6**, 810.
3. J. R. Heath and M. A. Ratner, *Phys. Today*, 2003, **56**, 43.
4. (a) D. L. Pearson, L. Jones, J. S. Schumm and J. M. Tour, *Synth. Met.*, 1997, **84**, 303; (b) J. M. Tour, A. M. Rawlett, M. Kozaki, Y. X. Yao, R. C. Jagessar, S. M. Dirk, D. W. Price, M. A. Reed, C. W. Zhou, J. Chen, W. Y. Wang and I. Campbell, *Chem. Eur. J.*, 2001, **7**, 5118; (c) J. C. Cuevas and E. Scheer, *Molecular Electronics: An Introduction to Theory and Experiment*, World Scientific Publishing Company, 2010.
5. R. P. Feynman, *Eng. Sci.*, 1960, **23**, 22.
6. J. M. Tour, M. Kozaki and J. M. Seminario, *J. Am. Chem. Soc.*, 1998, **120**, 8486.
7. D. J. Wold and C. D. Frisbie, *J. Am. Chem. Soc.*, 2000, **122**, 2970.

8. J. G. Kushmerick, D. B. Holt, J. C. Yang, J. Naciri, M. H. Moore and R. Shashidhar, *Phys. Rev. Lett.*, 2002, **89**, 086802.
9. (a) V. W. W. Yam, *Acc. Chem. Res.*, 2002, **35**, 555; (b) C. K. Hui, B. W. K. Chu, N. Y. Zhu and V. W. W. Yam, *Inorg. Chem.*, 2002, **41**, 6178; (c) V. W.-W. Yam and K. M.-C. Wong, in *Top. Curr. Chem.*, ed. L. d. Cola, 2005, **257**, 1; (d) H. Lang, P. Zoufala, S. Klaib, A. del Villar and G. Rheinwald, *J. Organomet. Chem.*, 2007, **692**, 4168; (e) H. Lang, A. del Villar, T. Stein, P. Zoufala, T. Ruffer and G. Rheinwald, *J. Organomet. Chem.*, 2007, **692**, 5203; (f) K. Onitsuka, N. Ohara, F. Takei and S. Takahashi, *Organometallics*, 2008, **27**, 25; (g) S. K. Yip, C. L. Chan, W. H. Lam, K. K. Cheung and V. W. W. Yam, *Photochem. Photobiol. Sci.*, 2007, **6**, 365; (h) M. Z. Asuncion, M. F. Roll and R. M. Laine, *Macromolecules*, 2008; (i) Y. Furusho and E. Yashima, *Chem. Rec.*, 2007, **7**, 1.
10. (a) D. Neuhauser and R. Baer, *J. Am. Chem. Soc.*, 2002, **124**, 4200; (b) R. Baer and D. Neuhauser, *Chem. Phys.*, 2002, **281**, 353; (c) M. Magoga and C. Joachim, *Phys. Rev. B*, 1999, **59**, 16011.
11. H. Vazquez, R. Skouta, S. Schneebeli, M. Kamenetska, R. Breslow, L. Venkataraman and M. S. Hybertsen, *Nat. Nanotechnol.*, 2012, **7**, 663.
12. (a) F. Chen, J. Hihath, Z. Huang, X. Li and N. J. Tao, *Annu. Rev. Phys. Chem.*, 2007, **58**, 535; (b) R. J. Nichols, W. Haiss, S. J. Higgins, E. Leary, S. Martin and D. Bethell, *Phys. Chem. Chem. Phys.*, 2010, **12**, 2801; (c) D. Allara and Y. Selzer, *Annu. Rev. Phys. Chem.*, 2006, **57**, 593.
13. C. Zhou, C. Muller, T. Burgin, J. Tour and M. Reed, *Science*, 1997, **278**, 252.
14. (a) B. Mantooth, K. Kelly, L. Bumm, J. Monnell, J. Stapleton and Z. Donhauser, *Science*, 2001, **292**, 2303; (b) D. K. James and J. M. Tour, *Chem. Mater.*, 2004, **16**, 4423; (c) B. Xu and N. J. Tao, *Science*, 2003, **301**, 1221.
15. L. Cheng, D. Nackashi, Y. Yao, A. Flatt, S. St Angelo and J. Tour, *J. Am. Chem. Soc.*, 2003, **125**, 13279.
16. B. Chen, A. Flatt, J. Stephenson, C. Doyle, J. Tour and J. He, *Nature Mater.*, 2006, **5**, 63.
17. (a) J. Fransson, O. M. Bengone, J. A. Larsson and J. C. Greer, *IEEE Trans. Nanotech.*, 2006, **5**, 745; (b) C. W. Bauschlicher and J. W. Lawson, *Theor. Chem. Acc.*, 2008, **119**, 429; (c) K. Walczak, *Phys. Status Solidi B*, 2007, **244**, 709.
18. (a) J. Cornil, J. Bredas and Y. Karzazi, *Adv. Func. Mater.*, 2002, **12**, 787; (b) K. Walczak, *Cent. Eur. J. Chem.*, 2004, **2**, 524; (c) A. Nitzan and M. A. Ratner, *Science*, 2003, **300**, 1384.
19. (a) F. Chen, X. Li, J. Hihath, Z. Huang and N. J. Tao, *J. Am. Chem. Soc.*, 2006, **128**, 15874; (b) B. Kim, J. M. Beebe, Y. Jun, X.-Y. Zhu and C. D. Frisbie, *J. Am. Chem. Soc.*, 2006, **128**, 4970; (c) K. Moth-Poulsen, L. Patrone, N. Stuhr-Hansen, J. B. Christensen, J.-P. Bourgoin and T. Bjørnholm, *Nano Lett.*, 2005, **5**, 783; (d) D. S. Seferos, A. S. Blum, J. G. Kushmerick and G. C. Bazan, *J. Am. Chem. Soc.*, 2006, **128**, 11260; (e) J. He, F. Chen, J. Li, O. F. Sankey, Y. Terazono, C. Herrero, D. Gust, T. A. Moore, A. L. Moore and S. M. Lindsay, *J. Am. Chem. Soc.*, 2005, **127**, 1384; (f) K. Liu, G. Li, X. Wang and F. Wang, *J. Phys. Chem. C*, 2008, **112**, 4342.
20. (a) L. Patrone, S. Palacin and J. P. Bourgoin, *Appl. Surf. Sci.*, 2003, **212-213**, 446; (b) S. Yasuda, S. Yoshida, J. Sasaki, Y. Okutsu, T. Nakamura, A. Taninaka, O. Takeuchi and H. Shigekawa, *J. Am. Chem. Soc.*, 2006, **128**, 7746.
21. J. M. Beebe, V. B. Engelkes, L. L. Miller and C. D. Frisbie, *J. Am. Chem. Soc.*, 2002, **124**, 11268.

22. L. Venkataraman, J. E. Klare, I. W. Tam, C. Nuckolls, M. S. Hybertsen and M. L. Steigerwald, *Nano Lett.*, 2006, **6**, 458.
23. (a) B. Xu and N. Tao, *Science*, 2003, **301**, 1221; (b) S. H. Chanteau and J. M. Tour, *Tetrahedron Lett.*, 2001, **42**, 3057; (c) C. Wang, A. S. Batsanov, M. R. Bryce, S. Martín, R. J. Nichols, S. J. Higgins, V. M. García-Suárez and C. J. Lambert, *J. Am. Chem. Soc.*, 2009, **131**, 15647.
24. J. He, B. Chen, A. K. Flatt, J. J. Stephenson, C. D. Doyle and J. M. Tour, *Nat. Mater.*, 2006, **5**, 63.
25. S. Marques-Gonzalez, D. S. Yufit, J. A. K. Howard, S. Martin, H. M. Osorio, V. M. Garcia-Suarez, R. J. Nichols, S. J. Higgins, P. Cea and P. J. Low, *Dalton Trans*, 2013, **42**, 338.
26. G. A. Koutsantonis, P. A. Schauer and B. W. Skelton, *Organometallics*, 2011, **30**, 2680.
27. M. J. Mio, L. C. Kopel, J. B. Braun, T. L. Gadzikwa, K. L. Hull, R. G. Brisbois, C. J. Markworth and P. A. Grieco, *Org. Lett.*, 2002, **4**, 3199.
28. T. Rueckes, K. Kim, E. Joselevich, G. Y. Tseng, C.-L. Cheung and C. M. Lieber, *Science*, 2000, **289**, 94.
29. M. U. Winters, E. Dahlstedt, H. E. Blades, C. J. Wilson, M. J. Frampton, H. L. Anderson and B. Albinsson, *J. Am. Chem. Soc.*, 2007, **129**, 4291.
30. (a) A. K. Mahapatro, G. U. Lee, K. J. Jeong and D. B. Janes, *Appl. Phys. Lett.*, 2009, **95**, 083106; (b) M. Taniguchi and T. Kawai, *Physica E*, 2006, **33**, 1.
31. L. T. Cai, H. Skulason, J. G. Kushmerick, S. K. Pollack, J. Naciri, R. Shashidhar, D. L. Allara, T. E. Mallouk and T. S. Mayer, *J. Phys. Chem. B*, 2004, **108**, 2827.
32. B. Kim, J. M. Beebe, C. Olivier, S. Rigaut, D. Touchard, J. G. Kushmerick, X.-Y. Zhu and C. D. Frisbie, *J. Phys. Chem. C*, 2007, **111**, 7521.
33. (a) J. M. Seminario, A. G. Zacarias and J. M. Tour, *J. Am. Chem. Soc.*, 2000, **122**, 3015; (b) K. Liu, X. Wang and F. Wang, *ACS Nano*, 2008, **2**, 2315.
34. (a) J. Chen, W. Wang, M. A. Reed, A. M. Rawlett, D. W. Price and J. M. Tour, *Appl. Phys. Lett.*, 2000, **77**, 1224; (b) Y. Selzer, M. A. Cabassi, T. S. Mayer and D. L. Allara, *Nanotechnology*, 2004, **15**, S483.
35. (a) N. Gergel-Hackett, N. Majumdar, Z. Martin, N. Swami, L. R. Harriott, J. C. Bean, G. Pattanaik, G. Zangari, Y. Zhu, I. Pu, Y. Yao and J. M. Tour, *J. Vac. Sci. Technol., A*, 2006, **24**, 1243; (b) Y. Selzer, L. Cai, M. A. Cabassi, Y. Yao, J. M. Tour, T. S. Mayer and D. L. Allara, *Nano Lett.*, 2005, **5**, 61; (c) Z. J. Donhauser, B. A. Mantooth, K. F. Kelly, L. A. Bumm, J. D. Monnell, J. J. Stapleton, D. W. Price Jr., A. M. Rawlett, D. L. Allara, J. M. Tour and P. S. Weiss, *Science*, 2001, **292**, 2303; (d) Z.-F. Shi, L.-J. Wang, H. Wang, X.-P. Cao and H.-L. Zhang, *Org. Lett.*, 2007, **9**, 595; (e) Y. Ie, M. Endou, S. K. Lee, R. Yamada, H. Tada and Y. Aso, *Angew. Chem., Int. Ed.*, 2011, **50**, 11980.
36. (a) T. Albrecht, K. Moth Poulsen, J. B. Christensen, J. Hjelm, T. Bjørnholm and J. Ulstrup, *J. Am. Chem. Soc.*, 2006, **128**, 6574; (b) S. Kubatkin, A. Danilov, M. Hjort, J. Cornil, J.-L. Brédas, N. Stuhr-Hansen, P. Hedegård and T. Bjørnholm, *Nature*, 2003, **425**, 698; (c) A. M. Kuznetsov, P. Sommer-Larsen and J. Ulstrup, *Surf. Sci.*, 1992, **275**, 52.
37. (a) M. A. Reed, J. Chen, A. M. Rawlett, D. W. Price and J. M. Tour, *Appl. Phys. Lett.*, 2001, **78**, 3735; (b) I.-W. P. Chen, M.-D. Fu, W.-H. Tseng, J.-Y. Yu, S.-H. Wu, C.-J. Ku, C.-h. Chen and S.-M. Peng, *Angew. Chem., Int. Ed. Engl.*, 2006, **45**, 5814.
38. (a) M. Elbing, R. Ochs, M. Koentopp, M. Fischer, C. v. Hänisch, F. Weigend, F. Evers, H. B. Weber and M. Mayor, *Proc. Natl. Acad. Sci. U. S. A.*, 2005, **102**, 8815; (b) I. Díez-Pérez,

J. Hihath, Y. Lee, L. Yu, L. Adamska, M. A. Kozhushner, I. I. Oleynik and N. J. Tao, *Nat. Chem.*, 2009, **1**, 635.
39. J. Park, A. N. Pasupathy, J. I. Goldsmith, C. Chang, Y. Yaish, J. R. Petta, M. Rinkoski, J. P. Sethna, H. D. Abruña, P. L. McEuen and D. C. Ralph, *Nature*, 2002, **417**, 722.
40. W. Liang, M. P. Shores, M. Bockrath, J. R. Long and H. Park, *Nature*, 2002, **417**, 725.
41. M. S. Inkpen and N. J. Long, in *Molecular Design and Applications of Photofunctional Polymers and Materials*, eds. W.-Y. Wong and A. S. Abd-El-Aziz, Royal Society of Chemistry, 2012.
42. R. Yamada, H. Kumazawa, T. Noutoshi, S. Tanaka and H. Tada, *Nano Lett.*, 2008, **8**, 1237.
43. V. Kaliginedi, P. Moreno-García, H. Valkenier, W. Hong, V. M. García-Suárez, P. Buiter, J. L. H. Otten, J. C. Hummelen, C. J. Lambert and T. Wandlowski, *J. Am. Chem. Soc.*, 2012, **134**, 5262.
44. P. J. Low, *Dalton Trans.*, 2005, 2821.
45. (a) T. Albrecht, A. Guckian, J. Ulstrup and J. G. Vos, *IEEE Trans. Nanotech.*, 2005, **4**, 430; (b) A. K. Mahapatro, J. Ying, T. Ren and D. B. Janes, *Nano Lett.*, 2008, **8**, 2131.
46. N. J. Long and C. K. Williams, *Angew. Chem., Int. Ed. Engl.*, 2003, **42**, 2586.
47. (a) K. Moth-Poulsen and T. Bjørnholm, *Nature Nanotech.*, 2009, **4**, 551; (b) R. Landauer, *Phys. Lett. A*, 1981, **85**, 91.
48. V. Geskin, A. Crispin, J. Cornil, R. Lazzaroni, W. Salaneck and X. Crispin, *J. Am. Chem. Soc.*, 2002, **124**, 8131.
49. Y. Xue and M. A. Ratner, *Int. J. Quantum Chem.*, 2005, **102**, 911.
50. (a) A. Aviram and M. A. Ratner, *Chem. Phys. Lett.*, 1974, **29**, 277; (b) M. D. Todd, A. Nitzan and M. A. Ratner, *J. Phys. Chem.*, 1993, **97**, 29.
51. H. M. McConnell, *J. Chem. Phys.*, 1961, **35**, 508.
52. M. Ratner and C. Joachim, *Nanotechnology*, 2004, **15**, 1065.
53. K. Liu, G. Li, X. Wang and F. Wang, *J. Phys. Chem. C*, 2008, **112**, 4342.
54. M. D. Newton and J. F. Smalley, *Phys. Chem. Chem. Phys.*, 2007, **9**, 555.
55. J. Zhang, A. M. Kuznetsov, I. G. Medvedev, Q. Chi, T. Albrecht, P. S. Jensen and J. Ulstrup, *Chem. Rev.*, 2008, **108**, 2737.
56. B. Kim, J. M. Beebe, C. Olivier, S. Rigaut, D. Touchard, J. G. Kushmerick, X. Y. Zhu and C. D. Frisbie, *J. Phys. Chem. C*, 2007, **111**, 7521.
57. (a) A. Cheong, A. E. Roitberg, V. Mujica and M. A. Ratner, *J. Photochem. Photobiol., A*, 1994, **82**, 81; (b) G. C. Solomon, D. Q. Andrews, T. Hansen, R. H. Goldsmith, M. R. Wasielewski, R. P. Van Duyne and M. A. Ratner, *J. Chem. Phys.*, 2008, **129**, 054701; (c) P. Sautet and C. Joachim, *Chem. Phys.*, 1989, **135**, 99; (d) S. H. Ke, W. T. Yang and H. U. Baranger, *Nano Lett.*, 2008, **8**, 3257.
58. (a) H. Weber, J. Reichert, M. Elbing, C. von Hanisch, D. Beckmann and M. Mayor, *Angew. Chem., Int. Ed. Engl.*, 2003, **42**, 5834; (b) M. Kiguchi, H. Nakamura, Y. Takahashi, T. Takahashi and T. Ohto, *J. Phys. Chem. C*, 2010, **114**, 22254.
59. D. Fracasso, H. Valkenier, J. C. Hummelen, G. C. Solomon and R. C. Chiechi, *J. Am. Chem. Soc.*, 2011, **133**, 9556.
60. G. C. Solomon, D. Q. Andrews, R. P. Van Duyne and M. A. Ratner, *J. Am. Chem. Soc.*, 2008, **130**, 7788.
61. (a) C. M. Guedon, H. Valkenier, T. Markussen, K. S. Thygesen, J. C. Hummelen and S. J. van der Molen, *Nat. Nanotechnol.*, 2012, **7**, 305; (b) S. V. Aradhya, J. S. Meisner, M. Krikorian, S. Ahn, R. Parameswaran, M. L. Steigerwald, C. Nuckolls and L. Venkataraman,

Nano Lett., 2012, **12**, 1643; (c) G. C. Solomon, D. Q. Andrews, R. H. Goldsmith, T. Hansen, M. R. Wasielewski, R. P. Van Duyne and M. A. Ratner, *J. Am. Chem. Soc.*, 2008, **130**, 17301; (d) D. Q. Andrews, G. C. Solomon, R. P. Van Duyne and M. A. Ratner, *J. Am. Chem. Soc.*, 2008, **130**, 17309.
62. D. Walter, D. Neuhauser and R. Baer, *Chem. Phys.*, 2004, **299**, 139.
63. J. G. Kushmerick, J. Naciri, J. C. Yang and R. Shashidhar, *Nano Lett.*, 2003, **3**, 897.
64. S. N. Yaliraki and M. A. Ratner, *J. Chem. Phys.*, 1998, **109**, 5036.
65. C. Joachim, *Nat. Nanotechnol.*, 2012, **7**, 620.
66. A. Błaszczyk, M. Chadim, C. von Hänisch and M. Mayor, *Eur. J. Org. Chem.*, 2006, **2006**, 3809.
67. S. S. Skourtis, D. H. Waldeck and D. N. Beratan, *J. Phys. Chem. B*, 2004, **108**, 15511.
68. R. H. Goldsmith, M. R. Wasielewski and M. A. Ratner, *J. Phys. Chem. B*, 2006, **110**, 20258.
69. (a) D. M. Cardamone, C. A. Stafford and S. Mazumdar, *Nano Lett.*, 2006, **6**, 2422; (b) C. A. Stafford, D. M. Cardamone and S. Mazumdar, *Nanotechnology*, 2007, **18**, 424014.
70. *US Pat.*, 0 215 861, 2007.
71. Y. Aharonov and D. Bohm, *Phys. Rev.*, 1959, **115**, 485.
72. B. Schwarzschild, *Phys. Today*, 1986, **39**, 17.
73. R. G. Chambers, *Phys. Rev. Lett.*, 1960, **5**, 3.
74. H. Batelaan and A. Tonomura, *Phys. Today*, 2009, **62**, 38.
75. R. A. Webb, S. Washburn, C. P. Umbach and R. B. Laibowitz, *Phys. Rev. Lett.*, 1985, **54**, 2696.
76. B. L. Al'tshuler, A. G. Aronov and B. Z. Spivak, *JETP Lett.*, 1981, **33**, 94.
77. V. Chandrasekhar, M. J. Rooks, S. Wind and D. E. Prober, *Phys. Rev. Lett.*, 1985, **55**, 1610.
78. A. Bachtold, C. Strunk, J.-P. Salvetat, J.-M. Bonard, L. Forro, T. Nussbaumer and C. Schonenberger, *Nature*, 1999, **397**, 673.
79. R. Baer, E. Rabani and O. Hod, *J. Am. Chem. Soc.*, 2005, **127**, 1648.
80. S. Zherlitsyn, B. Wustmann, T. Herrmannsdörfer and J. Wosnitza, *J. Low Temp. Phys.*, 2012, 1.
81. M. H. Harwood and D. W. Claridge, *Introduction to Organic Spectroscopy*, Oxford University Press, 1997.
82. O. Hod, R. Baer and E. Rabani, *J. Phys.-Condes. Matter*, 2008, **20**, 32.
83. M. Mayor and C. Didschies, *Angew. Chem., Int. Ed.*, 2003, **42**, 3176.
84. M. Iyoda, *Pure Appl. Chem.*, 2010, **82**, 831.
85. O. Hod, R. Baer and E. Rabani, *J. Phys. Chem. B*, 2004, **108**, 14807.
86. O. Hod, E. Rabani and R. Baer, *J. Chem. Phys.*, 2005, **123**, 051103.
87. (a) D. Rai, O. Hod and A. Nitzan, *J. Phys. Chem. Lett.*, 2011, **2**, 2118; (b) D. Rai, O. Hod and A. Nitzan, *Phys. Rev. B: Condens. Matter*, 2012, **85**, 155440.
88. F. Li, S. I. Yang, Y. Ciringh, J. Seth, C. H. Martin, D. L. Singh, D. Kim, R. R. Birge, D. F. Bocian, D. Holten and J. S. Lindsey, *J. Am. Chem. Soc.*, 1998, **120**, 10001.
89. D. L. Pearson and J. M. Tour, *J. Org. Chem.*, 1997, **62**, 1376.
90. (a) C. Wang, A. S. Batsanov, M. R. Bryce and I. Sage, *Synthesis*, 2003, **2003**, 2089; (b) S. Percec, R. Getty, W. Marshall, G. Skidd and R. French, *J. Polym. Sci., Part A: Polym. Chem.*, 2004, **42**, 541.
91. P. U. Müller, E. Weber, G. Rheinwald and W. Seichter, *Org. Biomol. Chem.*, 2005, **3**, 3757.

92. S. Z. Vatsadze, I. D. Titanyuk, A. V. Chernikov and N. V. Zyk, *Russ. Chem. Bull.*, 2004, **53**, 471.
93. C. Mechtler, M. Zirngast, W. Gaderbauer, A. Wallner, J. Baumgartner and C. Marschner, *J. Organomet. Chem.*, 2006, **691**, 150.
94. M. Bérubé and D. Poirier, *Org. Lett.*, 2004, **6**, 3127.
95. D. W. Price, S. M. Dirk, F. Maya and J. M. Tour, *Tetrahedron*, 2003, **59**, 2497.
96. (a) W. Zhang and J. S. Moore, *J. Am. Chem. Soc.*, 2005, **127**, 11863; (b) W. Zhang and J. S. Moore, *Adv. Synth. Catal.*, 2007, **349**, 93.
97. W. Zhang and J. S. Moore, *Angew. Chem., Int. Ed.*, 2006, **45**, 4416.
98. (a) W. J. Youngs, C. A. Tessier and J. D. Bradshaw, *Chem. Rev.*, 1999, **99**, 3153; (b) C. Grave and A. D. Schlüter, *Eur. J. Inorg. Chem.*, 2002, **2002**, 3075; (c) M. Iyoda, J. Yamakawa and M. J. Rahman, *Angew. Chem., Int. Ed.*, 2011, **50**, 10522.
99. J. Zhang, D. J. Pesak, J. L. Ludwick and J. S. Moore, *J. Am. Chem. Soc.*, 1994, **116**, 4227.
100. M. Kiguchi, K. Tahara, Y. Takahashi, K. Hasui and Y. Tobe, *Chem. Lett.*, 2010, **39**, 788.
101. (a) W. Haiss, H. van Zalinge, S. J. Higgins, D. Bethell, H. Höbenreich, D. J. Schiffrin and R. J. Nichols, *J. Am. Chem. Soc.*, 2003, **125**, 15294; (b) T. Albrecht, K. Moth-Poulsen, J. B. Christensen, A. Guckian, T. Bjørnholm, J. G. Vos and J. Ulstrup, *Faraday Discuss.*, 2006, **131**, 265.
102. W. Buchholz, *Commun. ACM*, 1959, **2**, 3.
103. Engineering Research Associates, *High-Speed Computing Devices*, McGraw-Hill, 1950.
104. D. E. Knuth, *The Art of Computer Programming, Volume 2: Seminumerical Algorithms* (2nd ed.), Addison-Wesley, 1981.
105. (a) G. Ma, X. Shen, L. Sun, R. Zhang, P. Wei, S. Sanvito and S. Hou, *Nanotechnology*, 2010, **21**, 495202; (b) D. Tang, Y. Wang, H. Yuan, L. Ci, W. Zhou and S. Xie, *Nanoscale Res. Lett.*, 2009, **4**, 538.

CHAPTER 2 : SYNTHESIS OF BRANCHED FERROCENE-CONTAINING COMPLEXES

2.1 ABSTRACT

The syntheses and electrochemical/optical properties of some branched and linear 1,1'-substituted ferrocene complexes are described *(Figure 2-1a* and *b)*. Metal centres were extended (and where relevant, connected) by arylethynyl spacers functionalised with trimethylsilyl (TMS), *tert*-butylthiol (S^{t}Bu) and *meta*-pyridyl moieties. Efforts towards a macrocyclic analogue *(Figure 2-1c*, obtained in trace quantities), are also discussed. As established in *Chapter 1*, such systems provide *two* well-defined molecular pathways for electron transfer, facilitating the study of quantum interference effects and other phenomena resulting from concurrent, and ultimately convergent, electron transport.

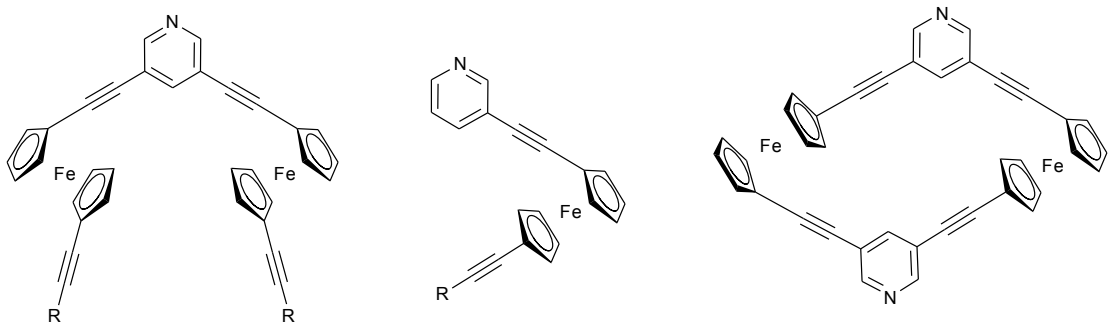

9, 10, 12 **3-5** **13**

(a) (b) (c)

Figure 2-1. Structures of (a) branched, (b) linear and (c) macrocyclic compounds prepared here (R = 3-pyridine, 4-(*tert*-butylthio)benzene, trimethylsilane).

Whilst previously published syntheses of related unsymmetrical materials are based on the isolation and onward reaction of 1-ethynyl-1'-iodoferrocene (prepared from 1,1'-diiodoferrocene (**1**) and substoichiometric quantities of ethynyltriisopropylsilane[1]), a different approach was

taken here, using monosubstituted products produced by reaction of the relevant alkyne with a 5-fold excess of **1**. The latter was readily available in large quantities following novel application of a simple oxidative purification technique (extending an approach recently developed by Goeltz and Kubiak for iodoferrocene).[2]

2.2 OXIDATIVE PURIFICATION OF 1,1'-DIIODOFERROCENE

2.2.1 1,1'-Diiodoferrocene – a convenient starting material?

Haloferrocenes have a broad reactivity profile, permitting facile preparation of numerous ferrocene-incorporated compounds. Direct reactions from Fc-I include Suzuki,[3] Ullmann,[4] Negishi,[5] Stille[6] or Sonogashira[7] couplings, Pd-catalysed carbonylations,[8] aminocarbonylations[9] or phosphinations,[10] and copper-mediated processes forming ferrocenyl carboxylic acids[11] or aryl ethers[12] *(Scheme 2-1)*. Indirectly, synthetic possibilities are extended by ready conversion of halogen functionalities to lithium,[13] acetyl,[14] magnesium halide,[15] azide,[16] cyanide,[14] zinc-chloride,[17] mercury chloride,[18] trialkyltin[18a,19] or boronic acid[15] species *(Scheme 2-2)*. Ferrocenyl iodides may also be converted to their bromides and chlorides via halogen exchange with CuX (X = Br, Cl) in pyridine.[14]

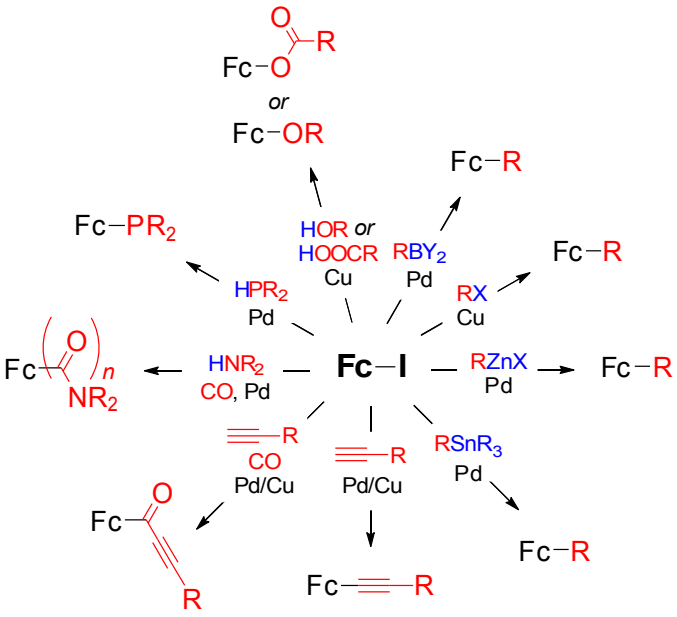

Scheme 2-1. Some Pd/Cu catalysed reactions of iodoferrocenes (R = aryl, alkyl, vinyl; Y = OH, OR; X = I, Br, Cl; *n* = 1, 2).

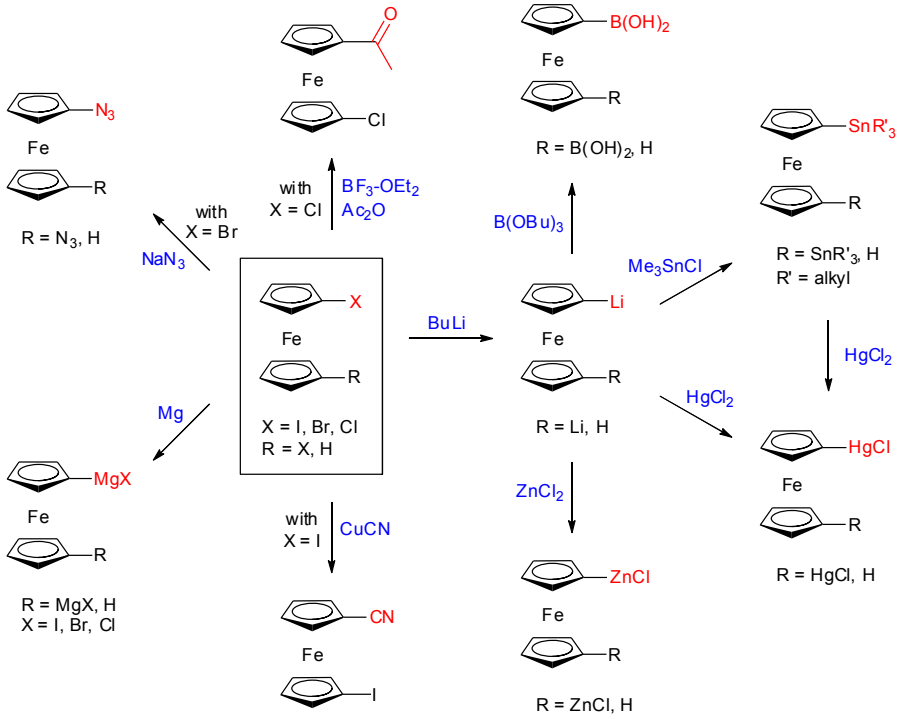

Scheme 2-2. Various reactive materials may be prepared from haloferrocenes in one or two steps.

For the above reasons, and its established utility in the preparation of related compounds *(vida infra)*, 1,1'-diiodoferrocene (**1**) was chosen as the primary starting material for syntheses of ferrocene-based molecular targets *(Chapter 1)*. However, obtaining large quantities of this complex is not straightforward. Typical routes – via 1,1'-chloromercuriferrocene,[20] 1,1'-dilithioferrocene,[21] or 1,l'-bis(tri-*n*-butylstannyl)ferrocene[22] – involve toxic starting materials/intermediates or provide the desired product in difficult to separate mixtures.[22a] Indeed, it has been this authors' experience that reactions of elemental iodine with 1,1'-dilithioferrocene-TMEDA[21a] generate a crude product consisting of ferrocene, iodoferrocene and **1** (in addition to 1,1'''-diiodobiferrocene and higher order ferrocenes), tedious to purify via conventional techniques. In telling examples from the literature, Kovar *et al.* recommend column chromatography (alumina grade II) *using a 2" x 18" column*,[21a] whereas others have suggested recrystallization from ethanol at -30°C.[23] Purification problems are likely a result of the monoferrocene series having similar polarities/solubilities, exacerbated by the fact that **1** is a liquid at room temperature (in remarkable contrast to iodoferrocene, bromoferrocene and 1,1'-dibromoferrocene, which are solids).

2.2.2 Oxidative purification

Perhaps unsurprisingly given the aforementioned context, a recent paper by Goeltz and Kubiak describing a new method *(Scheme 2-3a)* to purify iodoferrocene provoked substantial intrigue (many of the difficulties in isolating **1** are also incumbent here).[2] Taking a ferrocene/iodoferrocene mixture dissolved in pentane, they isolated the halogenated product by repeatedly washing the solution with aqueous $FeCl_3$ (a mild oxidant). This converted the ferrocene into ferrocenium chloride, which was readily extracted into the water layer and removed.

Whilst simple in practice, the approach is actually quite groundbreaking in exploiting the difference in oxidation potential between components for purification (~170 mV in this case). Crucially, by eliminating the need for careful column chromatography/recrystallization, syntheses could be run at scale – the published procedure generating 7.03 g iodoferrocene from 15 g ferrocene (28% yield).

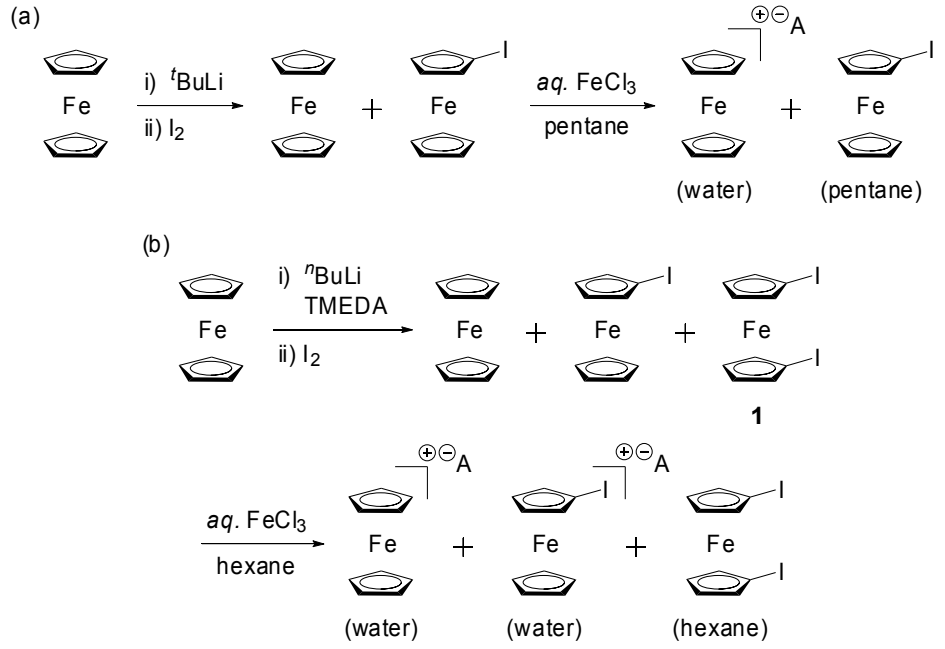

Scheme 2-3. Synthesis and oxidative purification of (a) iodoferrocene (Goeltz and Kubiak),[2] (b) **1** (this work) ($A^- = Cl^-$, $[FeCl_3]^-$ or $[FeCl_4]^-$).*

Application of this process to mixtures of ferrocene, iodoferrocene and **1** (generated from 1,1'-dilithioferrocene) was investigated by this author (following proof-of-principle experiments by a summer student, Mark Driver). Whilst initial attempts successfully employed AgOTf to remove contaminants (a slightly stronger oxidant – precipitating silver metal and generating ferrocenium triflates), it was soon found that the much cheaper $FeCl_3$ (used previously by Goeltz and Kubiak) would also oxidize iodoferrocene (and potentially, **1**) *(Scheme 2-3b)*. This critical result was not mentioned in the original paper regarding ferrocene/iodoferrocene mixtures,[2] and leaves samples at risk of complete oxidation if the procedure is applied too rigorously.

It was found that washing ~33 g of crude material (from 21.14 g ferrocene via 1,1'-dilithioferrocene-TMEDA) with 0.5 M aqueous $FeCl_3$ (10 x 200 mL) eliminated all ferrocene and iodoferrocene contaminants (*Figure 2-2*, full experimental procedures given in *Chapter 8)*. Elution of the resulting material through a short silica column (3″ x 4″) with *n*-hexane easily removed oxidized components, higher order ferrocenes, and grease, providing 9.54 g (19% yield)

* *n*-Hexane solutions of pure FcH and FcI were each oxidised with *aq.* $FeCl_3$ and the resulting aqueous phases analysed by mass spectrometry. Peaks attributable to $[FcH]^+$ and $[FcI]^+$ were observed in positive ion mode, with those attributable to $FeCl_4^-$ and $FeCl_3^-$ seen in negative ion mode.

of pure **1** by collection of the primary orange-red band. No significant impurities were observed by ^{1}H NMR *(Figure 2-4)* and the product was further characterized by ^{13}C{^{1}H} NMR and accurate mass/elemental analyses.

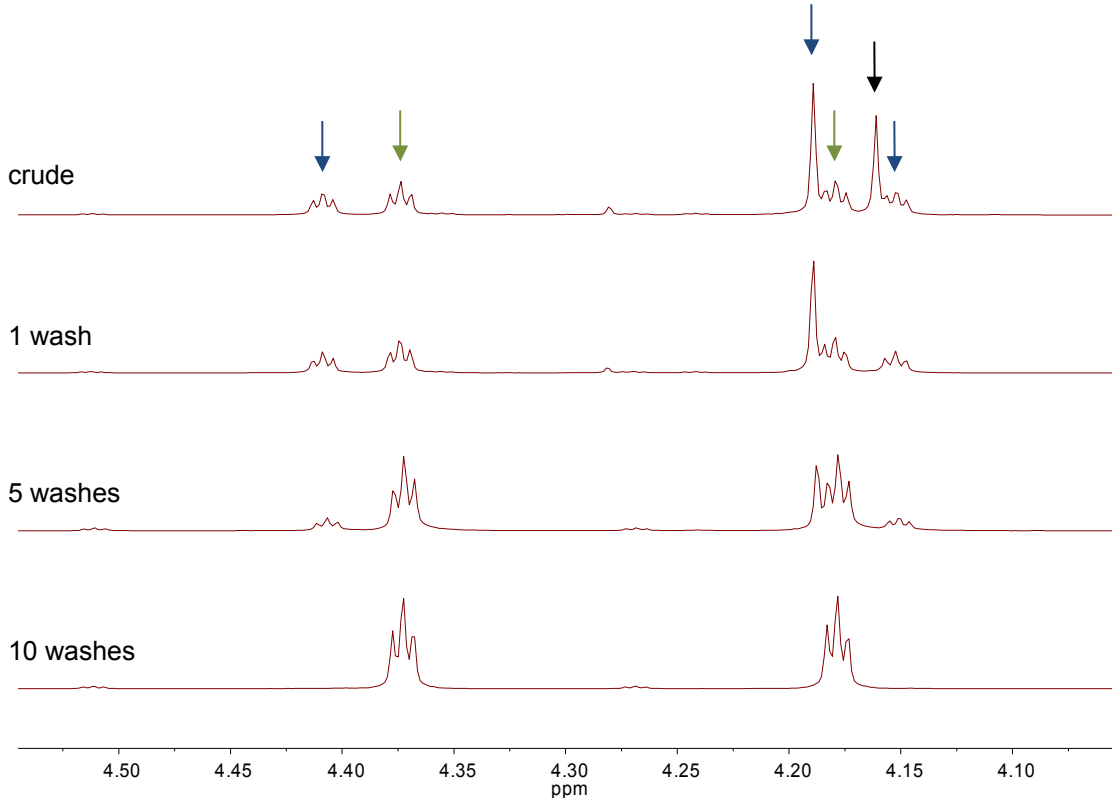

Figure 2-2. Selected ^{1}H NMR spectra showing the elimination of ferrocene (black arrow, after 1 wash with 0.5 M aqueous $FeCl_3$) and iodoferrocene (blue arrows, after 10 washes) from their mixture with **1** (green arrows).

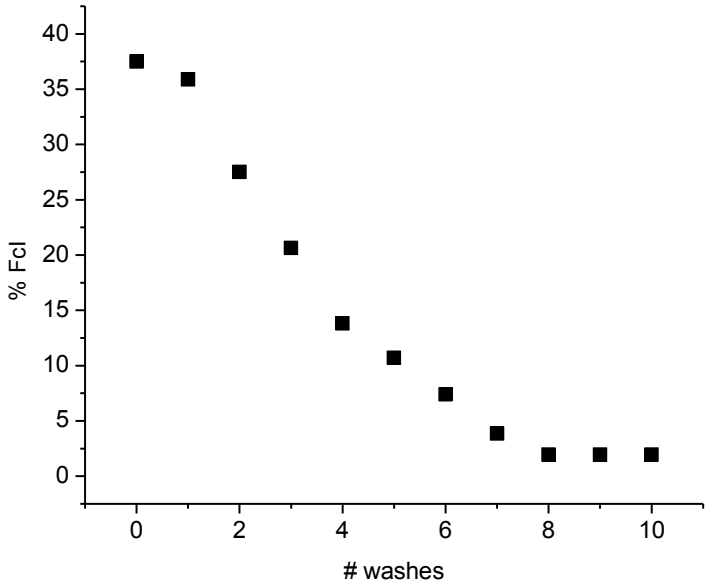

Figure 2-3. A graph showing the decreasing percentage of iodoferrocene (FcI) in the crude product (estimated by ^{1}H NMR, where % FcI + % **1** taken as 100%) with successive washings of 200 mL 0.5 M aqueous $FeCl_3$.

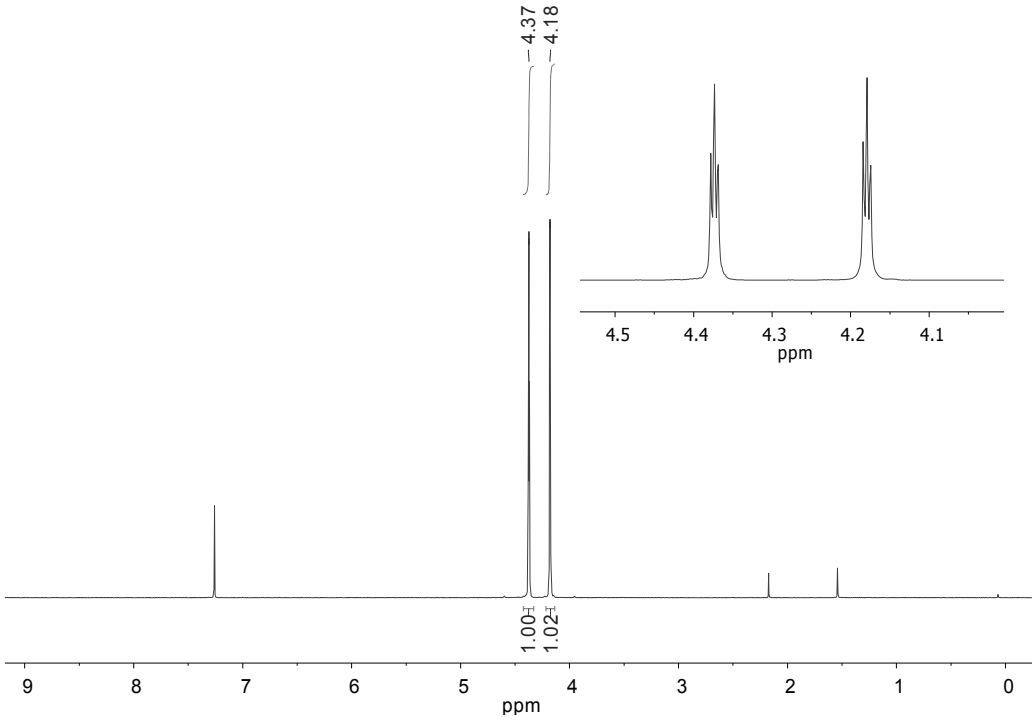

Figure 2-4. ^{1}H NMR spectrum of pure 1,1'-diiodoferrocene (**1**).

In this process ferrocene is rapidly oxidised first – evidenced by the disappearance of its singlet ^{1}H NMR resonance in *Figure 2-2* after only 1 wash, and the short induction period in *Figure 2-3*. Iodoferrocene is subsequently oxidised (relatively slowly), until only **1** remains. This observed order (FcH > FcI > fcI_2) follows the increasing redox potential of these species as measured by cyclic voltammetry *(Figure 2-5* with raw data in *Table 2-1)*. Each complex exhibits reversible behaviour ($i_p^a/i_p^c \approx 1$, $i_p \propto V_s^{1/2}$), with measured differences (in CH_3CN) of 155 mV and 132 mV between the oxidation potentials of ferrocene/iodoferrocene and iodoferrocene/**1**, respectively.

This 'oxidative purification' methodology (adapted for bromoferrocene and 1,1'-dibromoferrocene by a colleague, Shuoren Du) has recently been published.[24]

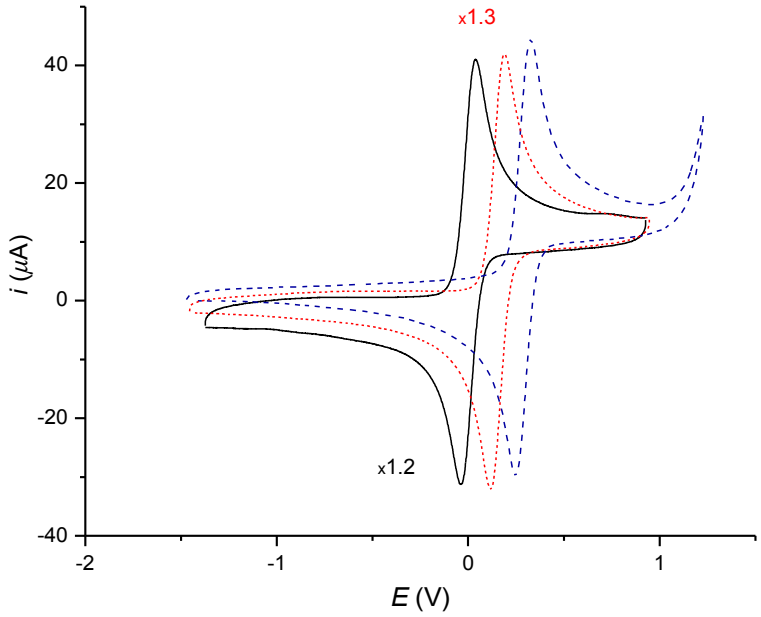

Figure 2-5. Cyclic voltammograms of ferrocene (black solid line), iodoferrocene (red dotted line), and pure **1** (blue dashed line) (potentials reported versus $[FcH]^+/[FcH]$) – current scaled for clarity.

Table 2-1. Electrochemical data for iodoferrocene and 1,1'-diiodoferrocene (**1**).[a]

compound	E_{pa} (V)	E_{pc} (V)	ΔE (V)[b]	i_p^a/i_p^c	$E_{1/2}$ (V)[c]
FcI	0.116	0.194	0.078	1.00	0.155
fcI_2 (**1**)	0.250	0.323	0.073	1.04	0.287

[a] For scan rate = 0.1 Vs^{-1}. $Bu_4N^+PF_6^-$ (0.1 M) in MeCN; WE: glassy carbon; RE, CE: Pt. All potentials (error = ±0.02 V) assigned to the Fe(II)/Fe(III) redox couple and reported relative to an internal $[FcH]^+$/[FcH] reference. [b] $\Delta E > 0.060$ V due to a small uncompensated solution resistance effect. [c] $E_{1/2} = ½(E_{pa} + E_{pc})$.

With large quantities of **1** now readily available, the synthesis of some novel 1,1'-substituted ferrocene-containing complexes for molecular electronics was pursued *(Section 2.3)*.

2.3 BRANCHED COMPLEXES FOR MOLECULAR ELECTRONICS

Ferrocene is often utilized within studies of molecular electronics – likely popularised by its robust nature, facile synthetic modification and well defined reversible electrochemistry (providing complexes typically stable in both 0/1+ states). Rotation of the Cp rings with respect to each other also adds a conformational flexibility that is not provided by other commonly used redox active centres. It has been speculated that, by bending, the same ferrocene complex could bridge electrode nanogaps of different sizes[25] – though this also increases the complexity of molecular junction preparation (observed experimentally,[26] and discussed later), and such deviations from linearity are considered to lower conductance through the molecule.[27] Others have commented that ferrocene derivatives are a good size to fit supramolecular hosts such as cyclodextrins,[28] useful for preparations of *shielded* molecular wires.

Significant work has been reported regarding syntheses of 1,1'-substituted ferrocene complexes functionalised with terminal moieties for surface binding. Examples with thioacetate,[25,29] *tert*-butylthiol,[30] 3-pyridine,[31] 4-pyridine,[31] or amine[21c] end groups are known *(Figure 2-6)*, typically incorporating ferrocene as part of a oligo(phenyleneethynylene) (OPE) backbone.

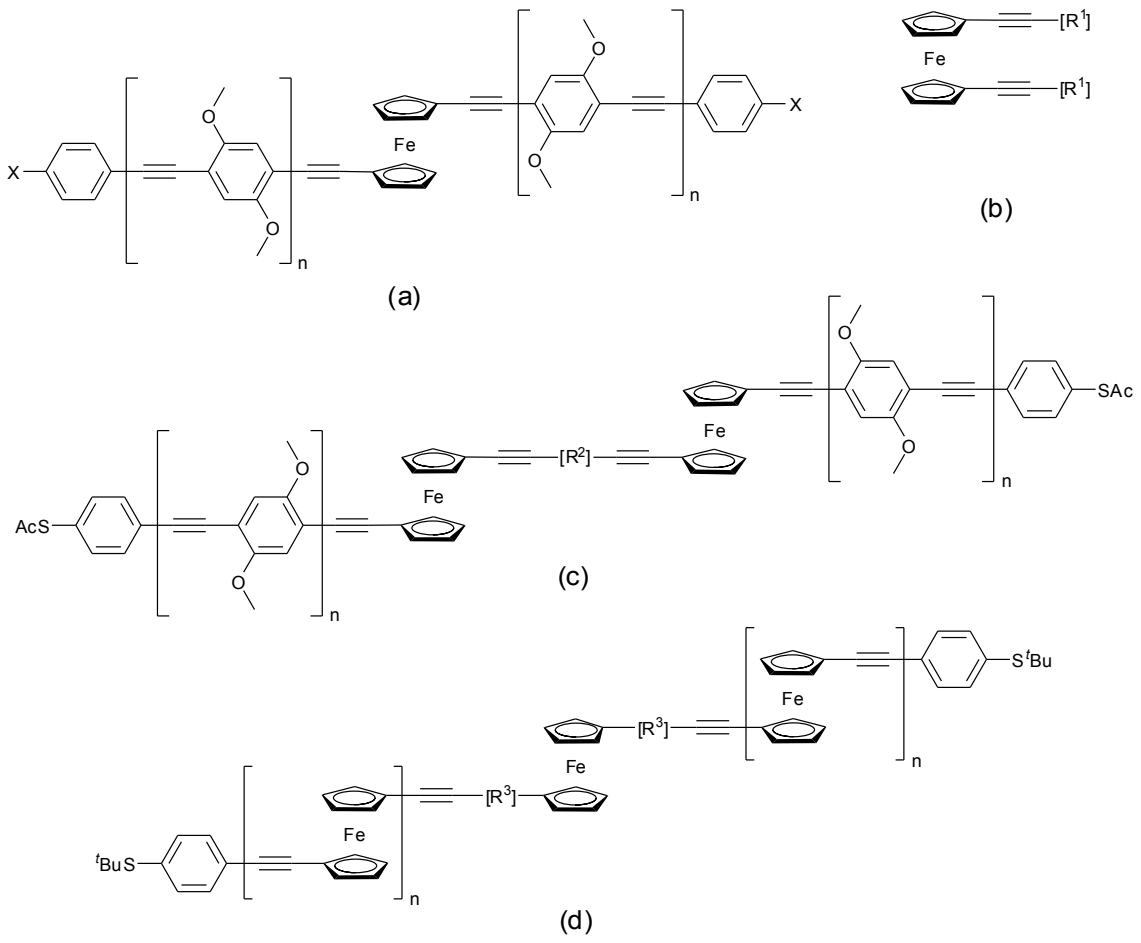

Figure 2-6. Some 1,1'-substituted ferrocene-based 'molecular electronic' components (X = SAc, NH_2; n = 0-2; R^1 = 3-pyridine, 4-pyridine, 4-(thioacetyl)benzene, 4-(thio-*tert*-butyl)benzene; R^2 = 1,4-benzene, 2,5-dimethoxy-1,4-benzene, 2,5-pyridine, *N*-methyl-2,5-pyridinium, 4,4'-azobenzene; R^3 = 1,4-benzene, 2,5-dimethoxy-1,4-benzene, 2,5-thiophene).

Motivation for much of this work came in 2001 from Engtrakul and Sita,[32] who proposed an electron-hopping mechanism for molecular rectification in diferrocene complexes linked by an *N*-methyl-2,5-diethynylpyridinium bridge. The electronic asymmetry induced creates a difference in redox potential between the attached ferrocene centres (confirmed by electrochemical studies of mono-ferrocene analogues), which is thought to generate an energy barrier for electron transport in one direction (facilitating it in the other).[†] Analogous dithiol derivatives suitable for junction measurements have since been synthesized *(Figure 2-6c*, R^2 =

[†] Mechanisms of rectification in redox systems have been discussed by Kuznetsov and Ulstrup;[33] the concept of single-molecule rectification was initially proposed by Aviram and Ratner in 1974.[34]

N-methyl-2,5-pyridine),[1] and a theoretical investigation by others was supportive of the concept.[35]

Intriguing results from relevant single-molecule conductance measurements provided further stimulus. In a seminal paper, Getty *et al.* found that a ferrocene-containing oligo(phenylethynyl)dithiolate compound *(Figure 2-6a*, X = SAc; n = 1) demonstrated a higher (indeed, "near-perfect") conductance than an all-organic analogue in gold nanogap junctions.[27] This was attributed to the presence of a low-lying molecular orbital, in resonance with the electrode Fermi levels at low bias and extending across the entire complex. Xiao and co-workers later investigated the properties of cysteamine-terminated ferrocene complexes using electrochemical STM, where changes in current were attributed to switching between low-conductance reduced, and high-conductance oxidised states.[36] Computational studies have also examined 1,1'-dicarboxyferrocene bound by aluminium electrodes,[37] and 1,1'-, and 1,3-dithioferrocenes linking silver or gold electrodes.[28,38] Electron transport through such systems was found to be affected by the identity and position of the end groups (1,3-substitution > 1,1'-substitution), as well as the nature of the termini-surface binding (*e.g.* at single adatoms, step edges or small islands).

In other related work, ferrocene-terminated alkanethiol monolayers have been shown to exhibit negative differential resistance (NDR) (*i.e.* decreasing current with increasing voltage).[39] This was explained via a resonant tunnelling process (as observed in semiconductor physics) – where the probability of electrons moving from one electrode to the other through a quantum well (in this case the ferrocene molecular orbitals) is controlled by tunnelling barriers that separate it from the electrical contacts.[39] Wassel *et al.* tested this hypothesis, finding that modulation of the tunnelling barriers – by functionalizing STM tips with insulating alkanethiol matrices, or encapsulating the ferrocene head groups with β-cyclodextrin – attenuated the NDR effect.[40] A similar result was obtained in a theoretical study by changing the STM tip-molecule separation.[41] The use of analogous monolayers as *memory devices* has also been considered. Such films may be oxidised at the ferrocene head group using low voltages, with charge-retention times readily tuned by changing the length or structure of the insulating linker (changing the tunnelling probability).[42]

Complexes have also seen significant use outside of the molecular junction. Following connection of two or more ferrocene (or other redox-active) termini, the rate of electron transfer

across a molecular bridge may be probed by generation and study of the 'mixed-valence' species (a topic explored further in *Chapter 6)*. This property has been linked to molecular conductance by theoretical treatments,[43] and experiment.[26] Short, conjugated bridges typically give delocalised systems (Robin and Day Class III,[44] with a shared valence state), whereas others provide valence-trapped (Class I) or intermediate, thermally activated valence exchange states (Class II). Communication through extended atom metal chains,[45] titanacycles,[46] Pt[47] and Ru[48] complexes, porphyrins,[49] and conjugated organics such as thiadiazoles,[50] thiophenes, furans, pyrrols,[51] or alkynes[52] has been investigated using ferrocene end groups. With other redox centres, the utility of ferrocene as a bridging moiety has been explored.[53]

2.3.1 Motivation for this work

As described in *Chapter 1*, interesting quantum effects may be observed in branched molecules that provide two or more well-defined paths for electron transfer through a junction. Of particular relevance here are the theoretical investigations of Magoga and Joachim, who found that conductance through a macrocycle was greater than the sum of the conductance through its individual branches (*i.e.* a *constructivelike* interference effect) *(Figure 2-7a)*.[54] They also demonstrated the importance of being able to control electron transfer through single branches in elucidating these types of effects (in their case by rotation of a single phenyl ring out of plane, breaking its π-conjugation). This ability is of additional importance in real-world systems, potentially permitting the exploitation of quantum interference as a conductance switching mechanism.

Experimental analogues of their theoretical series are proposed *(Figure 2-7b)* – modelled on the ferrocene OPE motif utilised successfully elsewhere, with pyridyl moieties for surface binding. Critically, it was considered that conductance through the individual branches of such complexes could be altered via redox events at the ferrocene centre (shifting the metal frontier orbitals in or out of alignment with the rest of the molecule).

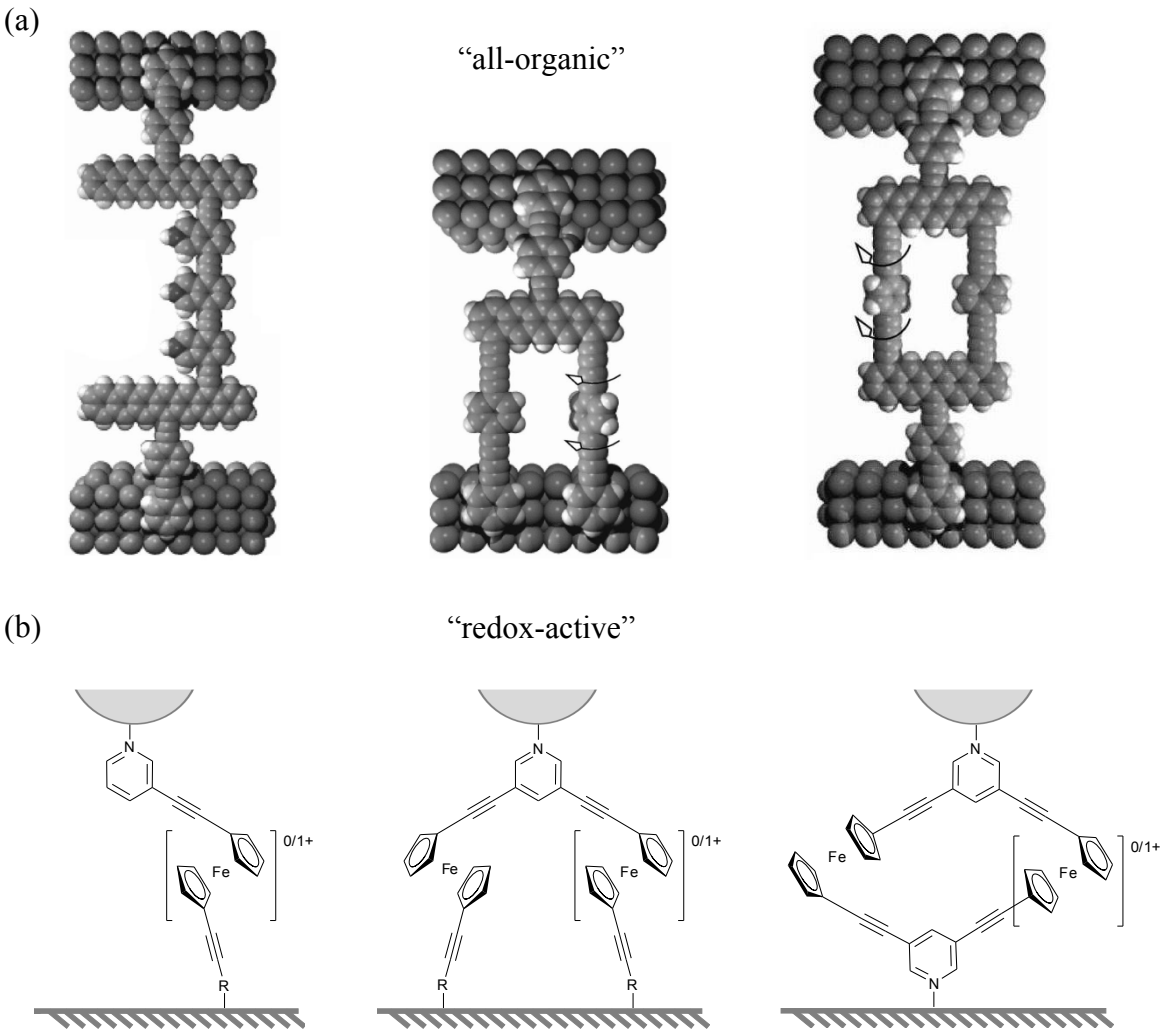

Figure 2-7. Linear, branched and macrocyclic systems for molecular electronics – (a) example theoretical structures investigated by Magoga and Joachim (phenyl rotation disrupting branch conductance),[54] (b) experimental analogues proposed here (redox events changing branch conductance, R = 3-pyridyl, 4-thioacetylbenzene). Figures (top) reprinted from reference [54] with permission. Copyright 1999 by the American Physical Society.

Admittedly, achieving the desired orientations of linear and branched all-pyridyl structures within molecular junctions might prove difficult due to competitive surface coordination and Cp ring rotation *(Figure 2-8)*. In the worst cases, complexes might bind by all moieties to the surface, presenting no opportunities for chemisorbed contact to a top electrode. To guard against such problems, mixed pyridyl/thiolate-terminated analogues were also considered. It was reasoned that these would be more likely to have a preferred surface orientation due to the

formation of strong thiolate-electrode bonds (assuming close packing of the monolayer and reversible binding of the pyridyl moiety) *(Figure 2-9)*. Surface selectivity could be enhanced further if the pyridyl nitrogen was protonated, or otherwise protected, prior to thiolate self-assembly.

Zhou *et al*. recently found that a useful general solution to such problems was to insert single complexes into defect sites of an insulating alkanethiol monolayer.[26]

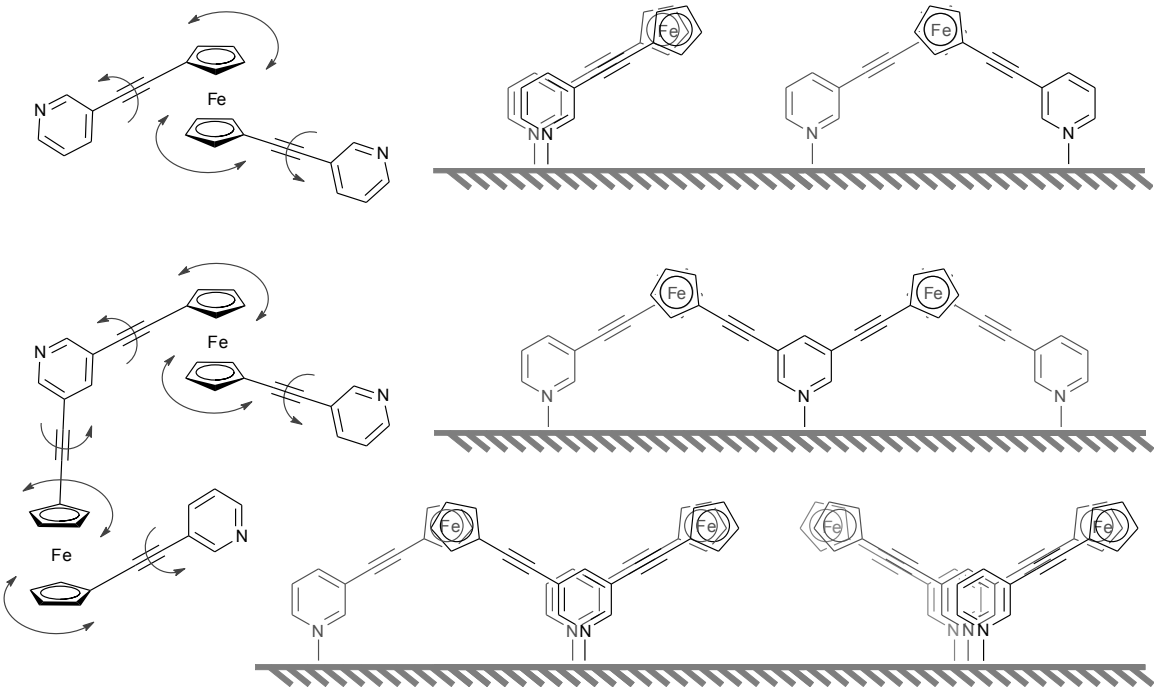

Figure 2-8. As well as the desired configuration *(Figure 2-7b)*, other surface-bound isomers of pyridyl-terminated ferrocene complexes may be expected.

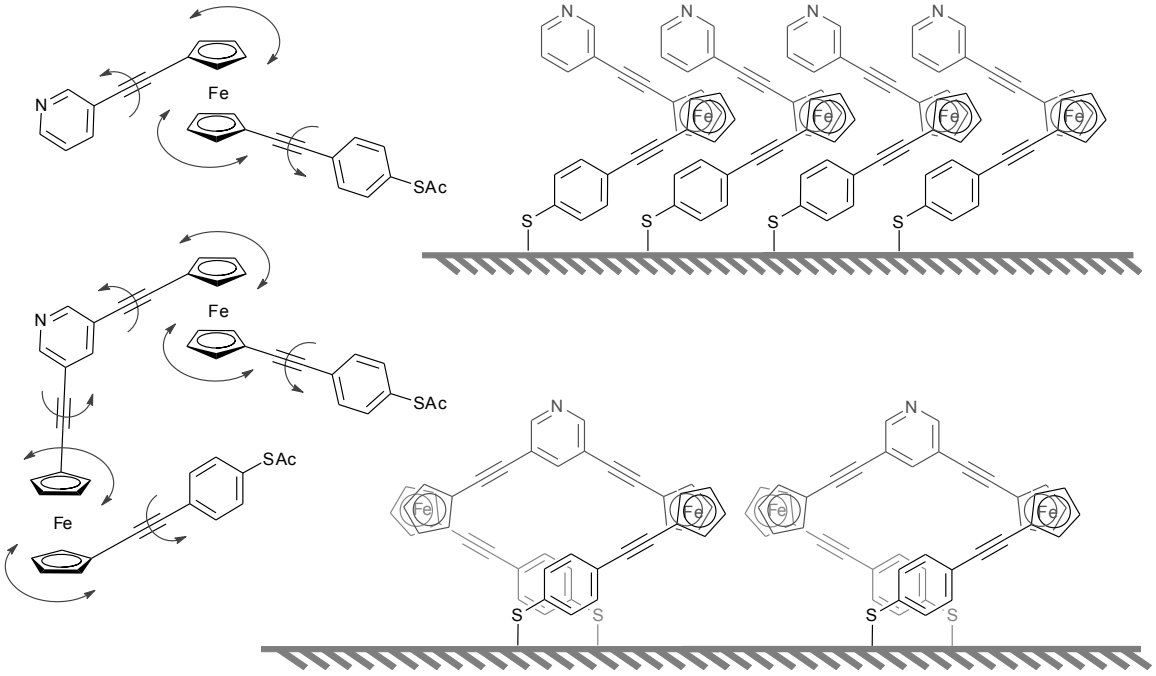

Figure 2-9. With mixed pyridyl/thiolate-terminated complexes, one orientation should be favoured.

2.3.2 Retrosynthetic considerations

Whilst every complex in *Figure 2-6* has been prepared via Sonogashira cross-coupling from **1**, these reactions are not always as straightforward as those found with typical aryl halides. When working with any iodoferrocenes, the following idiosyncrasies should be taken into account.

Routes via 1,1'-diethynylferrocene are impossible. This (otherwise useful) intermediate has never been isolated, somewhat limiting syntheses of ferrocene materials compared to those of prototypical OPE-type molecular wires (which readily involve cross-couplings of 1,4-diethynylbenzene*, Scheme 2-4)*.[55] Desilylation of the precursor, 1,1'-bis(trimethylsilyl)ethynylferrocene, results *only* in ferrocenophanes via base-mediated intramolecular cyclization *(Scheme 2-5)*.[56] Difficulties have also been reported in the desilylation of an 1-arylethynyl-1'-(trimethylsilyl)ethynylferrocene (*e.g. Scheme 2-6)*, presumably due to an analogous reaction.[1]

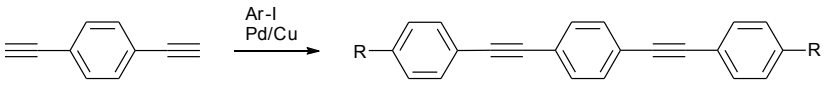

Scheme 2-4. Synthesis of OPE-type structures may readily proceed via 1,4-diethynylbenzene (R = phenylene(ethynylene) oligomers,[55a] SAc,[55b] NH_2[55c]).

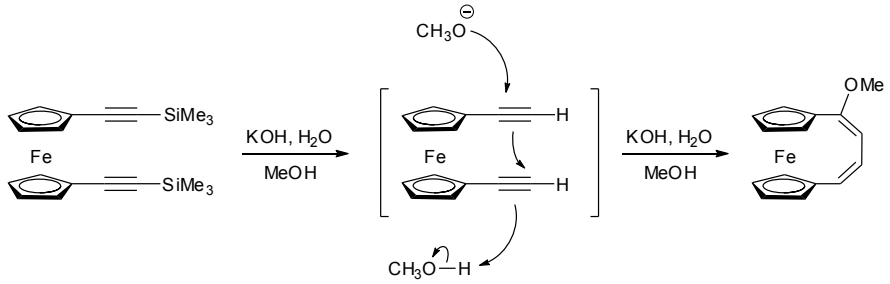

Scheme 2-5. The generation of ferrocenophanes following attempted preparation of 1,1'-diethynylferrocene.[56]

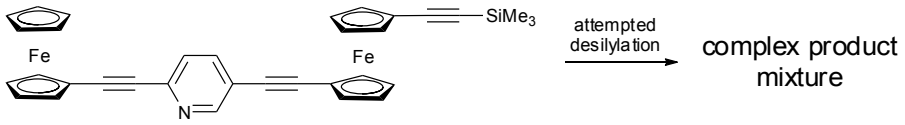

Scheme 2-6. Attempted desilylations of this 1-arylethynyl-1'-(trimethylsilyl)ethynylferrocene complex did not yield the desired product.[1]

Remarkably, 1,1'-bis(1,4-ethynylbenzene)diethynylferrocenes,[1] 1-iodo-1'-ethynylferrocene[29,57] and 1,1'''-diethynylbiferrocene[58] are stable under basic conditions *(Figure 2-10a-c*, respectively). These may be prepared from their silylated precursors and reacted on using conventional cross-coupling methodologies.

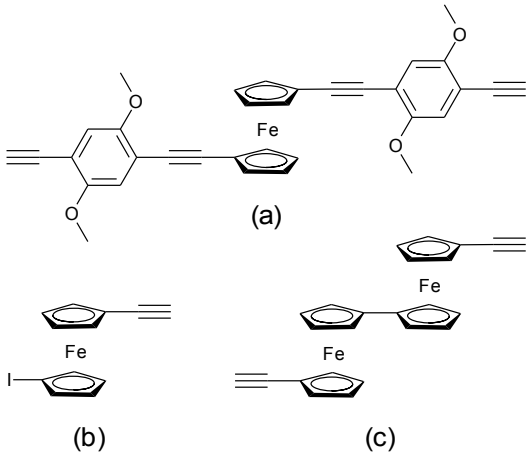

Figure 2-10. Some stable ferrocene-containing terminal alkyne complexes.

Incorporation of the thioacetate group is problematic. Attempts (described in *Chapter 3)* to cross-couple **1** and 1-ethynyl-4-thioacetylbenzene *(Scheme 2-7a)* proved unsuccessful. Others have also noted failed reactions of Fc-I and terminal alkynes in the presence of SAc (*e.g. Scheme 2-7b)*.[29-30] In *Chapter 3*, it is shown that this is due to a previously unknown competing Pd-catalysed reaction between the thioacetate group and terminal alkyne(s). The Sonogashira cross coupling of Fc–I is blocked in the presence of SAc, presumably because the rate of oxidative addition to Pd(0) follows the order Ar–I > Ar–Br > S–Ac > Fc–I.

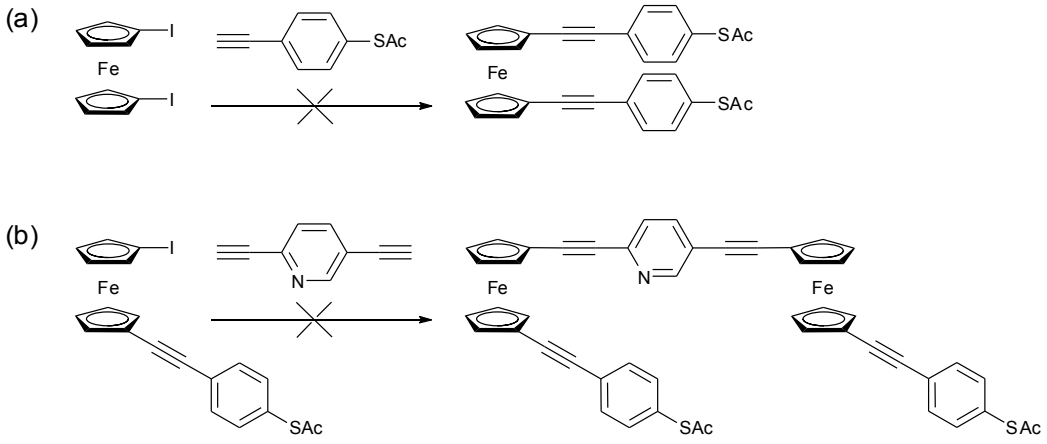

Scheme 2-7. Unsuccessful attempts to synthesise thioacetyl-terminated ferrocene complexes via Sonogashira cross-coupling.

To avoid the thioacetate–alkyne reaction, *tert*-butylthiol moieties may be incorporated instead and converted to thioacetate after other synthetic manipulations are complete (via established methods using $AlCl_3$,[59] BBr_3[60] or Br_2[61]). This approach has been successfully employed elsewhere with OPE-type components.[62] Whilst several relevant ferrocene complexes have been prepared *(Figure 2-6)*,[30] problems in conversion of their protecting *tert*-butyl groups to acetyls have been reported (plausibly due to side-reactions at the metal centre).[63] Indeed, only two successful applications of this strategy in ferrocene-containing compounds are known.[64]

Other routes are more successful but less ideal. Certainly, the coupling of 1-iodo-4-thioacetylbenzene with ferrocene-containing terminal alkynes (*e.g. Figure 2-10a)* is straightforward,[29] but 1-thioacetyl-4-ethynylbenzene units can only be incorporated with at least one arylethynyl moiety between themselves and the cyclopentadienyl ring. Direct connection of the 1-ethynyl-4-thioacetylbenzene motif to ferrocene *is* possible via Stille coupling *(Scheme 2-8)*,[25] though much less convenient.

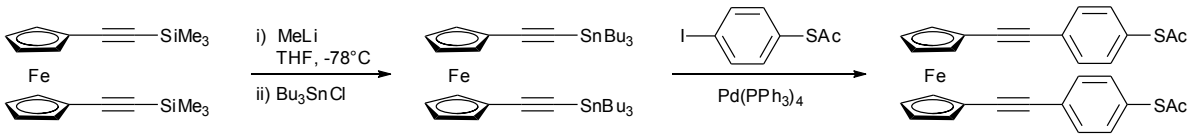

Scheme 2-8. The synthesis of thioacetyl-terminated ferrocene complexes may be realised using Stille coupling.[25]

Sonogashira reactions of iodoferrocenes are typically low yielding. As discussed at length in the next chapter, the common application of $PdCl_2(PPh_3)_2$ as a catalyst in Sonogashira cross-couplings with iodoferrocenes is rather inefficient. Whilst not taken into account for reactions here, it is shown in *Chapter 3* that yields are likely to be *significantly* improved by: (i) maximising reactant concentration, or ii) using a $PdCl_2(MeCN)_2/P(^tBu)_3$ catalyst combination. From **1**, it has sometimes also been observed that cross-coupling of the second iodo functionality is slower than the first.[29,65] Other side-reactions may also cause problems, such as hydrodehalogenation *(vida infra* and *Chapter 3)*.

2.3.3 Synthesis

Synthesis of linear and branched compounds

Novel linear *(Scheme 2-9)* and branched *(Scheme 2-10)* complexes were prepared via successive Sonogashira cross-couplings starting from **1**. *Meta*-pyridyl functionalities were incorporated into every material, with both trimethylsilyl- or *tert*-butylthiol-terminated structures prepared as possible precursors to their thioacetate equivalents. All reagents were commercially available except **1** (purified as previously described, *Scheme 2-3b)*, 1-(*tert*-butylsulfanyl)-4-ethynylbenzene[60,66] *(Scheme 2-11)* and 3,5-diethynylpyridine[67] *(Scheme 2-12)*, which were prepared via literature methods.

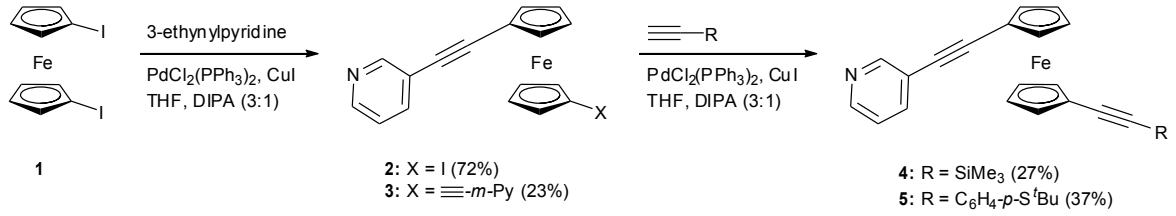

Scheme 2-9. Synthetic route to linear ferrocene complexes (**3**-**5**), proceeding via the unsymmetrical 1-iodo-1'-(3-pyridyl)ethynylferrocene (**2**).

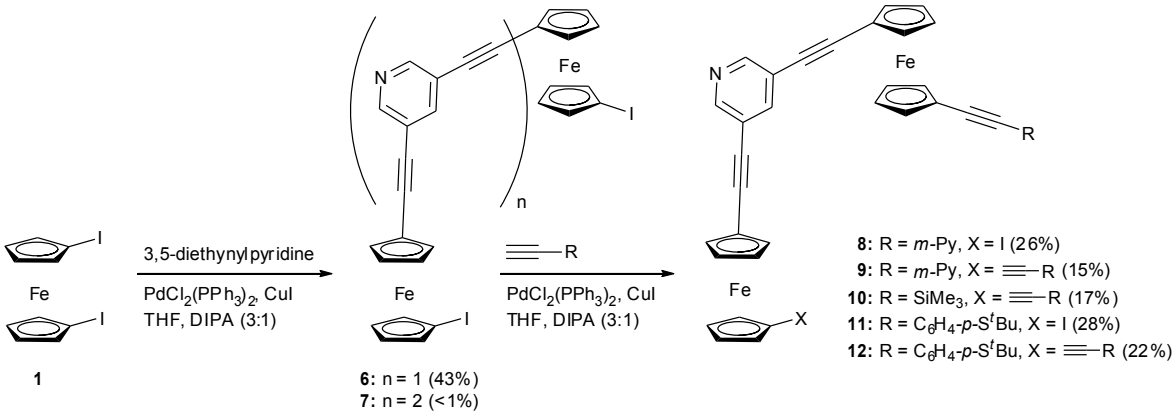

Scheme 2-10. Synthetic route to branched ferrocene complexes (**8**-**12**), proceeding via bis[1-iodoferrocene]-1'-(μ-3,5-diethynylpyridine) (**6**).

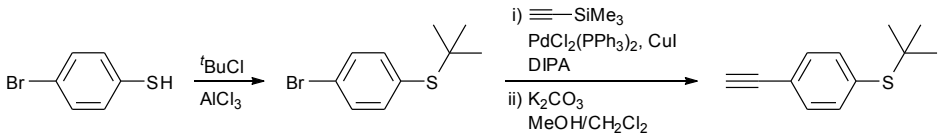

Scheme 2-11. Synthesis of 1-(*tert*-butylsulfanyl)-4-ethynylbenzene, adapted from literature methods.[60,66]

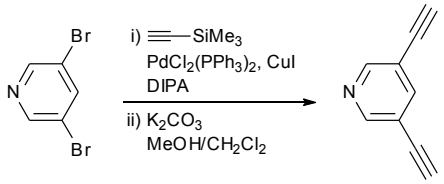

Scheme 2-12. Adapted two-step synthesis of 3,5-diethynylpyridine, from commerically available 3,5-dibromopyridine.[67]

Exploiting the large quantities made available by oxidative purification, asymmetrical intermediates **2** and **6** were synthesised using a five-fold excess of **1** (per alkyne functionality). Unreacted material was easily recovered by chromatography, and yields were typically around 60-70% per bond formed (in attempts with lower **1**-to-alkyne ratios, yields were significantly reduced). It is noted that **2** has been prepared before, albeit via cross coupling of 3-iodopyridine with 1-ethynyl-1'-iodoferrocene.[1]

Desired 1,1'-bis(arylethynyl)ferrocenes (linear: **4**, **5**; branched: **9**, **10**, **12**) were subsequently prepared from **2** and **6** respectively, via reaction with appropriate terminal alkynes. The symmetrical linear complex **3** was conveniently obtained directly from **1** using an excess of 3-ethynylpyridine (via a modified procedure[31]). Yields from cross-coupling of the second iodo-functionality were typically lower (15-37%), particularly in the branched series as mono-substituted products were also formed (**8**, **11**). (These two-terminal complexes contain a free Fc-I moiety, and could readily be reacted on to produce materials containing *three different* terminal groups.)

Two side reactions are of particular note. Complexes containing Fc-I were frequently contaminated with small quantities of their hydrodehalogenated analogues (*i.e. Scheme 2-10*, where X = H), their presence indicated via accurate mass analyses and singlet Cp–*H* resonances in ^{1}H NMR spectra (discussed further in *Chapter 3)*. Also, partial homocoupling of 3,5-

diethynylpyridine occurred if reagents were mixed (in the absence of solvent/amine) prior to removal of oxygen. An early synthesis of **6** thus also provided **7** (subsequent synthetic methods ensured complete removal of oxygen prior to catalyst addition).

Attempts to convert the *tert*-butylthio functionalities of **5** and **12** into thioacetate using the BBr_3 method[60,62] proved unsuccessful. Whilst the product formed from **5** showed a promising ^1H NMR spectrum (resonances attributable to ^{t}Bu now absent, with a new signal at ~2.5 ppm arguably due to Ac), mass spectrometric analysis showed no clear molecular ion for the desired product (or **5**). Even considering the possibility of additional borane adduct formation (via the pyridyl nitrogen) did not aid peak assignments (though the presence of boron was confirmed by ^{11}B NMR). Similar experiments using **12** also did not yield a clear ^1H NMR spectrum. Future work in this area should first establish suitable conditions for thiolate ^{t}Bu-Ac exchange using simpler ferrocene complexes.

Key to isolating most of these pyridyl-containing materials (via column chromatography) was the use of neutral grade V Alumina as a stationary phase. This permitted the use of reasonably non-polar CH_2Cl_2/*n*-hexane eluent combinations, affording superior resolution between components. After purification, all complexes were characterised by ^1H *(vida infra)* and $^{13}C\{^1H\}$ NMR *(Table 2-2)*, IR[‡], mass spec[§] and elemental analysis, where appropriate (full details in *Chapter 8*, with NMR spectra provided in *Appendix A)*.

[‡] Characteristic bands at 2207-2219 cm^{-1} for $\nu(C\equiv C)_{aryl}$ and ~2150 cm^{-1} for $\nu(C\equiv C)_{TMS}$.

[§] $[M+H]^+$ was always observed.

Table 2-2. Characteristic chemical shift ranges of $^{13}C\{^{1}H\}$ NMR resonances for the 1,1'-substituted complexes prepared here (R = C≡C–Ar, C≡C–Py).

nuclei environment	δ (ppm)
pyridyl/aryl	153-120
alkyne	104-82
Cp (*C*–H)	77-70
Cp (*C*–R)	68-66
Cp (*C*–I)	42-40
S(*C*(CH$_3$)$_3$)	46.5, 31.1
Si(CH$_3$)$_3$	0.3

The Cp–*H* region of ^{1}H NMR spectra provides useful insight into the identity of complexes, being highly diagnostic of the number and substitution of ferrocene centres *(Figure 2-11)*. This may be exemplified by first considering simple systems. In ferrocene, only a singlet is observed due to fast rotation of the Cp rings and equivalence of the ten Cp–*H* proton environments *(Figure 2-11a)*. When a substituent is introduced at one ring (as in the case of iodoferrocene), its remaining protons give two *pseudo*-triplet resonances (an AA'XX' pattern) accounting for two protons each (with a singlet resonance again provided by the unsubstituted ring, but now integrating for five protons) *(Figure 2-11b)*. Whilst the two protons in each A/X environment are chemically equivalent, they are *magnetically inequivalent*, because A (A') couples differently to both X (X') and X' (X), and X (X') couples differently to A (A') and A' (A). The observed *pseudo*-triplet pattern results from incomplete resolution of a 'doublet of doublets' splitting motif *(Figure 2-12)*. In 1,1'-substituted ferrocenes where the substituent is the same (*e.g.* **1**, *Figure 2-11dc)*, two *pseudo*-triplets only are observed, each integrating for four protons (the rings are again equivalent due to rapid rotation).

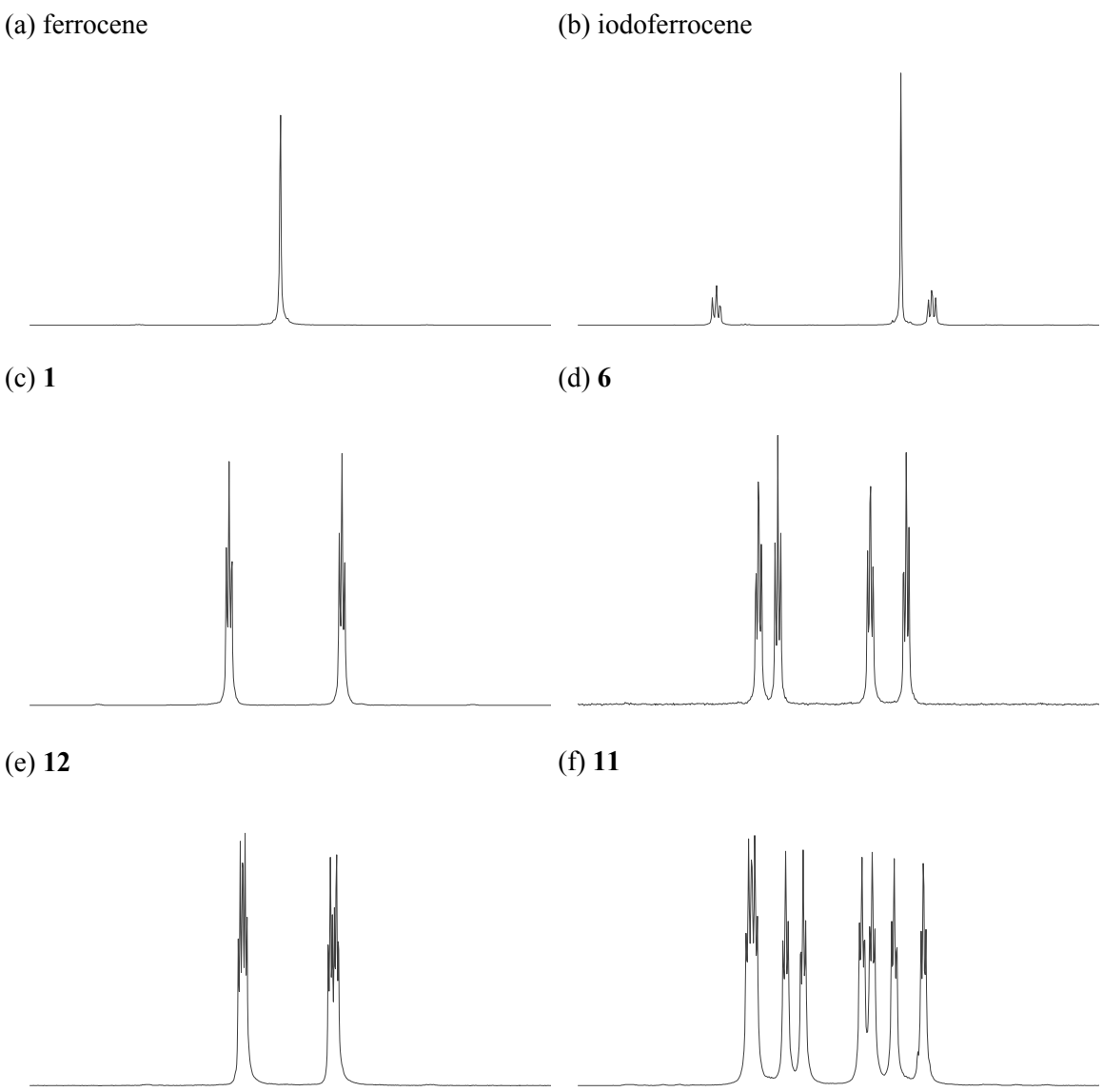

Figure 2-11. ^{1}H NMR spectra (Cp–*H* region) of selected 1,1'-substituted ferrocene complexes.

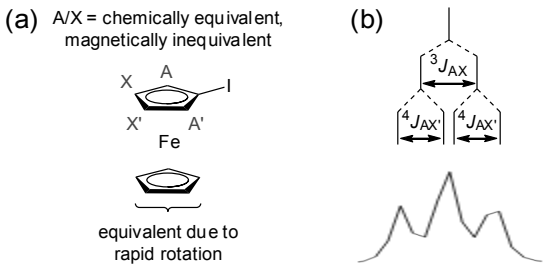

Figure 2-12. Magnetic inequivalence and rapid ring rotation (a) result in *pseudo*-triplet (b) and singlet resonances in the ^{1}H NMR spectra of substituted ferrocenes.

More intricate coupling patterns are now easily interpreted. A 1,1'-substituted ferrocene complex with different substituents exhibits four separate *pseudo*-triplet resonances (such as for **6**, *Figure 2-11d*) – and in the case of similar, yet chemically distinct substituents, these resonances approach each other and may overlap (such as for **12**, *Figure 2-11e)*. Complex **11**, containing two ferrocene centres each with a different set of substituents (iodo/pyridylethynyl, arylethynyl/pyridylethynyl), contains 8 different Cp-*H* environments/*pseudo*-triplet resonances *(Figure 2-11f)*.

In addition to the above, incorporation of *tert*-butylthiophenyl, 3,5- and 3-pyridyl moieties were evidenced by the appearance of characteristic resonances in the aromatic region of spectra *(Figure 2-13)*. *Tert*-butylthio and trimethylsilyl groups also provided distinctive singlets ($SC(CH_3)_3$, δ 1.3 ppm; $Si(CH_3)_3$, δ 0.2 ppm).

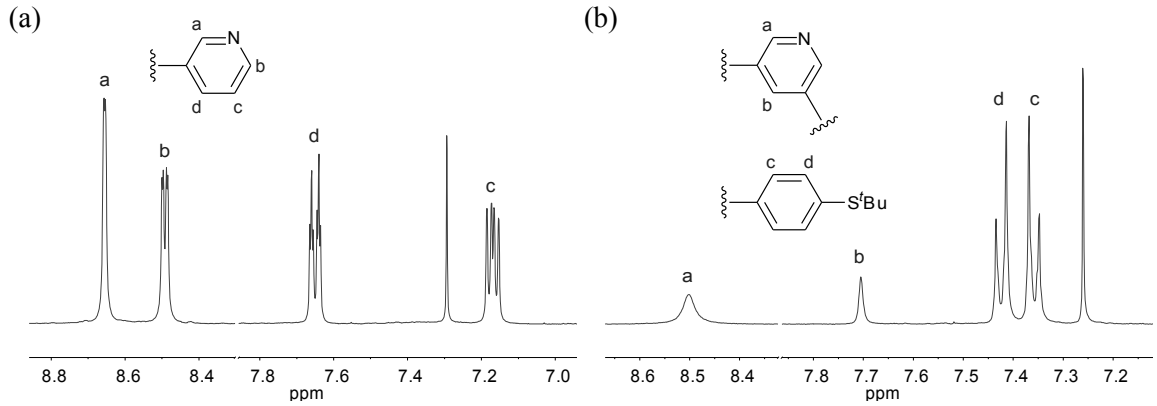

Figure 2-13. Selected ^{1}H NMR spectra showing typical resonances for (a) 3-pyridyl moieties (from complex **3**) and (b) 3,5-pyridyl and *tert*-butylthiophenyl moieties (from complex **12**). Resonances of complexes functionalised with (bulky) *tert*-butylthiophenyl groups were broadened, possibly due to hindered rotation of the Cp rings.

Synthesis of a ferrocene macrocycle

Despite reasonably facile syntheses of its linear and branched analogues, preparation of a pyridyl-containing ferrocene macrocycle proved difficult. Certainly, initial equimolar reactions of **1** and 3,5-diethynylpyridine failed completely, resulting only in multi-component products difficult to separate and analyze *(Scheme 2-12)*. (Perhaps unsurprising given that the approach required formation of four bonds in one step, with significant quantities of reagents also likely consumed by oligo-/polymerizations.)

Greater success was found by employing **6** (an intermediate 'half-macrocycle') as the starting material, though normal/high-dilution syntheses (all reagents combined at the start) only yielded trace amounts of **13** in crude form (identified by ^{1}H NMR and accurate mass measurements). No changes to reactant concentration, or purification technique (column chromatography on SiO_2, Alumina grade II/V) led to significant improvements in the isolated yield.

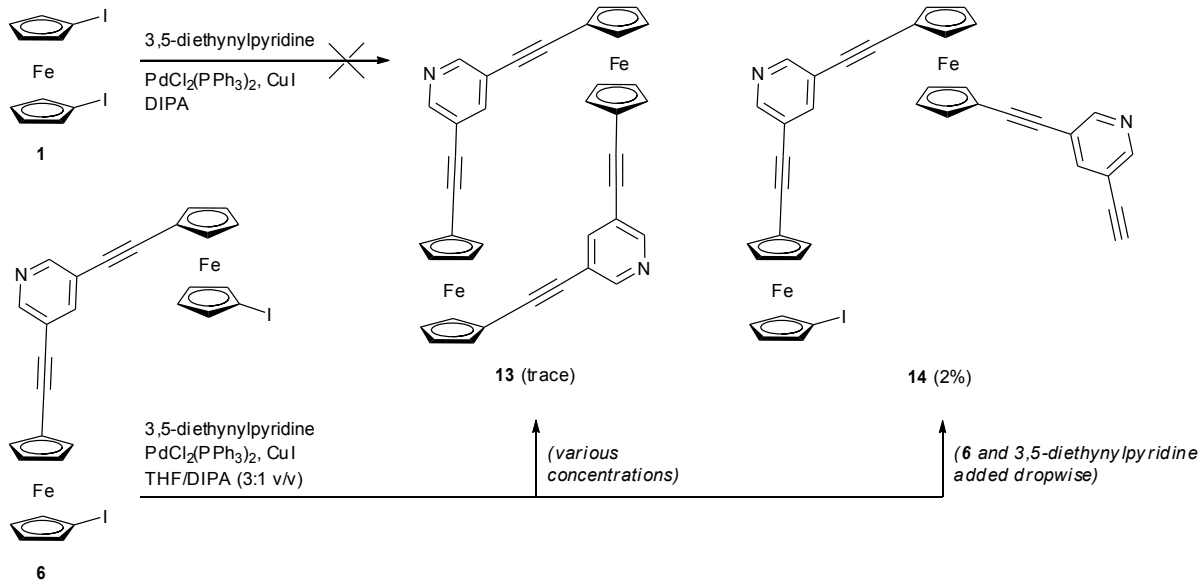

Scheme 2-13. Attempted syntheses of a ferrocene macrocycle – closed (**13**) and open (**14**) structures were partially isolated in small quantities.

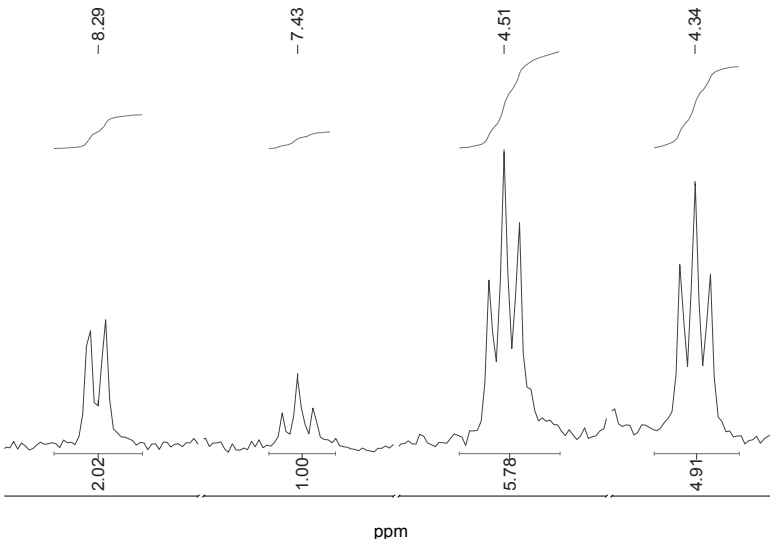

Figure 2-14. ^{1}H NMR ($CDCl_3$) resonances attributed to **13** (taken from the crude spectrum), showing patterns characteristic of 3,5-diethynylpyridyl *(Figure 2-13)* and symmetrically 1,1'-substituted ferrocenes *(Figure 2-11c)*. This sample also exhibited a mass peak at m/z 619.0560 ($[M+H]^+$ Calc. = 619.0591). The higher than theoretical integration of Cp–*H* resonances is due to overlap with impurity peaks resonances from a co-eluting unidentified side-product *(Figure 2-16)*.

Attempts at *pseudo*-high dilution syntheses of **13** (3,5-diethynylpyridine and **6** added dropwise) yielded the open macrocycle **14**, obtained in reasonable purity but only ~2% yield. The ^{1}H NMR spectrum of this material featured a characteristic C≡C–*H* resonance at δ 3.21 ppm, a Cp–*H* pattern similar to that of complex **11** *(Figure 2-11f,* albeit with greater pseudo-triplet overlap) and an aromatic region consistent with two 3,5-diethynylpyridyl moieties (one symmetrically, one asymmetrically substituted) *(Figure 2-15)*. IR[**] and accurate mass analyses[††] also supported the proposed structure. In theory, **14** could be reacted on to produce **13**, but was never isolated in sufficient quantities.

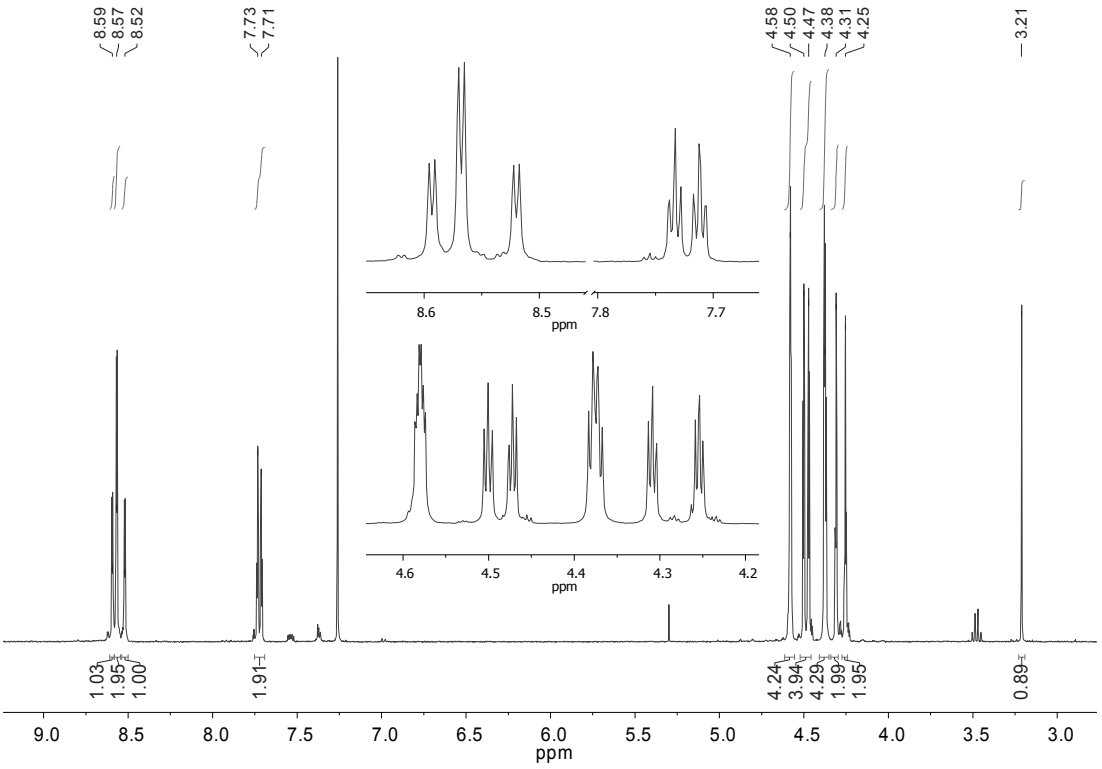

Figure 2-15. The ^{1}H NMR ($CDCl_3$) spectrum of open macrocycle **14**.

In most attempted syntheses of **13**, significant amounts of **6** were recovered[‡‡] and several minor side-products observed. Aside from **14**, the majority of compounds were not easily identified by modifying/combining starting materials via known reactions (*e.g.*

[**] Bands at 3287 ν(C≡C–H) and 2216 cm^{-1} for ν(C≡C)$_{aryl}$.

[††] *m/z* 746.9688 ([M+H]$^{+}$ Calc.: 746.9683).

[‡‡] Albeit contaminated with small quantities of hydrodehalogenated material.

hydrodehalogenation, homocoupling of the alkyne). One such example is a frequently observed material that eluted immediately prior to **13**. Despite exhibiting a ^{1}H NMR spectrum clearly suggestive of two asymmetrically substituted ferrocene centres (such as **11** or **14**), and three 3,5-diethynylpyridyl moieties (two asymmetrically, one symmetrically substituted) *(Figure 2-16)*, molecular weights of plausible structures were not consistent with the mass peaks observed (779, 723, 663 *m/z)*. Obtained yields were not enough for further characterisation.

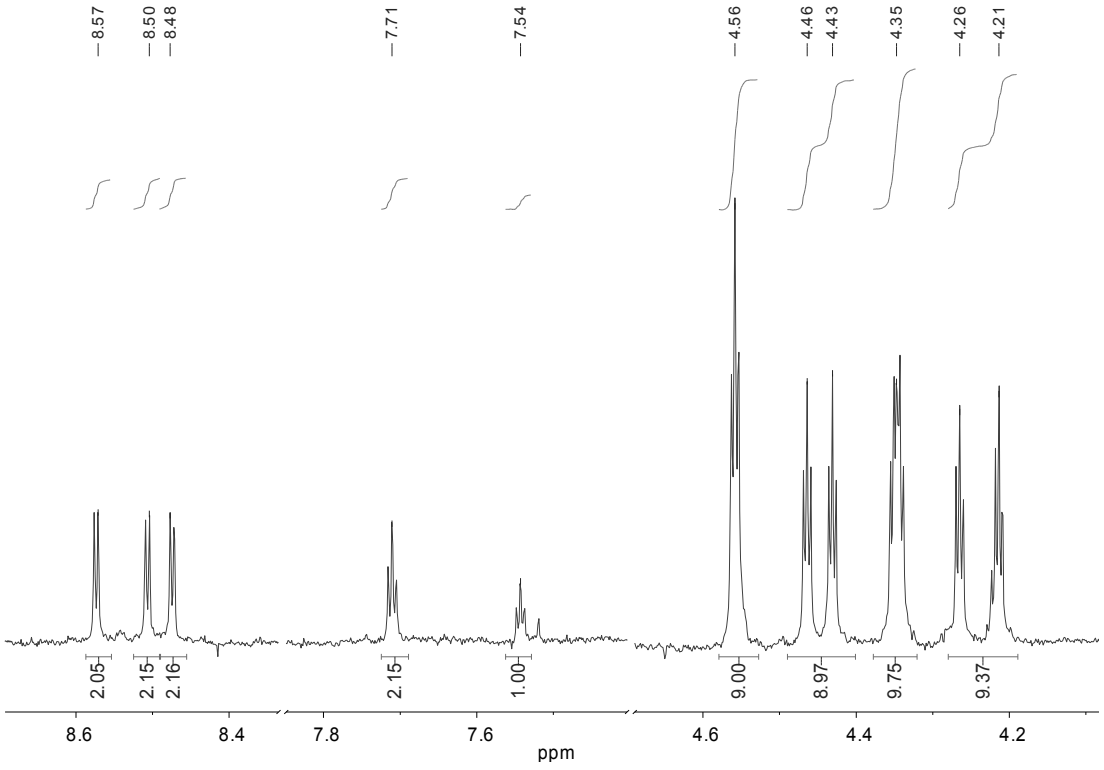

Figure 2-16. Selected resonances from the ^{1}H NMR spectrum ($CDCl_3$) of an unknown side-product commonly isolated in syntheses of **13**.

With their isolation, it is evident that both **13**, and its intermediate **14**, are reasonably stable materials. Poor yields, and the observation of competitive side-reactions, are thus attributed to low rates of Sonogashira cross-coupling.

Following detailed investigation of a model reaction in *Chapter 3*, it is hoped that enhanced reaction rates provided by application of the $PdCl_2(MeCN)_2$/P(^{t}Bu)$_3$ catalyst combination *(Chapter 3, Figure 3-4)* will improve future syntheses of these materials. With $PdCl_2(PPh_3)_2$,

there is a trade-off between i) high dilution, low yielding syntheses that permit macrocycle production, and ii) low-dilution, high yielding syntheses that favour oligo-/polymerisations *(Chapter 3, Figure 3-1)*.

2.3.4 Electrochemistry

The redox properties of selected materials (and **1**, for comparison) were investigated via cyclic voltammetry in CH_2Cl_2, with data summarised in *(Table 2-1)*. Complexes demonstrated close to reversible behaviour ($i_p^a/i_p^c \approx 1$, $i_p \propto V_s^{1/2}$) though ΔE was found to vary with scan rate (V_s) (in the reversible case, this relationship should be independent with $\Delta E \approx 0.059/n$ V) *(Figure 2-17)*. As **1** had shown reversible behaviour in MeCN solution, uncompensated resistance effects (R_u) were considered a possible cause of this deviation – the applied voltage contains an iR_s term (R_s = solution resistance, $R_{s(CH2Cl2)} > R_{s(MeCN)}$), that is sometimes non-negligible in non-aqueous solvents.[68] Correction of measured potentials (using a value of $R_s \approx 1$ KΩ, *estimated* from AC impedance spectroscopy) adjusted scans towards the ideal, but did not compensate completely – suggesting that not all R_u had been accounted for using the estimated value (or that R_u was not the only factor influencing these results).

Table 2-3. Electrochemical data for some 1,1'-substituted ferrocene complexes.[a]

compound	E_{pa} (V)	E_{pc} (V)	ΔE (V)	i_p^a/i_p^c	$E_{1/2}$[b] (V)
fcI_2 (**1**)	0.371	0.291	0.080	0.98	0.331
fcI(C≡C–*m*–Py) (**2**)	0.320	0.248	0.073	0.94	0.284
$fc(C{\equiv}C–m–Py)_2$ (**3**)	0.314	0.245	0.068	1.05	0.280
fc(C≡C–*m*–Py)(C≡C–$SiMe_3$) (**4**)	0.281	0.233	0.048	1.06	0.257
fc(C≡C–*m*–Py)(C≡C–*p*-C_6H_4–S′Bu) (**5**)	0.286	0.226	0.060	1.05	0.256
(μ-3,5-Py)(C≡C–[fc]–I)$_2$ (**6**)	0.325	0.273	0.051	0.92	0.299
(μ-3,5-Py)(C≡C–[fc]–C≡C–*m*-Py)$_2$ (**9**)[c]	0.361	0.280	0.081	1.05	0.320
(μ-3,5-Py)(C≡C–[fc]–C≡C–$SiMe_3$)$_2$ (**10**)	0.310	0.245	0.065	1.00	0.278
(μ-3,5-Py)(C≡C–[fc]–C≡C–*p*-C_6H_4–S′Bu)$_2$ (**12**)	0.291	0.227	0.063	1.05	0.259

[a] For scan rate = 0.1 Vs^{-1}. $Bu_4N^+PF_6^-$ (0.1 M) in CH_2Cl_2; WE: glassy carbon; RE, CE: Pt. All potentials assigned to the Fe(II)/Fe(III) redox couple, measured against an internal $[FeCp_2]^+/[FeCp_2]$ reference, reported relative to $[FeCp_2]^+/[FeCp_2]$ and corrected for iR_s. [b] $E_{1/2} = ½(E_{pa} + E_{pc})$. [c] Measured against an internal $[FeCp^*_2]^+/[FeCp^*_2]$ reference, reported relative to $[FeCp_2]^+/[FeCp_2]$ (0.495 V *vs.* $[FeCp^*_2]^+/[FeCp^*_2]$ in our system).

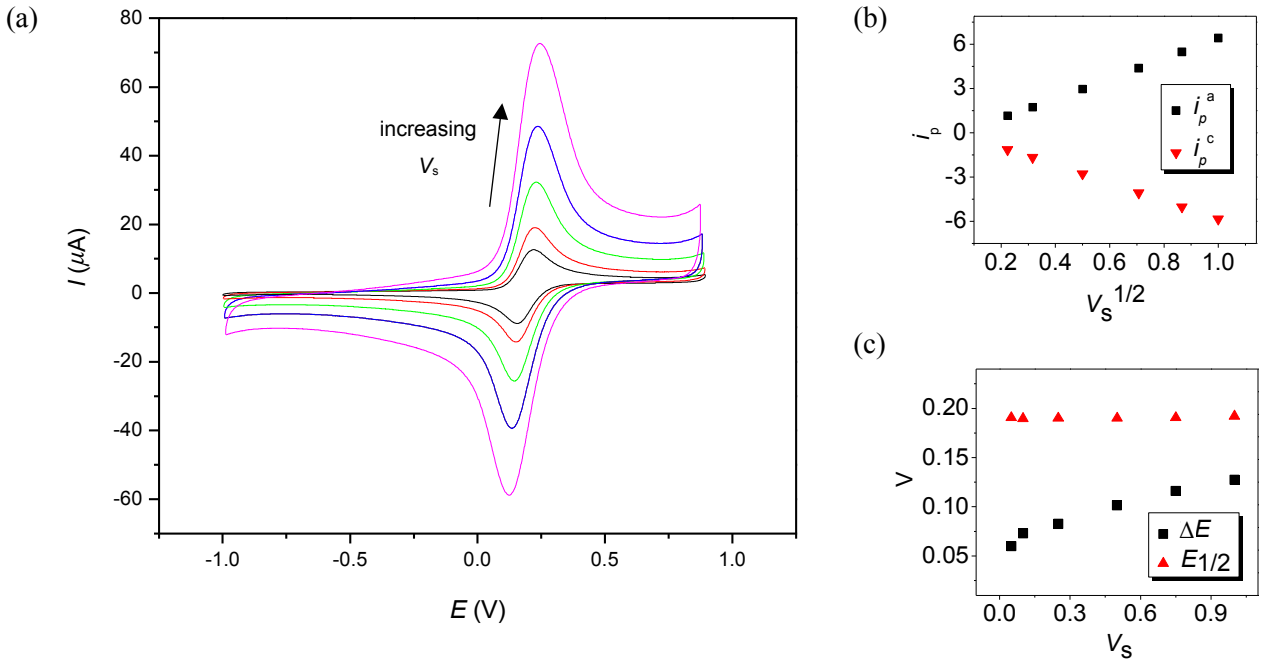

Figure 2-17. (a) Typical cyclic voltammograms for the (arylethynyl)ferrocene complexes studied here (these examples from **5**), showing variation of ΔE with increasing scan rate (corrected for R_u). (b) Plots of i_p versus $V_s^{1/2}$, and (c) $E_{1/2}$ and ΔE versus V_s.

$E_{1/2}$ values were comparable to those of (arylethynyl)ferrocenes reported elsewhere,[29-30,32] with all complexes demonstrating a higher redox potential than ferrocene due to the electron withdrawing nature of their iodo/alkynyl substituents. The relative trend iodo > pyridyl > $SiMe_3$ > aryl–S^{t}Bu was also established, observed in both linear and branched series.

In the bimetallic complexes, no electronic communication between ferrocene centres was apparent ($\Delta E_{1/2} \cong 0$). This is consistent with observations elsewhere – in 3,5-diethynylpyridine bridged $Fe(dppe)_2Cp^*$ complexes ($\Delta E_{1/2}$ = 0.11 V, compared with 0.72 V with butadiynyl bridges),[69] or between ferrocene centres linked by 3,5-benzene[70] or 2,5-diethynylpyridine ($\Delta E_{1/2} \cong 0$).[1] *Meta*-substituted bridges are not ideal mediators of electron transfer,[71] and the ferrocene moiety consistently exhibits lower $\Delta E_{1/2}$ (through the same bridge) in comparison to other redox centres *(Chapter 6)*.

It is worthy of further note that the redox waves for **3** and **8** rapidly became irreversible if too strong an oxidising voltage was applied (plausibly due to further reaction of the oxidised species in solution, or modification of the electrode surface). Other complexes were generally more

tolerant of the applied voltage range. Use of ferrocene as an internal reference for **9** was not possible due to a reaction between the oxidized species.

2.3.5 UV-vis spectroscopy

The occupied molecular orbitals of ethynylpyridines have been probed by photoelectron spectroscopy[72] and their frontier orbitals investigated theoretically.[73] The UV-vis absorption spectra of 3-ethynylpyridine (3-EP) and 3,5-diethynylpyridine (3,5-DEP) show broad, structured bands at around 275 nm and 292 nm, respectively (arguably the result of HOMO–LUMO π–π* transitions) *(Figure 2-18)*. Obtained data is summarised in *Table 2-4*. HOMO–LUMO gaps for a range of ethynylpyridines were recently calculated – with values of 5.40 eV (230 nm) and 5.16 eV (~241 nm) suggested for 3-EP and 3,5-DEP, respectively (deviations are plausibly due to solvent effects).[73]

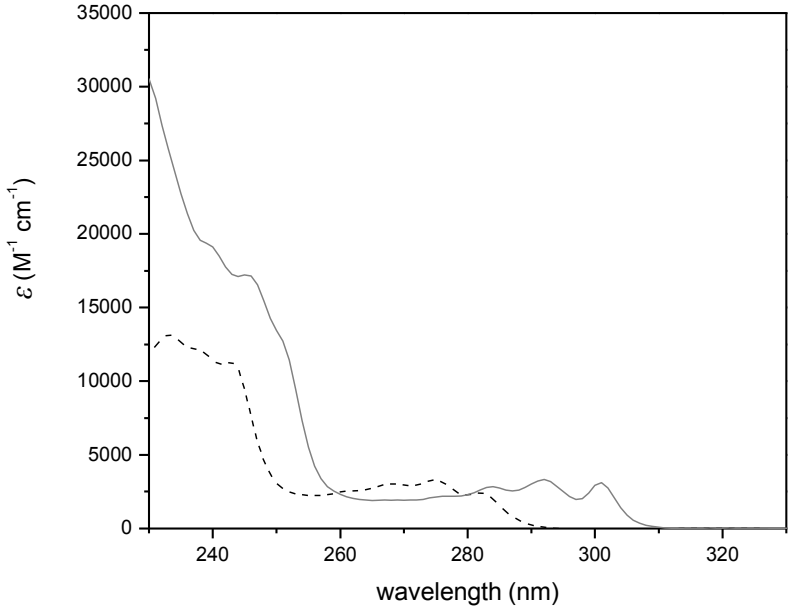

Figure 2-18. UV-vis spectra (in CH_2Cl_2) of 3-ethynylpyridine (dashed line) and 3,5-diethynylpyridine (solid line).

Table 2-4. Electronic spectral data for ethynylpyridine ligands.[a]

compound	λ_{max} /nm (ε /M^{-1} cm^{-1})[b]
3-EP	233 (13221), 244 (10844), 260 (2459), 269 (3015), 275 (3305), 282 (2454)
3,5-DEP	248infl (15443), 276 (2186), 284 (2839), 292 (3331), 301 (3112)

[a] Recorded at room temperature in CH_2Cl_2, using quartz cells with a pathlength of 10 mm. [b] Where possible, spectra were deconvoluted into composite Gaussian bands[§§] to obtain λ_{max} values. All extinction coefficients were taken from the experimental data at these wavelengths.

The electronic structure of ferrocene has been extensively studied and its UV-vis spectrum fully assigned, providing a useful starting point for interpretation of related spectra.[74] From the electronic configuration of its frontier orbitals *(Figure 2-19)* – $(1e_{2g})^4(2a_{1g})^2(2e_{1g}*)^0$ – three spin-allowed d–d transitions are expected. $^1A_{1g} \rightarrow a^1E_{1g}$ and $^1A_{1g} \rightarrow {}^1E_{2g}$ are unresolved and assigned to a band at 442 nm (measured in THF), with $^1A_{1g} \rightarrow b^1E_{1g}$ responsible for a band at 325 nm. These are formally Laporte-forbidden and weak. A more intense, higher energy band is observed at 200 nm (measured in isopentane), provided by a ligand-to-metal charge transfer (LMCT) transition, with shoulders at 240 nm and 265 nm attributed to metal-to-ligand charge transfer (MLCT) and LMCT transitions, respectively. Additional features may be observed in electron accepting solvents (such as halogenated hydrocarbons, or ethyl 2-cyanoacrylate), provided by intermolecular charge-transfer-to-solvent (CTTS) transitions (forming ferrocenium).[74c]

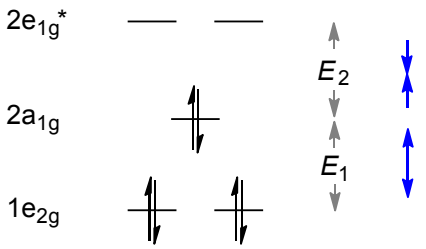

Figure 2-19. A qualitative frontier molecular orbital diagram for ferrocene, adapted from Yamahuchi *et al.*[74c] Anticipated changes in relative orbital energies (E_1, E_2) with increasingly electron-withdrawing substituents are denoted by blue arrows.[75]

Interpreting the optical absorption spectra of substituted ferrocenes is a process generally complicated by differences between their electronic structures and that of the parent complex.

[§§] Using the 'Fit Plot' tool of *MagicPlot Student v2.3*.

For example, in studying a series of 1-ferrocenes, Zhang *et al.* found that staggered conformations (D_{5d} symmetry) were preferred over the eclipsed conformation favoured by ferrocene (D_{5h} symmetry), changing the symmetry of interactions between Fe and the Cp ligand(s).[76] They also observed that substitution of Cp^- results in significant changes to the energies of its frontier orbitals, ultimately reducing 1-ferrocene HOMO(a_{1g})–LUMO(e_{1g}) gaps relative to the parent compound. This is in agreement with work by Dowben and co-workers concerning 1,1'-dichloro- and 1,1'-dibromoferrocene (symmetrical systems with electron-withdrawing substituents), which indicated that the greater the electron withdrawing power of the Cp ring substituent, the greater the mixing of Fe $d_{x2-y2,\ xy}$ and Cp(e_{2g})π orbitals, reducing E_2(a_{1g}–e_{1g}), and increasing E_1(e_{2g}–a_{1g}) and E_3($e_{1g(a)}$–$e_{1g(b)}$) *(Figure 2-19*, E_3 not shown).

Spectra of the asymmetrical, 1,1'-substituted linear complexes **2-5** are shown in *Figure 2-20*, with spectra of branched compounds **6**, **8**, **10** and **12** given in *Figure 2-21* (both figures include spectra of **1** and the relevant ethynylpyridine ligand for comparison). Obtained data is summarised in *Table 2-5*. With reference to features observed for ferrocene, and assuming a similar electronic structure, weak bands at 290 nm and 444 nm in the spectrum of **1** may be assigned to analogous d–d transitions. Interestingly, the latter band undergoes sequential bathochromatic shifts upon substitution of iodides with the alkynes, such that in mixed alkyne/iodo complexes (**2**, **6**) it is observed at 449-451 nm, and in 1,1'-bis(arylethynyl)ferrocenes at 454-456 nm.

The slight shoulder seen at 319 nm in the spectrum of **1** is tentatively attributed to a CTTS transition. Notably, shoulders at similar wavelengths are observed for all complexes.

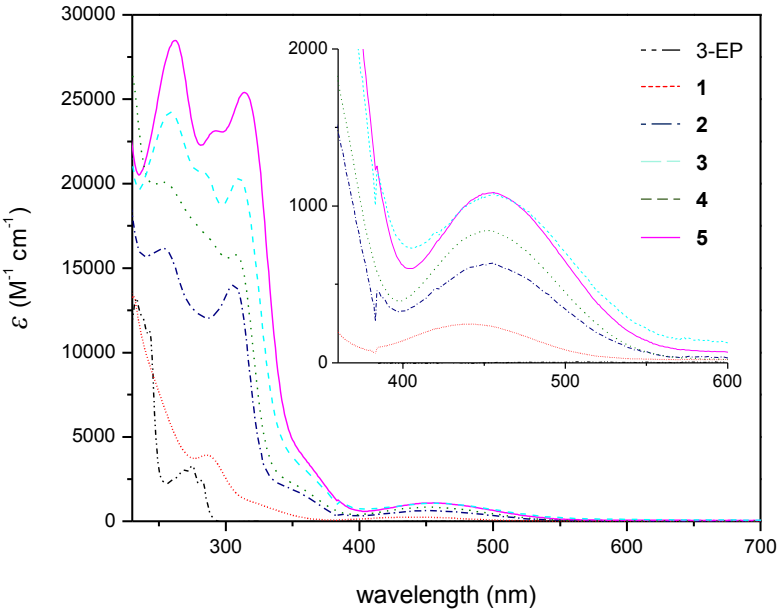

Figure 2-20. UV-vis spectra (in CH_2Cl_2) of linear complexes **2-5**, 3-ethynylpyridine, and **1** – inset, absorptions in the visible region magnified.

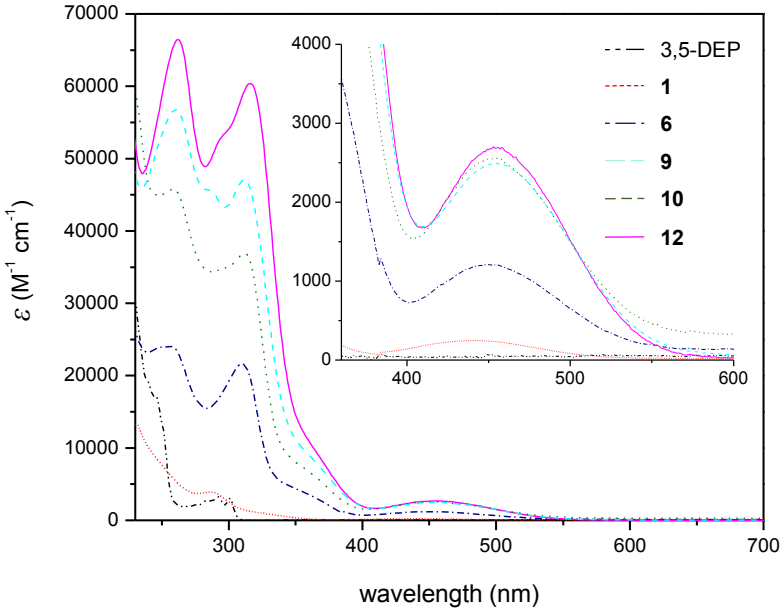

Figure 2-21. UV-vis spectra (in CH_2Cl_2) of branched complexes **6**, **9**, **10**, **12**, 3,5-diethynylpyridine, and **1** – inset, absorptions in the visible region magnified.

Table 2-5. Electronic spectral data of selected ferrocene complexes.[a]

compound	λ_{max} /nm (ε /M^{-1} cm^{-1})[b]
fcI_2 (**1**)	290 (3782), 319sh (1169), 444 (246)
fcI(C≡C–*m*–-Py) (**2**)	253 (16171), 307 (14000), 353sh (1768), 451 (624)
fc(C≡C–*m*–$Py)_2$ (**3**)	259 (24248), 287sh (20447), 312 (20226), 348sh (3995), 455 (1076)
fc(C≡C–*m*–Py)(C≡C–$SiMe_3$) (**4**)	254 (20076), 281sh (17308), 313 (14878), 350sh (2248), 454 (839)
fc(C≡C–*m*–Py)(C≡C–*p*–C_6H_4–S′Bu) (**5**)	262 (28484), 292 (23123), 317 (25158), 356 (4040), 456 (1085)
(μ-3,5-Py)(C≡C–[fc]–$I)_2$ (**6**)	251 (23918), 310 (21687), 352sh (4232), 449 (1211)
(μ-3,5-Py)(C≡C–[fc]–C≡C–*m*–$Py)_2$ (**9**)	263 (56422), 289sh (45177), 313 (47038), 354sh (10212), 456 (2486)
(μ-3,5-Py)(C≡C–[fc]–C≡C–$SiMe_3)_2$ (**10**)	259 (45793), 295infl (34770), 316 (35807), 344 (9090), 456 (2554)
(μ-3,5-Py)(C≡C–[fc]–C≡C–*p*–C_6H_4–S′$Bu)_2$ (**12**)	263 (66375), 293 (52553), 317 (60307), 356sh (12128), 456 (2693)

[a] Recorded at room temperature in CH_2Cl_2, using quartz cells with a pathlength of 10 mm. [b] Where possible, spectra were deconvoluted into composite Gaussian bands[§§] to obtain λ_{max} values. All extinction coefficients were taken from the experimental data at these wavelengths.

In all alkyne-functionalised complexes, intense bands are apparent between 250-350 nm, overshadowing the (much weaker) d–d transitions expected in that region. Similar features have been observed elsewhere in 1-substituted Fc–C≡C–R complexes (R = H, Ph, napthyl, anthryl, pyrenyl, perylenyl),[77] 1,1-ferrocene dicarboxylate M(II) salts,[78] and benzoyl-substituted derivatives.[74c] Due to their intensity ($\varepsilon \approx 12500 - 67500$ M^{-1} cm^{-1}), and the significantly weaker bands for **1** and the free ethynylpyridine ligands, these are attributed to LMCT/MLCT transitions facilitated by alkyne modification of Cp. Interestingly, in both the linear and branched series ε follows the trend aryl–S′Bu > pyridyl > $SiMe_3$ > I/pyridyl. For bands around 257 nm and 312 nm, λ_{max} follows a similar trend, except $SiMe_3$ > pyridyl for the latter. Intensities for bands in the branched series are approximately double those for the linear complexes.

2.4 CONCLUSION

Novel application of a facile oxidative purification method[2] enabled the preparation of pure **1** in large quantities using non-toxic materials. To exemplify its utility, an alternative and general approach to the synthesis of asymmetrical ferrocenes was demonstrated via Sonogashira cross-couplings of a 5-fold excess of **1** with terminal alkynes. The resulting 1-iodo-1'-(arylethynyl)ferrocenes were produced in good yields and converted to a series of linear and branched 1,1'-bis(arylethynyl)ferrocenes, which, along with a macrocyclic analogue (obtained in trace quantities), have applications in the future study of charge transport in complex, branched molecular structures. Whilst the incorporation of pyridyl groups posed no synthetic problems, difficulties were encountered in converting *tert*-butylthio moieties to their thioacetyl analogues (using the BBr_3 method[60,62]). Furthermore, yields when cross-coupling 1-iodo-1'-(arylethynyl)ferrocenes were generally low, particularly in the macrocyclization attempts. Future work should focus on applying the findings of *Chapter 3* in improving the rate (and yields) of such reactions.

Electrochemical studies revealed close to reversible redox activity for all the complexes, in good agreement with the known literature. Electronic communication between redox centres was not expected and not observed (both are oxidized at the same potential). The electron-withdrawing nature of Cp substituents were inferred from $E_{1/2}$ measurements, following the trend iodo > pyridyl > $SiMe_3$ > aryl–S^{t}Bu in both the linear and branched series. UV-vis spectra were not straightforward to interpret, but clearly exhibited features characteristic of ferrocene, in addition to intense MLCT/LMCT bands resulting from alkyne substitution of Cp. For some bands, variations in λ_{max} and ε also largely followed the substituent trends determined from cyclic voltammetry. Further analysis of such transitions will prove useful in understanding how the electronic structure of ferrocene changes upon substitution, and with different substituents.

2.5 REFERENCES

1. C. Engtrakul and L. R. Sita, *Organometallics*, 2008, **27**, 927.
2. J. C. Goeltz and C. P. Kubiak, *Organometallics*, 2011, **30**, 3908.
3. C. Imrie, C. Loubser, P. Engelbrecht and C. W. McCleland, *J. Chem. Soc., Perkin Trans. 1*, 1999, 2513.

4. M. D. Rausch, *J. Org. Chem.*, 1961, **26**, 1802.
5. M. Roemer and D. Lentz, *Chem. Commun.*, 2011, **47**, 7239.
6. M. Roemer and D. Lentz, *Eur. J. Inorg. Chem.*, 2008, **2008**, 4875.
7. A. Kasahara, T. Izumi and M. Maemura, *Bull. Chem. Soc. Jpn.*, 1977, **50**, 1021.
8. C. Fehér, Á. Kuik, L. Márk, L. Kollár and R. Skoda-Földes, *J. Organomet. Chem.*, 2009, **694**, 4036.
9. Z. Szarka, R. Skoda-Földes and L. Kollár, *Tetrahedron Lett.*, 2001, **42**, 739.
10. N. F. Blank, J. R. Moncarz, T. J. Brunker, C. Scriban, B. J. Anderson, O. Amir, D. S. Glueck, L. N. Zakharov, J. A. Golen, C. D. Incarvito and A. L. Rheingold, *J. Am. Chem. Soc.*, 2007, **129**, 6847.
11. M. Sato, H. Nakahara, K. Fukuda and S. Akabori, *J. Chem. Soc., Chem. Commun.*, 1988, 24.
12. M. R. an der Heiden, G. D. Frey and H. Plenio, *Organometallics*, 2004, **23**, 3548.
13. A. R. Koray, M. Ertas and Ö. Bekaroglu, *J. Organomet. Chem.*, 1987, **319**, 99.
14. M. Sato, T. Ito, I. Motoyama, K. Watanabe and K. Hata, *Bull. Chem. Soc. Jpn.*, 1969, **42**, 1976.
15. H. Shechter and J. F. Helling, *J. Org. Chem.*, 1961, **26**, 1034.
16. A. Shafir, M. P. Power, G. D. Whitener and J. Arnold, *Organometallics*, 2000, **19**, 3978.
17. (a) M. T. Lee, B. M. Foxman and M. Rosenblum, *Organometallics*, 1985, **4**, 539; (b) M. E. Huttenloch, J. Diebold, U. Rief, H. H. Brintzinger, A. M. Gilbert and T. J. Katz, *Organometallics*, 1992, **11**, 3600.
18. (a) R. M. G. Roberts, J. Silver and J. Azizian, *J. Organomet. Chem.*, 1986, **303**, 387; (b) B. E. Carpenter, W. E. Piers and R. McDonald, *Can. J. Chem.*, 2001, **79**, 291.
19. N. Lenze, B. Neumann, A. Salmon, A. Stammler, H.-G. Stammler and P. Jutzi, *J. Organomet. Chem.*, 2001, **619**, 74.
20. (a) A. N. Nesmeyanov, E. G. Perevalova and O. A. Nesmeyanova, *Dokl. Akad. Nauk SSSR*, 1955, **100**, 1099; (b) A. N. Nesmeyanov, V. A. Sazonova and V. I. Romanenko, *Dokl. Akad. Nauk SSSR*, 1965, **161**, 1085; (c) R. W. Fish and M. Rosenblum, *J. Org. Chem.*, 1965, **30**, 1253; (d) R. W. Wagner, T. E. Johnson and J. S. Lindsey, *Tetrahedron*, 1997, **53**, 6755.
21. (a) R. F. Kovar, M. D. Rausch and H. Rosenberg, *Organomet. Chem. Synth.*, 1971, **1**, 173; (b) M. Kai, I. Motoyama, M. Katada, Y. Masuda and H. Sano, *Chem. Lett.*, 1988, 1037; (c) Q. Lu, X.-H. Wang and F.-S. Wang, *Chin. J. Appl. Chem.*, 2011, **28**, 136; (d) M. A. Bakar, N. N. Sergeeva, T. Juillard and M. O. Senge, *Organometallics*, 2011, **30**, 3225.
22. (a) I. R. Butler, S. B. Wilkes, S. J. Mcdonald, L. J. Hobson, A. Taralp and C. P. Wilde, *Polyhedron*, 1993, **12**, 129; (b) P. Park, A. J. Lough and D. A. Foucher, *Macromolecules*, 2002, **35**, 3810; (c) C.-H. Andersson, L. Nyholm and H. Grennberg, *Dalton Trans.*, 2012, **41**, 2374.
23. S. Sorriso, G. Cardaci and S. M. Murgia, *J. Organomet. Chem.*, 1972, **44**, 181.
24. M. S. Inkpen, S. Du, M. Driver, T. Albrecht and N. J. Long, *Dalton Trans.*, 2013, **42**, 2813.
25. M. Vollmann and H. Butenschon, *C. R. Chim.*, 2005, **8**, 1282.
26. X.-S. Zhou, L. Liu, P. Fortgang, A.-S. Lefevre, A. Serra-Muns, N. Raouafi, C. Amatore, B.-W. Mao, E. Maisonhaute and B. Schöllhorn, *J. Am. Chem. Soc.*, 2011, **133**, 7509.
27. S. A. Getty, C. Engtrakul, L. Wang, R. Liu, S.-H. Ke, H. U. Baranger, W. Yang, M. S. Fuhrer and L. R. Sita, *Phys. Rev. B*, 2005, **71**, 241401.

28. T. Uehara, R. V. Belosludov, A. A. Farajian, H. Mizuseki and Y. Kawazoe, *Jpn. J. Appl. Phys.*, 2006, **45**, 3768.
29. C. Engtrakul and L. R. Sita, *Organometallics*, 2008, **27**, 927.
30. (a) J. Ma, M. Vollmann, H. Menzel, S. Pohle and H. Butenschön, *J. Inorg. Organomet. Polym. Mater.*, 2008, **18**, 41; (b) I. Baumgardt and H. Butenschön, *Eur. J. Inorg. Chem.*, 2010, **2010**, 1076.
31. E. Lindner, R. Zong and K. Eichele, Phosphorus, *Sulfur Silicon Relat. Elem.*, 2001, **169**, 219.
32. C. Engtrakul and L. R. Sita, *Nano Lett.*, 2001, **1**, 541.
33. A. M. Kuznetsov and J. Ulstrup, *J. Chem. Phys.*, 2002, **116**, 2149.
34. A. Aviram and M. A. Ratner, *Chem. Phys. Lett.*, 1974, **29**, 277.
35. F. Ding, S. Chen and H. Wang, *Materials*, 2010, **3**, 2668.
36. X. Xiao, D. Brune, J. He, S. Lindsay, C. B. Gorman and N. Tao, *Chem. Phys.*, 2006, **326**, 138.
37. C. Morari, I. Rungger, A. R. Rocha, S. Sanvito, S. Melinte and G.-M. Rignanese, *ACS Nano*, 2009, **3**, 4137.
38. T. Bredow, C. Tegenkamp, H. Pfnur, J. Meyer, V. V. Maslyuk and I. Mertig, *J. Chem. Phys.*, 2008, **128**, 064704.
39. C. B. Gorman, R. L. Carroll and R. R. Fuierer, *Langmuir*, 2001, **17**, 6923.
40. R. A. Wassel, G. M. Credo, R. R. Fuierer, D. L. Feldheim and C. B. Gorman, *J. Am. Chem. Soc.*, 2003, **126**, 295.
41. S. Wang, W. Lu, Q. Zhao and J. Bernholc, *Phys. Rev. B*, 2006, **74**, 195430.
42. Q. Li, G. Mathur, M. Homsi, S. Surthi, V. Misra, V. Malinovskii, K.-H. Schweikart, L. Yu, J. S. Lindsey, Z. Liu, R. B. Dabke, A. Yasseri, D. F. Bocian and W. G. Kuhr, *Appl. Phys. Lett.*, 2002, **81**, 1494.
43. (a) A. Nitzan, *J. Phys. Chem. A*, 2001, **105**, 2677; (b) A. Nitzan, *Isr. J. Chem.*, 2002, **42**, 163; (c) M. C. Traub, B. S. Brunschwig and N. S. Lewis, *J. Phys. Chem. B*, 2007, **111**, 6676.
44. M. B. Robin and P. Day, *Adv. Inorg. Chem.*, 1968, **10**, 247.
45. J. F. Berry, F. A. Cotton and C. A. Murillo, *Organometallics*, 2004, **23**, 2503.
46. K. Kaleta, A. Hildebrandt, F. Strehler, P. Arndt, H. Jiao, A. Spannenberg, H. Lang and U. Rosenthal, *Angew. Chem., Int. Ed.*, 2011, **50**, 11248.
47. (a) G. Vives, A. Carella, S. Sistach, J.-P. Launay and G. Rapenne, *New J. Chem.*, 2006, **30**, 1429; (b) D. Osella, R. Gobetto, C. Nervi, M. Ravera, R. D'Amato and M. V. Russo, *Inorg. Chem. Commun.*, 1998, **1**, 239; (c) Á. Díez, E. Lalinde, M. T. Moreno and S. Sánchez, *Dalton Trans.*, 2009, 3434; (d) M. Lohan, B. Milde, S. Heider, J. M. Speck, S. Krauße, D. Schaarschmidt, T. Rüffer and H. Lang, *Organometallics*, 2012, **31**, 2310.
48. (a) N. D. Jones, M. O. Wolf and D. M. Giaquinta, *Organometallics*, 1997, **16**, 1352; (b) M. C. B. Colbert, J. Lewis, N. J. Long, P. R. Raithby, A. J. P. White and D. J. Williams, *J. Chem. Soc., Dalton Trans.*, 1997, 99; (c) Y. Zhu, O. Clot, M. O. Wolf and G. P. A. Yap, *J. Am. Chem. Soc.*, 1998, **120**, 1812; (d) C. Lebreton, D. Touchard, L. L. Pichon, A. Daridor, L. Toupet and P. H. Dixneuf, *Inorg. Chim. Acta*, 1998, **272**, 188.
49. A. Auger, A. J. Muller and J. C. Swarts, *Dalton Trans.*, 2007, 3623.
50. A. Hildebrandt, D. Schaarschmidt, L. van As, J. C. Swarts and H. Lang, *Inorg. Chim. Acta*, 2011, **374**, 112.

51. (a) A. Hildebrandt and H. Lang, *Dalton Trans.*, 2011, **40**, 11831; (b) A. Hildebrandt, D. Schaarschmidt and H. Lang, *Organometallics*, 2011, **30**, 556; (c) A. Hildebrandt, D. Schaarschmidt, R. Claus and H. Lang, *Inorg. Chem.*, 2011; (d) J. M. Speck, R. Claus, A. Hildebrandt, T. Rüffer, E. Erasmus, L. van As, J. C. Swarts and H. Lang, *Organometallics*, 2012, **31**, 6373.
52. A. Donoli, A. Bisello, R. Cardena, A. Ceccon, M. Bassetti, A. D'Annibale, C. Pasquini, A. Raneri and S. Santi, *Inorg. Chim. Acta*, 2011, **374**, 442.
53. (a) N. J. Long, A. J. Martin, R. Vilar, A. J. P. White, D. J. Williams and M. Younus, *Organometallics*, 1999, **18**, 4261; (b) M. I. Bruce, P. J. Low, F. Hartl, P. A. Humphrey, F. de Montigny, M. Jevric, C. Lapinte, G. J. Perkins, R. L. Roberts, B. W. Skelton and A. H. White, *Organometallics*, 2005, **24**, 5241; (c) Y. Fan, I. P.-C. Liu, P. E. Fanwick and T. Ren, *Organometallics*, 2009, **28**, 3959.
54. M. Magoga and C. Joachim, *Phys. Rev. B*, 1999, **59**, 16011.
55. (a) J. M. Tour, *Acc. Chem. Res.*, 2000, **33**, 791; (b) Y. Ito, A. Miyazaki, K. Takai, V. Sivamurugan, T. Maeno, T. Kadono, M. Kitano, Y. Ogawa, N. Nakamura, M. Hara, S. Valiyaveettil and T. Enoki, *J. Am. Chem. Soc.*, 2011, **133**, 11470; (c) M. C. Martos-Maldonado, I. Quesada-Soriano, J. M. Casas-Solvas, L. García-Fuentes and A. Vargas-Berenguel, *Eur. J. Org. Chem.*, 2012, **2012**, 2560.
56. J. K. Pudelski and M. R. Callstrom, *Organometallics*, 1992, **11**, 2757.
57. (a) M. Rosenblum, N. M. Brawn, D. Ciappenelli and J. Tancrede, *J. Organomet. Chem.*, 1970, **24**, 469; (b) I. R. Butler, A. L. Boyes, G. Kelly, S. C. Quayle, T. Herzig and J. Szewczyk, *Inorg. Chem. Commun.*, 1999, **2**, 403.
58. M. C. B. Colbert, D. Hodgson, J. Lewis, P. R. Raithby and N. J. Long, *Polyhedron*, 1995, **14**, 2759.
59. I. A. Aliev, G. A. Kalabin and N. Ghelis, *Sulfur Lett.*, 1991, **12**, 123.
60. N. Stuhr Hansen, *Synth. Commun.*, 2003, **33**, 641.
61. A. Blaszczyk, M. Elbing and M. Mayor, *Org. Biomol. Chem.*, 2004, **2**, 2722.
62. N. Stuhr-Hansen, J. K. Sørensen, K. Moth-Poulsen, J. B. Christensen, T. Bjørnholm and M. B. Nielsen, *Tetrahedron*, 2005, **61**, 12288.
63. H. Butenschön, Personal Communuication, 2012.
64. (a) O. Oms, T. Jarrosson, L. H. Tong, A. Vaccaro, G. Bernardinelli and A. F. Williams, *Chem. Eur. J.*, 2009, **15**, 5012; (b) J. B. Heilmann, E. A. Hillard, M.-A. Plamont, P. Pigeon, M. Bolte, G. Jaouen and A. Vessières, *J. Organomet. Chem.*, 2008, **693**, 1716.
65. A. D. Woods, G. Alcalde, V. B. Golovko, C. M. Halliwell, M. J. Mays and J. M. Rawson, *Organometallics*, 2005, **24**, 628.
66. E. H. van Dijk, D. J. T. Myles, M. H. van der Veen and J. C. Hummelen, *Org. Lett.*, 2006, **8**, 2333.
67. E. Bosch and C. L. Barnes, *Organometallics*, 2000, **19**, 5522.
68. A. J. Bard and L. Y. Faulkner, Electrochemical Methods (2nd ed.), Wiley, 2004.
69. (a) K. Costuas, O. Cador, F. Justaud, S. Le Stang, F. Paul, A. Monari, S. Evangelisti, L. Toupet, C. Lapinte and J.-F. Halet, *Inorg. Chem.*, 2011, **50**, 12601; (b) N. Lenarvor, L. Toupet and C. Lapinte, *J. Am. Chem. Soc.*, 1995, **117**, 7129.
70. A. K. Diallo, C. Absalon, J. Ruiz and D. Astruc, *J. Am. Chem. Soc.*, 2010, **133**, 629.
71. H. Weber, J. Reichert, M. Elbing, C. von Hanisch, D. Beckmann and M. Mayor, *Angew. Chem., Int. Ed. Engl.*, 2003, **42**, 5834.
72. S. C. Ng, I. Novak, X. You and W. Huang, *J. Phys. Chem. A*, 1998, **102**, 904.

73. R. K. Singh and M. K. Mishra, *Int. J. Quantum Chem.*, 2012, **112**, 426.
74. (a) H. B. Gray, Y. S. Sohn and N. Hendrickson, *J. Am. Chem. Soc.*, 1971, **93**, 3603; (b) N. Rösch and K. H. Johnson, *Chem. Phys. Lett.*, 1974, **24**, 179; (c) Y. Yamaguchi, W. Ding, C. T. Sanderson, M. L. Borden, M. J. Morgan and C. Kutal, *Coord. Chem. Rev.*, 2007, **251**, 515.
75. P. A. Dowben, D. C. Driscoll, R. S. Tate and N. M. Boag, *Organometallics*, 1988, **7**, 305.
76. G. Zhang, H. Zhang, M. Sun, Y. Liu, X. Pang, X. Yu, B. Liu and Z. Li, *J. Comput. Chem.*, 2007, **28**, 2260.
77. A. H. Flood, C. J. McAdam, K. C. Gordon, H. G. Kjaergaard, A. M. Manning, B. H. Robinson and J. Simpson, *Polyhedron*, 2007, **26**, 448.
78. J. Kuhnert, T. Ruffer, P. Ecorchard, B. Brauer, Y. Lan, A. K. Powell and H. Lang, *Dalton Trans.*, 2009, **4499**, 4499.

CHAPTER 3 : SONOGASHIRA CROSS-COUPLING WITH 1,1'-DIIODOFERROCENE

3.1 ABSTRACT

The Sonogashira cross-coupling of ethynylbenzene and 1,1'-diiodoferrocene was studied as a model system to understand and improve the typically low yielding reactions between iodoferrocenes and terminal alkynes in general *(Scheme 3-1)*. Concentration, temperature, solvent (3 examples), amine (3 examples), and phosphine ligand (14 examples) were systematically varied to examine their effects. Using $PdCl_2(PPh_3)_2$ as catalyst (with CuI, DIPA, THF), conversion of starting material was found to be rather sensitive to concentration and temperature. Furthermore, it was discovered that the $PdCl_2(MeCN)_2/P(^tBu)_3$ combination is unique in providing a *substantial* rate increase over $PdCl_2(MeCN)_2/PPh_3$ or $PdCl_2(PPh_3)_2$ systems.

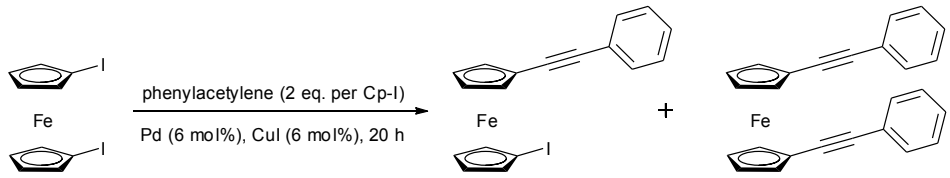

Scheme 3-1. Model reaction used to study the Sonogashira cross-coupling of iodoferrocenes and terminal alkynes.

Subsequent attempts to cross-couple 4-ethynylphenylthioacetate with 1,1'-diiodoferrocene – a reaction which has (unexpectedly) not yet drawn comment from the literature – resulted in unexpected cyclization of the alkynyl reagent, and the realisation of a new route to β-phenylthioketones in general *(Scheme 3-2)*.

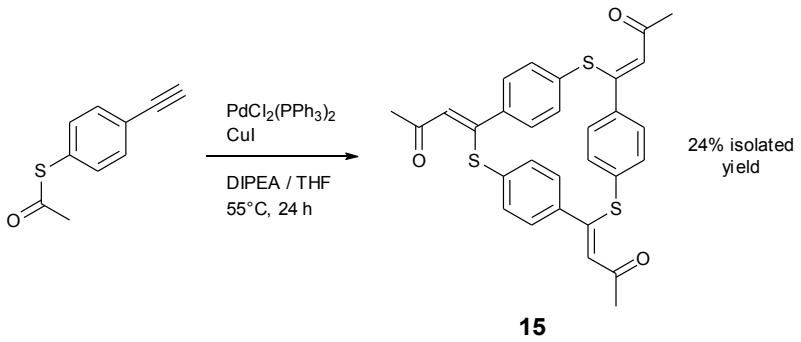

Scheme 3-2. A novel cyclic product is formed via oligomerization of 4-ethynylphenylthioacetate under Sonogashira conditions.

3.2 BACKGROUND

As discussed in *Chapter 2*, the broad reactivity of the Fc–I moiety makes iodinated ferrocene materials highly useful precursors to ferrocene-incorporated compounds. Whilst facile access to large quantities of iodoferrocene[1] and now 1,1'-diiodoferrocene *(Chapter 2)* increases their utility, full synthetic exploitation may only be realized through optimizing onward reaction conditions (enabling high product yields).

Improving the reactivity of iodoferrocenes under Sonogashira cross-coupling conditions *(Scheme 3-3)* was considered a primary target. Convenient and widely applicable, the reaction (with iodoferrocenes) has been used to construct compounds for molecular[2] and organic[3] electronics, the study of intramolecular electron transfer,[4] photo-[5] and electrochemical-sensing,[6] catalysis (pincer complexes),[7] and artificial bio-receptors.[8] It is worth noting that just two years after the seminal 1975 papers concerning aryl iodides by Heck,[9] Cassar[10] and Sonogashira *et al.*,[11] cross-coupling of iodoferrocenes was under investigation.[12]

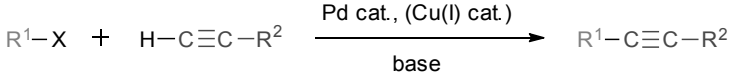

R^1 = aryl, heteroaryl, vinyl
R^2 = aryl, heteroaryl, alkenyl, alkyl, SiR_3
X = I, Br, Cl, OTf

Scheme 3-3. The Pd/Cu co-catalysed Sonogashira reaction.

Further inspiration for studying this reaction was borne out of frustrations when applying it to related materials in *Chapter 2* (low yields, problematic synthetic routes). Of particular interest was improving access to cyclo[bis[1,1'-bis(*μ*-3,5-diethynylpyridine)ferrocene]] (**13**) – impracticable under current coupling conditions – and developing a convenient route to installing the 4-ethynylphenylthioacetate motif at Fc–I *(Scheme 3-4)*.*

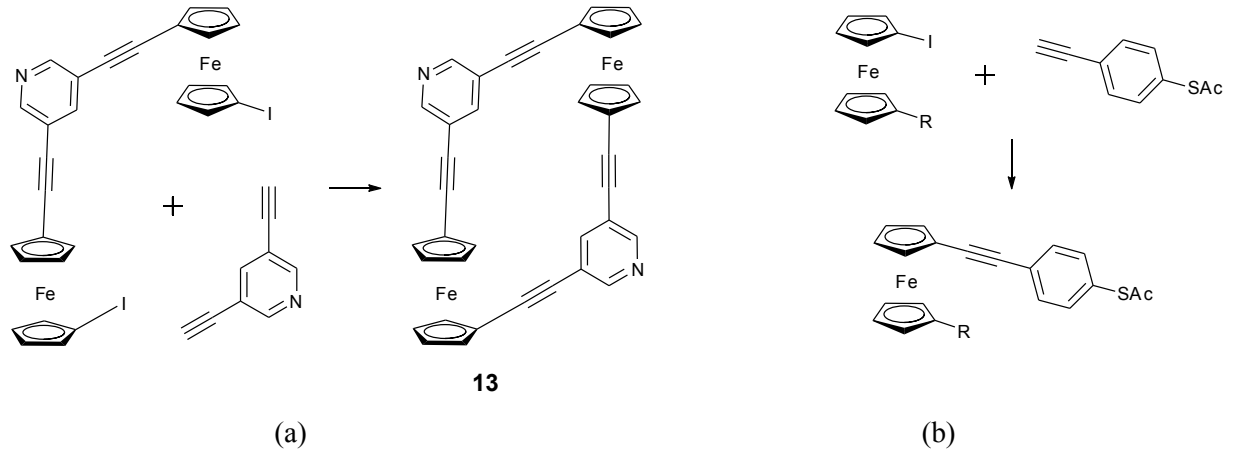

Scheme 3-4. Proposed routes to (a) cyclo[bis[1,1'-bis(*μ*-3,5-diethynylpyridine)ferrocene]] (**14**) and (b) ferrocenyl(4-ethynylphenylthioacetate) complexes.

Recent advances in Sonogashira cross-coupling have been comprehensively reviewed elsewhere.[13] Whilst some aspects of the catalytic cycle *(Scheme 3-5)* are still in contention, most researchers agree that the classical process is Pd(0)/Cu(I) co-catalysed, with oxidative addition of the aryl halide to the Pd(0) centre identified as the rate-determining step. The active Pd(0) catalyst may be added in the form of $Pd(0)L_x$, or generated *in situ* from $PdCl_2L_X$ by any one of several postulated reduction pathways (*e.g.* oxidation of amine/phosphine, homocoupling of terminal alkyne).

* Thioacetate groups have the capability to spontaneously form strong S-Au bonds upon contact with a gold surface, useful to anchor and electronically connect ferrocene-based molecular electronic components to macroscopic (gold) electrodes for testing.

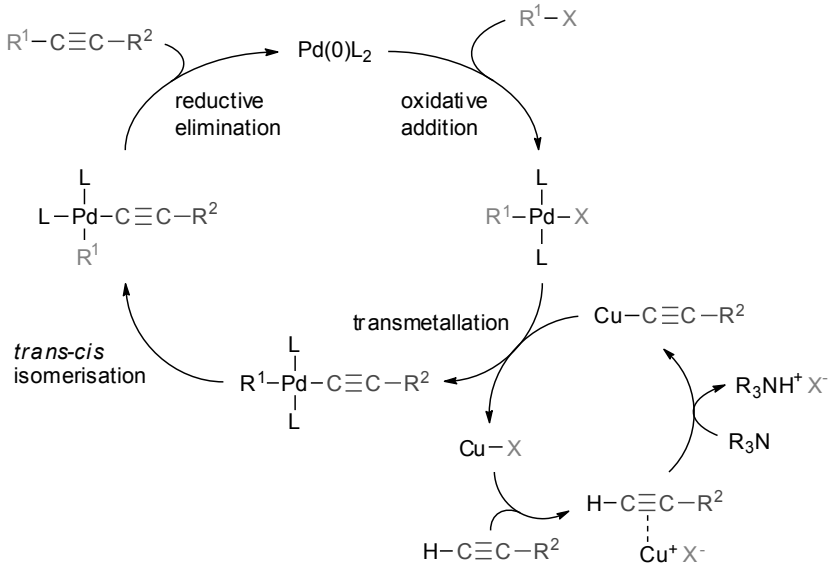

Scheme 3-5. Catalytic cycle for the Pd/Cu co-catalysed Sonogashira reaction.

A key question when considering the aptitude of iodoferrocenes towards Sonogashira cross-coupling is where Fc–I sits within the well-established aryl halides/triflate rate series (where I > OTf > Br >> Cl). Whilst it might be naively supposed that Fc–I would react at a similar rate as Ar–I, this is shown experimentally to be wholly incorrect. Aryl iodides will cross-couple with terminal alkynes extremely rapidly under most circumstances, resulting in high to quantitative yields, even at room temperature. In contrast, iodoferrocenes at elevated temperatures give typically low to moderate product yields, as seen here *(Chapter 2)* and in various published examples *(vida supra)*. This less than ideal reactivity has drawn comment,[14] even cited as motivation to explore alternative strategies for ferrocene incorporation (such as alkyne cross-metathesis,[15] Suzuki coupling of bromoferrocenes[16] or the (reverse) coupling of ethynylferrocenes with aryl iodides[17]). From 1,1'-diiodoferrocene it has also sometimes been observed that cross-couplings of the second iodo functionality are more difficult than the first *(Scheme 3-6)*[2c,18] – reasoned to be due to the solubility of the resulting compounds, or steric hindrance.[14]

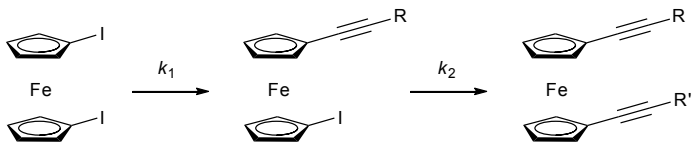

Scheme 3-6. Proposed rate difference (k_1>k_2) between the first and second cross-coupling steps of 1,1'-diiodoferrocene.

Literature syntheses with iodoferrocenes usually employ the convenient $PdCl_2(PPh_3)_2$/CuI catalytic system in DIPA/THF, with changes in ligands, catalyst loading, temperature, concentration, solvent and amine making it difficult to ratify the superiority of any particular set of conditions. Only one paper[19] describes (largely unsuccessful) attempts with Buchwald and Fu's $Pd(PhCN)_2Cl_2/P(^tBu)_3$ combination – utilized elsewhere to rapidly cross-couple aryl-bromides at room temperature.[20] González-Cabello *et al.* used a (copper-free) $Pd_2(dba)_3/AsPh_3$ combination to integrate iodoferrocene and 1,1'-diiodoferrocene with modified phthalocyanines in good, though not exceptional, yields.[4a] In attempting to optimise the Sonogashira cross coupling of 1,1'-diiodoferrocene and phenylacetylene *(Scheme 3-1)*, the aforementioned parameters will be controlled and where appropriate, systematically varied.

3.3 RESULTS AND DISCUSSION

3.3.1 Effects of concentration

Experiments varying concentration were run in DIPA/THF (1:3 v/v) with $PdCl_2(PPh_3)_2$/CuI, given their routine use in the literature (full procedures and methods are provided in *Chapter 8)*. It was further reasoned that assessment of the DIPA/THF system was more useful to the practicing synthetic chemist – due to its superior solubilizing power – than that of DIPA alone (acting as both amine *and* solvent).

The effect of concentration on the conversion of 1,1'-diiodoferrocene to its mono- and di-substituted products *(Scheme 3-1)* is shown in *Figure 3-1* (raw data in *Table 3-1)*. The formation of unexpected side products is discussed in *section 3.3.4*. Temperatures represent that of the oil bath heating the reaction vessel, with internal temperatures limited by the boiling points of DIPA (~84°C) and THF (66°C). It is apparent that reducing concentration significantly reduces the

yield of the di-substituted product, with the mono-substituted compound becoming dominant below concentrations of ~7 mM.

For completeness, changing the solvent system from DIPA/THF (1:3 v/v) to DIPA was shown to have little or no effect at high concentration/temperature (entries 1 and 2, *Table 3-1)*. High concentrations even enabled significant cross-coupling at room temperature (entry 6, *Table 3-1)*.

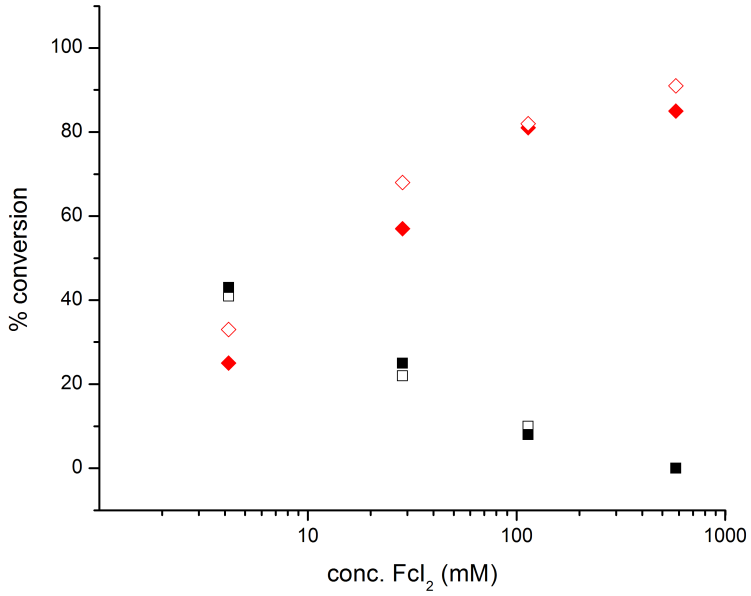

Figure 3-1. Effects of changing concentration on the conversion of fcI_2 to fcI(C≡CPh) (black squares) and $fc(C{\equiv}CPh)_2$ (red diamonds), entries 2-5, *Table 3-1*. Solid symbols = run 1, open symbols = run 2.

Table 3-1. Effects of changing concentration on reaction yield.[a]

				% conversion[b]		
#	amine/solvent	T /°C	[fcI_2] /mM	fcI(C≡CPh)	$fc(C{\equiv}CPh)_2$	side products
1	DIPA	90	580	1	85	15
2	DIPA/THF (1:3 v/v)	80	580	0	88	12
3	DIPA/THF (1:3 v/v)	80	114	9	82	8
4	DIPA/THF (1:3 v/v)	80	28	24	63	9
5	DIPA/THF (1:3 v/v)	80	4	42	29	8
6	DIPA/THF (1:3 v/v)	rt	580	46	10	7

[a] All reactions were run for 20 h and performed with 6 mol% $Pd(PPh_3)_2Cl_2$, 6 mol% CuI and 400 mol% phenylacetylene (2 equivalents per iodo functionality), relative to fcI_2. [b] Conversion obtained via ^{1}H NMR, given here as the average of two runs.

These results provide a plausible reason for the wide variability of published yields using similar solvents and catalysts, the relationship between concentration and yield (if general) should indeed be a key consideration of future syntheses with iodoferrocenes. Yet whilst simple structures may be easily reacted under such conditions due to their ready availability in large quantities, advanced materials prepared by multi-step syntheses are typically only available in much smaller amounts. In these cases it becomes rapidly impracticable to work with the small solvent volumes necessary for high yields and as such it is desirable to increase the rate of reaction beyond that of the $PdCl_2(PPh_3)_2$, DIPA, THF system.

3.3.2 Effects of amine and solvent

Variations in reaction medium were assessed with $PdCl_2(PPh_3)_2$ at room temperature where the ~25% total conversion of 1,1'-diiodoferrocene previously observed with $PdCl_2(PPh_3)_2$ in THF/DIPA (1:3 v/v) (entry 6, *Table 3-1*) permits facile discrimination between changes in rate as a function of increased or decreased yields. *Figure 3-2* shows the differences (with THF) using DIPA, DEA, DIPEA and TEA, with *Figure 3-3* showing the effects (with DIPA) of changing from THF to toluene or CH_2Cl_2 (raw data in *Table 3-2)*. Whilst nothing challenges the commonly used DIPA/THF combination, it is interesting to note that bulkier amines (DIPA, DIPEA) seem to fare better within their class of amine (secondary/tertiary), with DIPA (a bulky secondary amine) providing a higher yield than DIPEA (a bulky tertiary amine). Significant increases in side product formation are also observed with DEA (entry 9, *Table 3-2)*, discussed further in section 3.3.4.

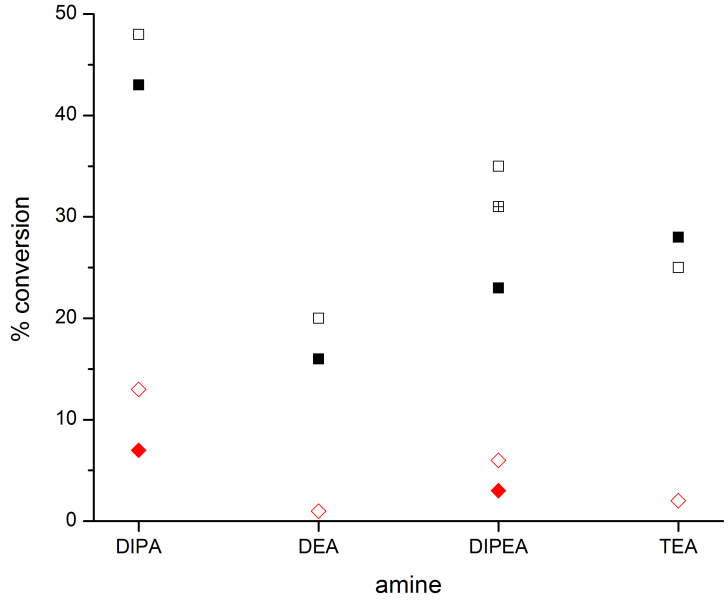

Figure 3-2. Effects of changing amine on the conversion of fcI_2 to fcI(C≡CPh) (black squares) and $fc(C{\equiv}CPh)_2$ (red diamonds), entries 6-9, *Table 3-2*. Solid symbols = run 1, open symbols = run 2, crossed symbols = run 3 (DIPEA only).

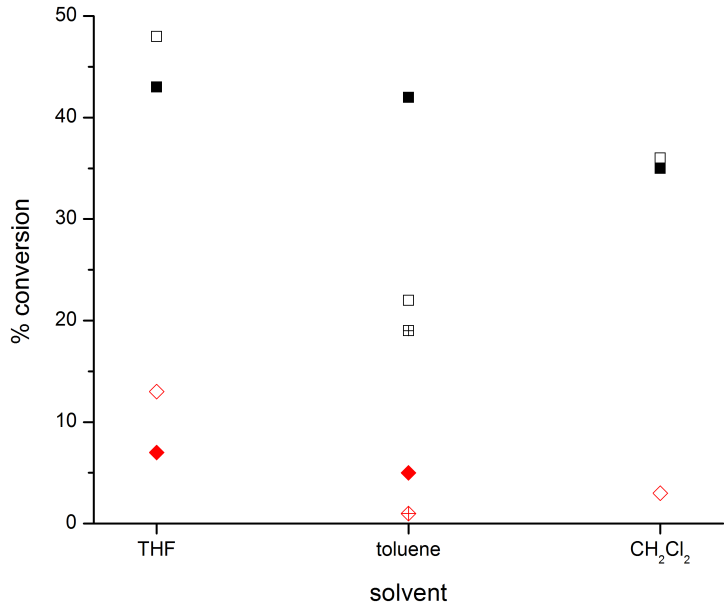

Figure 3-3. Effects of changing solvent on the conversion of fcI_2 to fcI(C≡CPh) (black squares) and $fc(C{\equiv}CPh)_2$ (red diamonds), entries 6,10-11, *Table 3-2*. Solid symbols = run 1, open symbols = run 2, crossed symbols = run 3 (toluene only).

Table 3-2. Effects of changing amine and solvent on reaction yield.[a]

		% conversion[b]		
#	amine/solvent (1:3 v/v)	fcI(C≡CPh)	fc(C≡CPh)$_2$	side products
6	DIPA/THF	46	10	7
7	TEA/THF	27	2	13
8[c]	DIPEA/THF	30	4	12
9	DEA/THF	18	1	29
10[c]	DIPA/toluene	28	2	8
11	DIPA/CH_2Cl_2	36	3	4

[a] All reactions were run for 20 hours at room temperature and performed with 6 mol% $PdCl_2(PPh_3)_2$ catalyst, 6 mol% CuI and 400 mol% phenylacetylene (2 equivalents per iodo functionality), relative to fcI_2 (concentration = 580 mM). [b] Conversion obtained via ^{1}H NMR, given here as the average of two runs (unless otherwise stated). [c]Conversion given as the average of three runs.

3.3.3 Effects of phosphines

The steric and electronic properties of phosphine (and other) ligands used in catalysis are known to have a profound influence on the rate and overall success of the reaction. P(^{t}Bu)$_3$ for example, a sterically bulky and highly electron rich mono-dentate phosphine, is notable for remarkable rate enhancements in Pd-catalysed couplings.[20-21] It is generally considered that bulky phosphines favour mono-ligated Pd(0) complexes,[22] highly active towards oxidative addition and promoting reductive elimination.[23]

The role of the phosphine ligand here was explored using a $PdCl_2(MeCN)_2$ pre-catalyst and free phosphine (L), forming the desired $PdCl_2L_2$ complex *in situ* via displacement of MeCN. Extra care was taken in this set of experiments given the highly air-sensitive nature of many electron-rich phosphines (being easily oxidised to R_3P=O). DIPA and phenylacetylene were each distilled and deoxygenated by sparging with N_2 or freeze-pump-thaw cycles, respectively.[†] The order of addition of reagents and solvents was also adjusted to ensure complete removal of all oxygen prior to introduction of the ligand (see *Chapter 8)*.

[†] DIPA (sparged with N_2, dried over 3A molecular sieves) and phenylacetylene in previous experiments were essentially used as received. The high yields of previous runs and comparison between controls (entry 12, *Table 3-3* and entry 6, *Table 3-1)* indicate the $PdCl_2(PPh_3)_2$/phenylacetylene system is highly tolerant of small quantities of dissolved oxygen and other (deleterious) impurities.

Yields achieved using the preformed $Pd(PPh_3)_2Cl_2$ catalyst and the $Pd(MeCN)_2Cl_2/PPh_3$ combination were highly comparable (entries 12 and 13, *Table 3-3)*, indicating in the latter case that the desired $PdCl_2(PPh_3)_2$ complex was indeed formed under the reaction conditions. With the rate determining step of the catalytic cycle for iodoferrocenes unknown, and previous investigations with $P(^tBu)_3$ reported as largely unsuccessful,[19] the systematic variation of phosphine ligand (14 examples) was undertaken with an aim of exploring a broad steric and electronic landscape (raw data in *Table 3-3)*. Plotting Tolman cone angles (θ) and electronic parameters (ν_{el}) of the phosphine ligands[24] versus product yield gives useful insights into the relative contributions of these factors to the rate of reaction *(Figure 3-4)*.

Table 3-3. Effects of changing phosphine on reaction yield.[a]

		% conversion[b]			phosphine	
#	catalytic system	fcI(C≡CPh)	fc(C≡CPh)$_2$	side products	θ (°)	ν_{el} (cm^{-1})
12	$Pd(PPh_3)_2Cl_2$	39	5	10	145	2068.9
13	$Pd(MeCN)_2Cl_2/PPh_3$	35	4	11	145	2068.9
14	$Pd(MeCN)_2Cl_2/P(C_6H_4$-*p*-$Cl)_3$	18	1	10	145	2072.8
15	$Pd(MeCN)_2Cl_2/P(C_6H_4$-*p*-$OMe)_3$	22	1	8	145	2066.1
16	$Pd(MeCN)_2Cl_2/P($*p*-tolyl$)_3$	29	3	10	145	2066.7
17	$Pd(MeCN)_2Cl_2/P($*o*-tolyl$)_3$	2	0	2	194	2066.6
18	$Pd(MeCN)_2Cl_2/PPh_2($*o*-tolyl$)$	21	2	9	161	2068.1
19	$Pd(MeCN)_2Cl_2/PPh_2Me$	1	0	5	136	2067.0
20	$Pd(MeCN)_2Cl_2/PPh_2(C_6F_5)$	6	0	0	158	2074.8
21	$Pd(MeCN)_2Cl_2/P(C_6F_5)_3$	2	0	2	184	2090.9
22	$Pd(MeCN)_2Cl_2/PBz_3$	0	0	0	165	2066.4
23	$Pd(MeCN)_2Cl_2/PCy_3$	0	0	2	170	2056.4
24	$Pd(MeCN)_2Cl_2/P(^nBu)_3$	0	0	0	132	2060.3
25	$Pd(MeCN)_2Cl_2/P(^tBu)_3$	3	93	4	182	2056.1
26	$Pd(MeCN)_2Cl_2/P(O\text{-}^iPr)_3$	1	0	4	130	2075.9

[a] All reactions were run for 20 hours at room temperature and performed with 6 mol% Pd catalyst, 6 mol % CuI, 12 mol% phosphine (where applicable) and 400 mol% phenylacetylene (2 equivalents per iodo functionality), relative to fcI_2 (concentration = 580 mM). [b] Conversion obtained via ^{1}H NMR, average of two runs (difference of ≤5% between runs).

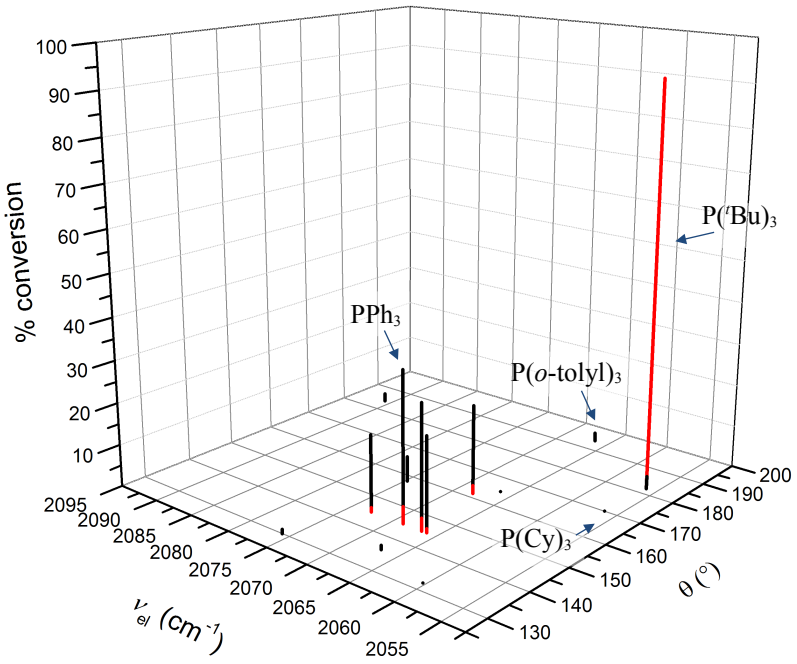

Figure 3-4. A 3D map of the effect of phosphine ligand on reaction conversion – plotted on the z-axis where the height of black bars = % fcI(C≡CPh), red bars = % fc(C≡CPh)$_2$. Decreasing values of ν_{el} indicate increasing electron-donating ability of the ligand (Tolman electronic parameter), increasing θ values indicates increasing steric bulk (Tolman cone angle).[24]

This investigation exposes a significant number of phosphines with little or no aptitude for the cross-coupling of iodoferrocenes at room temperature. That said, several of medium bulk and electronic-donating ability, with PPh_3 being most efficient, form reasonably active catalysts providing 20-40% of 1-iodo-1'-(phenylethynyl)ferrocene and ≤5 of 1,1'-bis(phenylethynyl)ferrocene under these conditions. Small departures from the sterics/electronics of PPh_3 result in (sometimes quite dramatic) rate decreases.

Perhaps most remarkable is the unique behaviour of P(^{t}Bu)$_3$, providing near quantitative conversion of 1,1-diiodoferrocene to 1,1'-bis(phenyl)ethynylferrocene (entry 25, *Table 3-3)* – a result that can only be attributed to the ligand's exceptional combination of extreme steric bulk and electron donating ability (given the poor results with P(*o*-tolyl)$_3$ and PCy_3, entries 17 and 23 *Table 3-3)*. Further insights may be gained from observations of the reaction solutions. Whereas most phosphines gave a readily stirred black suspension for the duration of the run (20 h), with P(^{t}Bu)$_3$ the mixture rapidly took on a red colour, solidifying with precipitate and becoming hot to

the touch after only 15 min. Additional studies are needed to more accurately explore the effects of this catalyst combination – improved yields at high dilutions are anticipated, with or without additional rate enhancements that may be provided by increasing reaction temperature.

Despite significant successes elsewhere,[20-21] this result is perhaps surprising given previous reports of largely unsuccessful Sonogashira cross couplings with iodoferrocenes and $PdCl_2(PhCN)_2/P(^tBu)_3$.[19] However, closer inspection of the specific syntheses involved *(Scheme 3-7)* provide reasonable explanations. For *Scheme 3-7(a)* it is shown later *(section 3.4)* that thioacetyl groups and terminal alkynes are generally incompatible when attempting cross-coupling with iodoferrocenes, and with *Scheme 3-7(b)* the approach is not straightforward, with difunctional reagents quite possibly leading to oligo- or polymerisation products.

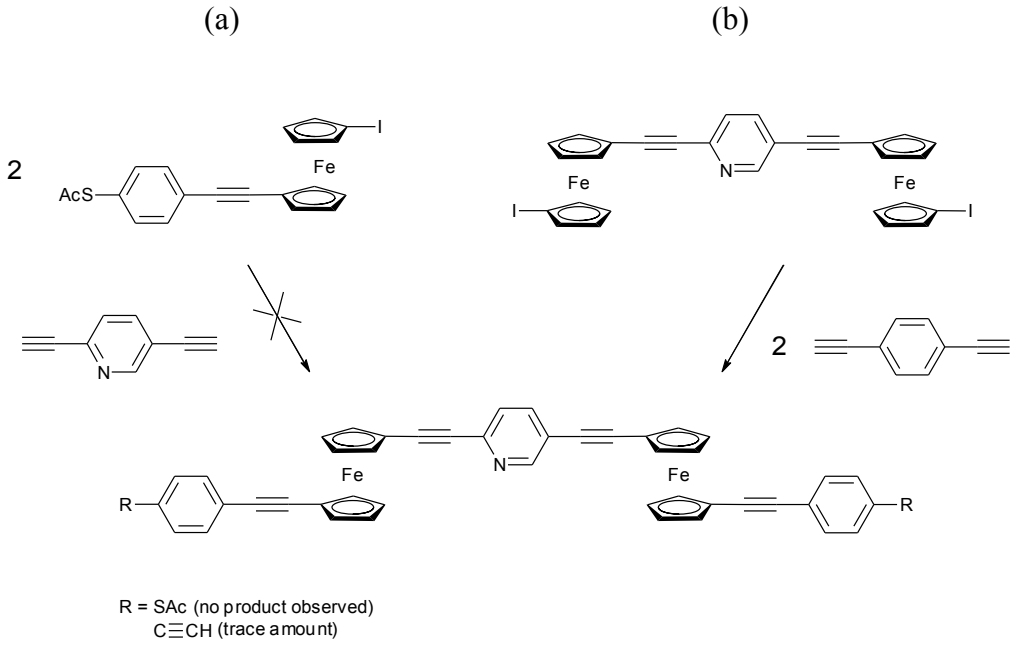

Scheme 3-7. Attempted cross-coupling reactions with $PdCl_2(PhCN)_2/P(^tBu)_3$, reported by Engtrakul and Sita in 2008.[19]

3.3.4 Comments on side products

By full or partial isolation, ^1H NMR and accurate mass spectrometric analyses *(Chapter 8)*, crude mixtures from typical runs were shown to contain iodoferrocene, (phenylethynyl)ferrocene, and even ferrocene, in addition to the expected two cross-coupled

products and unreacted starting material *(Scheme 3-1)*. These limit the full conversion of 1,1'-diiodoferrocene to the desired cross-coupled compounds *(Table 3-1-Table 3-3)*, and are likely formed via conversion of the Fc–I bond to Fc–H under Sonogashira conditions *(Scheme 3-8)*. It should be reiterated here with confidence that no iodoferrocene/ferrocene impurities were present in the 1,1'-diiodoferrocene starting material used *(Chapter 2)*.

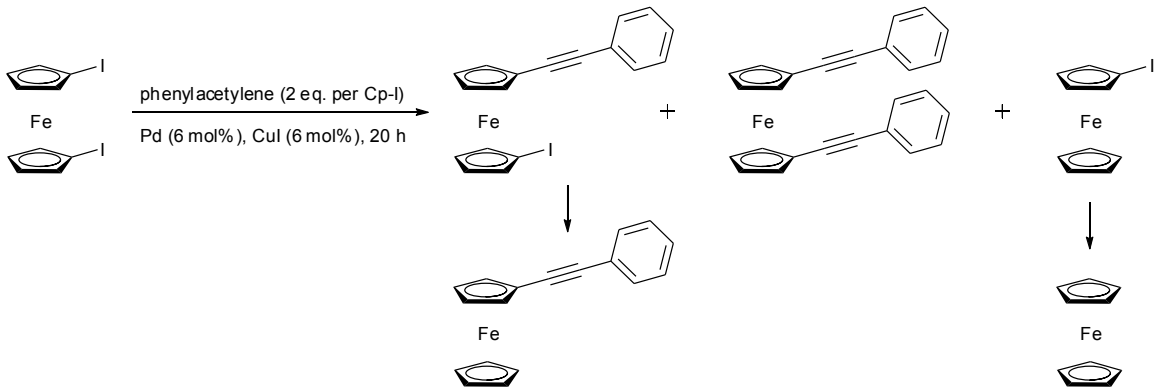

Scheme 3-8. The apparent conversion of Cp–I to Cp–H under Sonogashira conditions is hypothesised to generate side products as shown.

Such hydrodehalogenation side reactions have been noted in Sonogashira cross-couplings of fluorinated aryl halides,[25] very recently investigated in detail by Orbach *et al.*[26] Studying the reaction shown in *Scheme 3-9*, labelling studies with THF-d_8 (containing trace water isotopomers) and THF-d_8/D_2O (6:1 v/v) were used to implicate (adventitious) water as the hydrogen source. No hydrodehalogenation took place in rigorously dried THF-d_8, though it was observed in anhydrous DMF (50 ppm water). The phosphine appeared to play an important role. Whereas full conversion of the fluorinated aryl bromide to the aryl hydride was ultimately achieved by reaction of the former with $Pd(PEt_3)_4$ (1 eq.) or PEt_3 (3 eq.) in THF/H_2O (6:1 v/v) after 5 min, no reaction was observed with $Pd(PPh_3)_4$ (1 eq.) under these conditions, and extended reaction times and elevated temperatures (43 h, 100°C) were required to achieve 43% conversion with PPh_3 (3 eq.). Hydrodehalogenation was not observed under any of the above conditions with non-fluorinated arylbromides. It was postulated that this reaction proceeds via formation of a phosphonium salt ([aryl–PR_3]Br), followed by hydrolysis with water (forming R_3P=O and HBr).

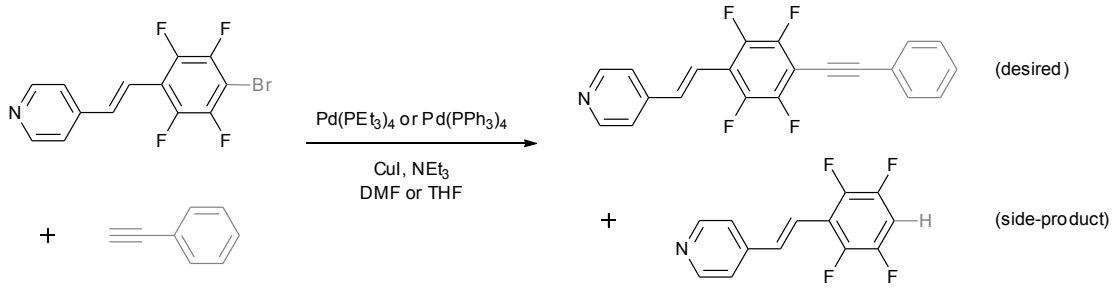

Scheme 3-9. The reaction used by Orbach *et al.* to study hydrodehalogenation of fluorinated aryl halides under Sonogashira conditions.

In experiments performed by this author with iodoferrocenes, room temperature runs using either phenylacetylene-d_1/THF or phenylacetylene/THF-d_8 showed no observable labelled products by ^{1}H NMR – though in the former case the acetylenic proton of unreacted phenylacetylene is clearly observed in the crude product spectrum (indicating proton/deuterium exchange under the reaction conditions). Reactions in toluene or CH_2Cl_2 *(Table 3-2)* resulted in comparable quantities of hydrodehalogenated products, suggesting that the solvent is an unlikely source of hydrogen. Broader variations with amine *(Table 3-2*, DEA providing significantly more side products than the others) were observed, suggesting this component plays some role. In agreement with the findings of Orbach *et al.* the extent of hydrodehalogenation appears dependant on the nature of the Pd/phosphine combination – with side product formation linked to the rate of cross-coupling in most cases *(Table 3-3)*.

Though reasonable efforts were made to dry the amine and solvent used in all reactions (over 3A molecular sieves and drying columns, respectively), (adventitious) water cannot yet be ruled out as a plausible hydrogen source here. Hydrodehalogenation was never observed in any 'standard' Sonogashira cross-couplings of aryl-iodides or bromides using the very same lab solvents *(Chapters 2, 4 and 5)*, implicating iodoferrocenes are a special case in addition to the aforementioned fluorinated aryl halides.

3.4 REACTIONS WITH 4-ETHYNYLPHENYLTHIOACETATE

3.4.1 Motivation

The thioacetate functionality is extremely useful within molecular electronics for physically and electronically connecting molecules to macroscopic (gold) electrodes for testing. This and analogous moieties have been installed in 1-iodo-1'-ethynylferrocene or iodoferrocenes by cross-coupling reactions using 4-iodophenylthioacetate[19]/1-(*tert*-butylsulfanyl)-4-iodobenzene,[2a,16] or 1-(*tert*-butylsulfanyl)-4-ethynylbenzene *(Chapter 2)*, respectively. Though two successful published examples exist,[27] difficulties converting the robust S^{t}Bu group into SAc (via established methods using $AlCl_3$,[28] BBr_3[29] or Br_2[30]) in ferrocene-containing materials have been reported.[31] Eager to circumvent these potential problems and other limitations *(Chapter 2)*, the synthesis of 1,1'-bis(4-thioacetylphenyl)ethynylferrocene from 1,1'-diiodoferrocene and 4-ethynylphenylthioacetate under Sonogashira conditions was investigated here *(Scheme 3-10)*. Somewhat surprisingly, this relatively simple approach had not drawn comment from others in the field.

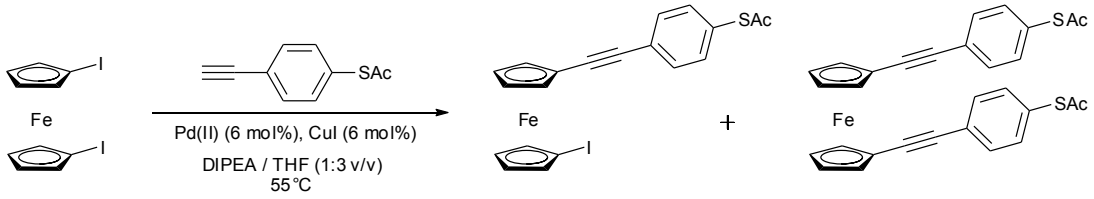

Scheme 3-10. Investigated synthesis of 1,1'-bis(4-thioacetylphenyl)ethynylferrocene.

THF/DIPEA was used in these experiments to avoid deacetylation of the SAc group.[32] This readily occurs with DIPA at 50°C, whereas 4-iodophenylthioacetate/4-ethynylphenylthioacetate can be cross-coupled with alkynes/aryl iodides using *tertiary* amines at moderate temperatures (*e.g.* DIPEA, 55°C).[2c,32-33] Even without the rapid rate increase provided by P(^{t}Bu)$_3$, moderate yields of the desired products from *Scheme 3-10* were anticipated based upon reactions using $PdCl_2(PPh_3)_2$ and phenylacetylene – employing extended reactions times or moderate heating *(Table 3-4)*.

Table 3-4. Effects of longer reaction times and moderate heating on reaction yield.[a]

				% conversion[b]		
#	amine/solvent (1:3 v/v)	T /°C	time /h	fcI(C≡CPh)	fc(C≡CPh)$_2$	side products
6	DIPA/THF	rt	20	46	10	7
27	DIPA/THF	rt	60	46	29	15
8	DIPEA/THF	rt	20	30	4	12
28	DIPEA/THF	55	20	44	32	12

[a] All reactions were performed with 6 mol% $Pd(PPh_3)_2Cl_2$, 6 mol% CuI and 400 mol% phenylacetylene (2 equivalents per iodo functionality), relative to fcI_2 (concentration = 580 mM). [b] Conversion obtained via ^{1}H NMR, average of two runs.

3.4.2 Unexpected alkyne carbochalcogenation reaction

Surprisingly, it appears the desired Sonogashira cross-couplings between iodoferrocenes and 4-ethynylphenylthioacetate are unfeasible due to a more rapid side reaction. The crude ^{1}H NMR spectrum resulting from the reaction in *Scheme 3-10* showed only 1,1'-diiodoferrocene starting material after 24 h, albeit with the notable absence of resonances attributable to 4-ethynylphenylthioacetate. Upon closer inspection, three new resonances at approximately δ 7.0, 6.4 and 2.3 ppm (CD_2Cl_2) were identified, integrating in the ratio 4:1:3 – runs at room temperature with the $PdCl_2(PPh_3)_2$/P(^{t}Bu)$_3$ combination gave similar results.

A pale yellow solid with matching spectral features *(Figure 3-5)* was isolated by column chromatography, giving a molecular ion ($[M+H]^+$) of exactly three times the mass of 4-ethynylphenylthioacetate. With two ^{1}H NMR resonances arguably aromatic, and apparent retention of the acetyl functionality (given the resonance at 2.3 ppm and a C=O absorption at 1659 cm^{-1} in the IR spectrum), this was initially considered to be the alkyne trimerization product shown in *Figure 3-6(a)* (given the significant literature precedent[34]). The correct structure was however, ultimately shown by X-ray crystallographic analysis to be that of the novel cyclic β-phenylthioketone (**15**) depicted in *Figure 3-6(b)* and *Figure 3-7* (with the lower 'aromatic' resonance at 6.42 ppm actually resulting from a vinylic proton). The overall reaction may be described as *syn* addition of the acetyl and thiolate to the carbon-carbon triple bond (accompanied by cleavage of the S-Ac bond, and reduction to C=C).

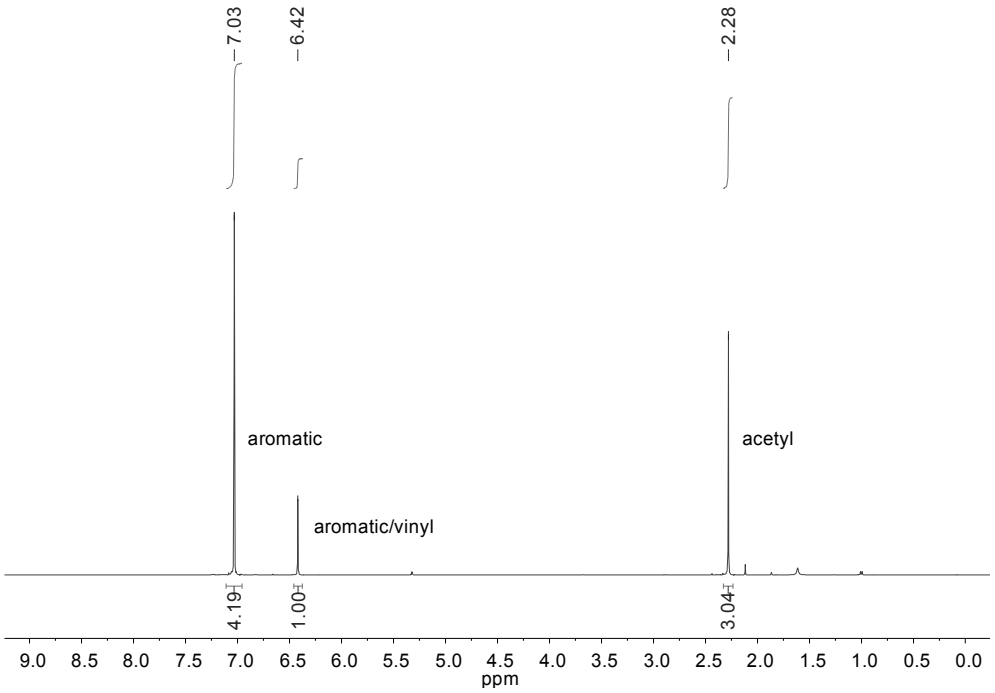

Figure 3-5. ^{1}H NMR spectrum (CD_2Cl_2) of **15**, a product unexpectedly produced from the reaction attempted in *Scheme 3-10*.

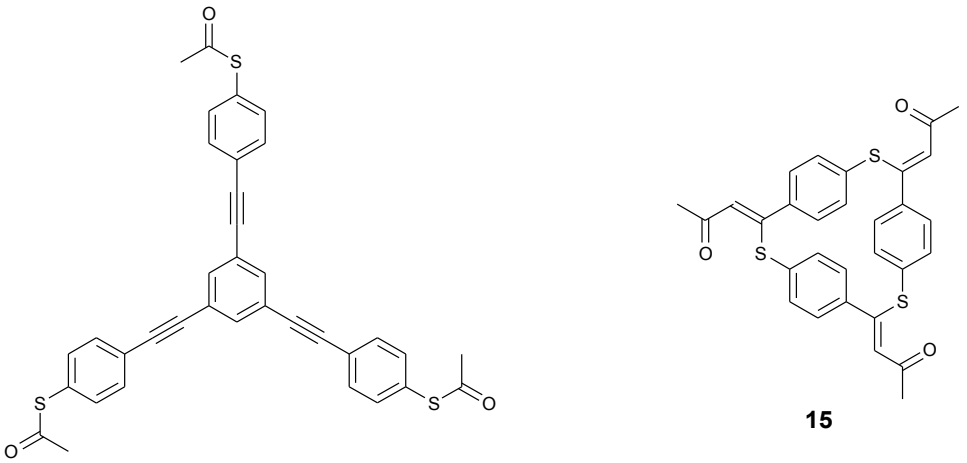

Figure 3-6. (a) The alkyne trimerization product of 4-ethynylphenylthioacetate, initially (incorrectly) considered as the isolated side-product from the attempted reaction shown in *Scheme 3-10*. (b) The correct structure as verified by X-ray crystallography.

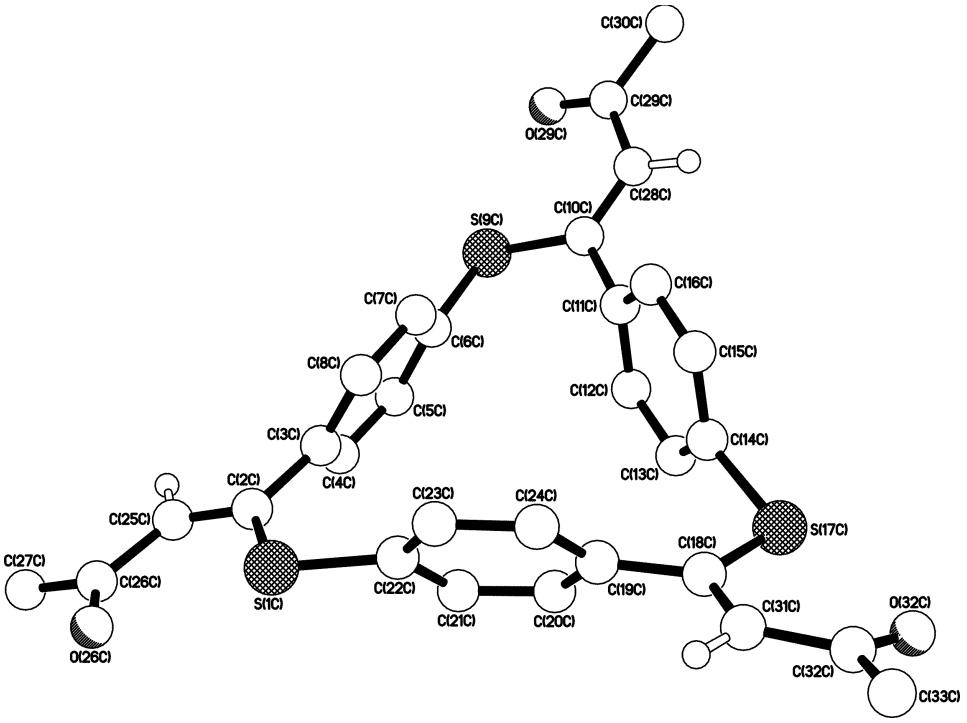

Figure 3-7. X-ray crystal structure of **15**. Whilst only the trimer was observed, the presence of higher order cycles cannot be ruled out.

To verify and explore this result further, phenylthioacetate and phenylacetylene (monofunctional analogues of 4-ethynylphenylthioacetate) were reacted under similar conditions in the absence of 1,1'-diiodoferrocene *(Scheme 3-11)*. Here, the addition product was formed as a mixture of *Z* (81%) and *E* (19%) isomers in 80% isolated yield – in contrast to the cyclic product which was isolated in 24% yield, consisting of all *Z* isomers. This was confirmed by comparison to published $^{1}H/^{13}C\{^{1}H\}$ NMR data[35] and full characterisation including elemental analysis *(Chapter 8)*. Further experiments omitting each reagent systematically showed that $PdCl_2(PPh_3)_2$, CuI and DIPEA were all necessary for the reaction to occur in THF at a reasonable rate (proceeding sluggishly in the absence of CuI, and not at all without $PdCl_2(PPh_3)_2$).

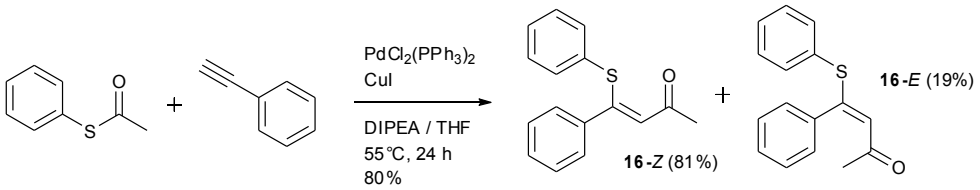

Scheme 3-11. Phenylthioacetate and phenylacetylene, monofunctional analogues of 4-ethynylphenylthioacetate, were reacted to form the addition product **16** in 80% isolated yield.

This result was compared to other syntheses of **16** from the literature *(Table 3-5)*. Whilst yields and *E/Z* ratios appear comparable, starting materials are acetylenic ketones/nucleophilic thiolates and reactions are not transition-metal catalysed.

Table 3-5. Typical literature syntheses of **16**, compared to the new Pd/Cu catalysed route.

#	reagents	conditions	T /°C	yield /% (*E/Z*)	ref
1	Ph–C≡CH, C_6H_5SAc	$PdCl_2(PPh_3)_2$, CuI, DIPEA/THF, 24 h	55	80 (19/81)	this work
2	Ph–C≡C–COMe, PhSNa	stirring, 10-15 min	rt	92 (22/78)	*35*
3	Ph–C≡C–COMe, PhSH	MeONa (cat.), diethyl ether, 5 h	0	75 (0/100)	*36*

Methods for the carbochalcogenation of alkynes using (primarily) Pd, Rh or Pt-mediated approaches were reviewed in 2006 by Kuniyasu and Kambe[37] and in 2010 by Bichler and Love[38]. It seems $R^1C(O)CH=C(R^2)S(R^3)$-type structures are often prepared via CO insertion mechanisms. Known processes for preparing materials similar to **16** directly from thioesters and terminal alkynes *(Scheme 3-12*, where R^1 = alkyl, aryl, OMe) are summarised in *Table 3-6*. The majority use more forcing conditions than the approach described here. Such transformations are reportedly of general interest for the syntheses of novel materials, and may provide insights into mechanisms of metal-catalysed oil desulfurization.[39]

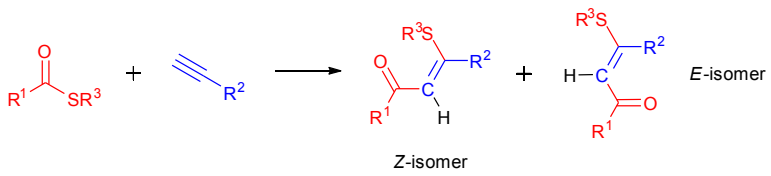

Scheme 3-12. Route to $R^1C(O)CH=C(R^2)S(R^3)$ compounds from thioesters and terminal alkynes (for **16**: R^1 = Me, R^2 = Ph, R^3 = Ph).

Table 3-6. Processes for preparing materials similar to **16** directly from thioesters and terminal alkynes (where R^1 = alkyl, aryl, OMe).

#	reagents	conditions	time /h	T /°C	ref
1	Ph–C≡CH, C_6H_5SAc	$PdCl_2(PPh_3)_2$, CuI, DIPEA/THF	24	55	this work
2	*n*-C_8H_{17}–C≡CH, $R^3SC(O)R^1$	$RhH(PPh_3)_4$, Et_2PhP, DMSO	12	100	*40*
3	R^2–C≡CH, $R^3SC(O)CF_3$ R^2–C≡CH, $R^3SC(O)R^1$	$Pt(PPh_3)_4$, xylene $Pd(dba)_2$/dppe, benzene	10 20	139 80	*41*
4	R^2–C≡CH, $R^3SC(O)R^1$	$PdCl_2$, CuI, K_2CO_3, Et_3N, DMF	0.66	80	*42*
5[a]	R^2–C≡CH, PhS–COOMe	$Pd(PCy_3)_2$, toluene	20	110	*39*
6	R^2–C≡CH, $[(CH_3)_2SC(O)R^1]BF_4^-$	i) CH_2Cl_2, (ii) TEA	1-25	–60-0	*43*

[a] Other $PdCl_2L_2$ (L = phosphine) and $RhCl(PPh_3)_3$/$RhCl(cod)(PPh_3)$ complexes catalysed this reaction, albeit with inferior performance.

3.4.3 Mechanistic considerations

Two reaction mechanisms may be contemplated. The first is an adaption of catalytic cycles proposed by Hua and Minami *et al. (Scheme 3-13)*.[39,41] Here oxidative addition of thioester to a Pd(0) centre results in cleavage of the R^3S–$C(O)R^1$ bond, whereby alkynyl insertion into Pd-S, *trans-cis* isomerisation and C-C bond-forming reductive elimination steps generate the *Z* isomer. For a related Pd-catalysed process, Hua *et al.* postulated that this product could then also oxidatively add to Pd(0) (cleaving the vinyl C-S bond), presumably forming a zwitterionic carbene complex that facilitates *Z-E* isomerisation (by analogy to related Rh,[44] Rh/Co[45] and Pd[46] systems), liberating the *E* isomer via reductive elimination.

Such a scheme is plausible but does not fully take into account the apparent roles played here by DIPEA or CuI *(vida supra)*, though it could be argued that these generate and maintain the active Pd(0) catalyst from $PdCl_2(PPh_3)_2$. This theory might be tested to some extent using a pre-

formed Pd(0) catalyst such as $Pd(PPh_3)_4$. DIPEA coordination to the Pd centre may also play a role – reversible reactions between secondary/primary amines and *trans*-$RPdX(PPh_3)_2$ species are known to form *trans*-$RPdX(PPh_3)$(amine) complexes (and PPh_3).[47]

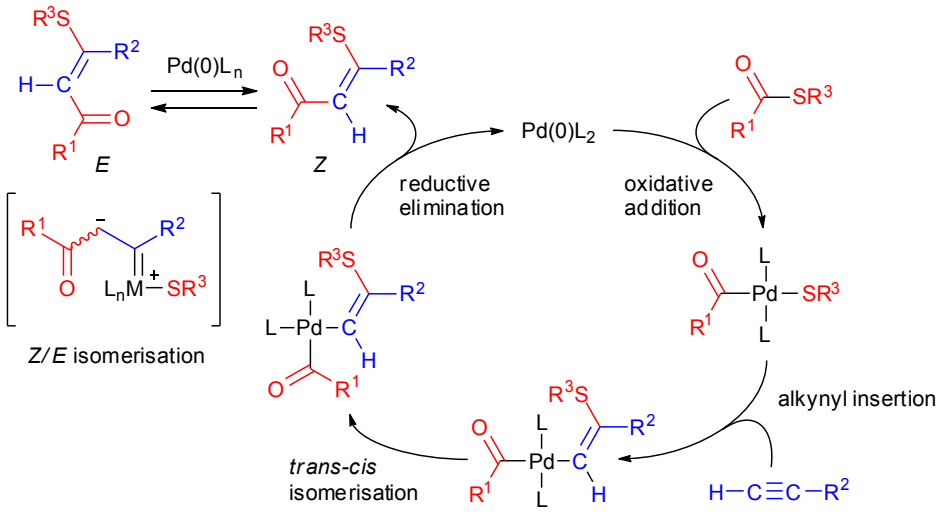

Scheme 3-13. One proposed catalytic cycle for carbothiolation, adapted from publications by Hua and Minami *et al.*[39,41]

A second mechanism is suggested by Tokuyama and Minami *et al. (Scheme 3-14).*[42,48] Here oxidative addition of thioester to the active Pd(0) centre cleaves the R^3S–$C(O)R^1$ bond, and transmetallation with Cu(I)-alkyne substitutes the bound thiolate which is captured by Cu(I) (plausibly returned to the catalytic cycle via thiolate transfer to the amine forming a quaternary salt). Subsequent *trans-cis* isomerisation followed by reductive elimination generates a cross-coupled alkyne-acetyl intermediate that subsequently reacts with the thiolate (as Cu(I)-thiolate or R_3NH-thiolate) via nucleophilic conjugate addition, generating the observed product. This scheme fully accounts for the apparent roles played here by $PdCl_2(PPh_3)_2$, CuI, and DIPEA *(vida supra)*, and bears some resemblance to the stoichiometric syntheses of **16** described in *Table 3-5*.

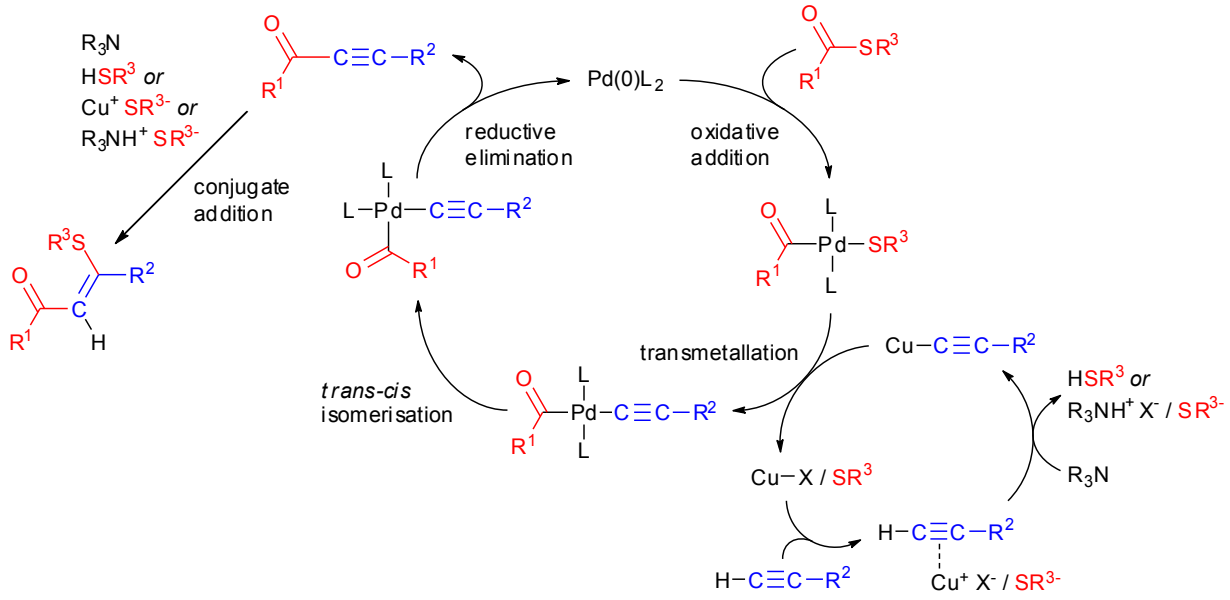

Scheme 3-14. A second possible mechanism, producing cross-coupled acetyl-alkyne and thiolate products that subsequently react under basic conditions to produce $R^1C(O)CH=C(R^2)S(R^3)$-type compounds (interpreted from work by Tokuyama and Minami *et al.*[42,48]).

The aryl-acetyl formation/thiolate nucleophilic conjugate addition mechanism takes into account the following experimental observations. Minami and co-workers identified and later isolated both alkynyl ketone and β-thio-αβ-unsaturated ketone intermediates en route to the synthesis of a variety of 2,3-dihydrothiopyran-4-one derivatives from thioesters and terminal alkynes *(Scheme 3-15)*.[42] It was found that the alkynyl ketone (**I-a**, *Scheme 3-15)* could be converted (in the presence of TEA and thiol, generated from the thioester) to the β-thio-αβ-unsaturated ketone (**I-b**, *Scheme 3-15)* via base catalysed nucleophilic conjugate addition. As **I-b** was also transformed into the final product via a base catalysed process, it was considered that the only role of Pd/Cu could have been in cross-coupling the thioester to the terminal alkyne (*i.e.* in forming **I-a**).

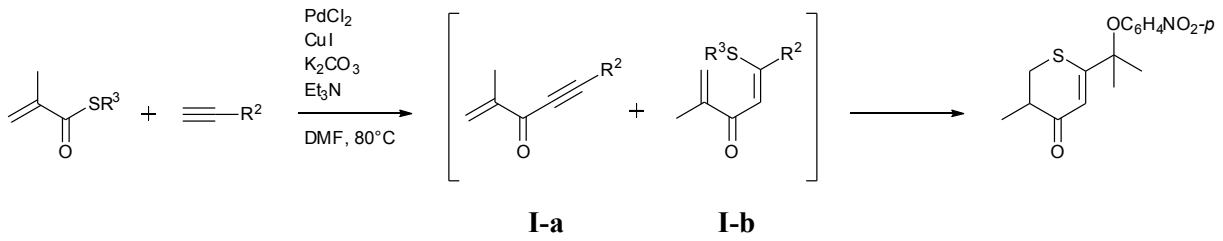

Scheme 3-15. Intermediates isolated (by Minami *et al.*) en route to 2,3-dihydrothiopyran-4-ones, from the reaction between a thioester and terminal alkyne (R^2 = $C(OH)Me_2$, R^3 = $C_6H_4NO_2$-*p*).[42]

Such a cross-coupling reaction had been described in 2003 by Tokuyama and co-workers *(Scheme 3-16)*, where they suggested a mechanism involving transmetallation between acylpalladium and cuprous acetylide species.[48] Their experiments showed both Pd and (an excess of) CuI was necessary to provide decent yields of cross-coupled products – further indicating that the Cu(I) likely traps the thiolate, preventing it from poisoning the Pd(0) centre. They also observed a conjugate addition by-product (from the reaction of 'ethanethiol' and a 1-alkynyl ketone) in one experiment with a prolonged reaction time.

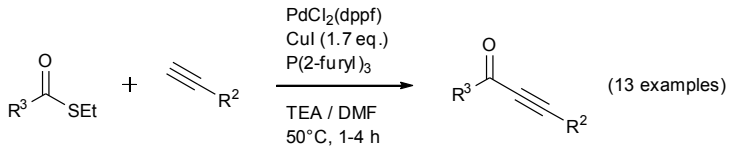

Scheme 3-16. The palladium-catalysed cross-coupling of thiol esters with terminal alkynes provides 1-alkynyl ketones.[48]

3.5 CONCLUSION

The Sonogashira cross-coupling of iodoferrocenes was explored systematically using the model system of 1,1'-diiodoferrocene and phenylacetylene, providing key insights into this often lamented reaction that should prove useful in future syntheses of ferrocenyl alkynes. Yields were found to be extremely sensitive to concentration, with excellent conversion achieved with ≥580 mM 1,1'-diiodoferrocene using a $PdCl_2(PPh_3)_2$ catalyst in refluxing THF/DIPA (3:1 v/v) *(Table 3-1)*. Even better yields were provided by a $PdCl_2(MeCN)_2$/$P(^tBu)_3$ combination *at room*

temperature (Table 3-3), suggesting the possibility of high yielding syntheses with iodoferrocenes at much lower concentrations (<580 mM). If realised, such conditions should facilitate access to improved quantities of the ferrocene macrocycle (**13**, *Chapter 2)*.‡ Somewhat inconveniently, significant conversion of the Fc–I functionality to Fc–H was observed under a range of conditions (plausibly due to the reaction of adventitious water). This limits yields due to side-product formation, and may complicate purification procedures.

Efforts to cross-couple 4-ethynylphenylthioacetate with 1,1'-diiodoferrocene resulted only in production of a cyclic β-phenylthioketone (**15**) via oligomerization of the ligand. This unanticipated reaction can be described as *syn* addition of the acetyl and thiolate groups to C≡C, and may be explained in terms of alkyne insertion *(Scheme 3-13)* or aryl-acetyl formation/thiolate nucleophilic conjugate addition mechanisms *(Scheme 3-14)*. It is plausible that the desired reaction *(Scheme 3-10)* does not take place because oxidative addition of Fc-I to Pd(0) is blocked by the more rapid oxidative addition of thioacetate. Noting previously successful cross-couplings between 4-ethynylphenylthioacetate and aryl bromides/iodides, it may be inferred that rates of oxidation addition to Pd(0) follow the series Ar–I > Ar–Br > S–Ac > Fc–I. With the convenient cross-coupling reaction between iodoferrocenes and 4-ethynylphenylthioacetate proven unfeasible, attention should now turn to other methods for preparing (thioacetylphenyl)ethynylferrocenes from Fc–I, ideally through finding a compatible method for conversion of S^{t}Bu precursors.

3.6 REFERENCES

1. J. C. Goeltz and C. P. Kubiak, *Organometallics*, 2011, **30**, 3908.
2. (a) J. Ma, M. Vollmann, H. Menzel, S. Pohle and H. Butenschön, *J. Inorg. Organomet. Polym. Mater.*, 2008, **18**, 41; (b) Q. Lu, X.-H. Wang and F.-S. Wang, *Chin. J. Appl. Chem.*, 2011, **28**, 136; (c) C. Engtrakul and L. R. Sita, *Organometallics*, 2008, **27**, 927; (d) T.-Y. Dong, S.-W. Chang, S.-F. Lin, M.-C. Lin, Y.-S. Wen and L. Lee, *Organometallics*, 2006, **25**, 2018; (e) E. Lindner, R. Zong and K. Eichele, *Phosphorus, Sulfur Silicon Relat. Elem.*, 2001, **169**, 219.

‡ As described in *Chapter 2*, high dilution syntheses using $PdCl_2(PPh_3)_2$ provided **13** in trace quantities only (plausibly due to the reduced rate of cross-coupling at these concentrations). Analogous reactions using the $PdCl_2(MeCN)_2/P(^tBu)_3$ combination have not yet been attempted due to time restrictions.

3. T. Michinobu, H. Kumazawa, K. Noguchi and K. Shigehara, *Macromolecules*, 2009, **42**, 5903.
4. (a) A. González-Cabello, P. Vázquez and T. Torres, *J. Organomet. Chem.*, 2001, **637–639**, 751; (b) K.-Q. Wu, J. Guo, J.-F. Yan, L. L. Xie, F.-B. Xu, S. Bai, P. Nockemann and Y.-F. Yuan, *Organometallics*, 2011, **30**, 3504; (c) C.-H. Andersson, L. Nyholm and H. Grennberg, *Dalton Trans*, 2012, **41**, 2374; (d) M. Lohan, P. Ecorchard, T. Ruffer, F. Justaud, C. Lapinte and H. Lang, *Organometallics*, 2009, **28**, 1878; (e) E. Lindner, R. Zong, K. Eichele and M. Ströbele, *J. Organomet. Chem.*, 2002, **660**, 78; (f) W.-M. Xue, Fritz E. Kühn, E. Herdtweck and Q. Li, *Eur. J. Inorg. Chem.*, 2001, **2001**, 213; (g) L.-A. Hore, C. J. McAdam, J. L. Kerr, N. W. Duffy, B. H. Robinson and J. Simpson, *Organometallics*, 2000, **19**, 5039.
5. (a) M. Takase and M. Inouye, *Chem. Commun.*, 2001, 2432; (b) M. Takase and M. Inouye, *Mol. Cryst. Liq. Cryst. Sci. Technol., Sect. A*, 2000, **344**, 313.
6. R. Ikeda, S. Kitagawa, J. Chiba and M. Inouye, *Chem. Eur. J.*, 2009, **15**, 7048.
7. S. Köcher, B. Walfort, G. P. M. van Klink, G. van Koten and H. Lang, *J. Organomet. Chem.*, 2006, **691**, 3955.
8. M. Inouye, M.-a. S. Itoh and H. Nakazumi, *J. Org. Chem.*, 1999, **64**, 9393.
9. H. A. Dieck and F. R. Heck, *J. Organomet. Chem.*, 1975, **93**, 259.
10. L. Cassar, *J. Organomet. Chem.*, 1975, **93**, 253.
11. K. Sonogashira, Y. Tohda and N. Hagihara, *Tetrahedron Lett.*, 1975, **16**, 4467.
12. A. Kasahara, T. Izumi and M. Maemura, *Bull. Chem. Soc. Jpn.*, 1977, **50**, 1021.
13. (a) R. Chinchilla and C. Nájera, *Chem. Rev.*, 2007, **107**, 874; (b) K. Sonogashira, *J. Organomet. Chem.*, 2002, **653**, 46; (c) R. Chinchilla and C. Najera, *Chem. Soc. Rev.*, 2011, **40**, 5084.
14. V. Mamane, *Mini-Rev. Org. Chem.*, 2008, **5**, 303.
15. J. Ma, B. Kühn, T. Hackl and H. Butenschön, *Chem. Eur. J.*, 2010, **16**, 1859.
16. I. Baumgardt and H. Butenschön, *Eur. J. Inorg. Chem.*, 2010, **2010**, 1076.
17. J. C. Torres, R. A. Pilli, M. D. Vargas, F. A. Violante, S. J. Garden and A. C. Pinto, *Tetrahedron*, 2002, **58**, 4487.
18. A. D. Woods, G. Alcalde, V. B. Golovko, C. M. Halliwell, M. J. Mays and J. M. Rawson, *Organometallics*, 2005, **24**, 628.
19. C. Engtrakul and L. R. Sita, *Organometallics*, 2008, **27**, 927.
20. T. Hundertmark, A. F. Littke, S. L. Buchwald and G. C. Fu, *Org. Lett.*, 2000, **2**, 1729.
21. M. Nishiyama, T. Yamamoto and Y. Koie, *Tetrahedron Lett.*, 1998, **39**, 617.
22. J. P. Stambuli, M. Bühl and J. F. Hartwig, *J. Am. Chem. Soc.*, 2002, **124**, 9346.
23. M. Schilz and H. Plenio, *J. Org. Chem.*, 2012, **77**, 2798.
24. C. A. Tolman, *Chem. Rev.*, 1977, **77**, 313.
25. (a) A. C. Albéniz, P. Espinet, B. Martín-Ruiz and D. Milstein, *J. Am. Chem. Soc.*, 2001, **123**, 11504; (b) P. Nguyen, Z. Yuan, L. Agocs, G. Lesley and T. B. Marder, *Inorg. Chim. Acta*, 1994, **220**, 289.
26. M. Orbach, J. Choudhury, M. Lahav, O. V. Zenkina, Y. Diskin-Posner, G. Leitus, M. A. Iron and M. E. van der Boom, *Organometallics*, 2011, **31**, 1271.
27. (a) O. Oms, T. Jarrosson, L. H. Tong, A. Vaccaro, G. Bernardinelli and A. F. Williams, *Chem. Eur. J.*, 2009, **15**, 5012; (b) J. B. Heilmann, E. A. Hillard, M.-A. Plamont, P. Pigeon, M. Bolte, G. Jaouen and A. Vessières, *J. Organomet. Chem.*, 2008, **693**, 1716.
28. I. A. Aliev, G. A. Kalabin and N. Ghelis, *Sulfur Lett.*, 1991, **12**, 123.

29. N. Stuhr Hansen, *Synth. Commun.*, 2003, **33**, 641.
30. A. Blaszczyk, M. Elbing and M. Mayor, *Org. Biomol. Chem.*, 2004, **2**, 2722.
31. H. Butenschön, Personal Communication, 2012.
32. R. P. Hsung, J. R. Babcock, C. E. D. Chidsey and L. R. Sita, *Tetrahedron Lett.*, 1995, **36**, 4525.
33. (a) D. L. Pearson and J. M. Tour, *J. Org. Chem.*, 1997, **62**, 1376; (b) L. Jones, J. S. Schumm and J. M. Tour, *J. Org. Chem.*, 1997, **62**, 1388; (c) C. B. Gorman, J. C. Smith, M. W. Hager, B. L. Parkhurst, H. Sierzputowska-Gracz and C. A. Haney, *J. Am. Chem. Soc.*, 1999, **121**, 9958; (d) H. Weber, J. Reichert, M. Elbing, C. von Hanisch, D. Beckmann and M. Mayor, *Angew. Chem., Int. Ed. Engl.*, 2003, **42**, 5834; (e) Z.-F. Shi, L.-J. Wang, H. Wang, X.-P. Cao and H.-L. Zhang, *Org. Lett.*, 2007, **9**, 595.
34. G. Dominguez and J. Perez-Castells, *Chem. Soc. Rev.*, 2011, **40**, 3430.
35. G. Perin, S. R. Mendes, M. S. Silva, E. J. Lenardão, R. G. Jacob and P. C. d. Santos, *Synth. Commun.*, 2006, **36**, 2587.
36. T. Nishio and Y. Omote, *J. Chem. Soc., Perkin Trans. 1 (1972-1999)*, 1981, 934.
37. H. Kuniyasu and N. Kambe, *Chem. Lett.*, 2006, **35**, 1320.
38. P. Bichler and J. Love, *Top. Curr. Chem.*, 2010, **31**, 39.
39. R. Hua, H. Takeda, S.-y. Onozawa, Y. Abe and M. Tanaka, *J. Am. Chem. Soc.*, 2001, **123**, 2899.
40. M. Arisawa, Y. Igarashi, H. Kobayashi, T. Yamada, K. Bando, T. Ichikawa and M. Yamaguchi, *Tetrahedron*, 2011, **67**, 7846.
41. Y. Minami, H. Kuniyasu, K. Miyafuji and N. Kambe, *Chem. Commun.*, 2009, 3080.
42. Y. Minami, H. Kuniyasu and N. Kambe, *Org. Lett.*, 2008, **10**, 2469.
43. V. G. Nenaidenko, P. V. Verteletskii, M. V. Lebedev, N. E. Shevchenko and E. S. Balenkova, *Russ. J. Org. Chem.*, 1998, **34**, 974.
44. K. A. Brady and T. A. Nile, *J. Organomet. Chem.*, 1981, **206**, 299.
45. I. Ojima, N. Clos, R. J. Donovan and P. Ingallina, *Organometallics*, 1990, **9**, 3127.
46. M. Murakami, T. Yoshida, S. Kawanami and Y. Ito, *J. Am. Chem. Soc.*, 1995, **117**, 6408.
47. A. Jutand, S. Négri and A. Principaud, *Eur. J. Inorg. Chem.*, 2005, **2005**, 631.
48. H. Tokuyama, T. Miyazaki, S. Yokoshima and T. Fukuyama, *Synlett*, 2003, 1512.

CHAPTER 4 : SYNTHESIS OF LINEAR PYRIDYL-TERMINATED RUTHENIUM COMPLEXES

4.1 ABSTRACT

In this chapter, the synthesis of some *trans*-$RuCl_{2-x}(dppe)_2(C{\equiv}C{-}R)_x$ complexes is discussed (dppe = 1,2-bis(diphenylphosphino)ethane; R = C_5H_4N, $[C_5H_4N{-}CH_3]^+$ and C_6H_5; x = 1, 2). Intended as precursors for a broader study of related linear multi- and hetero-metallic complexes (Ru, Os), difficulties utilizing 4-ethynylpyridine as a ligand somewhat limited progress. Whilst desired products could be made (as indicated by $^1H/^{31}P\{^1H\}$ NMR, and mass spectrometry), they contained significant impurities that were not easily removed. In contrast, analogous reactions with phenylacetylene proceeded cleanly, suggesting contaminants were formed from side reactions at the basic and nucleophilic pyridyl nitrogen.

Eventually, the unique combination of *cis*-$RuCl_2(dppe)_2$ and 4-ethynylpyridine (*vs*. other combinations with $[RuCl(dppe)_2]OTf$/4-ethynylpyridinium chloride) was found to provide a separable mixture, facilitating isolation of **17** in 68% yield *(Scheme 4-1,* top). Two general strategies for circumventing this problem were also explored, i) a protecting group approach using *N*-methyl-4-ethynylpyridinium triflate (**19**) *(Scheme 4-1*, bottom), and ii) a $16e^-$ centre avoidance rule *(Chapter 5)*. Selected complexes were further characterised by electrochemistry and UV-vis spectroscopy.

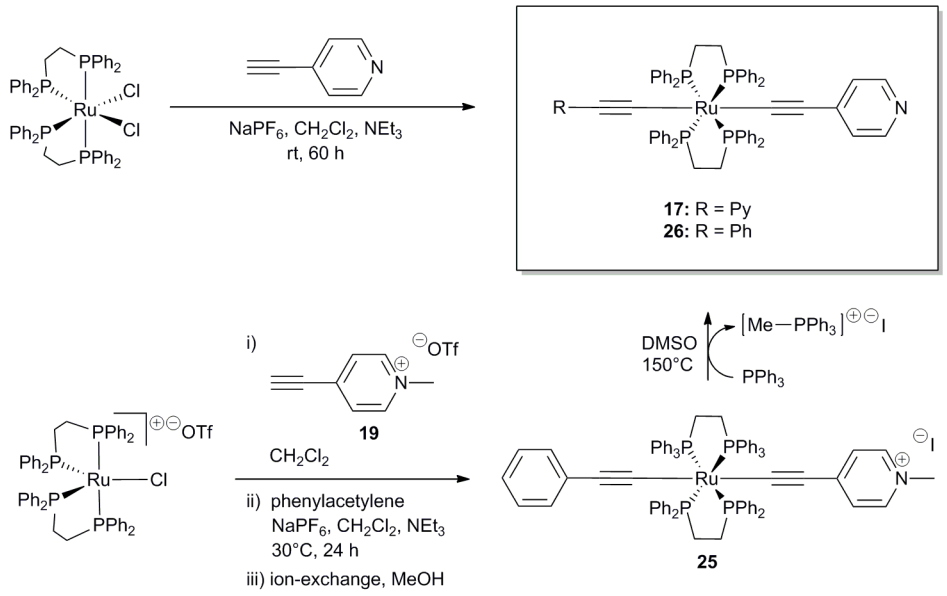

Scheme 4-1. Two approaches to the synthesis of pyridyl-terminated $Ru(dppe)_2$ complexes (a third methodology is explored experimentally in *Chapter 5)*.

4.2 BIS(ALKYNYL) RUTHENIUM COMPLEXES AS MOLECULAR ELECTRONIC COMPONENTS

4.2.1 Background

Ruthenium bis-alkynyl complexes are commonly studied as molecular electronic components. Akin to ferrocene systems *(Chapter 2)*, they are relatively air and moisture stable and exhibit reversible redox chemistry at low potentials. Furthermore, due to the linear and rigid nature of alkynyl ligands, and their fixed *trans* orientation at the metal centre, junction fabrication with these complexes is significantly more straightforward than with those containing more flexible ferrocene-based species (see *Chapter 2)*. It is also generally accepted that such compounds will function as good molecular conductors. Ruthenium metal d-orbitals are thought to be of suitable symmetry and energy for effective mixing with the frontier orbitals of conjugated ligands (*e.g.* polyynes, OPEs),[1] resulting in smaller HOMO-LUMO gaps (E_g) and as a result, higher conductance (assuming low R_0).[2] This is in contrast to platinum analogues –

$Pt(PEt_3)_2$ once declared a "true insulating centre" [3] – whose effectiveness as mediators of electron transport is currently the subject of conflicting reports.[4]

Relevant known examples feature $Ru(dppm)_2$,[5] Ru(16-TMC),[6] $Ru(dppe)_2$,[1,7] $Ru(dmpe)_2$[8] or $Ru_2(ap)_4$[2b,9] centres typically incorporated into OPE-type structures and comprising thioacetate, pyridyl, isocyanide, thioalkylsilyl or amino end groups for surface binding (dppm = 1,2-bis(diphenylphosphino)methane, 16-TMC = 1,5,9,13-tetramethyl-1,5,9,13-tetraazacyclohexadecane, dmpe = 1,2-bis(dimethylphosphino)methane, ap = 2-anilinopyridinate) *(Figure 4-1)*.

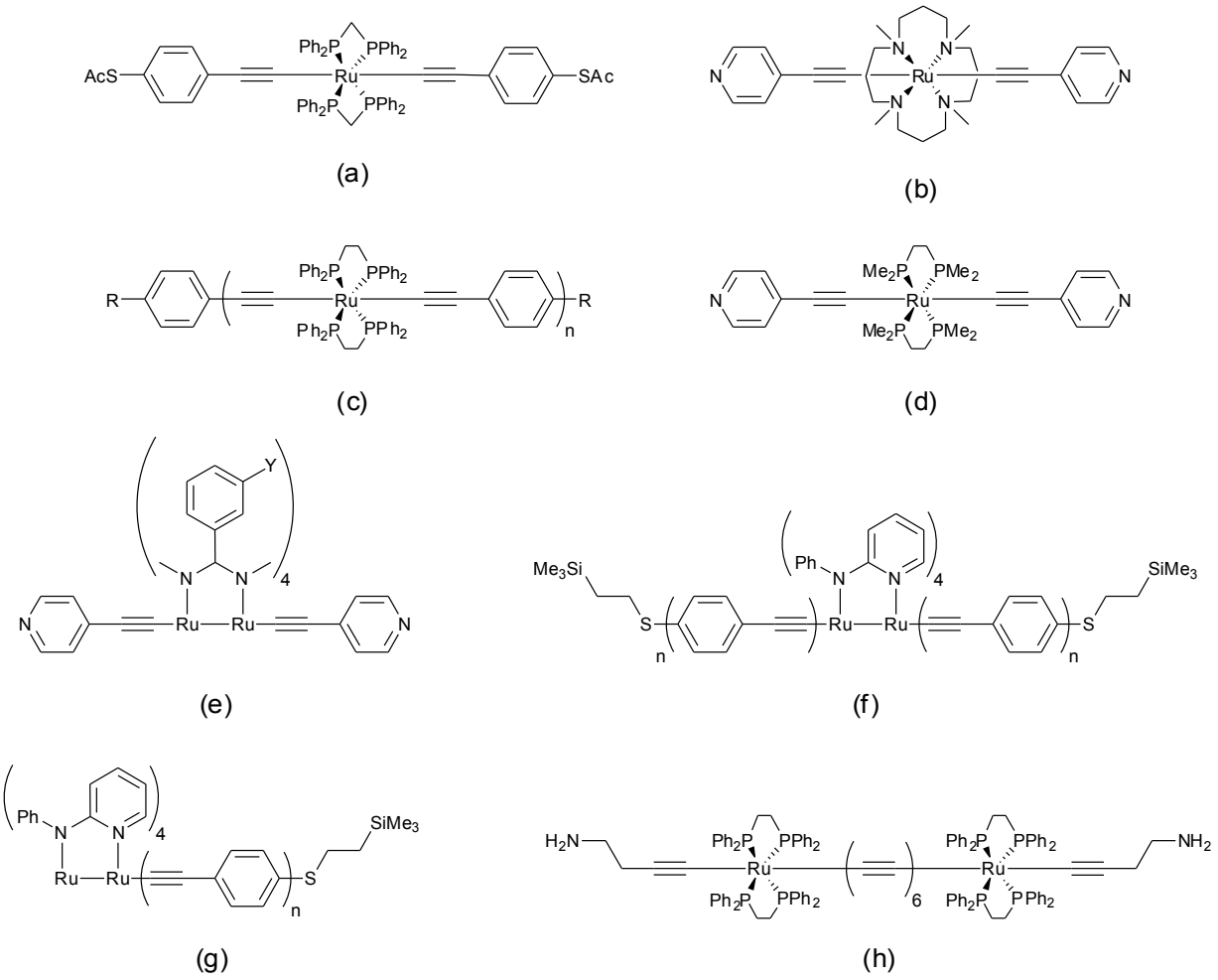

Figure 4-1. Some ruthenium σ-alkynyl complexes with terminal surface binding groups (R = NC, CH_2–SAc, O–$(CH_2)_6$–SAc; Y = H, OMe; $n_{(f,\,g)}$ = 1, 2; $n_{(c)}$ = 1-3).

4.2.2 Relevant junction conductance measurements

In 2005, Blum *et al.* studied individual or small groups of $Ru_2(ap)_4[\sigma(C{\equiv}CC_6H_4)_2S^-]$ *(Figure 4-1g*, n = 1) inserted into a self-assembled monolayer of undecanethiol.[2b] Whilst only a moderately low value of β = 0.59-0.88 (± 0.08-0.12) $Å^{-1}$ was obtained (using the STM apparent height method), in their setup, this was 15-45% smaller than that obtained for an all-organic analogue, suggesting the ruthenium compound was a superior 'molecular wire'. Similar results were obtained by Liu and co-workers in their studies of a thiolate-terminated $Ru(dppm)_2$ complex *(Figure 4-1a*, where $\beta = 1.01 \pm 0.25$ $Å^{-1}$ for Ru *vs.* 1.11 ± 0.18 $Å^{-1}$ for OPE).[5b]

Conductance measurements of electromigrated nanogap junctions containing molecules of *trans*-$Ru_2(ap)_4[\sigma(C{\equiv}CC_6H_4)_nS^-]_2$ *(Figure 4-1f*, n = 1, 2), revealed peaks (G_p) at specific voltages. These correlated with redox events of the molecule as measured by solution voltammetry,[9a] and were attributed to the alignment of molecular HOMO/LUMO energy levels and the metal electrode E_F with applied bias (*i.e. resonant* tunnelling).

Such features were also observed in a series of $Ru(dppe)_2$ complexes functionalised with terminal isocyanide (–NC) groups *(Figure 4-1c*, R = NC).[7b] The electron transfer properties of their Au-bound monolayers were investigated as a function of molecular length and temperature, exhibiting a value of $\beta = 0.09$ $Å^{-1}$ (at ambient temperature, from plots of resistance *vs.* molecular length) – encouragingly low compared to that of typical conjugated organic wires (β = 0.06–0.63 $Å^{-1}$, *Table 1-1)* and significantly smaller than that obtained for $Ru_2(ap)_4[\sigma(C{\equiv}CC_6H_4)_2S^-]$.[2b] However, an exceptionally large contact resistance ($R_0 = 4.2 \times 10^8$ Ω) was extrapolated from the data, attributed to the nature of the Au-CN linkage. Whilst charge transfer through the mono- and di-nuclear complexes was shown to be largely independent of temperature (suggestive of a tunnelling mechanism), Coulomb blockade-like behaviour was observed for the tri-nuclear complex at 5 K (attributed to the large R_0, which would favour charge localisation on the molecule). Related thiolate-terminated complexes were subsequently studied (*Figure 4-1c*, R = CH_2–SAc, O–$(CH_2)_6$–SAc), showing reduced contact resistances (1.01×10^5, 1.44×10^6 Ω), with comparable β values (0.1-0.16 $Å^{-1}$) and length/temperature-dependant transport mechanisms.[7c]

Electron transfer through these materials likely occurs via hole-mediated mechanisms, as inferred by correlation of G_p with molecular *oxidation* events observed in solution voltammetry (note however that G_p occurs where E_F is in resonance with a molecular level, not at the equilibrium potential). Furthermore, density functional theory calculations of a thiolate-

terminated Ru(dppm)$_2$ complex *(Figure 4-1a)* showed the HOMO spanned the whole length of the molecule, in contrast to the LUMO which was localised on the metal centre.[5b] With the Ru(dppe)$_2$ complexes of the Rigaut/Frisbie groups *(Figure 4-1c)*, hole-mediated processes were alluded to in explanations as to why the thiolate-terminated compounds exhibit lower R_0 than their isocyanide analogues, *i.e.* that the orientation of the Au–S dipole brings the HOMO closer to E_F, reducing ΔE_{DA}.[7c]

4.2.3 Synthetic methodology

Reviewed by Long and Williams in 2003,[10] M–C≡C–R σ-bond forming routes include: i) dehydrohalogenation (often Cu^I catalysed);[11] ii) metathesis using trimethylstannyl reagents (sometimes Pd^0 catalysed);[12] iii) displacement using alkali-/alkali-earth-metal alkynyl complexes;[13] iv) methane,[14] v) N_2,[15] or vi) H_2 elimination;[16] vii) vinylidene formation;[17] viii) use of R–C≡C^+ synthons (from alkynyliodinium triflates);[18] ix) the sodium methoxide method;[19] x) alkynyl ligand exchange;[20] and xi) C–C bond activation;[21] amongst others *(Scheme 4-2)*.

Only a handful of methods are known for the controlled synthesis of *asymmetric* bis-alkynyl metal centres,* however. Metal/ligand specific, approaches are now established for Ru(dppe)$_2$,[17b,c] Ru(dmpe)$_2$,[22] Fe(dmpe),[23] Os(dppm)$_2$,[24] W(dppe)$_2$,[25] Mn(dmpe)$_2$[26] and $Ru_2(ap)_4$[27] centres. These have been utilised in most syntheses of multi-metallic molecular electronic components (which typically proceed via asymmetric intermediates).

* Though these may be prepared via stoichiometric control of reagents, lengthy purification is often required to isolate desired materials from the mixtures that readily form.

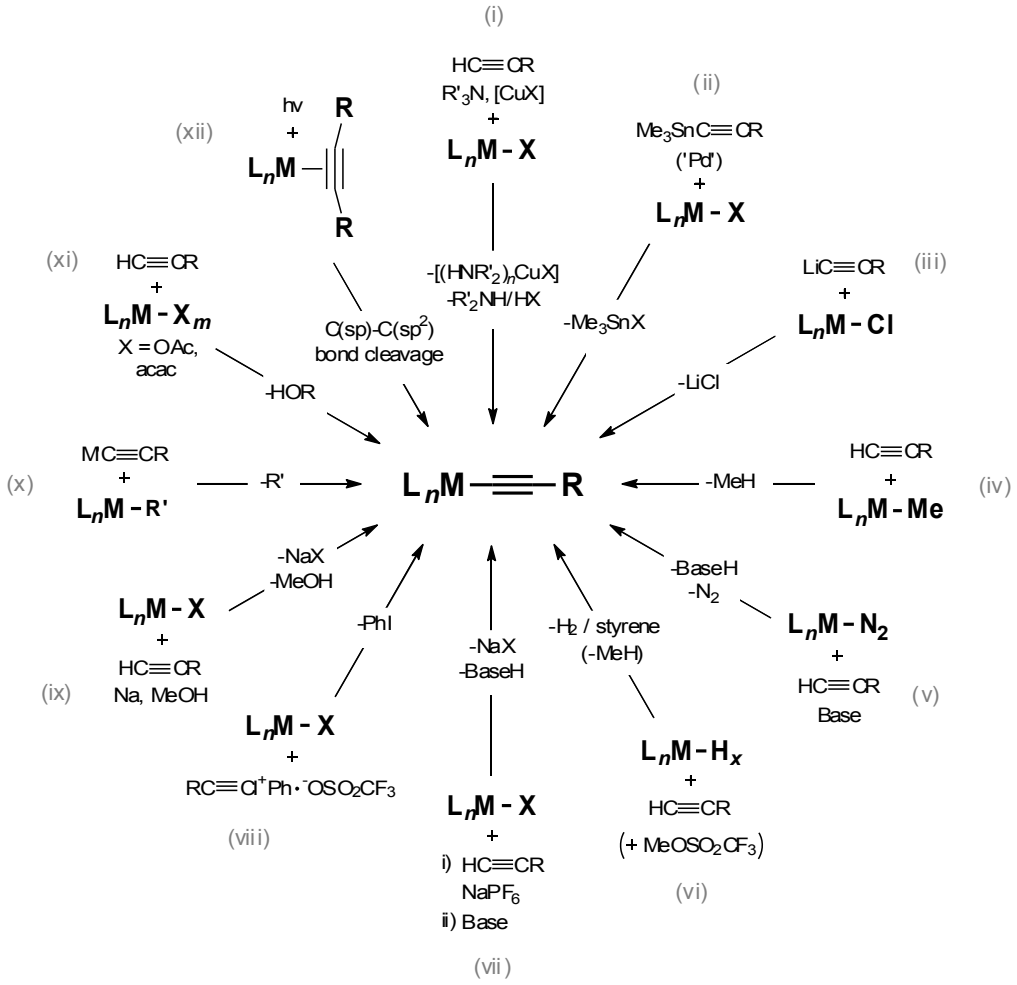

Scheme 4-2. A survey of M–C≡C–R σ-bond forming routes (roman numerals refer to descriptions in the bulk text).[28]

For producing asymmetrical ruthenium-containing systems (the focus of this work), vinylidene formation is arguably the most convenient method *(Scheme 4-2*, vii). This utilizes readily prepared chloride complex precursors (rather than hydride, dinitrogen, or methylated variants) and terminal alkynes (rather than their lithiated or stannylated equivalents) (*Scheme 4-2*). Pioneered by Dixneuf and co-workers in the 1990s,[17b,c] work then and since has shown that different ruthenium starting materials (*cis*-$RuCl_2(dppe)_2$/[RuCl(dppe)]OTf), halide abstracting agents ($NaPF_6$ or AgOTf) or base (1,8-diazabicycloundec-7-ene, NEt_3, KO^tBu, alumina) may be successfully used, with reactions typically run in CH_2Cl_2 or MeOH.

The mechanism of this process, particularly relevant to discussions later, is thought to involve η^2-coordination of alkyne to a 5-coordinate, 16e$^-$ ruthenium centre (previously generated by abstraction of chloride by $NaPF_6$ or similar salt, and loss of NaCl) *(Scheme 4-3)*. This species then undergoes a 1,2-hydrogen shift[29] to form the vinylidene which may subsequently be isolated (in the absence of base). Deprotonation affords the mono-alkynyl species, which can be further reacted with additional alkyne, halide abstracting agent and base (typically NEt_3) to yield the desired *trans*-bis-alkynyl complex.

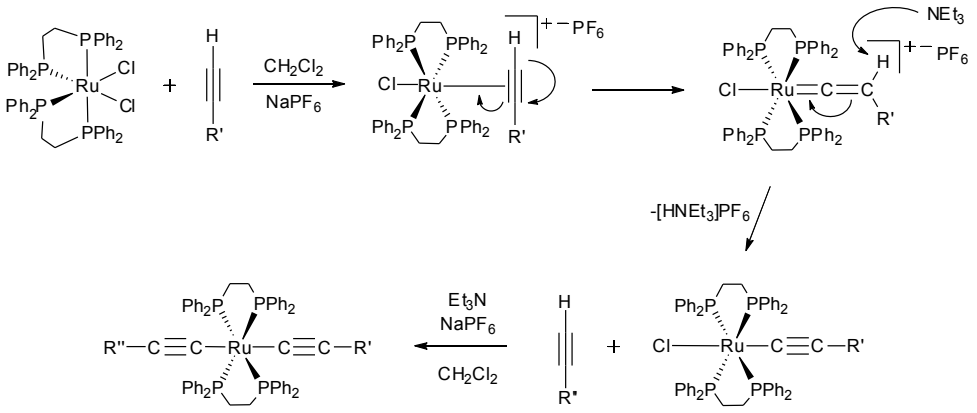

Scheme 4-3. Step-wise mechanism of bis-acetylide formation using Ru(dppe)$_2$ centres.[1a,17c,29-30]

It should be stressed that *trans*-$RuCl_2$(dppe)$_2$ and *cis*-$RuCl_2$(dppm)$_2$ are largely unsuitable starting materials for such syntheses. It was reported that reactions between *trans*-$RuCl_2$(dppe)$_2$ and terminal acetylenes required 5-7 days to form vinylidene species, compared with 6-12 hours with *cis*-$RuCl_2$(dppe)$_2$.[24] This may be attributed to the *trans effect* (as coordinated phosphorus ligands have a greater *trans*-directing influence than chloride),[31] or be because *cis* to *trans* isomerisation during acetylide addition is a driving force.[24] Furthermore, bis-alkynyl species are not readily prepared in good yields from mono-alkynyl dppm complexes (*e.g. trans*–RuCl(C≡CR)(dppm)$_2$).[17b,c,32]

4.2.4 Motivation for this work

The synthesis of linear analogues *(Figure 4-2a)* was considered a prudent endeavour prior to the preparation of branched and macrocyclic Ru(dppe)$_2$-containing complexes *(Chapter 5)*. As in

Chapter 2, it was intended that the 3,5-diethynylpyridyl motif should provide branching/surface-binding functions, yet it was unclear whether terminal pyridyl moieties could be successfully incorporated into $Ru(dppe)_2$-containing structures.

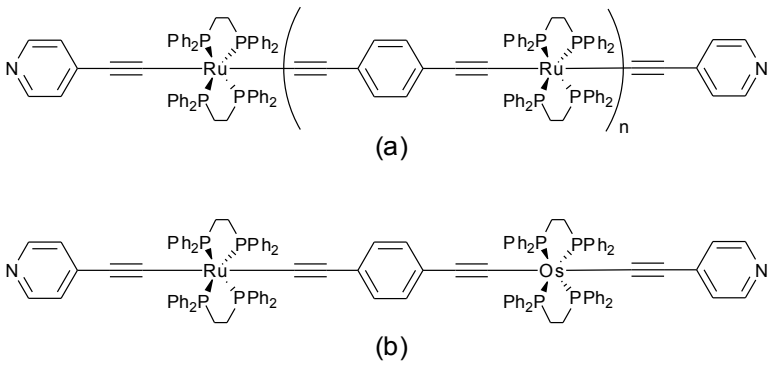

Figure 4-2. Target linear ruthenium and osmium complexes, designed as molecular wires (a) or diodes (b) (n = 0, 1, 2).

Conceived as two-terminal molecular wires in their own right – not single branched analogues of macrocyclic systems (*i.e. Chapter 2, Figure 2-7)* – 4-pyridyl moieties were chosen as terminal groups to facilitate perpendicular coordination on electrode surfaces. An all-ruthenium series was envisaged *(Figure 4-2a)*, to explore the effects of the pyridyl group on contact resistance (in line with aforementioned publications by Rigaut/Frisbie *et al.*[7b,c]), with heterometallic (Ru, Os) analogues *(Figure 4-2b)* intended as single-molecule diodes (as a result of their inherent electronic asymmetry, see *Chapter 2)*.

4.3 SYNTHESIS

Following strategies successfully utilized elsewhere,[1] syntheses of pyridyl-terminated linear molecular targets *(Figure 4-2)* were planned as shown in *Scheme 4-4* (the intended route to trinuclear complexes is not shown, but would proceed similarly).[†]

[†] Several other routes were of course plausible (but not explored), such as from $RuCl(dppm)_2(\mu\text{-}C{\equiv}C{-}C_6H_4{-}C{\equiv}C)OsCl(dppm)_2$ (a chloride-terminated analogue of *Figure 4-2b*, prepared previously by Younus *et al.*[33]).

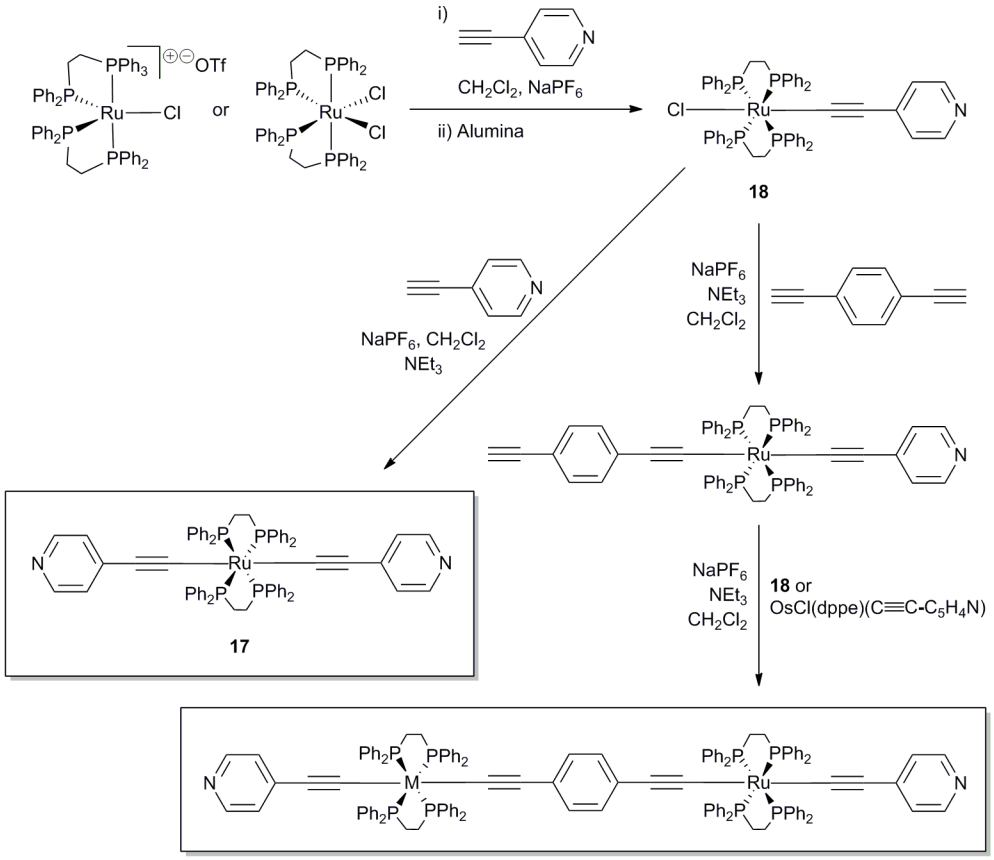

Scheme 4-4. Proposed route to pyridyl-terminated $M(dppe)_2$ complexes (M = Ru, Os).

4.3.1 [RuCl(dppe)$_2$]OTf and *cis*-RuCl$_2$(dppe)$_2$

Preparation of *cis*-$RuCl_2(dppe)_2$ was initially challenging. Several publications clearly indicate its synthesis should proceed via ligand exchange of $RuCl_2(dmso)_4$ with dppe, following the method of Chaudret *et al.* for *cis*-$RuCl_2(dppm)_2$.[34] Whilst this is a convenient way to prepare the latter, attempts here using dppe typically yielded a difficult to separate mixture of *cis*- and *trans*-isomers *(Figure 4-3a*, and noted previously[24]*),* the latter being most thermodynamically stable. During the course of these investigations similar findings were corroborated by Fox *et al.*,[30] who developed a more reliable synthesis *(Scheme 4-5)*. Their route (from $RuCl_3{\cdot}nH_2O$) was successfully used to prepare all the ruthenium starting materials required for this work *(Figure 4-3b-d)*.

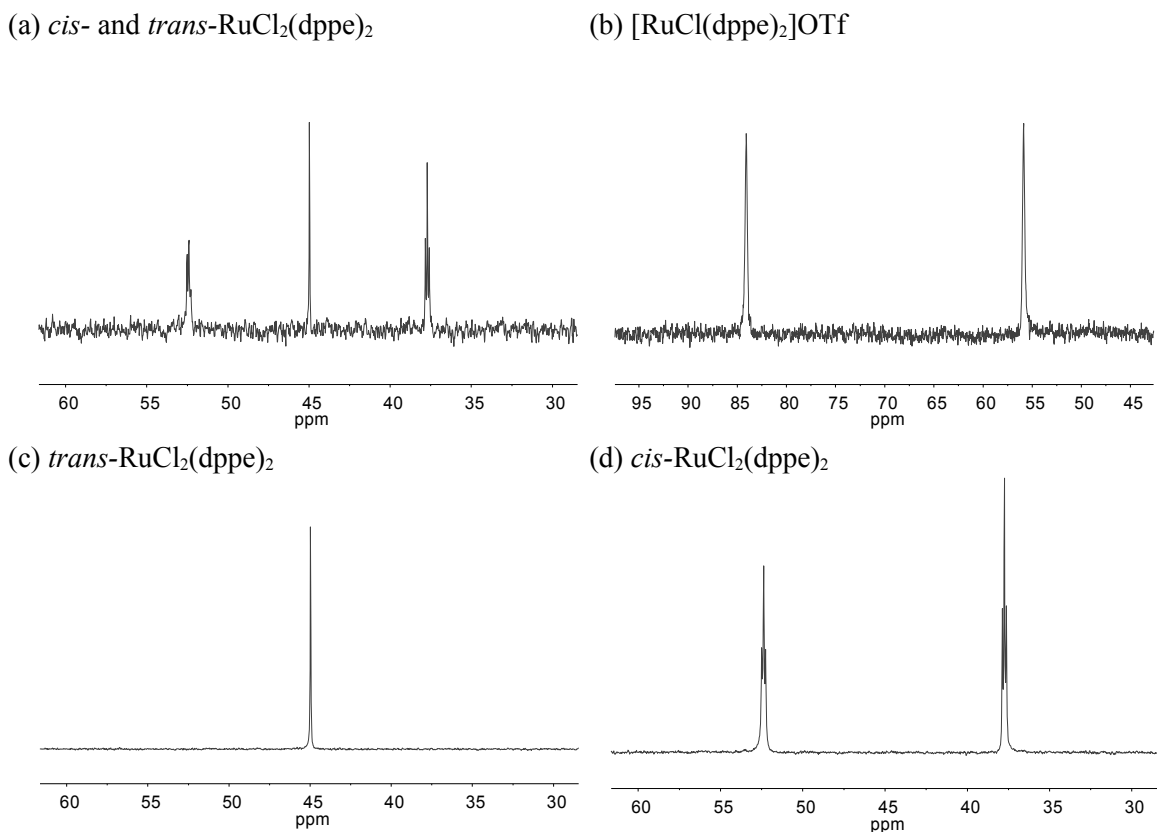

Figure 4-3. $^{31}P\{^{1}H\}$ NMR spectra of (a) the mixture of *cis*- and *trans*-$RuCl_2(dppe)_2$ produced from $RuCl_2(dmso)_4$/dppe,[34] and (b) pure $[RuCl(dppe)_2]OTf$, (c) *trans*-$RuCl_2(dppe)_2$ and (d) *cis*-$RuCl_2(dppe)_2$ prepared using the method of Fox *et al.*[30]

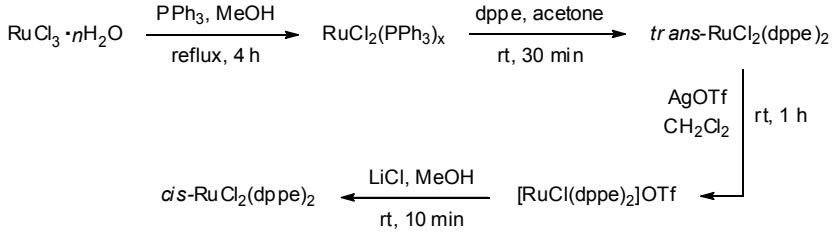

Scheme 4-5. A robust synthesis of $[RuCl(dppe)_2]OTf$ and *cis*–$RuCl_2(dppe)_2$ (x = 3, 4).[30] The first step typically produced either $RuCl_2(PPh_3)_3$, $RuCl_2(PPh_3)_4$, or a mixture (deduced from its $^{31}P\{^{1}H\}$ NMR spectrum[35]), but all materials could be successfully reacted on to form *trans*-$RuCl_2(dppe)_2$.

4.3.2 Syntheses with 4-ethynylpyridine

Preparation of the ligand

Though alternative precursors were commercially available (*i.e.* 4-ethynylpyridinium chloride, 4-bromopyridinium chloride, 4-vinylpyridine[36]), 4-ethynylpyridine was routinely and conveniently prepared on the gram-scale from 4-aminopyridine *(Scheme 4-6)*.[37] In this procedure a modified Sandmeyer reaction was used to generate 4-iodopyridine, which was rapidly reacted on via Sonogashira coupling with trimethylsilylacetylene (to avoid potential decomposition via onium polymerisation[38]). After desilylation, crude material was sublimed at ~60°C/1 mmHg to provide the product as a colourless crystalline solid.

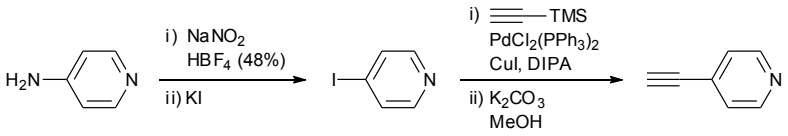

Scheme 4-6. A reproducible synthesis of 4-ethynylpyridine.[37]

Formation of σ-alkynyl complexes

The synthesis of $RuCl(dppe)_2(C{\equiv}C{-}C_5H_4N)$ (**18**) from reaction of 4-ethynylpyridine and $[RuCl(dppe)_2]OTf$ *(Scheme 4-4*, step 1) was not as straightforward. Though it was evident from $^1H/^{31}P\{^1H\}$ NMR and mass spectra that the desired complex had formed, significant impurities were always produced *(Figure 4-4a)*. Considerable efforts to avoid their formation (by varying reactant ratios, relative solvent quantity, reaction time, etc) or to remove them from the bulk material using column chromatography/fractional recrystallization, proved futile. Such persistent contaminants were not observed using phenylacetylene *(Figure 4-4b)*, so their formation was attributed to side-reactions at the basic and nucleophilic pyridyl nitrogen *(Scheme 4-7)*.

Similar problems had been anticipated or encountered elsewhere. In their successful syntheses of isocyanide-terminated complexes *(Figure 4-2c*, R = NC), Olivier *et al.* justified use of protecting groups to "avoid any complexation of the isocyanide function to 16-electron ruthenium intermediates".[1a] Furthermore, from $[RuCl(dppe)_2]OTf$, Fox *et al.* observed formation of bis-alkynyl species when using 4–ethynylaniline (due to the ligands' basicity), and of various

side-products with 4–ethynylbenzonitrile (attributed to "competitive coordination and chloride substitution reactions involving the nitrile moiety").[30]

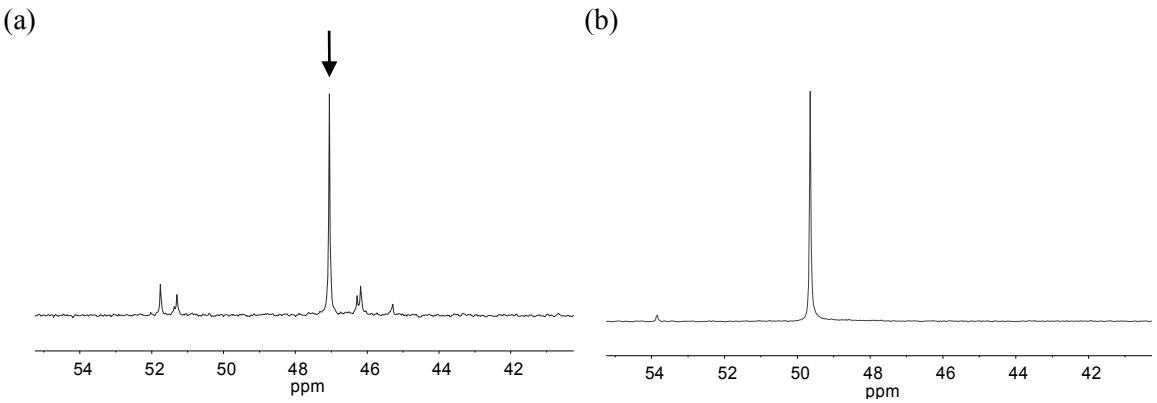

Figure 4-4. Selected $^{31}P\{^{1}H\}$ NMR spectra ($CDCl_3$) showing resonances attributable to (a) crude **18** prepared from $[RuCl(dppe)_2]OTf$/4-ethynylpyridine (product indicated by arrow), (b) $RuCl(dppe)_2(C{\equiv}C–C_6H_5)$ (~97% pure) from $[RuCl(dppe)_2]OTf$/phenylacetylene.

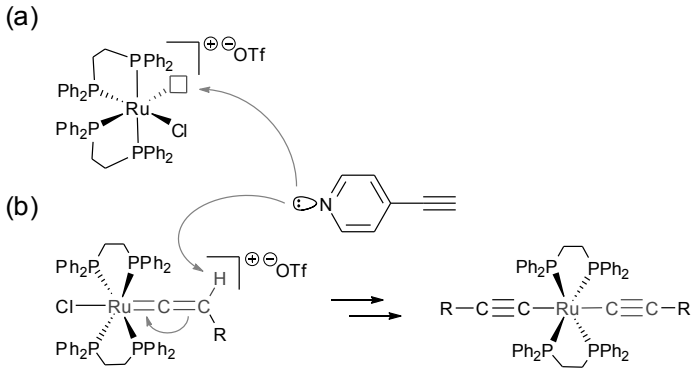

Scheme 4-7. Potential side reactions in ruthenium σ-alkynyl bond formation when using 4-ethynylpyridine.

Eventually, in trying all the combinations of reasonable starting materials,[‡] the reaction of 4-ethynylpyridine and *cis*-$RuCl_2(dppe)_2$ permitted isolation of an otherwise clean mixture of **18** (75%) and $Ru(dppe)_2(C{\equiv}C–C_5H_4N)_2$ (**17**, 25%) *(Scheme 4-4) (Figure 4-5a)*. Whilst side reactions

[‡] $[RuCl(dppe)]OTf$, *cis*-$RuCl_2(dppe)_2$, 4-ethynylpyridine, 4-ethynylpyridinium chloride. The reaction of $[RuCl(dppe)]OTf$ and 4-ethynylpyridinium chloride produced even more impurities, plausibly due to nucleophilic attack of chloride at the metal centre.

were still evident, the majority of impurities could now be removed by column chromatography (alumina grade II, CH_2Cl_2/MeOH [95:5]). So far, efforts to isolate **18** from its mixture with **17** have proven unsuccessful, but the latter could be obtained in pure form following extended stirring of *cis*-$RuCl_2(dppe)_2$ with excess 4-ethynylpyridine, $NaPF_6$ and NEt_3 *(Scheme 4-1*, top) *(Figure 4-5b)*.

Bis-acetylide formation in the absence of added base may be reasonably explained by deprotonation of the vinylidene intermediate by the basic pyridyl moiety, facilitating coordination of a second 4-ethynylpyridine ligand (*i.e. Scheme 4-7b)*. This has been observed with some pyridyl-terminated $CpRu(PPh_3)_2$ vinylidenes/acetylides.[39] Alternatively, a more unusual hypothesis (though in line with similar observations discussed later) entertains the possibility that bis-acetylide formation may have occurred on the alumina column prior to or during elution.

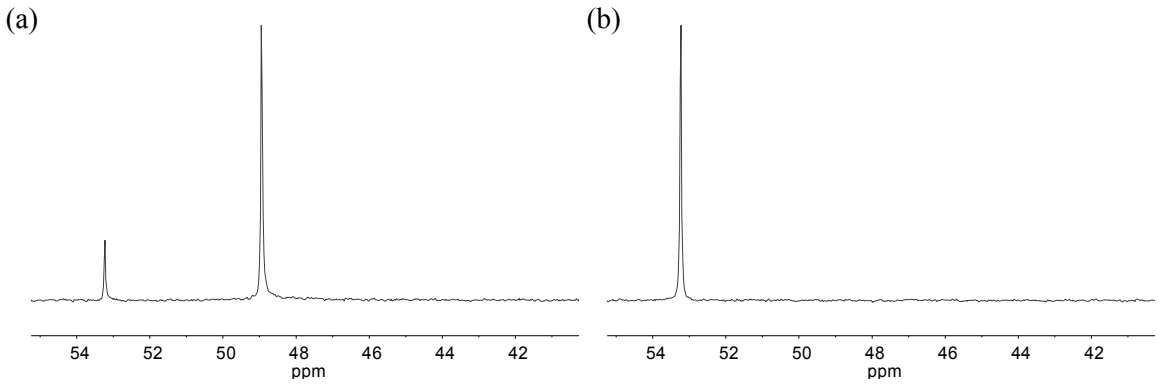

Figure 4-5. Selected $^{31}P\{^1H\}$ NMR spectra ($CDCl_3$) showing resonances attributable to (a) a mixture of **17**/**18** and (b) pure **17** prepared from *cis*-$RuCl_2(dppe)_2$/4-ethynylpyridine.

Complexes were identified by integration of relevant pyridyl, phenyl and CH_2 resonances in their ^1H NMR spectra *(e.g. Figure 4-6)*, $^{31}P\{^1H\}$ NMR resonances at approximately δ 49 and 53 ppm (indicative of mono- and bis-alkynyl $Ru(dppe)_2$ complexes, respectively) *(Figure 4-5)* and further characterised by IR spectroscopy, $^{13}C\{^1H\}$ NMR and accurate mass/elemental analyses (see *Chapter 8* for full details). Single crystal X-ray analysis of **17** confirmed correct structural assignment *(Figure 4-7)*, with bond lengths and angles (including the slight deviation from

linearity exhibited by the coordinated acetylenic ligands[12c]) typical of similar complexes *(Table 4-1)*.

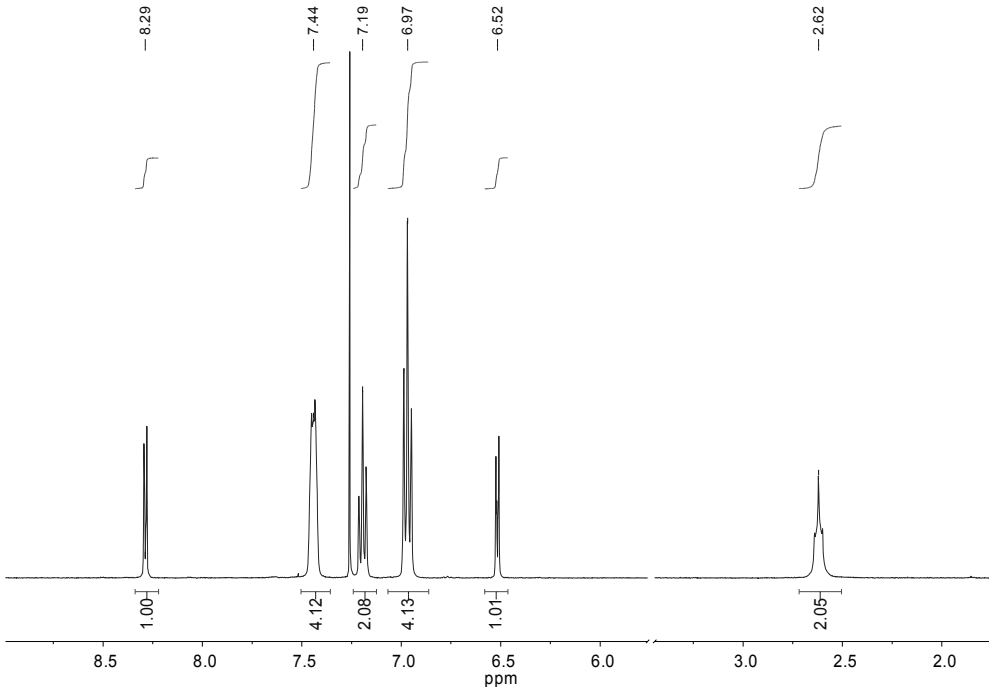

Figure 4-6. The ^{1}H NMR spectrum ($CDCl_3$) of **17**. Doublets at δ 8.29 and 6.52 ppm correspond to Py–*H*, the broad multiplet at 2.62 is assigned to C*H*$_2$ (dppe), and the remaining aromatic resonances attributed to Ph–*H* (dppe).

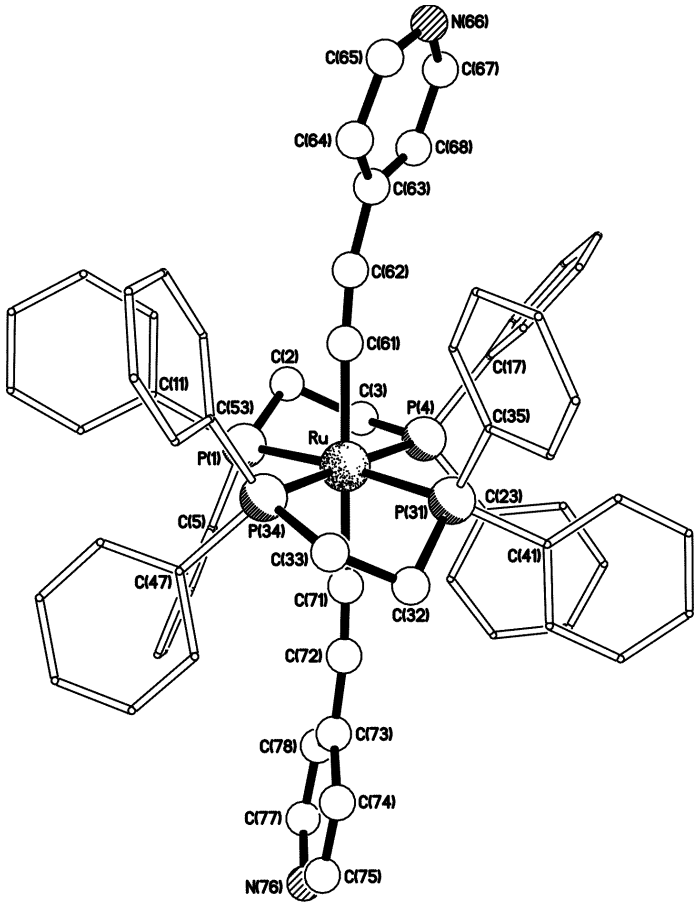

Figure 4-7. X-ray crystal structure of **17** (hydrogen atoms removed for clarity).

Table 4-1. Selected bond lengths and angles for some symmetrical ruthenium bis-acetylide complexes.

complex	Ru–C (Å)	Ru–P (Å)	C≡C (Å)	C≡C–R (°)[a]	ref
$Ru(dppe)_2(C{\equiv}C{-}C_6H_5)_2$	2.060	2.356	1.207	173.23	*12c*
	2.064	2.360	1.194	166.07	
		2.363			
		2.362			
$Ru(dmpe)_2(C{\equiv}C{-}C_5H_4\text{-}p\text{-}{}^t\!Bu)_2$	2.057	2.306	1.218	176.81	*40*
	2.057	2.309	1.224	175.03	
		2.317			
		2.306			
$Ru(dppe)_2(C{\equiv}C{-}C_5H_4N)_2$ (**17**)	2.052	2.365	1.220	164.81	this work
	2.052	2.357	1.223	171.47	
		2.357			
		2.368			

[a] Defined by the plane of the aromatic ring to the plane of the C≡C bond.

Given the numerous examples of σ-alkynyl pyridyl-terminated ruthenium complexes known *(Figure 4-8*, in addition to *Figure 4-2b* and *d)*,[21,23,42,44] the general difficulties encountered here in preparing analogous $Ru(dppe)_2$-containing materials are perhaps surprising. However, with different ancillary ligands (16-TMC, dmpe, dppm, Cp/PPh_3), or alternative σ-alkynyl bond forming reactions (*e.g.* the sodium methoxide method), syntheses are potentially shielded against pyridyl coordination/deprotonation problems. Whilst it might be suggested that such methods could be harnessed in preparing the target molecules of this chapter, none compare favourably with the $Ru(dppe)_2$/vinylidene approach when, as in this case, high yielding preparations of unsymmetrical bis-alkynyl complexes are paramount.

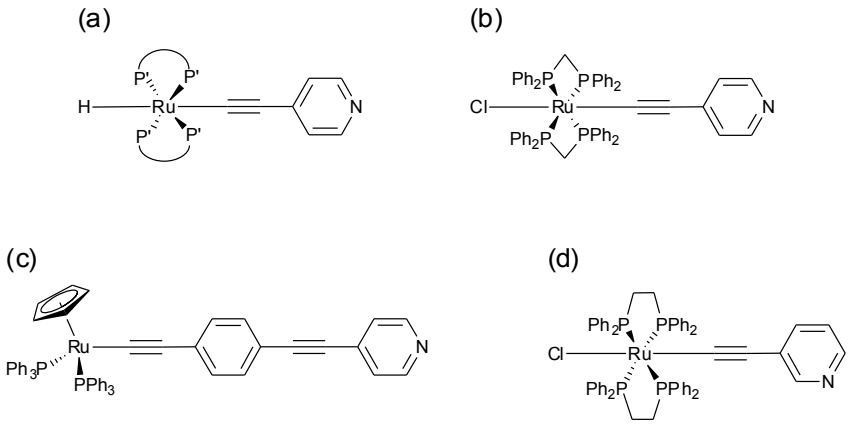

Figure 4-8. Further examples of pyridyl-terminated ruthenium complexes (P'–P' = dppe, dppm).

Instability of pyridyl-terminated Ru(dppe)$_2$ complexes in CH_2Cl_2

Following their isolation it became apparent that **17**, and pyridyl-terminated Ru(dppe)$_2$ complexes in general, visually react/decompose upon extended contact with CH_2Cl_2 (changing colour from bright yellow to red, or darkening).[§] Similar observations were noted with CH_2Cl_2 solutions of RuCl(dppm)$_2$(C≡C–C_5H_4N) *(Figure 4-8b)*, tentatively attributed by the authors to protonation of the pendant pyridyl nitrogen (*i.e. Figure 4-9a)*.[41] An alternative explanation may be the formation of methylenebispyridinium dichlorides *(Figure 4-9b)*, via a reaction analogous to that recently observed between organic pyridines and CH_2Cl_2 under ambient conditions.[42] In stark contrast, these materials exhibit a significantly higher stability in $CHCl_3$.

[§] This is particularly remarkable considering they are synthesised in CH_2Cl_2, and that single crystals of **17** for X-ray diffraction were grown from vapour diffusion of diethyl ether into an oxygenated CH_2Cl_2 solution.

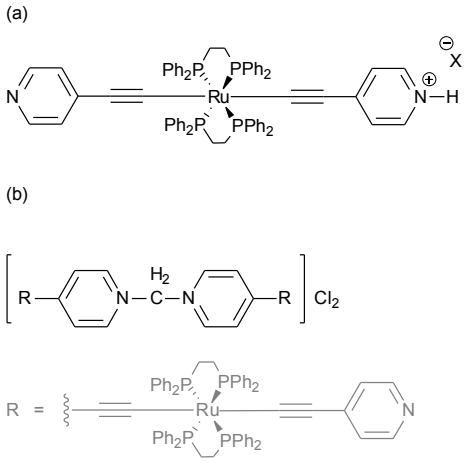

Figure 4-9. Plausible products formed by reaction/decomposition of **17** in CH_2Cl_2: (a) protonation,[41] (b) formation of methylenebispyridinium dichlorides.[42]

Of further intrigue, the reaction between **17** and CH_2Cl_2 is either more rapid at lower concentrations, or exhibits a significant kinetic isotope effect. No colour change in a saturated CD_2Cl_2 solution was observed over several days, though the slow formation of new aromatic peaks could be monitored by ^1H NMR spectroscopy *(Figure 4-11)*. In contrast, dilute CH_2Cl_2 solutions of **17** (for UV-vis spectroscopy) changed colour from yellow to pale red after just 1 day. This is explicitly shown by their measured absorption spectra *(Figure 4-10)*, whereby an intense band at 435 nm is entirely replaced by a broader, weaker one at 528 nm. Assuming both transitions are attributable to MLCT bands, this bathochromic shift indicates greater electron withdrawing ligand character *(section 4.5)*, as would be expected following protonation/quaternization of the pyridyl nitrogen.

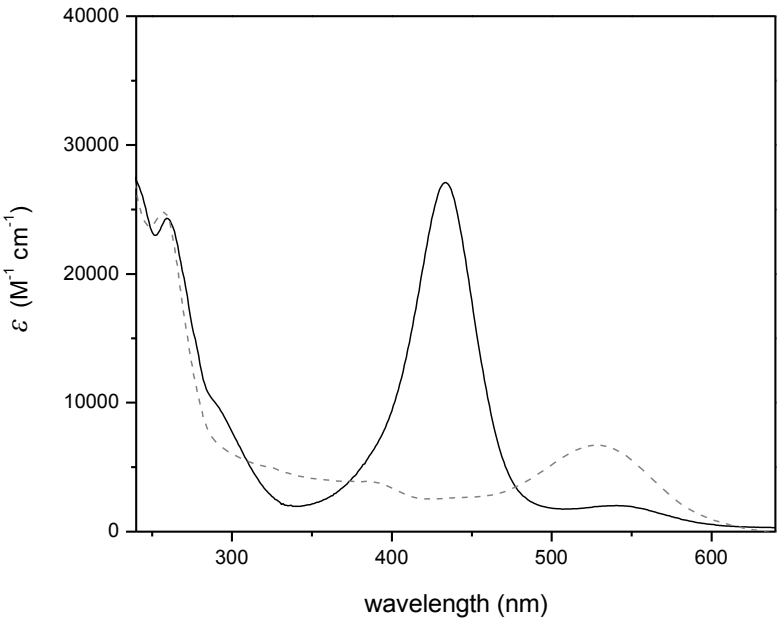

Figure 4-10. UV-vis spectra of **17** in CH_2Cl_2 – measured after initial dissolution (black solid line, yellow solution), and 1 day (red dashed line, pale red solution).

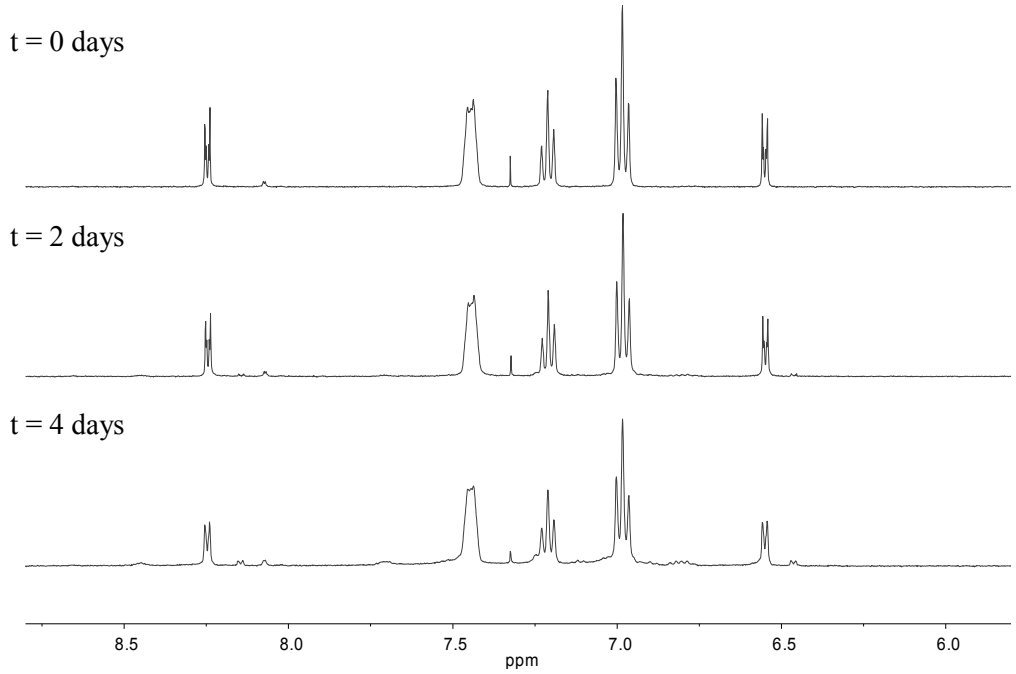

Figure 4-11. Selected $^{1}H/^{31}P\{^{1}H\}$ NMR spectra of **17** (aromatic region, CD_2Cl_2) recorded over several days.

4.3.3 A 'protecting group' strategy (reactions using *N*-methyl-4-ethynylpyridinium triflate)

It is apparent that utilization of 4-ethynylpyridine as a traditional acetylide ligand has some fundamental disadvantages and limitations. The development of alternative, more synthetically robust approaches to pyridyl-terminated alkynyl complexes was desirable,[**] and this section thus describes efforts towards a protecting group strategy. If the lone pair of the pyridyl nitrogen could be preoccupied until it was needed for surface binding, syntheses such as those shown in *Scheme 4-4* could likely proceed with fewer complications.

Synthesis of a protected 4-ethynylpyridine ligand

Several moieties may be installed at a pyridyl nitrogen, via protonation[43] (forming pyridinium halides), alkylation[44] (*N*-alkyl pyridinium halides), borane complexation[45] (pyridine-borane adducts) or oxidation[46] (pyridine *N*-oxides). These can be removed as and when is required using the appropriate reagents/conditions *(Scheme 4-8)*.[††]

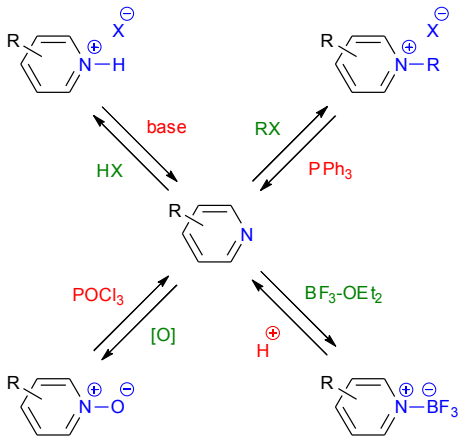

Scheme 4-8. Some protecting group approaches for pyridine.

[**] Specifically for $Ru(dppe)_2$, but methods could be broadly applicable.

[††] Coordination to a metal centre was also considered as a protecting group approach, such as in known examples where the 4-ethynylpyridine motif is bound to $W(CO)_nL$ (n = 3-5; L = CO, PPh_3, $P(OMe)_3$, PMe_3, dppe),[39,47] or $[Re(2,2'\text{-bipy})(CO)_3]PF_6$ centres.[39] However, methods to selectively remove these metal fragments are not known, and the stability of such complexes under subsequent reaction conditions was questionable.

As a protecting group in this context, pyridinium halides are of no real use as they would be deprotonated during bis-acetylide formation *(Scheme 4-3)*. Pyridine *N*-oxides were also deemed unsuitable as their metal coordination via oxygen is well known, potentially offering no benefit over the free amine.

Alkylation and borane complexation seemed reasonable options, but presented problems specific to the terminal alkyne functionality. Whilst nitrogen quaternization may proceed without significant event for many substituted pyridines, with 4-ethynylpyridine this has been observed to activate the carbon-carbon triple bond towards polyacetylene formation *(Scheme 4-9a)*.[48] It was also considered that use of BH_3 in forming borane adducts could result in anti-Markovnikov hydroboration products *(Scheme 4-9b)*.[49] Indeed, attempts reacting 4-ethynylpyridine with 1-chloropropane (heating in ethanol) or 1-bromobutane (heating in toluene) produced dark black/blue (polymerized) products that were only significantly soluble in DMSO. Syntheses with $BH_3{\cdot}SMe_2$ or $BF_3{\cdot}OEt_2$ (at ambient temperature in ether[45b]) also proved largely unsuccessful.

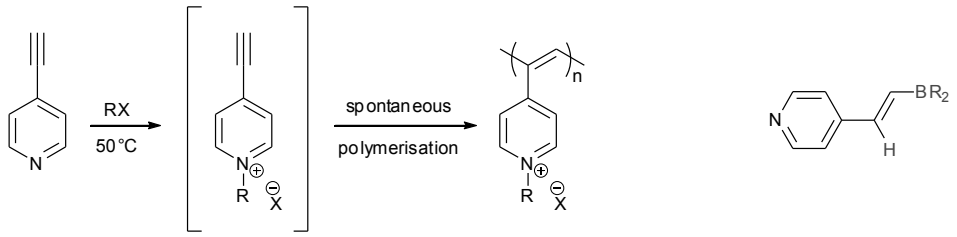

Scheme 4-9. Problems with alkylation or borane complexation of 4-ethynylpyridine: (a) activation of C≡C towards polyacetylene formation,[48] and (b) hydroboration product(s) with BH_3.[49]

Only one stable example of 4-ethynylpyridine with a quaternized nitrogen is known (aside from metal complex adducts, *e.g.* Re(2,2'-bipy)$(CO)_3$(Py–C≡C–H)[39]). Remarkably, two syntheses of this rather unique *N*-methyl-4-ethynylpyridinium cation, as triflate[50] (**19**) and iodide/perchlorate[51] salts, were published independently in 1992. Both utilize low temperatures (0°C), suggesting formation of polyacetylenes upon nitrogen quaternization is in some part thermally activated. With slight modification[52] of the procedure for **19**, the triflate and iodide

salts of *N*-methyl-4-ethynylpyridinium were obtained as off-white and dark solids, respectively *(Scheme 4-10)*.

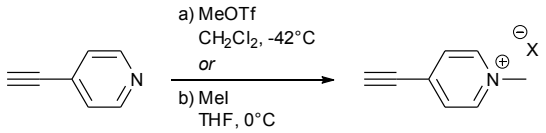

Scheme 4-10. Syntheses of *N*-methyl-4-ethynylpyridinium triflate (**19**, X = OTf) and *N*-methyl-4-ethynylpyridinium iodide (X = I).

Formation of σ-alkynyl complexes

Using *N*-methyl-4-ethynylpyridinium triflate, syntheses of σ-alkynyl complexes from $[RuCl(dppe)_2]OTf$ proceeded cleanly *(Scheme 4-11)*, supporting the hypothesis that the nitrogen lone pair was the cause of impurities in previous experiments.[‡‡] Deprotonation of the intermediate vinylidene species (**22**) and removal of excess ligand (alumina grade II, acetone) provided $[RuCl(dppe)_2(C_5H_4N–CH_3)]OTf$ (**20**) in 57% yield. Retention of *N*-methyl functionalities and triflate anions was confirmed by the presence of singlet resonances at approximately δ 4.1 ppm (Py–CH_3) and δ -79 ppm (S–CF_3) in their ^1H and $^{19}F\{^1H\}$ NMR spectra, respectively. Whilst **22** could not be isolated by chromatography (forming **20**) or recrystallization (co-crystallising with **19**), crystals suitable for X-ray analysis were obtained, confirming its structure *(Figure 4-12)*.

[‡‡] Reaction of *N*-methyl-4-ethynylpyridinium iodide with $[RuCl(dppe)_2]OTf$ resulted in even more side-products than with 4-ethynylpyridine, presumably due to the nucleophilicity of the iodide anion (relative to halides, triflate is weakly coordinating and non-nucleophilic[53]).

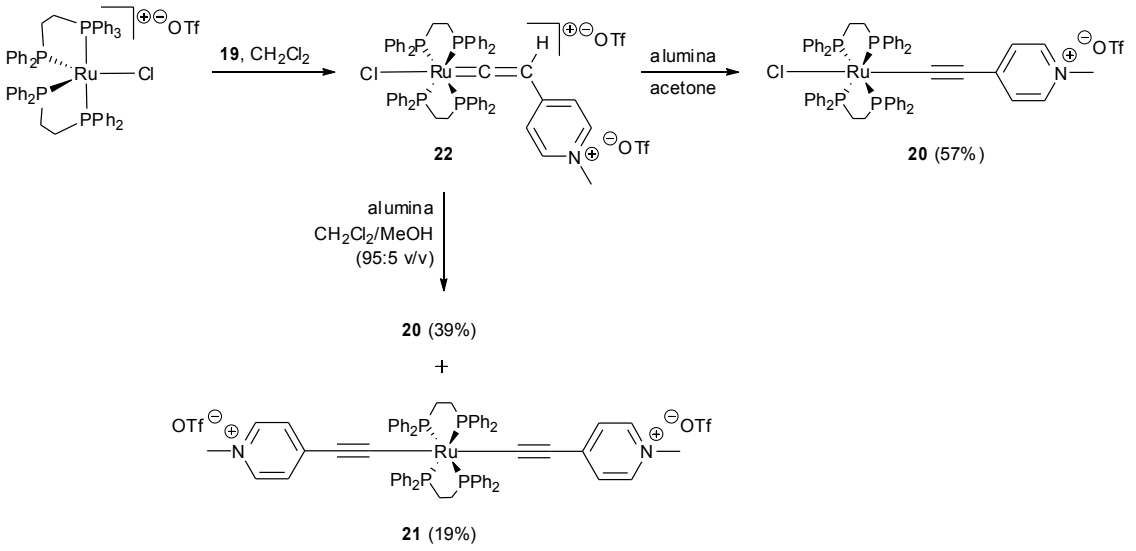

Scheme 4-11. Synthesis of some *N*-methyl-4-ethynylpyridinium triflate Ru(dppe)$_2$ complexes.

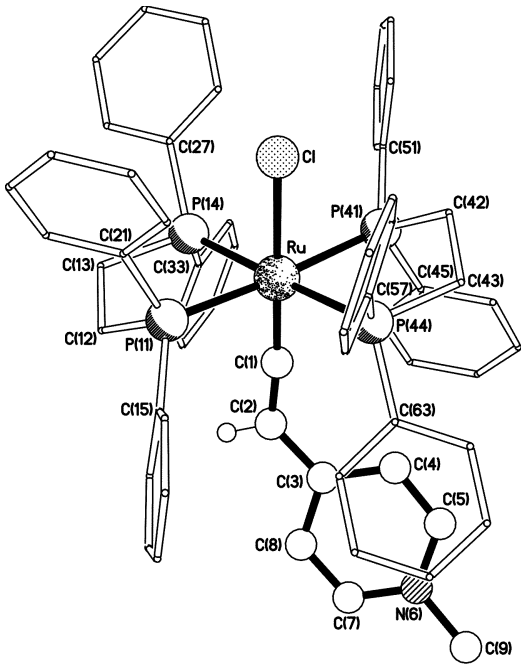

Figure 4-12. Crystal structure of [RuCl(dppe)$_2$(=C=C(H)–C$_5$H$_4$N–CH$_3$)]$^{2+}$ (**22**$^{2+}$). Hydrogen atoms (except the vinylidene proton), counter-ions and co-crystallised **19** removed for clarity.

Remarkably, if **22** was eluted through alumina using CH_2Cl_2/MeOH (95:5 v/v) instead of acetone, a mixture of **20** and the bis-acetylide, $[RuCl(dppe)_2(C_5H_4N–CH_3)_2][OTf]_2$ (**21**) was obtained. This is again suggestive that bis-acetylide formation can occur on the alumina column prior to or during elution *(vida supra)*. Previous attempts to synthesize **21** (via reaction of **20** with **19** in the presence of NEt_3 and $NaPF_6$) had failed, with control experiments showing that **19** rapidly decomposes in NEt_3/CH_2Cl_2. Unlike samples of **17**/**18**, **20**/**21** could be separated by careful fractional recrystallization (CH_2Cl_2/*n*-hexane).

Such reactions are the first to employ *N*-methyl-4-ethynylpyridinium as a ligand. Whilst some 4-(*N*-alkylpyridine)ethynyl-coordinated complexes are known *(Figure 4-13)*, they were all prepared from reaction of 4-pyridylacetylide precursors with RI (R = Me, $C_{10}H_{21}$).[9b,47b,54]

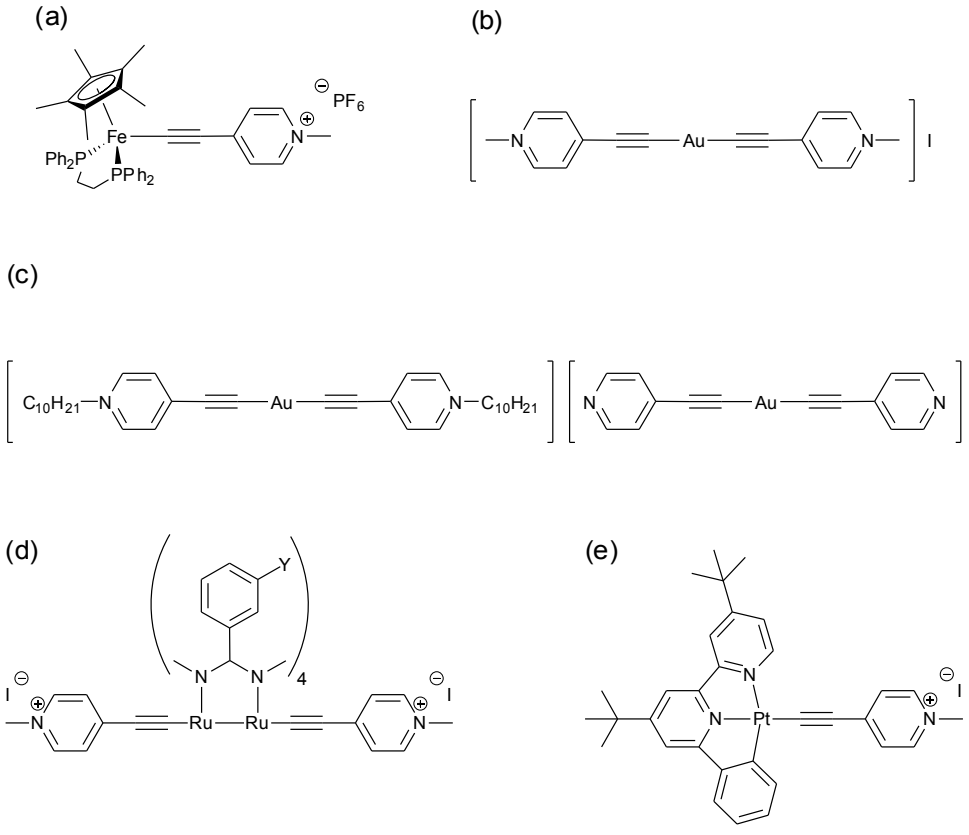

Figure 4-13. Previously determined examples of 4-(*N*-alkylpyridine)ethynyl-coordinated complexes.

Anion exchange and demethylation

Clearly fulfilling their desired role as protecting moieties, identifying a suitable method to remove the *N*-methyl groups of these complexes was now of interest. Whilst the 'reverse Menschutkin[§§] reaction' has been achieved with *N*-alkylated organic pyridines via numerous methods – dry-heating (≥300°C),[56] heating (106-215°C) in various solvents (*e.g.* *N*-methylimidazole,[57] pyridine, pyrolidine, or morpholine,[58] dimethylformamide,[59] or pyridinium chloride[60]), or treatment with xanthate[58] or various nitrogen-based/halide nucleophiles[57,61] – a common and relatively mild approach involves the 'soft' nucleophile PPh_3 (forming the free amine and phosphonium halide). This latter process has been studied mechanistically and kinetically by several groups.[60,62]

First reported by Ho in 1973,[63] such reactions were initially considered to involve nucleophilic attack by PPh_3 at the *N*-methyl group.[62b] It was later determined by Deady and Korytsky that the active dealkylation agent is actually the halide counterion, generating free alkyl halide which is rapidly consumed by reaction with PPh_3 – this prevents reverse quaternization and drives the reaction to completion *(Scheme 4-12)*.[62c] It has been observed, by correlation of reaction rates and Hammett constants for 3- and 4-substituted pyridines, that the less basic the amine the faster the rate of demethylation.[62b] Others have also shown[62a] that *N*-benzylpyridinium bromides are dealkylated more rapidly than *N*-methylpyridinium iodides (though this is arguably more due to the halide than the alkyl substituent[62c]).

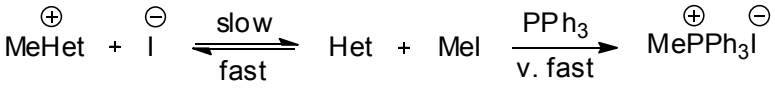

Scheme 4-12. Proposed dealkylation mechanism of *N*-heterocycles.[62c]

Accepting the above mechanism, it was clear that the non-nucleophilic triflate anions of **20**/**21** were unsuitable for demethylation attempts using PPh_3. As halides could not be installed directly due to side reactions *(vida supra)*, it was desirable to exchange the triflate anions of complexes after they had been synthesised. This was ultimately achieved using a halide-

[§§] Alternative spellings: Menshutkin, Menšutkin.[55]

functionalised anion exchange resin *(Figure 4-14)*,[***] in a procedure based upon that of Lamarque *et al.*[64] [RuCl(dppe)$_2$(C$_5$H$_4$N–CH$_3$)]Cl (**23**) was thus provided in essentially quantitative yield simply by dissolving **20** in methanol and eluting the solution dropwise through the resin (full experimental procedures in *Chapter 8)*. Triflate-chloride exchange was confirmed by loss of the ν(S=O) band and singlet C*F*$_3$ resonance in the products IR and ^{19}F NMR spectra, by elemental analysis, and X-ray crystallography *(Figure 4-15)*. Interestingly, if less polar solvents such as CH_2Cl_2, acetone or acetonitrile were used to elute **20** through the resin, no ion-exchange was observed.

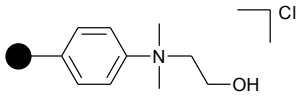

Figure 4-14. The quaternized amine functionality of Amberlite IRA-400 (shown); incorporated within a polystyrene/divinylbenzene copolymer.

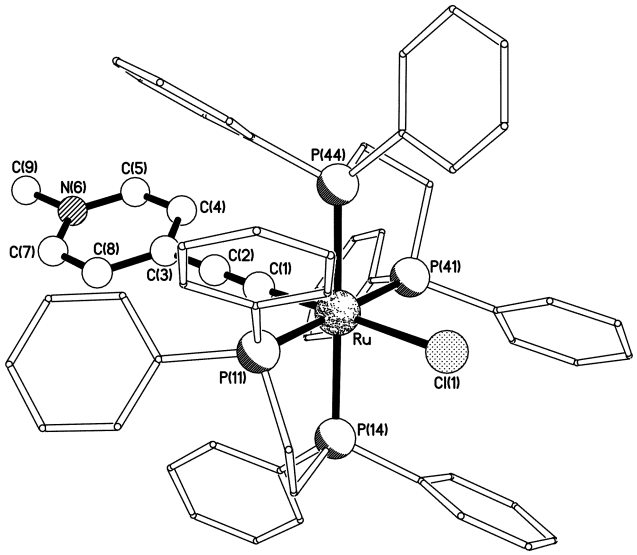

Figure 4-15. Crystal structure of [RuCl(dppe)$_2$(C≡C–C$_5$H$_4$N–CH$_3$)]Cl (**23**). Hydrogen atoms and chloride counter-ion removed for clarity.

[***] Amberlite IRA 410, a strongly basic anion exchange resin (the chloride form is commerically available). Attempts of stirring **20**/**21** with halide salts in acetonitrile had proved ineffective for anion exchange.

Though the reverse quaternization reactions of *N*-methylpyridinium chlorides had not been examined previously, it was considered that they might be faster than with other halides (given the superior rates observed with *N*-alkylpyridinium bromides *vs.* iodides[62c]). However, all attempts at demethylation of **23** using PPh_3 (10 eq.) failed – either at ambient temperatures (over several days in acetonitrile, acetone or chloroform), or with more forcing conditions (acetonitrile, overnight, 80°C; toluene, 3 days, 110°C; DMSO, overnight, 150°C). Though the thermal stability of **23** was encouraging, with no substantial decompositions observed during any of these investigations, apparent solvent coordination was observed with acetonitrile. Furthermore, attempted syntheses of the iodide analogue of **20**/**23** (using an iodide-functionalised ion-exchange resin[†††]) were complicated by incomplete reaction (or Ru–Cl/Ru–I exchange).

A more robust iodide/bromide-containing complex was required for testing, prompting the two-step synthesis of $[Ru(dppe)_2(C{\equiv}C{-}C_6H_5)(C{\equiv}C{-}C_5H_4N{-}CH_3)]I$ (**25**) from **20** *(Scheme 4-13)*. Chloride substitution with phenylacetylene indeed afforded $[Ru(dppe)_2(C{\equiv}C{-}C_6H_5)(C{\equiv}C{-}C_5H_4N{-}CH_3)]OTf$ (**24**) (further demonstrating the utility of the methyl triflate adduct as a suitable protecting group), and subsequent anion exchange using an iodide-functionalised resin provided **25**. Notably, bis-acetylide formation in this case required gentle heating/higher concentrations to drive the reaction to completion. All products were characterised by the usual methods (with the conversion of triflate to iodide again confirmed by IR, $^{19}F\{^1H\}$ NMR and elemental analyses). The solubility of $[Ru(dppe)_2(C{\equiv}C{-}C_6H_5)(C{\equiv}C{-}C_5H_4N{-}CH_3)]X$ was also greatly increased upon exchange of triflate for iodide.

[†††] This was generated by dropwise elution of a 5-10% w/w aqueous solution of KI through the chloride form of Amberlite IRA.

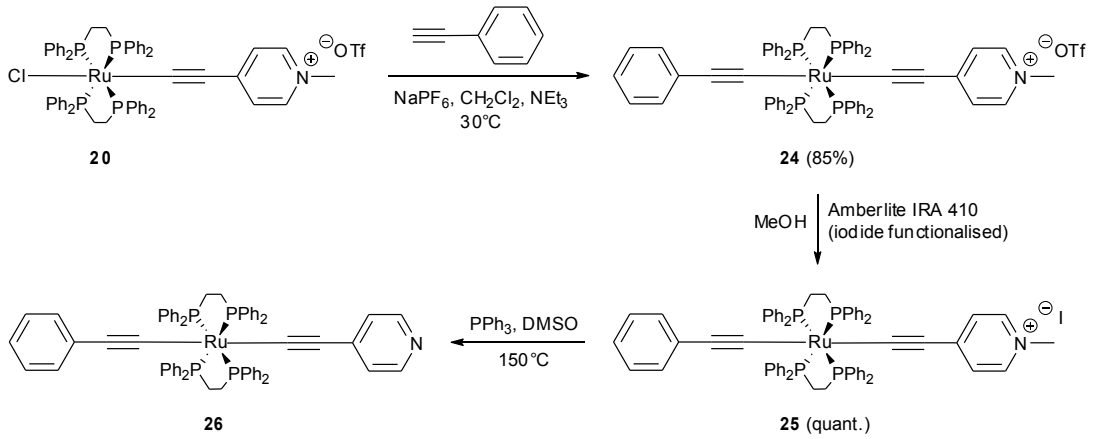

Scheme 4-13. Synthetic route to $Ru(dppe)_2(C{\equiv}C{-}C_6H_5)(C{\equiv}C{-}C_5H_4N)$ (**26**) in three steps from **20**.

Demethylation attempts using **25** proved more encouraging than with **23**. In an NMR-scale experiment, **25** (0.002 mM) and PPh_3 (0.015 mM) were heated in DMSO-d_6 at 150°C (no reaction was observed after 24 h at 120°C). ^1H and $^{31}P\{^1H\}$ NMR spectra were taken at 20 h and 84 h, whereby new resonances attributable to $[MePPh_3]I$[65] were observed *(Figure 4-16a)*. Similar observations were made for a *N*-methylpyridinium iodide[66]/PPh_3 control *(Figure 4-16b)*. However, multiple overlapping resonances in the aromatic region made it difficult to identify new peaks that could be attributed to the demethylated complex, **26** *(Scheme 4-13)*, and it is not clear if this is stable under the reaction conditions (multiple peaks were observed in the $^{31}P\{^1H\}$ NMR spectrum). Further work is required to confirm the formation of **26** via this approach. Assuming that the $[MePPh_3]I$ is stable, integration of reactant and product methyl peaks suggests that 35% of **25** and 61% of *N*-methylpyridinium iodide had been demethylated after 84 h.

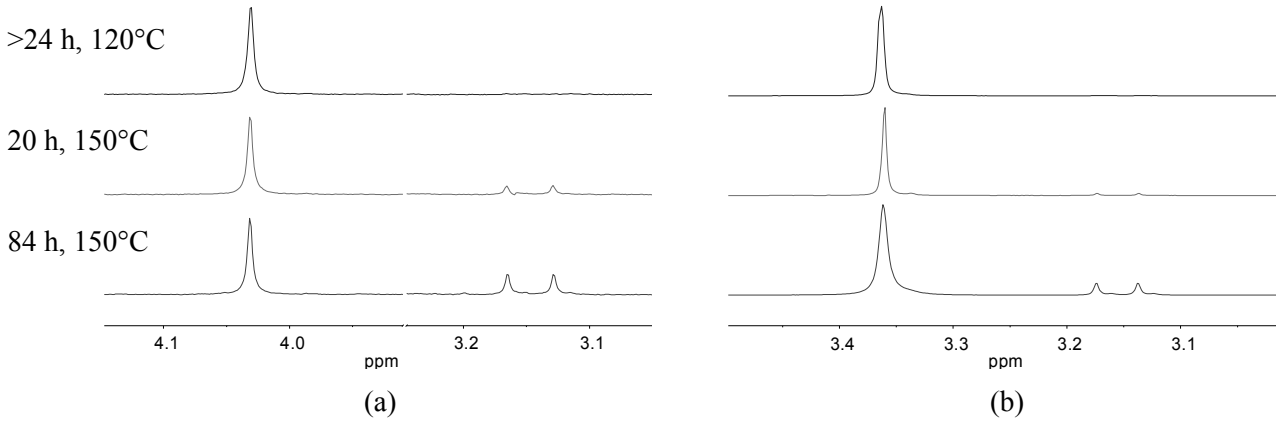

Figure 4-16. ^{1}H NMR spectra showing selected resonances for attempted demethylation of (a) **25**, (b) *N*-methylpyridinium iodide (singlets = N–CH_3; doublets at δ ~3.15 ppm = P–CH_3) .

These experiments demonstrate the utility and plausibility of a protecting group approach to the syntheses of pyridyl-terminated Ru(dppe)$_2$ complexes. However, prior to useful practical application, the process requires additional development. Triflate/halide exchange processes are severely limited by the low solubility of the triflate salts in methanol – only 0.040 g of **24** could be dissolved in ~700 mL. Ideally, alternative eluting solvent(s) that facilitate anion exchange may be found, otherwise complexes should be designed to include solubilising moieties. Furthermore, using DMSO (bp = 189°C) as a solvent for the demethylation reaction is almost certainly bound to cause product purification issues. A comparable approach (*e.g.* using acetonitrile, bp = 82°C) would be preferable.

4.4 ELECTROCHEMISTRY

The redox properties of **17**, **20**, **21** and **24** were investigated via cyclic voltammetry in $CHCl_3$ (given the instability of **17** in CH_2Cl_2). Data for these and some analogous literature complexes are provided in *Table 4-2*. All compounds exhibited close to reversible redox features ($i_p \propto V_s^{1/2}$) at potentials approximately 0.26-0.59 V positive of $[FcH]^+/[FcH]$. These were assigned to the Ru(II)/Ru(III) couple. As in *Chapter 2*, estimation of R_s using AC impedance spectroscopy and correction for iR_s greatly adjusted the observed behaviour towards reversibility ($\Delta E \approx 0.059/n$ V).

Additional reactions were encountered at oxidising potentials ~200 mV more positive than the tail of the anodic wave, affecting the reversible processes. These could not be fully resolved, due to the proximity of observed features to solvent oxidation, but are attributed to irreversible largely metal-based oxidations (presumably Ru(III) to Ru(IV), typically seen >0.80 V positive of Ru(II)/Ru(III)[8b,30]). Limiting the oxidative voltage resolved these issues, but led to difficulties in defining the baseline for the cathodic wave, resulting in apparent $i_p^a/i_p^c > 1$ in the majority of cases. It should be noted that subsequent scans were observed to stabilise, indicating that no significant changes to the electrode surface were occurring during these experiments.

Table 4-2. Electrochemical data for some ruthenium complexes.[a]

compound	E_{pa} (V)	E_{pc} (V)	ΔE (V)	i_p^a/i_p^c	$E_{1/2}$[b] (V)	ref
trans-$RuCl_2(dppe)_2$[c]	/	/	/	/	0.04	*67*
$RuCl(dppe)_2(C{\equiv}C{-}C_6H_5)$[c]	/	/	/	/	0.01	*30*
	/	/	/	/	-0.01	*67*
$Ru(dppe)_2(C{\equiv}C{-}C_6H_5)_2$[c]	/	/	/	/	0.00	*67*
trans-$RuCl_2(dmpe)_2$[c]	/	/	0.070	/	-0.05	*8b*
$Ru(dmpe)_2(C{\equiv}C{-}C_5H_4N)_2$[c]	/	/	0.070	/	0.03	*8b*
$Ru(dppe)_2(C{\equiv}C{-}C_5H_4N)_2$ (**17**)	0.312	0.227	0.085	1.32	0.269	this work
$[RuCl(dppe)_2(C{\equiv}C{-}C_5H_4N{-}CH_3)]OTf$ (**20**)	0.479	0.392	0.087	1.07	0.435	this work
$[Ru(dppe)_2(C{\equiv}C{-}C_5H_4N{-}CH_3)_2][OTf]_2$ (**21**)	0.629	0.554	0.075	1.14	0.591	this work
$[Ru(dppe)_2(C{\equiv}C{-}C_6H_5)(C{\equiv}C{-}C_5H_4N{-}CH_3)]OTf$ (**24**)	0.307	0.238	0.069	1.19	0.272	this work

[a] For scan rate = 0.1 Vs^{-1}. $Bu_4N^+PF_6^-$ (0.1 M) in $CHCl_3$ (unless otherwise stated); WE: glassy carbon; RE, CE: Pt. All potentials assigned to the Ru(II)/Ru(III) redox couple, reported relative to $[FcH]^+/[FcH]$ and corrected for iR_s. [b] $E_{1/2} = ½(E_{pa} + E_{pc})$. [c] In CH_2Cl_2 with $Bu_4N^+PF_6^-$ or $Bu_4N^+BF_4^-$.

It can be seen from *Table 4-2* that changing chloride for phenylacetylide ligand(s) results in decreased $E_{1/2}$ values (as in the $RuCl_{2-x}(dppe)_2(C{\equiv}C{-}C_6H_5)_x$ series, and between **20**/**24**), whereas with chloride-pyridylacetylide exchange a positive shift is observed (*trans*-$RuCl_2(diphos)_2$ to $Ru(diphos)_2(C{\equiv}C{-}C_5H_4N)_2$, diphos = dmpe, dppe). The particularly large magnitude between the $E_{1/2}$ of **17** and analogous $Ru(dppe)_2$ or $Ru(dmpe)_2$ complexes (0.23-0.28 V) may in part be due to the latter being measured in CH_2Cl_2 not $CHCl_3$ (or due to unaccounted for reactions between $Ru(dmpe)_2(C{\equiv}C{-}C_5H_4N)_2$ and CH_2Cl_2).

Compounds containing *N*-methyl-4-pyridylacetylide have $E_{1/2}$ values greatly shifted towards more positive potentials. As might be expected, the close proximity of the quaternized nitrogen makes these metal complexes significantly more difficult to oxidize.

4.5 UV-VIS SPECTROSCOPY

The absorption spectra of all novel complexes synthesized here (and *trans*-$RuCl_2(dppe)_2$, for comparison) were measured in $CHCl_3$. These are shown for symmetrical and unsymmetrical complexes in *Figure 4-17* and *Figure 4-18*, respectively, with data summarized in *Table 4-3*.

Though $RuCl_2(dppe)_2$ *(Figure 4-17)* does not on initial inspection appear to have any significant absorptions in the visible region, an expanded view reveals an extremely weak band ($\varepsilon \approx 60$ M^{-1} cm^{-1}, observed under these conditions at 450 nm), credited with provision of its yellow colour.[68] This was assigned by Chatt and Hayter to a $^1A_{lg} \rightarrow {}^1E_g$ transition, and corresponds to the promotion of an electron from the t_{2g} to e_g orbital (respectively the HOMO and LUMO for this, as well as other low spin d^6 octahedral complexes).

With the majority of compounds studied here, such Laporte-forbidden d-d transitions are obscured by intense, broad/overlapping (non-Gaussian) absorptions at similar energies. These correspond to transitions from ruthenium based molecular orbitals to ligand π* orbitals (MLCT bands).[1b,8b] In **17**, they are centred at 359 nm, whereas a bathochromic shift to 456 nm, or 468-471 nm is observed with $[C{\equiv}C{-}C_5H_4N{-}CH_3]OTf/Cl$ or $[C{\equiv}C{-}C_5H_4N{-}CH_3]OTf/C{\equiv}C{-}C_6H_5$ containing materials, respectively. This is expected for MLCT processes as the electron withdrawing character of the ligand increases,[69] clearly correlated elsewhere in a series of $RuCp^*(dppe)(C{\equiv}C{-}C_6H_4X)$ (X = NO_2, CN, F, H, OMe, NH_2) complexes.[70]

Observed in all spectra are multiple/overlapping absorptions at high energies, typical of such materials and attributed to dppe-centred (*i.e.* intra ligand, π-π*/n-π*) transitions.[1b,68] Interestingly, changing the counter-ions of complexes **20** and **24** (from triflate to chloride and iodide, respectively), is seen to affect absorptions in this region *(Figure 4-18)*.

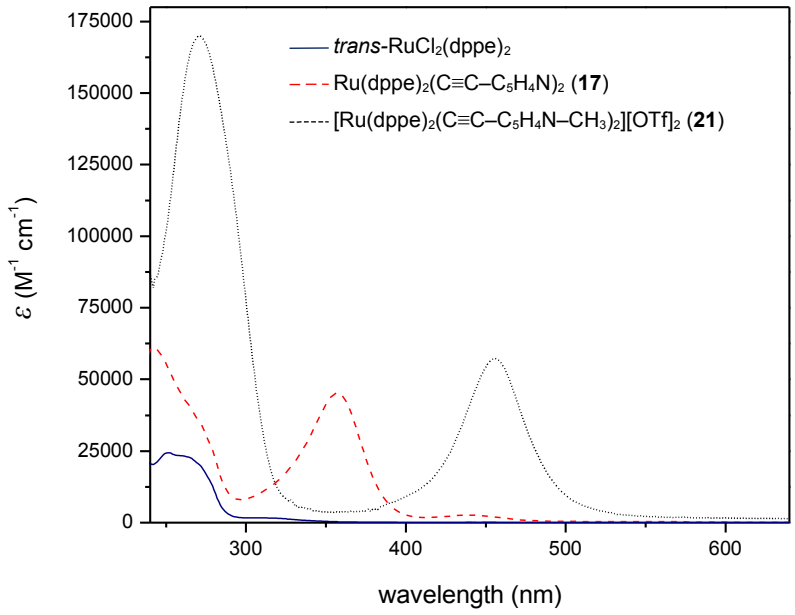

Figure 4-17. UV-vis spectra (in $CHCl_3$) of symmetrical ruthenium complexes: *trans*-$RuCl_2(dppe)_2$, **17** and **21**.

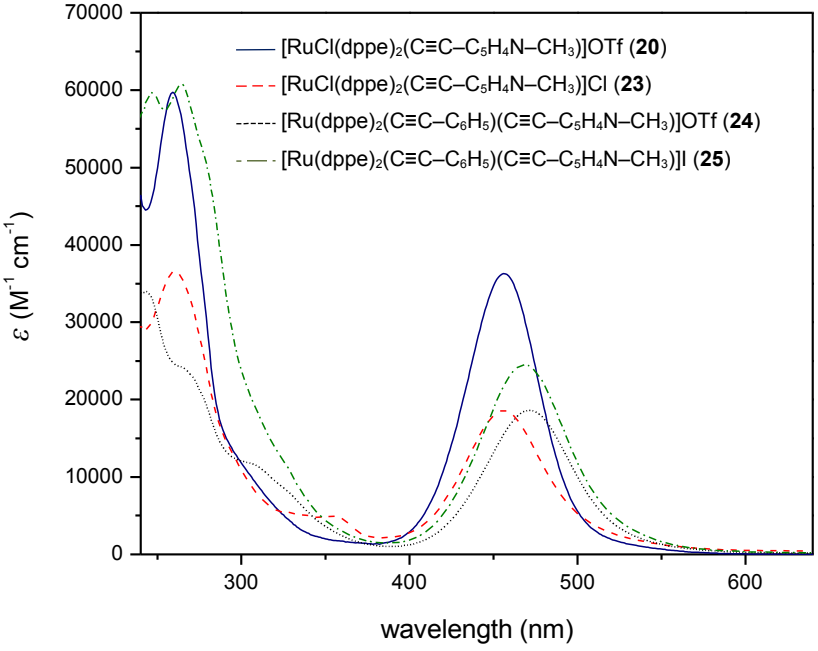

Figure 4-18. UV-vis spectra (in $CHCl_3$) of unsymmetrical ruthenium complexes: **20**, **21**, **24** and **25**.

Table 4-3. Electronic spectral data of selected ruthenium complexes and ligands.[a]

compound	λ_{max} /nm (ε /M^{-1} cm^{-1})[b]
trans-$RuCl_2(dppe)_2$	249 (24005), 263infl (23025), 277sh (14989), 306 (1609), 450 (57)
$Ru(dppe)_2(C{\equiv}C{-}C_5H_4N)_2$ (**17**)	274sh (31879), 342sh (32325), 359 (44957), 439 (2577), 502infl (372)
$[H{-}C{\equiv}C{-}C_5H_4N{-}CH_3]OTf$ (**19**)[c]	260sh, 263infl, 268, 275sh, 283sh
$[RuCl(dppe)_2(C{\equiv}C{-}C_5H_4N{-}CH_3)]OTf$ (**20**)	262 (58442), 456 (36299)
$[Ru(dppe)_2(C{\equiv}C{-}C_5H_4N{-}CH_3)_2][OTf]_2$ (**21**)	272 (169614), 456 (57303),
$[RuCl(dppe)_2(C{\equiv}C{-}C_5H_4N{-}CH_3)]Cl$ (**23**)	261 (36514), 300sh (10885), 325sh (5434), 358 (4842), 456 (18596)
$[Ru(dppe)_2(C{\equiv}C{-}C_6H_5)(C{\equiv}C{-}C_5H_4N{-}CH_3)]OTf$ (**24**)	243 (34040), 268sh (23624), 299sh (12119), 471 (18626)
$[Ru(dppe)_2(C{\equiv}C{-}C_6H_5)(C{\equiv}C{-}C_5H_4N{-}CH_3)]I$ (**25**)	246 (59680), 264 (60792), 304sh (21199), 468 (24531)

[a] Recorded at room temperature in $CHCl_3$, using quartz cells with a pathlength of 10 mm. [b] Where possible, spectra were deconvoluted into composite Gaussian bands‡‡‡ to obtain λ_{max} values. All extinction coefficients were taken from the experimental data at these wavelengths. [c] Sparingly soluble in $CHCl_3$, observed λ_{max} values from a saturated solution provided for comparison.

4.6 CONCLUSION

Incorporation of the 4-ethynylpyridine ligand into $Ru(dppe)_2$ σ-alkynyl complexes proved surprising difficult due to the formation of various unknown impurities, hindering progress in the synthesis of extended structures. Though the bis-alkynyl, **17**, was eventually isolated in pure form, its preparation was far from robust (and the compound was observed to further react/decompose in contact with CH_2Cl_2). Reasoning that contaminants were likely formed due to side reactions at the pyridyl nitrogen, a protecting group strategy was pursued using *N*-methyl-4-ethynylpyridinium triflate (**19**) (a uniquely stable quaternized 4-ethynylpyridine). In support of the previous hypothesis, this was here employed as a ligand for the first time, and with none of the problems encountered using the free amine.

Of additional interest, formation of bis-alkynyl complexes was observed when the vinylidene complexes **22** or $[RuCl(dppe)_2(=C{=}C(H)\text{-}C_5H_4N)]OTf$ were eluted through alumina using

‡‡‡ Using the 'Fit Plot' tool of *MagicPlot Student v2.3*.

CH_2Cl_2/MeOH (95:5 v/v). Further studies are required to examine the reproducibility of this rather unusual apparent reaction.

In exploring methods to remove the *N*-methyl groups of protected pyridyl ruthenium complexes, it was found that their triflate anions could be readily exchanged for halides (Cl, I) by elution of the salt through an appropriate anion exchange resin. Though **23** (a mono-alkynyl Cl^- salt) could not be demethylated with PPh_3, an analogous approach using **25** (a bis-alkynyl I^- salt) proved successful. Though this work provides a 'proof of concept' for the protecting group approach in syntheses with 4-ethynylpyridine, further development of reaction conditions with model systems is required prior to its useful practical application.

Cyclic voltammetry and UV-vis spectroscopy showed that these materials have redox/electronic properties typical of analogous ruthenium acetylides, albeit with increased $E_{1/2}$ values and red-shifted absorptions (relative to $RuCl_{2-x}(C{\equiv}C{-}C_6H_5)_x$). Though measurements in the same solvent are required, 4-ethynylpyridine and *N*-methyl-4-ethynylpyridine appear to be remarkably electron-withdrawing ligands, the latter comparable even to 1-ethynyl-4-nitrobenzene (for $RuCl(dppe)_2(C{\equiv}C{-}C_6H_4{-}NO_2)$, $E_{1/2}$ = 0.20 V[30] and λ_{max} ($Ru \rightarrow C_6H_4NO_2$) = 482 nm[71] in CH_2Cl_2).

Observations and insights provided by the study of these linear systems proved extremely useful in addressing the preparation of more complex branched and macrocyclic $Ru(dppe)_2$ analogues (discussed in *Chapter 5)*. For these compounds, an entirely different synthetic approach (*i.e.* $16e^-$ centre avoidance) was utilised.

4.7 REFERENCES

1. (a) C. Olivier, B. Kim, D. Touchard and S. Rigaut, *Organometallics*, 2008, **27**, 509; (b) A. Benameur, P. Brignou, E. Di Piazza, Y.-M. Hervault, L. Norel and S. Rigaut, *New J. Chem.*, 2011, **35**, 2105.
2. (a) A. Salomon, D. Cahen, S. Lindsay, J. Tomfohr, V. B. Engelkes and C. D. Frisbie, *Adv. Mater.*, 2003, **15**, 1881; (b) A. Blum, T. Ren, D. A. Parish, S. A. Trammell, M. H. Moore, J. G. Kushmerick, G.-L. Xu, J. R. Deschamps, S. K. Pollack and R. Shashidhar, *J. Am. Chem. Soc.*, 2005, **127**, 10010..
3. P. Siemsen, U. Gubler, C. Bosshard, P. Günter and F. Diederich, *Chem. Eur. J.*, 2001, **7**, 1333.
4. (a) C. Stroh, M. Mayor, C. v. Hänisch and P. Turek, *Chem. Commun.*, 2004, 2050; (b) M. Mayor, C. von Hänisch, H. B. Weber, J. Reichert and D. Beckmann, *Angew. Chem., Int. Ed.*, 2002, **41**, 1183; (c) T. L. Schull, J. G. Kushmerick, C. H. Patterson, C. George, M. H.

Moore, S. K. Pollack and R. Shashidhar, *J. Am. Chem. Soc.*, 2003, **125**, 3202; (d) G. Vives, A. Carella, S. Sistach, J.-P. Launay and G. Rapenne, *New J. Chem.*, 2006, **30**, 1429; (e) S. C. Jones, V. Coropceanu, S. Barlow, T. Kinnibrugh, T. Timofeeva, J. L. Brédas and S. R. Marder, *J. Am. Chem. Soc.*, 2004, **126**, 11782.

5. (a) H.-W. Lin, X.-H. Wang, X.-J. Zhao, J. Li and F.-S. Wang, *Synth. Met.*, 2003, **135-136**, 239; (b) K. Liu, X. Wang and F. Wang, *ACS Nano*, 2008, **2**, 2315.
6. M.-Y. Choi, M. C. W. Chan, S.-M. Peng, K.-K. Cheung and C.-M. Che, *Chem. Commun.*, 2000, 1259.
7. (a) H. Qi, A. Gupta, B. C. Noll, G. L. Snider, Y. Lu, C. Lent and T. P. Fehlner, *J. Am. Chem. Soc.*, 2005, **127**, 15218; (b) B. Kim, J. M. Beebe, C. Olivier, S. Rigaut, D. Touchard, J. G. Kushmerick, X.-Y. Zhu and C. D. Frisbie, *J. Phys. Chem. C*, 2007, **111**, 7521; (c) L. Luo, A. Benameur, P. Brignou, S. H. Choi, S. Rigaut and C. D. Frisbie, *J. Phys. Chem. C*, 2011, **115**, 19955.
8. (a) J.-L. Zuo, E. Herdtweck, F. F. d. Biani, A. M. Santos and F. E. Kühn, *New J. Chem.*, 2002, **26**, 889; (b) F. E. Kühn, J.-L. Zuo, F. F. d. Biani, A. M. Santos, Y. Zhang, J. Zhao, A. Sandulache and E. Herdtweck, *New J. Chem.*, 2004, **28**, 43.
9. (a) A. K. Mahapatro, J. Ying, T. Ren and D. B. Janes, *Nano Lett.*, 2008, **8**, 2131; (b) Jie-Wen Ying and T. Ren, *J. Organomet. Chem.*, 2008, **693**, 1449.
10. N. J. Long and C. K. Williams, *Angew. Chem., Int. Ed. Engl.*, 2003, **42**, 2586.
11. (a) K. Sonogashira, S. Takahashi and N. Hagihara, *Macromolecules*, 1977, **10**, 879; (b) P. J. Kim, H. Masai, K. Sonogashira and N. Hagihara, *Inorg. Nucl. Chem. Lett.*, 1970, **6**, 181; (c) K. Sonogashira, T. Yatake, Y. Tohda, S. Takahashi and N. Hagihara, *J. Chem. Soc., Chem. Commun.*, 1977, 291.
12. (a) B. Cetinkaya, M. F. Lappert, J. McMeeking and D. E. Palmer, *J. Chem. Soc., Dalton Trans.*, 1973, 1202; (b) S. J. Davies, B. F. G. Johnson, M. S. Khan and J. Lewis, *J. Chem. Soc., Chem. Commun.*, 1991, 187; (c) Z. Atherton, C. W. Faulkner, S. L. Ingham, A. K. Kakkar, M. S. Khan, J. Lewis, N. J. Long and P. R. Raithby, *J. Organomet. Chem.*, 1993, **462**, 265.
13. (a) M. L. H. Green, *Organometallic Compounds* (3rd. ed.), ed. G. E. Coates, M. L. H. Green and K. Wade, Methuen, 1968; (b) A. López-Hernández, K. Venkatesan, H. W. Schmalle and H. Berke, *Monatsh. Chem.*, 2009, **140**, 845.
14. (a) D. Zargarian, P. Chow, N. J. Taylor and T. B. Marder, *J. Chem. Soc., Chem. Commun.*, 1989, 540; (b) H. B. Fyfe, M. Mlekuz, D. Zargarian, N. J. Taylor and T. B. Marder, *J. Chem. Soc., Chem. Commun.*, 1991, 188; (c) H.-F. Klein and H. H. Karsch, *Chem. Ber.*, 1975, **108**, 944.
15. C. Bianchini, M. Peruzzini, A. Vacca and F. Zanobini, *Organometallics*, 1991, **10**, 3697.
16. (a) C. Bianchini, F. Laschi, F. Ottaviani, M. Peruzzini and P. Zanello, *Organometallics*, 1988, **7**, 1660; (b) L. D. Field and A. V. George, *J. Organomet. Chem.*, 1993, **454**, 217; (c) C. Bianchini, P. Frediani, D. Masi, M. Peruzzini and F. Zanobini, *Organometallics*, 1994, **13**, 4616.
17. (a) P. Haquette, N. Pirio, D. Touchard, L. Toupet and P. H. Dixneuf, *J. Chem. Soc., Chem. Commun.*, 1993, 163; (b) D. Touchard, C. Morice, V. Cadierno, P. Haquette, L. Toupet and P. H. Dixneuf, *J. Chem. Soc., Chem. Commun.*, 1994, 859; (c) D. Touchard, P. Haquette, S. Guesmi, L. L. Pichon, A. Daridor, L. Toupet and P. H. Dixneuf, *Organometallics*, 1997, **16**, 3640.
18. P. J. Stang and C. M. Crittell, *Organometallics*, 1990, **9**, 3191.

19. (a) L. D. Field, A. V. George, F. Laschi, E. Y. Malouf and P. Zanello, *J. Organomet. Chem.*, 1992, **435**, 347; (b) M.-Y. Choi, M. C.-W. Chan, S. Zhang, K.-K. Cheung, C.-M. Che and K.-Y. Wong, *Organometallics*, 1999, **18**, 2074.
20. R. J. Cross and M. F. Davidson, *J. Chem. Soc., Dalton Trans.*, 1986, 411.
21. C. Müller, C. N. Iverson, R. J. Lachicotte and W. D. Jones, *J. Am. Chem. Soc.*, 2001, **123**, 9718.
22. (a) L. D. Field, A. M. Magill, T. K. Shearer, S. J. Dalgarno and P. Turner, *Organometallics*, 2007, **26**, 4776; (b) L. D. Field, A. V. George, D. C. R. Hockless, G. R. Purches and A. H. White, *J. Chem. Soc., Dalton Trans.*, 1996, 2011; (c) L. D. Field, A. M. Magill, T. K. Shearer, S. B. Colbran, S. T. Lee, S. J. Dalgarno and M. M. Bhadbhade, *Organometallics*, 2010, **29**, 957.
23. L. D. Field, A. J. Turnbull and P. Turner, *J. Am. Chem. Soc.*, 2002, **124**, 3692.
24. M. Younus, N. J. Long, P. R. Raithby, J. Lewis, N. A. Page, A. J. P. White, D. J. Williams, M. C. B. Colbert, A. J. Hodge, M. S. Khan and D. G. Parker, *J. Organomet. Chem.*, 1999, **578**, 198.
25. (a) S. N. Semenov, O. Blacque, T. Fox, K. Venkatesan and H. Berke, *J. Am. Chem. Soc.*, 2010, **132**, 3115; (b) S. N. Semenov, S. F. Taghipourian, O. Blacque, T. Fox, K. Venkatesan and H. Berke, *J. Am. Chem. Soc.*, 2010, **132**, 7584.
26. (a) F. J. Fernández, M. Alfonso, H. W. Schmalle and H. Berke, *Organometallics*, 2001, **20**, 3122; (b) K. Venkatesan, T. Fox, H. W. Schmalle and H. Berke, *Organometallics*, 2005, **24**, 2834.
27. (a) A. R. Chakravarty and F. A. Cotton, *Inorg. Chim. Acta*, 1986, **113**, 19; (b) G. Xu and T. Ren, *J. Organomet. Chem.*, 2002, **655**, 239.
28. M. S. Inkpen and N. J. Long, in *Molecular Design and Applications of Photofunctional Polymers and Materials*, eds. W.-Y. Wong and A. S. Abd-El-Aziz, Royal Society of Chemistry, 2012.
29. M. Bassetti, V. Cadierno, J. Gimeno and C. Pasquini, *Organometallics*, 2008, **27**, 5009.
30. M. A. Fox, J. E. Harris, S. Heider, V. Pérez-Gregorio, M. E. Zakrzewska, J. D. Farmer, D. S. Yufit, J. A. K. Howard and P. J. Low, *J. Organomet. Chem.*, 2009, **694**, 2350.
31. F. A. Cotton and G. W. Wilkinson, *Advanced Inorganic Chemistry* (3rd ed.), Interscience, 1972.
32. D. Touchard, P. Haquette, N. Pirio, L. Toupet and P. H. Dixneuf, *Organometallics*, 1993, **12**, 3132.
33. M. Younus, N. J. Long, P. R. Raithby and J. Lewis, *J. Organomet. Chem.*, 1998, **570**, 55.
34. B. Chaudret, G. Commenges and R. Poilblanc, *J. Chem. Soc., Dalton Trans.*, 1984, 1635.
35. K. G. Caulton, *J. Am. Chem. Soc.*, 1974, **96**, 3005.
36. N. R. Champness, A. N. Khlobystov, A. G. Majuga, M. Schröder and N. V. Zyk, *Tetrahedron Lett.*, 1999, **40**, 5413.
37. (a) C. Coudret, *Synth. Commun.*, 1996, **26**, 3543; (b) S. H. Chanteau and J. M. Tour, *Tetrahedron Lett.*, 2001, **42**, 3057.
38. A. A. Berlin and E. F. Razvodovskii, *J. Polym. Sci., Part C: Polym. Symp.*, 1967, **16**, 369.
39. I.-Y. Wu, J. T. Lin, J. Luo, S.-S. Sun, C.-S. Li, K. J. Lin, C. Tsai, C.-C. Hsu and J.-L. Lin, *Organometallics*, 1997, **16**, 2038.
40. L. D. Field, A. M. Magill, T. K. Shearer, S. J. Dalgarno and M. M. Bhadbhade, *Eur. J. Inorg. Chem.*, 2011, **2011**, 3503.
41. Q. Ge and T. S. A. Hor, *Dalton Trans.*, 2008, 2929.

42. A. B. Rudine, M. G. Walter and C. C. Wamser, *J. Org. Chem.*, 2010, **75**, 4292.
43. T. Eicher and S. Hauptmann, *The Chemistry of Heterocycles: Structure, Reactions, Syntheses, and Applications* (2nd ed.), Wiley VCH, 2003.
44. (a) A. B. Prescott, *J. Am. Chem. Soc.*, 1895, **18**, 91; (b) *US Pat.*, 4 115 390, 1978; (c) M. Khodaei and E. Nazari, *Chem. Lett.*, 2010, **39**, 390.
45. (a) P. A. v. d. Meulen and H. A. Heller, *J. Am. Chem. Soc.*, 1932, **54**, 4404; (b) M. J. G. Lesley, A. Woodward, N. J. Taylor, T. B. Marder, I. Cazenobe, I. Ledoux, J. Zyss, A. Thornton, D. W. Bruce and A. K. Kakkar, *Chem. Mater.*, 1998, **10**, 1355; (c) M. A. Zajac, *J. Org. Chem.*, 2008, **73**, 6899.
46. S. Youssif, *ARKIVOC*, 2001, 242.
47. (a) J. T. Lin, J. J. Wu, C.-S. Li, Y. S. Wen and K.-J. Lin, *Organometallics*, 1996, **15**, 5028; (b) S. Le Stang, D. Lenz, F. Paul and C. Lapinte, *J. Organomet. Chem.*, 1999, **572**, 189.
48. S. Subramanyam and A. Blumstein, *Macromolecules*, 1991, **24**, 2668.
49. J. Clayden, N. Greeves, S. Warren and P. Wothers, *Organic Chemistry* (1st ed.), Oxford University Press, 2001.
50. S. Rubinsztajn, W. K. Fife and M. Zeldin, *Tetrahedron Lett.*, 1992, **33**, 1821.
51. A. S. Kalgutkar and N. Castagnoli, *J. Med. Chem.*, 1992, **35**, 4165.
52. B. Tuesuwan and S. M. Kerwin, *Biochemistry*, 2006, **45**, 7265.
53. C. A. Reed, *Acc. Chem. Res.*, 2009, **43**, 121.
54. (a) M. Ferrer, L. Rodríguez, O. Rossell, F. Pina, J. C. Lima, M. F. Bardia and X. Solans, *J. Organomet. Chem.*, 2003, **678**, 82; (b) M. Ferrer, L. Rodríguez, O. Rossell, F. Pina, J. C. Lima, M. F. Bardia and X. Solans, *J. Organomet. Chem.*, 2004, **689**, 270; (c) M. Ferrer, M. Mounir, L. Rodríguez, O. Rossell, S. Coco, P. Gómez-Sal and A. Martín, *J. Organomet. Chem.*, 2005, **690**, 2200; (d) C. Latouche, P.-H. Lanoe, J. A. G. Williams, V. Guerchais, A. Boucekkine and J.-L. Fillaut, *New J. Chem.*, 2011, **35**, 2196.
55. (a) N. Menschutkin, *Z. Phys. Chem.*, 1890, **6**, 41; (b) K. J. Stanger, J.-J. Lee and B. D. Smith, *J. Org. Chem.*, 2007, **72**, 9663.
56. P. A. Claret and G. H. Williams, *J. Chem. Soc. C*, 1969, 146.
57. L. W. Deady and W. L. Finlayson, *Synth. Commun.*, 1980, **10**, 947.
58. A. R. Katritzky and S. S. Thind, *J. Chem. Soc., Perkin Trans. 1*, 1980, 1895.
59. D. Aumann and L. W. Deady, *J. Chem. Soc., Chem. Commun.*, 1973, 32.
60. A. Ruiz, P. Rocca, F. Marsais, A. Godard and G. Quéguiner, *Tetrahedron Lett.*, 1997, **38**, 6205.
61. A. R. Katritzky, G. Musumarra, K. Sakizadeh and M. Misic-Vukovic, *J. Org. Chem.*, 1981, **46**, 3820.
62. (a) J. P. Kutney and R. Greenhouse, *Synth. Commun.*, 1975, **5**, 119; (b) U. Berg, R. Gallo and J. Metzger, *J. Org. Chem.*, 1976, **41**, 2621; (c) L. W. Deady and O. L. Korytsky, *Tetrahedron Lett.*, 1979, **20**, 451; (d) M. Sawada, Y. Takai, C. Chong, T. Hanafusa, S. Misumi and Y. Tsuno, *Tetrahedron Lett.*, 1985, **26**, 5065; (e) L. Deady, W. Finlayson and O. Korytsky, *Aust. J. Chem.*, 1979, **32**, 1735; (f) L. W. Deady, *Aust. J. Chem.*, 1981, **34**, 163; (g) M. Shibagaki, H. Matsushita and H. Kaneko, *Heterocycles*, 1983, **20**, 497; (h) M. Sawada, Y. Takai, C. Chong, T. Hanafusa and S. Misumi, *Anal. Chem.*, 1986, **58**, 231.
63. T.-L. Ho, *Synth. Commun.*, 1973, **3**, 99.
64. (a) *US Pat.*, 0 204 467, 2010; (b) M. Lopez, J. Coca and H. Sastre, *J. Chem. Eng. Data*, 1992, **37**, 274.
65. C. Lichtenberg, M. Elfferding and J. Sundermeyer, *Eur. J. Inorg. Chem.*, 2010, **2010**, 3117.

66. S. Huang, J. C. S. Wong, A. K. C. Leung, Y. M. Chan, L. Wong, M. R. Fernendez, A. K. Miller and W. Wu, *Tetrahedron Lett.*, 2009, **50**, 5018.
67. C. E. Powell, M. P. Cifuentes, J. P. Morrall, R. Stranger, M. G. Humphrey, M. Samoc, B. Luther-Davies and G. A. Heath, *J. Am. Chem. Soc.*, 2002, **125**, 602.
68. D. M. Klassen and G. A. Crosby, *J. Mol. Spectrosc.*, 1968, **25**, 398.
69. K. Costuas, F. Paul, L. Toupet, J.-F. Halet and C. Lapinte, *Organometallics*, 2004, **23**, 2053.
70. F. Paul, B. G. Ellis, M. I. Bruce, L. Toupet, T. Roisnel, K. Costuas, J.-F. Halet and C. Lapinte, *Organometallics*, 2005, **25**, 649.
71. N. Gauthier, N. Tchouar, F. Justaud, G. Argouarch, M. P. Cifuentes, L. Toupet, D. Touchard, J.-F. Halet, S. Rigaut, M. G. Humphrey, K. Costuas and F. Paul, *Organometallics*, 2009, **28**, 2253.

CHAPTER 5 : SYNTHESIS OF BRANCHED PYRIDYL-CONTAINING RUTHENIUM COMPLEXES

5.1 ABSTRACT

Efforts towards a macrocyclic, pyridyl-terminated Ru(dppe)$_2$ containing complex (**35**) are herein described *(Figure 5-1a)*. Inspired by the results of the previous chapter, these and the synthesis of its single branched analogue (**37**) successfully employ a 16e$^-$ centre avoidance rule, whereby pyridyl moieties are incorporated (via Sonogashira cross-coupling) only *after* ruthenium bis-acetylide centres have been constructed. This approach circumvents the problems encountered with pyridyl-containing alkynes when forming C–Ru bonds via the Dixneuf method – by providing no opportunities for (a) coordination of the pyridyl nitrogen to ruthenium, or (b) premature deprotonation of vinylidene species.

Initial progress in preparing fixed-shape macrocycles based on the *cis*-Ru(PP$_3$)(C≡C–R)$_2$ motif is also briefly detailed (PP$_3$ = tris[2-(diphenylphosphino)ethyl]phosphine) *(Figure 5-1b)*. This route was eventually abandoned in favour of those using *trans*-Ru(dppe)$_2$ centres, given the generally greater synthetic experience with these in forming bis-alkynyl complexes (particularly with pyridyl-containing acetylides, see *Chapter 4)*. Work thus far had however resulted in isolation of a new and unusual *trans*-RuCl$_2$(PP$_3$)$_2$ complex (**28**) (bearing pendant 'phosphorus arms') and the synthesis of a novel pyridyl-containing ligand (**27**), both of which will be discussed.

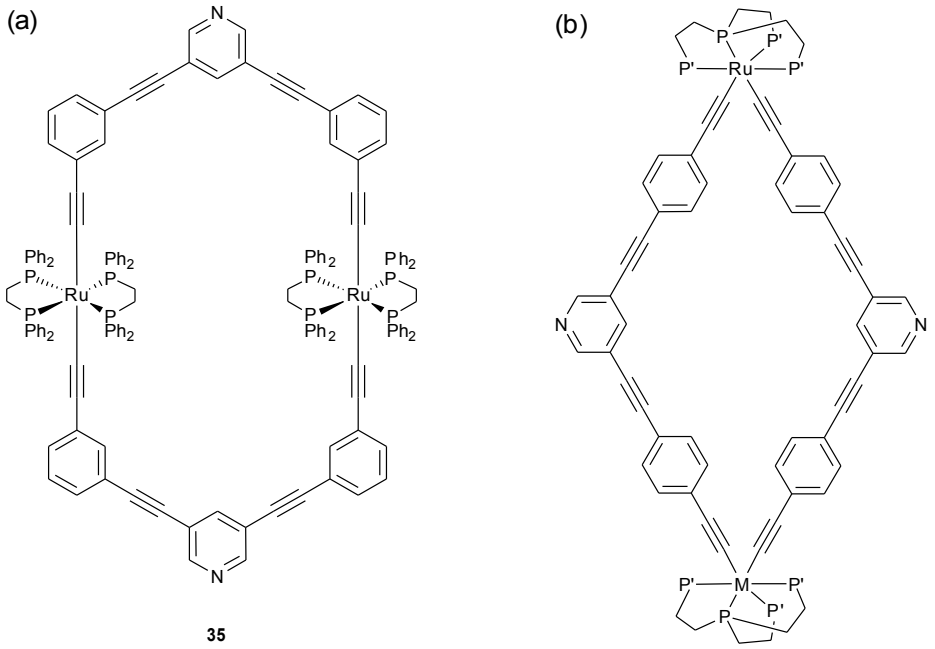

Figure 5-1. Target pyridyl-containing, macrocyclic complexes with (a) $Ru(dppe)_2$, or (b) $M(PP_3)$ centres (M = Ru, Os; P' = PPh_2).

5.2 OVERVIEW OF RELEVANT ARYLETHYNYL COMPOUNDS

The synthesis of fixed-shape/shape-persistent macrocyclic molecules is a broad area, reviewed comprehensively elsewhere (with key strategies and concepts discussed in *Chapter 1)*.[1] Known cyclic structures often comprise some but not all of the following characteristics: (i) a *conjugated backbone* to mediate electron transfer, (ii) *redox/photo-active centres* for molecular accessibility, and (iii) *surface binding groups* for self-assembly. These features, only in combination, provide a testable system on which conductance studies and related investigations may be undertaken, towards an improved understanding of molecular quantum interference effects *(Chapter 1)*.

In this section, a brief, representative overview of compounds, particularly those *specifically* relevant to the targets of this work, will be highlighted.

Compounds comprising 3,5-diethynylpyridine

As discussed in previous chapters, the 3,5-pyridyl motif is arguably the most accessible of all the possible 3,5-aryl functionalities (halo-, alkynyl-substituted, etc) with surface binding groups at the *ipso* position (*e.g.* –SAc, $–NH_2$, –COOH). It should therefore come as no surprise that several branched compounds containing 3,5-diethynylpyridyl are already known *(Figure 5-2* and *Figure 5-3)*.[2] Often, these approach the idealised structures shown in *Figure 5-1*.

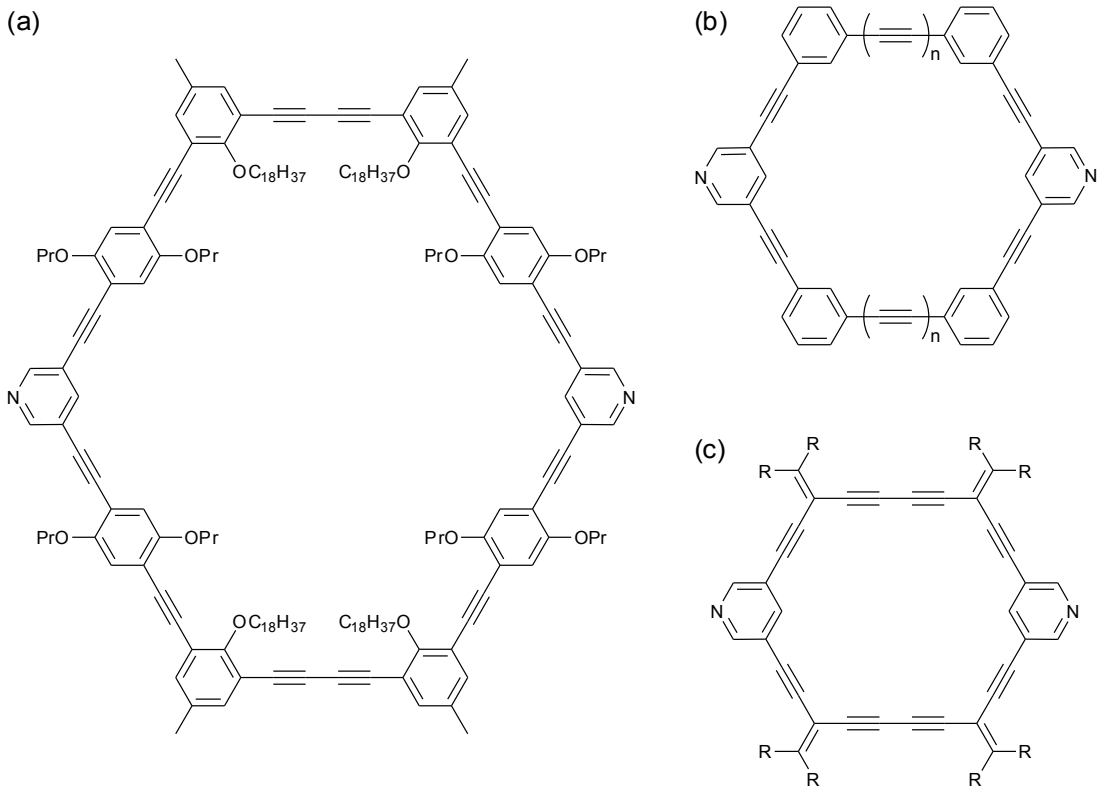

Figure 5-2. Conjugated, all-organic macrocycles containing the 3,5-diethynylpyridyl motif (R = Me, Ph, adamantylidene; n = 1, 2).[2b-e,2g,h,2j,2l]

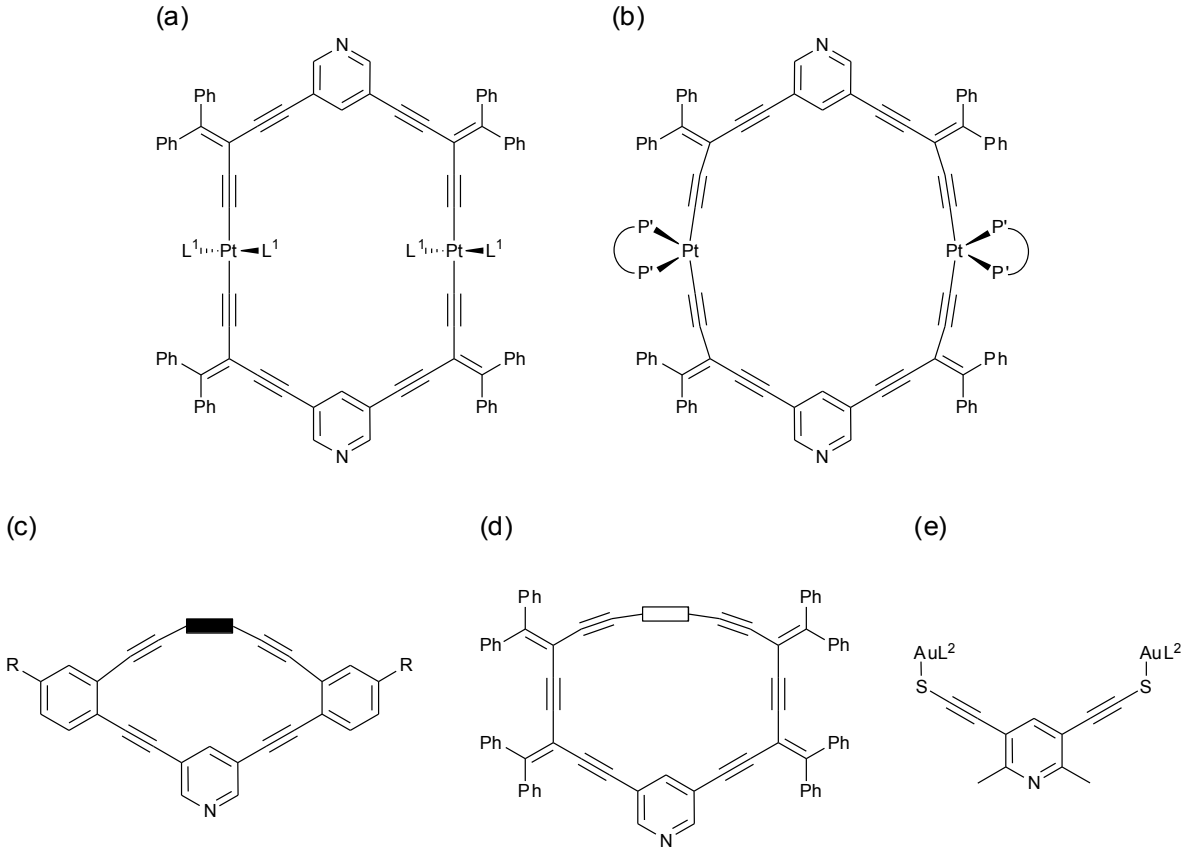

Figure 5-3. Some branched all-organic and Pt/Au-containing compounds with the 3,5-diethynylpyridyl motif (L^1 = PPh_3, PEt_3; P'–P' = *cis*-1,2-bis(diphenylphosphino)ethylene, (*S*,*S*)-chiraphos, (*R*,*R*)-chiraphos; R = H, ^{t}Bu; –■– = —, $Pt(PPh_3)_2$, $Pt(PEt_3)_2$; –□– = —, $Pt(PPh_3)_2$, (*S*,*S*)-chiraphos, (*R*,*R*)-chiraphos; L^2 = PPh_3, PPh_2Me, $PPhMe_2$, PMe_3, $AsPh_3$).[2a,2f,g,2i,2k-n]

Primarily these structures have been investigated as ligands for coordination chemistry (*e.g.* macrocyclic 4,4'-bipyridine analogues), and studied as potentially porous materials.[2e,2g,h,2l] Their *N*-complexes with Ru(porphyrinate),[2b,2d] $[Re(CO)_3(4,4'\text{-}t\text{-}Bu_2bpy)]PF_6$ (4,4'-*t*-Bu_2bpy = 4,4'-di-*tert*-butyl-2,2'-bipyridine),[2c] $Pt(PEt_3)_2$,[2e,2g] and $PtCl_2(SEt)$[2f] are known. On more than one occasion, solubility enhancement upon coordination of the pyridyl nitrogen has greatly facilitated isolation of the cycle.

Use of unmodified 3,5-diethynylpyridine as a ligand has been explored by Vicente *et al.* in a series of mono- and polymeric gold complexes, highlighting its multiple potential coordination modes.[3] Though non-conjugated, some interesting interlocked macrocycles have also been prepared from a coordinated 3,5-diethynylpyridine template.[4]

Macrocyclic arylethynyl materials

Whilst cyclic structures containing 3,5-diethynylpyridyl have been of growing interest over the last decade, those based on 1,3-diethynylbenzyl have been studied for nearly 40 years. The hexameric phenylene ethynylene macrocycle *(Figure 5-4a*, n = 6) may be taken as an example of progress. First obtained (4.6% yield) by Staab and Neunhoeffer in 1974 via Stephens–Castro coupling,[5] since then its extended family (*Figure 5-4a*, n = 3-8, 10, 12) has been prepared (in much improved yields) using a myriad of coupling techniques or alkyne metathesis.[6] With the latter, the hexamer was confirmed as the most thermodynamically stable oligomer (*vs.* smaller, n ≤ 5, or bigger, n ≥ 7, systems).[6i] Notably, with increasing ring size these compounds may adopt non-planar conformations to reduce strain *(Figure 5-4b)*.[7]

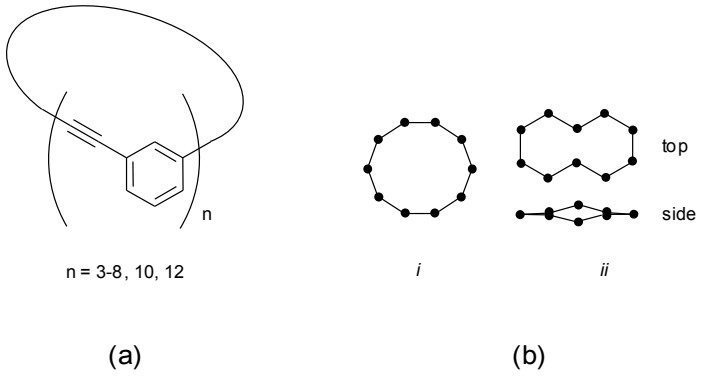

Figure 5-4. (a) The family of cyclic 1,3-phenylene ethynylene macrocycles. (b) Schematic diagrams of the possible planar *(i)* and non-planar *(ii)* conformations of the decameric 1,3-phenylene ethynylene macrocycle.[7]

Though they provide a straightforward starting point, it is implicit from the previous figures that moieties other than 1,3-aryls may be integrated into cyclic structures for the construct of 'angles'. *Strain-free* cycles have employed 1,3- and 1,2- substituted benzenes, substituted heterocycles, alkenes, cross-conjugated alkenes/alkanes, allenes, radialenes, and polycyclic aromatics/fused ring systems for such purposes, whereas *strained* systems have comprised these, and also alkynes, oligophenylenes, oligothiophenes, amongst others.[1b,1d]

5.3 FORCED-*CIS* GEOMETRIES (COMPLEXES WITH PP_3)

In postulating novel conjugated structures containing redox active centres, macrocyclic complexes of the type shown in *Figure 5-1b* were initially considered. In such materials the acetylide ligands would be forced into a stable *cis*-geometry by employing a tetradentate ancillary ligand (such as PP_3) at the metal centre. Though ruthenium *cis*-acetylide complexes with monophosphine ligands are known (*e.g.* PMe_3/$PPh_2(C{\equiv}C{-}R)$, where R = Ph, *p*-tolyl, Fc),[8] these have shown potential for isomerization into the *trans*-isomer (either thermally[8a] or photochemically[8b]) and are typically formed as *cis*/*trans* mixtures.

To the best of my knowledge there is only one report describing the syntheses of *cis* bis-acetylide complexes with $Ru(PP_3)$ centres.[9] These were prepared by Bianchini *et al.* in 1994 from the reaction of *cis*-$RuH_2(PP_3)$ with $X{-}C{\equiv}C{-}C_6H_5$ (X = H, elimination of H_2 method, *Scheme 4-2vi*; X = Li, displacement, *Scheme 4-2iii*). Whereas the bis-acetylide (air stable in solution) was accessed simply by heating reagents in toluene (with *excess* phenylacetylide), the mono-acetylide/hydride (air sensitive in solution) required *stoichiometric* control of reagents (with phenylacetylide), or use of lithium phenylacetylide. It was therefore of additional interest here to develop improved step-wise methods for the preparation of bis-alkynyl species from $RuX_2(PP_3)$, if possible.

Based on the established procedures in the first instance, a route from *cis*-$RuH_2(PP_3)$ to the desired homo-metallic macrocycle was envisaged as shown in *Scheme 5-1*.

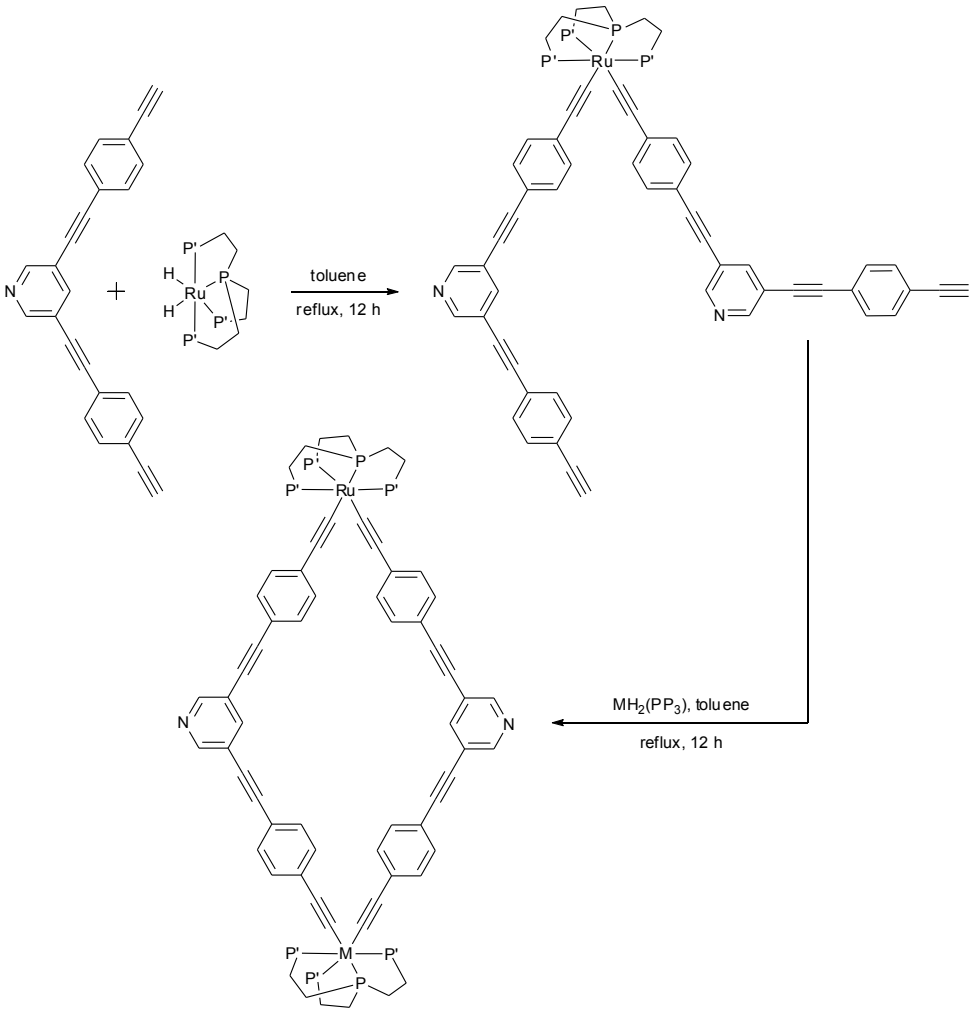

Scheme 5-1. Proposed synthesis of a macrocycle containing $M(PP_3)$ centres (M = Ru, Os), where the acetylide ligands are forced into a *cis*-geometry as a result of the coordinated tetradentate ancillary ligand (P' = PPh_2).

5.3.1 Progress towards $M(PP_3)$-containing macrocycles

Preparation of $MCl_2(PP_3)$ and formation of butenynyl complexes

As precursors to $MH_2(PP_3)$,* $MCl_2(PP_3)$ (M = Ru, Os) complexes were successfully synthesised[10-11] via ligand substitution of $RuCl_2(PPh_3)_3$[12] or $OsCl_2(PPh_3)_3$[13] *(Figure 5-5)*.†

* Not attempted here, from these materials the metal dihydrides may be prepared by reaction with $LiAlH_4$.[10]

† It has yet to be established whether $Os(PP_3)(C{\equiv}C{-}C_6H_5)_2$ complexes can also be produced via elimination of H_2/displacement reactions from $OsH_2(PPh_3)$.

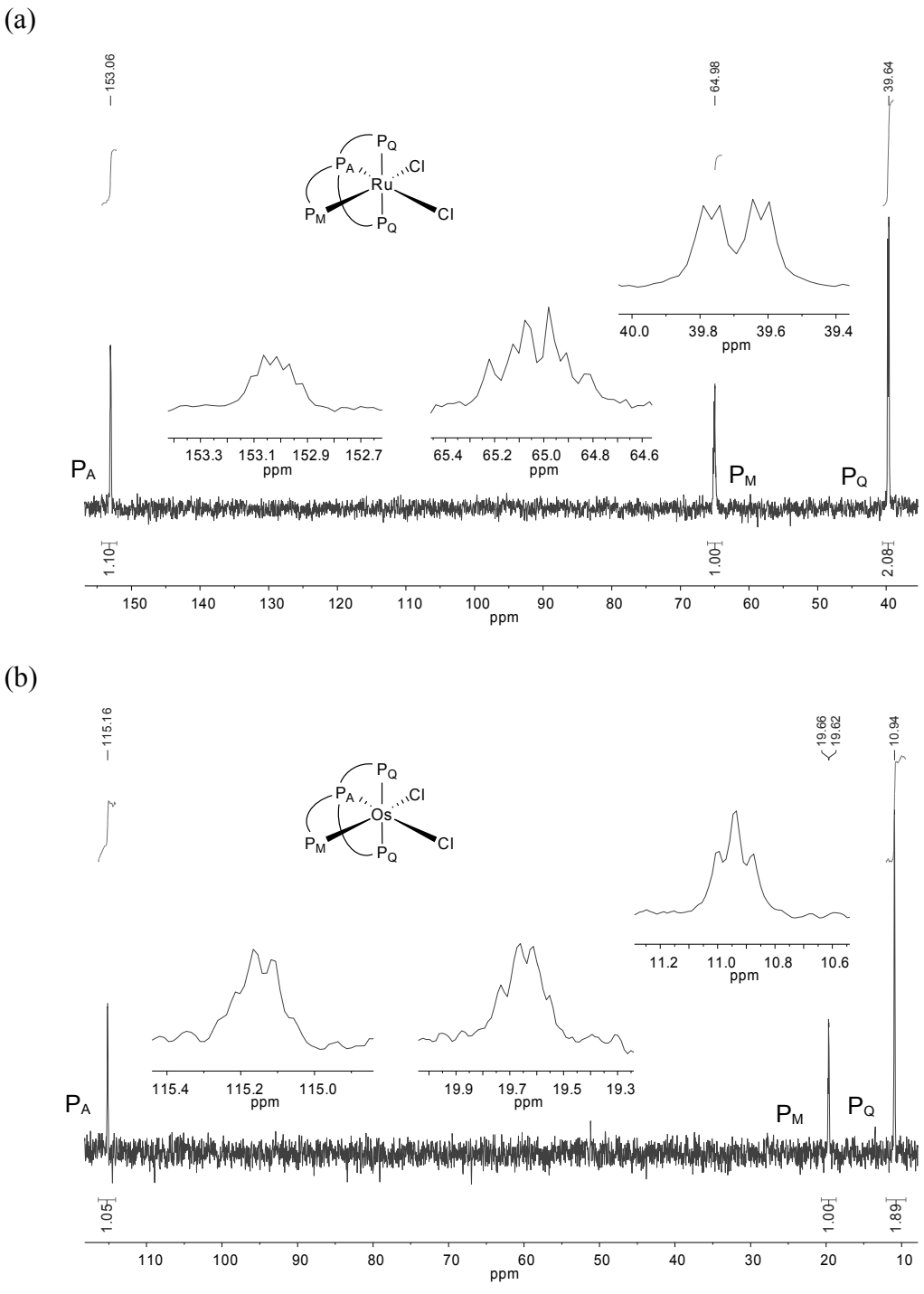

Figure 5-5. $^{31}P\{^{1}H\}$ NMR spectra ($CDCl_3$) of (a) $RuCl_2(PP_3)$ and (b) $OsCl_2(PP_3)$. The three phosphorus environments correspond to PPh_2 *trans* to PPh_2 (P_Q, resonance of approx. double intensity), PPh_2 *trans* to Cl (P_M), and the PR_3 apex (P_A).

Step-wise σ-alkynyl complex formation from the metal dichlorides (Dixneuf approach) was investigated *(Scheme 4-3)*. As *cis*-isomers they should be reasonably active in this context *(see section 4.2.3)*. However, reactions between $RuCl_2(PP_3)$ and terminal alkynes (C≡C–Ph, C≡C–$SiMe_3$) under typical conditions (CH_2Cl_2, $NaPF_6$, NEt_3) led only to the formation of butenynyl complexes (PF_6^- salts, *Scheme 5-2)*. Practically identical to known compounds (with BPh_4^- anions),[14] crude samples were identified via their $^{31}P\{^1H\}$ NMR spectra *(Figure 5-6* and *Figure 5-7*, with splitting patterns similar to $MCl_2(PP_3)$), but not further characterised. In retrospect their formation is perhaps not surprising, given that the syntheses of analogous complexes from $MCl_2(L)$ have previously been described (M = Fe,[15] Os[14c]; L = $P(CH_2CH_2PMe_3)_3$, dmpe, PP_3).

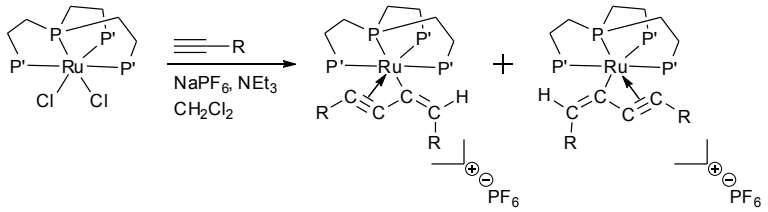

Scheme 5-2. Attempted syntheses of $Ru(PP_3)(C{\equiv}C{-}R)_2$ complexes via reaction of $RuCl_2(PP_3)$ and H–C≡C–R under Dixneuf conditions resulted instead in butenynyl complexes (R = Ph, $SiMe_3$; P' = PPh_2).

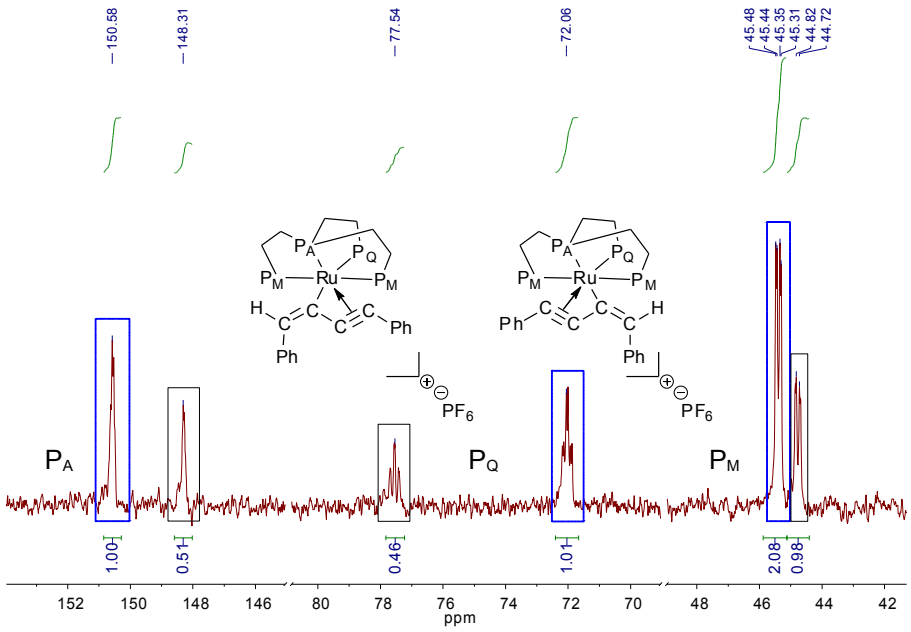

Figure 5-6. $^{31}P\{^{1}H\}$ NMR ($CDCl_3$) of $[(PP_3)Ru(\eta^3\text{–}PhC_3CHPh)]PF_6$, formed from reaction of phenylacetylene and $RuCl_2(PP_3)$ under Dixneuf conditions (resonances attributable to PF_6 excluded for clarity). As with the BF_4^- salt, this complex forms in a mixture of *E* and *Z* isomers (associated resonances indicated by rectangles).

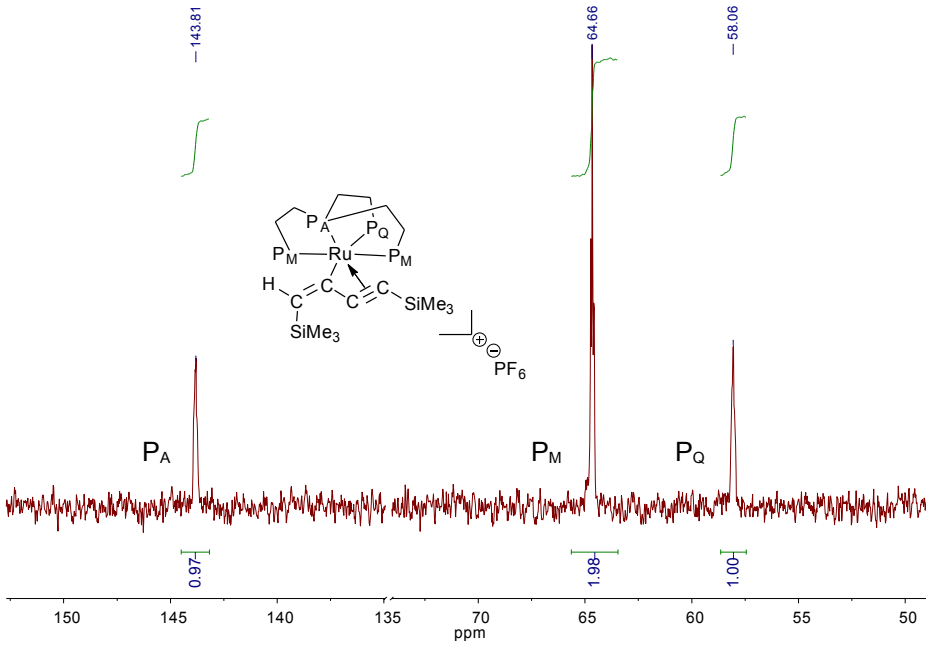

Figure 5-7. $^{31}P\{^{1}H\}$ NMR spectrum ($CDCl_3$) of $[(PP_3)Ru\{\eta^3\text{-}(SiMe_3)C_3CH(SiMe_3)\}]PF_6$, formed from reaction of trimethylsilylacetylene and $RuCl_2(PP_3)$ under Dixneuf conditions (resonances attributable to PF_6 excluded for clarity).

Ligand synthesis

Work towards the branched ligand presented in *Scheme 5-1* proceeded without significant difficulty. From 3,5-dibromopyridine, iterative Sonogashira cross-coupling/desilylation reactions with trimethylsilylacetylene and 1-bromo-4-(trimethylsilyl)ethynylbenzene (**L1**) (obtained from 1-bromo-4-iodobenzene via the literature procedure[16]) yielded the silyl-protected precursor **27** in three steps *(Scheme 5-3)*.‡ This novel compound was fully characterised by the usual methods and its UV-vis spectrum is shown in *Figure 5-9* (with data in *Table 5-1)* (for full experimental details see *Chapter 8)*. The characteristic 3,5-pyridyl motif (a doublet downfield to a triplet, 2:1 intensity) is clearly observed in its ^{1}H NMR spectrum *(Figure 5-8)*, as are singlet resonances for $Si(CH_3)_3$ (18H) and for Ar–*H* (8H) (the latter due to strong coupling effects, where $\Delta\delta/J << 0.5$§).

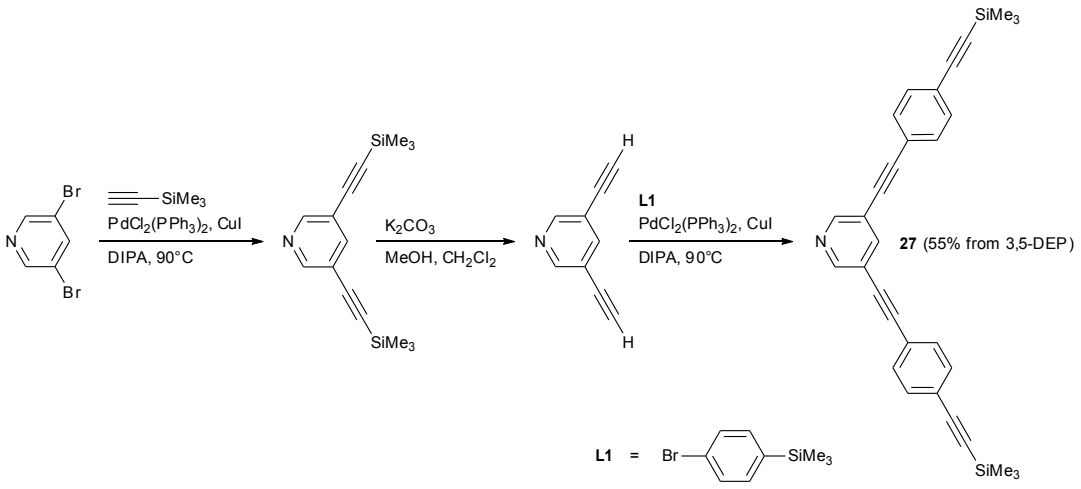

Scheme 5-3. Synthesis of a novel protected pyridyl ligand **27** (3,5-DEP = 3,5-diethynylpyridine).

‡ High reaction concentrations for the cross-couplings proved essential to the isolation of desired materials from their mixtures with monosubstituted reaction products (e.g. 3-bromo-5-(trimethylsilyl)ethynylpyridine and 3-ethynyl-5-[4-(trimethylsilyl)ethynylbenzene]ethynylpyridine).

§ This 'singlet' proton resonance correlates to two distinct carbon environments in 2D (HMQC) experiments.

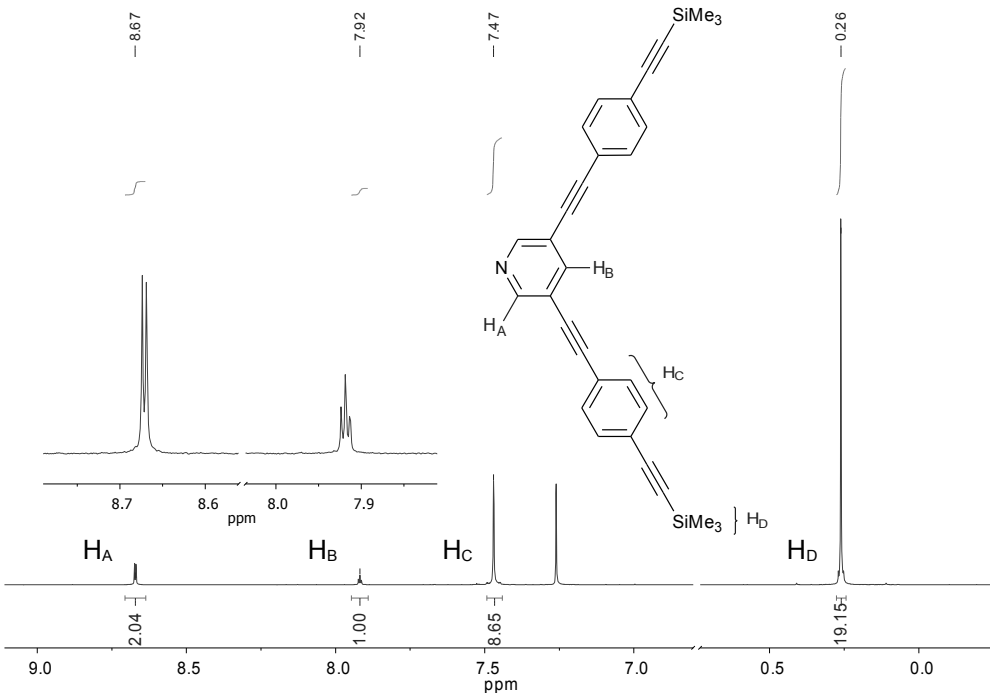

Figure 5-8. ^{1}H NMR spectrum ($CDCl_3$) of protected pyridyl ligand **27**.

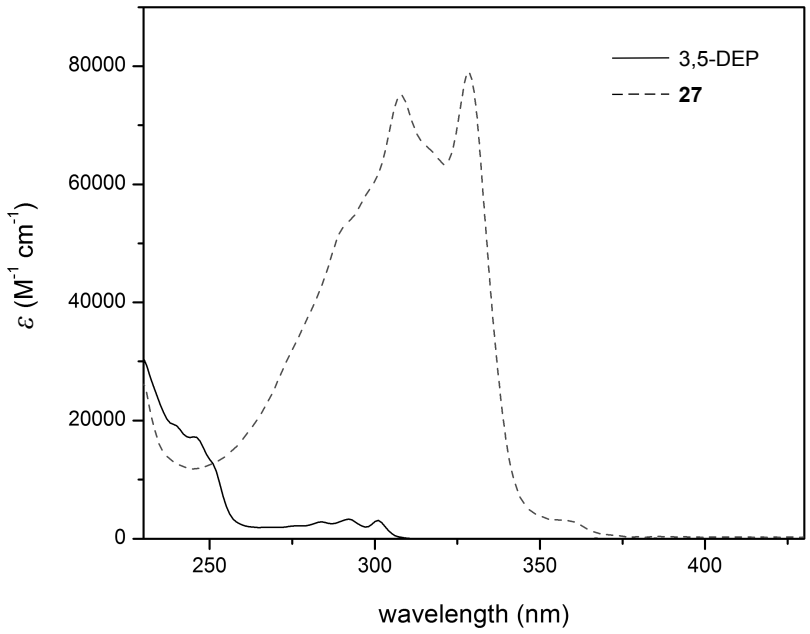

Figure 5-9. UV-vis spectra (in CH_2Cl_2) of 3,5-diethynylpyridine (3,5-DEP) and protected pyridyl ligand **27**. The increased conjugation pathway of the latter results in absorptions at lower energies (decreased HOMO-LUMO gap), and a significantly larger molar absorptivity is observed.

Table 5-1. Electronic spectral data of ethynylpyridine ligands.[a]

compound	λ_{max} /nm (ε /M^{-1} cm^{-1})[b]
3,5-DEP	248infl (15443), 276 (2186), 284 (2839), 292 (3331), 301 (3112)
27	281sh (39019), 292sh (53663), 298sh (58823), 308 (75213), 318sh (65224), 329 (78663), 359 (3069)

[a] Recorded at room temperature in CH_2Cl_2, using quartz cells with a pathlength of 10 mm. [b] Where possible, spectra were deconvoluted into composite Gaussian bands[**] to obtain λ_{max} values. All extinction coefficients were taken from the experimental data at these wavelengths.

Tactical shift to Ru(dppe)₂ systems

Despite modest progress to this point, efforts towards macrocycles based on $M(PP_3)$ were refocused to the syntheses of those based on $Ru(dppe)_2$. With the latter, starting materials are more conveniently prepared (*cis*-$RuCl_2(dppe)_2$/$[RuCl(dppe)_2]OTf$/terminal alkynes *vs.* metal hydrides/lithiated alkynes), step-wise bis-acetylide synthesis is readily achievable, and, following the work in *Chapter 4* (conducted in parallel), reactions between $Ru(dppe)_2$ centres and pyridyl-containing alkynes were now better understood. Though not of immediate concern, this transition from *cis*- to *trans*-ruthenium geometries also circumvented potential synthetic complications should undesirable butenynyl formation occur from *cis*-$M(PP_3)(C{\equiv}C{-}R)_2$ *(vida supra)*.

5.3.2 Metal complexes with pendant 'phosphorus arms'

Trans-*$RuCl_2(PP_3)_2$*

Prior to discussions of branched $Ru(dppe)_2$-containing compounds, the synthesis and properties of a new complex, *trans*-$RuCl_2(PP_3)_2$ (**28**), are worthy of note. This unusual compound was repeatedly isolated as a minor side product from syntheses of *cis*-$RuCl_2(PP_3)$ (where $RuCl_2(PPh_3)_3$ was reacted with PP_3 in slight excess), and could be synthesised directly from $RuCl_2(PPh_3)_3$ using ≥2 equivalents of PP_3 *(Scheme 5-4)*. Quite unusually it comprises two potentially *tetradentate* PP_3 ligands each coordinated through only *two* sites (in blatant disregard of the chelate effect), and as a result features four uncoordinated 'phosphorus arms'. Whether this bonding arrangement is due to steric/strain effects, or because *trans*-$RuCl_2(L_n)$ is

[**] Using the 'Fit Plot' tool of *MagicPlot Student v2.3*.

thermodynamically more stable than *cis*-$RuCl_2(L_n)$ (as observed with the isomers of $RuCl_2(dppe)_2$), is unclear. In addition to the usual methods, **28** was characterised by UV-vis spectroscopy *(Figure 5-10)*, X-ray crystallography *(Figure 5-11*, with selected bond lengths and angles provided in *Table 5-2)* and cyclic voltammetry *(Figure 5-12)*.

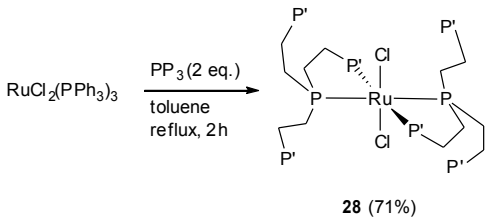

Scheme 5-4. Synthesis of $RuCl_2(PP_3)_2$ (with ~1 eq. PP_3, the mono-ligated $RuCl_2(PP_3)$ complex forms as the main product)

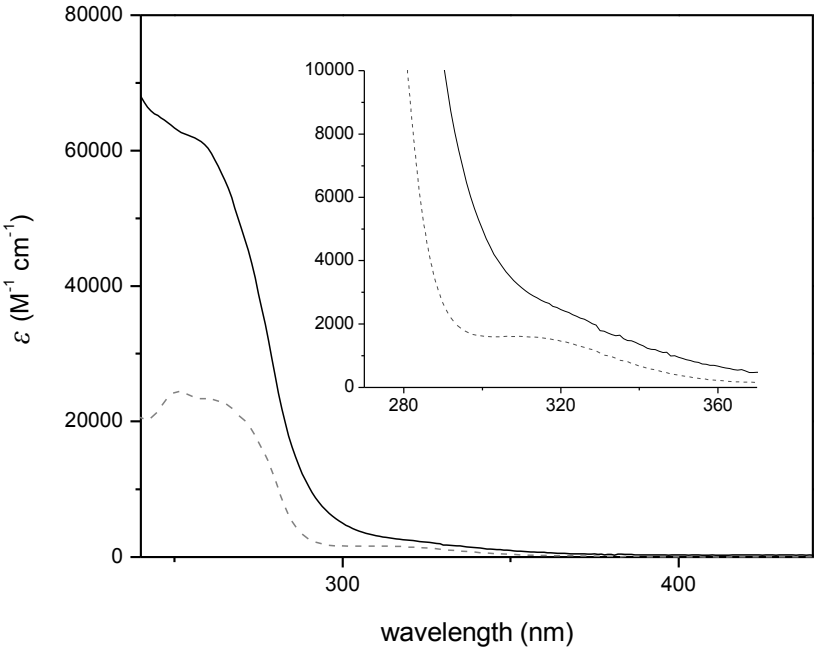

Figure 5-10**.** UV-vis spectrum of **28** in CH_2Cl_2 (solid line), and the spectrum of $RuCl_2(dppe)_2$ in $CHCl_3$ (dashed line) for comparison. Inset, absorptions in the visible region magnified. Similar features are observed in both cases; see *Chapter 4* for a relevant discussion.

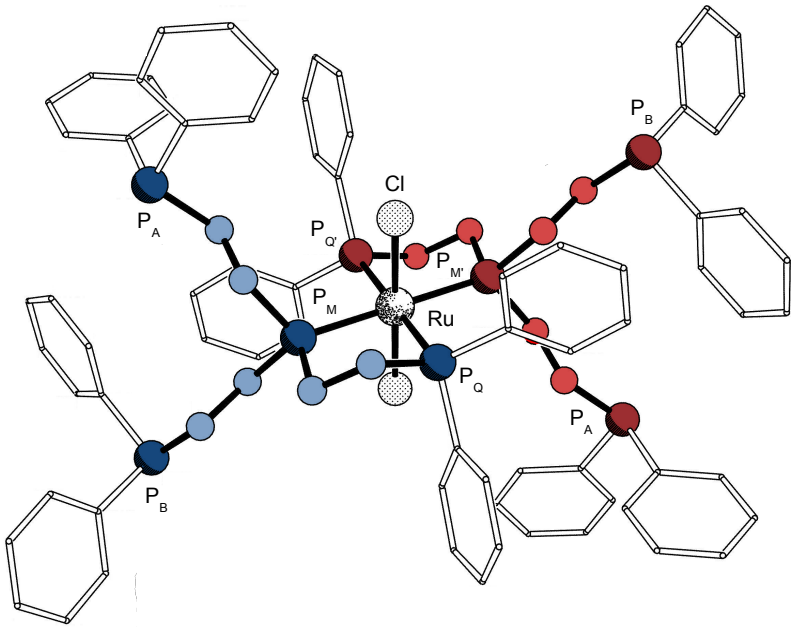

Figure 5-11. Crystal structure of $RuCl_2(PP_3)_2$ (**28**) (with hydrogen atoms omitted and colour added to the backbone of each ligand for clarity).

Table 5-2. Selected bond lengths and angles for *trans*-$RuCl_2(PP_3)_2$ (**28**) and analogous ruthenium complexes.

complex	Ru–Cl (Å)	Ru–P (Å)	P–Ru–Cl (°)[a]	P–Ru–P (°)[a]	ref
trans-$RuCl_2(depe)_2$	2.428	2.340	90.65	96.61	*17*
		2.338	89.35	83.39	
			92.63		
			87.37		
trans-$RuCl_2(dppe)_2$[b]	2.433	2.381	81.40	98.38	*18*
		2.356	94.19	81.62	
			98.60		
			98.38		
trans-$RuCl_2(PP_3)_2$ (**28**)	2.434	2.389	92.50	97.49	this work
		2.358	87.50	82.51	
			98.02		
			81.98		

[a] Angles provided are between *cis*-substituents, with the angle between *trans*-substituents always 180.0° in these examples. [b] Other X-ray crystal structures of this compound are known.[19]

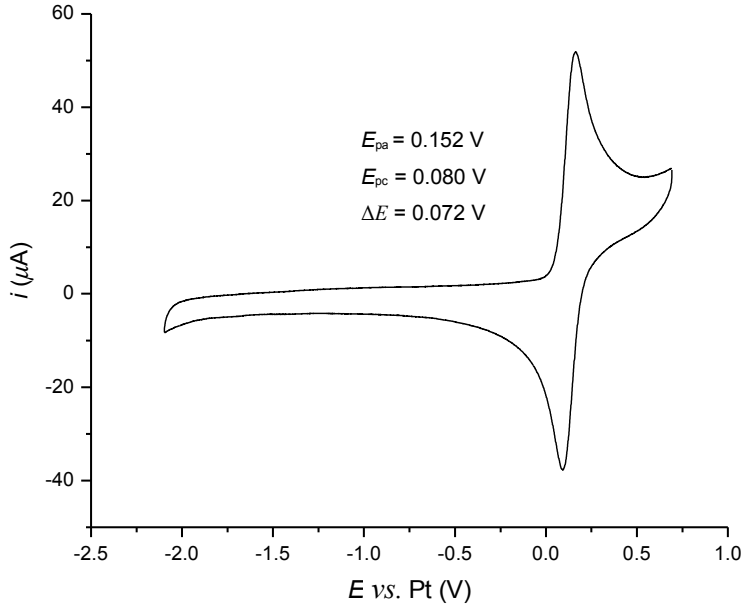

Figure 5-12. Cyclic voltammogram for $RuCl_2(PP_3)_2$ (**28**). Scan rate = 0.1 Vs^{-1}, $Bu_4N^+PF_4^-$ (0.1 M) in CH_2Cl_2 with glassy carbon working electrode and Pt-wire reference and counter electrodes. Potentials are corrected for iR_s and reversible redox features ($i_p \propto V_s^{1/2}$, $\Delta E \approx 0.059/n$ V) assigned to the Ru(II)/Ru(III) couple. $E_{1/2}$ = 0.116 V *vs.* $[FcH]^+/[FcH]$, measured against an internal $[FeCp^*_2]^+/[FeCp^*_2]$ reference (-0.495 V *vs.* $[FcH]^+/[FcH]$ in this system). As in *Chapter 4*, i_{pa}/i_{pc} = 1.1 (*i.e.* > 1) is attributed to difficulties in defining the baseline for the reduction wave.

The $^{31}P\{^1H\}$ NMR spectrum of this complex is particularly interesting *(Figure 5-13)*. Three resonances are observed with relative intensities 1:1:2 and a rather complicated splitting pattern. It is hypothesized that in **28** the pendant PPh_2 moieties of each ligand are *chemically* non-equivalent as they cannot be interchanged by any symmetry operation (the molecular point group is C_i), and the bound $P_M/P_{M'}$ and $P_Q/P_{Q'}$ nuclei are *magnetically* non-equivalent as $J_{MQ} \neq J_{MQ'}$ (*i.e.* an ABMQ-ABM'Q' system). The resonance at δ 49.57 ppm can thus be attributed to the apical phosphorus atoms, P_M ($P_{M'}$), appearing as a broad multiplet (unresolved dddd) due to ^2J coupling with $P_{Q'}$ (P_Q) and ^3J coupling with P_A, P_B and P_Q ($P_{Q'}$). Further upfield at δ 40.70 ppm appears a pseudo-triplet (unresolved dd) assigned to the coordinated PPh_2 group, $P_Q/P_{Q'}$, from coupling to P_M and $P_{M'}$. Finally, at δ −11.83 ppm there is another resonance, corresponding to the uncoordinated phosphorus atoms, P_A and P_B. As these have similar but non-identical chemical

shifts (also notably comparable to that of PPh$_2$ in the free ligand, at approximately δ –13 ppm), their overlapping doublets (from ^3J coupling to P_M/$P_{M'}$) appear as a triplet. $^{31}P\{^{31}P\}$ NMR experiments could be used to verify this explanation of the observed spectral characteristics.

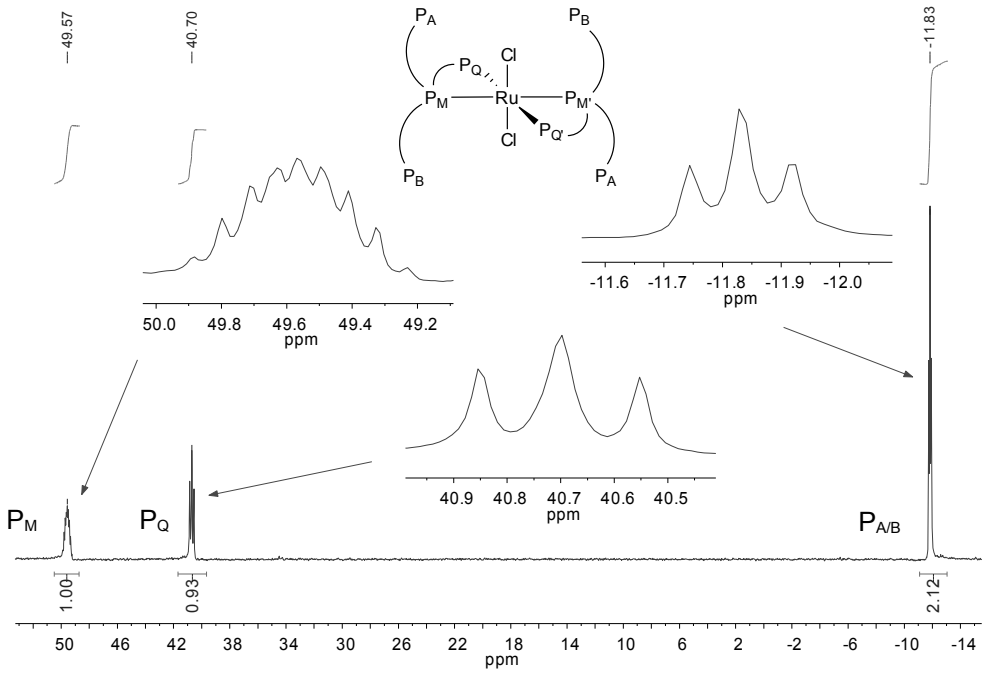

Figure 5-13. $^{31}P\{^1H\}$ NMR spectrum ($CDCl_3$) of $RuCl_2(PP_3)_2$ (P_X = PPh_2).

$MCl_2(PP_3)_2$ analogues

To the best of my knowledge, the only other mononuclear complexes with incompletely coordinated tripodal phosphines and a 1:2 metal to ligand ratio are $RuCl_2$(triphos)$_2$ (triphos = bis(diphenylphosphinoethyl)phenylphosphine),[20] $Mo(PP_3)_2$,[21] and $MX_2(L)_2$ (M = Pt, Pd; L = PP_3, tris[2-(diphenylphosphino)ethyl]amine; X = Cl, Br, I, NO_3)[22] *(Figure 5-14)*. This scarcity prompted investigations into the synthesis of additional group 8 species.

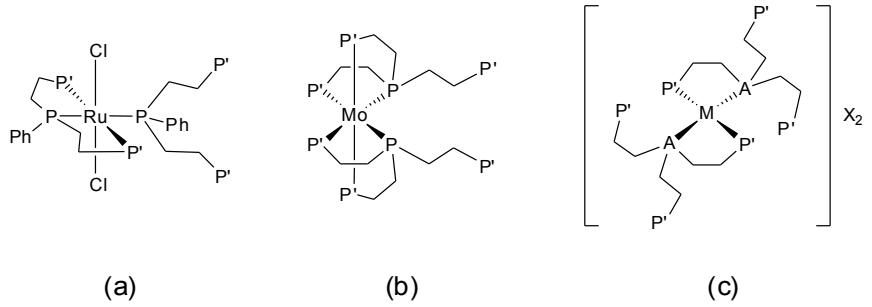

Figure 5-14. Mononuclear complexes with incompletely coordinated tripodal phosphines and a 1:2 metal to ligand ratio (P' = PPh_2; M = Pt, Pd; A = P, N; X = Cl, Br, I, NO_3).[20-22]

Noting that $RuCl_2(PP_3)_2$ was readily formed following identical reaction conditions to $RuCl_2(PP_3)$ (albeit with two equivalents PP_3 rather than one), the preparation of its Fe and Os congeners was attempted following the literature procedures for their mono-ligated complexes (*i.e.* heating PP_3 with $OsCl_2(PPh_3)_3$/$FeCl_2$ at reflux in 2-methoxyethanol/ethanol, respectively).[11,23] Unfortunately, these efforts produced only multiple product mixtures that could not be separated or identified (providing no clear evidence for the formation of $MCl_2(PP_3)_2$). It is however anticipated that the desired complexes *could* be formed using alternative literature procedures (*e.g.* for $FeCl_2(PP_3)$[24]), or suitable conditions deduced by systematic variation of solvent, temperature and reaction time. Indeed, whilst an inseparable mixture product was again obtained when PP_3 (2 eq.) was reacted with $OsCl_2(PPh_3)_3$ in hot toluene (the conditions used to prepare $RuCl_2(PP_3)_n$, n = 1, 2), in this case mass spectrometric analysis revealed a *m/z* fragment suggestive of $OsCl_2(PP_3)_2$.[††]

5.4 *TRANS*-ACETYLIDES (COMPLEXES WITH DPPE)

The simplest conceivable bimetallic *trans*-$Ru(dppe)_2$-containing macrocycle (**35**) (with a phenylene ethynylene backbone and pyridyl surface binding moieties) is shown in *Figure 5-15b*, alongside its single- (**37**) and double-branched analogues. Whilst conceptually similar to the ferrocene-based compounds of *Chapter 2* (and accordingly analogous to the theoretically investigated structures of Magoga and Joachim, *Figure 5-15a)*,[25] preparations of these ruthenium

[††] For $OsCl_2(PP_3)_2$ – ES+: *m/z* 1567 ($[M–Cl]^+$ calcd: 1567); for $RuCl_2(PP_3)_2$ – ES+: *m/z* 1513 ($[M]^+$ calcd: 1513), 1477 ($[M–Cl]^+$ calcd: 1477).

complexes were not expected to suffer from slow reaction rates (unlike Sonogashira cross couplings with Fc–I using traditional methods, see *Chapter 3)*, and it is considered that such complexes should prove easier to study in molecular junctions due to the fixed *trans* orientation of acetylide ligands at $Ru(dppe)_2$.

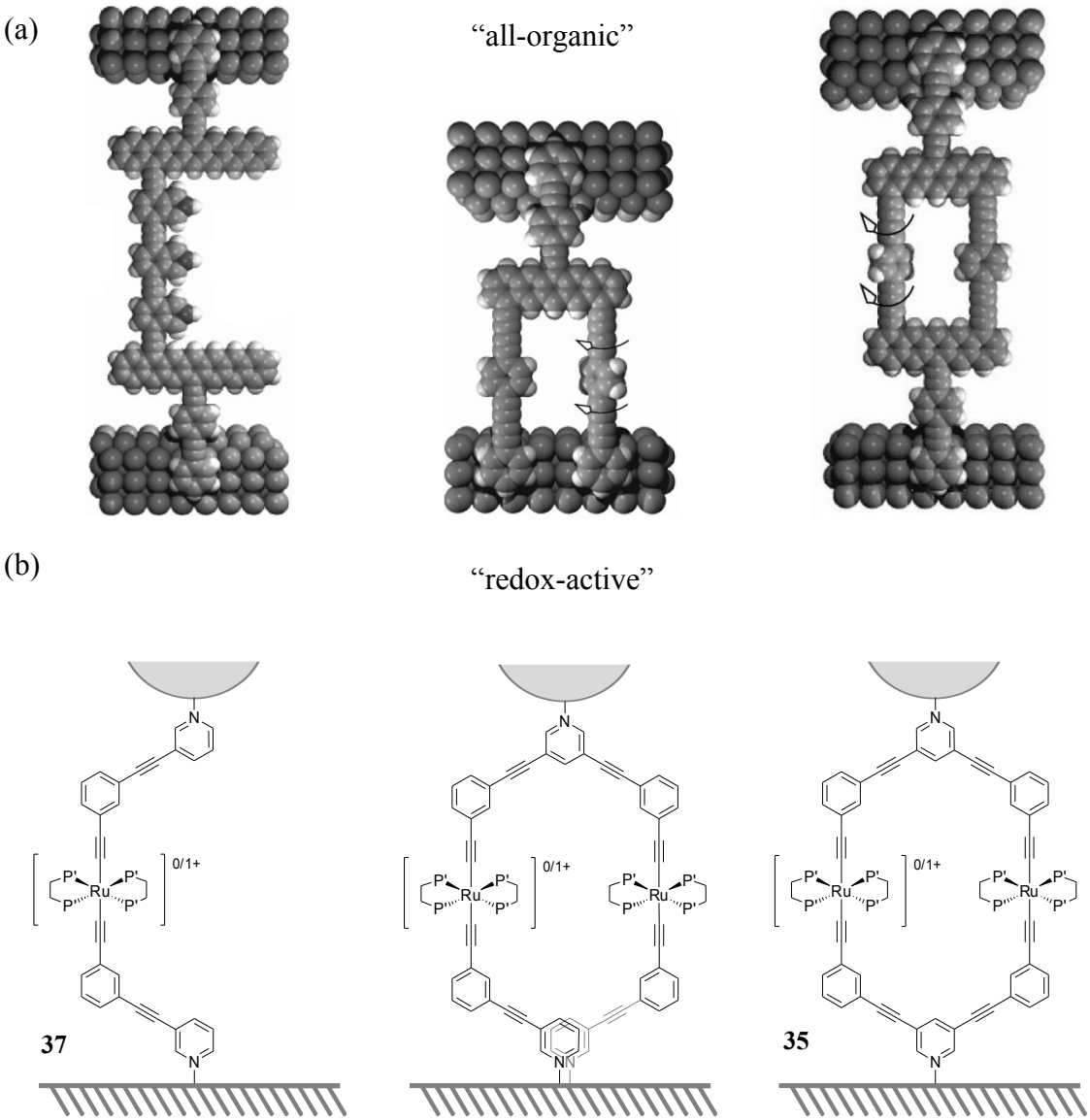

Figure 5-15. Linear, branched and macrocyclic systems for molecular electronics – (a) example "all-organic" theoretical structures investigated by Magoga and Joachim (phenyl rotation disrupting branch conductance),[25] (b) experimental "redox-active" analogues proposed here (redox events changing branch conductance, P' = PPh_2). Figures (top) reprinted from reference [25] with permission.

5.4.1 Synthesis

Initially the preparation of **35** was attempted via a two-step route, starting with the reaction of [RuCl(dppe)$_2$]OTf and 3,5-bis(1-ethynyl-3-phenylethynyl)pyridine[2c] (**L2**) *(Scheme 5-5)*. This produced a crude product exhibiting ^{1}H/^{31}P{^{1}H} NMR spectra strongly suggestive of the desired intermediate (**HC1**), however all attempts at its isolation proved futile. Given the difficulties using 4-ethynylpyridine with [RuCl(dppe)$_2$]OTf *(Chapter 4)*, it is likely that persistent impurities were again formed from side reactions at the pyridyl nitrogen (and in retrospect purifications may have been hindered by further decomposition/reaction of the material in CH_2Cl_2)

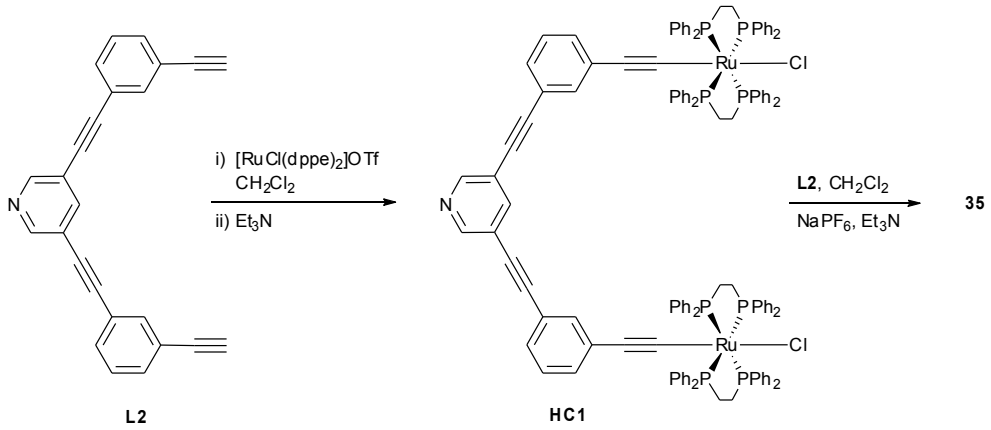

Scheme 5-5. An unsuccessful synthetic route to **35** – the intermediate (**HC1**) could not be isolated pure.

Much greater success was achieved using a step-wise approach that avoided contact of the pyridyl moiety with 16e$^-$ ruthenium centres *(Scheme 5-6)*. Here, [RuCl(dppe)$_2$]OTf[12] *(Scheme 4-5)* was reacted with 1-(triisopropylsilyl)ethynyl-3-ethynylbenzene[26] (**L3**, *Scheme 5-7)* to produce a vinylidene intermediate that was deprotonated (by elution through alumina) to yield the mono-acetylide **29** (79%). The asymmetrical bis-acetylide **32** (90%) was prepared from this by stirring with 1-ethynyl-3-iodobenzene (**31**, *Scheme 5-8)*, $NaPF_6$ and Et_3N. Room temperature Sonogashira cross-coupling[27] of the aryl iodide **31** with 3,5-diethynylpyridine (3,5-DEP, *Scheme 2-12)* resulted in **33** (61%), which was subsequently de-silylated[28] with tetrabutylammonium fluoride giving **34** (47%). The crude macrocycle **35** was obtained in reasonable yield (~40%, ≥80% pure by ^{1}H NMR) following cross-coupling of **34** with 3,5-diiodopyridine[29] (3,5-DIP, *Scheme 5-9)*.

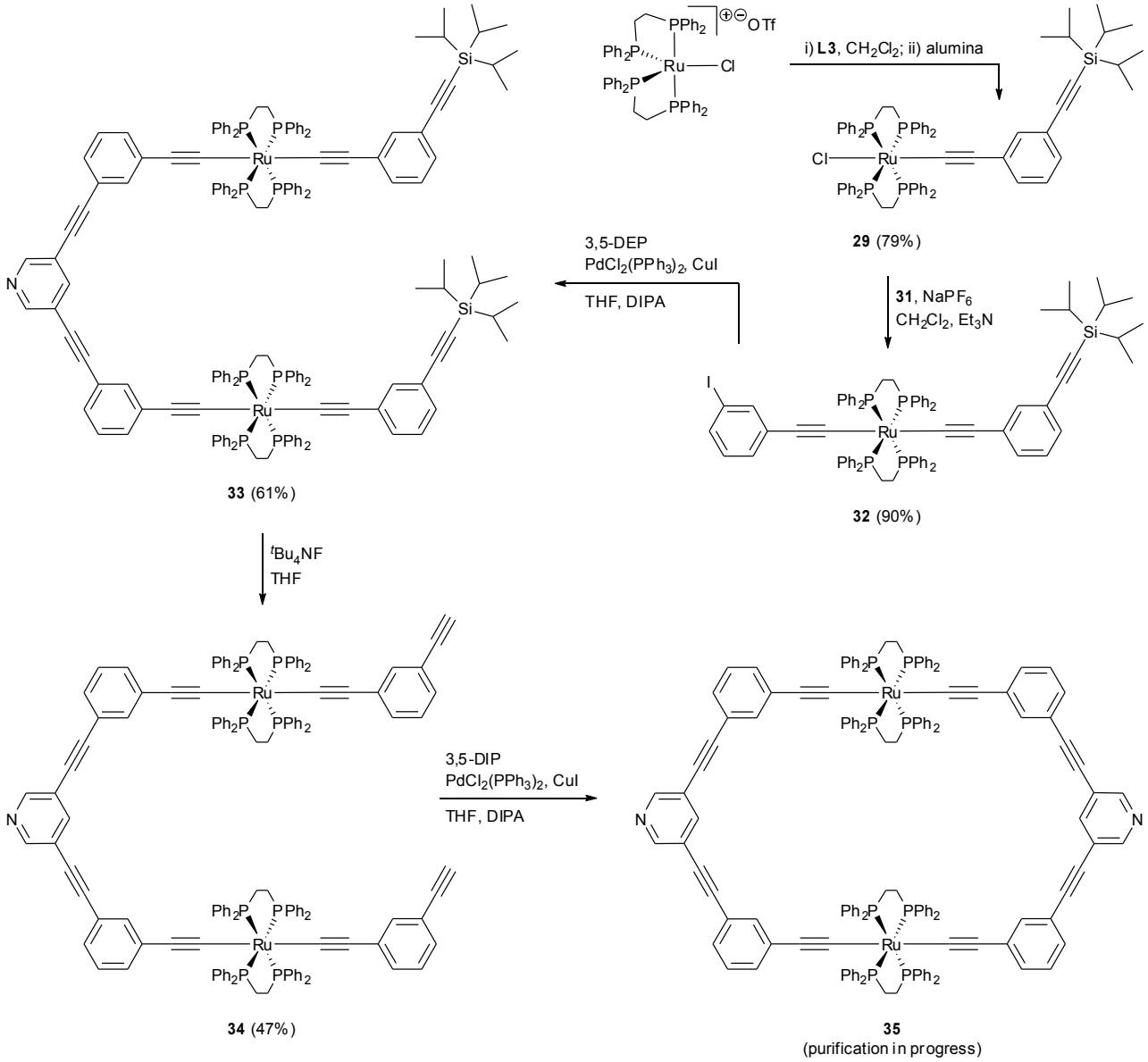

Scheme 5-6. A synthetic route to **35** that avoids contact of the pyridyl moiety with $16e^-$ ruthenium centres (**L3** = 1-(triisopropylsilyl)ethynyl-3-ethynylbenzene; 3,5-DEP = 3,5-diethynylpyridine; 3,5-DIP = 3,5-diiodopyridine).

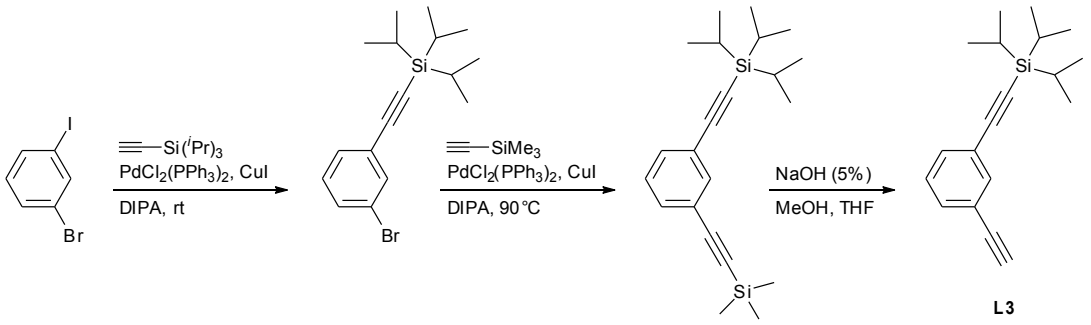

Scheme 5-7. Modified literature synthesis of 1-(triisopropylsilyl)ethynyl-3-ethynylbenzene (**L3**).[26]

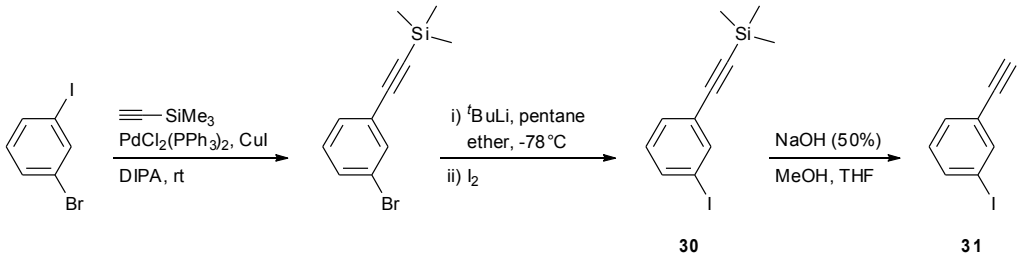

Scheme 5-8. Synthesis of 1-ethynyl-3-iodobenzene (**31**) (1-bromo-3-(trimethylsilyl)ethynylbenzene[30] prepared according to typical Sonogashira cross-coupling procedures).

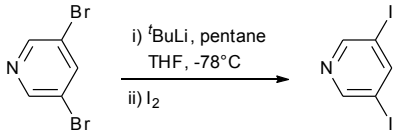

Scheme 5-9. Synthesis of 3,5-diiodopyridine (3,5-DIP). Whilst yields of 14-83.5% are reported for this approach,[29] attempts here provided <10% product.

Synthesis of the single-branched analogue was achieved in two steps via a similar approach. Reaction of *cis*-Ru(dppe)$_2$[12] *(Scheme 4-5)* and **31** with excess $NaPF_6$ and Et_3N over 2 days[27,31] provided **36** (78%), and subsequent cross-coupling with 3-ethynylpyridine (3-EP) resulted in **37** (85%).

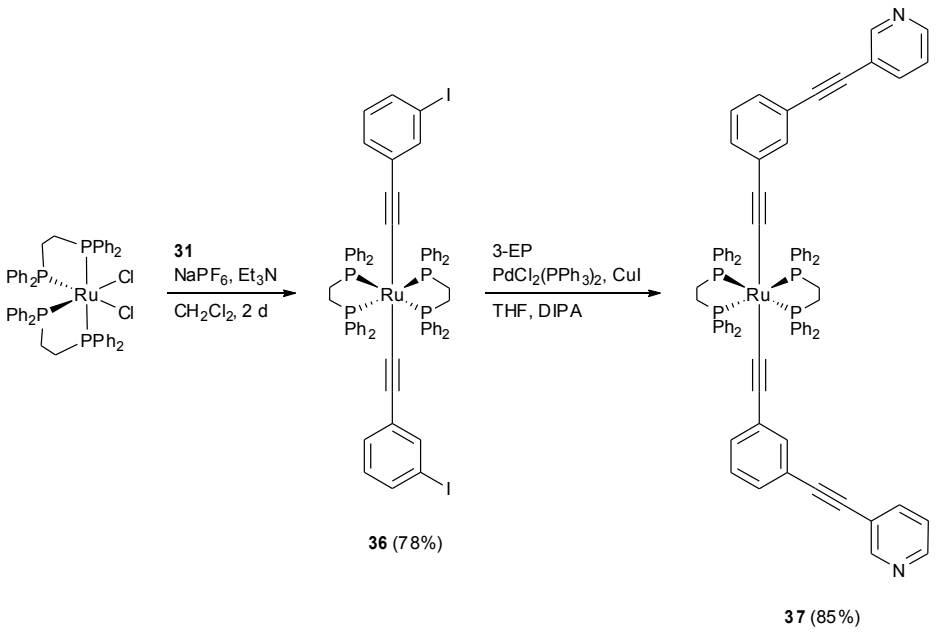

Scheme 5-10. Synthesis of single-branched complex **37** (3-EP = 3-ethynylpyridine).

These materials were all found to be air stable in the solid state, and could be manipulated in oxygenated solutions for short periods. However, once pyridyl moieties had been incorporated into complexes it proved essential to minimise their contact with oxygenated $CHCl_3$, and to avoid CH_2Cl_2 completely. The rapid decomposition of **33** and **34** in the latter was observed, though they were stable in $CDCl_3$ for several days (similar behaviour was noted for analogous linear ruthenium complexes, see *Chapter 4)*.

Whilst preparation of the double-branched analogue of **35** and **37** *(Figure 5-15)* has not yet been attempted, it is considered readily achievable via Sonogashira cross-coupling of **34** with 3-iodopyridine.

5.4.2 Characterization

All novel precursors to **35** (*i.e.* **29**, **32**, **33**, **34**, **36**) and **37** were characterised by $^{1}H/^{31}P\{^{1}H\}/^{13}C\{^{1}H\}$ NMR (selected spectra provided in *Figure 5-16*, *Figure 5-17* and *Figure 5-18*) and IR[‡‡] spectroscopy, mass spectrometric[§§] and elemental analyses (see *Chapter 8* for full

[‡‡] Characteristic bands at 2045-2063 cm^{-1} for ν(Ru–*C*≡*C*), ~2148 cm^{-1} for $\nu(C{\equiv}C)_{TIPS}$, ~2212 cm^{-1} for $\nu(C{\equiv}C)_{Py}$ and 3288 cm^{-1} for ν(C≡*C*–*H*).

[§§] $[M–Cl]^+$ observed with FAB+ for the mono-acetylide **29**, and $[M+H]^+$ or M^+ with ESI+ for the bis-acetylides.

details). Though isolation of **35** in pure form has not yet been achieved,*** its successful synthesis is supported by ^{1}H and $^{13}C\{^{1}H\}$ NMR spectroscopy *(Figure 5-19*, with the latter almost completely assigned through correlation experiments), as well as mass spectrometric analysis.

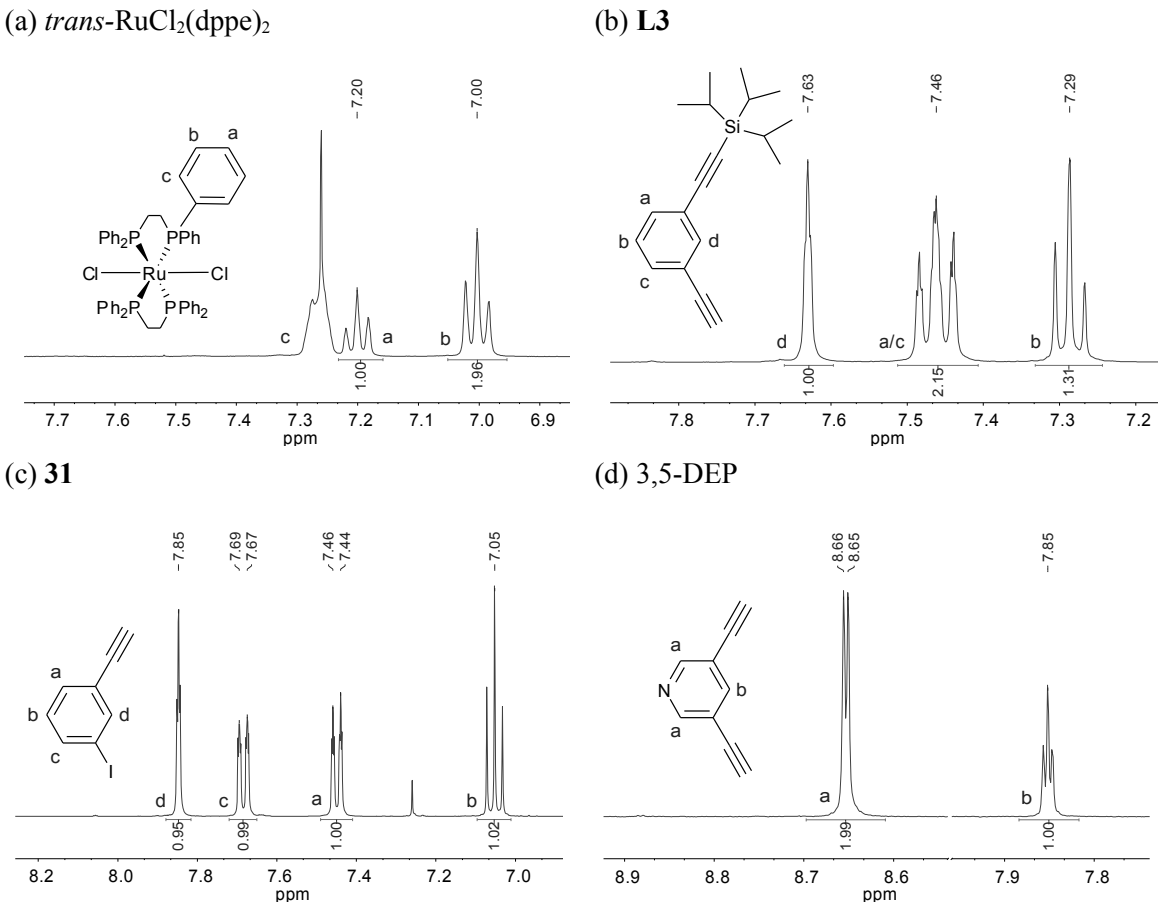

Figure 5-16. ^{1}H NMR spectra (aromatic region, $CDCl_3$) for: (a) *trans*-$RuCl_2(dppe)_2$ (for comparison), (b) 1-(triisopropylsilyl)ethynyl-3-ethynylbenzene (**L3**), (c) 1-ethynyl-3-iodobenzene (**31**) (d) 3,5-diethynylpyridine (3,5-DEP).

*** **35** decomposes on all grades of alumina (unlike **33**/**34**), and is remarkably soluble (hindering recrystallization attempts).

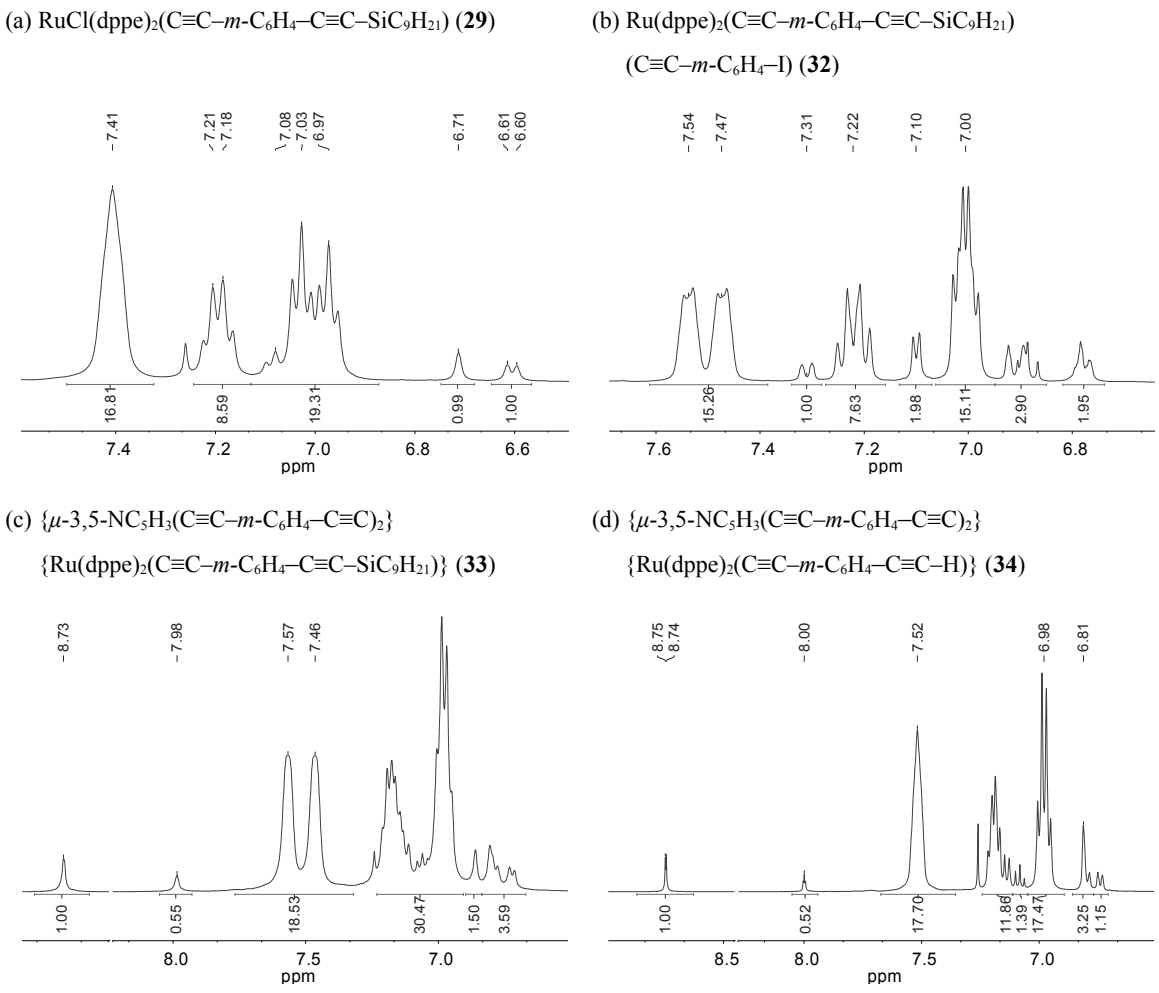

Figure 5-17. ^{1}H NMR spectra (aromatic region, $CDCl_3$) for: (a) **29**, (b) **32**, (c) **33** and (d) **34**.

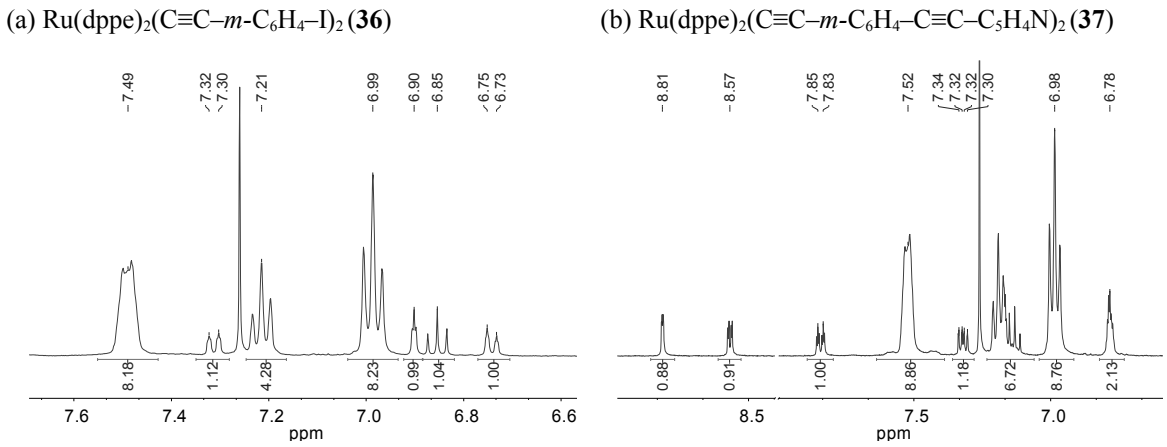

Figure 5-18. ^{1}H NMR spectra (aromatic region, $CDCl_3$) of the single branched complex **37** and its iodo precursor **36**.

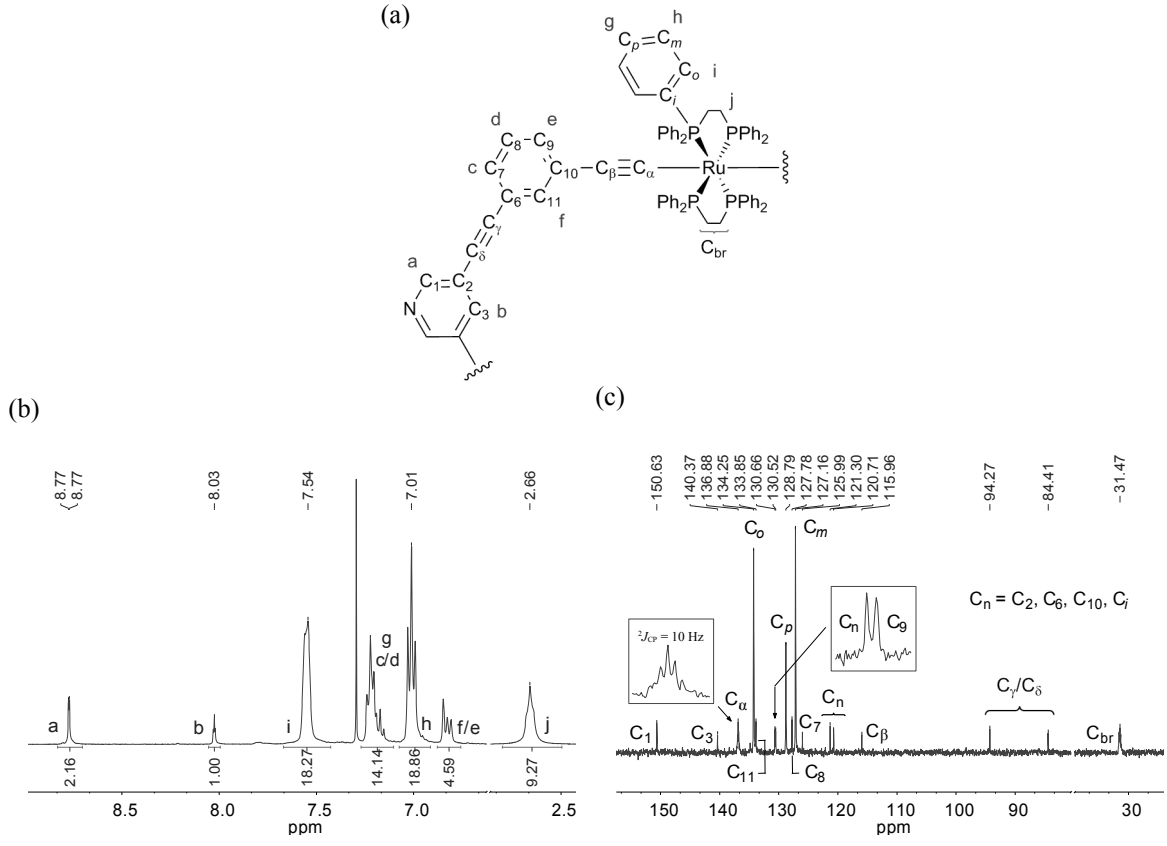

Figure 5-19. For crude macrocycle **35**: (a) ^{1}H (lowercase letters) and $^{13}C\{^{1}H\}$ (C_X) NMR labelling scheme used here, (b) ^{1}H NMR and (c) $^{13}C\{^{1}H\}$ NMR spectra ($CDCl_3$). One C_n resonance is not observed in this $^{13}C\{^{1}H\}$ NMR spectrum, possibly due to overlap with another.

The ^{1}H NMR spectrum of the symmetrical *trans*-$RuCl_2(dppe)_2$ complex *(Figure 5-16a)* provides a useful starting point for interpretation of more complicated spectra. Clearly visible in the aromatic region are three resonances corresponding to the phenyl protons of the dppe ligand, in *ortho* (overlapping with the residual solvent peak of $CDCl_3$), *para* and *meta* positions from downfield to upfield, respectively.[†††] Upon substitution of one of the chlorides, such as in **29** *(Figure 5-17a)*, axial asymmetry at the ruthenium centre is introduced. This results in chemical non-equivalence of the dppe ring protons, and a splitting of their resonances (this is observed in all analogous asymmetrical species, *e.g.* **32-34** in *Figure 5-17b-d)*. Upon completion of the macrocyclic structure (complex **35**), axial symmetry is returned to $Ru(dppe)_2$ and the phenyl peaks of the dppe ligands appear much as they did in *trans*-$RuCl_2(dppe)_2$ *(Figure 5-19b)* (albeit with C–H_o now shifted downfield by ~0.3 ppm).

From the examples given in *Figure 5-17* it is clear that for these species the aromatic region of ^{1}H NMR spectra can be troublesome to fully assign as a result of multiple overlapping ligand resonances *(Figure 5-16b-d)*. Those attributable to the 3,5-pyridyl (*e.g. Figure 5-16d)*, and to some extent the 3-pyridyl *(Figure 2-13a, Figure 5-18b)*, moieties are however well separated and particularly diagnostic. Of additional utility for complex identification are the distinct signals of the dppe CH_2 protons (br m, δ 2.6-2.7 ppm), as well as those attributable to isopropyl (br s, δ 1.20 ppm) or terminal alkyne (s, δ 3.06 ppm) functionalities, where appropriate. Interestingly, it appears that coordination of the terminal alkyne to ruthenium results in significant electron donation to the aromatic ligand. This is exemplified with particular clarity in the spectra of **29** and **36** *(Figure 5-17a* and *Figure 5-18a)*, where the resonances of proton environments closest to –C≡C–Ru are shifted substantially upfield compared to those in the free ligand *(Figure 5-16)*.

Though detailed assignment of ^{13}C{^{1}H} NMR spectra proved increasingly difficult as species became larger and more asymmetrical, characteristic resonances for dppe CH$_2$ and C_{Ar}–H environments, the quintet corresponding to C_a–Ru (though often broadened), and C_{Py}–H (for **33**, **34**, **35** and **37**) were identified in nearly every case. With high molecular symmetry, even for **35** (M_w ≈ 2447 Daltons), readily interpretable spectra were usually obtained (*e.g. Figure 5-19c)* ($Ru(dppe)_2(C{\equiv}C–C_6H_4$-*m*-$I)_2$ (**36**) proved an exception to this rule, as a result of its limited solubility in $CDCl_3/CD_2Cl_2$).

[†††] ^{1}H NMR (400 MHz, $CDCl_3$): δ (ppm) 7.27 (br m, 16H, Ph–H_o), 7.20 (t, 8H, Ph–H_p), 7.00 (t, 16H, Ph–H_m).[12]

All $^{31}P\{^{1}H\}$ NMR spectra showed a single singlet resonance corresponding to the equivalent PPh$_2$ nuclei of the dppe ligands – seen at δ 49.48 ppm for the mono-acetylide complex **29**, and at δ 52-54 ppm for the bis-acetylides.

5.4.3 Electrochemistry

The redox properties of **29**, **32**, **33**, **36** and **37** were investigated via cyclic voltammetry in $CHCl_3$ (given the instability of the pyridyl-containing compounds in CH_2Cl_2). Data for these and some analogous literature complexes are provided in *Table 5-3*. All compounds exhibited close to reversible redox features (and $i_p \propto V_s^{1/2}$, as expected for a solution-based redox process) at potentials 0.05-0.09 V positive of $[FcH]^+/[FcH]$, assigned to the Ru(II)/Ru(III) couple as a first approximation (ligand contributions to the HOMOs of these species should also be considered[32]). As in previous chapters, estimation of R_s using AC impedance spectroscopy and correction for iR_s greatly adjusted the observed behaviour towards reversibility ($\Delta E \approx 0.059/n$ V).

Table 5-3. Electrochemical data for selected Ru(dppe)$_2$ complexes.[a]

compound	E_{pa} (V)	E_{pc} (V)	ΔE (V)	i_p^a/i_p^c	$E_{1/2}$[b] (V)	ref
trans-RuCl$_2$(dppe)$_2$[c]	/	/	/	/	0.04	*32a*
RuCl(dppe)$_2$(C≡C–C$_6$H$_5$)[c]	/	/	/	/	0.01	*12*
	/	/	/	/	-0.01	*32a*
Ru(dppe)$_2$(C≡C–C$_6$H$_5$)$_2$[c]	/	/	/	/	0.00	*32a*
Ru(dppe)$_2$(C≡C–*m*-C$_6$H$_4$–I)$_2$ (**36**)	0.144	0.033	0.110	1.04	0.088	this work
Ru(dppe)$_2$(C≡C–*m*-C$_6$H$_4$–C≡C–C$_5$H$_4$N)$_2$ (**37**)	0.085	0.014	0.071	1.12	0.049	this work
RuCl(dppe)$_2$(C≡C–*m*-C$_6$H$_4$–C≡C–SiC$_9$H$_{21}$) (**29**)	0.099	0.008	0.091	1.02	0.054	this work
Ru(dppe)$_2$(C≡C–*m*-C$_6$H$_4$–C≡C–SiC$_9$H$_{21}$) (C≡C–*m*-C$_6$H$_4$–I) (**32**)	0.092	0.014	0.079	1.02	0.053	this work
{*μ*-3,5-NC$_5$H$_3$(C≡C–*m*-C$_6$H$_4$–C≡C)$_2$} {Ru(dppe)$_2$(C≡C–*m*-C$_6$H$_4$–C≡C–SiC$_9$H$_{21}$)} (**33**)	0.078	0.022	0.056	1.06	0.050	this work

[a] For scan rate = 0.1 Vs^{-1}. $Bu_4N^+PF_6^-$ (0.1 M) in $CHCl_3$; WE: glassy carbon; RE, CE: Pt. All potentials assigned to the Ru(II)/Ru(III) redox couple, measured against an internal $[FeCp^*_2]^+/[FeCp^*_2]$ reference, reported relative to $[FcH]^+/[FcH]$ (0.495 V *vs.* $[FeCp^*_2]^+/[FeCp^*_2]$ in this system) and corrected for iR_s drop. [b] $E_{1/2} = ½(E_{pa} + E_{pc})$. [c] In CH_2Cl_2 with $Bu_4N^+PF_6^-$ or $Bu_4N^+BF_4^-$.

From the $E_{1/2}$ values of these complexes (and in line with ^{1}H NMR observations), it seems all the acetylide ligands utilised here are to some extent electron-withdrawing – with **36** (ligated twice with C≡C–C_6H_4-*m*-I) proving hardest to oxidise. That said, the potentials of these *meta* bis-acetylides are more comparable to Ru(dppe)$_2$(C≡C–C_6H_5)$_2$ than the tertiary and quaternary *para* pyridyl-containing species of *Chapter 4*. It would be interesting in this context to compare $E_{1/2}$ for **36** and Ru(dppe)$_2$(C≡C–*p*-C_6H_4–I)$_2$,[27] but the latter was not characterized electrochemically.

Akin to their linear analogues *(Chapter 4)*, additional reactions were seen at higher oxidising potentials, affecting the reversible processes.[‡‡‡] These are also attributed to irreversible largely metal-based oxidations (presumably Ru(III) to Ru(IV), typically seen >0.80 V positive of Ru(II)/Ru(III)[12,33]). Not fully resolved in these experiments (due to the limits imposed by solvent oxidation), approximate onset potentials were observed at ~0.5 V *vs.* $[FcH]^+/[FcH]$.

Interestingly, an irreversible reduction wave was also noted at approximately -1.5 V for all of the complexes studied (*e.g. Figure 5-20)*. Not usually observed with analogous compounds (aside from those containing –NO_2, which demonstrate reductive features in this region[12,34]), these are tentatively assigned to Ru/dppe, or –C≡C–R based processes.[§§§] Typically, the LUMOs of such complexes are principally comprised of metal/ancillary ligand contributions,[32a-e] however they may also become completely ligand(π*) centred with increasing conjugation length of the acetylide component,[32c] or when this is functionalised with electron-withdrawing substituents (*e.g.* Ar–NO_2).[32f] Others have calculated the LUMO as M–C(σ*).[32g,h]

[‡‡‡] With step-wise increase of the overpotential, i_{pa}/i_{pc} became larger (>> 1). This is consistent with partial destruction of the Ru(III) species during the forward potential sweep – with less oxidised material available for reduction back to Ru(II), $i_{pa} > i_{pc}$.

[§§§] Rather than to reduction of oxygen/water – solutions were prepared using fresh solvent, thoroughly sparged with argon, and analogous features were not observed in blank experiments.

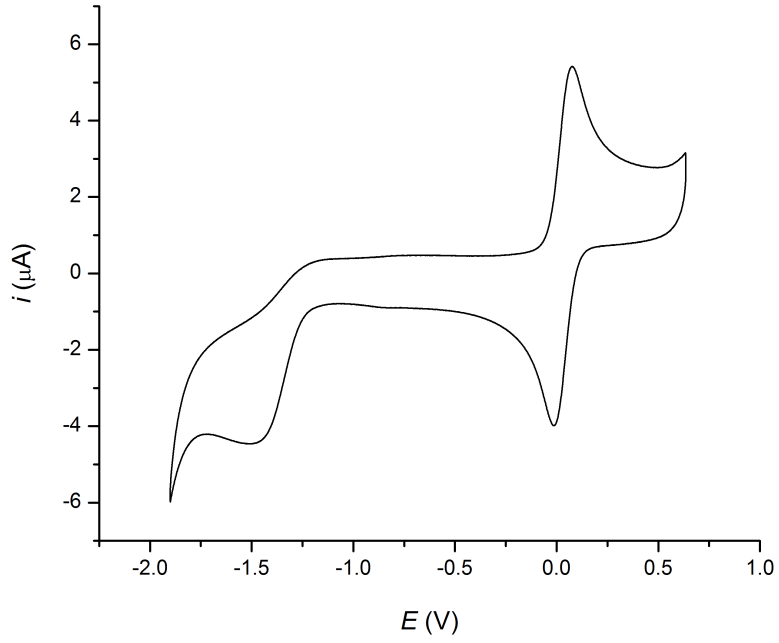

Figure 5-20. Cyclic voltammogram for **29** – similar irreversible reductive waves were observed for all acetylide complexes studied (potentials *vs.* $[FcH]^+/[FcH]$ and corrected for uncompensated resistance effects).

5.4.4 UV-vis spectroscopy

The absorption spectra of **36**, **37**, **29**, **32** and **33** were measured in $CHCl_3$. These are shown in *Figure 5-21* (the spectrum of *trans*-$RuCl_2(dppe)_2$ included for comparison), with data summarized in *Table 5-4*.

Similar to the linear complexes of *Chapter 4*, the majority of compounds studied here exhibit intense, broad/overlapping (non-Gaussian) absorptions centred around 325-350 nm. These correspond to transitions from ruthenium based molecular orbitals to ligand π* orbitals (MLCT bands).[31b,33] A bathochromic shift to higher wavelengths (lower energies), is seen for complexes containing the C≡C–C_6H_4-*m*-I ligand, in line with expectations for MLCT processes as the electron withdrawing character of the ligand increases.[35] Observed in all spectra are multiple/overlapping absorptions at high energies, typical of such materials and attributed to dppe-centred (*i.e.* intra ligand, π-π*/n-π*) transitions.[31b,36] Complexes containing acetylide ligands with extended conjugation (*e.g.* **37** and **33**), also display features in the region 275-325

nm suggestive of ligand based π-π* processes (red shifted due to decreased HOMO-LUMO gaps, similar features can be seen in the UV-vis spectrum of branched pyridyl ligand **27**, *Figure 5-9)*.

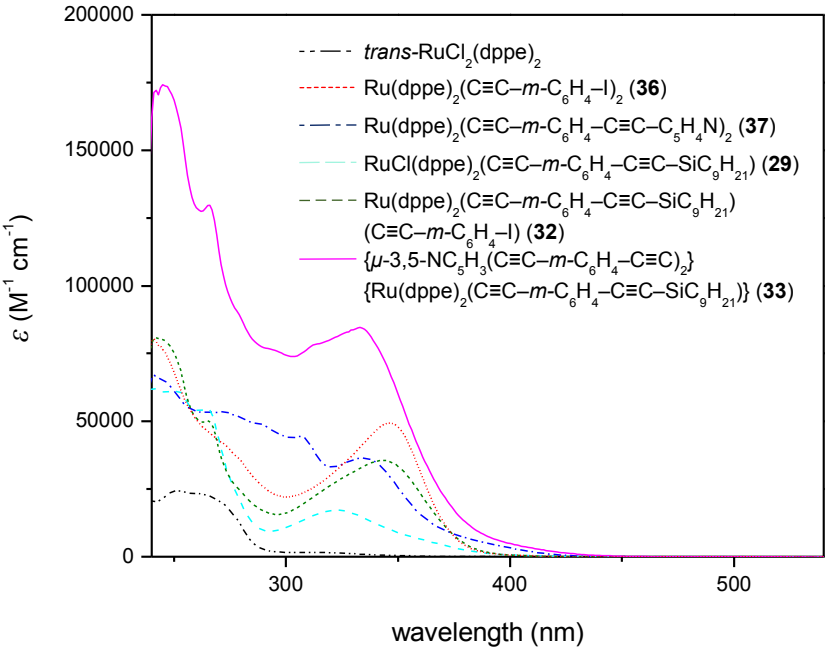

Figure 5-21. UV-vis spectra (in $CHCl_3$) of selected ruthenium complexes: *trans*-$RuCl_2(dppe)_2$, **36**, **37**, **29**, **32** and **33**.

Table 5-4. Electronic spectral data of selected ruthenium complexes and ligands.[a]

compound	λ_{max} /nm (ε /M^{-1} cm^{-1})[b]
trans-$RuCl_2(dppe)_2$	249 (24005), 263infl (23025), 277sh (14989), 306 (1609), 450 (57)
$Ru(dppe)_2(C{\equiv}C–$*m*$-C_6H_4–I)_2$ (**36**)	247sh (73752), 276sh (38458), 336sh (43093), 350 (47920)
$Ru(dppe)_2(C{\equiv}C–$*m*$-C_6H_4–C{\equiv}C–C_5H_4N)_2$ (**37**)	259sh (53920), 265 (53345), 273 (53496), 279sh (51790), 285infl (49514), 301sh (43963), 308 (44116), 334 (36434), 361sh (14850)
$RuCl(dppe)_2(C{\equiv}C–$*m*$-C_6H_4–C{\equiv}C–SiC_9H_{21})$ (**29**)	249 (60936), 253 (60997), 259sh (54219), 267 (52474), 320 (17024), 358sh (6883)
$Ru(dppe)_2(C{\equiv}C–$*m*$-C_6H_4–C{\equiv}C–SiC_9H_{21})$ $(C{\equiv}C–$*m*$-C_6H_4–I)$ (**32**)	244 (80600), 267(48737), 275sh (29063), 328sh (30367), 350sh (33335)
{μ-3,5-$NC_5H_3(C{\equiv}C–$*m*$-C_6H_4–C{\equiv}C)_2$} {$Ru(dppe)_2(C{\equiv}C–$*m*$-C_6H_4–C{\equiv}C–SiC_9H_{21})$} (**33**)	245 (174171), 266 (129733), 276sh (93527), 292 (76813), 311 (77597), 331 (84020), 351sh (57754)

[a] Recorded at room temperature in $CHCl_3$, using quartz cells with a pathlength of 10 mm. [b] Where possible, spectra were deconvoluted into composite Gaussian bands[****] to obtain λ_{max} values. All extinction coefficients were taken from the experimental data at these wavelengths.

5.5 CONCLUSION

Initial work towards macrocyclic ruthenium complexes containing the tetradentate PP_3 ligand resulted in the synthesis of an unusually coordinated *trans*-$RuCl_2(PP_3)_2$ complex (**28**) and a novel extended branched pyridyl ligand (**27**). Despite successes here and elsewhere with $[RuCl_2(dppe)_2]$/*cis*-$RuCl_2(dppe)_2$ starting materials, it was found that reactions between *cis*-$RuCl_2(PP_3)$ and terminal alkynes under Dixneuf conditions result only in butenynyl complexes. Future work towards the target structures shown in *Scheme 5-1* should focus on the published M–C bond formation approaches from $MH_2(PP_3)$ and X–C≡C–R (X = H, Li).[9]

With $Ru(dppe)_2$ centres, strict adherence to a $16e^-$ avoidance rule readily facilitated the incorporation of pyridyl-moieties into ligand frameworks (*e.g.* for **37** and **33**, via Sonogashira cross-coupling) in stark contrast to the significant problems encountered using 4-ethynylpyridine (*Chapter 4*). The simplicity of this approach, compared to those involving protecting groups, suggests that it might prove a useful general strategy for incorporating other nucleophilic/basic

[****] Using the 'Fit Plot' tool of *MagicPlot Student v2.3*.

moieties into $Ru(dppe)_2$ complexes. For example, it could circumvent protecting group approaches[37] when using isocyanide-termini, or enable the facile introduction of nitrile or amine functionalities (difficulties using these have been previously reported[12]).

$^1H/^{13}C\{^1H\}$ NMR spectra strongly suggest that the desired $Ru(dppe)_2$-containing macrocycle **35** has been prepared (albeit in ~80% purity). When contrasted with the difficulties encountered in synthesis of the ferrocene-based analogue (**13**, *Chapter 2)* the apparent ease of cyclization of **34**/3,5-DIP is quite remarkable. This may be attributed to the much greater rate of reaction for aryl iodides compared to ferrocenyl iodides in traditional Sonogashira cross-couplings, and further encourages future attempts to synthesise **13** using the $PdCl_2(MeCN)_2/P(^tBu)_3$ combination *(Chapter 3)*.

The electrochemical and absorption properties of these products (and novel precursors) are broadly as expected for their class of compounds, though atypical irreversible reductive features (thought to be Ru/dppe, or –C≡C–R based) were observed via cyclic voltammetry. Future work will focus on purification of **35** (*e.g.* via reverse-phase column chromatography, alternative recrystallization procedures), its full characterisation, and the synthesis of its double-branched equivalent. If successful, single-molecule conductance and related studies will be undertaken, in line with discussions in *Chapter 1*.

5.6 REFERENCES

1. (a) C. Grave and A. D. Schlüter, *Eur. J. Inorg. Chem.*, 2002, **2002**, 3075; (b) W. Zhang and J. S. Moore, *Angew. Chem., Int. Ed.*, 2006, **45**, 4416; (c) Y.-F. Han, W.-G. Jia, W.-B. Yu and G.-X. Jin, *Chem. Soc. Rev.*, 2009; (d) M. Iyoda, J. Yamakawa and M. J. Rahman, *Angew. Chem., Int. Ed.*, 2011, **50**, 10522.
2. (a) E. Bosch and C. L. Barnes, *Organometallics*, 2000, **19**, 5522; (b) K. Campbell, R. McDonald, N. R. Branda and R. R. Tykwinski, *Org. Lett.*, 2001, **3**, 1045; (c) S.-S. Sun and A. J. Lees, *Organometallics*, 2001, **20**, 2353; (d) K. Campbell, R. McDonald and R. R. Tykwinski, *J. Org. Chem.*, 2002, **67**, 1133; (e) K. Campbell, C. J. Kuehl, M. J. Ferguson, P. J. Stang and R. R. Tykwinski, *J. Am. Chem. Soc.*, 2002, **124**, 7266; (f) K. Campbell, R. McDonald, M. J. Ferguson and R. R. Tykwinski, *Organometallics*, 2003, **22**, 1353; (g) K. Campbell, K. J. Ooms, R. E. Wasylishen and R. R. Tykwinski, *Org. Lett.*, 2005, **7**, 3397; (h) K. J. Ooms, K. Campbell, R. R. Tykwinski and R. E. Wasylishen, *J. Mater. Chem.*, 2005, **15**, 4318; (i) C. A. Johnson Ii, B. A. Baker, O. B. Berryman, L. N. Zakharov, M. J. O'Connor and M. M. Haley, *J. Organomet. Chem.*, 2006, **691**, 413; (j) K. Becker, M. Fritzsche, S. Hoger and J. M. Lupton, *J. Phys. Chem. B*, 2008, **112**, 4849; (k) E. Cerrada, M. Laguna and N. Lardíes, *Eur. J. Inorg. Chem.*, 2009, **2009**, 137; (l) K. Campbell, K. J. Ooms, M. J. Ferguson, P. J. Stang, R. E. Wasylishen and R. R. Tykwinski, *Can. J. Chem.*, 2011, **89**, 1264; (m) K. Campbell, R. McDonald, M. J. Ferguson

and R. R. Tykwinski, *J. Organomet. Chem.*, 2003, **683**, 379; (n) K. Campbell, C. A. Johnson, R. McDonald, M. J. Ferguson, M. M. Haley and R. R. Tykwinski, *Angew. Chem., Int. Ed.*, 2004, **43**, 5967.

3. J. Vicente, M. T. Chicote, M. M. Alvarez-Falcon and D. Bautista, *Organometallics*, 2004, **23**, 5707.
4. Y. Furusho, T. Matsuyama, T. Takata, T. Moriuchi and T. Hirao, *Tetrahedron Lett.*, 2004, **45**, 9593.
5. H. A. Staab and K. Neunhoeffer, *Synthesis*, 1974, 424.
6. (a) J. S. Moore and J. S. Zhang, *Angew. Chem., Int. Ed. Engl.*, 1992, **31**, 922; (b) Z. Wu, S. Lee and J. S. Moore, *J. Am. Chem. Soc.*, 1992, **114**, 8730; (c) J. Zhang, D. J. Pesak, J. L. Ludwick and J. S. Moore, *J. Am. Chem. Soc.*, 1994, **116**, 4227; (d) Z. Wu and J. S. Moore, *Angew. Chem., Int. Ed.*, 1996, **35**, 297; (e) T. Kawase, N. Ueda, H. R. Darabi and M. Oda, *Angew. Chem., Int. Ed.*, 1996, **35**, 1556; (f) T. Kawase, N. Ueda and M. Oda, *Tetrahedron Lett.*, 1997, **38**, 6681; (g) T. Kawase, Y. Hosokawa, H. Kurata and M. Oda, *Chem. Lett.*, 1999, **28**, 745; (h) W. Zhang and J. S. Moore, *J. Am. Chem. Soc.*, 2004, **126**, 12796; (i) W. Zhang and J. S. Moore, *J. Am. Chem. Soc.*, 2005, **127**, 11863.
7. Y. Li, J. Zhao, X. Yin and G. Yin, *ChemPhysChem*, 2006, **7**, 2593.
8. (a) T. Rappert and A. Yamamoto, *Organometallics*, 1994, **13**, 4984; (b) L. Field, A. Magill, S. Dalgarno and P. Jensen, *Eur. J. Inorg. Chem.*, 2008, 4248; (c) J. s. Berenguer, M. a. Bernechea, J. Fernández, B. n. Gil, E. Lalinde, M. T. Moreno, S. Ruiz and S. Sánchez, *Organometallics*, 2011, **30**, 4665.
9. C. Bianchini, P. Frediani, D. Masi, M. Peruzzini and F. Zanobini, *Organometallics*, 1994, **13**, 4616.
10. C. Bianchini, P. Perez, M. Peruzzini, F. Zanobini and A. Vacca, *Inorg. Chem.*, 1991, **30**, 279.
11. C. Bianchini, K. Linn, D. Masi, M. Peruzzini, A. Polo, A. Vacca and F. Zanobini, *Inorg. Chem.*, 1993, **32**, 2366.
12. M. A. Fox, J. E. Harris, S. Heider, V. Pérez-Gregorio, M. E. Zakrzewska, J. D. Farmer, D. S. Yufit, J. A. K. Howard and P. J. Low, *J. Organomet. Chem.*, 2009, **694**, 2350.
13. S. Bhattacharya and C. G. Pierpont, *Inorg. Chem.*, 1991, **30**, 2906.
14. (a) C. Bianchini, C. Bohanna, M. A. Esteruelas, P. Frediani, A. Meli, L. A. Oro and M. Peruzzini, *Organometallics*, 1992, **11**, 3837; (b) C. Bianchini, M. Peruzzini, F. Zanobini, P. Frediani and A. Albinati, *J. Am. Chem. Soc.*, 1991, **113**, 5453; (c) P. Barbaro, C. Bianchini, M. Peruzzini, A. Polo, F. Zanobini and P. Frediani, *Inorg. Chim. Acta*, 1994, **220**, 5.
15. (a) L. D. Field, A. V. George and T. W. Hambley, *Inorg. Chem.*, 1990, **29**, 4565; (b) L. Field, B. Messerle, R. Smernik, T. Hambley and P. Turner, *J. Chem. Soc., Dalton Trans.*, 1999, 2557.
16. P. Blakskjaer and K. V. Gothelf, *Org. Biomol. Chem.*, 2006, **4**, 3442.
17. I. Buys, L. Field, A. George, T. Hambley and G. Purches, *Aust. J. Chem.*, 1995, **48**, 27.
18. C.-W. Chang, P.-C. Ting, Y.-C. Lin, G.-H. Lee and Y. Wang, *J. Organomet. Chem.*, 1998, **553**, 417.
19. (a) T. S. Lobana, R. Singh and E. R. T. Tiekink, *J. Coord. Chem.*, 1990, **21**, 225; (b) J. R. Polam and L. C. Porter, *J. Coord. Chem.*, 1993, **29**, 109; (c) B. M. Berven, G. A. Koutsantonis, B. W. Skelton, R. D. Trengove and A. H. White, *Inorg. Chem.*, 2009, **48**, 11832.
20. R. R. Guimerans, E. C. Hernandez, M. M. Olmstead and A. L. Balch, *Inorg. Chim. Acta*, 1989, **165**, 45.
21. M. Garcìa-Basallote, P. Valerga, M. C. Puerta-Vizcaíno, A. Romero, A. Vegas and M. Martínez-Ripoll, *J. Organomet. Chem.*, 1991, **420**, 371.
22. D. Fernández-Anca, M. I. García-Seijo and M. E. García-Fernández, *Dalton Trans*, 2010, **39**, 2327.

23. R. King, R. Kapoor, M. Saran and P. Kapoor, *Inorg. Chem.*, 1971, **10**, 1851.
24. L. D. Field, B. A. Messerle, R. J. Smernik, T. W. Hambley and P. Turner, *Inorg. Chem.*, 1997, **36**, 2884.
25. M. Magoga and C. Joachim, *Phys. Rev. B*, 1999, **59**, 16011.
26. S. Y.-L. Leung, A. Y.-Y. Tam, C.-H. Tao, H. S. Chow and V. W.-W. Yam, *J. Am. Chem. Soc.*, 2012, **134**, 1047.
27. A. Klein, O. Lavastre and J. Fiedler, *Organometallics*, 2006, **25**, 635.
28. O. Lavastre, J. Plass, P. Bachmann, S. Guesmi, C. Moinet and P. H. Dixneuf, *Organometallics*, 1997, **16**, 184.
29. (a) M. Winkler, B. Cakir and W. Sander, *J. Am. Chem. Soc.*, 2004, **126**, 6135; (b) J. E. Ormond-Prout, P. Smart and L. Brammer, *Cryst. Growth Des.*, 2011, **12**, 205.
30. M. Joshi, R. Tiwari and A. K. Verma, *Org. Lett.*, 2012, **14**, 1106.
31. (a) D. Touchard, P. Haquette, S. Guesmi, L. L. Pichon, A. Daridor, L. Toupet and P. H. Dixneuf, *Organometallics*, 1997, **16**, 3640; (b) A. Benameur, P. Brignou, E. Di Piazza, Y.-M. Hervault, L. Norel and S. Rigaut, *New J. Chem.*, 2011, **35**, 2105.
32. (a) C. E. Powell, M. P. Cifuentes, J. P. Morrall, R. Stranger, M. G. Humphrey, M. Samoc, B. Luther-Davies and G. A. Heath, *J. Am. Chem. Soc.*, 2002, **125**, 602; (b) M. A. Fox, R. L. Roberts, W. M. Khairul, F. Hartl and P. J. Low, *J. Organomet. Chem.*, 2007, **692**, 3277; (c) O. F. Koentjoro, R. Rousseau and P. J. Low, *Organometallics*, 2001, **20**, 4502; (d) M. A. Fox, R. L. Roberts, T. E. Baines, B. Le Guennic, J.-F. Halet, F. Hartl, D. S. Yufit, D. Albesa-Jové, J. A. K. Howard and P. J. Low, *J. Am. Chem. Soc.*, 2008, **130**, 3566; (e) D. J. Armitt, M. I. Bruce, M. Gaudio, N. N. Zaitseva, B. W. Skelton, A. H. White, B. Le Guennic, J. F. Halet, M. A. Fox, R. L. Roberts, F. Hartl and P. J. Low, *Dalton Trans.*, 2008, 6763; (f) F. Paul, B. G. Ellis, M. I. Bruce, L. Toupet, T. Roisnel, K. Costuas, J.-F. Halet and C. Lapinte, *Organometallics*, 2006, **25**, 649; (g) J. E. McGrady, T. Lovell, R. Stranger and M. G. Humphrey, *Organometallics*, 1997, **16**, 4004; (h) C. D. Delfs, R. Stranger, M. G. Humphrey and A. M. McDonagh, *J. Organomet. Chem.*, 2000, **607**, 208.
33. F. E. Kühn, J.-L. Zuo, F. F. d. Biani, A. M. Santos, Y. Zhang, J. Zhao, A. Sandulache and E. Herdtweck, *New J. Chem.*, 2004, **28**, 43.
34. N. Gauthier, N. Tchouar, F. Justaud, G. Argouarch, M. P. Cifuentes, L. Toupet, D. Touchard, J.-F. Halet, S. Rigaut, M. G. Humphrey, K. Costuas and F. Paul, *Organometallics*, 2009, **28**, 2253.
35. K. Costuas, F. Paul, L. Toupet, J.-F. Halet and C. Lapinte, *Organometallics*, 2004, **23**, 2053.
36. D. M. Klassen and G. A. Crosby, *J. Mol. Spectrosc.*, 1968, **25**, 398.
37. C. Olivier, B. Kim, D. Touchard and S. Rigaut, *Organometallics*, 2008, **27**, 509.

CHAPTER 6 : THERMODYNAMIC CORRELATIONS IN MIXED-VALENCE COMPLEXES

6.1 INTRODUCTION

This chapter marks a departure from the synthetic theme prevalent in the rest of this thesis. It is concerned instead with the thermodynamic properties of relevant 'mixed-valence' complexes (strictly, 'mixed-oxidation state' complexes,[1] *in which the number of electrons assigned to at least two atoms of the same element in a molecule in a localised bonding scheme is not integral*[2]); and the reasons for this are threefold.

First, and related to the branched synthetic targets discussed in *Chapter 2* and *5*, it was of interest to better understand the properties which will stabilise a mixed-valence complex relative to its isovalent states. Under such favourable circumstances oxidation of identical redox centres will occur at different potentials, with the difference between the first (E_1^0) and second (E_2^0) equilibrium potentials, $\Delta E_{1/2}^0$ (= $E_2^0 - E_1^0$), large enough to facilitate investigation of the properties of the mixed-valence. As can be seen from *Figure 2.7* and *Figure 5.15*, this is of fundamental importance when working with symmetrical branched binuclear complexes, where oxidation of each redox centre individually is required to change the conductance of a single branch (oxidized redox centre) relative to another (neutral redox centre). Thus far, electrochemical investigations of structurally similar compounds have exhibited $\Delta E_{1/2}^0 \approx 0$.

Secondly, this thesis has focussed entirely on syntheses of branched complexes comprising synthetically accessible iron ({$FeCp_2$}) and ruthenium ({$Ru(dppe)_2$}, {$Ru(PP_3)$}) centres. Whilst these have additional meritorious properties which support their incorporation within molecular electronic components (see *Chapter 2* and *4)*, questions pertaining to the effects of changing the metal centre and its ligand environment on critical electronic properties (such as molecular conductance) remain difficult to answer and are intriguing. To date, molecular junction measurements of metal acetylides are scarce (*e.g.* with Pt[3] and Ru[4] centres), and do not yet convey clear structure-property relationships. Fortunately, molecular conductance has been related to the rate of intramolecular electron transfer,[5] which may itself be assessed using the

properties of suitable mixed-valence models. The area of mixed-valence chemistry is thus of considerable *general* relevance to those working within molecular electronics.

Finally, in a recent related review[6] this author had observed that electron density at a metal centre ($M(L)_n$, where M represents a metal centre, and $(L)_n$ represents the ancillary ligand framework), *quantified* by ν(X) frequencies (X = C≡O, C≡N, C≡C) of their monometallic $\{M(L)_n\}$–R analogues (R = $^-$C≡O, $^-$C≡N, $^-$C≡C–C_6H_5), in some cases exhibited intriguing positive correlations with $\Delta E_{1/2}^0$ for analogous series of binuclear mixed-valence complexes containing the same bridge motif (see *section 6.3.2*, qualitative relationships had been previously noted by others[7]). The apparent relationship between $\Delta E_{1/2}^0$ and such a straightforward empirical measure (recorded for hundreds of different $M(L)_n$, *e.g.* for $M(L)_n$–C≡C–C_6H_5[8]), offered the tantalising suggestion that the former could be predicted for numerous as yet unknown bimetallic complexes. This could then guide researchers towards an 'ideal' molecular wire, assuming $\Delta E_{1/2}^0$ bore some relationship to the rate of electron transfer in that series. Fully aware that the link between electronic communication and $\Delta E_{1/2}^0$ is often called into question, it was of significant interest to explore this apparent association in greater detail. If the observed correlations might not be due to a proportional rate of electron transfer between redox centres, what then should they be attributed to?

Towards this end, a brief background to the study of mixed-valence systems *(section 6.2.1)*, and an overview of their properties in terms of electron transfer and intervalence charge transfer (IVCT) band analysis is provided *(section 6.2.2)*. In somewhat greater detail, $\Delta E_{1/2}^0$ and the many thermodynamic contributions to the free energy of comproportionation ($\Delta_{co}G^0$) are then discussed *(section 6.2.3)*. Following this, the previously mentioned apparent relationships between electron density at $M(L)_n$ and $\Delta E_{1/2}^0$ are presented for the homobimetallic complexes $[\{M(L)_n\}_2(\mu\text{-BL})]$ (where μ-BL = C_4 alkyne, C_4 alkene and C_8 alkyne). Collected data for bridges containing 1,4-phenylene or 2,5-thiophene units is also given, though with these systems ν(X) *vs.* $\Delta E_{1/2}^0$ relationships could not be established. Chosen as a representative case study, the C_4 alkyne series is investigated in further detail *(section 6.3.3)*. Within this context, relationships between electron density and the factors which stabilise/destabilise the mixed valence state are explored.

6.2 'MIXED-VALENCE' COMPLEXES

6.2.1 History and relevance

Though many 'mixed-valence' compounds are known throughout nature (Prussian blue, '$Fe_x^{III}[Fe^{II}(CN)_6]_y$', being a popular example), the first deliberately synthesized, stable example was the Creutz-Taube ion, $[\{(NH_3)_5Ru\}_2(\mu\text{-py})]^{5+}$ (py = pyrazine, *Figure 6-1,* **D**),[9] generated from one-electron oxidation of $[\{(NH_3)_5Ru\}_2(\mu\text{-py})]^{4+}$ and isolated as the tosylate salt.* In accordance with Marcus-Hush theory *(section 6.2.2)*,[10] this compound exhibited an absorption band that was not present in the fully reduced or fully oxidised states. Thus, the spectral feature was attributed to an IVCT transition, that is, the transition of an electron from the Ru^{II} centre to the Ru^{III} centre through the bridging pyrazine ligand. Its preparation followed on from many years of work exploring electron transfer processes via 'self-exchange' (*e.g.* $Fe^{2+} + Fe^{3+} \rightleftarrows Fe^{3+} + Fe^{2+}$) and 'cross-reactions' (*e.g.* $Fe^{2+} + Ce^{4+} \rightleftarrows Fe^{3+} + Ce^{3+}$) in solution,[11] and greatly simplified such investigations by eliminating diffusional aspects.

Indeed, since this work was presented an enormous (and still growing) number of analogous systems have been prepared and extensively studied. Related group 8 complexes with bridging ligands based on nitrogen, sulfur or oxygen donors have been the subject of substantial interest (being largely inert to substitution and stable in different oxidation states),[12] and systematic inquiries involving metal centres (clusters,[13] or redox-active organic structures[14]) linked by saturated or unsaturated hydrocarbons (*e.g.* fulvalene/fused ring systems, linear carbon chain bridges, or bridges containing additional metal centres) have also proved fruitful research areas.[7e,15] Some representative examples are shown in *Figure 6-1*. Given the large number of M^{II}/M^{III} systems investigated in this context, general discussions pertaining to mixed-valence complexes will typically refer to such species (*e.g.* $[M_1^{II}M_2^{III}]^{n+}$).

* For simplicity such complexes may be represented by the notation $[M_1^xM_2^y]$. As such, $[\{(NH_3)_5Ru\}(\mu\text{-py})\{Ru(NH_3)_5\}]^{n+}$ can be denoted by $[Ru_1^{II}Ru_2^{II}]$ for the fully reduced (n = 4) and $[Ru_1^{III}Ru_2^{III}]$ for the fully oxidized (n = 6) states. Mixed-valence complexes (in this case n = 5) can be denoted as $[Ru_1^{II}Ru_2^{III}]$, or $[Ru_1^{II1/2}Ru_2^{II1/2}]$ depending on whether the charge is considered localised or delocalised, respectively. More generally, $[R_1R_2]$, $[O_1O_2]$, $[O_1R_2]$ shall be used to signify reduced (= R) or oxidised (= O) centres in binuclear systems.

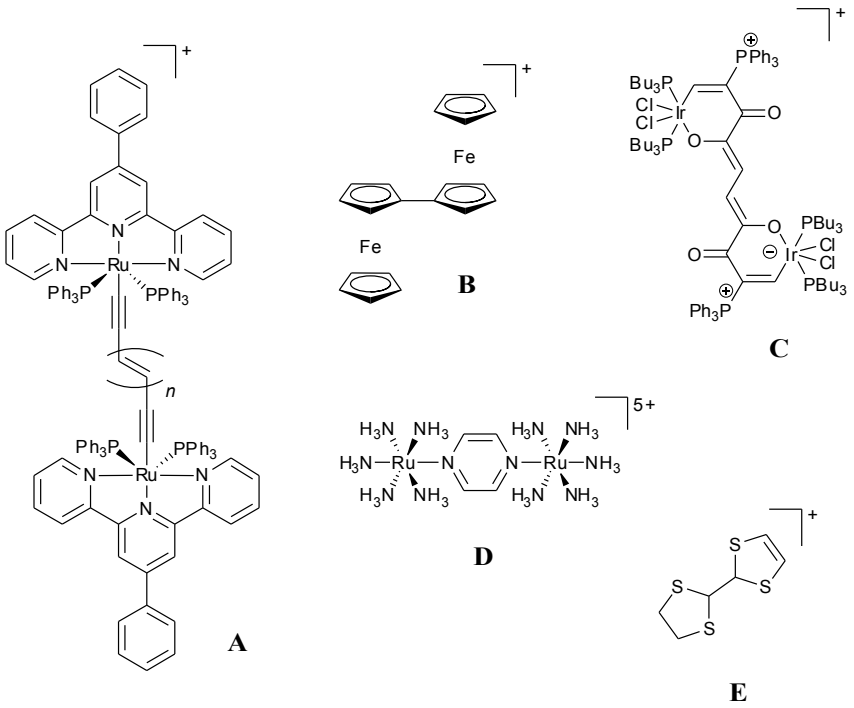

Figure 6-1. Some classical (**B**,[16] **D**,[9] **E**[16]) and modern (**A**,[17] **C**[18]) examples of mixed-valence complexes.

Today, investigations of mixed-valence complexes remain an area of intense interest for several reasons. As materials in their own right, they exhibit unusual magnetic and (often useful) optical properties,[1] and their study is vital to the ratification and development of improved electron transfer theories; they aid better understanding of related and important processes (*e.g.* in biological systems such as metalloenzymes/improved materials for molecular electronics). Overall, the field also provides useful translational insights into molecular reactivity, and links into the concepts of redox *non-innocent* ligand frameworks.[19]

6.2.2 Electron-transfer in mixed-valence complexes

Much in the same way that Eyring's transition state theory can be used to describe reactions involving *structural changes* (*i.e.* bond making/breaking processes), Marcus-Hush theory can be used to describe *electron transfer* reactions.[10] As the specific application of the latter to mixed-valence complexes has been thoroughly reviewed elsewhere,[12a,20] only key concepts pertinent to later discussions are provided here.

In Marcus theory, the electron transfer reaction (*e.g.* $[M_1^{II}M_2^{III}] \rightarrow [M_1^{III}M_2^{II}]$) may be

visualised by two parabola, representing Gibbs free energies for the 'reactant' (*i.e.* the reduced species/donor, centred at $X = 0$ on the reaction coordinate) and the 'product' (*i.e.* oxidised species/acceptor, centred at $X = 1$) states *vs.* nuclear configuration *(Figure 6-2)*.[†] At the minimum on the left hand parabola, the metal-ligand/ligand-ligand bond lengths and the surrounding solvent medium are said to be in the ground state nuclear configuration for the electron to exist on the reactant (if an electron resides on this curve it exists on the reactant). Likewise, at the minimum on the right hand parabola, the metal-ligand/ligand-ligand bond lengths and the surrounding solvent medium are considered to be in the ground state nuclear configuration for the electron to exist on the product (and if an electron resides on this curve it exists on the product).

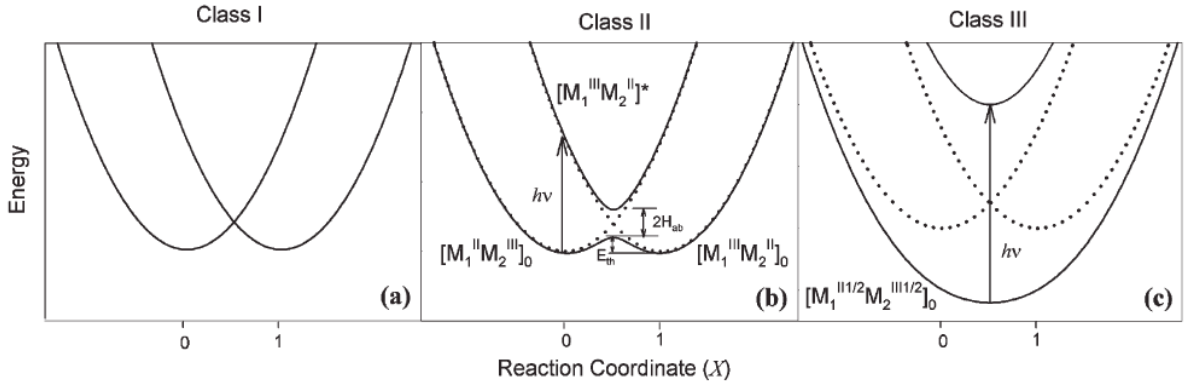

Figure 6-2. Potential energy curves for the reactant ($[M_1^{II}M_2^{III}]$, left hand parabola) and product ($[M_1^{III}M_2^{II}]$, right hand parabola) of electron transfer reactions in mixed-valence complexes (*e.g.* $[\{M(L)_n\}_2(\mu\text{-BL})]$). For (a), electronic coupling between the reactant and product states is negligible ($H_{ab} = 0$, diabatic limit, dotted lines in (b) and (c)), in (b) it is weak ($H_{ab} = \lambda/4$) and in (c) it is strong ($H_{ab} = 3\lambda/4$) (adiabatic regimes, solid lines). Figure reproduced from reference [20] by permission of The Royal Society of Chemistry (RSC).

Though no bonds are being broken or formed, an electron transfer reaction requires *changes* to the inner-sphere (*i.e.* metal-ligand and ligand-ligand bond lengths and angles) and outer-sphere (*i.e.* the surrounding solvent medium) environments (*e.g.* consider how bond lengths and solvent orientations might be different in $[Fe(OH_2)_6]^{2+}$ and $[Fe(OH_2)_6]^{3+}$). Electron transfer thus

[†] For identical reactant/product states, the difference in energy ($\Delta_r G^0$) between the reactant/product minima is zero.

requires an energy input to facilitate this change, and may occur via two mechanisms: a thermally activated, 'horizontal' process (following the lower potential energy curve in *Figure 6-2b* and *c)*, or 'vertically', with optical excitation (following the higher potential energy curve).

To satisfy the law of conservation of energy for the electron, electron transfer can only occur when the nuclear configuration of the reactant is such that its energy is the same as the energy of the product. This is this case (for symmetrical systems, $\Delta_r G^0 = 0$) at the intercept of reactant and product parabola ($X = 0.5$), where the energy difference between $X = 0$ and $X = 0.5$ is the activation energy (E_{th}) for the thermally activated process. At this energy an electron is now allowed to hop from the reactant to product curves, and it does so at a rate defined by eqn (6-1) (where k_{et} = rate of electron transfer, κ = transmission coefficient, υ = vibrational frequency with which the activated complex approaches the transition state, R = gas constant, T = temperature).[21]

$$k_{et} = \kappa \upsilon e^{-E_{th}/RT} \tag{6-1}$$

Alternatively, with light of sufficient energy ($h\nu$) the electron may be promoted from the reactant curve to the product curve at $X = 0$ (eqn (6-2)). In accordance with the Franck-Condon principle (which states that electronic motion can be considered instantaneous compared to nuclear motion), this forms an excited state ($[M_1^{III}M^{II}]^*$) where the electron resides on the acceptor (it is on the product curve) but the complex has the nuclear configuration of the donor (thus it is high in energy on the product curve). This is the optical excitation mechanism of electron transfer, and the absorption of light gives rise to an IVCT band unique to the mixed-valence species (it is not observed in the fully reduced/oxidised states). The energy of this transition is called the reorganisation energy (λ) (formally, *the energy change associated with molecular rearrangements that must take place so that the reactant can take on the equilibrium geometry of the product*[21]), comprised of outer-sphere (λ_o) and inner-sphere (λ_i) contributions, and can be related to the activation energy of the thermal process.[20]

$$[M_1^{II}M_2^{III}] \xrightarrow{h\nu} [M_1^{III}M_2^{II}]^* \tag{6-2}$$

From *Figure 6-2* it can be seen that the potential energy curves of reactant and product states

change under different circumstances. Notably, the extent of splitting at $X = 0.5$ is described by an electronic coupling parameter, H_{ab}. In the *diabatic* limit *(Figure 6-2a*) there is no mixing between reactant and product states, and the probability (and rate) of electron transfer is small (*i.e.* small κ and k_{et}, see eqn (6-1)). Robin and Day classified compounds exhibiting $H_{ab} = 0$ as belonging to Class I (complete charge localisation).[22] This may be the case where two redox centres are far apart, or when their interaction is symmetry or spin-forbidden (*e.g.* if linked by a long saturated hydrocarbon bridge). Alternatively, under favourable conditions (*e.g.* small separation, well-matched $(L)_nM$-bridge energies), electronic coupling between the product and reactant states will remove their degeneracy and produce two new *adiabatic* surfaces (solid lines in *Figure 6-2b*).‡ With greater electronic coupling, H_{ab} becomes larger, the minima of reactant and product states move closer together (eventually coalescing, *Figure 6-2c)*, and the rate of electron transfer will increase (the thermal barrier to electron transfer is reduced, ultimately to zero). Depending on the magnitude of H_{ab}, complexes may be assigned as Robin and Day Class II (partial charge localisation) or Class III (completely delocalised).

Hush related the properties of the IVCT band to the extent of electronic coupling.[10] For Gaussian-shaped bands of Class II systems, H_{ab} may be determined using eqn (6-3) (where $\Delta\nu_{1/2}$ is the bandwidth at half-height and r_{ab} is the distance between the two diabatic states).[20] IVCT bands in the Class II regime are weak ($\varepsilon_{max} \leq 5000$ M^{-1} cm^{-1}), solvent-dependant, and broad ($\Delta\nu_{1/2} \geq 2000$ cm^{-1}).[20]

$$H_{ab} = \frac{2.06 \times 10^{-2} \, (\nu_{max} \varepsilon_{max} \Delta\nu_{1/2})^{1/2}}{r_{ab}} \qquad (6\text{-}3)$$

With increasing electronic coupling (Robin and Day Class III, *Figure 6-2c*), the system is considered fully delocalised (as reactant and product minima coalesce, there is no longer a thermal barrier to electron transfer). In this regime $H_{ab} >> \lambda$ and the energy of the "IVCT band" now provides a direct measure of H_{ab} (*i.e.* $h\nu = 2H_{ab}$). The term "average valence" may be considered more appropriate here than "mixed-valence", with each metal centre formally assigned a charge of 2½ (*i.e.* $[M_1^{II1/2}M_2^{II1/2}]$).

Though often applied, the Hush model is not perfect for several reasons. Most importantly, the metal-metal separation ($r_{MM'}$, typically used for r_{ab}) may not be the true charge transfer

‡ In the same way that electron wavefunctions of individual hydrogen atoms couple to form H_2.

distance (*e.g.* if $r_{ab} < r_{MM'}$ due to delocalisation, H_{ab} will be underestimated), and interpretation of spectra is often complicated by additional overlapping IVCT and inter configurational transitions which hinder band-shape analyses.[20] Due to the band cut-off effect, as a Class II system approaches Class III use of eqn (6-3) to calculate H_{ab} will result in a further underestimation; this time related to $\Delta\nu_{1/2}$. Proper assignment of Class II and III systems, improved assessments of H_{ab}, and a desire to account for all experimentally observed spectral features have driven the development of new models for IVCT band analyses (*e.g.* three and four-state,[23] PKS,[24] Ondrechen[25]) and methods to assess delocalisation (*e.g.* spin density calculations,[2] the charge distribution parameter[26]).

A popular alternative to that of Hush is the "CNS" model,[27] which considers coupling mediated by the bridging ligand (superexchange formalism) and relies less on the properties of the IVCT band in determining the electronic coupling parameter. The latter is in this case denoted $H_{MM'}$ and can be determined using eqn (6-4). $H_{ML}/H_{M'L}$ are provided by eqn (6-3) (taking H_{ML} ($\cong H_{M'L}$) in place of H_{ab}, using the properties of the MLCT band) and ΔE_{ML} is the effective M–BL energy gap (provided by eqn (6-5) where ΔE_{MLCT} and ΔE_{IVCT} are the energies of the MLCT and IVCT bands, respectively). As coupling via superexchange occurs predominantly via either hole or electron transfer mechanisms, only the first or the second term in eqn (6-4) needs to be considered for any given system.

$$H_{MM'} = \frac{H_{ML}H_{M'L}}{2\Delta E_{ML}} + \frac{H_{LM}H_{LM'}}{2\Delta E_{LM}} \tag{6-4}$$

$$\frac{1}{\Delta E_{ML}} = \frac{1}{2}\left(\frac{1}{\Delta E_{MLCT}} - \frac{1}{\Delta E_{IVCT}}\right) \tag{6-5}$$

6.2.3 The electrochemical 'tool' (contributions to $\Delta_{co}G^0$)

In addition to optical investigations, the properties of mixed valence complexes may be studied using voltammetric methods. From such experiments it is often possible to extract the free energy of comproportionation ($\Delta_{co}G^0$), a parameter which is increased in proportion to the extent of electronic coupling between redox sites. However, the electrochemical approach *does*

not provide a direct measure of this, and use of it for such a purpose has been cautioned against.[2,20,28] Indeed, $\Delta_{co}G^0$ is composed of several factors, which can be summarised as eqn (6-6) (where $\Delta_{st}G^0$ = statistical, $\Delta_{el}G^0$ = electrostatic, $\Delta_{in}G^0$ = inductive, $\Delta_{re}G^0$ = resonance, $\Delta_{as}G^0$ = antiferromagnetic superexchange, $\Delta_{ip}G^0$ = ion-pairing, $\Delta_{so}G^0$ = solvation, $\Delta_{str}G^0$ = structural contributions). Of these, only $\Delta_{re}G^0$ can be linked to H_{ab}.

$$\Delta_{co}G^0 = \Delta_{st}G^0 + \Delta_{el}G^0 + \Delta_{in}G^0 + \Delta_{re}G^0 + \Delta_{as}G^0 + \Delta_{ip}G^0 + \Delta_{so}G^0 + \Delta_{str}G^0 \qquad (6\text{-}6)$$

Despite this, some authors have argued that with *careful* assessment of its contributories, $\Delta_{co}G^0$, as calculated from $\Delta E_{1/2}{}^0$, can at least be used to invoke trends in $\Delta_{re}G^0$ (the free energy of resonance exchange) in a series of structurally similar compounds.[12a,29] On occasion, differences in $\Delta E_{1/2}{}^0$ ($\Delta\Delta E_{1/2}{}^0$) have even been utilised to evaluate the Hush/CNS models.[29] (This hypothesis is further tested in *section 6.3.3* using complexes of the form $[\{M(L)_n\}_2(\mu\text{-}C{\equiv}C{-}C{\equiv}C)]$.)

In any case, it is of great importance to appreciate the factors which stabilize the mixed-valence state over its isovalent states. From a practical standpoint, the former must be isolated (via chemical oxidation) or generated *in situ* (using spectrochemical methods) to facilitate its study. Furthermore, to obtain accurate H_{ab} values from analyses of IVCT bands, the position of the comproportionation equilibrium shown in eqn (6-7) must be known.[§]

$$[M_1{}^{II}M_2{}^{II}] + [M_1{}^{III}M_2{}^{III}] \overset{K_{co}/4}{\rightleftharpoons} 2[M_1{}^{II}M_2{}^{III}] \qquad (6\text{-}7)$$

Thus, each of the contributing factors to $\Delta_{co}G^0$ will be discussed in detail here. This is to provide context for later discussions, and because no clear, comprehensive overview of them all can be found in the recent literature. Every effort has been made to provide accurate descriptions, clear definitions, and consistent equations (converted into SI units where appropriate), with

[§] It is necessary to adjust the intensity (ε_{max}) of the IVCT band to account for the actual amount of mixed-valence species in the composition (though this error is only significant when the comproportionation constant, K_{co}, is small). The proportion of the mixed-valence species ($[R_1O_2]$) in the composition at equilibrium, *i.e.* $[R_1O_2]/M_t$ (where M_t = total concentration of all species), is $K_{co}{}^{1/2}/(2 + K_{co}{}^{1/2})$ (NOTE: K_{co} adjusted for the statistical factor, *vida infra)*.

assumptions, approximations and unknowns highlighted. It should be stressed that whilst each factor is explored separately (in line with discussions elsewhere), this is for clarity only. As will be seen, several should be considered intimately related.

The comproportionation constant (K_{co}) *and the statistical factor* ($\Delta_{st}G^0$)

A symmetrical binuclear metal complex of the form [{M(L)$_n$}$_2$(μ-BL)] may exhibit different electrochemical responses depending on the identity of the metals, their ligand environment, and the extent of interaction[**] between the centres (here we will only consider complexes with two identical redox sites). In the case of isolated, non-interacting centres, oxidation of both will occur at the same applied potential, E^0 (eqn (6-8)). From this the reaction Gibbs energy ($\Delta_r G^0$) and the equilibrium constant (K) of the reaction may be determined, using eqn (6-9).

$$[M_1^{II}M_2^{II}] \underset{+2e^-}{\overset{E^0}{\rightleftharpoons}} [M_1^{III}M_2^{III}] \tag{6-8}$$

$$-nFE^0 = \Delta_r G^0 = -RT \ln K \tag{6-9}$$

When there is an interaction between the metal centres, oxidation of the complex is observed to proceed via two well-separated, one-electron processes (eqn (6-10)). For reasons discussed in detail later, the fully reduced and fully oxidized states are unstable with respect to comproportionation into the mixed-valence state. The difference in formal oxidation potentials, $\Delta E_{1/2}{}^0$ (= $E_2{}^0 - E_1{}^0$), can be related to the extent of interaction between the sites. This was shown by Richardson and Taube[30] (in an approach adapted from Sokol *et al.*[31] for four non-equivalent redox sites) using the method described below.[††]

[**] This is an oversimplification used only to introduce concepts. As will be seen, discussions of $\Delta E_{1/2}{}^0/K_{co}$ should primarily refer to the stability of the mixed-valence *vs.* isovalent states, rather than 'interaction' or 'communication' between redox centres.

[††] Their methods considered sequential reductions from a fully oxidised species. For consistency with the compounds described later in this chapter, we derive the relationship between $\Delta E_{1/2}{}^0$ and $\Delta_{co}G^0$ by considering sequential oxidations from a fully reduced species.

$$[M_1^{II}M_2^{II}] \underset{+1e^-}{\overset{E_1^0}{\rightleftharpoons}} [M_1^{II}M_2^{III}] \underset{+1e^-}{\overset{E_2^0}{\rightleftharpoons}} [M_1^{III}M_2^{III}] \qquad (6\text{-}10)$$

'fully-reduced' 'mixed-valence' 'fully-oxidized'

It should first be realised that the experimentally observed standard oxidation potentials (E_i^0) shown in eqn (6-10) are *macroscopic* parameters. When the fully reduced state is oxidized to the mixed-valence state, the value of E_1^0 is an algebraic combination of the *microscopic* potentials, that is, where e_1^0 is the oxidation potential for $R_1R_2 \rightarrow O_1R_2$, and e_2^0 is the oxidation potential for $R_1R_2 \rightarrow R_1O_2$. Though the equilibrium distribution of individual species in the same oxidation state *(i.e.* $[O_1R_2]$ and $[R_1O_2]$) cannot be determined at a given potential E, they may be described by microscopic equilibrium constants (k_i) *(Figure 6-3)* that are related to the microscopic standard potentials (e_i^0) by rearranged Nernst equations such as eqn (6-11).

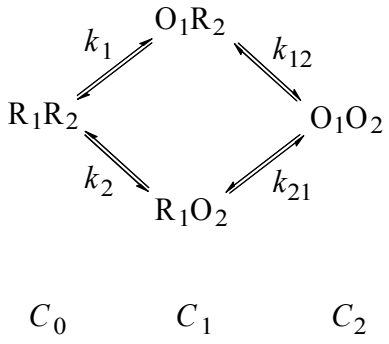

Figure 6-3. Microscopic equilibrium constants (k_i) relating species in different oxidation states (total concentration = C_n) following sequential one-electron oxidations of a dinuclear metal complex.

$$k_{12} = \frac{[O_1O_2]}{[O_1R_2]} = e^{\left[\frac{F(e_{12}^0 - E)}{RT}\right]} \qquad (6\text{-}11)$$

The macroscopic equilibrium constants (K_i) can be related to macroscopic standard potentials

(E_i^0) via analogous equations (*e.g.* eqn (6-12), where C_i/C_{i-1} is the total concentration of all species in a given oxidation state).

$$K_i = \frac{C_i}{C_{i-1}} = e^{\left[\frac{F(E_i^0 - E)}{RT}\right]} \tag{6-12}$$

Using these definitions for the microscopic and macroscopic equilibrium constants, it becomes possible to derive relationships between them (see eqn (6-13) and (6-14)).

$$K_1 = \frac{[O_1R_2] + [R_1O_2]}{[R_1R_2]} = k_1 + k_2 \tag{6-13}$$

Where,

$$k_1 = \frac{[O_1R_2]}{[R_1R_2]} \quad , \quad k_2 = \frac{[R_1O_2]}{[R_1R_2]}$$

$$K_2 = \frac{[O_1O_2]}{[O_1R_2] + [R_1O_2]} = (k_{12}^{-1} + k_{21}^{-1})^{-1} \quad (6\text{-}14)$$

Where,

$$k_{12} = \frac{[O_1O_2]}{[O_1R_2]} \quad , \quad k_{21} = \frac{[O_1O_2]}{[R_1O_2]} \quad \text{so} \quad k_{12}^{-1} = \frac{[O_1R_2]}{[O_1O_2]} \quad , \quad k_{21}^{-1} = \frac{[R_1O_2]}{[O_1O_2]}$$

Therefore,

$$k_{12}^{-1} + k_{21}^{-1} = \frac{[O_1R_2] + [R_1O_2]}{[O_1O_2]}$$

The difference in macroscopic potentials ($E_2^0 - E_1^0$) thus results in the combined Nernst equation shown in eqn (6-15). For the limiting case where $k_1 = k_2$ and $k_{12} = k_{21}$ (*i.e.* $[O_1R_2] = [R_1O_2]$), as would be expected if the redox sites were identical (*i.e.* $M(L)_n = M(L)_n$), then we can say $k_1 = k_2 = k$ and $k_{12} = k_{21} = k'$. This implies $K_1/K_2 = 4k/k'$, where the difference between k and k' reflects interaction between the sites (eqn (6-16)). By definition $4k/k'$ (K_{co}) is given by eqn (6-17), with $K_{co}/4$ describing the comproportionation equilibrium of eqn (6-18) (a generalised version of eqn (6-7)). As $\Delta E_{1/2}^0$ is positive, a negative free energy ($\Delta_{co}G^0$) can be calculated from eqn (6-19). This provides a measure of the stability of the mixed-valent species relative to the fully oxidized/reduced species. With no interaction between the sites (*i.e.* if $k\text{-}k' = 0$), then $k/k' = 1$ and $K_1/K_2 = 4$ (at room temperature, $\Delta E_{1/2}^0 = 35.6$ mV and $\Delta_{co}G^0 = -3.44$ kJ mol^{-1}). This is the so called "statistical factor", $\Delta_{st}G^0$.

$$\Delta E_{1/2}^0 = E_2^0 - E_1^0 = \frac{RT}{F} \ln\left(\frac{K_1}{K_2}\right) \quad (6\text{-}15)$$

$$\Delta E_{1/2}^0 = \frac{RT}{F} \ln\left(\frac{4k}{k'}\right) \quad (6\text{-}16)$$

$$\frac{4k}{k'} = K_{co} = \frac{4[O_1R_2]^2}{[O_1O_2][R_1R_2]} \tag{6-17}$$

$$[O_1O_2] + [R_1R_2] \overset{K_{co}/4}{\rightleftharpoons} 2[O_1R_2] \tag{6-18}$$

$$\Delta_{co}G^0 = -RT\ln\left(\frac{4k}{k'}\right) = -FE_{1/2}{}^0 \tag{6-19}$$

Where $K_{co} > 4$, the statistical factor can be corrected for either by dividing K_{co} (obtained from $\Delta E_{1/2}{}^0$) by 4, or by subtraction of $\Delta_{st}G^0$ (= -3.44 kJ mol^{-1}) from $\Delta_{co}G^0$. It should be further noted that because the equilibrium in question describes the generation of 2 moles of product, the free energy obtained from its equilibrium constant should be divided by 2 to provide the stabilization energy per 1 mole of product. This corrected stabilization energy term we shall call the total free energy, $\Delta_{to}G^0$ (eqn (6-20)).

$$\Delta_{to}G^0 = -\frac{1}{2}RT\ln\left(\frac{K_{co}}{4}\right) = -\frac{1}{2}\left(\Delta_{co}G^0 - \Delta_{st}G^0\right) \tag{6-20}$$

As $K_{co}/4$ represents the equilibrium position shown in eqn (6-7)/eqn (6-18), factors that influence the magnitude of $\Delta E_{1/2}{}^0$ (and subsequently, $K_{co}/4$, $\Delta_{to}G^0$, etc) can be considered as those which stabilize (or destabilize) the mixed-valence state relative to its isovalent states.

The electrostatic factor ($\Delta_{el}G°$)

Initial work in this area was conducted by Sutton, Sutton and Taube with the mixed-valence complex $[\{Ru(NH_3)_5\}_2(\mu\text{-}4,4'\text{-bipy})]^{5+}$, in trying to rationalize its calculated $\Delta_{de}G^0$ values (-0.20 kJ mol^{-1}, from analysis of its IVCT band using the Hush model) with much larger $\Delta_{to}G^0$ (-2.22 kJ mol^{-1}, from eqn (6-20)).[32] They recognized that the magnitude of electrostatic repulsion between the two positively charged metal centres of a given complex would change depending on its oxidation state. Conveniently, the difference in charges (z) between all species in a comproportionation equilibrium (in which each oxidation state is separated by a one electron change), is always equal to 1 (with the magnitude of the resulting energy term described as being

proportional to 1).[‡‡] As the greatest repulsive energy term occurs for the summed contributions of the isovalent states, the electrostatic factor favours formation of the mixed-valence species.

Initial estimations of the magnitude of $\Delta_{el}G°$ were made by calculating the energy (work) required to bring two point charges from infinite separation to a distance equivalent to the metal-metal separation when surrounded by a continuous dielectric medium (also taking into account the ionic strength of the solvent).[32-33] Thus the difference in electrostatic energy between the mixed-valence and isovalent states of a binuclear molecule can be determined using eqn (6-21) and (6-22) (adapted for SI units). Here, e = elementary charge (in C), ε_0 = vacuum permittivity (F m^{-1}), ε_r = relative permittivity, r_{12} = metal-metal separation (m), k_B = Boltzmann's constant (J K^{-1}), T = temperature (K), N_A = the Avogadro constant (mol^{-1}) and c = concentration (mol m^{-3}). As eqn (6-21) determines the energy difference (in J) from combining *four* molecules, Δw requires further manipulation to provide $\Delta_{el}G^0$ in kJ mol^{-1} (eqn (6-23)).

$$\Delta w = \frac{-e^2}{4\pi\varepsilon_0\varepsilon_r r_{12}(1 + \kappa r_{12})} \tag{6-21}$$

$$\kappa = \left(\frac{\varepsilon_0\varepsilon_r k_B T}{2N_A e^2 c}\right)^{-1/2} \tag{6-22}$$

$$\Delta_{el}G^0 = \frac{\Delta w N_A \text{ x } 10^{-3}}{4} \tag{6-23}$$

In the previous example (*i.e.* $[\{Ru(NH_3)_5\}_2(\mu\text{-}4,4'\text{-bipy})]^{5+}$) this provided $\Delta_{el}G^0 = 0.39$ kJ mol^{-1}, and the approach was considered to grossly underestimate $\Delta_{el}G^0$. In reality, the point charges are immersed in a molecular framework, which will likely not shield the charge between them as well as a solvent/double-layer of higher dielectric constant. Later work by Sutton and Taube therefore modelled this by embedding the charges in an ellipsoidal[34] cavity *(Figure 6-4)* of dielectric constant ε_i (= 2, simulating the molecular environment), surrounded by a medium of

[‡‡] The total electrostatic repulsion energy for the isovalent states of M^{2+}/M^{3+} systems is *proportional to 13* (that is, the sum of the repulsive energies calculated, for example using Coulomb's Law, is proportional to the squared charges of each isovalent state, *i.e.* $2^2 + 3^2$). For the mixed-valence species this is proportional to 12 (two molecules each containing z = 3+ and z = 2+, *i.e.* 2 x 6). If the fully reduced species is instead neutral, the difference in charges is still 1 but formally due to 1 ($0^2 + 1^2$) for the isovalent states and 0 (2 x 0) for the mixed-valence.

dielectric constant ε_s (= 125). This provided a higher estimate of $\Delta_{el}G^0$ = 0.59 kJ mol^{-1} (but notably still too small to fully account for $\Delta_{to}G^0$).[35]

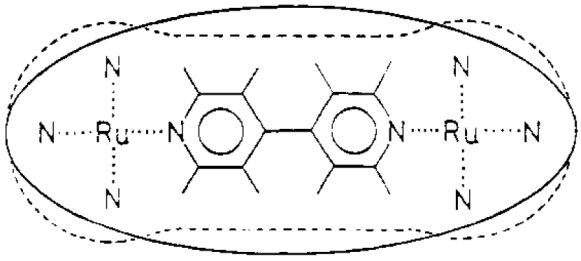

Figure 6-4. Ellipsoid model (solid line) of Sutton and Taube[35] used in their improved calculation of $\Delta_{el}G^0$ (dotted line = molecular geometry). Reprinted with permission from reference [35]. Copyright 1981 American Chemical Society.

Others have more recently employed a simpler dielectric continuum model that neglects ionic strength (eqn (6-24)).[29,36] Results obtained using eqn (6-21) and (6-24) are contrasted in *Figure 6-5*. In either case, it can be seen that $\Delta_{el}G^0$ is increased in solvents of low dielectric constant (quite significantly, compare values obtained using ε_r(water) = 80.10 *vs.* $\varepsilon_r(CH_2Cl_2)$ = 9.08 in *Figure 6-5)*, or with decreased ionic strength (a relatively minor effect – not shown). As the dielectric constant plays such an important role, the capacity for dissolved electrolyte to alter the dielectric response of a solvent should likely not be neglected in this context – ε_r of a 0.1 M solution of Bu_4NClO_4 in CH_2Cl_2 was found experimentally to be increased from the pure solvent (~9) to 12.5.[37]

$$\Delta w = \frac{-e^2}{4\pi\varepsilon_0\varepsilon_r r_{12}} \qquad (6\text{-}24)$$

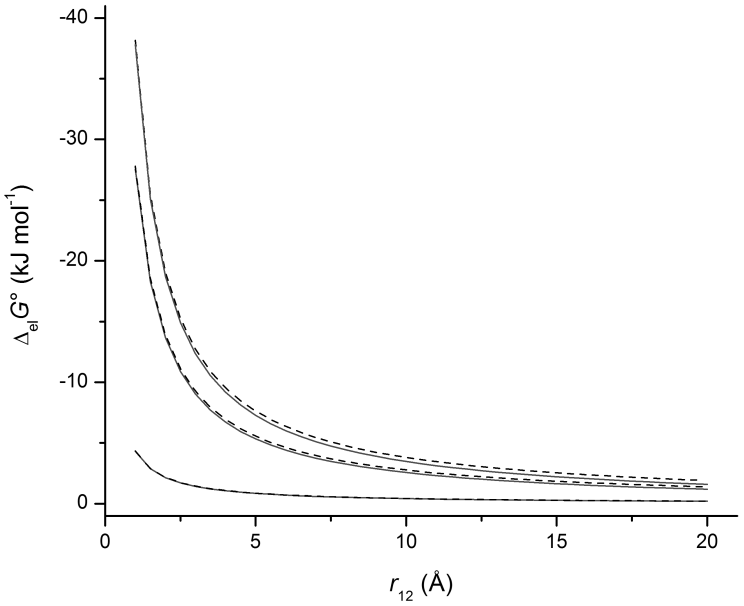

Figure 6-5. Distance (r_{12}) dependence of $\Delta_{el}E°$ in CH_2Cl_2 (ε_r = 9.1, top curves) CH_2Cl_2 + 0.1 M Bu_4NClO_4 (ε_r = 12.5, middle curves) and H_2O (ε_r = 80.1, bottom curves) calculated using continuum dielectric models that account for (eqn (6-21), solid lines) or disregard (eqn (6-24), dotted lines) ionic strength (T = 298 K, c = 0.1 mol m^{-3}).

In addition to errors resulting from modelling the solvent as a dielectric continuum and not taking into account the shape of the molecular cavity, a serious problem in determining accurate values using eqn (6-21) and (6-24) lies in assessing the true charge separation (particularly as $\Delta_{el}G°$ increases exponentially with decreasing r_{12}, *Figure 6-5)*. In line with previous discussions, using $r_{MM'} = r_{12}$ likely determines only the lower limit of electrostatic free energy within a system.

Inductive, or synergistic effects ($\Delta_{in}G°$)

Continuing with the previous example (*i.e.* $[\{Ru(NH_3)_5\}_2(\mu\text{-}4,4'\text{-bipy})]^{5+}$), to account for the remaining contributions to $\Delta_{to}G°$ Taube and co-workers conceived what are now described as inductive, or synergistic effects ($\Delta_{in}G°$).[30,35,38] In an interesting thought-experiment the step-wise assembly of isovalent and mixed-valence states from Ru^{II}, Ru^{III} and bridging ligand (μ-BL) components was considered. Though this is described using the redox centre (Ru^{II}) as a π-donor and the ligand as a π-acceptor, such arguments hold for the reverse case also.[39]

When a Ru^{II} centre and μ-BL are combined to $Ru_{(1)}^{II}$–μ-BL, the result is stabilization by back-bonding (electron transfer from the metal πd to the ligand π* orbitals). When a second Ru^{II} is bound to $Ru_{(1)}^{II}$–μ-BL (forming $Ru_{(1)}^{II}$–μ-BL–$Ru_{(2)}^{II}$), the extent of backbonding corresponding to addition of $Ru_{(2)}^{II}$ is not as great as that when adding $Ru_{(1)}^{II}$ (*Figure 6-6*, top). The consequence of this is that the fully reduced state does not achieve its lowest possible energy (and so is inherently electronically unstable). In other words, $Ru_{(2)}^{II}$ can be thought of as 'feeling' the electron density from $Ru_{(1)}^{II}$ inductively, and is thus more easily oxidized. If addition of Ru^{III} to $Ru_{(1)}^{II}$–μ-BL is now considered (forming $Ru_{(1)}^{II}$–μ-BL–$Ru_{(2)}^{III}$), the positive charge of $Ru_{(2)}^{III}$ results in a lowered π* orbital on μ-BL, increasing the $Ru_{(1)}^{II}$–μ-BL backbonding interaction and stabilizing the mixed-valence state (a push-pull effect,[33] *Figure 6-6*, bottom). Or alternatively, the electron-withdrawing $Ru_{(2)}^{III}$ centre is 'felt' through the ligand, making $Ru_{(1)}^{II}$ more difficult to oxidize. With $Ru_{(2)}^{II}$ easier to oxidize, and $Ru_{(1)}^{II}$ harder to oxidize, $\Delta E_{1/2}{}^{0}$ is increased.

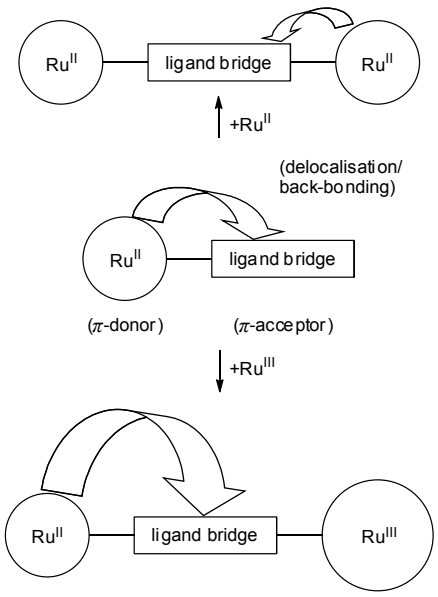

Figure 6-6. The inductive effect in Ru^{II}/Ru^{III} systems represented schematically.

These effects were confirmed through experiment, firstly by noting the increased basicity[40] and affinity for M^{2+} ions[41] of $[(NH_3)_5Ru(\mu\text{-py})]^{2+}$ relative to free py (indicating that electron-density changes from addition of Ru_1^{II} at one end of the ligand propagate through to the other end), and secondly by comparing Ru^{II}/Ru^{III} redox couples for the compound series shown in

Figure 6-7 (separating electron delocalization and inductive effects, as described in the figure caption).[35]

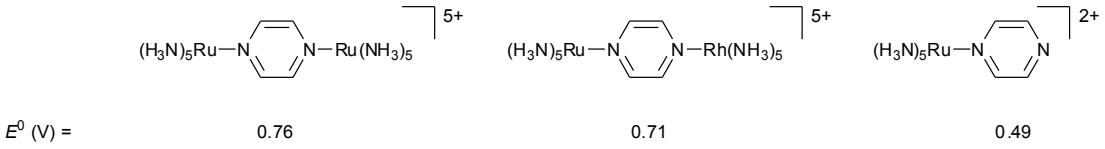

Figure 6-7. Selected complexes and potentials for their Ru^{II}/Ru^{III} redox couple (measured by potentiometric titration, reported relative to an Ag/AgCl reference electrode).[9,42] The potential of the mononuclear complex is much lower than for the dinuclear analogues containing (electron-withdrawing/π*-stabilising) Ru^{III} and Rh^{III} centres. As Rh^{III} is a d^6 metal it cannot participate in electron delocalisation, yet still exerts an influence similar to Ru^{III} on $E^0(Ru^{II}/Ru^{III})$.[35]

Whilst it is generally not possible to quantify $\Delta_{in}G°$ (it can only be estimated if one assumes $\Delta_{in}G° = \Delta_{to}G° - \Delta_{el}G° - \Delta_{re}G°$, etc[12a]), it can be argued that this contribution to $\Delta_{to}G°$ increases proportionally with $\Delta_{re}G$ or H_{ab}. These all rely upon efficient interactions between $(L)_nM$-ligand orbitals.

The free energy of resonance exchange ($\Delta_{re}G^0$)

As previously mentioned, when the two wavefunctions of the reactant and product states for an electron transfer reaction mix, they form upper and lower potential energy surfaces with a splitting at $X = 0.5$ which is equal to $2H_{ab}$ *(Figure 6-2).* When $H_{ab} \neq 0$ the minima on the combined ground state potential energy surface is reduced relative to its energetic position in the diabatic limit *(Figure 6-8)*. This decrease in energy may be described as the resonance stabilization energy attributable to delocalization of the valence, $\Delta_{re}G^0$, and accordingly will favour the mixed-valence over the isovalent states.

In the Class I/Class II regime *(Figure 6-8a)*, this contribution to $\Delta_{to}G^0$ is considered to be small[12a] and can be calculated for *one mole* of the mixed valence species from the properties of its IVCT band using eqn (6-25).[12a,20,27b,30] For borderline Class II/III ($H_{ab} \approx \lambda/2$) and very strongly coupled, Class III, systems ($H_{ab} >> \lambda/2$, *Figure 6-8b)*, this may be the dominant component of $\Delta_{to}G^0$, and is calculated via eqn (6-26)[12a,30] or (6-27),[20,27b] respectively.

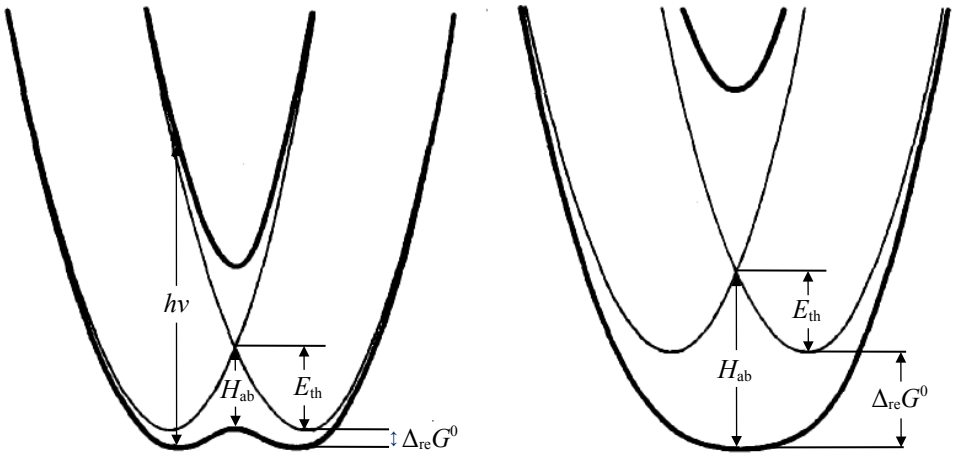

(a) (b)

Figure 6-8. Potential energy curves for symmetric class II (a) and class III (b) mixed-valence complexes (Class I = thin lines in each; $h\nu = \lambda$).[30] Figure adapted from Richardson and Taube,[30] with permission from Elsevier.

$$\Delta_{re}G^0 = -\frac{H_{ab}{}^2}{\lambda} = -\frac{H_{ab}{}^2}{\nu_{max}} \tag{6-25}$$

$$\Delta_{re}G^0 \approx -H_{ab} \approx -\frac{\nu_{max}}{2} \tag{6-26}$$

$$\Delta_{re}G^0 = -\left(H_{ab} - \frac{\lambda}{4}\right) = -\left(\frac{\nu_{max}}{2} - \frac{\lambda}{4}\right) \tag{6-27}$$

Antiferromagnetic superexchange ($\Delta_{as}G^0$)

Over the last two decades, an additional contribution to the position of mixed-valence equilibria has come into increasing focus. This involves *magnetic* coupling between unpaired ($m_s = \pm ½$) electrons on each redox centre,[43] and, as will be discussed, *reduces* $\Delta_{to}G^0$ by stabilizing the fully oxidized, $M_1^{III}M_2^{III}$, species (or more generally, *any* oxidation state that contains two unpaired electrons).[29,44]

The magnetic interaction between two spins, $\hat{S}_1$ and $\hat{S}_2$, on weakly coupled ions can be

described by the Heisenberg-Dirac-van Vleck Hamiltonian (eqn (6-28)).[43a,45] Here, $\mathcal{J}$ is the exchange coupling constant, which is positive if the spins are aligned parallel (↑↑, ferromagnetic coupling), and negative if the spins are anti-parallel (↑↓, antiferromagnetic coupling).

$$\mathcal{H} = -2\mathcal{J}\hat{\mathbf{S}}_1\hat{\mathbf{S}}_2 \tag{6-28}$$

Two spins $S_1 = S_2 = \pm½$ (= S_n) may be combined to provide a triplet state ($S_t = 1$) or a singlet state ($S_t = 0$). The energies of each state relative to their energy in the absence of interaction can then be calculated from the eigenvalues of $\mathcal{H}$ using eqn (6-29).[45a] It can be seen that when $\mathcal{J} < 0$ there is a singlet ground state (*i.e.* antiferromagnetic coupling is the major interaction),[§§] and that the singlet-triplet energy gap, E_{ST}, is $-2\mathcal{J}$ for both $\mathcal{J} < 0$ and $\mathcal{J} > 0$ (eqn (6-30)).[***] A representative energy level diagram for antiferromagnetic coupling is shown in *Figure 6-9*. Previous authors have used either $\mathcal{J}$ or $2\mathcal{J}$ as the stabilization energy conferred to $[M_2^{III}M_2^{III}]$ by this antiferromagnetic superexchange interaction (*i.e.* $\Delta_{as}G^0$).[29,44,47] Following the above discussion, it is suggested here that a more reasonable estimate is actually $\Delta_{as}G^0 = -3\mathcal{J}/2$ (assuming full population of the singlet state at the temperature of interest).

$$E(S_t) = -\mathcal{J}[S_t(S_t+1) - 2S_n(S_n + 1)] \tag{6-29}$$

$$E_{ST} = E(1) - E(0) = -\mathcal{J}/2 - 3\mathcal{J}/2 = -2\mathcal{J} \tag{6-30}$$

[§§] $\mathcal{J} < 0$ is usually the case when *two cations have lobes of singly occupied 3d-orbitals which point towards each other giving large overlap and hopping integrals* (from the Goodenough-Kanamori-Anderson rules).[45b,46]

[***] Depending on the form of the Hamiltonian used for derivation, E_{ST} may be defined in different ways. For example using $\mathcal{H} = -\mathcal{J}\hat{\mathbf{S}}_1\hat{\mathbf{S}}_2$, $E_{ST} = -\mathcal{J}$ (as is the case for the modified Bleaney-Bowers equation, *vida infra)*.

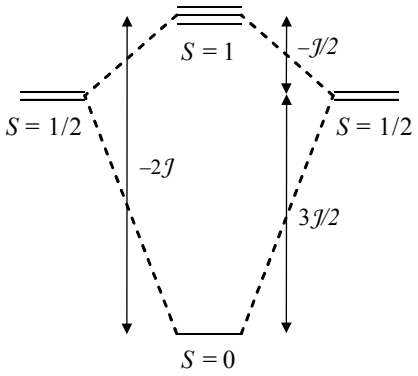

Figure 6-9. Energy level diagram for antiferromagnetic coupling ($\mathcal{J} < 0$) of two spins ($S_1 = S_2 = ½$, degeneracy given by $2S + 1$).

The magnitude of $\mathcal{J}$ may be estimated in several ways. Traditionally, this has been achieved by measuring the molar susceptibility, χ_m, of a solid sample as a function of temperature, T, and fitting the data using the Van Vleck equation (eqn (6-31), where μ_0 = vacuum permeability (N A^{-2}), N_A = Avogadro's constant (mol^{-1}), g = the Landé g-factor, μ_B = the Bohr magneton (J T^{-1}), k_B = Boltzmann's constant (J K^{-1}) and T = temperature (K)[†††]).[49] This may be modified to account for a proportion (ρ) of paramagnetic impurities, weak intermolecular interactions at low temperatures (by incorporation of a Weiss constant), and temperature independent paramagnetism (TIP) (eqn (6-32)).[47,50]

$$\chi_m = \frac{\mu_0 N_A g^2 {\mu_B}^2}{k_B T}\left[3 + \exp\left(\frac{-2\mathcal{J}}{k_B T}\right)\right]^{-1} \tag{6-31}$$

$$\chi_m = \frac{2\mu_0 N_A g^2 {\mu_B}^2}{k_B(T-\theta)}\left[3 + \exp\left(\frac{-2\mathcal{J}}{k_B T}\right)\right]^{-1}(1-\rho) + \frac{\mu_0 N_A g^2 {\mu_B}^2}{2k_B(T-\theta)}\rho + \text{TIP} \tag{6-32}$$

Substitution of eqn (6-31) into eqn (6-33) provides eqn (6-34) ($\mu_0 N_A \mu_B^2 / 3k_B = 1.5714 \times 10^{-6}$). Using the latter expression, Thompson and Ramaswamy showed that reasonable estimates of $\mathcal{J}$

[†††] To convert molar susceptibility from CGS (cm^3 mol^{-1}) to SI (m^3 mol^{-1}) requires multiplication by $4\pi \times 10^{-6}$.[48]

could be obtained for binuclear Cu^{II} complexes, measurements of their solid state room-temperature magnetic moments and known values of g and T. The inverse relationship between $\mathcal{J}$ and μ_{eff} may be easily rationalised: as $\mathcal{J}$ increases, thermal population of the triplet excited state decreases *(Figure 6-9)*, rendering the complex more diamagnetic through anti-parallel pairing of the electron spin dipoles.

$$\mu_{eff} = 797.73\sqrt{\chi_m T} \tag{6-33}$$

$$-2\mathcal{J} = k_B T \ln\left(\frac{3g^2}{\mu_{eff}{}^2} - 3\right) \tag{6-34}$$

Their approach was subsequently applied to binuclear Ru^{III} systems by Naklicki *et al.*,[43b] using a mean value of g chosen on the basis of values found for mononuclear Ru^{III} complexes. Notably, they measured mass susceptibilities, χ_g, *in solution* via the Evan's NMR method,[51] by applying his expression adapted[52] for modern spectrometers (where magnetic fields run parallel to the sample tube axis, rather than perpendicular) (eqn (6-35), where Δf = observed frequency shift of reference resonance (Hz), f = spectrometer frequency (Hz), m = mass of substance per volume of solution (kg m^{-3})).‡‡‡ Values of χ_g obtained in this manner may be converted to χ_m after applying a diamagnetic correction.[53]

$$\chi_g = \frac{-3\Delta f}{f m} \tag{6-35}$$

It is also possible to measure $\mathcal{J}$ directly via NMR, by measuring the chemical shift of resonances as a function of temperature, and fitting the data to eqn (6-36) (where H_{obs} = the frequency of the resonance being measured (Hz), H_{dia} = the frequency the same nucleus would have in a diamagnetic environment (Hz), H_0 = the resonance frequency of the nucleus (Hz), A = the hyperfine coupling constant between the electron and the nucleus in question (Hz), γ_C = the gyromagnetic ratio of the nucleus (Hz T^{-1}).[54]

‡‡‡ This simplified equation is valid if it can be assumed that the amount of solvent displaced by solute is very small (and thus the diamagnetic correction for the solvent is essentially the same in neat solvent and solution).[43b]

$$H_{obs} = H_{dia} + \frac{2g\mu_B H_0 A}{(\gamma_C/2\pi)k_B T}\left[3 + \exp\left(\frac{2J}{k_B T}\right)\right]^{-1} \quad (6\text{-}36)$$

Ion-pairing and medium effects

An improved awareness of the effect of solvents and counterions on $\Delta E_{1/2}^0$ has been provided by Geiger and co-workers in their systematic studies using model bis(fulvalene)dinickel (**C1**) and tetrakis(ferrocenyl)–nickel dithiolene (**C2**) complexes *(Figure 6-10)*.[28,55] The salient features of this insightful work show that $\Delta E_{1/2}^0$ for oxidation processes are maximized using a solvent of low polarity and donor number, with supporting electrolyte in low concentration comprising a large anion and a small cation (and *vice versa* in maximizing $\Delta E_{1/2}^0$ for reduction processes). Thus, the largest $\Delta E_{1/2}^0$ (= 0.85 V) observed for **C1** was in CH_2Cl_2/0.02 M Na($BArF_{24}$). Under these conditions, ion-pairing interactions between the electrolyte anions (cations) and the analyte cations (anions) were considered minimized.

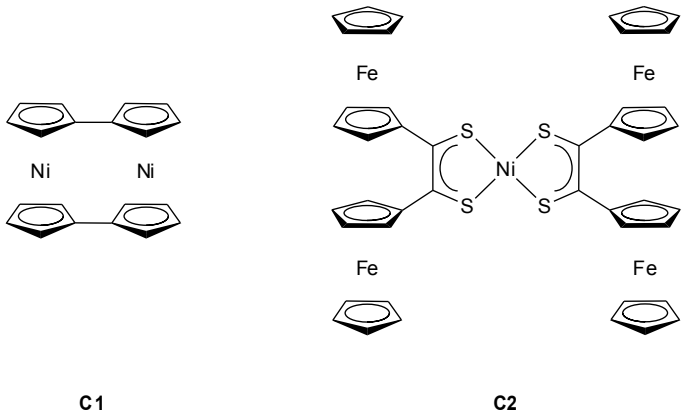

Figure 6-10. Model complexes used in the study of medium effects on $\Delta E_{1/2}^0$ by Geiger and co-workers.[28,55]

Changes in $\Delta E_{1/2}^0$ are determined by changes in the absolute values of E_1^0 and E_2^0 (eqn (6-10)). The effect of medium changes on the latter were thus rationalized by the equilibria and potential equations shown in *Figure 6-11* (for E_1^0), where with increased ion-pairing (*i.e.* larger K_{ip}) the oxidation equilibrium process is driven to the right (as Ox^+ is converted to OxA). This

shifts $E_n^{0'}$ to more negative potentials (in effect, with ion-pairing the analyte becomes easier to oxidize). The observation that changes in $E_2^{0'}$ with changing medium are significantly larger than changes in $E_1^{0'}$, was attributed by the authors to the increased charge density of the dication which accentuates ion-pairing effects (*i.e.* $K_{ip}([M_1M_2]^{2+}) >> K_{ip}([M_1M_2]^{+})$, as would be expected from simple electrostatic considerations).

$$\text{Red} \rightleftharpoons \text{Ox}^+ + e^- \qquad E_1^{\,0}$$

$$\text{Ox}^+ + \text{A}^- \rightleftharpoons \text{OxA} \qquad K_{ip}$$

$$E_1^{\,0'} = E_1^{\,0} - \frac{RT}{F} \ln\left(1 + K_{ip}[\text{A}^-]\right)$$

Figure 6-11. Ion-pairing effects can be rationalised in terms of an EC (electrochemical-chemical) mechanism (shown here for $E_1^{\,0}$ only).[56]

An alternative way of considering the effect of ion-pairing on $\Delta E_{1/2}^{\,0}$ is in terms of how this may stabilise the reactants and products of the comproportionation equilibria. Indeed, a complex network of competing equilibria can be envisaged *(Figure 6-12)*.[§§§] Here, ion-pairing can be qualitatively reasoned to confer a stabilizing energy on a charged species, or to reduce its concentration in the equilibrium (as in the model of Geiger and co-workers). To a reasonable first approximation, the favourable interaction of $[M_1^{III}M_2^{III}]^{2+}$ with one electrolyte anion (proportional to 4, using a simple electrostatic model *i.e.* Coulomb's law) will be greater than the favourable interaction of two $[M^{II}M^{III}]^{+}$ each with one electrolyte anion (proportional to 2), thus driving the equilibrium towards formation of the isovalent states, and decreasing $\Delta E_{1/2}^{\,0}$.

[§§§] This description neglects higher aggregates for simplification. Furthermore, analyte/electrolyte cations should also be considered in competition with donor solvents, and electrolyte anions in competition with acceptor solvents.

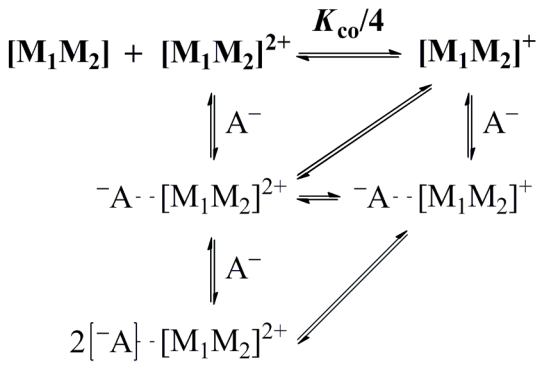

Figure 6-12. A complicated picture emerges when considering the effect of ion-pairing on the comproportionation equilibrium.

Thus, the effects of the surrounding medium on $\Delta E_{1/2}^0$ are impossible to ignore (further examples have been provided by others[57]). Comparisons between different complexes should be made extremely judiciously, in the same solvents and with the same electrolyte composition/concentration (though concentration is considered to have only a minor influence, with $\Delta E_{1/2}^0$ changing < 60 mV for **C1** in CH_2Cl_2 between 0.02 M and 0.10 M Na($BArF_{24}$)). With the same medium, $\Delta_{ip}G^0$ (a positive contribution to $\Delta_{to}G^0$, as increased ion-pairing stabilises the isovalent states) may be considered approximately constant – though this assumes the same extent of ion-pairing interaction between the electrolyte and *different* complexes.

From this analysis, it can be seen that $\Delta_{ip}G^0$ and $\Delta_{el}G^0$ are intimately related (see also solvation, below). They are both affected by changing solvent (via the dielectric constant, eqn (6-21) and (6-24)), and the latter is arguably reduced with improved screening of charges resulting from analyte-electrolyte ion-pairing interactions.

Solvation and enthalpy changes

Two other important contributions to $\Delta_{to}G^0$ are not always discussed in the context of those previously mentioned. These involve changes in the energy of ionic solvation, and any structural distortions (a largely enthalpic term) that might occur during redox processes. These factors typically take centre stage[14,58] in discussions of 'potential inversion'.[****]

[****] Normal potential ordering gives $E_1^0 < E_2^0$ ($\Delta E_{1/2}^0 > 0$) for oxidations and $E_1^0 < E_2^0$ ($\Delta E_{1/2}^0 < 0$) for reductions. This is due to the greater thermodynamic difficulty in adding a second electron/hole to an already charged species

Certainly, there will be significant changes in the solubility of a complex upon its oxidation or reduction. Though it overestimates solvation free energies (also neglecting hydrogen bonding, van der Waals interactions, etc),[59] the Born model can be used to invoke trends in energy changes (ΔG^0) upon moving a spherical ion from one medium (*i.e.* vacuum, gas, or solvent) to another. For one mole of ions moving from a vacuum to a solvent of dielectric ε_r (*i.e.* the free energy of ionic solvation), can be calculated using eqn (6-37) (where z = charge number of the ion, r_i = ionic radius).[60] At this point $\Delta_{so}G^0$ should be qualitatively distinguished from $\Delta_{el}G^0$ for clarity – it considers *favourable* ion-solvent interactions (an intermolecular term), whereas the latter intends only to describe intramolecular repulsive terms.

$$\Delta G^0 \text{ (ionic solvation)} = -\frac{N_A(ze)^2}{8\pi\varepsilon_0 r_i}\left[1-\left(\frac{1}{\varepsilon_r}\right)\right] \qquad (6\text{-}37)$$

Savéant and co-workers have considered three different ways the change in energy of solvation ($\Delta_{so}G^0$) may affect the comproportionation equilibria in molecules containing identical and independent reducible/oxidizable groups.[56a,61] Where the groups do not interact with each other *(Figure 6-13a)*, $\Delta_{so}G^0$ will be zero (two mixed-valence complexes each with one centre ze/r, *vs.* one fully oxidized complex with two centres ze/r). If the charge can instead be considered fully delocalized across the whole molecule, the molecule can be modelled as a large ion *(Figure 6-13b)*. As the solvation energy of an ion is proportional to the square of its charge (eqn (6-37)), the fully oxidized/reduced species now has a much greater free energy of solvation (assuming the same radius for ze = 1 and ze = 2), and this shifts the comproportionation equilibrium in favour of the isovalent species ($\Delta_{so}G^0$ proportional to -2 for the two mixed-valence complexes, and $\Delta_{so}G^0$ proportional to -4 for the fully oxidized complex).

for electrostatic or other reasons *(vida supra)*. In some cases however it is thermodynamically easier to add the second hole/electron, a phenomenon typically attributed to solvation effects or structural changes following oxidation/reduction. This decreases $\Delta E_{1/2}{}^0$ and can result in potential inversion, where $E_1{}^0 > E_2{}^0$ ($\Delta E_{1/2}{}^0 < 0$) for oxidations and $E_1{}^0 > E_2{}^0$ ($\Delta E_{1/2}{}^0 > 0$) for reductions. In these extreme cases, a single two-electron redox wave is observed in cyclic voltammetry experiments, with thinner peaks and a smaller peak-peak separation than expected for one-electron Nernstian waves.[56a]

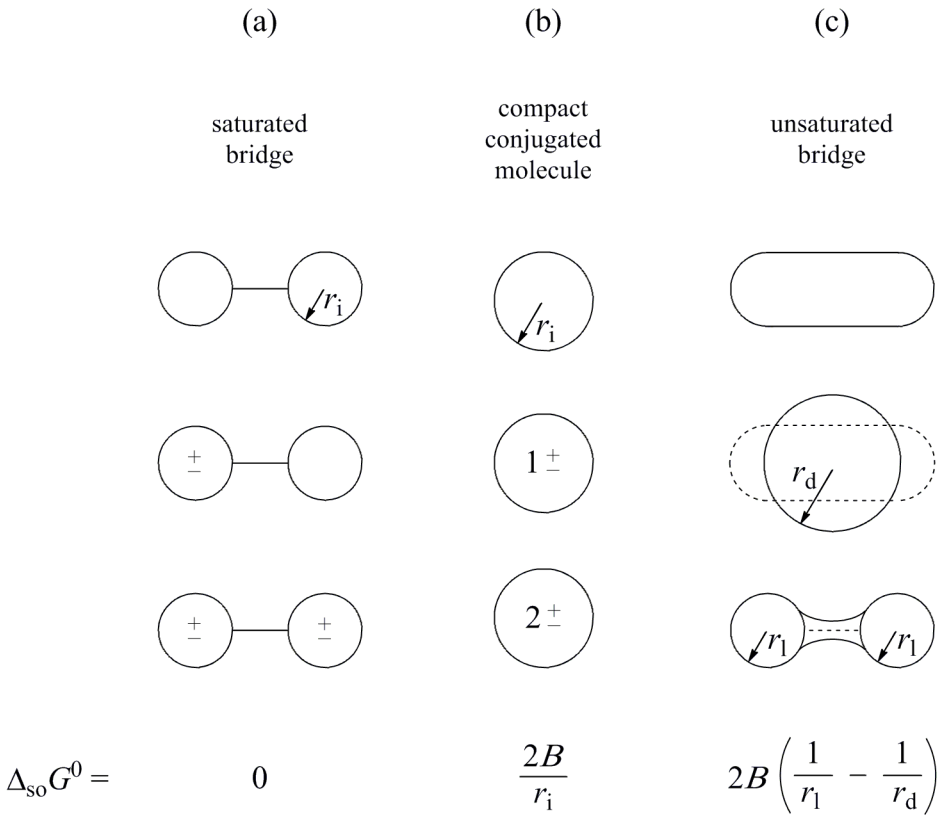

Figure 6-13. The variance of stabilisation energy, conferred to the isovalent states of the comproportionation equilibrium, that is attributable to changes in the free energy of solvation ($\Delta_{so}G^0$) with delocalisation of charge in sequentially oxidized (+) or reduced (–) complexes. Adapted from Savéant and co-workers.[56a,61]

A third possibility may be quite applicable to the complexes considered later in this work. When redox groups are separated by a long conjugated bridge, the single-charge of the mixed-valence species may be considered delocalized over a large area with radius r_d *(Figure 6-13c)*. Depending on the nature of the end-groups (electron-donating/withdrawing), charges may become localized at each end of the molecule in the fully oxidized/reduced species. If this should occur, $\Delta_{so}G^0 \propto -2/r_d$ for the mixed-valence state and $\Delta_{so}G^0 \propto -2/r_l$ for the isovalent states. With

increasing r_d relative to r_l (*i.e.* as the bridge is extended) the isovalent states become more and more stabilized (due to a larger free energy of solvation), decreasing $\Delta E_{1/2}^0$.

This effect was observed in *β*–carotene *(Figure 6-14a)* and simple analogues,[61] which exhibited potential inversion (*i.e.* $\Delta E_{1/2}^0 < 0$) when oxidized (due to hole localization in the end-groups, following model *Figure 6-13c)*, but successive one-electron waves when reduced (following model *Figure 6-13b)*. The opposite was seen in canthaxanthin *(Figure 6-14b)* – exhibiting potential inversion ($\Delta E_{1/2}^0 > 0$) when reduced (due to electron localization in the end-groups) and successive one-electron waves when oxidised. It was hypothesized by the authors that the effect of bridge extension on $\Delta_{so}G^0$ may accordingly play a critical role in reducing $\Delta E_{1/2}^0$, *in addition* to the more commonly cited factors such as decreasing electrostatic repulsion, resonance, induction, antiferromagnetic superexchange, etc.

(a)

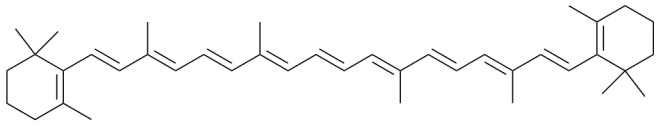

***β*–carotene**
(oxidations show potential inversion, sequential reductions)

(b)

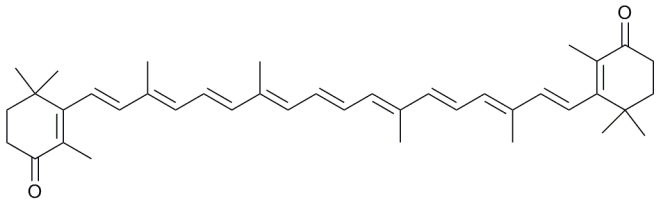

canthaxanthin
(reductions show potential inversion, sequential oxidations)

Figure 6-14. Carotenoids used in elucidating the solvation models shown in *Figure 6-13*.[61] For fully oxidised (a), holes are localised in the end groups due to the electron-donating methyl groups. In fully reduced (b), electrons are localised in the end groups due to electron-withdrawing carbonyl moieties. Charge is delocalised across the conjugated framework in all singly charged species, the dianion of (a) and the dication of (b).

Structural changes upon oxidation/reduction will also affect $\Delta E_{1/2}^0$, but to what extent likely requires assessment on a case-by-case basis. These can either be largely enthalpic in origin, associated with bond changes (*e.g.* single bonds to double bonds), and/or due to changes in

molecular shape that result from changes in bonding (*i.e.* impacting upon $\Delta_{so}G^0$). These effects can be assessed in the first instance by analysis of X-ray crystallographic data for successive oxidation states, or calculated via computational studies.[61] Several informative works may be consulted for further information and examples.[14,62]

Summary

For clarity, key aspects of each contribution to $\Delta_{to}G^0$ are summarised in *Table 6-1*. In attempting to make useful comparisons between sets of similar structures, it is imperative to correctly assess which components may be ignored (*e.g.* if $\Delta_{xx}G^0 << \Delta E_{1/2}{}^0$), and which might be assumed approximately constant across a series.

Table 6-1. Several factors may contribute to the position of the comproportionation equilibria – a summary.

contribution to $\Delta_{to}G^0$ ($\Delta_{to}G^0 = -½(\Delta_{co}G^0 - \Delta_{st}G^0)$)	sign[a]	magnitude (kJ mol^{-1})	relevant equation(s)
$\Delta_{el}G^0$ (electrostatic)	-ve	[b]	(6-23) (using (6-21) and (6-22), or (6-24))
$\Delta_{in}G^0$ (inductive)	-ve	/	/
$\Delta_{re}G^0$ (resonance)	-ve	[b]	(6-25) for Class II systems (6-26) for Class II/III systems (6-27) for Class III systems
$\Delta_{as}G^0$ (antiferromagnetic superexchange)	+ve	$-3\mathcal{J}/2$	(6-34) or (6-35) (from NMR studies)
$\Delta_{ip}G^0$ (ion-pairing)	+ve	[c]	/
$\Delta_{so}G^0$ (solvation)	+ve	[b]	*Figure 6-13a*, *b* or *c*
$\Delta_{str}G^0$ (structural)	system specific	/	/

[a] –ve will favour mixed-valence state, +ve will favour isovalent states. [b] Trends estimated using equations. [c] Minimised for oxidations using a solvent of low polarity and donor number, with supporting electrolyte in low concentration comprising a large anion and a small cation.

6.3 'ELECTRON DENSITY' *vs.* $\Delta E_{1/2}{}^0$

As previously discussed, changes in $\Delta E_{1/2}{}^0$ for complexes of the type [{M(L)$_n$}$_2$(μ-BL)], have on occasion been qualitatively attributed to differences in the electron density of the metal centre.[7] Furthermore, a correlation between electron density, from relevant ν(C≡C)/ν(C≡O)

values, and $\Delta E_{1/2}{}^{0}$ was noted for a small number of bisferrocenylacetylide complexes[63] – and a linear dependence between solvent donor number and $\Delta E_{1/2}{}^{0}$ in Ru pentamine complexes, noted (the greater Lewis basicity of the solvent, the greater the electron density at the metal centre).[64] The following sections expand upon our previous attempts to explore this relationship.[6] To the best of our knowledge no attempts to broadly quantify such trends have been made elsewhere (particularly with reference to metal σ alkynyl systems), and the potential association is intriguing.

6.3.1 Use of ν(X) to investigate the properties of M(L)$_n$

A convenient measure of electron density at the metal fragment {M(L)$_n$} was required, and for this it was considered that the IR stretching frequencies of diagnostic (isolobal) ligands such as carbonyl (C≡O), cyanide ($^{-}$C≡N), and to a lesser extent phenylacetylide ($^{-}$C≡C–C$_6$H$_5$), bound to mononuclear analogues of [{M(L)$_n$}$_2$(μ-BL)] species, *i.e.* {M(L)$_n$}–R (R = C≡O, $^{-}$C≡N, $^{-}$C≡C–C$_6$H$_5$), might prove good indicators *(Figure 6-15)*.[††††] Following Tolman's work on the electron-donating abilities of phosphines the inverse relationship between ν(C≡O) and the electron density at a metal centre (resulting largely from metal-to-ligand back-bonding) is well established.[65] As well as measuring electron density differences between {M(L)$_n$} where M = M and (L)$_n$ ≠ (L)$_n$, ν(X) were thought to be potentially indicative of orbital energetic/spatial changes where M ≠ M and (L)$_n$ = (L)$_n$. Data for relevant M(L)$_n$–R is provided in *Table 6-2*.

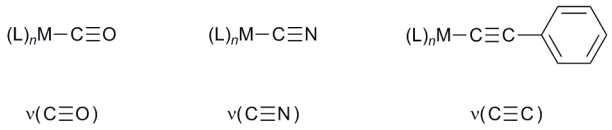

Figure 6-15. Mononuclear complexes and stretching frequencies used to quantify electron density at M(L)$_n$

[††††] IR spectroscopy has proved useful in other ways to probe the interactions between metal centres. For example, Geiger and co-workers utilised changes in the frequencies of IR active M(L)$_n$ (*e.g.* metal-bound carbonyl ligands) in different oxidation states to determine the extent of charge localisation between redox sites in valence trapped systems (the charge distribution parameter, Δp).[26]

Table 6-2. Selected infrared data for {$M(L)_n$}–R complexes (R = C≡O,[a] $^-$C≡N,[b] $^-$C≡C–C_6H_5[b]).

	IR data[c]								
$M(L)_n$	ν(C≡O)	complex (conditions)	ref	ν(C≡N)	complex (conditions)	ref	ν(C≡C)	complex (conditions)	ref
Fe(dppe)Cp*	1940	(unknown)	*66*	<2060[d]	Fe(CN)(dppe)Cp (unknown)	*67*	2054	/	*68*
Fe(dippe)Cp*	1928	[M']BPh_4 (Nujol mull)	*69*	/	/	/	2050	(Nujol mull)	*70*
Fe(dppe)Cp	1981	/	*71*	2060	(unknown)	*67*	2060	/	*72*
Fe(dppm)Cp	1983	/	*71*	/	/	/	2071	(THF)	*73*
							2065	(KBr)	
Fe(CO)(PMe_3)Cp	1955	[M']Br ($CHCl_3$)	*74*	/	/	/	/	/	/
	2054, 2009	[M']BF_4 ($C_2H_4Cl_2$)	*75*						
Fe(CO)(PPh_3)Cp	2010	/	*76*	2099	/	*77*	2085	(unknown)	*78*
Ru(dppe)Cp*	1972	/	*79*	2065	/	*80*	2071	/	*68*
Ru(dppm)Cp*	/	/	/	<2076[d]	Ru(CN)(dppm)Cp	*80*	2072	/	*81*
Ru(dppe)Cp	1990	/	*82*	2075	/	*80*	2082	(Nujol mull)	*83*
$Ru(PPh_3)_2Cp$	1986	($CHCl_3$)	*84*	2072	/	*80*	2068	(Nujol mull)	*83*
Ru(PPh_3)(PMe_3)Cp	1995	(Nujol mull)	*85*	/	/	/	2070	(Nujol mull)	*86*
Ru(dppf)Cp	1974	(KBr)	*87*	/	/	/	2112[e]	(KBr)	*87*
Os(dppe)Cp*	/	/	/	/	/	/	2085	(Nujol mull)	*88*
$Os(PPh_3)_2Cp$	/	/	/	2065	(KBr pellets)	*89*	2066	(Nujol mull)	*83*
Re(NO)(PPh_3)Cp*	2002	[M']BF_4 (CD_2Cl_2)	*90*	2090	(thin film)	*91*	/	/	/
Re(NO)(P(*p*-tol)$_3$)Cp*	2002	[M']BF_4	*92*	/	/	/	/	/	/
Re(NO)(PCy_3)Cp*	1993	[M']BF_4	*92*	/	/	/	/	/	/
Mo(dppe)(η-C_7H_7)	1958	/	*71*	2073	/	*93*	2025[f]	(unknown)	*94*
							2045	/	*95*
trans-$FeCl(depe)_2$	1906	[M']Cl (Nujol mull)	*96*	/	/	/	/	/	/
trans-$FeCl(dmpe)_2$	1938	[M']BPh_4 (Nujol mull)	*96*	/	/	/	2044	/	*97*
trans-$RuCl(dppe)_2$	1946	(KBr)	*98*	/	/	/	2072	/	*99*

Table 6-2 (continued)									
trans-RuCl(dppm)$_2$	1965	[M']BF$_4$ (Nujol mull)	*100*	/	/	/	2075	(KBr)	*101*
	1980	(Nujol mull)	*100*				2080	/	*102*
trans-OsCl(dppm)$_2$	1962	[M']SbF$_6$	*103*	/	/	/	2079	/	*102*
trans-CrCl(dmpe)$_2$	/	/	/	2082	(neat)	*104*	2032	(ATR)	*74*
Mn(dmpe)(C$_5$H$_4$Me)	/	/	/	/	/	/	2008	(KBr)	*105*

[a] As the $[M']^+[PF_6]^-$ salt in CH_2Cl_2 unless otherwise stated, where $[M']^+ = [\{M(L)_n\}–C{\equiv}O]^+$. [b] In CH_2Cl_2 unless otherwise stated. [c] In cm^{-1}. [d] Estimated from the IR frequency of the Cp analogue (-10 cm^{-1} based upon the difference between Ru(dppe)Cp* and Ru(dppe)Cp). [e] Not explicitly assigned by original authors. [f] Incorrectly reported value, corrected in subsequent publications.

Though the suitability of such parameters (*i.e.* ν(C≡C), particularly with terminal alkynes) to measure the extent of back-bonding has been called into question,[106] broadly this dataset can be seen to follow expected trends. Indeed, complexes bearing more electron rich Cp* ligands have lower IR frequencies than otherwise identical ones with Cp, and those with π-acceptor ligands such as CO or NO generally have much higher frequencies. Though a typical IR measurement might be expected to provide a value reproducible to approximately ±3 cm^{-1}, larger errors across *Table 6-2* may be expected. They have been collected from independent papers published throughout the last 50 years, were measured in different labs, with different instrumentation, and under different conditions. The effects of the latter appear most profound for the carbonyl series, where the changing counterion can be seen to play an important role (*e.g.* for $M(L)_n$ = Fe(CO)(PMe_3)Cp or *trans*-RuCl(dppm)$_2$). Where possible, values were taken for a common set of 'standard conditions' (= in CH_2Cl_2, and with the PF_6^- anion for C≡O complexes). It was considered that compilation of three diagnostic ligand series (ν(C≡O), ν(C≡N) and ν(C≡C)), rather than just one, would contribute to minimising potential errors.

6.3.2 Electrochemical data and correlations

We resolved to plot $\Delta E_{1/2}{}^0$ values for complexes of the type [{$M(L)_n$}$_2$(μ-BL)] (containing the same μ-BL) against ν(X) from their mononuclear analogues, {$M(L)_n$}–R. Chosen bridging ligand series were: –C≡C–C≡C– (C_4 alkyne), –C≡C–C≡C–C≡C–C≡C– (C_8 alkyne), –CH=CH–CH≡CH– (C_4 alkene), –C≡C–C_6H_4–C≡C– (phenylene) and –C≡C–C_4H_4S–C≡C– (thiophene). Though an extensive number of complexes of these types have been reported, their inclusion in this study was often not possible. Many known compounds have not been studied electrochemically, and of those that have, some show only quasi-reversible or irreversible features ($i_p{}^a/i_p{}^c \neq 1$). Furthermore, for a small number of complexes that exhibit reversible features, details of their {$M(L)_n$}–R (R = C≡O, $^-$C≡N, $^-$C≡C–C_6H_5) analogues have not yet been published (or are not easily established, *i.e.* for $(L)_nM$≡C–R species). Known complexes thus omitted from this inquiry are detailed in *Table 6-4*. Though data for –C≡C–/=C=C=/≡C–C≡ (C_2) bridges was also gathered, only two usable data points could be established *(Table 6-3)*.

Table 6-3. Electrochemical data[a] for complexes of the type [{M(L)$_n$}$_2$(μ-C$_2$)].

	CV data				
M(L)$_n$	E_1^0	E_2^0	$\Delta E_{1/2}^0$	conditions[b]	ref
Ru(dppe)Cp	-0.61	0.21	0.82	$Bu_4N^+PF_6^-/CH_2Cl_2$	*107*
Mn(dmpe)(C_5H_4Me)	-1.83	-0.85	0.99	$Bu_4N^+PF_6^-/CH_3CN$	*108*

[a] All redox potentials in volts relative to $[Cp_2Fe]^+/Cp_2Fe$. [b] Pt working electrode.

Relevant electrochemical data is given in *Table 6-5*-*Table 6-9*, with plots of $\Delta E_{1/2}^0$ against ν(X) (using the data from *Table 6-2)* presented in *Figure 6-16*-*Figure 6-18* for aliphatic systems. $\Delta E_{1/2}^0$ *vs*. ν(C≡O) is provided for aromatic systems in *Figure 6-19* (a representative example). For the aliphatic bridges, some intriguing correlations are observed (apparently linear with ν(C≡O)/ν(C≡N), and curved for ν(C≡C)), whereas no identifiable correlation can realistically be presented for the aromatic bridges considered. Reasonably justifiable anomalies across all datasets are highlighted in the figures and summarised in *Table 6-10*. Though it was not possible here to investigate all systems in sufficient detail, the C_4 alkyne bridged series was chosen for further analysis in an attempt to rationalise these apparent relationships. This follows in the next section.

Table 6-4. Known complexes of the type [{M(L)$_n$}$_2$(μ-BL)] not included in this study.

	M(L)$_n$		
μ-BL	Electrochemical experiments not conducted	Non-reversible electrochemistry ($i_p^a/i_p^c \neq 1$)	{M(L)$_n$}–X[a] analogues unknown
C_2	MX(PR$_3$) (M = Pt, Pd; X = Cl, I; R = Me, Et, ^{n}Bu, Ph;),[109] Fe(CO)$_2$Cp*,[110] HgR (R = Me, alkyl),[111] Au(PR$_3$),[112] [AuR]PPh$_4$ (R = CN, PhC≡C, MeC≡C, HC≡C),[113] Mn(CO)$_5$[114], [V(mes)$_3$]$^-$,[115] Cr(CO)$_3$Cp,[116] Ti(PMe$_3$)Cp$_2$,[117] Sm(thf)Cp*$_2$,[118] ScCp*$_2$,[119] [Pt(^{t}Bu$_3$-tpy)]OTf[120]	Ru(CO)$_2$Cp,[121] Re(CO)$_5$,[122] W(^{t}BuO$_3$)$_3$[123]	WCl(dmpe)$_2$[124]
C_4 alkyne	Fe(CO)$_2$Cp*,[125] Mo/W(CO)$_2$Tp',[b,126] Rh/Ir(P^{i}Pr$_3$)$_2$-type centres,[127] PtCl(PR$_3$)$_2$,[128] [Pt(^{t}Bu$_3$-tpy)]OTf,[120] Au(P(*p*-tol)$_3$),[129] [Rh(P^{n}Bu$_3$)$_4$]Cl,[130] Mo(CO)$_2$Cp[131]	Re(CO)$_3$(^{t}Bu$_2$bpy),[132] W(CO)$_3$Cp*/W(O)$_2$Cp*,[133] Au(PCy$_3$)[112d]	Mn(dmpe)$_2$R (R = I,[134] C≡C–H, C≡C–SiMe$_3$,[135] C≡C–SiEt$_3$, C≡C–Si^{i}Pr$_3$, C≡C–Si^{t}BuMe$_2$[136]), WI(dppe)$_2$,[137] Ru(PPh$_3$)$_2$(Ph-tpy)[17]
C_8 alkyne	Fe(CO)$_2$Cp*,[110c] M(CO)$_3$Cp (M = Mo, W),[138] [Pt(^{t}Bu$_3$-tpy)]PF$_6$,[120] Au(P(*p*-tol)$_3$)[129]	Ru(dpf)$_4$(C$_4$SiMe$_3$)$_2$,[c,139] Pt (PY$_3$)$_2$(R) (Y = *p*-tol, PPh$_2$X[d],[140] R = *p*-tol,[141] C$_6$F$_5$,[142] Cl[143];), Re(NO)(PR$_3$)Cp* (R = Ph, *p*-C$_6$H$_4$-^{t}Bu, *p*-C$_6$H$_4$-C$_6$H$_5$, PPh$_2$X[d])[7c,144]	Ru(PPh$_3$)$_2$(R)[e,145]
phenylene	MX(PR$_3$)$_2$ (M = Pd,[146] Pt;[146c,147] X = Cl, Br, I, NCS, H, OTf, C$_6$H$_5$; R = Et, Bu, *p*-tol, Ph;), [M(PR$_3$)$_2$L]X (M = Pd,[148] Pt;[147a] R = Et; L = PEt$_3$, Py, CO; X = ClO$_4$;), Pt(dppe)(C≡C-C$_6$H$_4$-C≡CH),[149] MR$_3$ (M = Sn, Pb; R = CH$_3$, C$_6$H$_5$;),[150] V(EtMe$_4$C$_5$H$_5$)$_2$,[151] M(PR$_3$) (M = Cu, Ag; R = Et, ^{n}Bu, Ph;),[152] Rh(P^{n}Bu$_3$)$_4$,[130,153] [Rh(PMe$_3$)(H)]Cl,[153] [MCl(CO)(PPh$_3$)$_2$(CH$_3$CN)]OTf (M = Ir, Rh),[154] Au(PR$_3$) (R = Me,[155] *p*-tol[156]), Cu(PR$_3$)$_2$ (R = Et, Ph),[157] RuCl(CO)(dppf),[f,158] [M(P(OEt)$_3$)$_5$]X (M = Ru,[159] Fe;[160] X = PF$_6$, BPh$_4$;), Ru(PPh$_3$)$_2$Cp,[161] Re(CO)$_2$P$_3$ (P = PPh(OEt)$_2$, PPh$_2$(OEt)),[162] Ir(η^3-CH$_2$CHCHPh)Cp*,[163] Ir(CO)$_2$(PPh$_3$)$_2$(CHCH$_2$)$_2$[164] Mn(C$_5$H$_4$Me)(tmeda),[165] Ir(η^2-C$_4$H$_4$)(CO)(PPh$_3$)$_2$[166]	Pt(NCN),[g,167] Au(PCy$_3$),[168] Pt(P(^{n}Bu)$_3$)$_2$(C≡C-C$_6$H$_5$),[169] U(NN'$_3$),[h,77] Fe(CO)$_2$Cp,[170] CoCl(cyclam)[171]	Ru(PPh$_3$)$_2$(R),[e,145] TiCp$_2$(CH$_2$SiMe$_3$)[172]
thiophene	M(CO)$_3$Cp (M = Mo, W),[173] M(CO)$_2$Cp (M = Fe, Ru),[173] Pt(Ph)(PEt$_3$)$_2$,[174] Fe(CO)$_2$CpR [R = CH$_3$, I, CC-C$_4$H$_4$S-CC-(Cp)W(CO)$_3$(CH$_3$), CC-C$_4$H$_4$S-CC-(Cp)Re(CO)$_3$],[175] MCl(PBu$_3$)$_2$ (M = Pd,[176] Pt[147b]), Au(PPh$_3$)$_2$,[177] HgR (R = Ph, Me),[178] Pt(CCPh)(P(*p*-tol)$_3$)$_2$,[179] Pt(*m,p*-CCPh(OR)$_3$) (R = *n*-C$_{12}$H$_{25}$),[180] Pt(PBu$_3$)$_2$(DPAF) (DPAF = diphenylamino-2,7-fluorenylene)[181]	Fe(CO)$_2$Cp,[170] Pt(PBu$_3$)$_2$[CC-C$_6$H$_4$-CC-Pt(Ph)(PBu$_3$)$_2$][169]	Ru(PPh$_3$)$_2$(R),[e,145] PtCl(PBu$_3$)$_2$(CC-C$_6$H$_4$R) (R = fulleropyrrolidine moiety)[182]
C_4 alkene	RuCl(CO)(NH$_3$)(PPh$_3$)$_2$,[183] Fe(CO)$_2$Cp,[184] RuCl$_2$(PCy$_3$)$_2$,[185]	RuCl(CO)(PPh$_3$)$_2$,[186] RuCl(CO)(PEt$_3$)$_3$,[186] RuCl(CO)(PPh$_3$)$_2$(NC$_5$H$_4$COOEt),[186]	/

[a] X = C≡O, C≡N. [b] Tp' = hydridotris(3,5-dimethylpyrazolyl)borate). [c] dpf = N,N'-diphenylformamidine. [d] X = alkyl link to PPh$_2$ ligand bound on other metal centre. [e] R = N-(benzoyl)-N'-(picolinylidene)-hydrazine or 4'-phenyl-2,2':6',2''-terpyridine. [f] dppf = 1,l'-bis(dipheny1phosphino)ferrocene. [g] NCN = [C$_6$H$_3$(Me$_2$NCH$_2$)$_2$-2,6]$^-$. [h] NN'$_3$ = N(CH$_2$CH$_2$NSi^{t}BuMe$_2$)$_3$.

Table 6-5. Electrochemical data[a] for complexes of the type [{M(L)$_n$}$_2$(μ-C≡C–C≡C)].

	CV data				
M(L)$_n$	E_1^0	E_2^0	$\Delta E_{1/2}^0$	conditions[b]	ref
Fe(dppe)Cp*	-1.10	-0.38	0.72	(unknown electrolyte)	*187*
	-1.14	-0.42	0.72	$Bu_4N^+PF_6^-$	*188*
Fe(dippe)Cp*[c]	-1.43	-0.64	0.79	$Bu_4N^+PF_6^-$	*7a*
Ru(dppe)Cp*	-0.89	-0.24	0.65	/	*189*
Ru(dppm)Cp*	-0.94	-0.31	0.63	/	*189*
Ru(dppe)Cp	-0.70	-0.11	0.59	$Bu_4N^+PF_6^-$	*7b*
Ru(PPh$_3$)$_2$Cp	-0.69	-0.05	0.64	[glassy carbon]	*190*
Ru(PPh$_3$)(PMe$_3$)Cp	-0.72	-0.13	0.59	[glassy carbon]	*190*
Ru(dppf)Cp	-0.68	-0.03	0.65	$Bu_4N^+PF_6^-$	*191*
Os(dppe)Cp*	-1.08	-0.47	0.61	$Bu_4N^+PF_6^-$	*88*
Os(PPh$_3$)$_2$Cp	-0.79	-0.30	0.49	THF	*192*
Re(NO)(PPh$_3$)Cp*	-0.50	-0.06	0.44	$Et_4N^+ClO_4^-$/CH_3CN	*193*
	-0.45	0.08	0.53	/	*7c*
Re(NO)(P(*p*-tol)$_3$)Cp*	-0.68	-0.15	0.53	/	*7c*
CrCl(dmpe)$_2$	/	/	0.00		*74*
Mo(dppe)(η-C$_7$H$_7$)	-1.02	-0.59	0.43	$Bu_4N^+PF_6^-$ [glassy carbon]	*50b*

[a] All redox potentials in volts relative to $[Cp_2Fe]^+/Cp_2Fe$. [b] $Bu_4N^+BF_4^-$ in CH_2Cl_2 with Pt working electrode unless otherwise stated. [c] dippe = 1,2-bis(diisopropylphosphino)ethane.

Table 6-6. Electrochemical data[a] for complexes of the type [{M(L)$_n$}$_2$(μ-C≡C–C≡C–C≡C–C≡C)].

	CV data				
M(L)$_n$	E_1^0	E_2^0	$\Delta E_{1/2}^0$	conditions[b]	ref
Fe(dppe)Cp*	-0.65	-0.22	0.43	$Bu_4N^+PF_6^-$	*194*
Ru(dppe)Cp*	-0.38	-0.03	0.35	/	*192*
Ru(PPh$_3$)$_2$Cp	-0.22	0.12	0.34	/	*192*
Os(PPh$_3$)$_2$Cp	-0.32	-0.11	0.21	THF	*192*
Re(NO)(P(*p*-tol)$_3$)Cp*	-0.30	-0.01	0.29	/	*7c*
Re(NO)(PCy$_3$)Cp*	-0.35	-0.03	0.32	/	*7c*

[a] All redox potentials in volts relative to $[Cp_2Fe]^+/Cp_2Fe$. [b] $Bu_4N^+BF_4^-$ in CH_2Cl_2 with Pt working electrode unless otherwise stated.

Table 6-7. Electrochemical data[a] for complexes of the type [{M(L)$_n$}$_2$(μ-CH=CHCH=CH)].

	CV data				
M(L)$_n$	E_1^0	E_2^0	$\Delta E_{1/2}^0$	conditions[b]	ref
Fe(dppe)Cp*	-1.25	-0.65	0.60	$Bu_4N^+PF_6^-$	*195*
Fe(dppe)Cp	-1.17	-0.70	0.47	$Bu_4N^+PF_6^-$	*195*
Fe(dppm)Cp	-1.17	-0.73	0.44	$Bu_4N^+PF_6^-$	*196*
Fe(PMe_3)(CO)Cp[c]	-0.67	-0.26	0.41	unknown, -78°C	*197*
Fe(PPh_3)(CO)Cp					
- isomer A	-0.54	-0.12	0.42	unknown, -78°C	*197*
- isomer B	-0.58	-0.13	0.45	unknown, -78°C	*197*

[a] All redox potentials in volts relative to $[Cp_2Fe]^+/Cp_2Fe$. [b] $Bu_4N^+BF_4^-$ in CH_2Cl_2 with Pt working electrode unless otherwise stated. [c] Mixture of diastereoisomers.

Table 6-8. Electrochemical data[a] for complexes of the type [{M(L)$_n$}$_2$(μ-phenylene)].

	CV data				
M(L)$_n$	E_1^0	E_2^0	$\Delta E_{1/2}^0$	conditions[b]	ref
Fe(dppe)Cp*	-0.74	-0.48	0.26	$Bu_4N^+PF_6^-$	*198*
	-0.76	-0.50	0.26	$Bu_4N^+PF_6^-$	*199*
Fe(dppe)Cp	-0.37	-0.15	0.22	[Pt disk]	*170*
	-0.50[c]	-0.29[c]	0.21	$Bu_4N^+PF_6^-$	*200*
Ru(dppe)Cp*	-0.50	-0.22	0.28	[Pt microdisk]	*201*
Ru(dppe)Cp	-0.32	-0.09	0.23	[Pt microdisk]	*201*
Ru(PPh_3)$_2$Cp	-0.30	-0.01	0.29	[Pt microdisk]	*201*
Ru(dppf)Cp	-0.27	-0.01	0.26	$Bu_4N^+PF_6^-$	*191*
Mo(dppe)(η-C_7H_7)	-0.84	-0.67	0.17	unknown	*202*
trans-FeCl(depe)$_2$	-0.63	-0.47	0.16	/	*203*
trans-FeCl(dmpe)$_2$	-0.70	-0.50	0.20	$Bu_4N^+ClO_4^-$	*204*
trans-RuCl(dppe)$_2$	-0.33	0.01	0.34	$Bu_4N^+PF_6^-$	*7d*
	-0.34	0.02	0.36	$Bu_4N^+PF_6^-$	*205*
trans-RuCl(dppm)$_2$	-0.30	0.00	0.30	/	*203*
	-0.34	-0.02	0.32	[Pt disk]	*206*
trans-OsCl(dppm)$_2$	-0.51	-0.21	0.30	/	*203*

[a] All redox potentials in volts relative to $[Cp_2Fe]^+/Cp_2Fe$. [b] $Bu_4N^+BF_4^-$ in CH_2Cl_2 with Pt working electrode unless otherwise stated. [c] Assuming $[Cp_2Fe]^+/Cp_2Fe$ = 0.50 V *vs.* $[Cp^*_2Fe]^+/Cp^*_2Fe$.

Table 6-9. Electrochemical data[a] for complexes of the type [{M(L)$_n$}$_2$(μ-thiophene)].

	CV data				
M(L)$_n$	E_1^0	E_2^0	$\Delta E_{1/2}^0$	conditions[b]	ref
trans-RuCl(dppm)$_2$	-0.47	-0.11	0.36	/	*203*
trans-OsCl(dppm)$_2$	-0.71	-0.19	0.32	/	*203*
Fe(dppe)Cp*	-0.85[c]	-0.51[c]	0.34	$Bu_4N^+PF_6^-$	*207*
Fe(dppe)Cp	-0.65[c]	-0.36[c]	0.29	[Pt disk]	*170*

[a] All redox potentials in volts relative to $[Cp_2Fe]^+/Cp_2Fe$. [b] $Bu_4N^+BF_4^-$ in CH_2Cl_2 with Pt working electrode unless otherwise stated. [c] Assuming $[Cp_2Fe]^+/Cp_2Fe$ = 0.460 V *vs.* SCE.

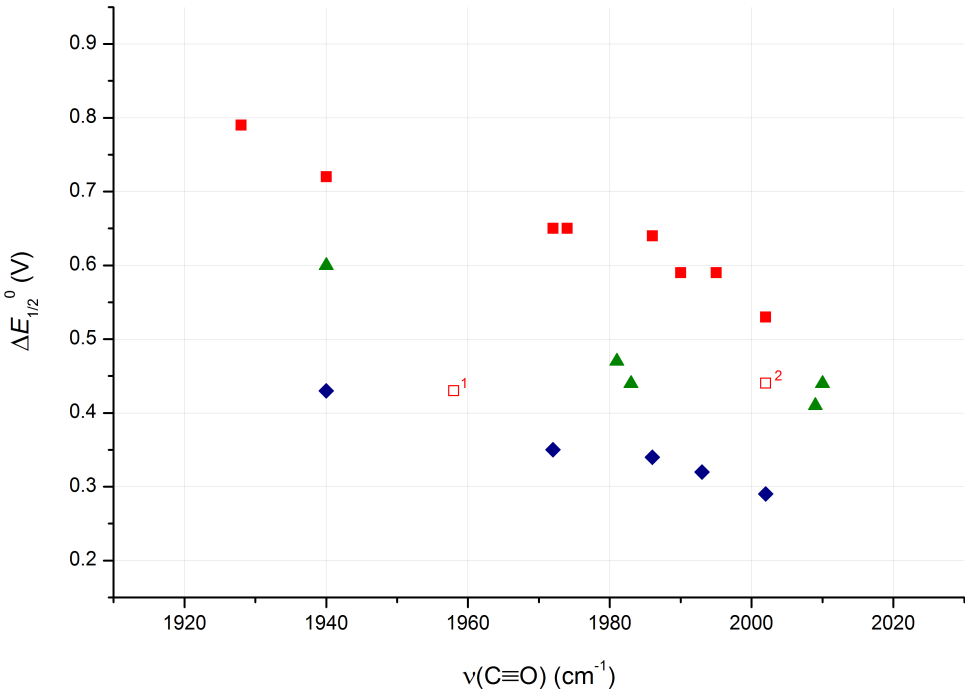

Figure 6-16. $\Delta E_{1/2}^0$ *vs.* ν(C≡O) for aliphatic bridges (solid squares = C_4 alkyne, triangles = C_4 alkene, diamonds = C_8 alkyne). Outliers (hollow squares) discussed in *Table 6-10*.

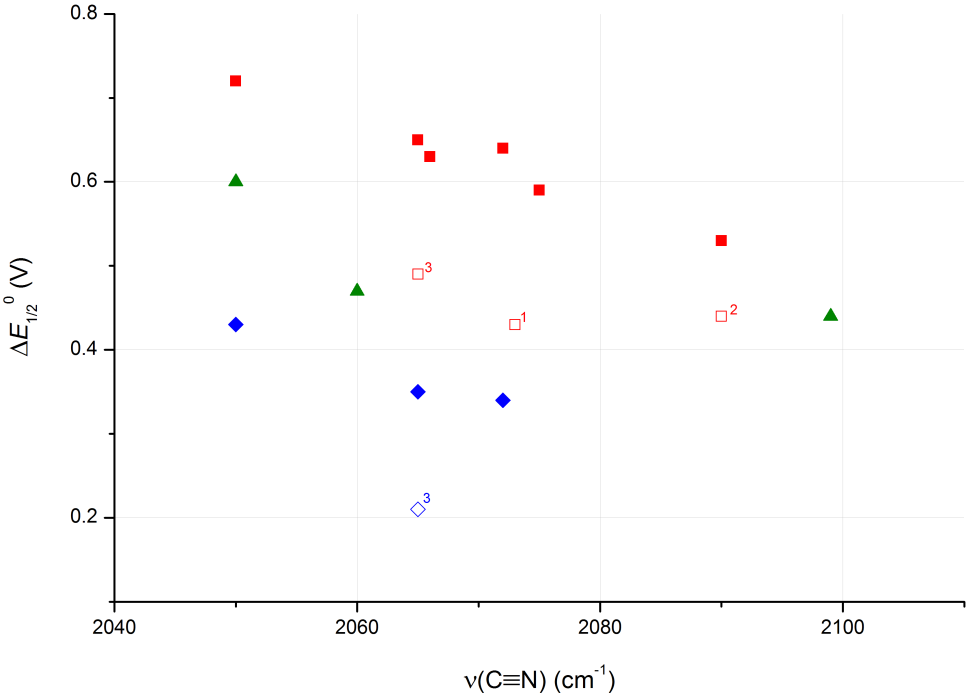

Figure 6-17. $\Delta E_{1/2}{}^{0}$ *vs.* ν(C≡N) for aliphatic bridges (solid squares = C_4 alkyne, triangles = C_4 alkene, diamonds = C_8 alkyne). Outliers (hollow shapes) discussed in *Table 6-10*.

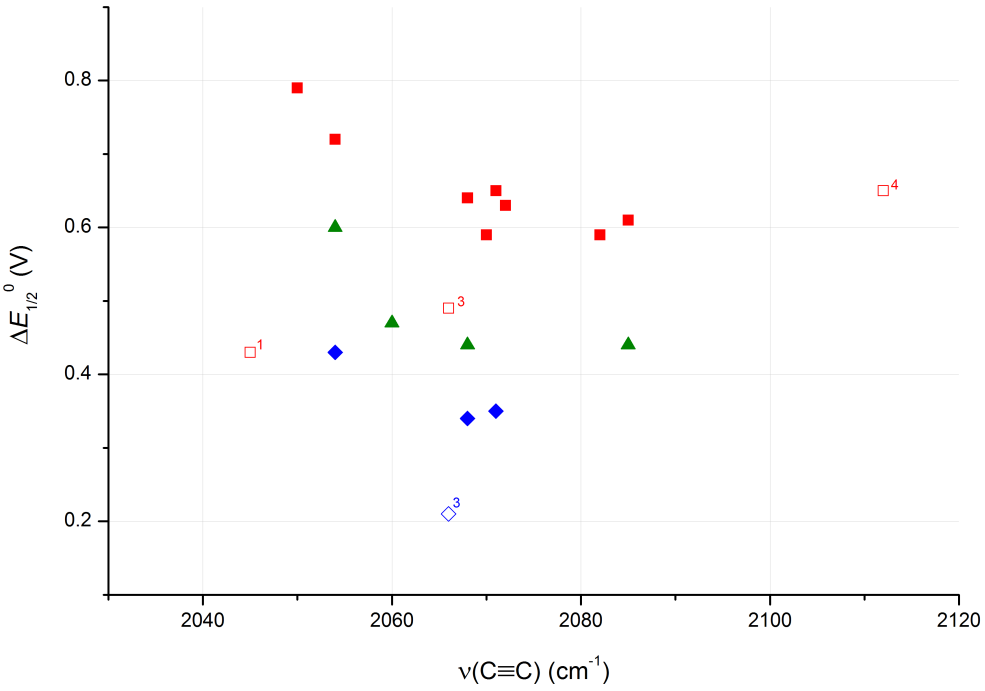

Figure 6-18. $\Delta E_{1/2}{}^{0}$ *vs.* ν(C≡C) for aliphatic bridges (solid squares = C_4 alkyne, triangles = C_4 alkene, diamonds = C_8 alkyne). Outliers (hollow shapes) discussed in *Table 6-10*.

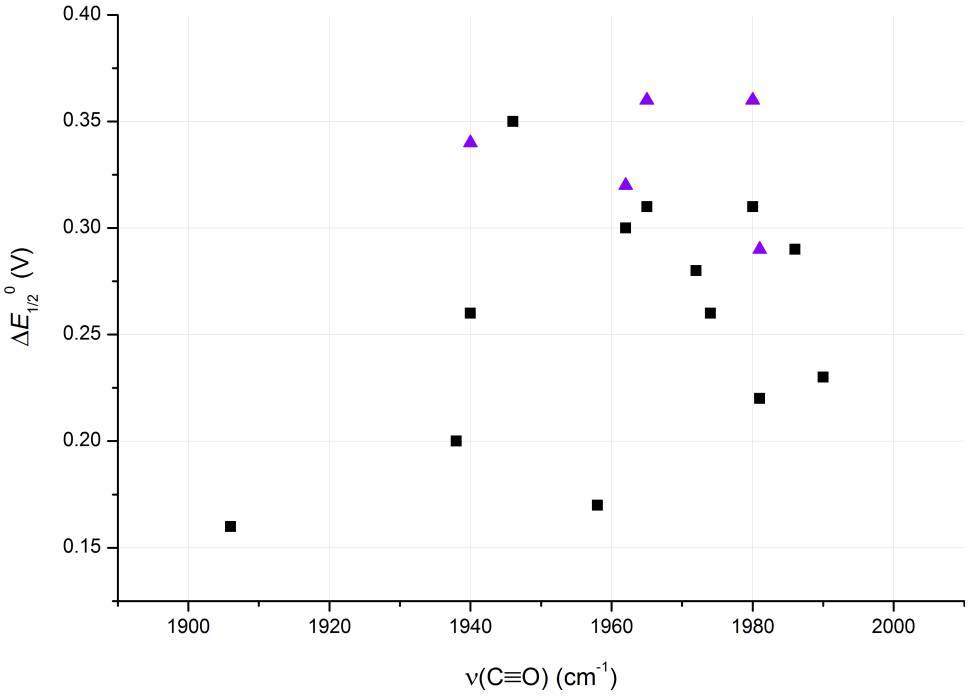

Figure 6-19. $\Delta E_{1/2}{}^{0}$ *vs.* ν(C≡O) for aromatic bridges (squares = phenylene, triangles = thiophene). Similar (non-correlative) results are obtained when plotting $\Delta E_{1/2}{}^{0}$ *vs.* ν(C≡N) or ν(C≡C).

Table 6-10. Reasonably justifiable anomalies summarised from all datasets.

#[a]	$M(L)_n$	suggested explanation
1	Mo(dppe)(η-C_7H_7)	group VI/d^4 metal with a different metal–acetylide bonding interaction (see later discussion)
2	Re(NO)(PPh_3)Cp*	different medium conditions ($Et_4N^+ClO_4^-$/CH_3CN)
3	Os(PPh_3)$_2$Cp	different medium conditions (THF)
4	Ru(dppf)Cp	ν(C≡C) of $M(L)_n$–C≡C–Ph not explicitly assigned by original authors

[a] From labelled points in *Figure 6-16-Figure 6-18*.

6.3.3 C_4 alkyne bridged complexes – a detailed analysis

The C_4 alkyne series was chosen as a case study to explore possible correlations between electron density/ν(X) and $\Delta_{xx}G^0$. In addition to electrochemical characterisation, the majority of complexes have been comprehensively studied (in numerous oxidation states) using a wide range of techniques including X-ray crystallography, UV-vis, near-IR, IR, NMR, EPR/ESR and Mössbauer spectroscopy, as well being probed computationally *(vida infra)*. Furthermore, most

of their mixed-valence complexes are considered to be Class III (fully delocalised) systems, which implies that $\Delta_{to}G^0$ includes a substantial contribution from $\Delta_{re}G^0$. For simplicity, discussion will initially focus on d^6 'piano stool' $M(L)_n$ fragments (*i.e.* ML_2Cp' (Cp' = Cp, Cp*) representing the bulk of this dataset), for reasons that will become evident.

Insights from molecular orbital considerations

It should first be explored what the variation of ν(X) in the mononuclear complexes might indicate from a molecular orbital standpoint. Whilst conventionally a decrease in ligand bond order may be interpreted in terms of an increased electron population in ligand π* orbitals (*i.e.* metal-to-ligand π backbonding), as we shall see this is not necessarily the case for metal σ alkynyl complexes. This has an impact both on the meaning of ν(C≡C), as well as the nature of inductive effects ($\Delta_{in}G^0$) for acetylide bridged mixed-valence systems.

Interactions between ML_2Cp' fragments (M = Ru,[208] Fe,[209] Re[209-210]) and acetylides can be qualitatively described by the same molecular orbital picture *(Figure 6-20)*. As depicted, the major interaction is between the metal d_{z^2} orbital and the lone pair (LP) of the acetylide ligand. This forms a strongly bonding (σ, filled) and an anti-bonding (σ*, unfilled) molecular orbital pair, and is responsible for the M–C single bond. 'Filled/filled' interactions between the metal d_{yz} and d_{xz} and ligand π bonding orbitals result in a stabilised (filled, bonding) and a destabilised (filled, anti-bonding) molecular orbital set, with the latter generating the HOMO and HOMO–1. The LUMO and LUMO+1 are mainly metal or alkynyl π* in nature depending on the extent of interactions between the metal d_{yz} and d_{xz} orbitals, and the ligand π* orbital pair. As they do not have appropriate symmetry for orbital interaction with the acetylide, the metal d_{xy} and $d_{x^2-y^2}$ orbitals are largely non-bonding. The large energy difference between the occupied metal π orbitals and the bridging ligand π* orbitals is considered to result in only weak π-type back backbonding effects.[211]

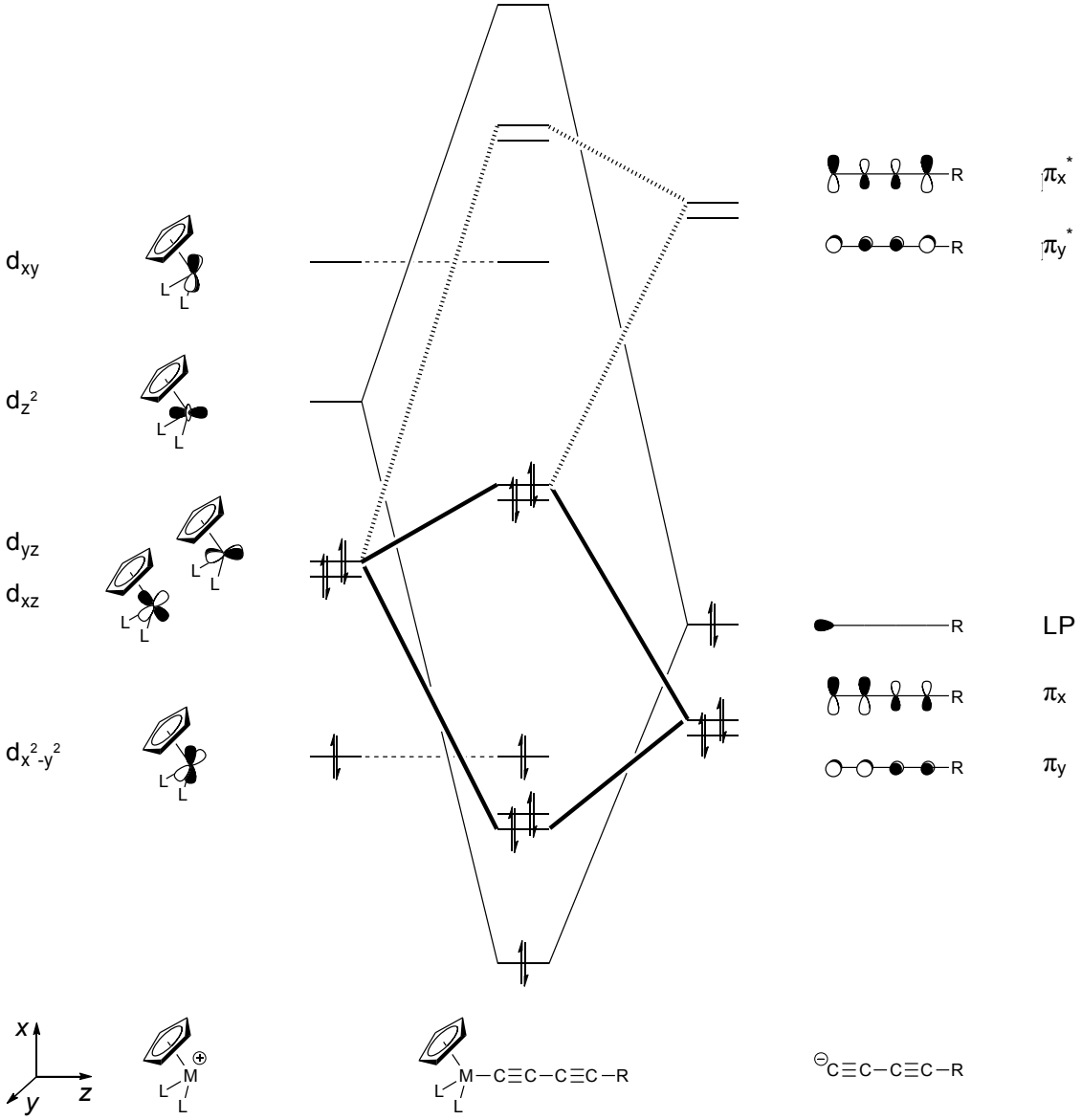

Figure 6-20. A qualitative molecular orbital diagram denoting the interactions between the frontier orbitals of a typical d^6 piano-stool $M(L)_n$ fragment and an acetylide ligand (adapted from references).[2,19c,208-209]

Several related studies on mononuclear acetylides (summarised in an excellent review by Manna, John and Hopkins[8]), also cast reasonable doubt over the extent to which metal π to ligand π* backbonding can be held responsible for changes in ν(C≡C) (or indeed, in C≡C bond lengths). Though some expected trends do appear reasonable in this context (*e.g.* for $M(L)_n$ = Fe(dippe)Cp*, ν(C≡C) = 2050 cm^{-1}; $M(L)_n$ = Fe(CO)(PPh_3)Cp, ν(C≡C) = 2085 cm^{-1}), from the

above molecular orbital picture ligand π to metal π *bonding* interactions (decreasing the electron population in ligand π), or bond polarisation effects ($M^{\delta+}$–$C^{\delta-}$)[§§§§] should have a greater influence. With increasing energy of the $M(L)_n$ orbitals (increasing π-basicity) relative to the 'fixed' energies of the ligand, metal π-ligand π* interactions will accordingly be enhanced, and metal π-ligand π interactions should decrease. These are opposing effects which further complicate interpretations of changing ν(C≡C) frequencies in terms of the metal-acetylide bonding picture.

Conversely, for established π-acceptors such as carbonyl or cyanide ligands changes in ν(C≡O)/ν(C≡N) can be almost exclusively attributed to π-back donation effects.[8] Thus, to a first approximation the ν(X) frequencies of monometallic complexes $M(L)_n$–X may be considered as an experimental probe of the energies of the $M(L)_n$ fragment relative to the bridging ligand (with ν(C≡O)/ν(C≡N) decidedly a more reliable measure). The difference in nature (weak π-acceptor/π-donor to predominantly π-acceptor) of the ligands in the monometallic series may also go some way to explain the poor correlation between ν(C≡O) and ν(C≡C) *(Figure 6-21)*, compared to that of ν(C≡O)/ν(C≡C) with ν(C≡N) *(Figure 6-22)*.

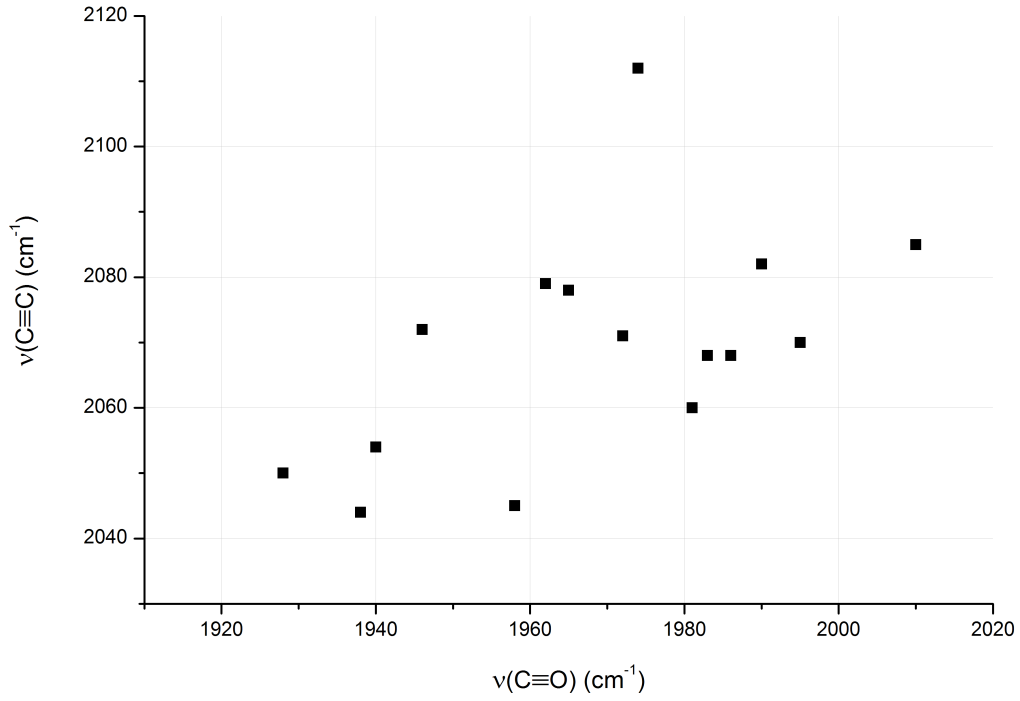

Figure 6-21. A plot of ν(C≡O) against ν(C≡C) (data from *Table 6-2)*.

[§§§§] The lone pair of the alkynyl anion, $^{-}C{\equiv}CR$, is slightly C≡C anti-bonding in character. With increasing polarisation of the $M^{\delta+}$–$C^{\delta-}$ bond, ν(C≡C) may be expected to decrease.[8]

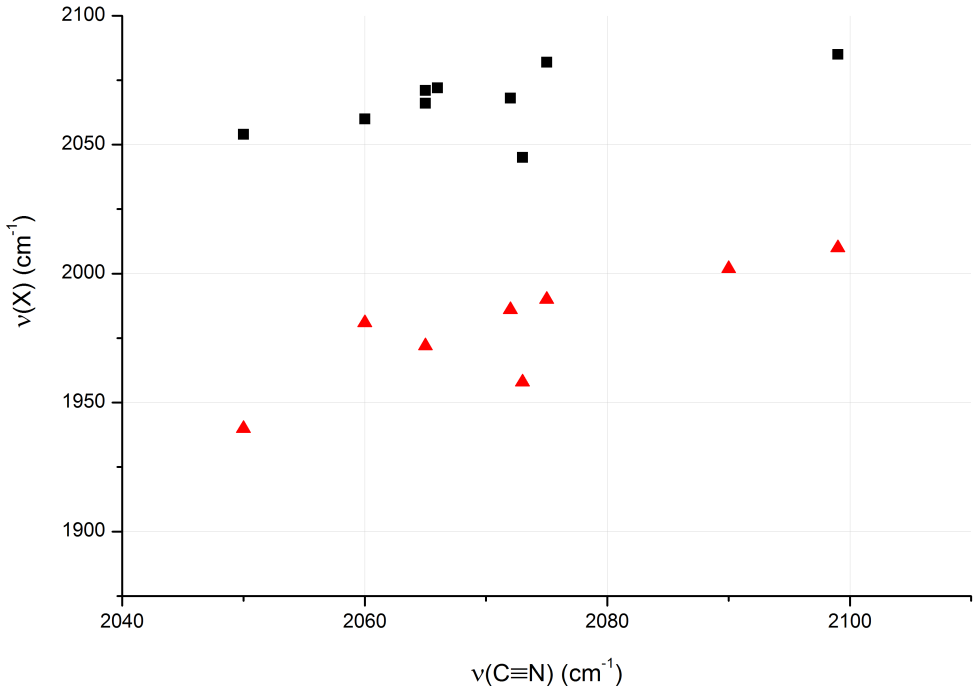

Figure 6-22. A plot of ν(C≡N) against ν(X) (black squares = ν(C≡C), red triangles = ν(C≡O)) (data from *Table 6-2)*.

Structural aspects

From the above molecular orbital picture, it is interesting to note that the HOMO and HOMO–1 are admixtures of metal and ligand π orbitals. Thus, when the complex is oxidised electron density will be removed from *both* the metal and the bridging ligand (an example of ligand *redox non-innocence*[2,19c]). As these MOs are anti-bonding between Ru–C_α and C_β–C_γ, and bonding between C_α–C_β, a decrease in electron occupancy of the HOMO/HOMO–1 should be expected to result in a shortening of the former bonds and a lengthening of the latter (as well as decreases in ν(C≡C)). This is generally evidenced in bond length changes observed experimentally via X-ray crystallographic studies *(Figure 6-23, Table 6-11)* and decreasing ν(C≡C) frequencies of the C_4 alkyne bridge upon oxidation *(Table 6-12)*, consistent with decreasing bond order (and notably inconsistent with a metal to acetylide π-backbonding model).[88,189-191] Successive oxidations (up to 4+ where $M(L)_n$ = $Ru(PR_3)_2Cp$[190]) are as a result considered to lead to carbenic/cumulenic, and potentially carbynic bridge structures *(Figure 6-24)*. It has however been suggested that the *extent* of changes in bond length/IR frequencies

(taken alone) are not necessarily a good indicator of assigning specific bond orders (*i.e.* acetylenic/cumulenic forms).[208a,209] Accordingly, further experimental evidence for the cumulenic bridge motif in $[\{Re(NO)(PPh_3)Cp^*\}(\mu\text{-}C_4)]^{n+}$ (n = 1, 2), for example, is provided by NMR, magnetic and computational studies, amongst other measures.[210]

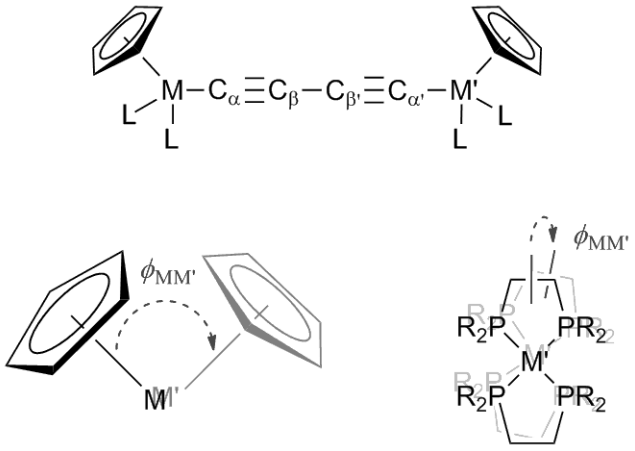

Figure 6-23. Labelling scheme used for structural parameters given in *Table 6-11*.

Table 6-11. Selected structural parameters[a] for complexes of the type $[\{M(L)_n\}_2(\mu\text{-}C_4)]^{n+}$ (n = 0, 1, 2).

$M(L)_n$	n	$r_{MM'}(S)$[b]	$r_{M\alpha}$ $r_{M'\alpha'}$	$r_{\alpha\beta}$ $r_{\alpha'\beta'}$	$r_{\beta\beta'}$	$r_{MM'}(B)$[c]	$\varphi_{MM'}$ (°)[d]	ref
Fe(dppe)Cp*	0	7.56	1.89 1.88	1.22 1.22	1.37	7.58	79	*209*
	1	7.44	1.83 1.83	1.24 1.24	1.36	7.50	180	*188*
Ru(dppe)Cp*	0	7.82	2.00 2.00	1.22 1.22	1.38	7.82	47	*189*
	1	7.63	1.93 1.93	1.25 1.25	1.34	7.70	180	
	2	7.48	1.86 1.86	1.28 1.27	1.29	7.56	40	
Ru(dppm)Cp*	0	7.83	2.02 2.02	1.22 1.22	1.39	7.87	68	*189*
Ru(dppe)Cp	0	7.75	2.01 2.02	1.22 1.22	1.40	7.87	39	*7b*
$Ru(PPh_3)_2Cp$[e]	0	7.80	1.99 1.99	1.22 1.23	1.38	7.81	178	*7b*
Ru(dppf)Cp	0	7.74	2.03 2.00	1.18 1.22	1.41	7.84	32	*191*
Os(dppe)Cp*	0	7.84	2.02 2.01	1.22 1.22	1.38	7.85	47	*88*
$Re(NO)(PPh_3)Cp^*$	0	7.83	2.04 2.04	1.20 1.20	1.39	7.87	108	*212*
	2	7.64	1.93 1.91	1.24 1.26	1.33	7.67	18	*209,212*
$CrCl(dmpe)_2$	0	7.44	1.79 1.79	1.30 1.30	1.27	7.45	169	*74*
	2	7.71	1.95 1.95	1.22 1.22	1.38	7.72	148	
Mo(dppe)(η-C_7H_7)	2	/	2.04 2.02	1.21 1.25	1.36	7.88	~81	*50b*

[a] Bond lengths (in Å, for clarity given to 2 decimal places only) and angles as defined in *Figure 6-23*. [b] Through space M–M' distance. [c] Through bond M–M' distance, with $r_{MM'}(S)$ an indicator of bridge curvature. [d] Included for completeness, variations in this (often contrasteric) torsion angle have been attributed to electronic conformation or crystallization effects[210,213] (often experimental values differ to geometries calculated in the gas phase[209]). [e] Other X-ray crystal structures of this compound have been obtained, with largely similar bond lengths and $\varphi_{MM'}$ either 26-32° *(cis)* or 178-180° *(trans)*.[161,213]

Table 6-12. Infrared stretching frequencies[a] for $[\{M(L)_n\}_2(\mu\text{-}C{\equiv}C{-}C{\equiv}C)]^{n+}$ and $[\{M(L)_n\}{-}C{\equiv}C{-}C_6H_5]^{n+}$ complexes.

		$[\{M(L)_n\}_2(\mu\text{-}C{\equiv}C{-}C{\equiv}C)]^{n+}$			$[\{M(L)_n\}{-}C{\equiv}C{-}C_6H_5]^{n+}$		
$M(L)_n$	*n*	ν(C≡C)	Δ*v*	ref [conditions]	ν(C≡C)	Δ*v*	ref [conditions]
Fe(dppe)Cp*	0	1955 1880		*214*	2053		*215* [Nujol mull]
	1	1973 1880			2021 1988		
	2	1950 2160			/	/	/
Ru(dppe)Cp*	0	1977sh 1963			2071 *or* 2072		*216*
	1	1860	-103		1930 *or* 1929	-141 *or* -143	
	2	1770	-90		/	/	/
$Ru(PPh_3)_2Cp$	0	1971 1956		*208a* [-50°C]	2074		*216b*
	1	1855			1937	-137	
	2	1767	-88		/	/	/
$Ru(PPh_3)(PMe_3)Cp$	0	1972 1957		*208a* [-50°C]	/	/	/
	1	1856			/	/	
	2	1767	-89		/	/	
Os(dppe)Cp*	0	1975sh 1965			/	/	/
	1	1860	-105		/	/	
	2	1781	-79		/	/	
$Re(NO)(PPh_3)Cp^*$	0	1964		*210*	/	/	/
	1	1872	-92		/	/	
	2	not obs.			/	/	
Mo(dppe)(η-C_7H_7)	0	/	/	/	2045		*95a*
	1	/	/		2032	-13	[$BF4^-$ salt]

[a] Measured in CH_2Cl_2 as the PF_6^- salt (unless otherwise stated), with frequencies in cm^{-1}.

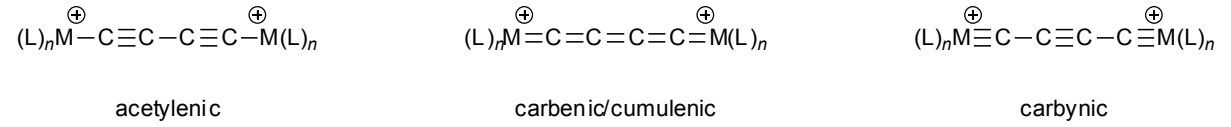

Figure 6-24. Potential structural forms of dicationic C_4 bridged species.

A further, particularly relevant, consequence of the previously mentioned bonding picture is that with decreasing electron density at $M(L)_n$ the percentage of bridging ligand character in the HOMO (and HOMO–1) of these complexes is found to increase *(Table 6-13)*. Upon oxidation, for extreme cases this could result in end-localised charges for electron-rich $M(L)_n$ and centrally-localised charge(s) for electron-poor $M(L)_n$ (with implications for $\Delta_{so}G^0$ contributions to comproportionation equilibria, in line with above discussions). Though metal character of these orbitals is expected to increase upon oxidation, similar trends in HOMO/HOMO-1 compositions between $M(L)_n$ fragments are observed in both neutral and dicationic species.[217]

Table 6-13. Selected molecular orbital compositions and singlet-triplet energy gaps (E_{ST}) for complexes of the type $[\{M(L)_n\}_2(\mu\text{-}C{\equiv}C{-}C{\equiv}C)]^{n+}$ (from density functional calculations).

	HOMO (n = 0)			HOMO-1 (n = 0)				
$M(L)_n$	M	C_4	$(L)_n$	M	C_4	$(L)_n$	E_{ST} (eV) (n = 2)	ref
Fe(dHpe)Cp	44	45	11	40	54	6	0.05	*209*
	41	46	13	36	52	12	-0.01	*88,217*
Ru(dHpe)Cp*	31	54	15	26	69	5	0.14	*208a*
Ru(dHpe)Cp	26	62	12	21	69	10	0.13	*88,217*
Os(dHpe)Cp	24	59	17	22	68	10	0.19	*88*
$Ru(PH_3)_2Cp$	27	59	14	25	69	6	0.10	*208a*
$Re(PH_3)(NO)Cp$	24	56	20	24	57	19	0.35	*209*
	32	54	14	6	66	28	0.43	*217*
$Ru(CO)_2Cp$*	14	76	10	10	86	4	0.13	*208a*
$Ru(CO)_2Cp$	13	79	8	10	87	3	-0.01	*208a*

Antiferromagnetic superexchange and resonance

Dications of C_4 bridged d^6 complexes are often found to be *diamagnetic (Table 6-14)*. Containing two unpaired electrons (one localised at each redox centre) this is perhaps a rather

unusual result, but can be interpreted as a consequence of strong antiferromagnetic superexchange coupling (see *section 6.2.3/Figure 6-9)*. This interaction provides a *singlet* ground state (*Scheme 6-1a)* and *triplet* excited state *(Scheme 6-1b)* which are in equilibrium at k_BT. With a small singlet-triplet energy gap (E_{ST}), paramagnetism will be observed even at low temperatures. This is found experimentally for [{Fe(dppe)Cp*}$_2$(μ-C$_4$)] (E_{ST} = 18 cm^{-1}),[47] where thermal population of the triplet state occurs even at 80 K.[47] When E_{ST} is large, at most only weak paramagnetism is encountered and the complex will exhibit primarily diamagnetic properties under ambient conditions (*e.g.* for [{Ru(dppe)Cp*}$_2$(μ-C$_4$)], E_{ST} = 850 cm^{-1}).[189,217] A low lying singlet state is thought to increase the proportion of the cumulenic resonance form, relative to the acetylenic one, in accordance with *Scheme 6-1*.[44]

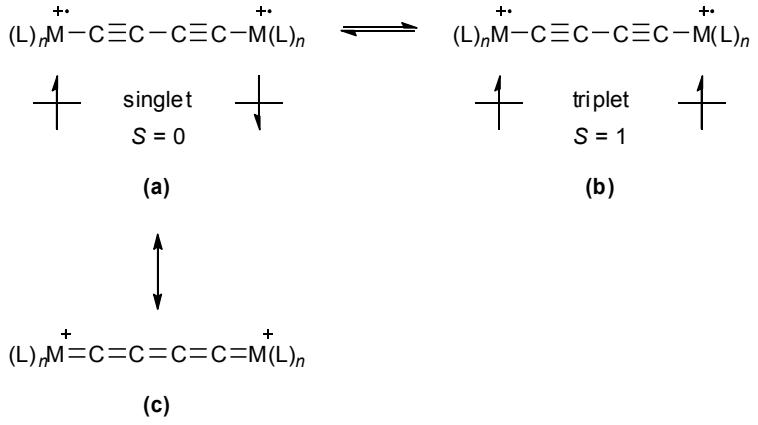

Scheme 6-1. Singlet/triplet/cumulene equilibria in dicationic diradical C$_4$ bridged complexes (adapted from ref).[44]

Experimentally determined values of E_{ST} (= -2$\mathcal{J}$) for dications of the C$_4$ bridged series (and/or other reported magnetic properties) are provided in *Table 6-14*. From this limited number of reports it appears that E_{ST} increases with decreasing electron density at M(L)$_n$. In contrast, computational studies on a wider range of complexes show no apparent correlation *(Table 6-13)*, though selected complexes do collaborate the experimental trend (*e.g.* M(L)$_n$ = Fe(dHpe)Cp < M(dHpe)Cp′ (M = Ru, Os) < Re(PH$_3$)(NO)Cp).

Table 6-14. Magnetic, NIR spectral data and critical observations of the mixed-valence state for complexes of the type $[\{M(L)_n\}_2(\mu\text{-}C_4)]^{n+}$ (n = 1, 2).

	magnetic properties[a]		NIR spectral characteristics[b]						
$M(L)_n$	$-2J$ (cm^{-1})	ref (method[c])	ν_{max} (cm^{-1})	ε_{max} (M^{-1} cm^{-1})	$\Delta\nu_{1/2}$ (cm^{-1})	H_{ab} (eV)[d]	additional comments	Class[e]	ref
Fe(dppe)Cp*	-18	*47* (I)	7704	12000	3260	0.19,[f] 0.47	delocalised on IR/Mössbauer time scales,[187] $\Delta\nu_{1/2}$ narrower than 'Hush limit'[g]	III	*188*
Fe(dippe)Cp*	-2	*218*	1318	14000	/	/	/	/	*7a*
Ru(dppe)Cp*	*predominantly diamagnetic*[189]		10195	9850	2440	0.63	$\Delta\nu_{1/2}$ narrower than 'Hush limit'[g]	III	*189*
			12240	6600	2600				
	-850	*217* (II)	14000	2200	3800				
Ru(dppm)Cp*	/	/	10165	14000	2036	0.63	$\Delta\nu_{1/2}$ narrower than 'Hush limit'[g]	III	*189*
			12100	9500	2456				
			14215	3500	3720				
$Ru(PPh_3)_2Cp$	diamagnetic properties[208a]		11400	8000	3600	0.71	delocalised on IR time scale,[190] $\Delta\nu_{1/2}$ narrower than 'Hush limit'[g]	III	*208a*
$Ru(PPh_3)(PMe_3)Cp$	/	/	11100	13400	3200	0.69	delocalised on IR time scale, $\Delta\nu_{1/2}$ narrower than 'Hush limit'[g]	III	*208a*
Ru(dppf)Cp	(could not be isolated)		11037	16400	3666	0.27,[f] 0.68	$\Delta\nu_{1/2}$ narrower than 'Hush limit'[g]	/	
Os(dppe)Cp*	diamagnetic[88]		19000		/	/	broad overlapping bands	/	*88*
			-8000						
			27800	11500					
$Re(NO)(PPh_3)Cp$*	diamagnetic[210]		8333	3200	1500	0.07,[f] 0.52	delocalised on IR, ESR, Raman time scales, $\Delta\nu_{1/2}$ narrower than 'Hush limit'[g]	III	*193, 210*
			10000	9400	1200	0.11,[f] 0.62			
			11325	15000	1800	0.18,[f] 0.70			
$Re(NO)(P(p\text{-}tol)_3)Cp$*	diamagnetic properties[7c]		8160	4800	1400	0.08,[f] 0.51	delocalised on IR, ESR time scales, $\Delta\nu_{1/2}$ narrower than 'Hush limit'[g]	III	*7c*
			9804	14000	1300	0.14,[f] 0.61			
			11200	24000	1500	0.21,[f] 0.69			
$CrCl(dmpe)_2$	paramagnetic[74]		/	/	/	/	mixed-valence complex found unstable toward disproportionation	/	*74*

Table 6-14 (continued)

Mo(dppe)(η-C_7H_7)	-406	*50b* (I)	3200 4400 9300 8500[h]	870 1750 1750 8440[h]	1200 1500 1370 900[h]	/	multiple, low intensity, solvatochromic NIR bands; localised on the X-band EPR time scale	II	*50b*

[a] For the fully oxidised species. [b] For the mixed-valence species, measured in CH_2Cl_2 and considered to be IVCT bands, unless otherwise stated. [c] I = best fit of a modified Bleaney–Bowers equation (polycrystalline samples). II = from variation of NMR chemical shifts *vs.* *T*.[217] [d] Calculated by the original authors from $H_{ab} = \nu_{max}/2$, unless otherwise stated. [e] Robin and Day Classification system, as defined by the original authors. [f] Calculated by the original authors from eqn (6-3) with r_{ab} defined as the through-space metal-metal distance ($r_{MM'}$). The latter was determined directly from the mixed-valence structure, or from the average of fully reduced and oxidized species, where appropriate (values provided in *Table 6-11)*. [g] An indicator of Class III systems, the Hush limit for Class II systems is calculated using $\Delta\nu_{1/2} = (2310\nu_{max})^{1/2}$. [h] Assigned as LMCT bands.

Remarkably, no linear trend with electron density can be established for the extent of electronic interaction between redox centres. Though the fragment $M(L)_n$ = Re(NO)(PPh_3)Cp* ($M(L)_n$–C≡O, ν(C≡O) = 2002 cm^{-1}; [{$M(L)_n$}(μ-C_4)], E_1^0 = -0.45 V) may be considered less electron rich than $M(L)_n$ = Fe(dppe)Cp* (ν(C≡O) = 1940 cm^{-1}, E_1^0 = -1.14 V), both of them have a lower calculated H_{ab} (= 0.52 eV and 0.47 eV, respectively) than a fragment of intermediate electron density, $M(L)_n$ = Ru(PPh_3)$_2$Cp (ν(C≡O) = 1986 cm^{-1}, E_1^0 = -0.69 V, H_{ab} = 0.71 eV). These electronic coupling parameters were obtained by the original authors from details of IVCT bands and application of Hush theory appropriate for Class III mixed-valence complexes. Further H_{ab} values (and other relevant properties) for this family of mixed-valence complexes are presented in *Table 6-14*.

Despite the established greater accuracy of IVCT band analyses over electrochemical measurements, it should be noted that the application of Hush theory to complexes which exhibit redox non-innocent ligands is questionable; as this is strictly only relevant for two-state systems with weakly interacting diabatic states.[2] Indeed, several of the examples provided in *Table 6-14* exhibit multiple bands in the near-IR region, further highlighting the fact that their spectral features should be interpreted as part of a three-, or four-state model[20] (such interrogations are currently beyond the scope of this work). Interestingly however, spin density calculations on related complexes (considered a more accurate measure of electron delocalisation where the bridge is involved in the redox process[2]) also largely agree with IVCT spectral band analyses for these compounds. That is, they suggest the single electron in C_4 alkyne bridged mixed valences complexes is less localised on the metal *vs.* the carbon bridge in the order [{Ru(dHpe)Cp}$_2$(μ-C_4)]$^+$ (0.352 *vs.* 0.562), [{Re(NO)(PH_3)Cp}$_2$(μ-C_4)]$^+$ (0.499 *vs.* 0.512) and [{Fe(dHpe)Cp}$_2$(μ-C_4)]$^+$ (0.650 *vs.* 0.398).[217]

'Rationalization' of $\Delta_{co}G^0$

The above discussions provide a reasonable basis on which the observed apparent trends between $\Delta_{co}G^0$ and electron density may be evaluated. First, the extent to which $\Delta E_{1/2}^0$ may deviate from a valid representation of electronic coupling in [{$M(L)_n$}$_2$(μ-C≡C–C≡C)] complexes is made explicitly clear by plotting both $\Delta_{to}G^0$ and $\Delta_{re}G^0$ against ν(C≡O) (*Figure 6-25*, with raw data tabulated in *Table 6-15)*. Whereas the former appears approximately linear (certainly within expected experimental errors in ν(C≡O) and $\Delta E_{1/2}^0$), the latter has at the very least a non-linear

relationship.[*****] Clearly, other contributions to $\Delta_{to}G^0$ must dominate, and each in turn will be considered.

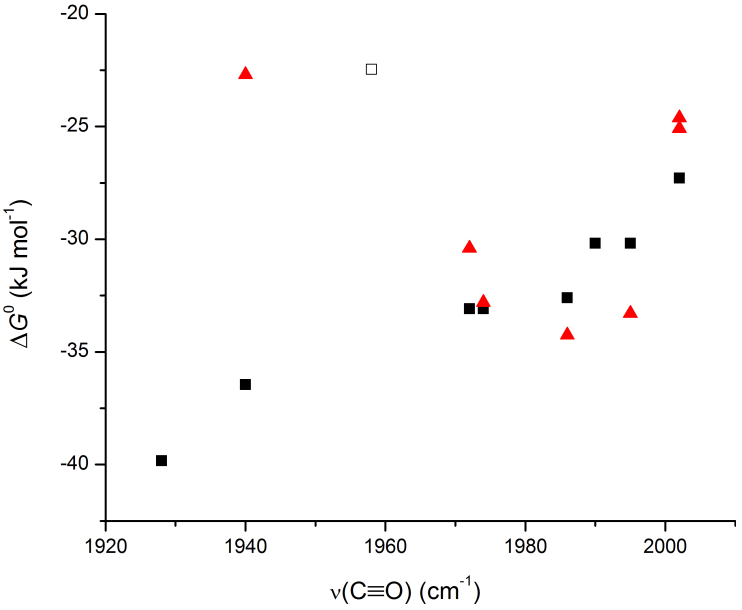

Figure 6-25. $\Delta_{to}G^0$ (squares) and $\Delta_{re}G^0$ (triangles) for [{M(L)$_n$}$_2$(μ-C≡C–C≡C)] complexes plotted against ν(X) for {M(L)$_n$}–R (raw data in *Table 6-2* and *Table 6-15*; hollow square, M(L)$_n$ = Mo(dppe)(C_7H_7)).

[*****] If it were not for the inherent inaccuracy in applying Hush theory to ligand redox-non innocent systems, it might be speculated that the minima in $\Delta_{re}G^0$ (representing a maxima in electronic coupling between the redox sites) is suggestive of a resonance interaction (*i.e.* an ideal energetic/spatial match) between the M(L)$_n$ and bridging ligand molecular orbitals where M(L)$_n$ = Ru(PPh_3)$_2$Cp.

Table 6-15. Calculable contributions[a] to $\Delta_{co}G^0$ for complexes of the type $[\{M(L)_n\}_2(\mu\text{-}C_4)]^{n+}$ (n = 0, 1, 2).

$M(L)_n$	$\Delta_{co}G^{0\,b}$	$\Delta_{to}G^{0\,c}$	$\Delta_{el}G^{0\,d}$	$\Delta_{re}G^{0\,e}$	$\Delta_{as}G^{0\,f}$
Fe(dppe)Cp*	-69.47	-36.45	-5.19	-22.69	0.16
Fe(dippe)Cp*	-76.22	-39.83	/	/	/
Ru(dppe)Cp*	-62.72	-33.08	-5.06	-30.40	7.63
Ru(dppm)Cp*	-60.79	-32.11	-4.93[h]	-30.40	/
Ru(dppe)Cp	-56.93	-30.18	-4.98[h]	/	/
$Ru(PPh_3)_2Cp$	-61.75	-32.60	-4.95[h]	-34.25	/
$Ru(PPh_3)(PMe_3)Cp$	-56.93	-30.18	/	-33.29	/
Ru(dppf)Cp	-62.72	-33.08	-4.99[h]	-32.81	/
Os(dppe)Cp*	-58.86	-31.15	-4.92[h]	/	/
$Os(PPh_3)_2Cp$	-47.28	-25.36	/	/	/
$Re(NO)(PPh_3)Cp^*$	-51.14	-27.29	-4.99[i]	-25.09	/
$Re(NO)(P(p\text{-}tol)_3)Cp^*$	-51.14[g]	-27.29	/	-24.61	/
$CrCl(dmpe)_2$	/	/	-5.09[i]	/	/
$Mo(dppe)(\eta\text{-}C_7H_7)$	-41.49	-22.46	/	/	3.65

[a] In kJ mol^{-1}. [b] Calculated using eqn (6-19) with $\Delta E_{1/2}{}^0$ values provided in *Table 6-5*. [c] Calculated using eqn (6-20). [d] Calculated using eqn (6-23) and (6-24) with ε_r = 9, T = 293 K and r_{12} taken as the metal-metal distance in the mixed-valence state *($r_{MM'}$, Table 6-11)*. [e] Calculated using eqn (6-26), where relevant assuming that the three observed IVCT bands are due to splitting of t_{2g} orbitals into Kramer's doublets (and thus taking the lowest energy IVCT transition to assess the extent of delocalisation in the ground state).[20,219] [f] Calculated using $\Delta_{as}G^0 = 3\mathcal{J}/2$ (from values provided in *Table 6-14)*. [g] Using $\Delta E_{1/2}{}^0$ = 0.53 V. [h] $r_{MM'}$ taken from the neutral complex. [i] $r_{MM'}$ taken as the average of the neutral and dicationic complexes.

In this series the only contributions to $\Delta_{co}G^0$ that may reasonably be attributed to changing electron density at $M(L)_n$ are $\Delta_{so}G^0$, $\Delta_{el}G^0$ and $\Delta_{in}G^0$. As mentioned previously, where the charge might be considered more centrally localised due to a largely bridge-centred oxidation (electron-poor $M(L)_n$), the complexes can be modelled as large spheres (shown for the extreme case in *Figure 6-13b)*. Here $\Delta_{so}G^0 \neq 0$, favouring the isovalent states. In the case of an electron rich $M(L)_n$ the charge can be considered more localised at the end groups, due to a greater metal-centred oxidation (*Figure 6-13a*). In this case, $\Delta_{so}G^0 = 0$, and will not affect $\Delta_{co}G^0$. Working to somewhat counter-act this contribution is $\Delta_{el}G^0$ (favouring the mixed-valence state), which might be expected to increase from a lower limit of ~5 kJ mol^{-1} *(Table 6-15*, calculated using $r_{MM'}$) as

the charges become more centrally localised and as a result are forced closer together (charge-charge distance << $r_{MM'}$).

The effect of $\Delta_{in}G^0$ is more difficult to gauge, even qualitatively. As described in *section 6.2.3* for a π-donor $M(L)_n$ and π-acceptor ligand, this should be expected to increase with increasing metal-to-ligand backbonding (of which ν(C≡O)/ν(C≡N) for $\{M(L)_n\}$–R provide an appropriate measure). However, as previously discussed, metal acetylides are better described in terms of a π-acceptor $M(L)_n$ and π-donor ligand combination (here the argument for an inductive effect would still apply, but in reversed form[39]). It is likely useful at this point to split $\Delta_{in}G^0$ into normal and reverse form contributions. With little aptitude for metal to ligand π backbonding, the contribution of $\Delta_{in}G^0_{reverse}$ to $\Delta_{co}G^0$ should decrease in the neutral state with increasing electron density at $M(L)_n$ (as the metal/ligand π orbitals move further apart in energy). Upon one-electron oxidation of the complex, the π-acceptor character of the bridge will be enhanced by the positive charge at $M_1(L)_n$, whereby greater π-backbonding will be possible from $M_2(L)_n$ in systems of higher electron density (and as the metal π-ligand π* orbitals move closer in energy, $\Delta_{in}G^0_{normal}$ will increase). If this latter effect outweighed the former it would support in some way the observed trend in $\Delta_{co}G^0$. Further experiments to probe the extent and nature of this interaction, along the line of Taube's experiments with cationic Rh d^6 complexes *(Figure 6-7)*, could greatly aid future discussions.

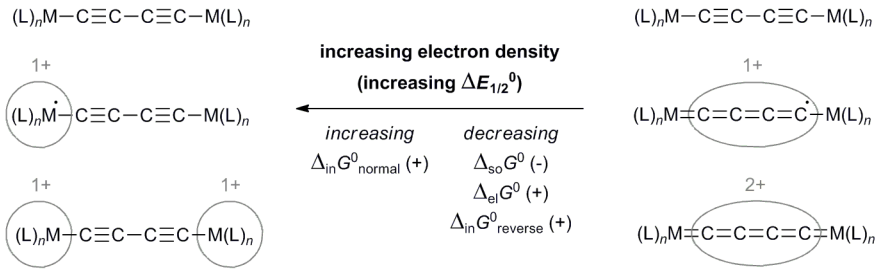

Figure 6-26. Overall thermodynamic picture for C_4 bridged d^6 piano stool $M(L)_n$ complexes (the sign in brackets following $\Delta_{xx}G^0$ indicates whether this contribution stabilises (+) or destabilises (-) the mixed-valence state).

Whilst the few experimentally determined values of $\Delta_{as}G^0$ are suggestive of a trend (appearing to increase in line with decreasing electron density, favouring the isovalent states),

this is not fully collaborated by computational work and requires further investigation.[†††††] Furthermore, current data for $\Delta_{re}G^0$ provides at best non-linear or unrelated relationships with respect to the energetic of frontier orbitals at $M(L)_n$. As all electrochemical measurements were taken under similar medium conditions, $\Delta_{ip}G^0$ may reasonably be assumed approximately constant *(Table 6-5)*.

In many ways, this makes the correlations suggested by plots of $\Delta E_{1/2}{}^0$ *vs.* ν(X) for aliphatic systems even more intriguing. It *could* be concluded at this stage that simple relationships between electron density and $\Delta E_{1/2}{}^0$ should not be expected for acetylide bridged dinuclear complexes; being currently observed for C_4/C_8 alkyne, and C_4 alkene bridges only as a result of similar, fortuitous trends in $\Delta_{re}G^0$ and $\Delta_{as}G^0$ (the magnitude of which can be quite significant; *e.g.* $\Delta_{as}G^0_{(calc)}$ = 33.77 kJ mol^{-1} for $[\{Re(PH_3)(NO)Cp\}_2(\mu\text{-}C_4)]^{2+}$, *Table 6-13)*. If this were correct, such correlations would not be anticipated to continue upon expansion of the dataset to other $M(L)_n$ (even with other d^6 piano stool compounds).

However, given the potential inapplicability of the two-state model to these systems (resulting in errors in H_{ab} and $\Delta_{re}G^0$) and the quite real possibility of a relationship between ν(X) and $\Delta_{as}G^0$, such a verdict requires additional verification. In particular, *experimental* determinations of E_{ST} and IVCT band properties for a greater number of d^6 piano stool $M(L)_n(\mu\text{-}C_4)$ complexes would prove very insightful. If linear trends between ν(X) and $\Delta E_{1/2}{}^0$ were observed to hold for a given series of complexes, voltammetric methods might yet prove surprisingly valuable as a handle for evaluating different models of electron transfer, and in establishing trends in $\Delta_{re}G^0$ for different $M(L)_n$-bridging combinations.

Comments on other C_4 bridged complexes

Considering the difficulties in establishing relationships between thermodynamic parameters for $M(L)_n$ of the same frontier orbital symmetry (*i.e.* d^6 piano stool and octahedral systems[19c]), it is perhaps not surprising that the $M(L)_n$ = Mo(dppe)(μ-C_7H_7) fragment, with different symmetry,

[†††††] Somewhat linked to $\Delta_{as}G^0$ (in accordance with *Scheme 6-1)*, is a possible difference in internal structural energy ($\Delta_{str}G^0$) when the cumulenic form of the mixed-valence and dicationic states are favoured over the acetylenic one (assuming an acetylenic form for the fully reduced state). Based upon the mean bond enthalpies $H_{(C-C)}$ = 348 kJ mol^{-1}, $H_{(C=C)}$ = 612 kJ mol^{-1}, and $H_{(C\equiv C)}$ = 838 kJ mol^{-1},[21] it is suggested that $\Delta_{str}G^0 \approx \sum(\Delta H^0_{products}) - \sum(\Delta H^0_{reactants}) \approx 3H_{(C=C)} - 2H_{(C\equiv C)} - H_{(C-C)} \approx$ -188 kJ mol^{-1}, which would favour the mixed valence state in the comproportionation equilibrium ($H_{(M-C)}$ and $H_{(M=C)}$ bond energies cancel out). Though this is an *extremely* rough approximation, which also neglects M–L contributions, it implies the magnitude of $\Delta_{as}G^0$ can in some cases be offset by enthalpic contributions to $\Delta_{co}G^0$.

appears as an outlier across the majority of datasets *(vida supra)*. Its acetylide complexes exhibit a different ordering of metal d orbitals as a result of strong interactions with the C_7H_7 ligand (the HOMO is now of d_{z^2} character), and there is a poor spatial overlap between the [Mo(dppe)(μ-C_7H_7)]$^+$ fragment and the acetylide frontier orbitals.[19c] This negatively impacts upon electronic communication across an acetylide bridge, as reflected in the fact that its C_4 mixed-valence complex has been assigned as Class II.[50b]

Berke and co-workers have applied efforts across several transition metals, most notably Mn, W and Cr. Whilst relevant ν(X) data was not available for any of these systems (as noted in *Table 6-4)*, it is expected that their (often quite significant) deviations from properties exhibited by the d^6 piano-stool series would likely facilitate further deviations from electron density *vs.* $\Delta E_{1/2}^0$ correlations. Thus, salient features are noted here for completeness.

Several compounds of the type [{Mn(dmpe)$_2$(R)}$_2$(μ-C_4)] (R = I,[134] C≡C–H, C≡C–SiMe$_3$,[135] C≡C–SiEt$_3$, C≡C–Si^{i}Pr$_3$ and C≡C–Si^{t}BuMe$_2$[136]) have been investigated over the last decade. Their neutral ([Mn^{II}Mn^{II}], d^5d^5) and mixed-valence complexes ([Mn^{II}Mn^{III}], d^5d^4) are typically low spin paramagnetic species (interestingly it was also found computationally that [{Mn(PH$_3$)$_4$I}$_2$(μ-C_4)] has a *triplet*, rather than singlet, ground state). As expected, the fully oxidized ([Mn^{III}Mn^{III}], d^4d^4) complexes are diamagnetic. Despite comparable values of $\Delta E_{1/2}^0$, the iodide complex ($\Delta E_{1/2}^0$ = 0.63 V; conditions unspecified) has been classified as Class II, and those terminated with –C≡C–H or –C≡C–SiMe$_3$ ($\Delta E_{1/2}^0$ = 0.58 or 0.55 V; THF, Au electrode) as Class III.

Quite recently the C_4 bridged tungsten complex, [I(dppe)$_2$W≡C–C≡C–C≡W(dppe)$_2$I]$^{n+}$ (n = 0, 1, 2),[137] was reported (an extended structure containing FeCl(depe)$_2$ end-groups has also been communicated).[220] A carbyne canonical structure persists through multiple oxidation states, with $\Delta E_{1/2}^0$ = 0.29 V (Au electrode); the mixed valence species assigned as Class II based upon apparent delocalisation on the EPR, but not IR, timescales. Both mono and dications are reportedly paramagnetic, with antiferromagnetic coupling observed for the latter (E_{ST} = 167 cm^{-1}). Related structurally are complexes of the type [{Cr(dmpe)$_2$R}$_2$(μ-C_4)]$^{n+}$ (R = Cl, I, C≡C–SiMe$_3$).[74] Remarkably, both chloride and trimethylsilylacetylide-terminated compounds exhibit only a single reversible redox wave in cyclic voltammetry studies (Au electrode, solvent unspecified), corresponding formally to a [Cr^{IV}Cr^{IV}] ⇄ [Cr^{III}Cr^{III}]$^{2+}$ + 2e$^-$ process (the carbyne form of the bridge in the fully reduced state changes to acetylenic in the fully oxidized state;

evidenced in part by X-ray crystallography, *Table 6-11)*. Though the apparent instability of the mixed-valence state with respect to disproportionation was attributed to a lack of electronic communication between the redox centres, it is not clear that this is the primary reason for $\Delta E_{1/2}^{0} \leq 0$ V. For example, taking the bond descriptions provided for the isovalent states (and assuming an intermediate cumulenic form in the mixed valence), $\Delta_{str}G^{0} \approx 4H_{(M=C)} - 2H_{(M\equiv C)} - H_{(M-C)} + 6H_{(C=C)} - 3H_{(C\equiv C)} - 3H_{(C-C)} \approx 4H_{(M=C)} - 2H_{(M\equiv C)} - H_{(M-C)} + 114$ kJ mol^{-1} (see previous footnote for assumptions/bond energies). This is almost certainly a positive value overall which should favour the isovalent states in the comproportionation equilibria (*e.g.* $\Delta_{str}G^{0} \approx 190$ kJ mol^{-1} taking $H_{(M=C)} = H_{(C=C)}$, $H_{(M\equiv C)} = H_{(C\equiv C)}$ and $H_{(M-C)} = H_{(C-C)}$).

Based upon these examples, the 'shotgun plots' observed between ν(X) and $\Delta E_{1/2}^{0}$ for the phenylene/thiophene series *(e.g. Figure 6-19)* might be partially explained by the greater variety of M(L)$_n$ that have been investigated with these bridges.

6.4 CONCLUSION

Correctly interpreting the properties of mixed-valence complexes is vital in developing accurate structure-property relationships, guiding subsequent synthetic efforts and better understanding electron transfer processes. Given that voltammetric methods remain one of the two most popular 'indicators' of electron delocalisation, fundamental to this area of work is a basic understanding of the properties that stabilise a mixed valence state with respect to disproportionation. Though easy to measure, $\Delta E_{1/2}^{0}$ represents a *complicated* equilibrium process, with multiple elements competing to stabilise or destabilise one oxidation state over another. Whilst at least seven (not counting the statistical factor) have so far been identified, in related work a comprehensive account of these is normally absent from discussions, and the magnitude of $\Delta E_{1/2}^{0}$ typically 'explained' by reference to only one or two. Here each have been discussed in turn – in the hope that more emphasis will be placed on the potential ambiguity of the electrochemical result, and also to help guide future work related to the branched complexes described previously in this thesis.

Succeeding primarily to exemplify the difficulties encountered in interpreting $\Delta E_{1/2}^{0}$, the apparent link between this and electron density at M(L)$_n$ was investigated further. Previously, it seemed this could be quantified for certain dinuclear bridged systems by using infrared

stretching frequencies (ν(X)) of the monometallic $M(L)_n$–R species (R = C≡O, $^-$C≡N, $^-$C≡C–C_6H_5).[6] However, it is apparent that not all factors contributing to $\Delta_{to}G^0$ may reasonably be linked to changes in electron density/ν(X) at present. Those that can, *i.e.* $\Delta_{so}G^0$, $\Delta_{el}G^0$ and $\Delta_{in}G^0$, *could* indeed produce such a relationship if they were the dominant contributions to $\Delta_{co}G^0$. Further studies are required to ratify relationships between electron density/ν(X) and $\Delta_{re}G^0$, $\Delta_{as}G^0$ and $\Delta_{str}G^0$ (some of which provide quite significant, calculable contributions), to further probe the utility of electrochemical methods for assessing electron delocalisation in d^6 piano stool $M(L)_n(\mu\text{-}C_4)$ complexes.

6.5 REFERENCES

1. P. Day, N. S. Hush and R. J. H. Clark, *Philos. Trans. R. Soc. A-Math. Phys. Eng. Sci.*, 2008, **366**, 5.
2. K. Costuas and S. Rigaut, *Dalton Trans.*, 2011, **40**, 5643.
3. (a) M. Mayor, C. von Hänisch, H. B. Weber, J. Reichert and D. Beckmann, *Angew. Chem., Int. Ed.*, 2002, **41**, 1183; (b) T. L. Schull, J. G. Kushmerick, C. H. Patterson, C. George, M. H. Moore, S. K. Pollack and R. Shashidhar, *J. Am. Chem. Soc.*, 2003, **125**, 3202.
4. (a) A. Blum, T. Ren, D. A. Parish, S. A. Trammell, M. H. Moore, J. G. Kushmerick, G.-L. Xu, J. R. Deschamps, S. K. Pollack and R. Shashidhar, *J. Am. Chem. Soc.*, 2005, **127**, 10010; (b) K. Liu, X. Wang and F. Wang, *ACS Nano*, 2008, **2**, 2315; (c) A. K. Mahapatro, J. Ying, T. Ren and D. B. Janes, *Nano Lett.*, 2008, **8**, 2131; (d) B. Kim, J. M. Beebe, C. Olivier, S. Rigaut, D. Touchard, J. G. Kushmerick, X.-Y. Zhu and C. D. Frisbie, *J. Phys. Chem. C*, 2007, **111**, 7521; (e) L. Luo, A. Benameur, P. Brignou, S. H. Choi, S. Rigaut and C. D. Frisbie, *J. Phys. Chem. C*, 2011, **115**, 19955.
5. (a) A. Nitzan, *J. Phys. Chem. A*, 2001, **105**, 2677; (b) A. Nitzan, *Isr. J. Chem.*, 2002, **42**, 163; (c) M. C. Traub, B. S. Brunschwig and N. S. Lewis, *J. Phys. Chem. B*, 2007, **111**, 6676.
6. M. S. Inkpen and N. J. Long, in *Molecular Design and Applications of Photofunctional Polymers and Materials*, eds. W.-Y. Wong and A. S. Abd-El-Aziz, Royal Society of Chemistry, 2012.
7. (a) M. Guillemot, L. Toupet and C. Lapinte, *Organometallics*, 1998, **17**, 1928; (b) M. I. Bruce, B. G. Ellis, M. Gaudio, C. Lapinte, G. Melino, F. Paul, B. W. Skelton, M. E. Smith, L. Toupet and A. H. White, *Dalton Trans.*, 2004, 1601; (c) W. E. Meyer, A. J. Amoroso, C. R. Horn, M. Jaeger and J. A. Gladysz, *Organometallics*, 2001, **20**, 1115; (d) A. Klein, O. Lavastre and J. Fiedler, *Organometallics*, 2006, **25**, 635; (e) P. Aguirre-Etcheverry and D. O'Hare, *Chem. Rev.*, 2010, **110**, 4839.
8. J. Manna, K. D. John and M. D. Hopkins, *Adv. Organomet. Chem.*, 1995, **38**, 79.
9. C. Creutz and H. Taube, *J. Am. Chem. Soc.*, 1969, **91**, 3988.
10. N. S. Hush, *Prog. Inorg. Chem.*, 1967, **8**, 391.
11. (a) H. Taube, *Angew. Chem., Int. Ed.*, 1984, **23**, 329; (b) R. A. Marcus, *Rev. Mod. Phys.*, 1993, **65**, 599.

12. (a) C. Creutz, *Prog. Inorg. Chem.*, 1983, **30**, 1; (b) W. Kaim and B. Sarkar, *Coord. Chem. Rev.*, 2007, **251**, 584; (c) K. Kalyanasundaram and M. K. Nazeeruddin, *Inorg. Chim. Acta*, 1994, **226**, 213; (d) M. D. Ward, *Chem. Soc. Rev.*, 1995, **24**, 121; (e) W. Kaim and G. K. Lahiri, *Angew. Chem., Int. Ed.*, 2007, **46**, 1778.
13. P. Low and N. Brown, *J. Cluster Sci.*, 2010, **21**, 235.
14. D. H. Evans, *Chem. Rev.*, 2008, **108**, 2113.
15. (a) D. Astruc, *Acc. Chem. Res.*, 1997, **30**, 383; (b) S. Barlow and D. O'Hare, *Chem. Rev.*, 1997, **97**, 637; (c) A. Ceccon, S. Santi, L. Orian and A. Bisello, *Coord. Chem. Rev.*, 2004, **248**, 683.
16. D. O. Cowan and F. Kaufman, *J. Am. Chem. Soc.*, 1970, **92**, 219.
17. L.-B. Gao, S.-H. Liu, L.-Y. Zhang, L.-X. Shi and Z.-N. Chen, *Organometallics*, 2005, **25**, 506.
18. L. Gong, L. Wu, Y. Lin, H. Zhang, F. Yang, T. Wen and H. Xia, *Dalton Trans*, 2007, 4122.
19. (a) M. D. Ward and J. A. McCleverty, *J. Chem. Soc., Dalton Trans.*, 2002, 275; (b) V. Lyaskovskyy and B. de Bruin, *ACS Catal.*, 2012, **2**, 270; (c) P. A. Schauer and P. J. Low, *Eur. J. Inorg. Chem.*, 2012, **2012**, 390.
20. D. M. D'Alessandro and F. R. Keene, *Chem. Soc. Rev.*, 2006, **35**, 424.
21. P. Atkins and J. de Paula, *Physical Chemistry* (7th ed.), Oxford University Press, 2002.
22. M. B. Robin and P. Day, *Adv. Inorg. Chem.*, 1968, **10**, 247.
23. B. S. Brunschwig, C. Creutz and N. Sutin, *Chem. Soc. Rev.*, 2002, **31**, 168.
24. S. B. Piepho, E. R. Krausz and P. N. Schatz, *J. Am. Chem. Soc.*, 1978, **100**, 2996.
25. (a) M. J. Ondrechen, J. Ko and L. J. Root, *J. Phys. Chem.*, 1984, **88**, 5919; (b) J. Ko and M. J. Ondrechen, *J. Am. Chem. Soc.*, 1985, **107**, 6161; (c) A. Ferretti, A. Lami, M. J. Ondrechen and G. Villani, *J. Phys. Chem.*, 1995, **99**, 10484.
26. (a) M. E. Stoll, S. R. Lovelace, W. E. Geiger, H. Schimanke, I. Hyla-Kryspin and R. Gleiter, *J. Am. Chem. Soc.*, 1999, **121**, 9343; (b) C. G. Atwood and W. E. Geiger, *J. Am. Chem. Soc.*, 2000, **122**, 5477.
27. (a) C. Creutz, M. D. Newton and N. Sutin, *J. Photochem. Photobiol., A*, 1994, **82**, 47; (b) B. S. Brunschwig and N. Sutin, *Coord. Chem. Rev.*, 1999, **187**, 233.
28. F. Barrière and W. E. Geiger, *J. Am. Chem. Soc.*, 2006, **128**, 3980.
29. C. E. B. Evans, M. L. Naklicki, A. R. Rezvani, C. A. White, V. V. Kondratiev and R. J. Crutchley, *J. Am. Chem. Soc.*, 1998, **120**, 13096.
30. D. E. Richardson and H. Taube, *Coord. Chem. Rev.*, 1984, **60**, 107.
31. W. F. Sokol, D. H. Evans, K. Niki and T. Yagi, *J. Electroanal. Chem. Interfacial Electrochem.*, 1980, **108**, 107.
32. J. E. Sutton, P. M. Sutton and H. Taube, *Inorg. Chem.*, 1979, **18**, 1017.
33. J. E. Sutton, Ph.D. Thesis, Stanford University, 1979.
34. (a) J. G. Kirkwood and F. H. Westheimer, *J. Chem. Phys.*, 1938, **6**, 506; (b) F. H. Westheimer and J. G. Kirkwood, *J. Chem. Phys.*, 1938, **6**, 513; (c) S. Ehrenson, *J. Am. Chem. Soc.*, 1976, **98**, 7510.
35. J. E. Sutton and H. Taube, *Inorg. Chem.*, 1981, **20**, 3125.
36. S. Ferrere and C. M. Elliott, *Inorg. Chem.*, 1995, **34**, 5818.
37. T. Sigvartsen, B. Gestblom, E. Noreland and J. Songstad, *Acta Chem. Scand.*, 1989, **43**, 103.
38. D. E. Richardson and H. Taube, *J. Am. Chem. Soc.*, 1983, **105**, 40.
39. W. Kaim and V. Kasack, *Inorg. Chem.*, 1990, **29**, 4696.

40. P. C. Ford, D. P. Rudd, R. Gaunder and H. Taube, *J. Am. Chem. Soc.*, 1968, **90**, 1187.
41. M. S. Pereira and J. M. Malin, *Inorg. Chem.*, 1974, **13**, 386.
42. C. Creutz and H. Taube, *J. Am. Chem. Soc.*, 1973, **95**, 1086.
43. (a) M. A. S. Aquino, F. L. Lee, E. J. Gabe, C. Bensimon, J. E. Greedan and R. J. Crutchley, *J. Am. Chem. Soc.*, 1992, **114**, 5130; (b) M. L. Naklicki, C. A. White, L. L. Plante, C. E. B. Evans and R. J. Crutchley, *Inorg. Chem.*, 1998, **37**, 1880.
44. C. Lapinte, *J. Organomet. Chem.*, 2008, **693**, 793.
45. (a) K. Fink, R. Fink and V. Staemmler, *Inorg. Chem.*, 1994, **33**, 6219; (b) K. M. D. Coey, *Magnetism and Magnetic Materials*, Cambridge University Press, 2010.
46. P. W. Anderson, *Phys. Rev.*, 1959, **115**, 2.
47. N. Le Narvor and C. Lapinte, *C. R. Acad. Sci., Ser. IIc: Chim.*, 1998, **1**, 745.
48. G. Pass and H. Sutcliffe, *J. Chem. Educ.*, 1971, **48**, 180.
49. (a) L. K. Thompson and B. S. Ramaswamy, *Inorg. Chem.*, 1986, **25**, 2664; (b) J. H. Van Vleck, *The Theory of Electric and Magnetic Susceptibilities*, Oxford University Press, 1932.
50. (a) B. Bleaney and K. D. Bowers, *Proc. R. Soc. London, Ser. A*, 1952, **214**, 451; (b) E. C. Fitzgerald, N. J. Brown, R. Edge, M. Helliwell, H. N. Roberts, F. Tuna, A. Beeby, D. Collison, P. J. Low and M. W. Whiteley, *Organometallics*, 2011, **31**, 157.
51. D. F. Evans, *J. Chem. Soc.*, 1959, 2003.
52. (a) W. D. Phillips and M. Poe, in *Methods Enzymol.*, ed. P. Anthony San, Academic Press, 1972, **24**, 304; (b) E. M. Schubert, *J. Chem. Educ.*, 1992, **69**, 62.
53. G. A. Bain and J. F. Berry, *J. Chem. Educ.*, 2008, **85**, 532.
54. (a) R. H. Holm and C. J. Hawkins, in *NMR of Paramagnetic Molecules*, eds. G. N. La Mar, W. D. Horrocks and R. H. Holm, Academic Press, New York, 1973; (b) A. D. Boersma, M. A. Phillippi and H. M. Goff, *J. Magn. Reson.*, 1984, **57**, 197; (c) G. C. Campbell and J. F. Haw, *Inorg. Chem.*, 1988, **27**, 3706; (d) F. A. Cotton, J. L. Eglin, B. Hong and C. A. James, *J. Am. Chem. Soc.*, 1992, **114**, 4915; (e) F. A. Cotton, J. L. Eglin, C. A. James and R. L. Luck, *Inorg. Chem.*, 1992, **31**, 5308.
55. F. Barrière, N. Camire, W. E. Geiger, U. T. Mueller-Westerhoff and R. Sanders, *J. Am. Chem. Soc.*, 2002, **124**, 7262.
56. (a) J.-M. Savéant, *Elements of Molecular and Biomolecular Electrochemistry*, John Wiley & Sons, Inc., 2006; (b) A. J. Bard and L. Y. Faulkner, *Electrochemical Methods* (2nd ed.), Wiley, 2004.
57. D. M. D'Alessandro and F. R. Keene, *Dalton Trans*, 2004, 3950.
58. D. H. Evans and M. W. Lehmann, *Acta Chem. Scand.*, 1999, **53**, 765.
59. J. R. Bontha and P. N. Pintauro, *J. Phys. Chem.*, 1992, **96**, 7778.
60. P. W. Atkins and A. J. MacDermott, *J. Chem. Educ.*, 1982, **59**, 359.
61. P. Hapiot, L. D. Kispert, V. V. Konovalov and J.-M. Savéant, *J. Am. Chem. Soc.*, 2001, **123**, 6669.
62. (a) N. Van Order, W. E. Geiger, T. E. Bitterwolf and A. L. Rheingold, *J. Am. Chem. Soc.*, 1987, **109**, 5680; (b) D. H. Evans and K. Hu, *J. Chem. Soc., Faraday Trans.*, 1996, **92**, 3983.
63. Y. Zhu, O. Clot, M. O. Wolf and G. P. A. Yap, *J. Am. Chem. Soc.*, 1998, **120**, 1812.
64. J. P. Chang, E. Y. Fung and J. C. Curtis, *Inorg. Chem.*, 1986, **25**, 4233.
65. C. A. Tolman, *Chem. Rev.*, 1977, **77**, 313.
66. D. Catheline and D. Astruc, *Organometallics*, 1984, **3**, 1094.

67. G. J. Baird and S. G. Davies, *J. Organomet. Chem.*, 1984, **262**, 215.
68. C. Bitcon and M. W. Whiteley, *J. Organomet. Chem.*, 1987, **336**, 385.
69. A. d. l. J. Leal, M. J. Tenorio, M. C. Puerta and P. Valerga, *Organometallics*, 1995, **14**, 3839.
70. M. Jimenez-Tenorio, M. C. Puerta and P. Valerga, *Organometallics*, 1994, **13**, 3330.
71. E. Isaacs and W. A. G. Graham, *J. Organomet. Chem.*, 1976, **120**, 407.
72. W. M. Khairul, M. A. Fox, N. N. Zaitseva, M. Gaudio, D. S. Yufit, B. W. Skelton, A. H. White, J. A. K. Howard, M. I. Bruce and P. J. Low, *Dalton Trans.*, 2009, 610.
73. M. Pilar Gamasa, J. Gimeno, E. Lastra, M. Lanfranchi and A. Tiripicchio, *J. Organomet. Chem.*, 1991, **405**, 333.
74. C. Egler-Lucas, O. Blacque, K. Venkatesan, A. López-Hernández and H. Berke, *Eur. J. Inorg. Chem.*, 2012, **2012**, 1536.
75. H. Schumann and L. Eguren, *J. Organomet. Chem.*, 1991, **403**, 183.
76. P. M. Treichel, R. L. Shubkin, K. W. Barnett and D. Reichard, *Inorg. Chem.*, 1966, **5**, 1177.
77. B. S. Newell, A. K. Rappé and M. P. Shores, *Inorg. Chem.*, 2010, **49**, 1595.
78. M. L. H. Green and T. Mole, *J. Organomet. Chem.*, 1968, **12**, 404.
79. M. I. Bruce, B. G. Ellis, B. W. Skelton and A. H. White, *J. Organomet. Chem.*, 2005, **690**, 792.
80. C. Nataro, J. Chen and R. J. Angelici, *Inorg. Chem.*, 1998, **37**, 1868.
81. M. I. Bruce, B. W. Skelton, A. H. White and N. N. Zaitseva, *J. Organomet. Chem.*, 2002, **650**, 141.
82. M. I. Bruce, M. G. Humphrey, G. A. Koutsantonis and M. J. Liddell, *J. Organomet. Chem.*, 1987, **326**, 247.
83. M. I. Bruce and R. C. Wallis, *Aust. J. Chem.*, 1979, **32**, 1471.
84. M. I. Bruce, M. G. Humphrey and M. J. Liddell, *J. Organomet. Chem.*, 1987, **321**, 91.
85. S. G. Davies and S. J. Simpson, *J. Chem. Soc., Dalton Trans.*, 1984, 993.
86. M. I. Bruce, F. S. Wong, B. W. Skelton and A. H. White, *J. Chem. Soc., Dalton Trans.*, 1982, 2203.
87. M. Sato and M. Sekino, *J. Organomet. Chem.*, 1993, **444**, 185.
88. M. I. Bruce, K. Costuas, T. Davin, J.-F. Halet, K. A. Kramarczuk, P. J. Low, B. K. Nicholson, G. J. Perkins, R. L. Roberts, B. W. Skelton, M. E. Smith and A. H. White, *Dalton Trans.*, 2007, 5387.
89. W. M. Laidlaw and R. G. Denning, *J. Organomet. Chem.*, 1993, **463**, 199.
90. A. T. Patton, C. E. Strouse, C. B. Knobler and J. A. Gladysz, *J. Am. Chem. Soc.*, 1983, **105**, 5804.
91. T.-S. Peng, C. H. Winter and J. A. Gladysz, *Inorg. Chem.*, 1994, **33**, 2534.
92. W. E. Meyer, A. J. Amoroso, M. Jaeger, J. L. Bras, W.-T. Wong and J. A. Gladysz, *J. Organomet. Chem.*, 2000, **616**, 44.
93. G. M. Aston, S. Badriya, R. D. Farley, R. W. Grime, S. J. Ledger, F. E. Mabbs, E. J. L. McInnes, H. W. Morris, A. Ricalton, C. C. Rowlands, K. Wagner and M. W. Whiteley, *J. Chem. Soc., Dalton Trans.*, 1999, 4379.
94. J. S. Adams, M. Cunningham and M. W. Whiteley, *J. Organomet. Chem.*, 1985, **293**, C13.
95. (a) J. S. Adams, C. Bitcon, J. R. Brown, D. Collison, M. Cunningham and M. W. Whiteley, *J. Chem. Soc., Dalton Trans.*, 1987, 3049; (b) N. J. Brown, D. Collison, R. Edge, E. C. Fitzgerald, M. Helliwell, J. A. K. Howard, H. N. Lancashire, P. J. Low, J. J. W. McDouall, J. Raftery, C. A. Smith, D. S. Yufit and M. W. Whiteley, *Organometallics*, 2010, **29**, 1261.

96. J. M. Bellerby, M. J. Mays and P. L. Sears, *J. Chem. Soc., Dalton Trans.*, 1976, 1232.
97. A. Hills, D. L. Hughes, M. Jimenez-Tenorio and G. J. Leigh, *J. Organomet. Chem.*, 1990, **391**, C41.
98. B. Gómez-Lor, A. Santos, M. Ruiz and A. M. Echavarren, *Eur. J. Inorg. Chem.*, 2001, **2001**, 2305.
99. S. Ingham, M. Khan, J. Lewis, N. Long, P. Raithby and C. Faulkner, *J. Organomet. Chem.*, 1994, **482**, 139.
100. J. T. Mague and J. P. Mitchener, *Inorg. Chem.*, 1972, **11**, 2714.
101. D. Touchard, P. Haquette, N. Pirio, L. Toupet and P. H. Dixneuf, *Organometallics*, 1993, **12**, 3132.
102. A. J. Hodge, S. L. Ingham, A. K. Kakkar, M. S. Khan, J. Lewis, N. J. Long, D. G. Parker and P. R. Raithby, *J. Organomet. Chem.*, 1995, **488**, 205.
103. G. Smith, D. J. Cole-Hamilton, M. Thornton-Pett and M. B. Hursthouse, *J. Chem. Soc., Dalton Trans.*, 1985, 387.
104. H. I. Karunadasa, K. D. Arquero, L. A. Berben and J. R. Long, *Inorg. Chem.*, 2010, **49**, 4738.
105. D. Unseld, V. V. Krivykh, K. Heinze, F. Wild, G. Artus, H. Schmalle and H. Berke, *Organometallics*, 1999, **18**, 1525.
106. C. D. Delfs, R. Stranger, M. G. Humphrey and A. M. McDonagh, *J. Organomet. Chem.*, 2000, **607**, 208.
107. M. I. Bruce, K. Costuas, B. G. Ellis, J.-F. Halet, P. J. Low, B. Moubaraki, K. S. Murray, N. Ouddaï, G. J. Perkins, B. W. Skelton and A. H. White, *Organometallics*, 2007, **26**, 3735.
108. S. Kheradmandan, K. Venkatesan, O. Blacque, H. W. Schmalle and H. Berke, *Chem. Eur. J.*, 2004, **10**, 4872.
109. (a) H. Ogawa, K. Onitsuka, T. Joh, S. Takahashi, Y. Yamamoto and H. Yamazaki, *Organometallics*, 1988, **7**, 2257; (b) K. Suenkel, U. Birk and C. Robl, *Organometallics*, 1994, **13**, 1679.
110. (a) M. Akita, M. Terada, S. Oyama and Y. Moro-oka, *Organometallics*, 1990, **9**, 816; (b) M. Akita, M. Terada, S. Oyama, S. Sugimoto and Y. Moro-oka, *Organometallics*, 1991, **10**, 1561; (c) M. Akita, M.-C. Chung, A. Sakurai, S. Sugimoto, M. Terada, M. Tanaka and Y. Moro-oka, *Organometallics*, 1997, **16**, 4882.
111. R. J. Spahr, R. R. Vogt and J. A. Nieuwland, *J. Am. Chem. Soc.*, 1933, **55**, 2465.
112. (a) R. J. Cross, M. F. Davidson and A. J. McLennan, *J. Organomet. Chem.*, 1984, **265**, C37; (b) R.-Y. Liau, A. Schier and H. Schmidbaur, *Organometallics*, 2003, **22**, 3199; (c) M. I. Bruce, K. R. Grundy, M. J. Liddell, M. R. Snow and E. R. T. Tiekink, *J. Organomet. Chem.*, 1988, **344**, C49; (d) C. M. Che, H. Y. Chao, V. M. Miskowski, Y. Li and K. K. Cheung, *J. Am. Chem. Soc.*, 2001, **123**, 4985.
113. R. Nast, P. Schneller and A. Hengefeld, *J. Organomet. Chem.*, 1981, **214**, 273.
114. J. A. Davies, M. El-ghanam, A. A. Pinkerton and D. A. Smith, *J. Organomet. Chem.*, 1991, **409**, 367.
115. G. Kreisel, P. Scholz and W. Seidel, *Z. Anorg. Allg. Chem.*, 1980, **460**, 51.
116. N. A. Ustynyuk, V. N. Vinogradova and D. N. Kravtsov, *Metalloorg. Khim.*, 1988, **1**, 85.
117. P. Binger, P. Müller, P. Philipps, B. Gabor, R. Mynott, A. T. Herrmann, F. Langhauser and C. Krüger, *Chem. Ber.*, 1992, **125**, 2209.
118. W. J. Evans, G. W. Rabe and J. W. Ziller, *J. Organomet. Chem.*, 1994, **483**, 21.
119. M. S. Clair, W. P. Schaefer and J. E. Bercaw, *Organometallics*, 1991, **10**, 525.

120. V. W.-W. Yam, K. M.-C. Wong and N. Zhu, *Angew. Chem., Int. Ed. Engl.*, 2003, **42**, 1400.
121. G. A. Koutsantonis and J. P. Selegue, *J. Am. Chem. Soc.*, 1991, **113**, 2316.
122. J. Heidrich, M. Steimann, M. Appel, W. Beck, J. R. Phillips and W. C. Trogler, *Organometallics*, 1990, **9**, 1296.
123. K. G. Caulton, R. H. Cayton, M. H. Chisholm, J. C. Huffman, E. B. Lobkovsky and Z. Xue, *Organometallics*, 1992, **11**, 321.
124. J. Sun, S. E. Shaner, M. K. Jones, D. C. O'Hanlon, J. S. Mugridge and M. D. Hopkins, *Inorg. Chem.*, 2010, **49**, 1687.
125. M. Akita, M.-C. Chung, A. Sakurai and Y. Moro-oka, *Chem. Commun.*, 2000, 1285.
126. B. E. Woodworth, P. S. White and J. L. Templeton, *J. Am. Chem. Soc.*, 1997, **119**, 828.
127. (a) J. Gil-Rubio, M. Laubender and H. Werner, *Organometallics*, 1998, **17**, 1202; (b) J. Gil-Rubio, M. Laubender and H. Werner, *Organometallics*, 2000, **19**, 1365; (c) H. Werner, R. W. Lass, O. Gevert and J. Wolf, *Organometallics*, 1997, **16**, 4077; (d) B. Callejas-Gaspar, M. Laubender and H. Werner, *J. Organomet. Chem.*, 2003, **684**, 144.
128. K. Onitsuka, N. Ose, F. Ozawa and S. Takahashi, *J. Organomet. Chem.*, 1999, **578**, 169.
129. M. I. Bruce, M. Jevric, B. W. Skelton, M. E. Smith, A. H. White and N. N. Zaitseva, *J. Organomet. Chem.*, 2006, **691**, 361.
130. H. B. Fyfe, M. Mlekuz, D. Zargarian, N. J. Taylor and T. B. Marder, *J. Chem. Soc., Chem. Commun.*, 1991, 188.
131. M. I. Bruce, M. Ke and P. J. Low, *Chem. Commun.*, 1996, 2405.
132. V. W. W. Yam, V. C. Y. Lau and K. K. Cheung, *Organometallics*, 1996, **15**, 1740.
133. R. L. Roberts, H. Puschmann, J. A. K. Howard, J. H. Yamamoto, A. J. Carty and P. J. Low, *Dalton Trans.*, 2003, 1099.
134. S. Kheradmandan, K. Heinze, H. W. Schmalle and H. Berke, *Angew. Chem., Int. Ed. Engl.*, 1999, **38**, 2270.
135. F. J. Fernández, K. Venkatesan, O. Blacque, M. Alfonso, H. W. Schmalle and H. Berke, *Chem. Eur. J.*, 2003, **9**, 6192.
136. K. Venkatesan, T. Fox, H. W. Schmalle and H. Berke, *Organometallics*, 2005, **24**, 2834.
137. S. N. Semenov, O. Blacque, T. Fox, K. Venkatesan and H. Berke, *J. Am. Chem. Soc.*, 2010, **132**, 3115.
138. M. I. Bruce, M. Ke, P. J. Low, B. W. Skelton and A. H. White, *Organometallics*, 1998, **17**, 3539.
139. K.-T. Wong, J.-M. Lehn, S.-M. Peng and G.-H. Lee, *Chem. Commun.*, 2000, 2259.
140. J. Stahl, J. C. Bohling, E. B. Bauer, T. B. Peters, W. Mohr, J. M. Martín-Alvarez, F. Hampel and J. A. Gladysz, *Angew. Chem., Int. Ed. Engl.*, 2002, **41**, 1872.
141. T. B. Peters, J. C. Bohling, A. M. Arif and J. A. Gladysz, *Organometallics*, 1999, **18**, 3261.
142. W. Mohr, J. Stahl, F. Hampel and J. A. Gladysz, *Chem. Eur. J.*, 2003, **9**, 3324.
143. Q. Zheng, F. Hampel and J. A. Gladysz, *Organometallics*, 2004, **23**, 5896.
144. (a) R. Dembinski, T. Bartik, B. Bartik, M. Jaeger and J. A. Gladysz, *J. Am. Chem. Soc.*, 2000, **122**, 810; (b) C. R. Horn and J. A. Gladysz, *Eur. J. Inorg. Chem.*, 2003, 2211.
145. L.-B. Gao, J. Kan, Y. Fan, L.-Y. Zhang, S.-H. Liu and Z.-N. Chen, *Inorg. Chem.*, 2007, **46**, 5651.
146. (a) R. Nast and A. Beyer, *J. Organomet. Chem.*, 1980, **194**, 125; (b) K. Onitsuka, H. Ogawa, T. Joh, S. Takahashi, Y. Yamamoto and H. Yamazaki, *J. Chem. Soc., Dalton Trans.*, 1991, 1531; (c) A. L. Groia, A. Ricci, M. Bassetti, D. Masi, C. Bianchini and C. L. Sterzo, *J. Organomet. Chem.*, 2003, **683**, 406.

147. (a) R. Nast and J. Moritz, *J. Organomet. Chem.*, 1976, **117**, 81; (b) M. I. Bruce, J. Davy, B. C. Hall, Y. J. v. Galen, B. W. Skelon and A. H. White, *Appl. Organomet. Chem.*, 2002, **16**, 559; (c) B. Olenyuk, M. D. Levin, J. A. Whiteford, J. E. Shield and P. J. Stang, *J. Am. Chem. Soc.*, 1999, **121**, 10434; (d) I. Ara, J. R. Berenguer, E. Eguizábal, J. Forniés, J. Gómez, E. Lalinde and J. M. Sáez-Rocher, *Organometallics*, 2000, **19**, 4385; (e) A. Köhler, J. S. Wilson, R. H. Friend, M. K. Al-Suti, M. S. Khan, A. Gerhard and H. Bässler, *J. Chem. Phys.*, 2002, **116**, 9457.
148. R. Nast and A. Beyer, *J. Organomet. Chem.*, 1980, **194**, 125.
149. N. J. Long, C. K. Wong and A. J. P. White, *Organometallics*, 2006, **25**, 2525.
150. R. Nast and H. Grouhi, *J. Organomet. Chem.*, 1979, **182**, 197.
151. F. H. Koehler, W. Proessdorf and U. Schubert, *Inorg. Chem.*, 1981, **20**, 4096.
152. E. C. Royer and M. C. Barral, *Inorg. Chim. Acta*, 1984, **90**, L47.
153. R. R. Tykwinski and P. J. Stang, *Organometallics*, 1994, **13**, 3203.
154. P. Stang and R. Tykwinski, *J. Am. Chem. Soc.*, 1992, **114**, 4411.
155. G. Jia, R. J. Puddephatt, J. D. Scott and J. J. Vittal, *Organometallics*, 1993, **12**, 3565.
156. V. W.-W. Yam and S. W.-K. Choi, *J. Chem. Soc., Dalton Trans.*, 1996, 4227.
157. K. Osakada, T. Takizawa, M. Tanaka and T. Yamamoto, *J. Organomet. Chem.*, 1994, **473**, 359.
158. A. Santos, J. Lopez, J. Montoya, P. Noheda, A. Romero and A. M. Echavarren, *Organometallics*, 1994, **13**, 3605.
159. G. Albertin, S. Antoniutti, E. Bordignon and M. Granzotto, *J. Organomet. Chem.*, 1999, **585**, 83.
160. G. Albertin, P. Agnoletto and S. Antoniutti, *Polyhedron*, 2002, **21**, 1755.
161. M. I. Bruce, B. C. Hall, B. D. Kelly, P. J. Low, B. W. Skelton and A. H. White, *J. Chem. Soc., Dalton Trans.*, 1999, 3719.
162. G. Albertin, S. Antoniutti, E. Bordignon and D. Bresolin, *J. Organomet. Chem.*, 2000, **609**, 10.
163. C. S. Chin, D. Chong, M. Kim and H. Lee, *Bull. Korean Chem. Soc.*, 2001, **22**, 739.
164. C. S. Chin, H. Lee, H. Park and M. Kim, *Organometallics*, 2002, **21**, 3889.
165. S. Kheradmandan, T. Fox, Helmut W. Schmalle, K. Venkatesan and H. Berke, *Eur. J. Inorg. Chem.*, 2004, **2004**, 3544.
166. C. S. Chin, M. Kim, H. Lee, S. Noh and K. M. Ok, *Organometallics*, 2002, **21**, 4785.
167. G. v. Koten, S. Back, M. H. Lutz, A. L. Spek and H. Lang, *J. Organomet. Chem.*, 2001, **620**, 227.
168. H.-Y. Chao, W. Lu, Y. Li, M. C. W. Chan, C.-M. Che, K.-K. Cheung and N. Zhu, *J. Am. Chem. Soc.*, 2002, **124**, 14696.
169. T. Cardolaccia, A. M. Funston, M. E. Kose, J. M. Keller, M. J. R. and K. S. Schanze, *J. Phys. Chem. B*, 2007, **111**, 10871.
170. L. Medei, L. Orian, O. V. Semeikin, M. G. Peterleitner, N. A. Ustynyuk, S. Santi, C. Durante, A. Ricci and C. L. Sterzo, *Eur. J. Inorg. Chem.*, 2006, 2582.
171. W. A. Hoffert, M. K. Kabir, E. A. Hill, S. M. Mueller and M. P. Shores, *Inorg. Chim. Acta*, 2012, **380**, 174.
172. S. Back, R. A. Gossage, G. Rheinwald, I. del Río, H. Lang and G. van Koten, *J. Organomet. Chem.*, 1999, **582**, 126.
173. E. Viola, C. L. Sterzo, R. Crescenzi and G. Frachey, *J. Organomet. Chem.*, 1995, **493**, C9.

174. J. Lewis, N. J. Long, P. R. Raithby, G. P. Shields, W.-Y. Wong and M. Younus, *J. Chem. Soc., Dalton Trans.*, 1997, 4283.
175. A. Buttinelli, E. Viola, E. Antonelli and C. L. Sterzo, *Organometallics*, 1998, **17**, 2574.
176. P. Altamura, G. Giardina, C. L. Sterzo and M. V. Russo, *Organometallics*, 2001, **20**, 4360.
177. P. Li, B. Ahrens, K.-H. Choi, M. S. Khan, P. R. Raithby, P. J. Wilson and W.-Y. Wong, *CrystEngComm*, 2002, **4**, 405.
178. W.-Y. Wong, K.-H. Choi, G.-L. Lu and Z. Lin, *Organometallics*, 2002, **21**, 4475.
179. R. D'Amato, I. Fratoddi, A. Cappotto, P. Altamura, M. Delfini, C. Bianchetti, A. Bolasco, G. Polzonetti and M. V. Russo, *Organometallics*, 2004, **23**, 2860.
180. T. Cardolaccia, Y. Li and K. S. Schanze, *J. Am. Chem. Soc.*, 2008, **130**, 2535.
181. K.-Y. Kim, A. H. Shelton, M. Drobizhev, N. Makarov, A. Rebane and K. S. Schanze, *J. Phys. Chem. A*, 2010, **114**, 7003.
182. F. Guo, K. Ogawa, Y.-G. Kim, E. O. Danilov, F. N. Castellano, J. R. Reynolds and K. S. Schanze, *Phys. Chem. Chem. Phys.*, 2007, **9**, 2724.
183. H. P. Xia, R. C. Y. Yeung and G. C. Jia, *Organometallics*, 1998, **17**, 4762.
184. (a) M. R. Churchill and J. Wormald, *Inorg. Chem.*, 1969, **8**, 1936; (b) A. Sanders and W. P. Giering, *J. Organomet. Chem.*, 1976, **104**, 67.
185. X. Niu, L. Gopal, M. P. Masingale, D. A. Braden, B. S. Hudson and M. B. Sponsler, *Organometallics*, 2000, **19**, 649.
186. J. Maurer, R. Winter, B. Sarkar and S. Zalis, *J. Solid State Electrochem.*, 2005, **9**, 738.
187. N. L. Narvor and C. Lapinte, *J. Chem. Soc., Chem. Commun.*, 1993, 357.
188. N. Lenarvor, L. Toupet and C. Lapinte, *J. Am. Chem. Soc.*, 1995, **117**, 7129.
189. M. I. Bruce, B. G. Ellis, P. J. Low, B. W. Skelton and A. H. White, *Organometallics*, 2003, **22**, 3184.
190. M. I. Bruce, L. I. Denisovich, P. J. Low, S. M. Peregudova and N. A. Ustynyuk, *Mendeleev Commun.*, 1996, **6**, 200.
191. L.-B. Gao, L.-Y. Zhang, L.-X. Shi and Z.-N. Chen, *Organometallics*, 2005, **24**, 1678.
192. M. Bruce, K. Kramarczuk, B. Skelton and A. White, *J. Organomet. Chem.*, 2010, **695**, 469.
193. J. W. Seyler, W. Weng, Y. Zhou and J. A. Gladysz, *Organometallics*, 1993, **12**, 3802.
194. F. Coat and C. Lapinte, *Organometallics*, 1996, **15**, 477.
195. M.-C. Chung, X. Gu, B. A. Etzenhouser, A. M. Spuches, P. T. Rye, S. K. Seetharaman, D. J. Rose, J. Zubieta and M. B. Sponsler, *Organometallics*, 2003, **22**, 3485.
196. B. A. Etzenhouser, Q. Chen and M. B. Sponsler, *Organometallics*, 1994, **13**, 4176.
197. B. A. Etzenhouser, M. D. Cavanaugh, H. N. Spurgeon and M. B. Sponsler, *J. Am. Chem. Soc.*, 1994, **116**, 2221.
198. N. Lenarvor and C. Lapinte, *Organometallics*, 1995, **14**, 634.
199. Y. Matsuura, Y. Tanaka and M. Akita, *J. Organomet. Chem.*, 2009, **694**, 1840.
200. C. Ornelas, J. Ruiz and D. Astruc, *J. Organomet. Chem.*, 2009, **694**, 1219.
201. D. J. Armitt, M. I. Bruce, M. Gaudio, N. N. Zaitseva, B. W. Skelton, A. H. White, B. Le Guennic, J. F. Halet, M. A. Fox, R. L. Roberts, F. Hartl and P. J. Low, *Dalton Trans.*, 2008, 6763.
202. E. C. Fitzgerald, A. Ladjarafi, N. J. Brown, D. Collison, K. Costuas, R. Edge, J.-F. Halet, F. Justaud, P. J. Low, H. Meghezzi, T. Roisnel, M. W. Whiteley and C. Lapinte, *Organometallics*, 2011, **30**, 4180.
203. M. C. B. Colbert, J. Lewis, N. J. Long, P. R. Raithby, M. Younus, A. J. P. White, D. J.

Williams, N. N. Payne, L. Yellowlees, D. Beljonne, N. Chawdhury and R. H. Friend, *Organometallics*, 1998, **17**, 3034.
204. L. D. Field, A. V. George, F. Laschi, E. Y. Malouf and P. Zanello, *J. Organomet. Chem.*, 1992, **435**, 347.
205. O. Lavastre, J. Plass, P. Bachmann, S. Guesmi, C. Moinet and P. H. Dixneuf, *Organometallics*, 1997, **16**, 184.
206. S. K. Hurst, M. P. Cifuentes, A. M. McDonagh, M. G. Humphrey, M. Samoc, B. Luther-Davies, I. Asselberghs and A. Persoons, *J. Organomet. Chem.*, 2002, **642**, 259.
207. S. L. Stang, F. Paul and C. Lapinte, *Organometallics*, 2000, **19**, 1035.
208. (a) M. I. Bruce, P. J. Low, K. Costuas, J. F. Halet and S. P. Best, *J. Am. Chem. Soc.*, 2000, **122**, 1949; (b) O. F. Koentjoro, R. Rousseau and P. J. Low, *Organometallics*, 2001, **20**, 4502.
209. H. Jiao, K. Costuas, J. A. Gladysz, J.-F. Halet, M. Guillemot, L. Toupet, F. Paul and C. Lapinte, *J. Am. Chem. Soc.*, 2003, **125**, 9511.
210. M. Brady, W. Weng, Y. Zhou, J. W. Seyler, A. J. Amoroso, A. M. Arif, M. Böhme, G. Frenking and J. A. Gladysz, *J. Am. Chem. Soc.*, 1997, **119**, 775.
211. D. L. Lichtenberger, S. K. Renshaw, A. Wong and C. D. Tagge, *Organometallics*, 1993, **12**, 3522.
212. Y. Zhou, J. W. Seyler, W. Weng, A. M. Arif and J. A. Gladysz, *J. Am. Chem. Soc.*, 1993, **115**, 8509.
213. M. I. Bruce, P. Hinterding, E. R. T. Tiekink, B. W. Skelton and A. H. White, *J. Organomet. Chem.*, 1993, **450**, 209.
214. F. Coat, M.-A. Guillevic, L. Toupet, F. Paul and C. Lapinte, *Organometallics*, 1997, **16**, 5988.
215. R. Denis, L. Toupet, F. Paul and C. Lapinte, *Organometallics*, 2000, **19**, 4240.
216. (a) F. Paul, B. G. Ellis, M. I. Bruce, L. Toupet, T. Roisnel, K. Costuas, J.-F. Halet and C. Lapinte, *Organometallics*, 2006, **25**, 649; (b) M. A. Fox, R. L. Roberts, W. M. Khairul, F. Hartl and P. J. Low, *J. Organomet. Chem.*, 2007, **692**, 3277.
217. M. I. Bruce, K. Costuas, T. Davin, B. G. Ellis, J.-F. Halet, C. Lapinte, P. J. Low, M. E. Smith, B. W. Skelton, L. Toupet and A. H. White, *Organometallics*, 2005, **24**, 3864.
218. J.-F. Halet and C. Lapinte, *Coord. Chem. Rev.*, 2012, DOI: 10.1016/j.ccr.2012.09.007.
219. K. D. Demadis, C. M. Hartshorn and T. J. Meyer, *Chem. Rev.*, 2001, **101**, 2655.
220. S. N. Semenov, S. F. Taghipourian, O. Blacque, T. Fox, K. Venkatesan and H. Berke, *J. Am. Chem. Soc.*, 2010, **132**, 7584.

CHAPTER 7 : CONCLUSIONS AND FUTURE DIRECTIONS

This thesis has detailed synthetic efforts towards branched organometallic complexes for molecular electronics. These contain two well defined molecular pathways, enabling the future study of quantum interference effects and other phenomena resulting from concurrent, and ultimately convergent, electron transport processes. Critical in this context was the incorporation of *redox-active* groups, to enable the manipulation of electron transfer processes through individual branches.

As a 'conducting' backbone, arylethynyl ligands containing *meta*-pyridyl moieties proved extremely straightforward to synthesize. Though their incorporation into $\{FeCp_2\}$ and $\{Ru(dppe)_2\}$ complexes initially presented significant problems, successful methodologies have now been established. For ferrocene-based compounds, the low/moderate reactivity of Fc–I under typical Sonogashira cross-coupling conditions precluded high yields and led to difficulties in isolating the macrocycle (**13**) in anything but trace amounts. This issue was subsequently addressed by exploring the effects of concentration, solvent, base and phosphine ligand on a model reaction, finding that large rate improvements could be achieved using a $PdCl_2(MeCN)_2/P(^tBu)_3$ combination. Future work should revisit the synthesis of **13**, applying these new conditions. Other branched ferrocene-containing species were readily prepared (albeit in moderate yields), and a new route to β-phenylthioketones was discovered (precluding formation of the desirable Fc–C≡C–C_6H_4–SAc motif from iodoferrocenes and 4-ethynylphenylthioacetate).

With $\{Ru(dppe)_2\}$ centres, the bifunctional nature of 4-ethynylpyridine resulted in the production of multiple side-products during M–C bond formation. This motivated the pursuit of alternative, robust approaches to pyridyl-containing $\{Ru(dppe)_2\}$ complexes, though the linear complex $Ru(dppe)_2(C{\equiv}C{-}C_5H_4N)_2$ (**17**) was ultimately prepared via normal methods. Protecting group strategies for 4-ethynylpyridine proved only moderately successful – *N*-methyl-4-ethynylpyridinium triflate was readily utilised as a monofunctional ligand, but demethylation of the resulting complexes was not straightforward. Greater success was found employing a $16e^-$ avoidance rule, limiting contact between the basic/nucleophilic nitrogen and coordinatively

unsaturated metal centres. This strategy facilitated the syntheses of macrocyclic (**35**) and single-branched (**37**) ruthenium-containing compounds, albeit in ~80% purity in the former case. Subsequent efforts should focus on obtaining **35** in pure form, and in extending this approach to preparations of the double-branched species.

Factors affecting the comproportionation equilibria were also reviewed; the generation of macrocyclic mixed-valence complexes being of substantial importance for future studies. It is apparent that medium effects are the most readily harnessed in influencing the magnitude of $\Delta E_{1/2}^{0}$, other contributions to $\Delta_{co}G^{0}$ being largely intrinsic to the complex under investigation. Subsequent work should therefore explore isolation of the mixed-valence states in double-branched and macrocyclic systems by minimising ΔG_{ip}^{0} (*e.g.* by using $Na(BArF_{24})$ as an electrolyte). Using $CH_2Cl_2/Bu_4N^+PF_6^-$ solutions, no separation of redox potentials was observed for any of the dinuclear complexes investigated. Junction measurements of these materials may prove useful in further probing the questionable link between $\Delta E_{1/2}^{0}$ and k_{et}/H_{ab} (discussed at length in *Chapter 6)*.

Though this work has only attempted syntheses of symmetrical species, it would be of great interest to study their asymmetrical analogues. These may, for example, provide an initial destructive interference state that could be switched off by redox processes. As shown in *Figure 7-1*, electronic asymmetry could be introduced in numerous ways; using different metals, alternative ancillary ligands, or even perfluorinated aryl moieties. Macrocyclic structures bearing weakly coupled termini (*e.g.* $-(CH_2)_n-SAc$) could also prove interesting, as these might exhibit conductance switching by application of a magnetic field (in line with discussions in *Chapter 1)*. It is hypothesized that the majority of these compounds could be synthesized following a similar route as for **35** *(Scheme 5-6)*, albeit using 3-bromo-5-iodopyridine to facilitate the controlled addition of each ligand 'arm'.

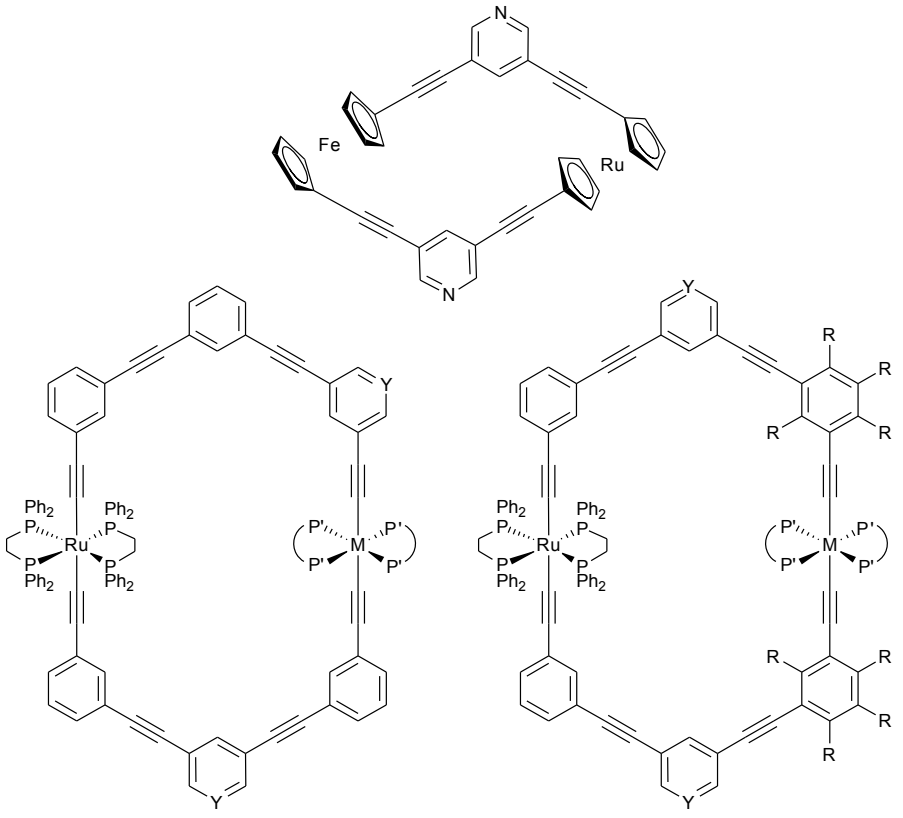

Figure 7-1. Some potentially interesting synthetic targets for future studies (M = Fe, Ru, Os; P′–P′ = dppe, depe, dppf; R = H, F; Y = N, C–$(CH_2)_n$–SAc).

In conclusion, it is clear that the synthesis of conducting macrocycles containing redox centres and surface binding moieties is not a straightforward enterprise. However, this work has made substantial progress in understanding how best to obtain these materials, and tantalising evidence for their formation is provided. The macrocyclic structure-type (two node regime) has hardly been explored experimentally in junction measurements, an endeavour which is of substantial interest in verifying theoretical studies, exploring new mechanisms for conductance switching and ultimately improving our understanding of charge transport through complex molecular architectures. This should prove a fascinating area of discovery in years to come.

CHAPTER 8 : EXPERIMENTAL

8.1 GENERAL

8.1.1 Conditions and materials

All preparations were carried out using standard Schlenk line and air-sensitive chemistry techniques under an atmosphere of nitrogen. No special precautions were taken to exclude air or moisture during workup, unless otherwise stated. Solvents used in reactions were sparged with nitrogen and dried with alumina beads, Q5 Copper catalyst on molecular sieves, or 3A molecular sieves,[1] where appropriate. Silica and neutral alumina of Brockmann activity I (0% H_2O), activity II (3% H_2O) or V (15% H_2O) were used for chromatographic separations. $PdCl_2(PPh_3)_2$,[2] 3,5-diethynylpyridine,[3] 1-(*tert*-butylsulfanyl)-4-ethynylbenzene,[4] $PdCl_2(MeCN)_2$, 4-ethynylphenylthioacetate,[5] 4-ethynylpyridine,[6] *cis*-$RuCl_2(dppe)_2$,[7] $[RuCl(dppe)_2]OTf$,[7] *N*-methyl-pyridinium iodide,[8] 1-bromo-4-(trimethylsilyl)ethynylbenzene,[9] $RuCl_2(PPh_3)_4$,[7] 1-(triisopropylsilyl)ethynyl-3-ethynylbenzene[10] and 3,5-diiodopyridine[11] were prepared via literature methods from commercially available starting materials. All other materials were purchased from commercial suppliers and used without further purification.

8.1.2 Instrumentation

^1H, $^{13}C\{^1H\}$, $^{31}P\{^1H\}$ and $^{19}F\{^1H\}$ NMR spectra were recorded at ambient temperature on a Bruker 400 MHz spectrometer and internally referenced to the residual solvent peaks of $CDCl_3$ at δ 7.26 (^1H) and 77.16 ppm ($^{13}C\{^1H\}$); CD_2Cl_2 at δ 5.32 (^1H) and 53.84 ($^{13}C\{^1H\}$) ppm; DMSO-d_6 at δ 2.50 (^1H) and 39.52 ($^{13}C\{^1H\}$) ppm; D_2O at δ 4.79 ppm (^1H);[12] or externally to 85% phosphoric acid (0.00 ppm). $^{13}C\{^1H\}$ spectra were fully assigned where possible using 2D correlation spectroscopy; this could not achieved in some cases due to insufficient sample quantity, solubility limitations or overlapping resonances. UV-vis and IR spectra were recorded on a PerkinElmer LAMBDA 25 UV/vis spectrophotometer or a PerkinElmer Spectrum 100 FT-IR spectrometer, respectively (the majority of UV-vis data is tabulated in the chapters). Mass spectrometry analyses were conducted by the Mass Spectrometry Service, Imperial College

London, the Mass Spectrometry Facility, University College London, and the EPSRC National Mass Spectrometry Service Centre (NMSSC), Swansea. Microanalyses were carried out by Stephen Boyer of the Science Centre, London Metropolitan University, or Alan Dickerson of the Department of Chemistry, University of Cambridge, for all novel compounds isolated in sufficient purity and yield. Some compounds did not produce satisfactory analyses, despite drying under vacuum for extended periods. For similar large compounds elsewhere, it has been argued that this is inevitable due to included solvent.[13] Here, NMR spectroscopy, mass spectrometry and cyclic voltammetric studies (see previous chapters) support the *absence* of unreacted materials/side products, unless otherwise stated.

Cyclic voltammograms were recorded under an atmosphere of argon in MeCN/0.1 M $^{n}Bu_4NPF_6$ on a CHI760C potentiostat (CH Instruments, Austin, Texas) with a glassy carbon disc as working electrode (diameter = 2.5 or 5 mm), and Pt-wire as reference and counter electrodes respectively. Analyte solutions were between 0.1-1 mM. Potentials are reported relative to $[FeCp_2]^+/[FeCp_2]$, measured against an internal $[FeCp_2]^+/[FeCp_2]$ or $[FeCp^*_2]^+/[FeCp^*_2]$ reference, where appropriate.

8.2 COMPOUNDS SYNTHESISED IN CHAPTER 2

8.2.1 1,1'-Diiodoferrocene (1)

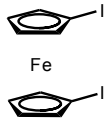

1

A mixture of ferrocene (21.14 g, 113.6 mmol), *n*-hexane (100 mL) and TMEDA (37.7 mL, 251.4 mmol) was stirred in an oven-dried 1 L three-necked flask and cooled to 0°C (ice-bath). 2.5 M ^{n}BuLi in hexanes (100 mL, 250 mmol) was added via cannula over 5 min, whereby the suspension was slowly raised to ambient temperature and stirred overnight. The resulting bright orange suspension (1,1'-dilithioferrocene-TMEDA) was cooled to -78°C (acetone/dry ice) and a solution of I_2 (62.51 g, 246.3 mmol) in diethyl ether (350 mL) added over ~15 min. After warming to 0°C, the reaction was quenched with water (100 mL) and stirred for a further 15 min. The mixture was extracted with water (3 x 200 mL), dried over $MgSO_4$, and filtered through Celite to provide a dark red oil (~33 g) after solvent removal.

The crude product was extracted into *n*-hexane (300 mL) and washed successively with 0.5 M aqueous $FeCl_3$ (~10 x 200 mL). When FcH/FcI contaminants had been removed (composition

monitored by ^{1}H NMR spectroscopy between washings), the organic phase was extracted with water until the washings were colourless, dried over $MgSO_4$, filtered through Celite and evaporated to reveal a brown oil. Further purification via column chromatography (silica, *n*-hexane, 3″ x 4″) and drying *in vacuo* at 50°C yielded pure fcI_2 as a dark orange oil (9.54 g, 19%). ^{1}H NMR (400 MHz, $CDCl_3$): δ (ppm) 4.18 (pseudo-t, $J_{\alpha\beta}$ = ~1.7 Hz, 4H, Cp–*H*), 4.37 (pseudo-t, $J_{\alpha\beta}$ = ~1.8 Hz, 4H, Cp–*H*). ^{13}C{^{1}H} NMR (100 MHz, $CDCl_3$): δ (ppm) 40.42 (Cp–I, *C*–I), 72.41 (Cp–I, *C*–H), 77.72 (Cp–I, *C*–H). HR-MS EI+: *m/z* 437.8065, ([M]$^+$ Calc.: 437.8065). (Found: C, 27.58; H, 1.72. Calc. for $C_{10}H_8FeI_2$: C, 27.43; H, 1.84%).

8.2.2 1-(3-Pyridyl)ethynyl-1'-iodoferrocene (2)

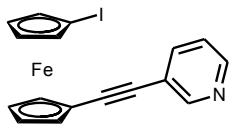

2

A solution of **1** (3.22 g, 7.35 mmol) in DIPA (8 mL) was sparged with nitrogen and added to a flask containing 3-ethynylpyridine (0.153 g, 1.48 mmol), $PdCl_2(PPh_3)_2$ (0.044 g, 0.06 mmol) and CuI (0.027 g, 0.142 mmol). Residual **1** was washed into the reaction flask with additional DIPA (4 x 2 mL) and the mixture stirred at 90°C for 24 h. After cooling and solvent removal the crude material was purified by column chromatography (silica; *n*-hexane→CH_2Cl_2→CH_2Cl_2:diethyl ether [3:1]) eluting first unreacted **1**, then **2** as a orange-red solid (0.44 g, 72%). Spectroscopic data was consistent with that reported previously.[14] ^{1}H NMR (400 MHz, $CDCl_3$): δ (ppm) 4.24 (pseudo-t, $J_{\alpha\beta}$ = 1.9 Hz, 2H, Cp–*H*), 4.30 (pseudo-t, $J_{\alpha\beta}$ = 1.9 Hz, 2H, Cp–*H*), 4.46 (pseudo-t, $J_{\alpha\beta}$ = ~1.8 Hz, 2H, Cp–*H*), 4.49 (pseudo-t, $J_{\alpha\beta}$ = 1.9 Hz, 2H, Cp–*H*), 7.26 (ddd, 1H, Py–H_m), 7.79 (dt, *J* = 7.9, 1.8 Hz, 1H, Py–H_p), 8.53 (dd, *J* = 4.8, 1.4 Hz, 1H, Py–H_o), 8.76 (d, *J* = 1.4 Hz, 1H, Py–$H_{o'}$). ^{13}C{^{1}H} NMR (100 MHz, $CDCl_3$): δ (ppm) 41.42 (Cp, *C*–I), 66.83 (Cp, *C*–C≡C), 71.01 (Cp, *C*–H), 72.32 (Cp, *C*–H), 74.30 (Cp, *C*–H), 76.56 (Cp, *C*–H), 83.73 (C≡C), 90.90 (C≡C), 121.15 (Py, *C*–C≡C), 123.15 (Py, *C*–H_m), 138.35 (Py, *C*–H_p), 148.21 (Py, *C*–H_o), 152.25 (Py, *C*–$H_{o'}$). IR (ATR): ν (cm^{-1}) 2209 (C≡C). HR-MS ES+: *m/z* 413.9430, ([M+H]$^+$ Calc.: 413.9442).

8.2.3 1,1'-Bis(3-pyridyl)ethynylferrocene (3)

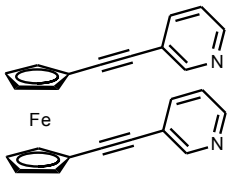

3

To a degassed (freeze-pump-thaw) solution of 1 (0.21 g, 0.480 mmol) in THF (1 mL) and DIPA (0.33 mL) was added 3-ethynylpyridine (0.153 g, 1.484 mmol), $PdCl_2(PPh_3)_2$ (0.007 g, 0.010 mmol) and CuI (0.004 g, 0.021 mmol) against N_2. After stirring at 80°C for 24 h, the mixture was cooled, solvent removed and the residue purified by column chromatography (alumina grade V; DCM:*n*-hexane [2:8→1:0]). Eluting as separate bands in the following order were **1**, **2** (0.076 g, 38% after recrystallization from CH_2Cl_2/*n*-hexane; typically contaminated with approximately 5% 3-pyridylethynylferrocene), and **3**. The latter was further purified by recrystallization (CH_2Cl_2/*n*-hexane) and isolated as an orange-red solid (0.043 g, 23%). Spectroscopic data was consistent with that reported previously.[15] ^{1}H NMR (400 MHz, $CDCl_3$): δ (ppm) 4.36 (pseudo-t, $J_{\alpha\beta}$ = ~1.8 Hz, 4H, Cp–*H*), 4.57 (pseudo-t, $J_{\alpha\beta}$ = 1.9 Hz, 4H, Cp–*H*), 7.14 (ddd, *J* = 7.7, 4.9 Hz, 2H, Py–H_m), 7.62 (dt, *J* = 7.9, 1.8 Hz, 2H, Py–H_p), 8.46 (dd, *J* = 4.8, 1.4 Hz, 2H, Py–H_o), 8.62 (d, *J* = 1.4 Hz, 2H, Py–$H_{o'}$). ^{13}C{^{1}H} NMR (100 MHz, $CDCl_3$): δ (ppm) 66.69 (Cp, *C*–C≡C), 71.20 (Cp, *C*–H), 73.19 (Cp, *C*–H), 83.68 (C≡C), 90.66 (C≡C), 121.04 (Py, *C*–C≡C), 123.05 (Py, *C*–H_m), 138.10 (Py, *C*–H_p), 147.99 (Py, *C*–H_o), 152.08 (Py, *C*–$H_{o'}$). IR (ATR): ν (cm^{-1}) 2207 (C≡C). HR-MS ES+: *m/z* 389.0746, ($[M+H]^+$ Calc.: 389.0741).

8.2.4 1-(3-Pyridyl)ethynyl-1'-(trimethylsilyl)ethynylferrocene (4)

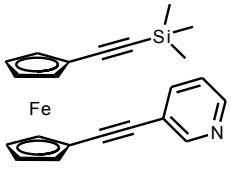

4

Trimethylsilylacetylene (0.05 mL, 0.354 mmol) and DIPA (1.3 mL) were added to a suspension of **2** (0.094 g, 0.228 mmol), $PdCl_2(PPh_3)_2$ (0.004 g, 0.006 mmol) and CuI (0.002 g, 0.011 mmol) in THF (4 mL). After stirring at 80°C for 24 h, the mixture was cooled, solvent removed and the residue purified by column chromatography (silica; CH_2Cl_2/diethyl ether [3:1]) to provide **4** as an orange-red solid (0.024 g, 27%). ^{1}H NMR (400 MHz, $CDCl_3$): δ (ppm) 0.20 (s, 9H, Si–CH_3), 4.28 (pseudo-t, $J_{\alpha\beta}$ = ~1.8 Hz, 2H, Cp–*H*), 4.31 (pseudo-t, $J_{\alpha\beta}$ = 1.9 Hz, 2H, Cp–*H*), 4.48 (pseudo-t, $J_{\alpha\beta}$ = 1.9 Hz, 2H, Cp–*H*), 4.51 (pseudo-t, $J_{\alpha\beta}$ = 1.9 Hz, 2H, Cp–*H*), 7.25 (ddd, 1H, Py–H_m), 7.76 (dt, *J* = 7.9, 1.7 Hz, 1H, Py–H_p), 8.52 (dd, *J* = 4.8, 1.3 Hz, 1H, Py–H_o), 8.72 (d, *J* = 1.2 Hz, 1H, Py–$H_{o'}$). ^{13}C{^{1}H} NMR (100 MHz, $CDCl_3$): δ (ppm) 0.30 (Si–CH_3), 65.72 (Cp, *C*–C≡C), 66.53 (Cp, *C*–C≡C), 71.25 (Cp, *C*–H), 71.88 (Cp, *C*–H), 73.56 (Cp, *C*–H), 73.66 (Cp, *C*–H),

83.08 (C≡C), 91.36 (C≡C), 91.70 (C≡C), 103.18 (C≡C), 121.22 (Py, *C*–C≡C), 123.13 (Py, *C*–H_m), 138.28 (Py, *C*–H_p), 148.14 (Py, *C*–H_o), 152.22 (Py, *C*–$H_{o'}$). IR (ATR): ν (cm^{-1}) 2151 (Si–*C*≡*C*), 2213 (Py–*C*≡*C*). HR-MS ES+: *m/z* 384.0860, ($[M+H]^+$ Calc.: 384.0871). (Found: C, 68.08; H, 5.46; N, 3.61. Calc. for $C_{22}H_{21}FeNSi$: C, 68.93; H, 5.52; N, 3.65%).

8.2.5 1-(3-Pyridyl)ethynyl-1'-[1-(phenyl-4-*tert*-butylsulfanyl)]ethynylferrocene (5)

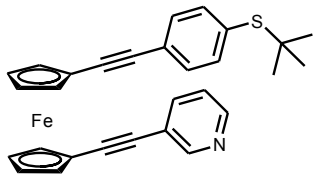

5

A solution of 1-(*tert*-butylsulfanyl)-4-ethynylbenzene (0.24 g, 1.26 mmol) in DIPA (4 mL) was sparged with nitrogen and added to a flask containing **2** (0.272 g, 0.659 mmol), $PdCl_2(PPh_3)_2$ (0.010 g, 0.014 mmol) and CuI (0.01 g, 0.052 mmol). Residual alkyne was washed into the reaction mixture with THF (3 x 4 mL) and the suspension stirred at 80°C for 21 h. After cooling and solvent removal the crude material was purified by column chromatography (silica; CH_2Cl_2/diethyl ether [8:2]) to provide **5** as an orange-red solid (0.115 g, 37%). ^{1}H NMR (400 MHz, $CDCl_3$): δ (ppm) 1.29 (s, 9H, C–CH_3), 4.34 (pseudo-t, 2H, Cp–*H*), 4.36 (pseudo-t, 2H, Cp–*H*), 4.56 (pseudo-t, 2H, Cp–*H*), 4.57 (pseudo-t, 2H, Cp–*H*), 7.15 (ddd, 1H, Py–H_m), 7.34 (d, *J* = 8.2 Hz, 2H, Ar–*H*), 7.40 (d, *J* = 8.2 Hz, 2H, Ar–*H*), 7.64 (dt, *J* = 7.8 Hz, 1H, Py–H_p), 8.49 (dd, 1H, Py–H_o), 8.69 (d, 1H, Py–$H_{o'}$). ^{13}C{^{1}H} NMR (100 MHz, $CDCl_3$): δ (ppm) 31.11 (C–*C*H_3), 46.51 (*C*–CH_3), 66.45 (Cp, *C*–C≡C), 67.23 (Cp, *C*–C≡C), 71.11 (Cp, *C*–H), 71.25 (Cp, *C*–H), 73.16 (Cp, *C*–H), 73.20 (Cp, *C*–H), 83.58 (C≡C), 86.50 (C≡C), 88.75 (C≡C), 90.91 (C≡C), 121.47 (br, Py, *C*–C≡C), 123.26 (br, Ar, *C*–C≡C), 124.21 (Py, *C*–H_m), 131.33 (Ar, *C*–H), 132.58 (Ar, *C*–S), 137.30 (Ar, *C*–H), 138.13 (Py, *C*–H_p), 147.94 (Py, *C*–H_o), 152.09 (Py, *C*–$H_{o'}$). IR (ATR): ν (cm^{-1}) 2207 (C≡C). HR-MS ES+: *m/z* 476.1139, ($[M+H]^+$ Calc.: 476.1135). (Found: C, 72.52; H, 5.26; N, 2.87. Calc. for $C_{29}H_{25}FeNS$: C, 73.26; H, 5.30; N, 2.95%).

8.2.6 (μ-3,5-Py)(C≡C–[fc]–I)$_2$ (6)

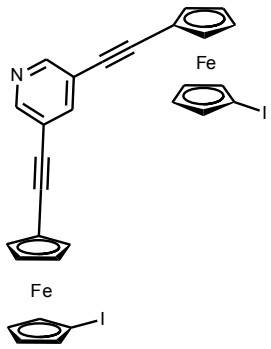

6

With an identical procedure to the synthesis of **2**, the crude product was produced using **1** (13.87 g, 31.54 mmol), 3,5-diethynylpyridine (0.398 g, 3.130 mmol), $PdCl_2(PPh_3)_2$ (0.137 g, 0.l95 mmol), CuI (0.097 g, 0.509 mmol) and DIPA (20 mL, 3 x 10 mL). This was purified via column chromotography (silica; *n*-hexane→CH_2Cl_2), first eluting unreacted **1**. Recrystallisation (CH_2Cl_2/*n*-hexane) and drying *in vacuo* provided the pure material as an orange-red solid (1.00 g, 43%). ^{1}H NMR (400 MHz, $CDCl_3$): δ (ppm) 4.25 (pseudo-t, $J_{\alpha\beta}$ = ~1.8 Hz, 4H, Cp–*H*), 4.31 (pseudo-t, $J_{\alpha\beta}$ = 1.8 Hz, 4H, Cp–*H*), 4.47 (pseudo-t, $J_{\alpha\beta}$ = 1.9 Hz, 4H, Cp–*H*), 4.50 (pseudo-t, $J_{\alpha\beta}$ = 1.8 Hz, 4H, Cp–*H*), 7.90 (t, *J* = 2 Hz, 1H, Py–H_p), 8.64 (d, *J* = 2 Hz, 1H, Py–H_o). ^{13}C{^{1}H} NMR (100 MHz, $CDCl_3$): δ (ppm) 41.48 (Cp, *C*–I), 66.60 (Cp, *C*–C≡C), 71.05 (Cp, *C*–H), 72.43 (Cp, *C*–H), 74.38 (Cp, *C*–H), 76.62 (Cp, *C*–H), 83.18 (C≡C), 91.63 (C≡C), 120.98 (Py, *C*–C≡C), 140.23 (Py, *C*–H_p), 150.35 (Py, *C*–H_o). MS ES+: *m/z* 748, ([M+H]$^+$ Calc.: 748). IR (ATR): ν (cm^{-1}) 2215 (Py–*C*≡*C*). (Found: C, 46.48; H, 2.54; N, 1.64. Calc. for $C_{29}H_{19}Fe_2I_2N$: C, 46.63; H, 2.56; N, 1.88%).

8.2.7 (μ-3,5-Py–C≡C–C≡C–3,5-Py)(C≡C–[fc]–I)$_2$ (7)

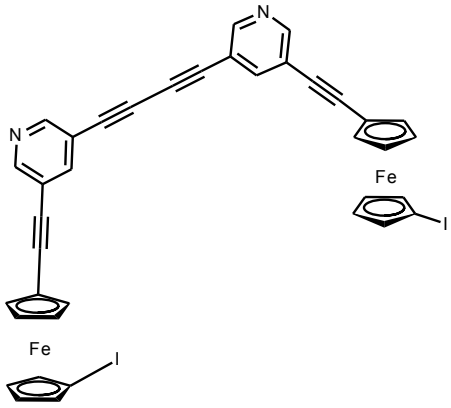

7

Combined in air, a mixture of **1** (2.39 g, 5.43 mmol), 3,5-diethynylpyridine (0.068 g, 0.535 mmol), $PdCl_2(PPh_3)_2$ (0.009 g, 0.013 mmol), and CuI (0.006 g, 0.032 mmol) was placed under an atmosphere of nitrogen and DIPA (10 mL) added After stirring at 90°C for 24 h, the suspension was cooled, solvent removed, and the crude residue purified by column chromatography (silica; *n*-hexane→CH_2Cl_2). This eluted unreacted **1**, **6**, and then the title product which was isolated as a red-orange solid (0.001 g, <1%) after recrystallisation (CH_2Cl_2/*n*-hexane) and drying *in vacuo*. ^{1}H NMR (400 MHz, $CDCl_3$): δ (ppm) 4.25 (pseudo-t, $J_{\alpha\beta}$ = ~1.8 Hz, 4H, Cp–*H*), 4.32 (pseudo-t, $J_{\alpha\beta}$ = 1.9 Hz, 4H, Cp–*H*), 4.47 (pseudo-t, $J_{\alpha\beta}$ = 1.9 Hz, 4H, Cp–*H*), 4.50 (pseudo-t, $J_{\alpha\beta}$ = 1.9 Hz, 4H, Cp–*H*), 7.92 (t, *J* = 2 Hz,

2H, Py–H_p), 8.67 (d, J = 1.7 Hz, 2H, Py–H_o), 8.71 (d, J = 1.7 Hz, 2H, Py–$H_{o'}$). $^{13}C\{^1H\}$ NMR (100 MHz, $CDCl_3$): δ (ppm) 71.05 (Cp, *C*–H), 72.50 (Cp, *C*–H), 74.45 (Cp, *C*–H), 76.67 (Cp, *C*–H). IR (ATR): ν (cm^{-1}) 2216 (Py–*C*≡*C*). HR-MS ES+: *m/z* 872.8698, ($[M+H]^+$ Calc.: 872.8650).

8.2.8 (*μ*-3,5-Py){(C≡C–[fc]–C≡C–*m*–Py)(C≡C–[fc]–I)} (8) and (*μ*-3,5-Py)(C≡C–[fc]–C≡C–*m*–Py)$_2$ (9)

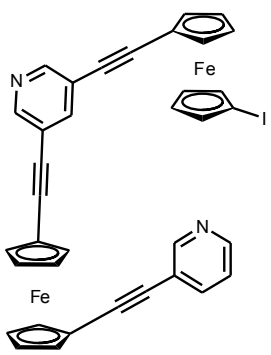

8

THF (6 mL) and DIPA (2 mL) were added to a flask containing **6** (0.106 g, 0.142 mmol), 3-ethynylpyridine (0.045 g, 0.436 mmol), $PdCl_2(PPh_3)_2$ (0.004 g, 0.006 mmol) and CuI (0.002 g, 0.011 mmol). After stirring at 80°C for 24 h, the suspension was cooled, solvent removed, and the crude residue purified by column chromatography (alumina grade V; petroleum ether/CH_2Cl_2 [1:1→0:1]). Following elution of unreacted **6**, a second orange fraction was collected which provided **8** (contaminated with approximately 20% of the hydrodehalogenated analogue) as an orange-red solid (0.034 g, 26%) after recrystallisation (CH_2Cl_2/*n*-hexane). ^1H NMR (400 MHz, $CDCl_3$): δ (ppm) 4.25 (pseudo-t, $J_{αβ}$ = ~1.8 Hz, 2H, Cp–*H*), 4.31 (pseudo-t, $J_{αβ}$ = 1.8 Hz, 2H, Cp–*H*), 4.37 (m, 4H, Cp–*H*), 4.47 (pseudo-t, $J_{αβ}$ = 1.9 Hz, 2H, Cp–*H*), 4.50 (pseudo-t, $J_{αβ}$ = 1.9 Hz, 2H, Cp–*H*), 4.58 (m, 4H, Cp–*H*), 7.17 (ddd, J = 7.8, 4.9 Hz, 1H, 3-Py–H_m), 7.64 (m, 1H, 3-Py–H_p), 7.74 (t, J = 2 Hz, 1H, 3,5-Py–H_p), 8.48 (m, 1H, 3-Py–H_o), 8.52 (d, J = 2 Hz, 1H, 3,5-Py–H_o), 8.58 (d, J = 2 Hz, 1H, 3,5-Py–$H_{o'}$), 8.65 (m, 1H, 3-Py–$H_{o'}$). $^{13}C\{^1H\}$ NMR (100 MHz, $CDCl_3$): δ (ppm) 41.43 (Cp, *C*–I), 66.37 (Cp, *C*–C≡C), 66.63 (Cp, *C*–C≡C), 66.70 (Cp, *C*–C≡C), 71.06 (Cp, *C*–H), 71.29 (Cp, *C*–H), 71.37 (Cp, *C*–H), 72.44 (Cp, *C*–H), 73.23 (Cp, *C*–H), 73.26 (Cp, *C*–H), 74.36 (Cp, *C*–H), 76.61 (Cp, *C*–H), 83.07 (C≡C), 83.13 (C≡C), 83.77 (C≡C), 90.62 (C≡C), 91.40 (C≡C), 91.59 (C≡C), 120.70 (Py, *C*–C≡C), 120.99 (Py, *C*–C≡C), 123.09 (3-Py, *C*–H_m), 138.07 (3-Py, *C*–H_p), 140.01 (3,5-Py, *C*–H_p), 148.13 (3-Py, *C*–H_o), 150.15 (3,5-Py, *C*–H_o), 152.11 (3-Py, *C*–$H_{o'}$). IR (ATR): ν (cm^{-1}) 2211 (C≡C). HR-MS ES+: *m/z* 722.9684 ($[M+H]^+$ Calc.: 722.9683).

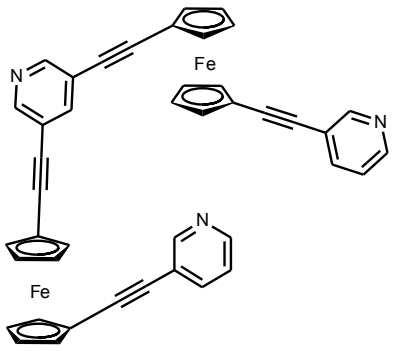

9

From a third orange band, **9** was isolated as an orange-red solid (0.015 g, 15%) after recrystallisation (CH_2Cl_2/*n*-hexane). ^{1}H NMR (400 MHz, $CDCl_3$): δ (ppm) 4.37 (m, 8H, Cp–*H*), 4.58 (m, 8H, Cp–*H*), 7.17 (ddd, *J* = 7.7, 4.9 Hz, 2H, 3-Py–H_m), 7.60 (t, *J* = 1.8 Hz, 1H, 3,5-Py–H_p), 7.63 (dt, *J* = 7.8, 1.6 Hz, 2H, 3-Py–H_p), 8.47 (m, 4H, overlapping 3-Py–H_o and 3,5-Py–H_o), 8.65 (d, 2H, 3-Py–$H_{o'}$). ^{13}C{^{1}H} NMR (100 MHz, $CDCl_3$): δ (ppm) 66.35 (Cp, *C*–C≡C), 66.64 (Cp, *C*–C≡C), 71.35 (Cp, *C*–H), 71.42 (Cp, *C*–H), 73.24 (Cp, *C*–H), 73.27 (Cp, *C*–H), 82.99 (C≡C), 83.70 (C≡C), 90.71 (C≡C), 91.45 (C≡C), 120.60 (Py, *C*–C≡C), 120.99 (Py, *C*–C≡C), 123.08 (3-Py, *C*–H_m), 138.13 (3-Py, *C*–H_p), 139.87 (3,5-Py, *C*–H_p), 148.11 (3-Py, *C*–H_o), 149.95 (3,5-Py, *C*–H_o), 152.09 (3-Py, *C*–$H_{o'}$). IR (ATR): ν (cm^{-1}) 2210 (C≡C). HR-MS ES+: *m/z* 698.0987, ($[M+H]^+$ Calc.: 698.0982).

8.2.9 (*μ*-3,5-Py)(C≡C–[fc]–C≡C–$SiMe_3$)$_2$ (10)

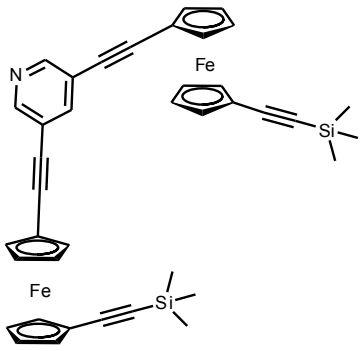

10

With an identical procedure to the synthesis of **4**, the crude product was produced using **6** (0.95 g, 1.272 mmol), trimethylsilylacetylene (0.72 mL, 5.09 mmol) $PdCl_2(PPh_3)_2$ (0.040 g, 0.057 mmol), CuI (0.017 g, 0.090 mmol), DIPA (20 mL) and THF (40 mL). This was purified by column chromatography (silica; CH_2Cl_2) providing **10** as an orange solid (0.25 g, 29%) of ~85% purity. A sample of analytical purity (0.15 g, 17%) could be isolated following further column chromatography (alumina grade V, CH_2Cl_2/*n*-hexane [1:1]) and careful selection of fractions using ^{1}H NMR spectroscopy. ^{1}H NMR (400 MHz, $CDCl_3$): δ (ppm) 0.21 (s, 18H, Si–CH_3), 4.28 (pseudo-t, $J_{\alpha\beta}$ = 1.8 Hz, 4H, Cp–*H*), 4.31 (pseudo-t, $J_{\alpha\beta}$ = ~1.8 Hz, 4H, Cp–*H*), 4.48 (pseudo-t, $J_{\alpha\beta}$ = 1.8 Hz, 4H, Cp–*H*), 4.51 (pseudo-t, $J_{\alpha\beta}$ = ~1.8 Hz, 4H, Cp–*H*), 7.85 (t, *J* = 2 Hz, 1H, Py–H_p), 8.61 (d, *J* = 2 Hz, 2H, Py–H_o). ^{13}C{^{1}H} NMR (100 MHz, $CDCl_3$): δ (ppm) 0.34 (Si–CH_3), 65.47 (Cp, *C*–C≡C), 66.61 (Cp, *C*–C≡C), 71.30 (Cp, *C*–H), 72.02 (Cp, *C*–H), 73.61 (Cp, *C*–H), 73.68 (Cp, *C*–H), 82.46 (C≡C), 91.79 (C≡C), 93.04 (C≡C), 103.13 (C≡C), 120.79 (Py, *C*–C≡C), 140.20 (Py, *C*–H_p), 150.16 (Py, *C*–H_o). IR (ATR): ν (cm^{-1}) 2150 (Si–*C*≡*C*), 2219 (Py–*C*≡*C*). HR-MS ES+: *m/z* 688.1240

([M+H]$^+$ Calc.: 688.1242). (Found: C, 68.07; H, 5.34; N, 2.07. Calc. for $C_{39}H_{37}Fe_2NSi_2$: C, 68.13; H, 5.42; N, 2.04%). The mono-substituted compound was not isolated/observed.

8.2.10 (μ-3,5-Py){(C≡C–[fc]–C≡C–*p*-C_6H_4–S^{t}Bu)(C≡C–[fc]–I) (11) and (μ-3,5-Py)(C≡C–[fc]–C≡C–*p*-C_6H_4–S^{t}Bu)$_2$ (12)

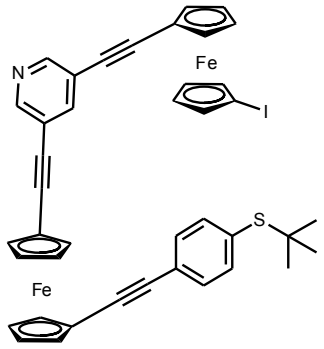

11

With an identical procedure to the synthesis of **5**, the crude product was obtained using **6** (0.461 g, 0.617 mmol), 1-(*tert*-butylsulfanyl)-4-ethynylbenzene (0.35 g, 1.84 mmol), $PdCl_2(PPh_3)_2$ (0.015 g, 0.021 mmol) CuI (0.010 g, 0.053 mmol), DIPA (8 mL) and THF (3 x 8 mL). This was purified by column chromatography (alumina grade V; CH_2Cl_2/*n*-hexane [7:3→1:0]), eluting unreacted **6**, then **11** (the first of two closely eluting bands) as an orange solid (0.14 g, 28%). ^{1}H NMR (400 MHz, $CDCl_3$): δ (ppm) 1.28 (s, 9H, C–C*H*$_3$), 4.25 (pseudo-t, $J_{\alpha\beta}$ = ~1.8 Hz, 2H, Cp–*H*), 4.31 (pseudo-t, $J_{\alpha\beta}$ = 1.8 Hz, 2H, Cp–*H*), 4.35 (pseudo-t, $J_{\alpha\beta}$ = 1.8 Hz, 2H, Cp–*H*), 4.37 (pseudo-t, $J_{\alpha\beta}$ = 1.8 Hz, 2H, Cp–*H*), 4.47 (pseudo-t, $J_{\alpha\beta}$ = ~1.8 Hz, 2H, Cp–*H*), 4.50 (pseudo-t, $J_{\alpha\beta}$ = 1.9 Hz, 2H, Cp–*H*), 4.57 (m, 4H, Cp–*H*), 7.35 (d, *J* = 8.2 Hz, 2H, Ar–*H*), 7.42 (d, *J* = 8.2 Hz, 2H, Ar–*H*), 7.79 (t, 1H, Py–*H*), 8.57 (br m, 2H, Py–*H*). ^{13}C{^{1}H} NMR (100 MHz, $CDCl_3$) δ (ppm) 31.14 (C–*C*H$_3$), 41.40 (Cp, *C*–I), 46.48 (*C*–CH$_3$), 66.17 (Cp, *C*–C≡C), 66.63 (Cp, *C*–C≡C), 67.30 (Cp, *C*–C≡C), 71.08 (Cp, *C*–H), 71.15 (Cp, *C*–H), 71.37 (Cp, *C*–H), 72.44 (Cp, *C*–H), 73.16 (Cp, *C*–H), 73.25 (Cp, *C*–H), 74.37 (Cp, *C*–H), 76.59 (Cp, *C*–H), 82.96 (C≡C), 83.13 (C≡C), 86.61 (C≡C), 88.63 (C≡C), 91.53 (C≡C), 91.58 (C≡C), 120.65 (Py, *C*–C≡C), 124.12 (Ar, *C*–C≡C), 131.30 (Ar, *C*–H), 132.69 (Ar, *C*–S), 137.31 (Ar, *C*–H), 140.07 (Py, *C*–H$_p$), 150.13 (Py, *C*–H$_o$). IR (ATR): ν (cm^{-1}) 2218 (Ar–*C*≡*C*). HR-MS ES+: *m/z* 810.0077 ([M+H]$^+$ Calc.: 810.0077).

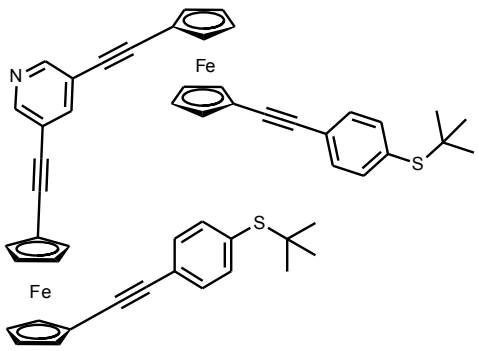

12

Careful selection of fractions from the third band (using ^{1}H NMR spectroscopy) provided **12** as an orange-red solid (0.12 g, 22%). ^{1}H NMR (400 MHz, $CDCl_3$): δ (ppm) 1.28 (s, 18H, C–C*H*$_3$), 4.36 (m, 8H, Cp–*H*), 4.57 (m, 8H, Cp–*H*), 7.36 (d, *J* = 8.2 Hz, 2H, Ar–*H*), 7.43 (d, *J* = 8.2 Hz, 2H, Ar–*H*), 7.70 (t, 1H, Py–*H*$_p$), 8.50 (d, 2H, Py–*H*$_o$). ^{13}C{^{1}H} NMR (100 MHz, $CDCl_3$): δ (ppm) 31.14 (C–

*C*H$_3$), 46.49 (*C*–CH$_3$), 66.16 (Cp, *C*–C≡C), 67.21 (Cp, *C*–C≡C), 71.25 (Cp, *C*–H), 71.44 (Cp, *C*–H), 73.19 (Cp, *C*–H), 73.28 (Cp, *C*–H), 82.90 (C≡C), 86.55 (C≡C), 88.72 (C≡C), 91.58 (C≡C), 120.62 (Py, *C*–C≡C), 124.15 (Ar, *C*–C≡C), 131.32 (Ar, *C*–H), 132.73 (Ar, *C*–S), 137.33 (Ar, *C*–H), 140.01 (Py, *C*–H$_p$), 150.01 (Py, *C*–H$_o$). IR (ATR): ν (cm^{-1}) 2218 (Ar–*C*≡*C*). HR-MS ES+: *m/z* 872.1795 ([M+H]$^+$ Calc.: 872.1770).

8.2.11 Evidence for a ferrocene macrocycle (13)

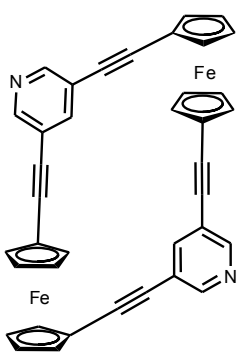

13

Representative procedure: DIPA (45 mL) and THF (65 mL) were added to a flask containing **6** (0.53 g, 0.710 mmol), 3,5-diethynylpyridine (0.105 g, 0.826 mmol) $PdCl_2(PPh_3)_2$ (0.023 g, 0.033 mmol) and CuI (0.005 g, 0.026 mmol). After stirring at 80°C for 48 h the reaction mixture was dried *in vacuo*, extracted with CH_2Cl_2, and the crude material purified using column chromatography (silica; CH_2Cl_2/diethyl ether [0:1→6:4]). Following elution of unreacted **6** and various coloured bands of unknown composition, **13** was identified in trace quantities. *Band eluting immediately prior to **13** (unknown composition):* ^{1}H NMR (400 MHz, $CDCl_3$): δ (ppm) 4.21 (pseudo-t, $J_{\alpha\beta}$ = ~1.8 Hz, 4H, Cp–*H*), 4.26 (pseudo-t, $J_{\alpha\beta}$ = 1.9 Hz, 4H, Cp–*H*), 4.35 (m, 8H, Cp–*H*), 4.43 (pseudo-t, $J_{\alpha\beta}$ = 1.9 Hz, 4H, Cp–*H*), 4.46 (pseudo-t, $J_{\alpha\beta}$ = 1.9 Hz, 4H, Cp–*H*), 4.45 (pseudo-t, $J_{\alpha\beta}$ = 1.9 Hz, 8H, Cp–*H*), 7.54 (t, *J* = 2.1 Hz, 1H, Py–*H*), 7.71 (t, *J* = 2.2, 2 Hz, 2H, Py–*H*), 8.47 (d, *J* = 2 Hz, 2H, Py–*H*), 8.51 (d, *J* = 2 Hz, 2H, Py–*H*), 8.57 (d, *J* = 2 Hz, 2H, Py–*H*). HR-MS ESI+: *m/z* 722.9742, 779.0026. ***13***: ^{1}H NMR (400 MHz, $CDCl_3$): δ (ppm) 4.34 (pseudo-t, $J_{\alpha\beta}$ = 1.9 Hz, 8H, Cp–*H*), 4.51 (pseudo-t, $J_{\alpha\beta}$ = 1.9 Hz, 8H, Cp–*H*), 7.43 (t, *J* = 4 Hz, 2H, Py–*H*$_p$), 8.29 (d, *J* = 2 Hz, 4H, Py–*H*$_o$). HR-MS ES+: *m/z* 619.0591, ([M+H]$^+$ Calc.: 619.0560). No significant improvements to the yield or purity of the title compound were observed despite multiple attempts using this method, varying reaction concentration or trying different column purification procedures (*e.g.* silica, alumina grades II/V, CH_2Cl_2/diethyl ether, CH_2Cl_2/MeOH).

8.2.12 An 'open' ferrocene macrocycle (14)

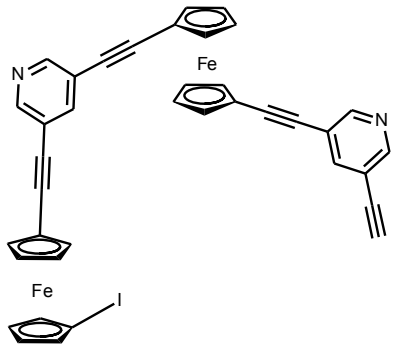

14

A solution of **6** (0.50 g, 0.669 mmol) and 3,5-diethynylpyridine (0.088 g, 0.692 mmol) in THF (35 mL) was added dropwise over 24 h to a mixture of $PdCl_2(PPh_3)_2$ (0.020 g, 0.028 mmol) and CuI (0.050 g, 0.026 mmol) in DIPA (10 mL) stirred at 90°C. After a further 24 h at 90°C the reaction was cooled and solvent removed, whereby the residue extracted with CH_2Cl_2 and filtered (Celite). The crude mixture was purified by column chromatography (silica; CH_2Cl_2/MeOH [1:0→99:1]), eluting unreacted **6**, various coloured bands of unknown composition, and crude **14**. The latter further purified by column chromatography (silica; CH_2Cl_2/diethyl ether [9:1]), recrystallized (CH_2Cl_2/*n*-hexane) and dried *in vacuo* to provide **14** as a bright orange solid (~10 mg, 2%) of purity sufficient for spectroscopic characterisation. ^{1}H NMR (400 MHz, $CDCl_3$): δ (ppm) 3.21 (s, 1H, C≡C–*H*), 4.25 (pseudo-t, $J_{\alpha\beta}$ = ~1.8 Hz, 2H, Cp–*H*), 4.31 (pseudo-t, $J_{\alpha\beta}$ = 1.9 Hz, 2H, Cp–*H*), 4.38 (m, 4H, Cp–*H*), 4.47 (pseudo-t, $J_{\alpha\beta}$ = ~1.8 Hz, 2H, Cp–*H*), 4.50 (pseudo-t, $J_{\alpha\beta}$ = 1.9 Hz, 2H, Cp–*H*), 4.58 (m, 4H, Cp–*H*), 7.71 (t, *J* = ~2 Hz, 1H, Py–H_p), 7.73 (t, *J* = 2 Hz, 1H, Py–H_p), 8.52 (d, *J* = 2 Hz, 1H, Py–H_o), 8.57 (d, *J* = 2 Hz, 2H, Py–H_o), 8.59 (d, *J* = 2 Hz, 2H, Py–H_o). ^{13}C{^{1}H} NMR (100 MHz, $CDCl_3$): δ (ppm) 71.09 (Cp, *C*–H), 71.40 (Cp, *C*–H), 71.44 (Cp, *C*–H), 72.45 (Cp, *C*–H), 73.25 (Cp, *C*–H), 74.37 (Cp, *C*–H), 76.60 (Cp, *C*–H), 81.33 (C≡*C*–H), 139.94 (Py, *C*–H_p), 140.87 (Py, *C*–H_p), 150.14 (Py, *C*–H_o), 150.31 (Py, *C*–H_o), 150.86 (Py, *C*–H_o), 151.11 (Py, *C*–H_o). IR (ATR): ν (cm^{-1}) 2216 (*C*≡*C*), 3287 (C≡*C*–*H*). HR-MS ES+: *m/z* 746.9688 ($[M+H]^+$ Calc.: 746.9683).

8.3 COMPOUNDS SYNTHESISED IN CHAPTER 3

8.3.1 Sonogashira cross-coupling reactions with phenylacetylene

Typical procedure using $PdCl_2(PPh_3)_2$ catalyst. THF and the relevant amine were added to a flask containing **1** (0.51 g, 1.16 mmol), $PdCl_2(PPh_3)_2$ (0.050 g, 0.071 mmol) and CuI (0.014 g, 0.073 mmol). The mixture was sparged with nitrogen, whereby phenylacetylene (0.51 mL, 4.64 mmol) was added and the resulting black suspension stirred at the appropriate temperature for 20 h. The mixture was subsequently opened to air and reagent grade CH_2Cl_2 (5 mL) was added

(NOTE: large solvent volumes were evaporated to dryness first). An aliquot (~1 mL) was taken, eluted through a silica plug using CH_2Cl_2, dried, and analyzed by ^{1}H NMR *(vida infra)*.

Typical procedure using $PdCl_2(MeCN)_2$ catalyst. THF (0.75 mL) was added to a flask containing **1** (0.25 g, 0.57 mmol), $PdCl_2(MeCN)_2$ (0.009 g, 0.035 mmol) and copper iodide (0.007 g, 0.037 mmol). The mixture was sparged with nitrogen, whereby phosphine ligand (0.070 mmol), freshly distilled and deoxygenated DIPA (0.25 mL), and phenylacetylene (0.25 mL, 2.27 mmol) were added (in that order). The resulting black suspension was stirred at the appropriate temperature for 20 h, after which time the mixture was opened to air and reagent grade CH_2Cl_2 (5 mL) was added (NOTE: large solvent volumes were evaporated to dryness first). An aliquot (~1 mL) was taken, eluted through a silica plug using CH_2Cl_2, dried, and analyzed by ^{1}H NMR *(vida infra)*.

Partial isolation of reaction products by column chromatography. Column chromatography (silica; CH_2Cl_2/*n*-hexane [1:4]) of the dried residue yielded several bands of co-eluting ferrocene-containing components. These were identified by high resolution mass spectrometry and characteristic cyclopentadienyl ^{1}H NMR resonances *(Figure 8-1)*.[16] Band 1: Unreacted **1** (**A**) and iodoferrocene (**B**). ^{1}H NMR (400 MHz, $CDCl_3$): δ (ppm) 4.15 (pseudo-t, $J_{\alpha\beta}$ = ~1.8 Hz, 2H, **B**), 4.18 (pseudo-t, $J_{\alpha\beta}$ = 1.8 Hz, 4H, **A**), 4.19 (s, 5H, **B**), 4.37 (pseudo-t, $J_{\alpha\beta}$ = ~1.8 Hz, 4H, **A**), 4.41 (pseudo-t, $J_{\alpha\beta}$ = 1.7 Hz, 2H, **B**). HR-MS ES+: *m/z* 311.9113 ($[M]^+$ Calc.: 311.9098, **B**), 437.8072 ($[M]^+$ Calc.: 437.8065, **A**). Band 2: (phenylethynyl)ferrocene (**C**) and 1-iodo-1'-(phenylethynyl)ferrocene (**D**). ^{1}H NMR (400 MHz, $CDCl_3$): δ (ppm) 4.23 (pseudo-t, $J_{\alpha\beta}$ = ~1.8 Hz, 2H, **D**), 4.25 (s, 5H, **C**), 4.26 (pseudo-t, $J_{\alpha\beta}$ = 1.9 Hz, 2H, **D**), 4.45 (pseudo-t, $J_{\alpha\beta}$ = ~1.8 Hz, 2H, **D**), 4.47 (pseudo-t, $J_{\alpha\beta}$ = 1.8 Hz, 2H, **D**), 4.50 (pseudo-t, $J_{\alpha\beta}$ = 1.9 Hz, 2H, **C**) (NOTE: a pseudo-t, 2H for **C** is obscured by overlapping resonances for **D**). HR-MS ES+: *m/z* 286.0446 ($[M]^+$ Calc.: 286.0445, **C**), 412.9482 ($[M+H]^+$ Calc.: 412.9490, **D**). Band 3: 1,1'-bis(phenylethynyl)ferrocene (**E**). ^{1}H NMR (400 MHz, $CDCl_3$): δ (ppm) 4.32 (pseudo-t, $J_{\alpha\beta}$ = 1.8 Hz, 4H, **E**), 4.55 (pseudo-t, $J_{\alpha\beta}$ = 1.9 Hz, 4H, **E**). HR-MS ES+: *m/z* 387.0821 ($[M+H]^+$ Calc.: 387.0836, **E**).

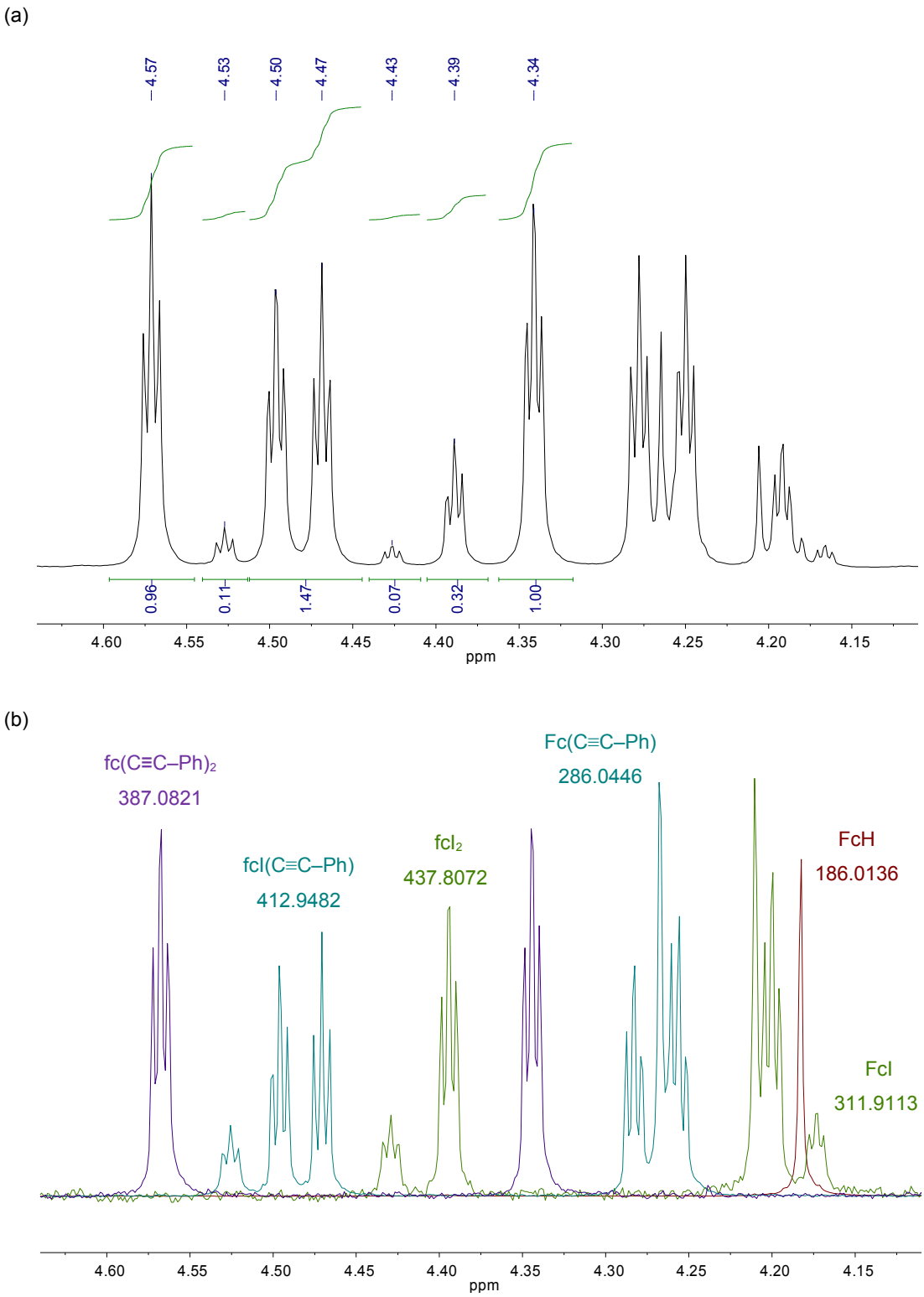

Figure 8-1. A comparison of the ^{1}H NMR spectra of (a) the crude mixture resulting from a typical catalysis run, and (b) the superposition of isolated and partially isolated components from the mixture. Accurate mass spectroscopic analyses support ^{1}H NMR resonance assignments.

8.3.2 Method of analyzing product composition

The % composition of individual species in the mixture was obtained from the ratio of the integral value representing a single proton intensity for that component (representative of the number of moles of that component) and an integral value representing the sum of all the single proton intensities (representative of the total number of moles) for all species (eqn (8.1)). A worked example for the spectrum in *Figure 8-1a* is given in *Table 8-1* (sum of single proton intensities = 0.778).

$$\% \text{ component} = 100 \times \frac{\text{single proton intensity of component}}{\text{sum of single proton intensities for all components}} \quad (8.1)$$

Table 8-1. A worked example showing % composition of components calculated from the ^{1}H NMR spectrum in *Figure 8-1a*.

component	integrated resonance	division factor	single proton intensity	% composition
FcI	4.43 (0.07)	2	0.035	4
fcI_2	4.39 (0.32)	4	0.080	10
Fc(C≡C–Ph)	4.53 (0.11)	2	0.055	7
fcI(C≡C–Ph)	4.47, 4.50 (1.47)	4	0.368	47
$fc(C{\equiv}C{-}Ph)_2$	4.57 (0.96)	4	0.240	31

8.3.3 Cyclization product of 4-ethynylphenylthioacetate (15)

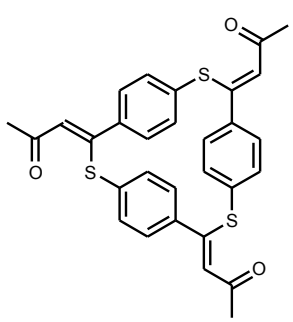

15

A solution of 4-ethynylphenylthioacetate (0.21 g, 1.19 mmol) in THF (0.4 mL) and DIPEA (0.2 mL) was degassed (freeze-pump-thaw). $PdCl_2(PPh_3)_2$ (0.022 g, 0.031 mmol) and CuI (0.007 g, 0.037 mmol) were added against nitrogen and the mixture stirred at 55°C for 24 h. After cooling and solvent removal, the crude material was purified by column chromatography (silica; CH_2Cl_2/diethyl ether [19:1]) and dried *in vacuo* to provide **15** as a bright yellow solid (0.05 g, 24%). Crystals suitable for X-ray diffraction were grown by diffusion of diethyl ether into a CH_2Cl_2 solution. ^{1}H NMR (400 MHz, CD_2Cl_2): δ (ppm) 2.28 (s, 9H, C*H*$_3$), 6.42 (s, 3H, C=C*H*), 7.03 (s, 12H, Ar–*H*).

$^{13}C\{^{1}H\}$ NMR (100 MHz, CD_2Cl_2): δ (ppm) 30.84 (*C*H_3), 125.87 (C=*C*H), 129.59 (Ar, *C*–H), 133.81 (Ar, *C*–H), 134.27 (Ar, *C*–R), 138.76 (Ar, *C*–R), 155.83 (*C*=CH), 196.03 (*C*=O). IR (ATR): ν (cm^{-1}) 1659 (C=O). UV-vis (CH_2Cl_2): λ_{max}/nm (ε/M^{-1} cm^{-1}) 303sh (31554), 325 (47443), 363sh (11759). HR-MS ES+: *m/z* 529.0955, ($[M+H]^+$ Calc.: 529.0966). (Found: C, 68.11; H, 4.56. Calc. for $C_{30}H_{24}O_3S_3$: C, 68.15; H, 4.58%).

8.3.4 Mixture of isomers (16-*Z* and 16-*E*)

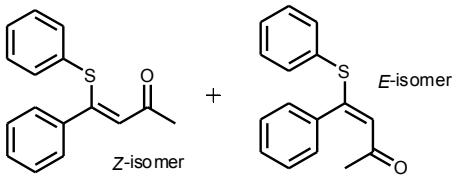

16

A mixture of THF (1 mL), DIPEA (0.5 mL), $PdCl_2(PPh_3)_2$ (0.070 g, 0.100 mmol) and CuI (0.019 g, 0.100 mmol) was sparged with nitrogen. S-phenylthioacetate (0.44 mL, 3.25 mmol) and phenylacetylene (0.40 mL, 3.64 mmol) were added after 5 and 10 minutes, respectively. Upon addition of the latter, the suspension immediately changed colour from yellow to dark red. After stirring at 55°C for 24 h, the mixture was cooled, solvent removed, and the residue purified by column chromatography (silica; ethyl acetate/petroleum benzine [1:9]) to provide **16** (a mixture of *Z/E* isomers [81/19]) as a soft yellow solid (0.66 g, 80%). Spectroscopic data was consistent with that reported previously.[17] ^{1}H NMR (400 MHz, $CDCl_3$): δ (ppm) 1.72 (s, 3H, C*H*$_3$, *E*), 2.35 (s, 3H, C*H*$_3$, *Z*), 5.71 (s, 1H, C=C*H*, *E*), 6.49 (s, 1H, C=C*H*, *Z*), 6.95-7.60 (m, 10H, Ph–*H*). $^{13}C\{^{1}H\}$ NMR (100 MHz, $CDCl_3$): δ (ppm) 30.25 (*C*H_3, *E*), 30.86 (*C*H_3, *Z*), 123.12 (C=*C*H, *E*), 123.54 (C=*C*H, *Z*), 127.85 (Ph), 127.96 (Ph), 128.46 (Ph), 128.62 (Ph), 128.92 (Ph), 129.01 (Ph), 129.68 (Ph), 129.97 (Ph), 130.10 (Ph), 132.63 (Ph), 134.31 (Ph), 135.52 (Ph), 138.40 (Ph), 159.34 (*C*=CH), 196.40 (*C*=O). IR (ATR): ν (cm^{-1}) 1646 (C=O), 1659 (C=O). HR-MS ES+: *m/z* 255.0844, ($[M+H]^+$ Calc.: 255.0844). (Found: C, 75.63; H, 5.58. Calc. for $C_{16}H_{14}OS$: C, 75.55; H, 5.55%).

8.4 COMPOUNDS SYNTHESISED IN CHAPTER 4

8.4.1 *Trans*-Ru(dppe)$_2$(C≡C–C$_5$H$_5$N)$_2$ (17)

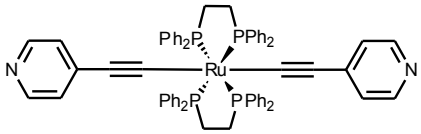

17

A mixture of 4-ethynylpyridine (0.058 g, 0.562 mmol), *cis*-$RuCl_2(dppe)_2$ (0.168 g, 0.173 mmol) $NaPF_6$ (0.117 g, 0.697 mmol) and Et_3N (0.15 mL, 0.826 mmol) in CH_2Cl_2 (5 mL) was stirred at room temperature for 3 days. The resulting pink suspension was dried *in vacuo* and filtered through an alumina grade II plug in CH_2Cl_2/MeOH (95:5). The crude product was further purified by column chromatography (alumina grade V; CH_2Cl_2), the eluting yellow band recrystallized (CH_2Cl_2/*n*-hexane) and dried *in vacuo* to yield **17** as a bright yellow solid (0.13 g, 68%). Crystals suitable for X-ray diffraction were grown by vapour diffusion of diethyl ether into a CH_2Cl_2 solution. ^{1}H NMR (400 MHz, $CDCl_3$): δ (ppm) 2.62 (br s, 8H, CH_2), 6.52 (dd, J = 4.6, ~1.5 Hz, 4H, Py–H_m), 6.97 (t, J = 7.6 Hz, 16H, Ph–H_m), 7.19 (t, J = 7.4 Hz, 8H, Ph–H_p), 7.44 (br m, 16H, Ph–H_o), 8.28 (d, J = 4.5, 1.5 Hz, 4H, Py–H_o). ^{31}P{^{1}H} NMR (162 MHz, $CDCl_3$): δ (ppm) 53.23 (s, *P*Ph$_2$). ^{13}C{^{1}H} NMR (100 MHz, $CDCl_3$): 31.45 (m, $|^1J_{CP} + {}^3J_{CP}|$ = 12 Hz, *C*H$_2$), 116.02 (Ru–C≡*C*), 124.73 (Py, *C*–H$_m$), 127.35 (Ph, *C*–H$_m$), 129.10 (Ph, *C*–H$_p$), 134.13 (Ph, *C*–H$_o$), 136.43 (quint., $^2J_{CP}$ = 10 Hz, Ru–*C*≡C–), 137.36 (Ar, *C*–R), 148.99 (Py, *C*–H$_o$). IR (ATR): ν (cm^{-1}) 2054 (C≡C). HR-MS ES+: *m/z* 1103.2539, ([M+H]$^+$ Calc.: 1103.2516). (Found: C, 71.49; H, 5.17; N, 2.57. Calc. for $C_{66}H_{56}N_2P_4Ru$: C, 71.92; H, 5.12; N, 2.54%).

8.4.2 Evidence for *trans*-RuCl(dppe)$_2$(C≡C–C$_5$H$_4$N) (18)

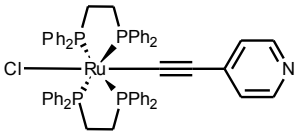

18

A mixture of 4-ethynylpyridine (0.023 g, 0.223 mmol), *cis*-$RuCl_2(dppe)_2$ (0.101 g, 0.104 mmol) and $NaPF_6$ (0.0419 g, 0.249 mmol) in CH_2Cl_2 (3 mL) was stirred at room temperature for 24 h then dried *in vacuo*. The brown residue was washed with diethyl ether (3 x 5 mL) extracted with CH_2Cl_2 (3 x 6 mL) and loaded onto an alumina (grade II) column. Elution with CH_2Cl_2/MeOH (95:5), collection of the yellow band and solvent removal provided a yellow solid (0.08 g) apparently comprising a mixture of the mono- (**18**, 75%) and bis-acetylide (**17**, 25%). This was not easily separated by recrystallization (CH_2Cl_2/*n*-hexane) or column chromatography

(alumina grade V; $CHCl_3$/*n*-hexane). In addition to features attributable to **17**, the following were tentatively assigned to **18**. ^{1}H NMR (400 MHz, $CDCl_3$): δ (ppm) 2.67 (br m, 8H, CH_2), 6.35 (d, *J* = 6.1 Hz, 2H, Py–H_m), 6.95 (t, 8H, Ph–H_m), 7.02 (t, 8H, Ph–H_p), 7.15-7.24 (t, 8H, Ph–*H*), 7.36 (br m, 16H, Ph–H_o), 8.22 (d, *J* = 6 Hz, 2H, Py–H_o). ^{31}P{^{1}H} NMR (162 MHz, $CDCl_3$): δ (ppm) 48.95 (s, *P*Ph_2).

8.4.3 *N*-methyl-4-ethynylpyridinium triflate (19)

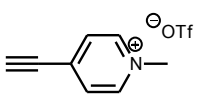

19

A solution of 4-ethynylpyridine (1.00 g, 9.70 mmol) in diethyl ether (40 mL) was cooled to -41°C (acetonitrile/dry ice) whereby methyl triflate (1.45 mL, 12.81 mmol) in diethyl ether (20 mL) was added dropwise. The resulting suspension was raised to room temperature, filtered, washed thoroughly with diethyl ether and dried *in vacuo* to give **19** as an off-white solid (2.06 g, 79%). Spectroscopic data was consistent with that reported previously.[18] ^{1}H NMR (400 MHz, $CDCl_3$): δ (ppm) 3.99 (s, 1H, C≡C–*H*), 4.54 (s, 3H, N–CH_3), 7.97 (d, *J* = 6 Hz, 2H, Py–H_m), 8.85 (d, *J* = 6.7 Hz, 2H, Py–H_o). ^{1}H NMR (400 MHz, D_2O): δ (ppm) 4.32 (s, 3H, N–CH_3), 4.37 (weak s, 1H, C≡C–*H*), 8.03 (d, *J* = 6.6 Hz, 2H, Py–H_m), 8.72 (d, *J* = 6.6 Hz, 2H, Py–H_o). ^{13}C{^{1}H} NMR (100 MHz, D_2O): δ (ppm) 48.01 (N–*C*H_3), 78.39, 92.00, 118.01, 121.16, 130.29 (Py, *C*–H_m), 139.34, 144.97 (Py, *C*–H_o). ^{19}F{^{1}H} NMR (377 MHz, $CDCl_3$): δ (ppm) -78.98 (s, CF_3). IR (ATR): ν (cm^{-1}) 2117 *(C≡C)*, 3234 (C≡*C*–*H*). HR-MS EI+: *m/z* 118.06472 ($[M]^+$ Calc.: 118.06513).

8.4.4 *Trans*-[RuCl(dppe)$_2$(C≡C–C_5H_4N–CH_3)][OTf] (20), *trans*-[Ru(dppe)$_2$(C≡C–C_5H_4N–CH_3)$_2$][OTf]$_2$ (21) and [RuCl(dppe)$_2$(=C=C(H)–C_5H_4N–CH_3)][OTf]$_2$ (22)

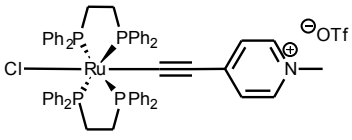

20

Typical procedure: A mixture of **19** (0.407 g, 1.523 mmol) and [RuCl(dppe)$_2$]OTf (1.498 g, 1.384 mmol) in CH_2Cl_2 (14 mL) was stirred overnight at room temperature. After removal of solvent, purification of the crude product was approached in three ways. *Method A.* The vinylidene intermediate was deprotonated and separated from unreacted **19** by column chromatography (alumina grade II; acetone), recrystallized (CH_2Cl_2/*n*-hexane) and dried *in vacuo* to give the title compound as a pale orange solid (0.94 g, 57%) of purity suitable for subsequent reactions. An analytical sample could be obtained by recrystallization from

CH_2Cl_2/MeOH, washing with MeOH and diethyl ether, and drying *in vacuo*. ^{1}H NMR (400 MHz, $CDCl_3$): δ (ppm) 2.69 (br m, 8H, CH_2), 4.09 (s, 3H, N–CH_3), 6.11 (d, J = 6.8 Hz, 2H, Py–H_m), 6.98 (t, 8H, Ph–H_m), 7.06 (m, 16H, Ph–H), 7.25 (m, 8H, Ph–H), 7.48 (br m, 8H, Ph–H_o), 8.02 (d, J = 6.8 Hz, 2H, Py–H_o). ^{31}P{^{1}H} NMR (162 MHz, CD_2Cl_2): δ (ppm) 46.59 (s, PPh$_2$). ^{13}C{^{1}H} NMR (100 MHz, $CDCl_3$): δ (ppm) 30.20 (m, $|^1J_{CP} + {}^3J_{CP}|$ = 11 Hz, CH$_2$), 46.54 (N–CH$_3$), 127.23 (Py, C–H$_m$), 127.57 (Ph, C–H$_m$), 127.84 (Ph, C–H$_m$), 129.73 (Ph, C–H$_p$), 129.84 (Ph, C–H$_p$), 133.56 (Ph, C–H$_o$), 134.46 (Ph, C–H$_o$), 141.90 (Py, C–H$_o$). ^{19}F{^{1}H} NMR (377 MHz, $CDCl_3$): δ (ppm) -78.88 (s, CF_3). IR (ATR): ν (cm^{-1}) 2005 (Ru–C≡C). MS ES+: *m/z* 1050, ([M–OTf]$^+$ Calc.: 1050). (Found: C, 60.50; H, 4.53; N, 1.19. Calc. for $C_{61}H_{55}ClF_3NO_3P_4RuS$: C, 61.08; H, 4.62; N, 1.17%).

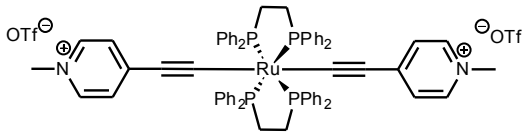

21

Method B. The vinylidene intermediate was loaded onto an alumina (grade II) column in CH_2Cl_2, and eluted with CH_2Cl_2/MeOH (95:5 v/v). The isolated orange fraction contained a mixture of the mono- and bis-alkynyl species, which could be separated by fractional recrystallization (CH_2Cl_2/*n*-hexane) with the bis-alkynyl complex (**21**) precipitating out first as a yellow solid. This was further purified by recrystallization from CH_2Cl_2/$CHCl_3$ at -20°C, washed with a minimum amount of $CHCl_3$ and dried *in vacuo* to provide a yellow-orange powder (0.07 g, 19% – based on 0.138 g, 0.516 mmol **19**). ^{1}H NMR (400 MHz, CD_2Cl_2): δ (ppm) 2.64 (m, 8H, CH_2), 4.17 (s, 6H, N–CH_3), 6.60 (d, J = 6.8 Hz, 4H, Py–H_m), 7.05 (t, J = 7.5 Hz, 16H, Ph–H_m), 7.30 (m, 24H, Ph–H), 8.18 (d, J = 6.9 Hz, 4H, Py–H_o). ^{31}P{^{1}H} NMR (162 MHz, CD_2Cl_2): δ (ppm) 52.97 (s, PPh$_2$). ^{13}C{^{1}H} NMR (100 MHz, CD_2Cl_2): δ (ppm) 30.96 (CH$_2$), 47.26 (N–CH$_3$), 128.21 (Ph, C–H$_m$), 130.39 (Ph, C–H$_p$), 133.89 (Ph, C–H$_o$), 133.89 (Py, C–H$_o$). ^{19}F{^{1}H} NMR (377 MHz, CD_2Cl_2): δ (ppm) -78.91 (s, CF_3). IR (ATR): ν (cm^{-1}) 2021 (Ru–C≡C). MS ES+: *m/z* 566, ([M]$^{2+}$ Calc.: 566). (Found: C, 58.66; H, 4.32; N, 2.04. Calc. for $C_{70}H_{62}F_6N_2O_6P_4RuS_2$: C, 58.78; H, 4.37; N, 1.96%).

20 was isolated as a second orange fraction from the fractional recrystallization procedure, washed with methanol (2 x 50 mL), ether, and *n*-hexane to provide a orange solid (0.22 g, 39% – based on 0.503 g, 0.465 mmol of [RuCl(dppe)$_2$]OTf). Spectroscopic features were identical to those observed previously.

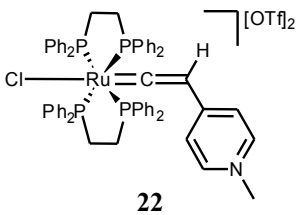

22

Method C. Filtration of the solution prior to deprotonation provided a mixture of the vinylidene intermediate (**22**) and unreacted **19**. Crystals suitable for X-ray diffraction were obtained by slow diffusion of *n*-hexane into a CH_2Cl_2 solution. Co-crystallisation of both components indicated this was not a useful purification procedure. ^{1}H NMR (400 MHz, $CDCl_3$): δ (ppm) 3.09 (br m, 4H, CH_2), 3.82 (s, 3H, N–CH_3), 5.89 (d, J = 6.7 Hz, 2H, Py–H_m), 6.15 (quint., $^4J_{HP}$ = 2.7 Hz, 1H, C=CH), 7.00-7.48 (m, 40H, Ph–H) 7.94 (d, J = 6.4 Hz, 2H, Py–H_o). ^{31}P{^{1}H} NMR (162 MHz, $CDCl_3$): δ (ppm) 33.16 (s, PPh$_2$).

8.4.5 *Trans*-[RuCl(dppe)$_2$(C≡C–C$_5$H$_4$N–CH$_3$)]Cl (23)

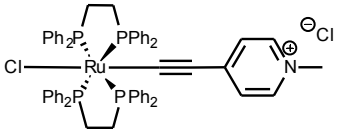

23

A 20 mL volume of Amberlite IRA 410 (strongly basic anion exchange resin, chloride form) was washed sequentially with water (3 x 100 mL), acetone (3 x 20 mL), petroleum benzine (3 x 20 mL), acetone (3 x 20 mL) and methanol (3 x 20 mL). A solution of **20** (0.033 g, 0.028 mmol) in methanol (150 mL) was eluted dropwise through the resin and dried *in vacuo* to yield the title compound as an orange-red solid in quantitative yield. Crystals suitable for X-ray diffraction were grown from slow diffusion of *n*-hexane into a $CDCl_3$ solution. ^{1}H NMR (400 MHz, $CDCl_3$): δ (ppm) 2.68 (br m, 8H, CH_2), 4.34 (s, 3H, N–CH_3), 6.16 (d, J = 6.5 Hz, 2H, Py–H_m), 6.97 (t, 8H, Ph–H_m), 7.01-7.14 (m, 16H, Ph–H), 7.24 (m, 8H, Ph–H), 7.44 (br m, 8H, Ph–H_o), 8.48 (d, J = 6.6 Hz, 2H, Py–H_o). ^{31}P{^{1}H} NMR (162 MHz, $CDCl_3$): δ (ppm) 47.22 (s, PPh$_2$). ^{13}C{^{1}H} NMR (100 MHz, $CDCl_3$): δ (ppm) 30.20 (m, $|^1J_{CP} + {}^3J_{CP}|$ = 10 Hz, CH$_2$), 46.76 (N–CH$_3$), 127.01 (Py, C–H$_m$), 127.53 (Ph, C–H$_m$), 127.79 (Ph, C–H$_m$), 129.68 (Ph, C–H$_p$), 129.80 (Ph, C–H$_p$), 133.59 (Ar, C–R), 134.41 (Ph, C–H$_o$), 134.50 (Ph, C–H$_o$), 134.78 (br, Ru–C≡C), 142.36 (Py, C–H$_o$). IR (ATR): ν (cm^{-1}) 2018 (Ru–C≡C). HR-MS ES+: *m/z* 1050.2028, ([M]$^+$ Calc.: 1050.2017). (Found: C, 66.44; H, 5.16; N, 1.35. Calc. for $C_{60}H_{55}Cl_2NP_4Ru$: C, 66.36; H, 5.10; N, 1.29%).

8.4.6 *Trans*-[Ru(dppe)$_2$(C≡C–C$_6$H$_5$)(C≡C–C$_5$H$_4$N–CH$_3$)]OTf (24)

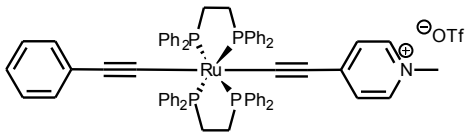

24

A mixture of **20** (0.101 g, 0.084 mmol), phenylacetylene (0.02 mL, 0.182 mmol), $NaPF_6$ (0.058 g, 0.345 mmol) and Et_3N (0.05 mL, 0.357 mmol) in CH_2Cl_2 (3 mL) was stirred for 24 h at 30°C, whereby the suspension was filtered and solvent removed. The crude material was recrystallized (CH_2Cl_2/*n*-hexane), washed with *n*-hexane (3 x 20 mL), ethanol (1 x 20 mL) and ether (3 x 20 mL) to provide **24** as an orange-red solid (0.09 g, 85%). ^{1}H NMR (400 MHz, $CDCl_3$): δ (ppm) 2.61 (br m, 8H, CH_2), 4.04 (s, 3H, N–CH_3), 6.23 (d, *J* = 6.8 Hz, 2H, Py–H_m), 6.90-7.30 (m, 37H, Ph–*H*), 7.81 (br m, 8H, Ph–H_o), 7.89 (d, *J* = 6.8 Hz, 2H, Py–H_o). ^{31}P{^{1}H} NMR (162 MHz, $CDCl_3$): δ (ppm) 52.45 (s, *P*Ph$_2$). ^{13}C{^{1}H} NMR (100 MHz, $CDCl_3$): δ (ppm) 31.28 (br, *C*H$_2$), ~46.75 (N–*C*H$_3$), 127.36 (Py, *C*–H$_m$), 127.62 (Ph, *C*–H), 127.99 (Ph, *C*–H), 129.53 (Ph, *C*–H), 129.92 (Ph, *C*–H), 133.40 (Ph, *C*–H), 134.48 (Ph, *C*–H$_o$), 141.70 (Py, *C*–H$_o$). ^{19}F{^{1}H} NMR (377 MHz, CD_2Cl_2): δ (ppm) -71.96 (s, CF_3), -73.86 (s, CF_3). IR (ATR): ν (cm^{-1}) 1998 (Ru–*C*≡*C*), 2018 (Ru–*C*≡*C*). HR-MS ES+: *m/z* 1116.2747, ([M–OTf]$^+$ Calc.: 1116.2720). (Found: C, 58.11; H, 4.28; N, 1.01. Calc. for $C_{69}H_{60}F_3NO_3P_4RuS$: C, 65.50; H, 4.78; N, 1.11%).

8.4.7 *Trans*-[Ru(dppe)$_2$(C≡C–C$_6$H$_5$)(C≡C–C$_5$H$_4$N–CH$_3$)]I (25)

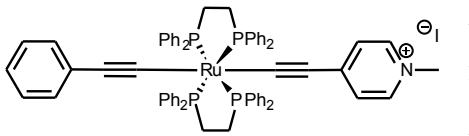

25

A 10% w/w solution of potassium iodide in water (100 mL) was eluted dropwise through a 20 mL dry volume of Amberlite IRA 410 (strongly basic anion exchange resin, chloride form) over ~45 min. The resin was washed with water (3 x 100 mL), acetone (3 x 20 mL), petroleum benzine (3 x 20 mL), acetone (3 x 20 mL) and methanol (3 x 20 mL). A solution of **24** (0.040 g, 0.032 mmol) in methanol (700 mL) was eluted dropwise through the resin and dried (alumina grade II, CH_2Cl_2/MeOH [95:5] → *in vacuo*) to yield the title compound as a red solid (0.030 g, 75%). ^{1}H NMR (400 MHz, $CDCl_3$): δ (ppm) 2.61 (br m, 8H, CH_2), 4.36 (s, 3H, N–CH_3), 6.26 (d, *J* = 6.7 Hz, 2H, Py–H_m), 6.9-7.3 (m, 37H, Ph–*H*), 7.77 (br m, 8H, Ph–H_o), 8.48 (d, *J* = 6.7 Hz, 2H, Py–H_o). ^{31}P{^{1}H} NMR (162 MHz, $CDCl_3$): δ (ppm) 52.59 (s, *P*Ph$_2$). IR (ATR): ν (cm^{-1}) 2020 (br, Ru–*C*≡*C*). HR-MS ES+: *m/z*

1116.3842 ([M–I]$^+$ Calc.: 1116.2720). MS ES–: *m/z* 126.9 (weak) (I^- Calc.: 126.9). (Found: C, 67.58; H, 5.37; N, 1.15. Calc. for $C_{68}H_{60}INP_4Ru$: C, 65.70; H, 4.87; N, 1.13%).

8.4.8 Attempted demethylation reactions (26)

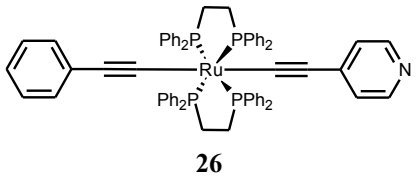

26

A mixture of **25** (0.002 g, 0.002 mmol) and PPh_3 (0.004 g, 0.015 mmol) in DMSO-d_6 (~0.6 mL) was heated under a constant pressure of nitrogen at 150°C. After 1-3 days, resonances attributable to [Me–PPh_3]I[19] were observed in $^1H/^{31}P\{^1H\}$ NMR spectra. Those of **26** were not easily identified in the crude spectrum. ^1H NMR (400 MHz, DMSO-d_6): δ (ppm) 3.15 (d, $^2J_{HP}$ = 15 Hz, 3H, P–CH_3). $^{31}P\{^1H\}$ NMR (162 MHz, DMSO-d_6): δ (ppm) 22.68 (s, *P*MePh$_3$). For comparison, an analogous experiment using *N*-methylpyridinium iodide (0.002 g, 0.009 mmol) and PPh_3 (0.022 g, 0.085 mmol) was run concurrently. ^1H NMR (400 MHz, DMSO-d_6): δ (ppm) 3.16 (d, $^2J_{HP}$ = 15 Hz, 3H, P–CH_3). $^{31}P\{^1H\}$ NMR (162 MHz, DMSO-d_6): δ (ppm) 22.68 (s, *P*MePh$_3$).

8.5 COMPOUNDS SYNTHESISED IN CHAPTER 5

8.5.1 Bis[4-(trimethylsilyl)ethynylbenzene]-3,5-diethynylpyridine (27)

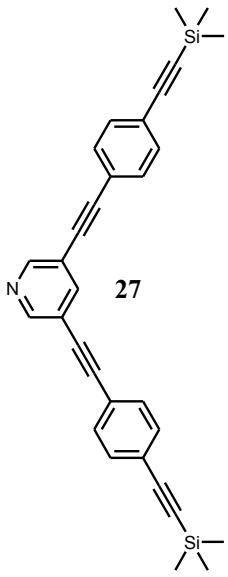

27

A mixture of 3,5-diethynylpyridine (0.122 g, 0.960 mmol), 1-bromo-4-(trimethylsilyl)ethynylbenzene (0.730 g, 2.881 mmol), $PdCl_2(PPh_3)_2$ (0.027 g, 0.038 mmol), CuI (0.015 g, 0.076 mmol) and DIPA (5 mL) was stirred at 90°C for 36 h. After solvent removal the crude residue was purified by column chromatography (silica; CH_2Cl_2) to provide **27** as a pale yellow solid (0.25 g, 55%). ^1H NMR (400 MHz, $CDCl_3$): δ (ppm) 0.26 (s, 18H, Si–CH_3), 7.47 (s, 8H, Ar–*H*), 7.92 (t, *J* = 2 Hz, 1H, Py–H_p), 8.67 (d, *J* = 2 Hz, 2H, Py–H_o). $^{13}C\{^1H\}$ NMR (100 MHz, $CDCl_3$): δ (ppm) 0.03 (Si–*C*H_3), 87.07 (C≡C), 93.06 (C≡C), 97.01 (C≡C), 104.51 (C≡C), 120.07 (Ar, *C*–C≡C), 122.36 (Ar, *C*–C≡C), 123.90 (Ar, *C*–C≡C), 131.67 (Ph, *C*–H), 132.14 (Ph, *C*–H), 140.65 (Py, *C*–H_p), 151.06 (Py, *C*–H_o). IR (ATR): ν (cm^{-1}) 2154 (Si–*C*≡*C*), 2212

(wk, Py–*C*≡*C*). HR-MS ES+: *m/z* 472.1909, ([M+H]$^+$ Calc.: 472.1917). (Found: C, 78.82; H, 6.34; N, 3.09. Calc. for $C_{31}H_{29}NSi_2$: C, 78.93; H, 6.20; N, 2.97%).

8.5.2 *Trans*-$RuCl_2(PP_3)_2$ (28)

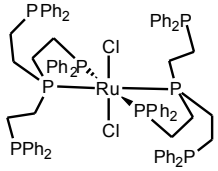

28

A solution of $RuCl_2(PPh_3)_4$ (0.150 g, 0.123 mmol) and PP_3 (0.214 g, 0.319 mmol) in toluene (1 mL) was heated in an oil bath at 120°C for 2 h. After cooling, the toluene solution was filtered through cotton wool into a clean glass vial, using CH_2Cl_2 (3 mL) to extract residual material from the reaction flask. Diethyl ether (20 mL) was layered above the toluene/CH_2Cl_2 solution, forming yellow crystals after 6 days. The solution was decanted, the solid material washed with diethyl ether (1 x 15 mL) and acetone (1 x 15 mL) and dried *in vacuo* to provide **28** as a yellow-orange powder (0.133 g, 71%). Crystals suitable for X–ray diffraction were obtained by slow diffusion of diethyl ether into a CH_2Cl_2 solution of **28**. ^{1}H NMR (400 MHz, $CDCl_3$): δ (ppm) 1.45 (br m, 4H, CH_2), 1.77 (br m, 12H, CH_2), 1.94 (br m, 4H, CH_2), 2.53 (br m, 4H, CH_2), 6.98 (t, *J* = 7.6 Hz, 8H, Ph–*H*), 7.12 (t, *J* = 7.4 Hz, 4H, Ph–*H*), 7.15-7.30 (m, 40H, Ph–*H*), 7.56 (m, 8H, Ph–*H*). ^{31}P{^{1}H} NMR (162 MHz, $CDCl_3$) d (ppm) -11.79 (t, $^3J_{PP}$ = ~13 Hz, 4P, free *P*Ph_2), 40.73 (t, $|^2J_{PP} + {}^3J_{PP}|$ = 24 Hz, 2P, bound *P*Ph_2), 49.54 (m, 2P, bridgehead *P*). ^{13}C{^{1}H} NMR (100 MHz, $CDCl_3$): δ (ppm) 20.37 (*C*H_2), 22.41 (*C*H_2), 22.55 (*C*H_2), 127.44 (Ph, *C*–H), 128.43 (Ph, *C*–H), 128.48 (Ph, *C*–H), 128.53 (Ph, *C*–H), 128.73 (Ph, *C*–H), 129.29 (Ph, *C*–H), 132.64 (Ph, *C*–H), 132.82 (Ph, *C*–H), 133.10 (Ph, *C*–H), 133.28 (Ph, *C*–H), 134.37 (Ph, *C*–H), 136.80 (Ph, *C*–H). UV-vis (CH_2Cl_2): λ_{max}/nm (ε/M^{-1} cm^{-1}) 255sh (62078) 305sh (3825). MS ES+: *m/z* 1513, ([M+H]$^+$ Calc.: 1513). (Found: C, 66.75; H, 5.66. Calc. for $C_{84}H_{84}Cl_2P_8Ru$: C, 66.67; H, 5.59%).

8.5.3 *Trans*-$RuCl(dppe)_2(C{\equiv}C–m\text{-}C_6H_4–C{\equiv}C–SiC_9H_{21})$ (29)

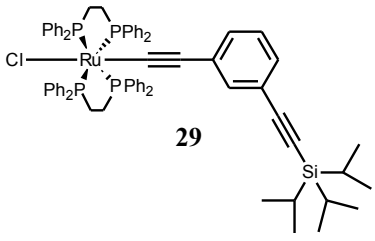

29

A solution of 1-(triisopropylsilyl)ethynyl-3-ethynylbenzene (0.37 g, 1.310 mmol) in CH_2Cl_2 (3 mL) was degassed (freeze-pump-thaw) and added to a flask containing [$RuCl(dppe)_2$]OTf (1.417 g, 1.309 mmol). Residual alkyne was washed into the reaction mixture with CH_2Cl_2 (4 x 3 mL), and the yellow suspension stirred for 20 h. After solvent removal, the crude material was washed with diethyl ether (3 x 20

mL), re-dissolved in CH_2Cl_2 and eluted through alumina (grade II). The yellow band was collected, recrystallized (CH_2Cl_2/*n*-hexane) and dried *in vacuo* to provide **29** as a pale yellow powder (1.25 g, 79%). ^{1}H NMR (400 MHz, $CDCl_3$): δ (ppm) 1.20 (s, 21H, Si–^{i}Pr), 2.67 (br s, 8H, CH_2), 6.61 (d, J = 7.5 Hz, 1H, Ar–*H*), 6.71 (s, 1H, Ar–*H*), 6.90-7.50 (m, 42H, Ar–*H*). ^{31}P{^{1}H} NMR (162 MHz, $CDCl_3$): δ (ppm) 49.48 (s, *P*Ph$_2$). ^{13}C{^{1}H} NMR (100 MHz, $CDCl_3$): δ (ppm) 11.55 (Si–^{i}Pr), 18.91 (Si–^{i}Pr), 30.86 (m, *C*H$_2$), 88.84 (C≡C), 108.04 (C≡C), 112.34 (Ru–C≡*C*), 122.49 (Ar, *C*–C≡C), 126.24 (Ar, *C*–C≡C), 127.12 (Ph, *C*–H$_m$), 127.36 (Ph, *C*–H$_m$), 127.44 (Ar, *C*–H), 128.92 (Ph, *C*–H$_p$), 129.01 (Ph, *C*–H$_p$), 130.04 (Ar, *C*–H), 134.23 (Ph, *C*–H$_o$), 134.68 (Ph, *C*–H$_o$), 135.94 (m), 136.49 (m). IR (ATR): ν (cm^{-1}) 2063 (Ru–*C*≡*C*), 2149 (Si–*C*≡*C*). MS FAB+: *m/z* 1179, ([M–Cl]$^+$ Calc.: 1179). (Found: C, 70.15; H, 6.05. Calc. for $C_{71}H_{73}ClP_4RuSi$: C, 70.20; H, 6.06%).

8.5.4 3-Iodo-ethynylbenzene (31)

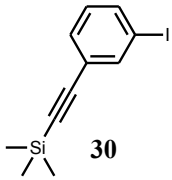

30

1.7 M ^{t}BuLi in pentane (13.4 mL, 22.78 mmol) was added dropwise to a solution of 3-bromo-(trimethylsilyl)ethynylbenzene (2.81 g, 11.10 mmol) in diethyl ether (100 mL) held at -78°C (acetone/dry ice). After 30 min, I_2 (5.79 g, 22.81 mmol) in diethyl ether (80 mL) was added, the mixture stirred a further 10 min at -78°C, then raised to room temperature and quenched with aqueous sodium thiosulphate (30% w/w, 100 mL). The organic layer was extracted with diethyl ether (3 x 50 mL) and the combined organic fractions were dried ($MgSO_4$) and filtered (Celite). Removal of solvent provided crude 3-iodo-(trimethylsilyl)ethynylbenzene as a pale orange liquid (3.41 g), used in the next step without further purification. Spectroscopic data was consistent with that reported previously.[20] ^{1}H NMR (400 MHz, $CDCl_3$): δ (ppm) 0.24 (s, 9H, Si–CH_3), 7.03 (t, J = 7.8 Hz, 1H, Ar–*H*), 7.41 (dt, J = 7.8, 1.3 Hz, 1H, Ar–*H*), 7.64 (ddd, J = 8.1, 1.8, 1 Hz, 1H, Ar–*H*), 7.82 (t, J = 1.6 Hz, 1H, Ar–*H*). ^{13}C{^{1}H} NMR (100 MHz, $CDCl_3$): δ (ppm) 0.14 (Si–*C*H$_3$), 93.50, 95.90, 103.15, 125.21 (*C*–C≡C), 129.71 (Ar, *C*–H), 131.02 (Ar, *C*–H), 137.49 (Ar, *C*–H), 140.54 (Ar, *C*–H). IR (ATR): ν (cm^{-1}) 2160 (*C*≡*C*). HR-MS EI+: *m/z* 299.98271 ([M]$^+$ Calc.: 299.98257).

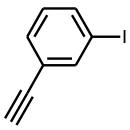

31

A mixture of crude 3-iodo-(trimethylsilyl)ethynylbenzene (3.41 g, ≤11.10 mmol) and 1M NaOH (6 mL, 6 mmol) in methanol/THF (120 mL, 1:1) was stirred overnight then neutralised with aqueous $NaHCO_3$ (3.5% w/w, 100 mL). After extraction with CH_2Cl_2 (3 x 100 mL), the combined fractions were dried ($MgSO_4$),

filtered (Celite) and purified by column chromatography (silica; petroleum benzine) to provide **31** as a pale yellow oil (1.84 g, 73% over two steps). Spectroscopic data was consistent with that reported previously.[20] ^{1}H NMR (400 MHz, $CDCl_3$): δ (ppm) 3.12 (s, 1H, C≡C–*H*), 7.05 (t, *J* = 7.9 Hz, 1H, Ar–*H*), 7.45 (dt, *J* = 7.7, 1.1 Hz, 1H, Ar–*H*), 7.68 (dt, *J* = 8.2, 1.3 Hz, 1H, Ar–*H*), 7.85 (t, *J* = 1.3 Hz, 1H, Ar–*H*). ^{13}C{^{1}H} NMR (100 MHz, $CDCl_3$): 78.69 (C≡*C*–H), 82.01, 93.69, 124.29 (Ar, *C*–C≡C), 129.95 (Ar, *C*–H), 131.38 (Ar, *C*–H), 138.00 (Ar, *C*–H), 140.82 (Ar, *C*–H). IR (ATR): ν (cm^{-1}) 3288 (C≡*C*–*H*). HR-MS EI+: *m/z* 227.94301 ([M]$^{+}$ Calc.: 227.94304).

8.5.5 *Trans*-Ru(dppe)$_2$(C≡C–*m*-C$_6$H$_4$–C≡C–SiC$_9$H$_{21}$)(C≡C–*m*-C$_6$H$_4$–I) (32)

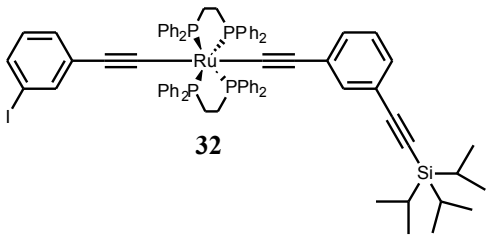

32

A solution of **31** (0.4 g, 1.75 mmol) in CH_2Cl_2 (3 mL) was degassed (freeze-pump-thaw) and added to a flask containing **29** (1.056 g, 0.869 mmol) and $NaPF_6$ (0.296 g, 1.762 mmol). Residual alkyne ligand was washed into the reaction flask with CH_2Cl_2 (3 x 2 mL), whereby additional CH_2Cl_2 (24 mL) and Et_3N (0.49 mL, 3.52 mmol) were added. After stirring overnight at room temperature, the yellow suspension was filtered and solvent removed. The residue was recrystallized (CH_2Cl_2/*n*-hexane) and washed with *n*-hexane (3 x 50 mL), MeOH (50 mL, portionwise) and diethyl ether (3 x 50 mL), providing **32** as a yellow powder (1.1 g, 90%). ^{1}H NMR (400 MHz, CD_2Cl_2): δ (ppm) 1.21 (s, 21H, Si–^{i}Pr), 2.61 (br s, 8H, C*H*$_2$), 6.78 (m, 2H, Ar–*H*), 6.89 (m, 3H, Ar–*H*), 7.01 (m, 16H, Ar–*H*), 7.10 (d, *J* = 4.8 Hz, 2H, Ar–*H*), 7.22 (m, 8H, Ar–*H*), 7.31 (d, 1H, Ar–*H*), 7.47 (br m, 8H, Ph–*H*$_o$), 7.54 (br m, 8H, Ph–*H*$_o$). ^{31}P{^{1}H} NMR (162 MHz, CD_2Cl_2): δ (ppm) 52.93 (s, *P*Ph$_2$). ^{13}C{^{1}H} NMR (100 MHz, CD_2Cl_2): δ (ppm) 11.82 (Si–^{i}Pr), 18.95 (Si–^{i}Pr), 31.76 (m, C*H*$_2$), 89.35 (C≡C), 93.94 (C≡C), 108.20 (C≡C), 122.93, 126.61, 127.50 (Ph, *C*–H$_m$), 127.94, 129.18, 129.53 (Ph, *C*–H$_p$), 130.23, 130.62 (Ar, *C*–H), 132.08, 132.50, 134.56 (Ph, *C*–H$_o$), 137.32 (m, Ru–*C*≡C), 139.71 (Ar, *C*–H). IR (ATR): ν (cm^{-1}) 2054 (Ru–*C*≡*C*), 2148 (Si–*C*≡*C*). MS MALDI+: *m/z* 1406.3 (weak) ([M]$^{+}$ Calc.: 1406.3). (Found: C, 67.25; H, 5.49. Calc. for $C_{79}H_{77}IP_4RuSi$: C, 67.47; H, 5.52%).

8.5.6 {*μ*-3,5-$NC_5H_3(C{\equiv}C–$*m*-$C_6H_4–C{\equiv}C)_2$}{$Ru(dppe)_2(C{\equiv}C–$*m*-$C_6H_4–C{\equiv}C–SiC_9H_{21})$} (33)

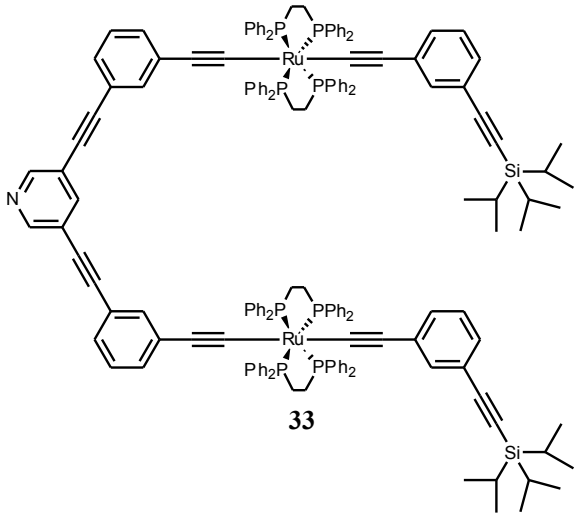

33

THF (9 mL) and DIPA (3 mL) were added to a mixture of **32** (1.030 g, 0.732 mmol), 3,5-diethynylpyridine (0.046 g, 0.362 mmol), $PdCl_2(PPh_3)_2$ (0.006 g, 0.009 mmol) and CuI (0.003 g, 0.016 mmol). The yellow suspension was stirred at room temperature for 45 h, whereby solvent was removed *in vacuo*. The residue was purified by column chromatography (alumina V, petroleum benzine/$CHCl_3$ [1:0→6:4]) to provide **33** as a yellow solid (0.60 g, 61%). ^{1}H NMR (400 MHz, $CDCl_3$): δ (ppm) 1.20 (s, 42H, Si–^{i}Pr), 2.60 (br s, 16H, CH_2), 6.72 (dt, 2H, Ar–*H*), 6.79 (m, 4H, Ar–*H*), 6.86 (br s, 2H, Ar–*H*), 6.98 (m, 32H, Ph–H_m), 7.06 (t, 2H, Ar–*H*), 7.10-7.23 (m, 22H, Ar–*H*), 7.46 (br m, 16H, Ph–H_o), 7.57 (br m, 16H, Ph–H_o), 7.98 (t, 1H, Py–H_p), 8.73 (d, 2H, Py–H_o). ^{31}P{^{1}H} NMR (162 MHz, $CDCl_3$): δ (ppm) 53.79 (s, *P*Ph_2). ^{13}C{^{1}H} NMR (100 MHz, $CDCl_3$): δ (ppm) 11.58 (Si–^{i}Pr), 18.92 (Si–^{i}Pr), 31.61 (m, *C*H_2), 84.48 (C≡C), 88.89 (C≡C), 108.09 (C≡C), 120.82 (Ar, *C*–C≡C), 121.40 (Ar, *C*–C≡C), 122.62 (Ar, *C*–C≡C), 126.05, 126.45, 127.25 (Ph, *C*–H_m), 127.54, 127.86, 128.82 (Ph, *C*–H_p), 128.89 (Ph, *C*–H_p), 129.95, 130.79, 133.93, 134.25 (Ph, *C*–H_o), 134.46 (Ph, *C*–H_o), 137.05 (m, Ru–*C*≡C), 140.47 (Py, *C*–H_p), 150.71 (Py, *C*–H_o). IR (ATR): ν (cm^{-1}) 2050 (Ru–*C*≡*C*), 2148 (Si–*C*≡*C*), 2213 (Py–*C*≡*C*). MS MALDI+: *m/z* 2684.8 (ex. weak) ([M+H]$^+$ Calc.: 2684.8). (Found: C, 73.92; H, 5.86; N, 0.51. Calc. for $C_{167}H_{157}NP_8Ru_2Si_2$: C, 74.73; H, 5.90; N, 0.52%).

8.5.7 {*μ*-3,5-NC_5H_3($C{\equiv}C$–*m*-C_6H_4–$C{\equiv}C$)$_2$}{Ru(dppe)$_2$($C{\equiv}C$–*m*-C_6H_4–$C{\equiv}C$–H)} (34)

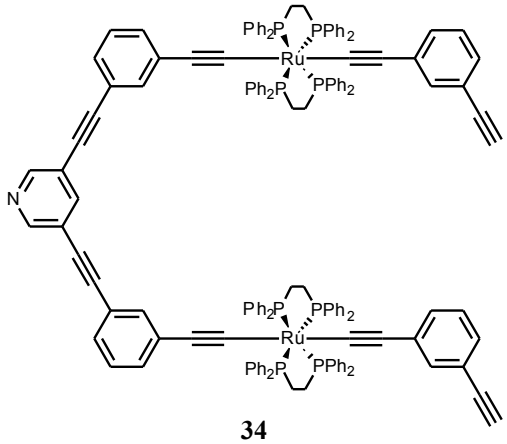

34

1.0 M TBAF in THF (0.45 mL, 0.45 mmol) was added dropwise to a solution of **33 (**0.55 g, 0.205 mmol) in THF (20 mL). After stirring at room temperature for 1.5 h, the yellow solution was dried *in vacuo* and redissolved in CH_2Cl_2. This was washed with water (1 x 50 mL), dried ($MgSO_4$), filtered (Celite) and purified by column chromatography (alumina grade V, *n*-hexane/$CHCl_3$ [1:0→8:2]) to provide **34** as a bright yellow solid (0.23 g, 47%). ^{1}H NMR (400 MHz, $CDCl_3$): δ (ppm) 2.63 (br s, 16H, C*H*$_2$), 3.06 (s, 2H, C≡C–*H*), 6.75-6.88 (m, 8H, Ar–*H*), 6.98 (m, 32H, Ar–*H*), 7.08-7.38 (m, 24H, Ar–*H*) 7.52 (br s, 32H, Ar–*H*$_o$), 8.00 (t, 1H, Py–*H*$_p$), 7.45 (d, 2H, Py–*H*$_o$). ^{31}P{^{1}H} NMR (162 MHz, $CDCl_3$): δ (ppm) 53.67 (s, *P*Ph_2). ^{13}C{^{1}H} NMR (100 MHz, $CDCl_3$): δ (ppm) 31.55 (m, *C*H_2), 76.10 (C≡*C*–H), 84.50 (C≡C), 94.34 (C≡C), 116.00 (Ru–C≡*C*), 120.80 (Ar, *C*–C≡C), 121.20 (Ar, *C*–C≡C). 121.37 (Ar, *C*–C≡C), 126.04, 126.59, 127.23 (Ph, *C*–H$_m$), 127.64, 127.86, 128.86 (Ph, *C*–H$_p$), 130.48, 130.56, 130.76, 133.96, 134.11, 134.32 (Ph, *C*–H$_o$), 136.95 (br m, Ru–*C*≡C), 140.48, 150.70 (Py, *C*–H$_p$), 153.67 (Py, *C*–H$_o$). IR (ATR): ν (cm^{-1}) 2045 (Ru–*C*≡*C*), 2213 (Py–*C*≡*C*), 3288 (C≡*C*–*H*). MS MALDI+: *m/z* 2372.1 ([M]$^+$ Calc.: 2371.5). (Found: C, 73.85; H, 5.04; N, 0.61. Calc. for $C_{149}H_{117}NP_8Ru_2$: C, 75.46; H, 4.97; N, 0.59%).

8.5.8 Evidence for cyclo{μ-3,5-$NC_5H_3(C{\equiv}C–m\text{-}C_6H_4–C{\equiv}C)_2\}_2\{Ru(dppe)_2\}_2$ (35)

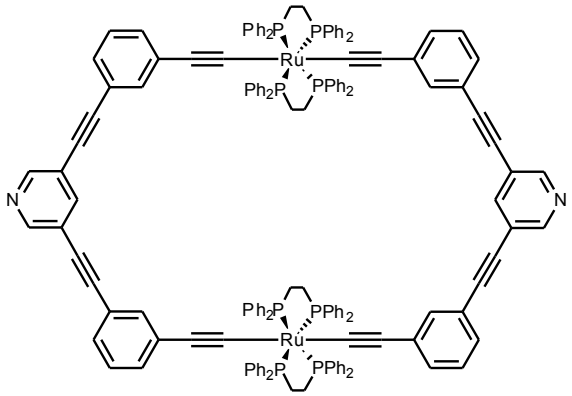

35

A mixture of **34** (0.181 g, 0.076 mmol), 3,5-diiodopyridine (0.025 g, 0.076 mmol), $PdCl_2(PPh_3)_2$ (0.002 g, 0.003 mmol), CuI (0.001 g, 0.005 mmol), THF (5 mL) and DIPA (1 mL) was stirred for 44 h at room temperature. Solvent was removed and the residue extracted into CH_2Cl_2. The solution was filtered through a short alumina (grade II) plug and dried *in vacuo*, providing **35** (0.08 g, 43%) in ~85% purity. Column chromatography on alumina (grade II and V, $CHCl_3$/*n*-hexane) appeared to degrade the compound. ^{1}H NMR (400 MHz, $CDCl_3$): δ (ppm) 2.62 (br m, 16H, CH_2), 6.77 (m, 8H, Ar–*H*), 6.98 (t, 32H, Ph–H_m), 7.10-7.24 (m, 24H, Ar-*H*), 7.51 (br m, 32H, Ph–H_o), 7.99 (t, 2H, Py–H_m), 8.74 (d, 4H, Py–H_o). ^{31}P{^{1}H} NMR (162 MHz, $CDCl_3$): δ (ppm) 53.66 (s, *P*Ph_2). ^{13}C{^{1}H} NMR (100 MHz, $CDCl_3$): δ (ppm) 31.56 (m, $|^1J_{CP} + {}^3J_{CP}|$ = 12 Hz, CH_2), 84.49 (C≡C), 94.36 (C≡C), 116.05 (Ru–C≡*C*), 120.80 (Ar, *C*–C≡C), 121.39 (Ar, *C*–C≡C), 126.08 (Ar, *C*–H), 127.25 (Ar, *C*–H_m), 127.87 (Ar, *C*–H), 128.87 (Ar, *C*–H_p), 130.61 (Ar, *C*–H), 130.74 (Ar, *C*–H), 133.94 (Ar, *C*–H), 134.33 (Ar, *C*–H_o), 136.97 (m, $^2J_{CP}$ = 10 Hz, Ru–*C*≡C), 140.46 (Py, *C*–H_p), 150.72 (Py, *C*–H_o). Further purification/characterisation is in progress.

8.5.9 *Trans*-$Ru(dppe)_2(C{\equiv}C–m\text{-}C_6H_4–C{\equiv}C–I)_2$ (36)

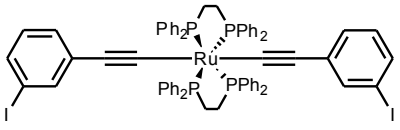

36

A solution of **31** (0.09 g, 0.395 mmol) in CH_2Cl_2 (3 mL) was degassed (freeze-pump-thaw) and added to a flask containing *cis*-$RuCl_2(dppe)_2$ (0.129 g, 0.133 mmol) and $NaPF_6$ (0.091 g, 0.542 mmol). Residual alkyne ligand was washed into the reaction flask with CH_2Cl_2 (4 x 3 mL), whereby Et_3N (0.11 mL, 0.79 mmol) was added. After stirring at room temperature for 3 days the yellow suspension was filtered and thoroughly extracted with CH_2Cl_2. The combined extracts were dried *in vacuo*, recrystallized (CH_2Cl_2/*n*-hexane) and washed with *n*-hexane, MeOH (3 x 10 mL) and diethyl ether (3 x 10 mL), providing **36** as a bright yellow solid (0.14 g, 78%). ^{1}H NMR (400 MHz, $CDCl_3$): δ (ppm) 2.58 (br m, 8H,

CH_2), 6.74 (dt, J = 7.8 Hz, 2H, Ar–H), 6.85 (t, J = 7.4 Hz, 2H, Ar–H), 6.90 (t, 2H, Ar–H), 6.99 (t, J = 7.6 Hz, 16H, Ph–H_m), 7.21 (t, J = 7.4 Hz, 8H, Ph–H_p), 7.32 (dt, J = 7.9 Hz, 2H, Ar–H), 7.49 (br m, 16H, Ph–H_o). $^{31}P\{^1H\}$ NMR (162 MHz, $CDCl_3$): δ (ppm) 53.62 (s, PPh$_2$). $^{13}C\{^1H\}$ NMR (100 MHz, $CDCl_3$): δ (ppm) 31.41 (m, CH$_2$), 93.86 (C≡C), 127.29 (Ph, C–H$_m$), 128.75 (Ar, C–H), 128.96 (Ph, C–H$_p$), 129.20 (Ar, C–H), 131.87 (Ar, C–H), 134.30 (Ph, C–H$_o$), 136.89 (m, $^2J_{CP}$ = ~10 Hz, Ru–C≡C), 139.53 (Ar, C–H). IR (ATR): ν (cm^{-1}) 2057 (Ru–C≡C). HR-MS ES+: *m/z* 1352.9144 ([M+H]$^+$ Calc.: 1353.0544). (Found: C, 57.43; H, 4.06. Calc. for $C_{68}H_{56}I_2P_4Ru$: C, 60.41; H, 4.18%).

8.5.10 *Trans*-Ru(dppe)$_2$(C≡C–*m*-C$_6$H$_4$–C≡C–C$_5$H$_4$N)$_2$ (37)

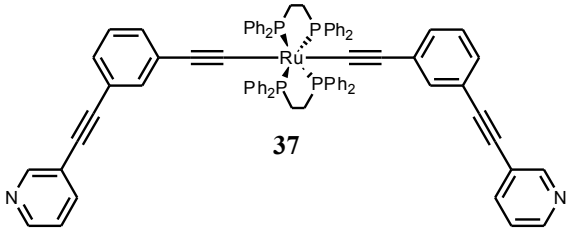

37

THF (3 mL) and DIPA (1 mL) were added to a mixture of **36** (0.080 g, 0.059 mmol), 3-ethynylpyridine (0.0139 g, 0.135 mmol), $PdCl_2(PPh_3)_2$ (0.001 g, 0.001 mmol) and CuI (0.001 g, 0.005 mmol). After stirring for 41 h at room temperature, the resulting suspension was dried *in vacuo*, re-dissolved in $CHCl_3$ and filtered through alumina (grade II). Recrystallization by slow diffusion of diethyl ether into a $CHCl_3$ solution provided **37**·Et$_2$O as bright yellow needles (0.065 g, 79%). ^1H NMR (400 MHz, $CDCl_3$): δ (ppm) 2.63 (br m, 8H, CH_2), 6.78 (m, 4H, Ar–H), 6.98 (t, J = 7.6 Hz, 16H, Ph–H_m), 7.09-7.24 (m, 12H, Ar–H), 7.32 (ddd, 2H, Py–H_m), 7.52 (br d, 16H, Ph–H_o), 7.84 (dt, J = 7.9, 1.9 Hz, 2H, Py–H_p), 8.56 (dd, J = 4.9, 1.5 Hz, 2H, Py–H_o), 8.81 (d, J = 1.6 Hz, 2H, Py–$H_{o'}$). $^{31}P\{^1H\}$ NMR (162 MHz, $CDCl_3$): δ (ppm) 53.69 (s, PPh$_2$). $^{13}C\{^1H\}$ NMR (100 MHz, $CDCl_3$): δ (ppm) 31.55 (m, $|^1J_{CP} + {}^3J_{CP}|$ = 12 Hz, CH_2), 85.07 (C≡C), 93.70 (C≡C), 116.04 Ru–C≡C), 121.12 (Ar, C–C≡C), 121.55 (Ar, C–C≡C), 123.24 (Py, C–H$_m$), 126.00 (Ar, C–H), 127.24 (Ph, C–H$_m$), 127.82 (Ar, C–H), 128.85 (Ph, C–H$_p$), 130.41 (Ar, C–H), 130.70 (Ar, C–H), 133.93 (Ar, C–H), 134.34 (Ar, C–H$_o$), 136.98 (m, $^2J_{CP}$ = 10 Hz, Ru–C≡C), 138.44 (Py, C–H$_p$), 148.47 (Py, C–H$_o$), 152.41 (Py, C–H$_{o'}$). IR (ATR): ν (cm^{-1}) 2057 (Ru–C≡C), 2211 (Py–C≡C). HR-MS ES+: *m/z* 1303.3086 ([M+H]$^+$ Calc.: 1303.3142). (Found: C, 73.66; H, 5.56; N, 1.97. Calc. for $C_{82}H_{64}N_2P_4Ru$ (**37**): C, 75.62; H, 4.95; N, 2.15. Calc. for $C_{86}H_{74}N_2OP_4Ru$ (**37**·Et$_2$O): C, 75.04; H, 5.42; N, 2.04%).

8.6 REFERENCES

1. D. B. G. Williams and M. Lawton, *J. Org. Chem.*, 2010, **75**, 8351.
2. (a) P. Four and F. Guibe, *J. Org. Chem.*, 1981, **46**, 4439; (b) O. Dangles, F. Guibe, G. Balavoine, S. Lavielle and A. Marquet, *J. Org. Chem.*, 1987, **52**, 4984.
3. E. Bosch and C. L. Barnes, *Organometallics*, 2000, **19**, 5522.
4. (a) N. Stuhr Hansen, *Synth. Commun.*, 2003, **33**, 641; (b) E. H. van Dijk, D. J. T. Myles, M. H. van der Veen and J. C. Hummelen, *Org. Lett.*, 2006, **8**, 2333.
5. Z.-F. Shi, L.-J. Wang, H. Wang, X.-P. Cao and H.-L. Zhang, *Org. Lett.*, 2007, **9**, 595.
6. (a) C. Coudret, *Synth. Commun.*, 1996, **26**, 3543; (b) S. H. Chanteau and J. M. Tour, *Tetrahedron Lett.*, 2001, **42**, 3057; (c) N. R. Champness, A. N. Khlobystov, A. G. Majuga, M. Schröder and N. V. Zyk, *Tetrahedron Lett.*, 1999, **40**, 5413.
7. M. A. Fox, J. E. Harris, S. Heider, V. Pérez-Gregorio, M. E. Zakrzewska, J. D. Farmer, D. S. Yufit, J. A. K. Howard and P. J. Low, *J. Organomet. Chem.*, 2009, **694**, 2350.
8. S. Huang, J. C. S. Wong, A. K. C. Leung, Y. M. Chan, L. Wong, M. R. Fernendez, A. K. Miller and W. Wu, *Tetrahedron Lett.*, 2009, **50**, 5018.
9. P. Blakskjaer and K. V. Gothelf, *Org. Biomol. Chem.*, 2006, **4**, 3442.
10. S. Y.-L. Leung, A. Y.-Y. Tam, C.-H. Tao, H. S. Chow and V. W.-W. Yam, *J. Am. Chem. Soc.*, 2012, **134**, 1047.
11. (a) M. Winkler, B. Cakir and W. Sander, *J. Am. Chem. Soc.*, 2004, **126**, 6135; (b) J. E. Ormond-Prout, P. Smart and L. Brammer, *Cryst. Growth Des.*, 2011, **12**, 205.
12. G. R. Fulmer, A. J. M. Miller, N. H. Sherden, H. E. Gottlieb, A. Nudelman, B. M. Stoltz, J. E. Bercaw and K. I. Goldberg, *Organometallics*, 2010, **29**, 2176.
13. C. Olivier, B. Kim, D. Touchard and S. Rigaut, *Organometallics*, 2008, **27**, 509.
14. C. Engtrakul and L. R. Sita, *Organometallics*, 2008, **27**, 927.
15. E. Lindner, R. Zong and K. Eichele, *Phosphorus, Sulfur Silicon Relat. Elem.*, 2001, **169**, 219.
16. (a) R. F. Kovar, M. D. Rausch and H. Rosenberg, *Organomet. Chem. Synth.*, 1971, **1**, 173; (b) V. P. Dyadchenko, M. A. Dyadchenko, V. N. Okulov and D. A. Lemenovskii, *J. Organomet. Chem.*, 2011, **696**, 468; (c) S. L. Ingham, M. S. Khan, J. Lewis, N. J. Long and P. R. Raithby, *J. Organomet. Chem.*, 1994, **470**, 153.
17. G. Perin, S. R. Mendes, M. S. Silva, E. J. Lenardão, R. G. Jacob and P. C. d. Santos, *Synth. Commun.*, 2006, **36**, 2587.
18. S. Rubinsztajn, W. K. Fife and M. Zeldin, *Tetrahedron Lett.*, 1992, **33**, 1821.
19. C. Lichtenberg, M. Elfferding and J. Sundermeyer, *Eur. J. Inorg. Chem.*, 2010, **2010**, 3117.
20. O. Lavastre, S. Cabioch, P. H. Dixneuf and J. Vohlidal, *Tetrahedron*, 1997, **53**, 7595.

APPENDICES (DIGITAL CONTENT)

A SELECTED NMR SPECTRA

APPENDIX A - SELECTED NMR SPECTRA.doc

Compounds prepared in Chapter 2.mnova

Compounds prepared in Chapter 3.mnova

Compounds prepared in Chapter 4.mnova

Compounds prepared in Chapter 5.mnova

B CRYSTALLOGRAPHIC DATA

15 (NL1204)	Cyclization product of 4-ethynylphenylthioacetate
17 (NL1207)	*Trans*-$Ru(dppe)_2(C{\equiv}C{-}C_5H_5N)_2$
22 (NL1002)	$[RuCl(dppe)_2(=C=C(H){-}C_5H_4N{-}CH_3)][OTf]_2$
23 (NL1110)	*Trans*-$[RuCl(dppe)_2(C{\equiv}C{-}C_5H_4N{-}CH_3)]Cl$
28 (NL0908)	*Trans*-$RuCl_2(PP_3)_2$

(folders contain .doc files with relevant crystal, refinement and structural data, .cif/.pdb files and .png images for each compound)

C PUBLICATIONS

The publications referenced on page 8 are provided here as .pdf files.

D COMPOUND GUIDE

This .pdf document contains labelled structures for all of the numbered compounds described in this thesis (3 pages).